frontiers | Research Topics

The regulation of environmental factors on the microbial cooperation

Edited by
Hao Li, Ruichang Gao, Wei Hu and Zhenlin Han

Published in
Frontiers in Microbiology

FRONTIERS EBOOK COPYRIGHT STATEMENT

The copyright in the text of individual articles in this ebook is the property of their respective authors or their respective institutions or funders. The copyright in graphics and images within each article may be subject to copyright of other parties. In both cases this is subject to a license granted to Frontiers.

The compilation of articles constituting this ebook is the property of Frontiers.

Each article within this ebook, and the ebook itself, are published under the most recent version of the Creative Commons CC-BY licence. The version current at the date of publication of this ebook is CC-BY 4.0. If the CC-BY licence is updated, the licence granted by Frontiers is automatically updated to the new version.

When exercising any right under the CC-BY licence, Frontiers must be attributed as the original publisher of the article or ebook, as applicable.

Authors have the responsibility of ensuring that any graphics or other materials which are the property of others may be included in the CC-BY licence, but this should be checked before relying on the CC-BY licence to reproduce those materials. Any copyright notices relating to those materials must be complied with.

Copyright and source acknowledgement notices may not be removed and must be displayed in any copy, derivative work or partial copy which includes the elements in question.

All copyright, and all rights therein, are protected by national and international copyright laws. The above represents a summary only. For further information please read Frontiers' Conditions for Website Use and Copyright Statement, and the applicable CC-BY licence.

ISSN 1664-8714
ISBN 978-2-8325-5775-4
DOI 10.3389/978-2-8325-5775-4

About Frontiers

Frontiers is more than just an open access publisher of scholarly articles: it is a pioneering approach to the world of academia, radically improving the way scholarly research is managed. The grand vision of Frontiers is a world where all people have an equal opportunity to seek, share and generate knowledge. Frontiers provides immediate and permanent online open access to all its publications, but this alone is not enough to realize our grand goals.

Frontiers journal series

The Frontiers journal series is a multi-tier and interdisciplinary set of open-access, online journals, promising a paradigm shift from the current review, selection and dissemination processes in academic publishing. All Frontiers journals are driven by researchers for researchers; therefore, they constitute a service to the scholarly community. At the same time, the *Frontiers journal series* operates on a revolutionary invention, the tiered publishing system, initially addressing specific communities of scholars, and gradually climbing up to broader public understanding, thus serving the interests of the lay society, too.

Dedication to quality

Each Frontiers article is a landmark of the highest quality, thanks to genuinely collaborative interactions between authors and review editors, who include some of the world's best academicians. Research must be certified by peers before entering a stream of knowledge that may eventually reach the public - and shape society; therefore, Frontiers only applies the most rigorous and unbiased reviews. Frontiers revolutionizes research publishing by freely delivering the most outstanding research, evaluated with no bias from both the academic and social point of view. By applying the most advanced information technologies, Frontiers is catapulting scholarly publishing into a new generation.

What are Frontiers Research Topics?

Frontiers Research Topics are very popular trademarks of the *Frontiers journals series*: they are collections of at least ten articles, all centered on a particular subject. With their unique mix of varied contributions from Original Research to Review Articles, Frontiers Research Topics unify the most influential researchers, the latest key findings and historical advances in a hot research area.

Find out more on how to host your own Frontiers Research Topic or contribute to one as an author by contacting the Frontiers editorial office: frontiersin.org/about/contact

The regulation of environmental factors on the microbial cooperation

Topic editors

Hao Li — Jining Medical University, China

Ruichang Gao — Jiangsu University, China

Wei Hu — Microbial Technology Institute/Shandong University, China

Zhenlin Han — University of Hawaii at Manoa, United States

Citation

Li, H., Gao, R., Hu, W., Han, Z., eds. (2024). *The regulation of environmental factors on the microbial cooperation*. Lausanne: Frontiers Media SA.

doi: 10.3389/978-2-8325-5775-4

Table of contents

frontiers | Frontiers in Microbiology

TYPE Original Research
PUBLISHED 09 October 2023
DOI 10.3389/fmicb.2023.1257924

Check for updates

OPEN ACCESS

EDITED BY
Ruichang Gao,
Jiangsu University, China

REVIEWED BY
Becky Nancy Aloo,
University of Eldoret, Kenya
Hansong Chen,
Zhejiang Normal University, China

*CORRESPONDENCE
Xiefeng Ye
✉ yexiefeng@henau.edu.cn

†These authors have contributed equally to this work

RECEIVED 13 July 2023
ACCEPTED 18 September 2023
PUBLISHED 09 October 2023

CITATION
Zhou H, Zhang M, Yang J, Wang J, Chen Y and Ye X (2023) Returning ryegrass to continuous cropping soil improves soil nutrients and soil microbiome, producing good-quality flue-cured tobacco.
Front. Microbiol. 14:1257924.
doi: 10.3389/fmicb.2023.1257924

COPYRIGHT
© 2023 Zhou, Zhang, Yang, Wang, Chen and Ye. This is an open-access article distributed under the terms of the Creative Commons Attribution License (CC BY). The use, distribution or reproduction in other forums is permitted, provided the original author(s) and the copyright owner(s) are credited and that the original publication in this journal is cited, in accordance with accepted academic practice. No use, distribution or reproduction is permitted which does not comply with these terms.

Returning ryegrass to continuous cropping soil improves soil nutrients and soil microbiome, producing good-quality flue-cured tobacco

Hanjun Zhou[1,2†], Mingjie Zhang[1†], Jiahao Yang[1], Jing Wang[1], Yulu Chen[1] and Xiefeng Ye[1*]

[1]Key Laboratory of Tobacco Cultivation of Tobacco Industry, National Tobacco Cultivation & Physiology & Biochemistry Research Centre, Tobacco Science College of Henan Agricultural University, Zhengzhou, China, [2]College of Natural Resources and Environment, Northwest A&F University, Yangling, China

The widespread and continuous cultivation of tobacco has led to soil degradation and reduced crop yields and quality. Green manure is an essential organic fertilizer that alleviates obstacles to continuous cultivation. However, the plant–soil microecological effects of green manure on flue-cured tobacco cultivation remain unclear. Thus, a positioning trail including two treatments, chemical fertilizer application only (treatment NPK) and chemical fertilizer application with turning ryegrass (treatment NPKG) was conducted, and the effect of ryegrass returning on the soil physicochemical properties, soil microbiome, crop yield, and quality of flue-cured tobacco in continuous cropping soil were investigated. Results showed that returning ryegrass to the field increased the thickness of soil humus layer from 13 cm to 15 cm, reduced the humus layer soil bulk density to 1.29 cm^3/g. Ryegrass tilled and returned to the field increased soil organic matter content by 6.89–7.92%, increased rhizosphere soil available phosphorus content by 2.22–17.96%, and converted the soil non-exchangeable potassium into potassium that was available for plant absorption and utilization. Ryegrass tilling and returning to the field increased the potassium content of middle leaves of flue-cured tobacco by 7.69–10.07%, the increased potassium content in flue-cured tobacco was accompanied by increased total sugar, reducing sugar, and the ratio of reducing sugar to nicotine, which facilitated the harmonization of the chemical composition of cured tobacco leaves. Moreover, the increased number of markedly improved operational taxonomic units enhanced the complexity of the soil bacterial community and its compactness after ryegrass tillage and their return to the field. The available potassium, available phosphorus, total potassium content, pH, and sampling period of the rhizosphere soil had considerable effects on the rhizosphere microbial. Ryegrass tilling and returning to the field changed the soil microbiome, which increased the abundance of bulk soil Proteobacteria, rhizosphere soil Fibrobacterota, and microbes with anti-pathogen activity (*Lysobacteria, Sphingomonas, Chaetomium, and Minimedusa*); and reduced the abundance of pathogenic fungi *Neocosmospore* genus in the soil. In brief, ryegrass returned to the field, improved soil microecology and restored soil nutrients, and established a new dynamic balance of soil ecology, thereby improving the quality of cultivated land and the quality of flue-cured tobacco.

KEYWORDS

ryegrass, flue-cured tobacco, soil microbiome, soil fertility, quality ryegrass, quality

1. Introduction

Flue-cured tobacco is an economically significant crop (Yang et al., 2015; Liu et al., 2020) and the main raw material for cigarette manufacturing. Its yield and quality play a crucial role in tobacco industry. Continuous cultivation is prevalent in areas ideal for tobacco cultivation, owing to factors such as fertile land resources, economic interests, and cultivation practices (Liu et al., 2020; Mirkarimi et al., 2021). Continuous cropping causes the soil to harden, the plow layer to become shallow, the organic matter content to decrease, the quality of soil fertility to decrease, and the level of land productivity to decline (Aparicio and Costa, 2007), resulting in significant economic losses and seriously affecting the sustainability of the tobacco industry.

Currently, a wide range of measures are used in field production to overcome continuous cropping challenges, including selecting appropriate cropping methods, such as rotation, intercropping, and cover crops (Yang et al., 2017; Li and Wu, 2018; Esmaeilzadeh-Salestani et al., 2021; Gao et al., 2022), proper soil fertilization, such as green manure (Huang et al., 2019; He et al., 2020; Chamkhi et al., 2022), and biological control (Liu et al., 2018). Green manure has been traditionally used since China's long history of agricultural production (Wang T. et al., 2022). De Santos et al. (2018) found that Melons intercropped with green manure not only produce cleaner fruit but also enhance the environment and economy. Yang et al. (2022) reported that replacing urea-N with green manure (*Astragalus sinicus* L.) mitigates CH_4 and NO_2 emissions in rice paddy. Green manure has attracted the interest of many researchers due to its ability to accomplish both food safety and green farming development (Kumar et al., 2011; Liang et al., 2022).

Soil microbiome play a crucial role in soil nutrient conversion, cycling, and maintaining soil ecological functions and health. Alterations in the microbial community are one of the main obstacles to continuous cropping in tobacco production (Chen et al., 2022). Green manure crops are organic fertilizers (Wang X. Y. et al., 2022) that can influence soil microbiome directly through the nutrients in the green manure itself, or indirectly through changes in soil and plant characteristics. Currently, researches on soil microbiology in tobacco field is still under continuous cropping conditions (Wang M. et al., 2022). Few studies have been conducted on the effects of green manure on soil characteristics, soil microbiome, and flue-cured tobacco yield and quality.

The Henan flue-cured tobacco growing region, which has a more than 100-year history of cultivation, is representative of China's strong-flavored flue-cured tobacco. The soil types in the Henan flue-cured tobacco growing region are mostly loamy, which is well aerated and has good water and fertilizer retention capacity. In recent years, the shortage of land resources has led to a severe succession of crops, resulting in soil degradation and poor nutrient availability for flue-cured tobacco plants. Therefore, it is essential to enhance the soil quality in the Henan flue-cured tobacco growing region in order to improve the yield of flue-cured tobacco. Ryegrass is an important source of green manure. In this study, a positioning trail including two treatments, chemical fertilizer application only (treatment NPK) and chemical fertilizer application with turning ryegrass (treatment NPKG) was conducted, and the effect of ryegrass returning on the growth and development of flue-cured tobacco, soil properties, and soil microbiome in continuous cropping soil were investigated. Further, the relationship between soil physicochemical properties and soil microbiome was analyzed. This research provides fundamental knowledge that mitigates the detrimental effects of continuous cultivation and enhances the quality and yield of flue-cured tobacco to promote sustainable agricultural production.

2. Materials and methods

2.1. Study area and experimental design

The investigation was conducted in the Science and Education Park of Henan Agricultural University (113°35′51″E, 34°52′13″N), Zhengzhou, China. It has a north temperate continental monsoon climate, with an average annual temperature of 14°C, an average annual rainfall of about 640 mm, a frost-free period of 220 days, and 2,400 h of annual sunlight. Ryegrass was planted for three seasons before the start of the positioning trial to ensure homogeneous soil fertility. The first ryegrass was sown on April 28, 2017, and was removed from the field on September 5, 2017. On September 22, 2017, the ryegrass was sown for the second time, and on May 10, it was removed from the field. Ryegrass was sown for the third time on May 26, and removed from the field on August 31, 2018. After homogenizing the fields, ryegrass was planted on October 27, 2018, and turned over on March 28, 2019. We started growing flue-cured tobacco in 2019 and returned the entire amount of ryegrass to the tilling plots planted with ryegrass. Before tilling, two 1 m^2 plots representing the overall growth of ryegrass in the plot were selected. The ryegrass was dug out with the roots, and the amount of tillage in each plot was counted after removing the soil and impurities. The ryegrass tilled in 2019, 2020, and 2021 were 6297.58, 7807.68, and 7496.53 kg/hm^2 (on dry a weight basis), respectively. Ryegrass was irrigated, tilled, and not fertilized during the planting period. The test soil was sandy loam with the following basic physicochemical properties: pH 7.57, organic matter (OM) 16.76 g/kg, total nitrogen (TN) 0.69 g/kg, alkaline nitrogen (AN) 32.40 mg/kg, available phosphorus (AP) 29.19 mg/kg, and available potassium (AK) 135.47 mg/kg.

Two treatments were tested: no ryegrass, chemical fertilizer application only (treatment NPK) and chemical fertilizer application with turning ryegrass (treatment NPKG). Each treatment was replicated three times for six plots, and each plot with an area of 66 m^2 (12 m × 5.5 m) was arranged in randomized groups. Cement slabs (100 × 50 × 4 cm, 80 cm buried in the soil) were set around the plot to prevent fertilizer and water from crossing the irrigation. The dosage of N was 52.5 kg/hm^2, N: P_2O_5: K_2O were 1: 2: 3. Special compound fertilizers (N: P_2O_5: K_2O = 8: 12: 20), potassium sulfate (K_2O 52%), and calcium magnesium phosphate (P_2O_5 16%) were used as base fertilizers, which were applied by band application before transplanting. Potassium nitrate (N: P_2O_5: K_2O = 13.5: 0: 44.5) was applied as topdressing and dissolved in water for hole application.

The tobacco variety tested was Zhongyan 100, with 110 cm row spacing and 50 cm plant spacing. Seedling transplantation was performed on April 30, 2020, and April 29, 2021, and harvesting was completed on September 15, 2020, and September 6, 2021. Other management measures were implemented in accordance with local management standards for quality tobacco leaves.

2.2. Sample collection and measurements

2.2.1. Soil sample collection

Bulk and rhizosphere soils were collected 45 and 75 days after transplanting the tobacco seedlings, respectively. Bulk soil collection: The middle position of two tobacco plants was collected at 0–20 cm using a soil auger. Five soil samples were collected from each plot and mixed as one sample. Rhizosphere soil collection: Sampling was carried out using destructive methods. The complete tobacco root system was dug and tapped to allow the loose soil combined with the roots to fall naturally. Then, the soil that was tightly combined with the root system (within 2 mm) was placed into the sampling bag, and the rhizosphere soil samples were collected. Three tobacco plants were selected from each plot to collect the rhizosphere soil, and the rhizosphere soil from the same treatment was mixed as one sample. Each soil sample was divided into two parts: one part was stored in a refrigerator at −80°C for high-throughput sequencing of soil microbrome, and the other was dried in the shade and screened for soil physicochemical indicators. After the flue-cured tobacco was mature and harvested, the soil profile was observed, and soil samples from different soil layers were collected to determine their bulk density.

2.2.2. Determination of physicochemical properties of soil

The ring-knife method was used to determine bulk soil density and soil pH was determined using a pH meter (soil: water = 1: 2.5) (Bao, 2000). AN and TN were determined using the diffusion and Kjeldahl methods, respectively; AP and total phosphorus (TP) were determined using the molybdenum antimony sulfate anti-colorimetric method and NaOH alkali fusion-molybdenum antimony anti-spectrophotometric method, respectively (Bao, 2000); and AK and total potassium (TK) were determined using the flame photometric method and the standards of NY/T87-1988 standards, respectively.

2.2.3. Flue-cured tobacco sample collection and determination

Before harvesting the flue-cured tobacco in 2020 and 2021, three representative tobacco plants were selected for each plot. The height, stem circumference, maximum leaf length, and maximum leaf width of each tobacco plant were determined according to the standard method of YC/T 142–2010. The selected tobacco plant was then centered on the stem base, and the surrounding 30 cm root belt soil was removed. The roots, stems, and leaves of the tobacco were separated and washed with tap water and deionized water. The tobacco plant was placed in an oven for 15 min at 105°C and then dried at 65°C until constant weight.

A continuous flow analyzer (AutoAnalyzer 3, Brown Ruby, Germany) was used to determine the total sugar, reducing sugar, nicotine, chlorine, and potassium contents of flue-cured tobacco leaves according to the standards YC/T159-2002, YC/T160-2002, YC/T217-2007, and YC/T162-2011, the ratio of potassium to chloride, the ratio of reducing sugar to nicotine, and the ratio of reducing sugar to total sugar.

2.2.4. DNA extraction, PCR amplification, and high-throughput sequencing

DNA was extracted from the soil samples using the MagPure Soil DNA KF Kit. Subsequently, the purity and concentration of DNA were detected by agarose gel electrophoresis, and PCR amplification was performed using specific primers with barcodes and high-efficiency, high-quality fidelity enzymes. Bacterial amplification was performed using 343F 5'-TACGGRAGGCAGCAG-3′ and 798R 5'-AGGGTATCTAATCCT-3′. The internal transcribed spacer (ITS) segments of fungal amplification, ITS1F 5'-CTTGGtcatttagaggaagtaa-3′ and ITS2 5'-GCTGCGTTCTTCATCGATGC-3′. Shanghai Ouyi Biomedical Technology was commissioned to perform the sequencing and biological information analysis using a MiSeq sequencer (Illumina). The raw tags were trimmed, merged, and assigned using the split library software (version 1.8.0) in QIIME to remove sequences with more than eight single-base repeats and sequences with lengths less than 200 bp to obtain clean tag sequences. The quality sequence valid tags obtained from the quality control were classified into operational taxonomic units (OTUs) based on 97% similarity using the Vsearch (version 2.4.2) software, and the most abundant sequence in each OTU was selected as the typical sequence of that OTU.

2.3. Statistical analysis

The least significant difference (LSD) test in one-way analysis of variance was used to analyze the differences and significance of soil physicochemical properties, flue-cured tobacco agronomic traits, dry matter accumulation, and soil microbial diversity among the different treatments. Co-occurrence network analysis was performed on OTUs with a total abundance in the top 200 to characterize the complex links between microbial communities. OTUs that were statistically significantly correlated were calculated using the "psych" package in R (Spearman coefficient $\rho \geq 0.7$, $p < 0.05$). The microbial co-occurrence networks for the different treatments were graphed using Gephi software (version 0.9.2), and the topological properties of the networks were calculated. Principal component analysis (PCoA) based on the Bray-Curtis distance matrix was used to analyze the differences in the beta diversity of the microbial community. Redundancy analysis (RDA) was performed using the "vegan" package in R (4.2.2) to assess the relationship between soil physicochemical factors and soil microbial communities. Linear discriminant analysis effect size (LEfSe) was used to search for biomarkers that differed significantly between treatments, with a linear discriminant analysis score of two.

3. Results

3.1. Soil forming layer profile and soil bulk density

The profile of the soil-forming layer and thicknesses of different soil-forming layers are shown in Figure 1 and Table 1, respectively. As shown in Figure 1, the soil profile of the NPKG treatment differed from that of the NPK treatment. Compared to the NPK treatment, the soil texture of the NPKG humus layer was looser. The deposition layer contained coarser particles and had higher soil compactness than the humus layer. The soil deposition layer of the NPKG treatment was more compact and contained more clay particles, but the soil particles were coarser than those of the NPK treatment. Table 1 shows that the thicknesses of the humus, leaching, deposition, and parent material layers in the NPKG treatment were 0–15 cm, 15–30 cm, 30–50 cm, and below 50 cm, respectively. The thicknesses of the humus, leaching, deposition, and parent material layers in the NPK treatment were

10.3389/fmicb.2023.1257924

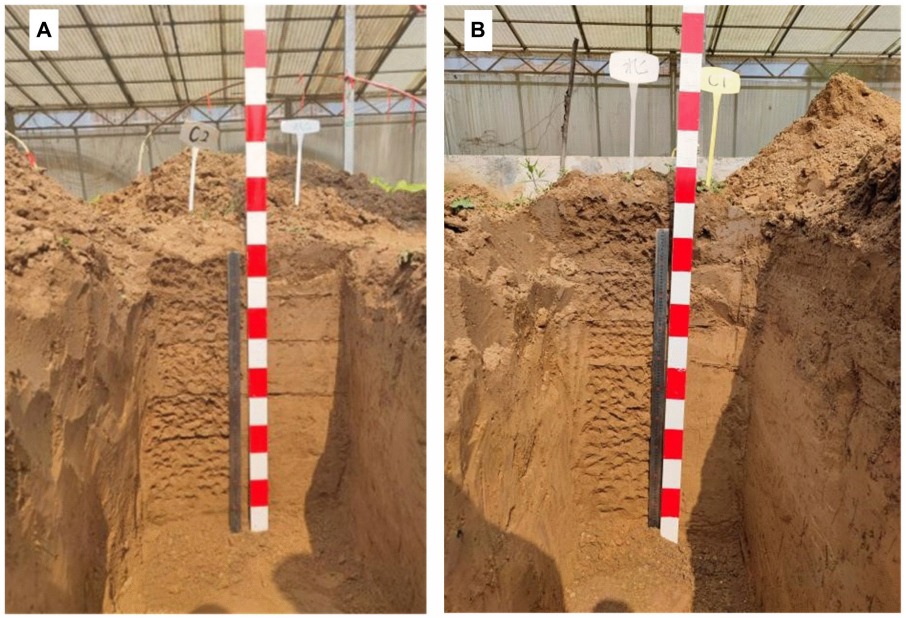

FIGURE 1
Soil profiles of **(A)** NPK and **(B)** NPKG. NPK, no ryegrass, chemical fertilizer application only; NPKG, chemical fertilizer application with turning ryegrass.

TABLE 1 **The thickness and soil bulk density of different soil generating layer.**

Soil generating layers	Soil generating layer thickness (cm)		Soil bulk density (cm^3/g)	
	NPK	NPKG	NPK	NPKG
Humus layer	0–13	0–15	1.33 + 0.010a	1.29 + 0.004b
Leaching layer	13–30	15–30	1.38 + 0.020a	1.33 + 0.016b
Deposition layer	30–45	30–50	1.44 + 0.050a	1.48 + 0.007a
Parent material layer	less than 45	less than 50	1.39 + 0.029a	1.30 + 0.024a

Different lowercase letters indicate significant difference between treatments NPK and NPKG ($P < 0.05$). NPK, no ryegrass, chemical fertilizer application only; NPKG, chemical fertilizer application with turning ryegrass.

0–13 cm, 13–30 cm, 30–45 cm, and < 45 cm, respectively. The thicknesses of the humus and deposition layers in the NPKG treatment were greater than those in the NPK treatment. Soil bulk density of the humus, leaching, and deposition layers showed increasing trends (Table 1). The soil bulk density of the humus and leaching layers of NPKG was significantly lower than that of NPK.

3.2. Soil fertility

Soil fertility is critical to crop yield and quality; it can be seen from Table 2 that tilling ryegrass in 2020 had no significant effect on either rhizosphere or bulk soil pH, while the pH of both rhizosphere and bulk soil decreased after turning and pressing ryegrass back into the field in 2021. At 45 days after transplanting in 2021, the bulk soil pH of the treatment NPKG was significantly lower than that of the treatment NPK. The soil AN content was 27.18–31.03 mg/kg for treatment NPK and 29.58–33.52 mg/kg for treatment NPKG between 2020 and 2021, where the AN content in rhizosphere soil was 11% higher for treatment NPKG than treatment NPK at 45 days after the transplant in 2020. The AN content of bulk soil was relatively high at 45 days after transplanting in 2020 and 2021, which showed a decreasing trend with the extension of the growth period. The soil AP content also decreased gradually as the growth period of the tobacco plants was prolonged. The AP content in bulk soil was 46.08–58.80 mg/kg in 2020 and 41.17–63.86 mg/kg in 2021, respectively. The AP content in rhizosphere soil was 56.46–66.60 mg/kg in 2020 and 56.67–74.90 mg/kg in 2021, respectively. The AP content was higher in the rhizosphere than in the bulk soil during each period, and rhizosphere soil AP content increased by 2.22–17.96%. As shown in Table 2, 45 days after transplanting in 2020 and 2021, the bulk and rhizosphere soil AK contents of the NPKG treatment were significantly higher than those of the NPK treatment. The soil AK content of treatment NPKG was 230.33–267.33 mg/kg and 270.67–380.80 mg/kg in 2020 and 2021, respectively. The results also indicated that the soil AK content increased with the number of years of ryegrass tillage. Soil OM content of treatment NPK and NPKG was 14.65–15.96 g/kg and 15.81–17.06 g/kg, respectively, and TN content was 0.81–0.90 g/kg and 0.85–0.98 g/kg, respectively (Table 2). The OM content of NPKG was 6.89–7.92% times higher than treatment NPK. There were no significant differences in soil TN and TP contents between treatments in most periods, except for significant differences between treatments in individual periods. There was also no significant difference in the soil TK content between the treatments. These results indicate that tilling ryegrass is beneficial for increasing the soil bulk and rapidly available rhizosphere nutrients, especially soil AK and rhizosphere soil AP content.

TABLE 2 Physicochemical properties of NPK and NPKG under different stages.

Stage		Treatment	pH	AN (mg/kg)	AP (mg/kg)	AK (mg/kg)	TN (g/kg)	TP (g/kg)	TK (g/kg)	OM (g/kg)
2020-45d	Bulk soil	NPK	7.67±0.13 a	28.93±1.07 b	53.84±3.86 b	175.00±12.29 c	0.86±0.02 a	1.10±0.00 c	17.09±0.13 a	15.62±0.41 b
		NPKG	7.70±0.06 a	32.90±1.40 a	58.80±5.28 ab	230.33±8.15 ab	0.93±0.04 a	1.13±0.01 bc	17.09±0.03 a	16.66±0.36 a
	Rhizosphere soil	NPK	7.72±0.03 a	28.31±1.17 b	63.86±3.97 ab	210.33±16.04 b	0.87±0.03 a	1.18±0.03 ab	17.30±0.15 a	15.70±0.36 b
		NPKG	7.60±0.02 a	31.43±1.42 ab	65.28±3.56 a	249.33±1.53 a	0.93±0.04 a	1.19±0.02 a	17.28±0.19 a	17.06±0.27 a
2020-75d	Bulk soil	NPK	7.89±0.09 a	27.88±1.99 a	46.08±0.77 c	194.00±24.27 b	0.84±0.03 a	1.12±0.03 b	16.73±0.17 a	15.89±0.48 a
		NPKG	7.88±0.05 a	30.68±1.65 a	50.76±2.48 bc	237.33±5.03 a	0.88±0.07 a	1.16±0.01 b	17.14±0.16 a	16.66±0.53 a
	Rhizosphere soil	NPK	7.74±0.07 ab	27.18±2.47 a	56.46±4.77 b	236.33±7.02 a	0.83±0.02 a	1.15±0.08 b	16.66±0.25 a	15.96±0.62 a
		NPKG	7.65±0.02 b	29.68±1.40 a	66.60±1.85 a	267.33±11.06 a	0.90±0.05 a	1.29±0.00 a	17.39±0.51 a	16.77±0.54 a
2021-45d	Bulk soil	NPK	7.80±0.04 a	31.03±0.42 b	54.74±1.69 c	254.33±23.50 b	0.90±0.02 ab	1.05±0.04 a	18.08±0.12 a	15.48±0.48 ab
		NPKG	7.60±0.12 b	33.52±0.64 a	63.86±5.68 bc	380.80±24.12 a	0.98±0.06 a	1.05±0.13 a	18.41±0.22 a	16.09±0.77 a
	Rhizosphere soil	NPK	7.88±0.06 a	28.61±1.11 c	67.30±3.52 ab	267.60±11.66 b	0.86±0.02 b	1.06±0.05 a	18.15±0.20 a	14.65±0.23 b
		NPKG	7.70±0.05 ab	29.82±0.73 bc	74.90±2.02 a	350.40±15.95 a	0.93±0.06 ab	1.04±0.09 a	18.08±0.40 a	15.81±0.47 a
2021-75d	Bulk soil	NPK	7.93±0.03 a	27.61±0.73 a	41.17±1.78 d	241.33±17.93 ab	0.85±0.02 a	1.22±0.12 a	17.74±0.10 a	15.30±0.42 b
		NPKG	7.86±0.03 a	29.82±1.92 a	47.85±2.02 c	299.33±11.37 a	0.88±0.03 a	1.10±0.09 a	17.85±0.21 a	16.58±0.24 a
	Rhizosphere soil	NPK	7.90±0.05 a	28.37±0.64 a	56.67±1.98 b	237.33±11.55 b	0.93±0.06 a	1.13±0.11 a	18.16±0.18 a	15.30±0.35 b
		NPKG	7.83±0.10 a	29.58±1.51 a	62.14±1.98 a	270.67±40.46 ab	0.90±0.04 a	1.09±0.07 a	17.85±0.22 a	16.19±0.86 ab

Different lowercase letters indicate the significant difference of soil physicochemical properties between treatments NPK and NPKG ($P < 0.05$). AN, alkaline nitrogen; AP, available phosphorus; AK, available potassium; TN, total nitrogen; TP, total phosphorus; TK, total potassium; OM, organic matter. NPK, no ryegrass, chemical fertilizer application only; NPKG, chemical fertilizer application with turning ryegrass.

10.3389/fmicb.2023.1257924

10.3389/fmicb.2023.1257924

3.3. Agronomic traits, dry matter accumulation, and chemical constituents of flue-cured tobacco

As shown in Figure 2, all agronomic traits in the NPKG treatment were better than those in the NPK treatment. The dry leaf weight in treatments NPK and NPKG were 89.7–106.4 g and 129.8–134.4 g, respectively. The root, stem, and leaf dry weights of NPKG in 2021 increased by 21.93, 13.80, and 28.45%, respectively, compared with those of the NPK treatment.

The chemical composition of the flue-cured tobacco leaves is shown in Table 3. The chlorine and nicotine contents of the leaves were 0.67–0.83% and 2.63–3.23%, respectively. Compared with the NPK treatment, NPKG reduced the nicotine content in the middle and upper leaves and increased the chloride content, but neither of the two treatments showed statistically significant differences in either indicator. The total sugar contents of the upper and middle leaves in the NPK treatment were 18.33–18.93% and 18.20–18.77%, respectively, whereas the total sugar contents of the upper and middle leaves in the NPKG treatment were 20.66–24.36% and 20.49–21.37%, respectively. The reducing sugar contents of NPK and NPKG were 13.37–14.94% and 15.09–16.20%, respectively. The reducing sugar to nicotine ratio of flue-cured tobacco was 4.34–4.71 and 5.14–5.73 for treatments NPK and NPKG, respectively. The reducing sugar content and the ratio of reducing sugar to nicotine in the NPKG treatment were significantly higher than those in the NPK treatment. The potassium content of the upper and middle leaves in the NPKG treatment increased by 3–10% compared to that in the NPK treatment. Ryegrass ripping and returning to the field increased the total sugar, reducing sugar and potassium content, and the reducing sugar-to-nicotine ratio in the upper and middle leaves, indicating that ryegrass turning and returning to the field is conducive to improving the quality of flue-cured tobacco leaves.

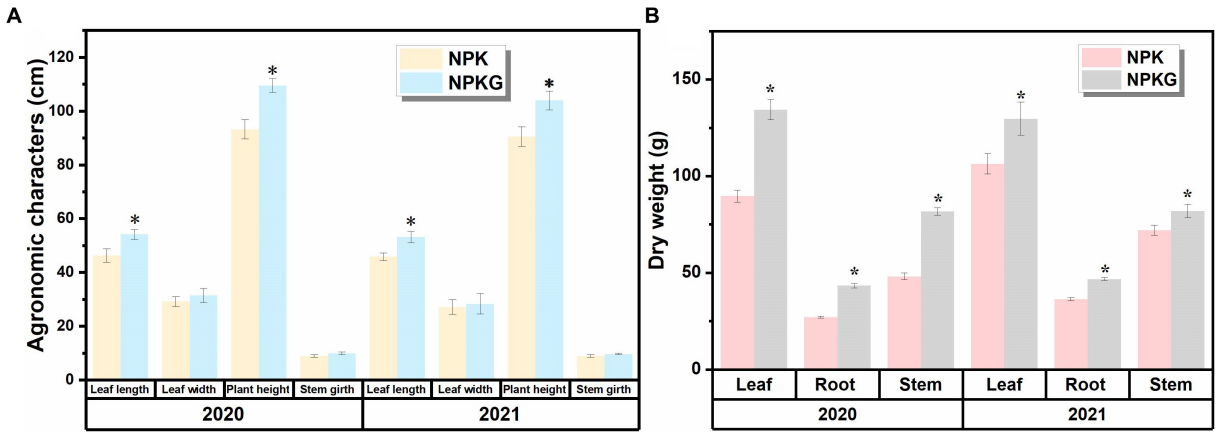

FIGURE 2
Flue-cured tobacco agronomic traits and dry matter accumulation of treatments **(A)** NPK and **(B)** NPKG. * represents $p < 0.05$. NPK, no ryegrass, chemical fertilizer application only; NPKG, chemical fertilizer application with turning ryegrass.

TABLE 3 Chemical composition of flue-cured tobacco.

			Chloride %	Nicotine %	Reducing sugar %	Total sugar %	Potassium %	Ratio of potassium to chloride	Ratio of reducing sugar to nicotine	Ratio of reducing sugar to total sugar
2020	Middle leaves	NPK	0.75a	3.16a	14.94b	18.77a	1.39b	1.88a	4.76b	0.64a
		NPKG	0.82a	2.88a	15.46a	21.37a	1.53a	1.87a	5.37a	0.68a
	Upper leaves	NPK	0.78a	3.23a	14.67b	18.93b	1.30b	1.68a	4.44b	0.75a
		NPKG	0.83a	3.10a	16.20a	24.36a	1.38a	1.67a	5.23a	0.66a
2021	Middle leaves	NPK	0.74a	2.84a	13.37b	18.20b	1.43b	1.94a	4.71b	0.73a
		NPKG	0.78a	2.63a	15.09a	20.49a	1.54a	1.98a	5.73a	0.74a
	Upper leaves	NPK	0.67a	3.17a	13.75b	18.33b	1.32a	1.95a	4.34b	0.75a
		NPKG	0.70a	3.09a	15.90a	20.66a	1.36a	1.93a	5.14a	0.77a

Different lowercase letters indicate the significant difference of flue-cured tobacco chemical composition between treatments NPK and NPKG ($p < 0.05$). NPK, no ryegrass, chemical fertilizer application only; NPKG, chemical fertilizer application with turning ryegrass.

10.3389/fmicb.2023.1257924

3.4. Analysis of soil microbial community diversity and co-occurrence network

The bacterial 16S rRNA gene V3–V4 region was sequenced using the Illumina HiSeq high-throughput sequencing platform, the tags were cleaned up after removing the chimeras, and the number of valid tags (valid sequences) data was obtained with a distribution of 65,558–72,622. The fungal ITS rRNA was sequenced, and the data volume of valid tags obtained by removing the chimeras of clean tags was distributed in 38,028–64,929 (Supplementary Table S1). There was no significant difference in the number of soil bacterial and fungal OTUs between the NPKG and NPK treatments. As shown in Supplementary Table S1, the coverage of each sample was above 96%, indicating that the sequencing depth reflects the actual microbial community. As shown in Supplementary Table S2, the Chao1 index of bulk and rhizosphere soil bacteria was notably higher in 2021 than in 2020; however, the Chao1 index of bulk soil fungi showed the opposite trend. The Chao1 index of bulk and rhizosphere soil fungi and bacteria tended to be higher than that of the NPK treatment at all periods after ryegrass tillage and return to the field.

Co-occurrence network analysis of the soil microbial community was conducted at the OTU level to further explore the complexity of the microbial community relationships among the different treatments. As shown in Figure 3, the numbers of soil bacterial edges for treatments NPKGB and NPKGR were 2,903 and 2011, respectively, which were 1.36 and 1.53 times higher than those for NPKB and NPKR, respectively. The average degree, graph density, and average clustering coefficient of the NPKGB and NPKGR treatments were

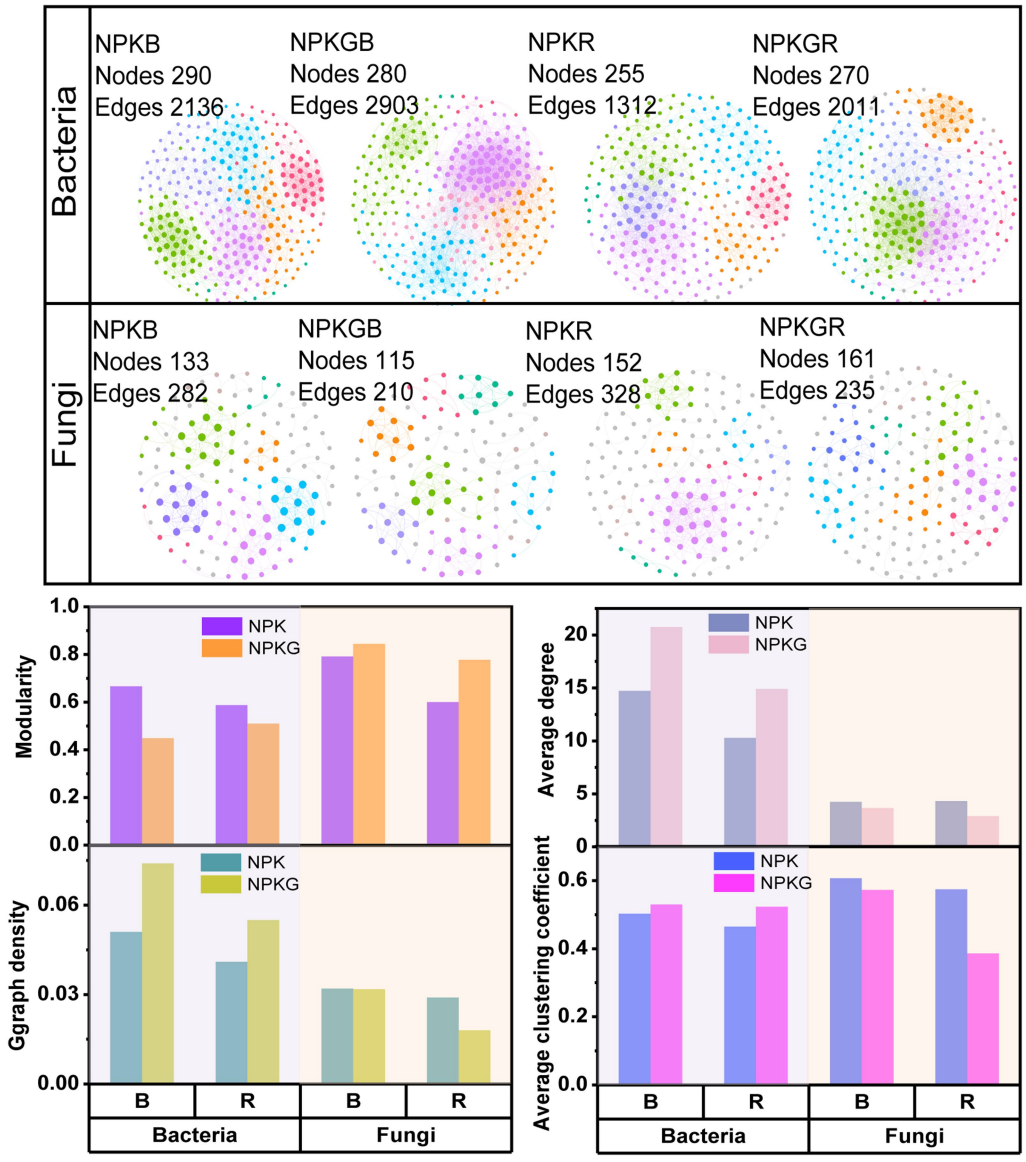

FIGURE 3
The co-occurrence networks and topological properties of bulk and rhizosphere soil bacteria and fungi between different treatments. Different colors represent different modules in the microbial networks. NPK, no ryegrass, chemical fertilizer application only; NPKG, chemical fertilizer application with turning ryegrass. B and R represent bulk soil and rhizosphere soil, respectively. NPKB, and NPKGB represent the bulk soil of the treatment NPK and NPKG, respectively; NPKR, and NPKGR represent the rhizosphere soil of the treatment NPK and NPKG, respectively.

higher than those of the NPKB and NPKR treatments, indicating that ryegrass tilling and returning to the field increased the interaction complexity of the soil bacterial co-occurrence network. The topological properties of the soil fungal co-occurrence network community after ryegrass rolling showed a trend opposite to that of the soil bacterial community. The number of edges and average clustering coefficient of the fungal co-occurrence network of bulk and rhizosphere soils with ryegrass in the field were lower than those without ryegrass. The results demonstrated that the soil bacterial community had higher complexity and stronger compactness after ryegrass tilling and its return to the field.

The response of the soil microbial community after ryegrass tillage and return to the field at the OTU level was specifically analyzed using volcano plots. As shown in Figure 4, the number of significantly increased OTUs in both bulk and rhizosphere soils substantially improved after ryegrass was turned and pressed into the field: 400 OTUs significantly increased and 184 OTUs significantly decreased in bulk soil bacteria, 316 OTUs significantly increased, and 233 OTUs significantly decreased in rhizosphere soil bacteria. In contrast, the number of significantly decreased OTUs was greater than that of significantly increased OTUs in the bulk soil fungi. A total of 206 OTUs significantly decreased, and 70 OTUs significantly increased after ryegrass tillage and return to the field. The results demonstrated the contribution of ryegrass to the increase in the soil bacterial community.

To further clarify the differences in the microbial community composition among the samples, the soil bacterial and fungal communities were analyzed by PCoA based on the Bray-Curtis algorithm, as shown in Figure 5. For both bulk and rhizosphere soil bacteria (Figures 5A,B), samples from the same year were clustered together, and samples from different treatments in 2021 were dispersed from each other. Treatments NPK1, NPK2, NPKG1, and NPKG2 clustered together, while there was no aggregation between treatments NPK1 and NPK3, indicating that the bulk and rhizosphere soil bacterial communities were highly variable between years and that tilling and returning ryegrass caused variation in the bulk soil bacterial community. For the PCoA analysis of bulk soil fungi, NPK1, NPK3, and NPK4 were combined. Treatments NPKG1, NPKG2, NPKG3, and NPKG4 tended to aggregate, indicating that returning ryegrass to the field changed the bulk soil fungal community.

PCoA was performed on the soil microbial communities of the NPK and NPKG treatments for the same period to further explore the timing effect on the soil microbial community after ryegrass tillage and return. As shown in Figure 6, there was no significant difference in the bacterial and fungal communities in the bulk and rhizosphere soils between the NPK and NPKG treatments during the first sampling period. The bulk and rhizosphere soil bacterial and fungal communities in the third and fourth sampling periods showed significant differences between the NPK and NPKG treatments ($p < 0.05$). The results indicated that ryegrass tilling and returning to the field for 3 years significantly changed the soil microbiome.

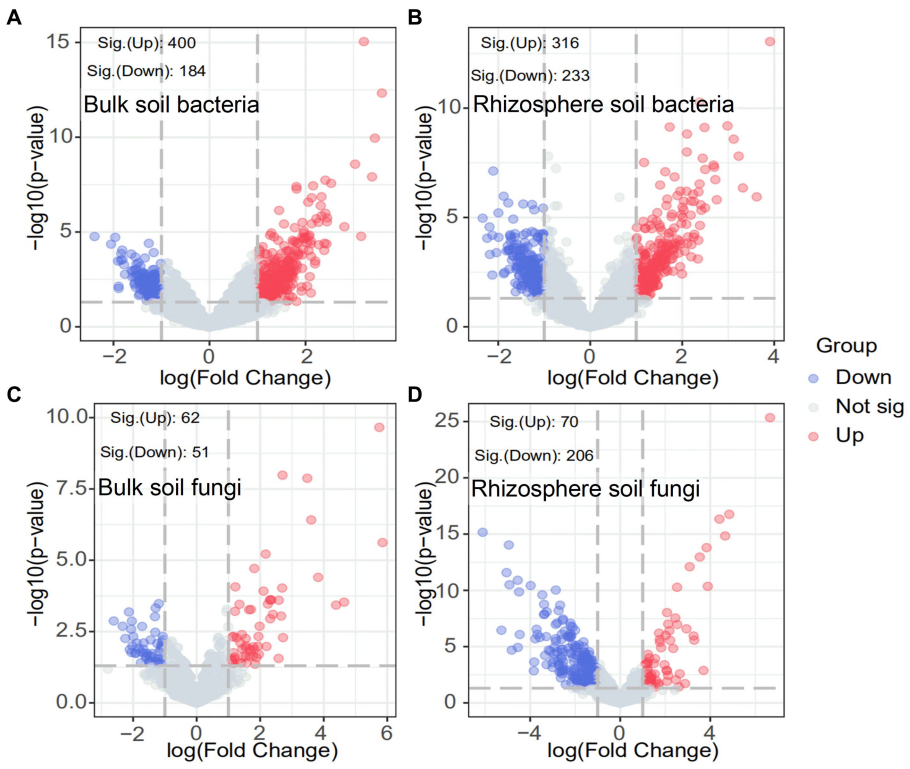

FIGURE 4
Volcano plots of bulk and rhizosphere soil bacteria **(A,B)** and fungi **(C,D)**. Blue circles indicate significantly decreased OTUs, red circles indicate significantly increased OTUs and gray circles indicate OTUs with no significant change.

10.3389/fmicb.2023.1257924

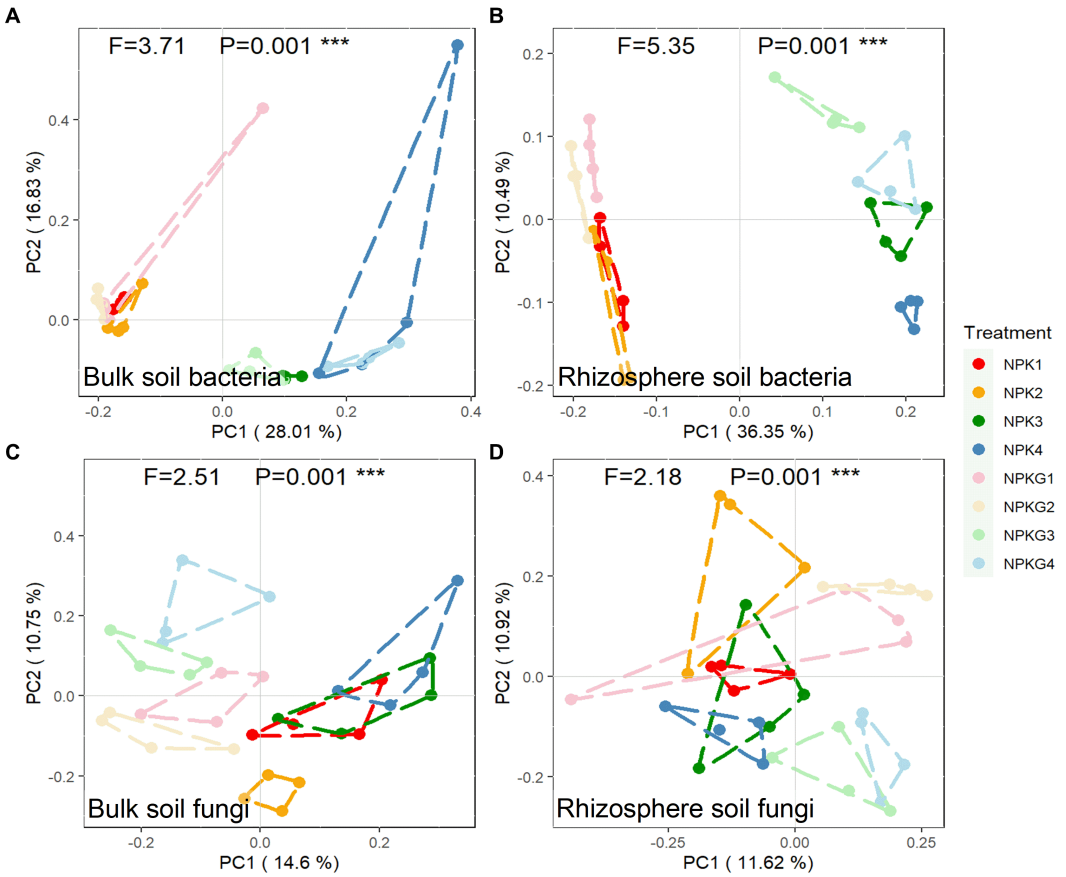

FIGURE 5
PCoA of **(A)** bulk soil bacteria, **(B)** rhizosphere soil bacteria, **(C)** bulk soil fungi, and **(D)** rhizosphere soil fungi community composition at OTU level (*n* = 4). NPK, no ryegrass, chemical fertilizer application only; NPKG, chemical fertilizer application with turning ryegrass. 1, 2, 3, and 4 in treatments represent 45 days and 75 days after transplanting in 2020, respectively, and 45 days and 75 days after transplanting in 2021.

3.5. Analysis of soil microbiome composition

The relative abundance and variance analyses of soil microbiome at the phylum level are shown in Figure 7. At the bacterial phylum level, the dominant bacteria (relative abundance >1%) in the bulk and rhizosphere soils were Proteobacteria, Bacteroidota, Gemmatimonadota, Actinobacteria, Firmicutes, Acidobacteria, Myxococcota, and Nitrospirota (Figure 7A). The LEfSe results showed that Gemmatimonadota, Latescibacterota, and Desulfobacterota were significantly reduced in the bulk and rhizosphere soils after ryegrass tillage and its return to the field. Bulk soil bacteria Proteobacteria and rhizosphere soil bacteria Fibrobacterota in the NPKG treatment were significantly higher than those in the NPK treatment group. At the fungal phylum level (Figure 7B), the fungi with an average relative abundance greater than 1% in bulk and rhizospheric soils were Ascomycota, Basidiomycota, Mortierellomycota, Rozellomycota, Glomeromycota, Chytridiomycota, Kickxellomycota, and Zoopagomycota. LEfSe results showed that the bulk soil fungi Zoopagomycota, Kickxellomycota, and rhizosphere soil Glomeromycota, Olpidiomycota, and Kickxellomycota were significantly reduced after ryegrass tillage and were returned to the field.

To further explore the changes in soil microbial communities, changes in soil microbial communities at the genus level were analyzed (Supplementary Figures S1, S2). At the bacterial genus level, the dominant bacterial genera shared by the bulk and rhizosphere soil was *Prevotella, Sphingomonas, AKAU4049, MND1, Muribaculaceae, S0134_terrestrial_group, Lysobacter, Nitrospira, Subgroup_7, Dongia*. The LEfSe results showed that tilling ryegrass significantly increased *Sphingomonas, Lysobacter,* and *Longimicrobiaceae* in bulk soil and *Sphingomonas* and *Pseudarthrobacter* in rhizosphere soil. The *AKAU4049* and *S0134_terrestrial_group* genera showed notable or extremely significant reductions in the bulk and rhizosphere soils.

At the fungal genus level, the dominant genera shared by the bulk and rhizosphere soils were *Mortierella, Chaetomium, Coprinellus, Neocosmospora, Minimedusa, Paurocotylis, Stachybotrys,* and *Preussia*. The soil fungi *Chaetomium, Minimedusa,* and *Paracylindrocarpon* increased significantly, whereas the bulk and rhizosphere soil fungi *Neocosmospora* markedly decreased after ryegrass tillage and its return to the field.

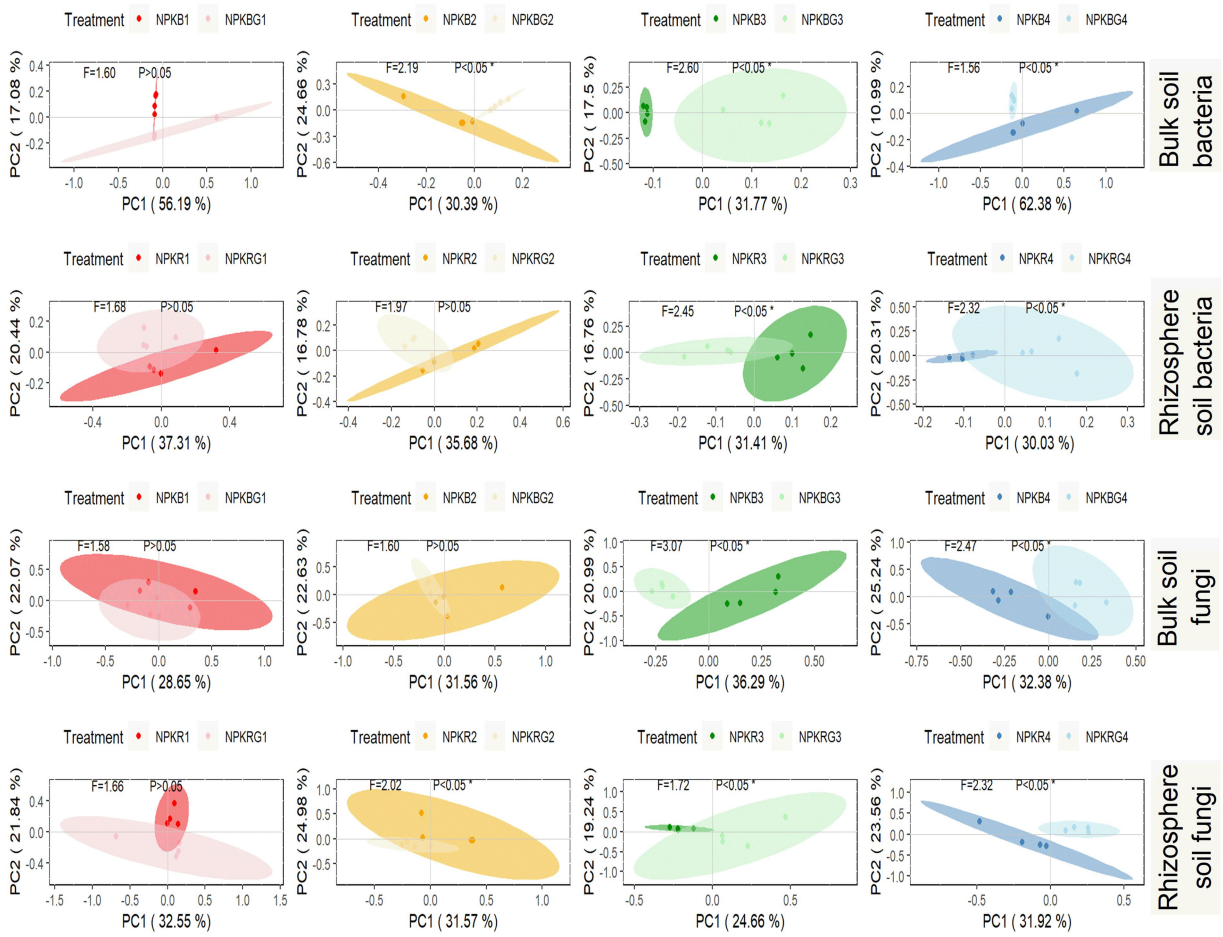

FIGURE 6
PCoA of bulk soil bacteria, rhizosphere soil bacteria, bulk soil fungi, and rhizosphere soil fungi community composition at OTU level. Ellipses are calculated with a confidence of 0.05. NPKB, and NPKBG represent the bulk soil of the treatment NPK and NPKG, respectively; NPKR, and NPKRG represent the rhizosphere soil of the treatment NPK and NPKG, respectively. 1, 2, 3, and 4 in treatments represent 45 days and 75 days after transplanting in 2020, respectively, and 45 days and 75 days after transplanting in 2021.

3.6. Correlation analysis between soil physicochemical properties and soil microbiome

To investigate the effects of soil environmental factors on the soil microbiome, RDA analyses were performed at the OTU level, and correlation heatmap analyses were conducted between the soil physicochemical properties and soil microbial community composition at the phylum level. As shown in Figure 8, the *p* values for all four models were less than 0.05, indicating that all soil environmental factors significantly affected soil microbiome. Figures 8A,C show that soil AK, TK, and OM significantly affected bulk soil bacterial and fungal communities. The rhizosphere soil AK, AP, and TK content, pH, and sampling period had significantly impacted on the rhizosphere soil microbial community. As shown in Figure 9, strongly correlations were observed between rhizosphere soil microbiome and rhizosphere soil nutrients. Rhizosphere soil pH showed strong positive correlations with the rhizosphere soil Firmicutes and Bacteroidota and highly significant negative correlations with the rhizosphere soil Proteobacteria, Actinobacteriota, and Fibrobacterota. Rhizosphere soil OM was significantly and positively correlated with the rhizosphere soil bacteria Proteobacteria and Fibrobacterota. Rhizosphere soil AK was significantly and adversely correlated with the rhizosphere soil fungi Kickxellomycota and bacteria Nitrospirota.

4. Discussion

4.1. Effects of returning ryegrass on soil layer construction and soil fertility

Generally, the soil profile is a comprehensive measure of the internal and external morphologies of soil. In this study, returning ryegrass to the field increased the thickness of the soil humus layer, and large soil particles were produced in the deposition layer. Returning ryegrass to the field also reduced the bulk density of soil humus and leaching layers. On the one hand, the well-developed and dense root system of ryegrass is deeply rooted in the soil to produce a drilling effect (Matocha et al., 2018; Pulido-Moncada et al., 2020), which reduces the soil density; on the other hand, the organic root exudates secreted by the roots of ryegrass dissolves the cohesives in the fragipan (Matocha et al., 2018).

The soil pH decreased after returning the ryegrass to the field, which was due to the ability of the ryegrass root system to secrete

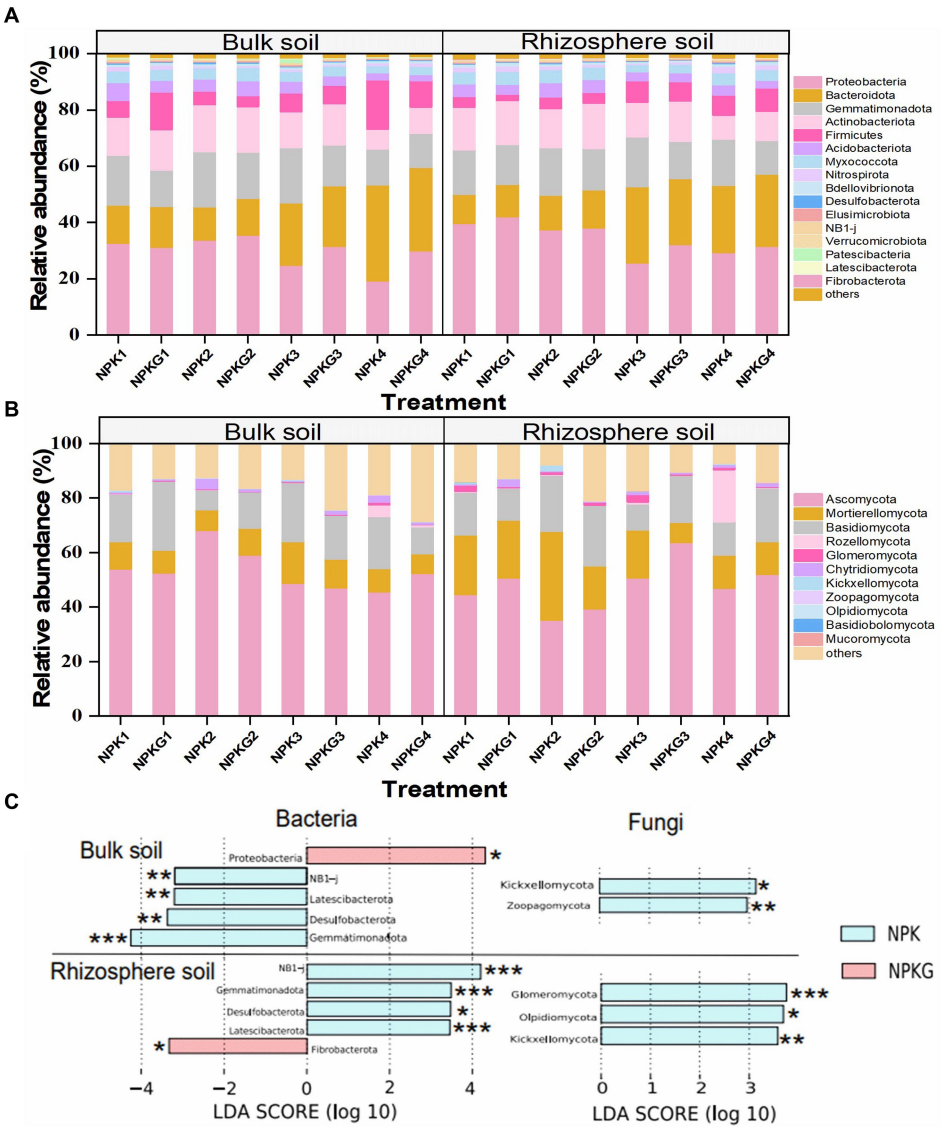

FIGURE 7
Relative abundance of the dominant **(A)** soil bacteria and **(B)** soil fungi at the phylum level. Biomarkers with statistical differences between treatment NPK and NPKG were determined by LEfSe **(C)**. * mean $P<0.05$, ** mean $P<0.01$, and *** mean $P<0.001$. NPK, no ryegrass, chemical fertilizer application only; NPKG, chemical fertilizer application with turning ryegrass. 1, 2, 3, and 4 in treatments represent 45 days and 75 days after transplanting in 2020, respectively, and 45 days and 75 days after transplanting in 2021.

small molecule organic acids (Matocha et al., 2018) and the ryegrass itself released organic acids during dry decomposition to reduce the soil pH (Matocha et al., 2018). The soil nitrogen content increased after the ryegrass was returned to the field, which is consistent with the results of He et al. (2020). The green manure returned to the field is decomposed into soil nutrients and mineralized into inorganic nitrogen by the soil microbiome (Daly et al., 2021). The positive correlation between rhizospheric soil AN and bacteria Proteobacteria substantiated the important role of the microbiome in soil-available nutrients. Ryegrass tillage and return promote an increase in soil AP content, mainly because of the organic acids released by ryegrass roots to convert soil TP into the available state of phosphorus (Hansen et al., 2021; Yang X. Y. et al., 2021). The continuous return of ryegrass also significantly increased soil AK content, which was closely related to the soil type and ryegrass. The main components of yellow-brown soil are illite and vermiculite, which contain potassium minerals that plants cannot absorb or use. On the one hand, the ryegrass that has been turned and returned to the field can directly expand the interlayer space of clay minerals and release the interlayer mineral potassium (Rezaeinejad et al., 2021). Besides, ryegrass is degraded into humus by microorganisms, which can cause the expansion of clay minerals, thereby reducing the potassium fixation strength of the soil to exogenous potassium. OM is an important indicator of soil fertility. In this study, returning ryegrass to the field increased soil OM content, which is closely related to the positive priming effect of ryegrass on soil organic carbon mineralization (Li et al., 2018). The addition of ryegrass promoted the formation of larger pores in sandy loam soil and stimulated the mineralization of natural organic carbon (Mendoza et al., 2022), and the organic acids released by ryegrass could liberate OM by dissolving soil protective mineral phases (Ding et al., 2021).

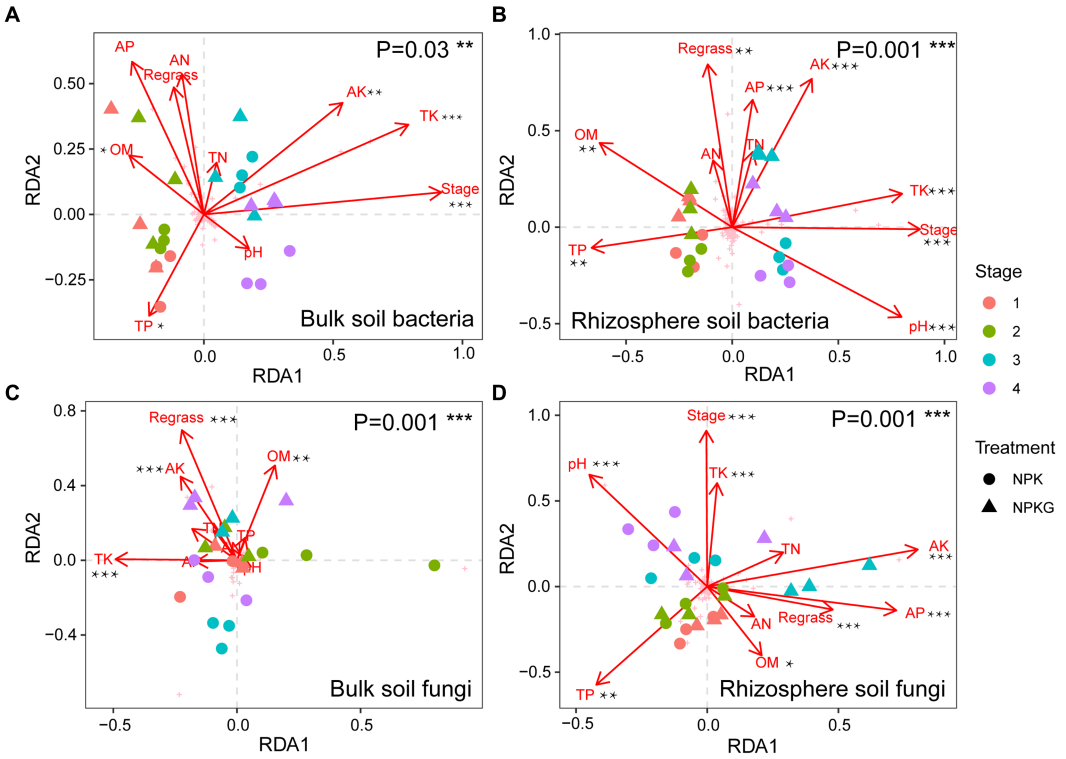

FIGURE 8
The correlation between microbial community structures bacteria **(A,B)** and fungi **(C,D)** and soil chemical properties based on RDA. NPK, no ryegrass, chemical fertilizer application only; NPKG, chemical fertilizer application with turning ryegrass. 1, 2, 3, and 4 in treatments represent 45 days and 75 days after transplanting in 2020, respectively, and 45 days and 75 days after transplanting in 2021. * mean $P<0.05$, ** mean $P<0.01$, and *** mean $P<0.001$.

4.2. Effects of returning ryegrass on agronomic characters and chemical constituents of flue-cured tobacco

The stem circumference, plant height, and dry matter weight of flue-cured tobacco were significantly higher after turning ryegrass, mainly because tilling ryegrass back into the field improved the soil structure and fertility. Ryegrass tillage increases the content of the rapidly AN, AP, AK, and OM in the soil, tillage of ryegrass reduces the soil bulk, loosens the soil, promotes root development, and enhances the ability of tobacco plants to absorb nutrients and water from the soil, thus facilitating the development and reproduction of tobacco plants. The content and coordination of the conventional chemical components in flue-cured tobacco leaves are important for their quality of tobacco leaves. Total sugar, reducing sugar, nicotine, chlorine, and potassium contents in tobacco measure the intrinsic quality, aroma, and taste of tobacco. In this study, ryegrass tillage increased the potassium content, which was closely related to the increase in soil AK content. Potassium in flue-cured tobacco is mainly derived from the soil system and is then absorbed into the body through the root system. The ratio of reducing sugar to nicotine is an important indicator for controlling the quality of cigarettes, which not only reflects the balance between acidic and alkaline substances in tobacco but also characterizes the coordination of the chemical composition of tobacco. In this study, returning ryegrass reduced the nicotine content, increased the potassium, total sugar, and reducing sugar contents, and reduced the sugar-to-nicotine ratio of flue-cured tobacco, indicating that returning ryegrass promotes harmonization of the chemical composition of flue-cured tobacco.

4.3. Effects of returning ryegrass on soil microbial community

An increase in soil fertility is inseparable from the contribution of the soil microbiome. In this study, the dominant phylum Proteobacteria increased after returning ryegrass, which is closely related to the organic carbon and OM produced by the decomposition of ryegrass in the soil. The strong positive correlation between rhizosphere soil OM content and Proteobacteria after ryegrass tillage and return to the field confirmed the response of Proteobacteria to soil OM, which is consistent with the findings of Li et al. (2019). Fibrobacterota is a cellulose-degrading bacterium (Ban et al., 2021), and an increase in Fibrobacterota in the rhizosphere soil after returning ryegrass promotes its degradation in the soil. Gemmatimonadetes, Latescibacterota, Desulfobacterota, and Kickxellomycota were dramatically reduced in both the bulk and rhizosphere soils after the ryegrass was tilled and pressed back into the field. Desulfobacterota and Kickxellomycota are anaerobes (Liu J. B. et al., 2022; Chen et al., 2023), and Latescibacterota decomposes complex organic compounds mainly under anaerobic conditions (Liu X. H. et al., 2022). Desulfobacterota, Latescibacterota, and

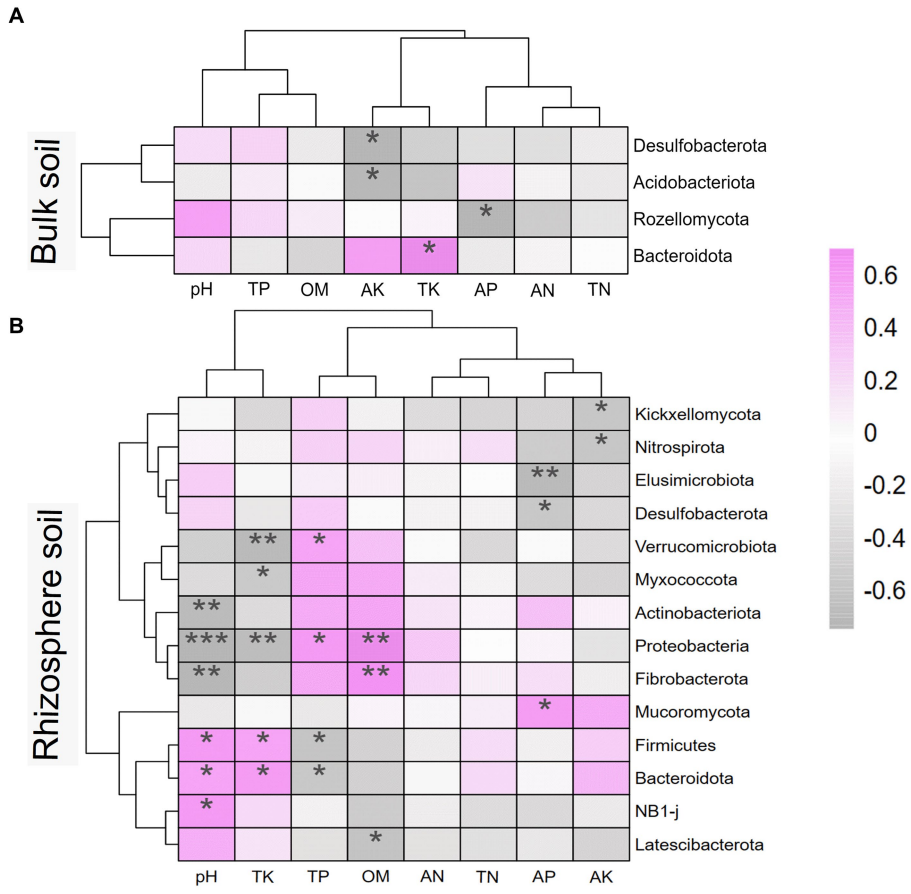

FIGURE 9
Heatmap of soil physicochemical properties and microbial communities at phylum level based on spearman correlation analysis. **(A)** is the bulk soil and **(B)** is the rhizosphere soil. * represents the correlation between soil microbiome and soil properties. * mean $P<0.05$, ** mean $P<0.01$, and *** mean $P<0.001$. AN, alkaline nitrogen; AP, available phosphorus; AK, available potassium; TN, total nitrogen; TP, total phosphorus; TK, total potassium; OM, organic matter.

Kickxellomycota decreased after returning to the ryegrass, indicating good aeration conditions in the soil. The significant negative relationship between Kickxellomycota and soil AK also demonstrated an increased soil pore structure. Gemmatimonadota prefers dry soil environments and exists in nutrient-poor environments. The reduction in Gemmatimonadota (including *S0134_terrestrial_group* genus and *AKAU4049* genus) in the soil after returning ryegrass also showed that the soil entropy of the returning ryegrass was suitable and rich in nutrients. Both *Lysobacter* and *Sphingomonas* genera were significantly higher in bulk soil with ryegrass than in soil without ryegrass. *Lysobacter* produces a variety of extracellular enzymes and metabolites with antagonistic activities against various soil-borne diseases. *Sphingomonas* also has the ability to degrade a wide range of organic pollutants (Yang Y. et al., 2021). An increased abundance of degrading microbiome indicates a reduced risk of crop damage by pests. The fungal genera *Chaetomium* and *Minimedusa* increased significantly, whereas *Neocosmospore* decreased in both the rhizosphere and bulk soil after returning ryegrass. *Chaetomium* not only promotes the degradation of OM, such as cellulose, cellulose disaccharides, and lignin but also has biocontrol effects on various plant pathogens. *Minimedusa* also has been shown to be effective against fungal diseases and has a good control effect (Wachowska and Rychcik, 2023). *Neocosmospore* is pathogenic genera that cause rot in the stems, roots, and tubers of Solanaceae crops (Sandoval-Denis et al., 2019; Custódio and Pereira, 2023). These results indicate that returning ryegrass to the field promotes soil aeration, increases the reproduction of microbiome with antibacterial functions, and inhibits the propagation of pathogenic microbiome.

5. Conclusion

Ryegrass tilling and returning to the field provides an important carbon source for soil microbiome and promotes microbiome reproduction. The large number of microbiome in turn promoted the decomposition of ryegrass, increased the thickness of the soil humus layer, and reduced the soil bulk density of the plow layer. Returning ryegrass into the field also provides a favorable environment for the reproduction of microbiome with antibacterial function that inhibits the propagation of pathogenic microorganisms and enhances the soil microorganism community toward the direction of making good use of soil nutrients, activating soil nutrients while establishing a new dynamic balance of soil nutrients, thereby improving the quality of cultivated land and raising the quality of flue-cured tobacco. This study provides a technical basis for using the winter idle time of continuous tobacco fields to plant and return ryegrass on limited arable land to alleviate the strain on arable land resources and improve tobacco yield and quality.

Data availability statement

The data presented in the study are deposited in the NCBI repository, under accession numbers PRJNA990362 and PRJNA994851.

Author contributions

HZ: Formal analysis, Writing – original draft. MZ: Investigation, Writing – original draft. JY: Data curation, Writing – review & editing. JW: Writing – review & editing. YC: Writing – review & editing. XY: Funding acquisition, Writing – review & editing, Conceptualization.

Funding

The author(s) declare financial support was received for the research, authorship, and/or publication of this article. This research was funded by the Key Laboratory for Tobacco Cultivation of Tobacco Industry of China (No. 30800665).

Conflict of interest

The authors declare that the research was conducted in the absence of any commercial or financial relationships that could be construed as a potential conflict of interest.

Publisher's note

All claims expressed in this article are solely those of the authors and do not necessarily represent those of their affiliated organizations, or those of the publisher, the editors and the reviewers. Any product that may be evaluated in this article, or claim that may be made by its manufacturer, is not guaranteed or endorsed by the publisher.

Supplementary material

The Supplementary material for this article can be found online at: https://www.frontiersin.org/articles/10.3389/fmicb.2023.1257924/full#supplementary-material

References

Aparicio, V., and Costa, J. L. (2007). Soil quality indicators under continuous cropping systems in the Argentinean pampas. *Soil Tillage Res.* 96, 155–165. doi: 10.1016/j.still.2007.05.006

Ban, Y. H., Li, X., Li, Y. Q., Li, X. Y., Li, X., Wang, X. J., et al. (2021). Comparative analysis of paddy straw-degrading consortia in China using high-throughput sequencing. *Appl. Soil Ecol.* 167:104077. doi: 10.1016/j.apsoil.2021.104077

Bao, S. (2000). *Soil and agricultural chemistry analysis*. China Agricultural Press: Beijing.

Chamkhi, I., Cheto, S., Geistlinger, J., Zeroual, Y., Kouisni, L., Bargaz, A., et al. (2022). Legume-based intercropping systems promote beneficial rhizobacterial community and crop yield under stressing conditions. *Ind. Crop. Prod.* 183:114958. doi: 10.1016/j.indcrop.2022.114958

Chen, L. M., Chen, S. S., Zhang, Y., Long, Y., Kong, X. Y., Wang, S. J., et al. (2023). Co-occurrence network of microbial communities affected by application of anaerobic fermentation residues during phytoremediation of ionic rare earth tailings area. *Sci. Total Environ.* 856:159223. doi: 10.1016/j.scitotenv.2022.159223

Chen, Y., Du, J., Li, Y., Tang, H., Yin, Z., Yang, L., et al. (2022). Evolutions and managements of soil microbial community structure drove by continuous cropping. *Front. Microbiol.* 13:839494. doi: 10.3389/fmicb.2022.839494

Custódio, F. A., and Pereira, O. L. (2023). First report of *Neocosmospora ipomoeae* causing basal stem rot on *Adenium obesum*. *Crop Prot.* 164:106138. doi: 10.1016/j.cropro.2022.106138

Daly, A. B., Jilling, A., Bowles, T. M., Buchkowski, R. W., Frey, S. D., Kallenbach, C. M., et al. (2021). A holistic framework integrating plant-microbe-mineral regulation of soil bioavailable nitrogen. *Biogeochemistry* 154, 211–229. doi: 10.1007/s10533-021-00793-9

De Santos, T. L., Nunes, A. B. A., Giongo, V., Da Barros, V. S., and De Figueirêdo, M. C. B. (2018). Cleaner fruit production with green manure: the case of Brazilian melons. *J. Clean. Prod.* 181, 260–270. doi: 10.1016/j.jclepro.2017.12.266

Ding, Y., Ye, Q. T., Liu, M. G., Shi, Z. Q., and Liang, Y. Z. (2021). Reductive release of Fe mineral-associated organic matter accelerated by oxalic acid. *Sci. Total Environ.* 763:142937. doi: 10.1016/j.scitotenv.2020.142937

Esmaeilzadeh-Salestani, K., Bahram, M., Seraj, R., Gohar, D., Tohidfar, M., Eremeev, V., et al. (2021). Cropping systems with higher organic carbon promote soil microbial diversity. *Agric. Ecosyst. Environ.* 319:107521. doi: 10.1016/j.agee.2021.107521

Gao, H., Tian, G., Khashi, U., Rahman, M., and Wu, F. (2022). Cover crop species composition alters the soil bacterial community in a continuous pepper cropping system. *Front. Microbiol.* 12:789034. doi: 10.3389/fmicb.2021.789034

Hansen, V., Eriksen, J., Jensen, L. S., Thorup-Kristensen, K., and Magid, J. (2021). Towards integrated cover crop management: N, P and S release from aboveground and belowground residues. *Agric. Ecosyst. Environ.* 313:107392. doi: 10.1016/j.agee.2021.107392

He, H., Li, W., Zhang, Y., Cheng, J., Jia, X., Li, S., et al. (2020). Effects of Italian ryegrass residues as green manure on soil properties and bacterial communities under an Italian ryegrass (*Lolium multiflorum* L.)-rice (*Oryza sativa* L.) rotation. *Soil Tillage Res.* 196:104487. doi: 10.1016/j.still.2019.104487

Huang, X., Jia, Z., Guo, J., Li, T., Sun, D., Meng, H., et al. (2019). Ten-year long-term organic fertilization enhances carbon sequestration and calcium-mediated stabilization of aggregate-associated organic carbon in a reclaimed Cambisol. *Geoderma* 355:113880. doi: 10.1016/j.geoderma.2019.113880

Kumar, N., Mina, B. L., Chandra, S., and Srivastva, A. K. (2011). In-situ green manuring for enhancing productivity, profitability and sustainability of upland rice. *Nutr. Cycl. Agroecosyst.* 90, 369–377. doi: 10.1007/s10705-011-9438-0

Li, X. M., Chen, Q. L., He, C., Shi, Q., Chen, S. C., Reid, B. J., et al. (2019). Organic carbon amendments affect the Chemodiversity of soil dissolved organic matter and its associations with soil microbial communities. *Environ. Sci. Technol.* 53, 50–59. doi: 10.1021/acs.est.8b04673

Li, S., and Wu, F. (2018). Diversity and co-occurrence patterns of soil bacterial and fungal communes in seven intercropping systems. *Front. Microbiol.* 9:1521. doi: 10.3389/fmicb.2018.01521

Li, L. J., Zhu-Barker, X., Ye, R., Doane, T. A., and Horwath, W. R. (2018). Soil microbial biomass size and soil carbon influence the priming effect from carbon inputs depending on nitrogen availability. *Soil Biol. Biochem.* 119, 41–49. doi: 10.1016/j.soilbio.2018.01.003

Liang, H., Li, S., Zhang, L., Xu, C. X., Lv, Y. H., Gao, S. J., et al. (2022). Long-term green manuring enhances crop N uptake and reduces N losses in rice production system. *Soil Tillage Res.* 220:105369. doi: 10.1016/j.still.2022.105369

Liu, J. B., Bao, Z., Wang, C. L., Wei, J. Y., Wei, Y. S., and Chen, M. X. (2022). Understanding of mercury and methylmercury transformation in sludge composting by metagenomic analysis. *Water Res.* 226:119204. doi: 10.1016/j.watres.2022.119204

Liu, G. C., Deng, L. M., Wu, R. J., Guo, S. P., Du, W. M., Yang, M. F., et al. (2020). Determination of nitrogen and phosphorus fertilisation rates for tobacco based on economic response and nutrient concentrations in local stream water. *Agric. Ecosyst. Environ.* 304:107136. doi: 10.1016/j.agee.2020.107136

Liu, K., McInroy, J. A., Hu, C. H., and Kloepper, J. W. (2018). Mixtures of plant-growth-promoting rhizobacteria enhance biological control of multiple plant diseases and plant-growth promotion in the presence of pathogens. *Plant Dis.* 102, 67–72. doi: 10.1094/PDIS-04-17-0478-RE

Liu, X. H., Zhang, S. Y., Cheng, R., Liu, R. Y., Liu, Z. B., and Yang, Q. (2022). Effects of nZVI and Fe_3O_4 NPs on anaerobic methanogenesis, microbial communities and metabolic pathways for treating domestic wastewater at ambient temperature. *J. Water Process. Eng.* 48:102845. doi: 10.1016/j.jwpe.2022.102845

Matocha, C., Karathanasis, T., Murdock, L. W., Grove, J. H., Goodman, J., and Call, D. (2018). Influence of ryegrass on physico-chemical properties of a fragipan soil. *Geoderma* 317, 32–38. doi: 10.1016/j.geoderma.2017.12.004

Mendoza, O., De Neve, S., and Deroo, H. S. (2022). Mineralisation of ryegrass and soil organic matter as affected by ryegrass application doses and changes in soil structure. *Biol. Fertil. Soils* 58, 679–691. doi: 10.1007/s00374-022-01654-9

Mirkarimi, S., Ardakani, Z., and Rostamian, R. (2021). Economic and environmental assessment of tobacco production in northern Iran. *Ind. Crop. Prod.* 161:113171. doi: 10.1016/j.indcrop.2020.113171

Pulido-Moncada, M., Katuwal, S., Ren, L., Cornelis, W., and Munkholm, L. (2020). Impact of potential bio-subsoilers on pore network of a severely compacted subsoil. *Geoderma* 363:114154. doi: 10.1016/j.geoderma.2019.114154

Rezaeinejad, R., Khademi, H., Ayoubi, S., and Mosaddeghi, M. R. (2021). Roots under water stress induce K release from phlogopite, bio-transforming to vermiculite. *Rhizosphere* 17:100310. doi: 10.1016/j.rhisph.2021.100310

Sandoval-Denis, M., Lombard, L., and Crous, P. W. (2019). Back to the roots: a reappraisal of Neocosmospora. *Persoonia* 43, 90–185. doi: 10.3767/persoonia.2019.43.04

Wachowska, U., and Rychcik, B. (2023). Plants control the structure of mycorrhizal and pathogenic fungal communities in soil in a 50-year maize monoculture experiment. *Plant Soil* 484, 133–153. doi: 10.1007/s11104-022-05779-6

Wang, T., Duan, Y., Liu, G. D., Shang, X. W., Liu, L. F., Zhang, K. X., et al. (2022). Tea plantation intercropping green manure enhances soil functional microbial abundance and multifunctionality resistance to drying-rewetting cycles. *Sci. Total Environ.* 810:151282. doi: 10.1016/j.scitotenv.2021.151282

Wang, X. Y., Duan, Y., Zhang, J., Ciampitti, I. A., Cui, J. W., Qiu, S. J., et al. (2022). Response of potato yield, soil chemical and microbial properties to different rotation sequences of green manure-potato cropping in North China. *Soil Tillage Res.* 217:105273. doi: 10.1016/j.still.2021.105273

Wang, M., Zhang, L., He, Y., Huang, L. K., Liu, L., Chen, D., et al. (2022). Soil fungal communities affect the chemical quality of flue-cured tobacco leaves in Bijie, Southwest China. *Sci Rep.* 12:2815. doi: 10.1038/s41598-022-06593-x

Yang, T., Barnett, R., Rockett, I., Yang, X., Wu, D., Zheng, W., et al. (2015). The impact of regional economic reliance on the tobacco industry on current smoking in China. *Health Place* 33, 159–171. doi: 10.1016/j.healthplace.2014.12.015

Yang, X. Y., Kong, Y. H., Guo, E. H., Chen, X., and Li, L. M. (2021). Organic acid regulation of inorganic phosphorus release from Mollisols with different organic matter contents. *Soil Use Manag.* 38, 576–583. doi: 10.1111/sum.12710

Yang, Y., Tong, Y. A., Liang, L. Y., Li, H. C., and Han, W. S. (2021). Dynamics of soil bacteria and fungi communities of dry land for 8 years with soil conservation management. *J. Environ. Manag.* 299:113544. doi: 10.1016/j.jenvman.2021.113544

Yang, W., Yao, L., Zhu, M. Z., Li, C. W., Li, S. Q., Wang, B., et al. (2022). Replacing urea-N with Chinese milk vetch (*Astragalus sinicus* L.) mitigates CH_4 and N_2O emissions in rice paddy. *Agric. Ecosyst. Environ.* 336:108033. doi: 10.1016/j.agee.2022.108033

Yang, H., Zhai, S., Li, Y., Zhou, J., He, R., Liu, J., et al. (2017). Waterlogging reduction and wheat yield increase through long-term ditch-buried straw return in a rice—wheat rotation system. *Field Crop Res.* 209, 189–197. doi: 10.1016/j.fcr.2017.05.012

frontiers | Frontiers in Microbiology

TYPE Original Research
PUBLISHED 19 October 2023
DOI 10.3389/fmicb.2023.1264619

Check for updates

OPEN ACCESS

EDITED BY
Wei Hu,
Shandong University, China

REVIEWED BY
Jie Lv,
Beijing University of Chemical Technology, China
Zhangran Chen,
Xiamen University, China

*CORRESPONDENCE
Jingping Niu
✉ niujingp@lzu.edu.cn
Tian Tian
✉ tiant@lzu.edu.cn

†These authors have contributed equally to this work and share first authorship

RECEIVED 21 July 2023
ACCEPTED 06 October 2023
PUBLISHED 19 October 2023

CITATION
Pei S, Feng L, Zhang Y, Liu J, Li J, Zheng Q, Liu X, Luo B, Ruan Y, Li H, Hu W, Niu J and Tian T (2023) Effects of long-term metal exposure on the structure and co-occurrence patterns of the oral microbiota of residents around a mining area.
Front. Microbiol. 14:1264619.
doi: 10.3389/fmicb.2023.1264619

COPYRIGHT
© 2023 Pei, Feng, Zhang, Liu, Li, Zheng, Liu, Luo, Ruan, Li, Hu, Niu and Tian. This is an open-access article distributed under the terms of the Creative Commons Attribution License (CC BY). The use, distribution or reproduction in other forums is permitted, provided the original author(s) and the copyright owner(s) are credited and that the original publication in this journal is cited, in accordance with accepted academic practice. No use, distribution or reproduction is permitted which does not comply with these terms.

Effects of long-term metal exposure on the structure and co-occurrence patterns of the oral microbiota of residents around a mining area

Shuwei Pei[1†], Lu Feng[2†], Yonghua Zhang[3], Jiangyun Liu[1], Jia Li[1], Qiwen Zheng[1], Xingrong Liu[1], Bin Luo[1], Ye Ruan[1], Huan Li[1], Weigang Hu[4], Jingping Niu[1*] and Tian Tian[1*]

[1]School of Public Health, Lanzhou University, Lanzhou, Gansu, China, [2]School of Stomatology, Lanzhou University, Lanzhou, Gansu, China, [3]Child Health Department, Lanzhou Maternal and Child Health Care Hospital, Lanzhou, Gansu, China, [4]State Key Laboratory of Herbage Improvement and Grassland Agro-Ecosystems, College of Ecology, Lanzhou University, Lanzhou, China

Objectives: The aim of our study was to investigate the impact of long-term exposure to heavy metals on the microbiome of the buccal mucosa, to unveil the link between environmental contamination and the oral microbial ecosystem, and to comprehend its potential health implications.

Methods: Subjects were divided into two groups: the exposure group and the control group. We collected samples of buccal mucosa, soil, and blood, and conducted microbial diversity analysis on both groups of oral samples using 16S rRNA gene sequencing. The concentrations of heavy metals in blood and soil samples were also determined. Additionally, microbial networks were constructed for the purpose of topological analysis.

Results: Due to long-term exposure to heavy metals, the relative abundance of *Rhodococcus*, *Delftia*, *Fusobacterium*, and *Peptostreptococcus* increased, while the abundance of *Streptococcus*, *Gemella*, *Prevotella*, *Granulicatella*, and *Porphyromonas* decreased. The concentrations of heavy metals in the blood (Pb, Cd, Hg, and Mo) were associated with the growth of *Rhodococcus*, *Delftia*, *Porphyromonas*, and *Gemella*. In addition, the relative abundances of some pathogenic bacteria, such as *Streptococcus anginosus*, *S. gordonii*, and *S. mutans*, were found to be enriched in the exposure group. Compared to the exposure group network, the control group network had a greater number of nodes, modules, interactive species, and keystone taxa. Module hubs and connectors in the control group converted into peripherals in the exposure group, indicating that keystone taxa changed. Metals in the blood (Pb, Cd, Hg, and Mo) were drivers of the microbial network of the buccal mucosa, which can have adverse effects on the network, thus providing conditions for the occurrence of certain diseases.

Conclusion: Long-term exposure to multiple metals perturbs normal bacterial communities in the buccal mucosa of residents in contaminated areas. This exposure reduces the complexity and stability of the microbial network and increases the risk of developing various diseases.

KEYWORDS

heavy metal, buccal mucosa, bacteria, keystone taxa, network analysis, 16S rRNA gene sequencing

1. Introduction

As one of the most important components of the national economy over the past several decades, the mining industry has played a major role in the rapid industrial transformation of China. However, due to a number of factors (e.g., lack of pollution control and ineffective enforcement of regulations), the metal mining industry has caused severe heavy metal contamination (Chen L. et al., 2022; Shi et al., 2022). These metal pollutants not only cause serious damage to natural resources such as land, water, and air but also pose a great threat to human health (Shao and Zhu, 2020).

Metal pollution is covert, persistent, and irreversible (Ghnaya et al., 2015). Once uncontrolledly discharged into soil and water, metals can persist for a long time (Li et al., 2014; Xia et al., 2019). Heavy metals that have been discharged accumulate in soil and water and eventually enter the human body through the food chain or in direct contact with the skin (Liu et al., 2013; Azimi et al., 2017). High concentrations of lead (Pb) can damage the human blood and nervous system (Ahamed and Siddiqui, 2007; Kumar et al., 2020). Mercury (Hg) can damage the nervous system when present in excess amounts (Driscoll et al., 2013), while cadmium (Cd) can impair kidney function and even cause cancer (Matović et al., 2015; García-Pérez et al., 2016). In addition, recent research has shown that heavy metal pollution also affects the structure of human microbial communities (Shao and Zhu, 2020; Zhang et al., 2023).

The oral cavity is one of the earliest organs in the body to be exposed to the external environment, and its internal microbiome is more susceptible to changes due to external factors such as diet, medicines, pollutants in the environment, and geographical location (Thomas et al., 2014; Dong et al., 2021; Gupta et al., 2022). Oral microbial communities are closely related to human health, affecting not only oral health but also the health of the whole body (Gao et al., 2018; Zhang Y. et al., 2018). Currently, it is believed that a number of diseases, including dental caries and periodontal diseases, are associated with imbalances in oral microorganisms (Wade, 2013; Curtis et al., 2020; Hajishengallis and Lamont, 2021). According to a previous report (Zhang et al., 2023), heavy metal pollution altered the abundance and diversity of the oral microbiome of mining residents and promoted the development of periodontitis. Studies have also shown that oral microbial disorders can lead to diabetes, Alzheimer's disease, cardiovascular disease, and cancer (Sudhakara et al., 2018; Irfan et al., 2020; Zhang et al., 2020). In addition, because they are at the beginning of the digestive tract, oral microbes have a close connection with intestinal microbes. Some oral bacteria were able to enter the gut through the enteral route or hematogenous route, affecting the intestinal microbiome and immune responses (Lu et al., 2023). For instance, *Porphyromonas gingivalis*, an oral anaerobic bacterium in the oral cavity, altered the composition of the intestinal microbiota when administered orally in mouse experiments (with an increased proportion of Bacteroidetes and a decreased proportion of Firmicutes), and this alteration is considered to be attributed to the increase of the serum endotoxin level resulting from *P. gingivalis* infection (Nakajima et al., 2015). Simultaneously, *P. gingivalis* also induces inflammation in intestinal tissues and disrupts the ratio of the T-helper 17 cell/T-regulatory cells in the colon (Wang T. et al., 2022).

Exposure to heavy metals can affect the structure of microbial communities in the oral cavity. Although many studies have investigated this topic in recent years, most have been limited to saliva and plaque samples. However, the oral mucosa is an important component of the oral cavity, has an extremely rich microbial population, and is closely associated with a variety of diseases (Chen J. et al., 2022; Wang S. et al., 2022). Therefore, studying changes in the structure of microbial communities in the oral mucosa under the influence of metal exposure is important for us to gain a deeper understanding of the effects of heavy metal exposure on oral microbial communities and the occurrence of related diseases.

Baiyin City, located in the province of Gansu, China, is known as the "Chinese Copper City" because of its rich resources of nonferrous metals. Due to the frequent mining activities of the last century, heavy metals have been released into the environment, causing severe pollution in the soil, water sources, and air (Yue et al., 2020). Contaminated crops, vegetables and animal foods enter the human body through the food chain, eventually causing heavy metals to accumulate in the local residents (Li et al., 2006; Zhao et al., 2020). In previous studies, the harmful effects of metal exposure on human and animal health in the area have been reported (Zhang et al., 2016; Zhang Q. et al., 2018). However, the effect of metal exposure on the human oral mucous microbiome is still unclear. Therefore, this paper reports the effects of long-term metal exposure on the microbial community structure and co-occurrence patterns of the oral mucous of local residents, filling the gap in epidemiological research on the interaction of heavy metals and buccal mucosal bacteria.

2. Materials and methods

2.1. Study area

Due to long-term nonferrous metal smelting and mining in the last century, the air, soil, surface water, and groundwater of Baiyin city, Gansu Province, are seriously polluted. We selected two adjacent villages in the region as representative contaminated areas: Minqin village and Shuanghe village (36°28′38.188″ N, 104°18′47.870″ E; 36°27′24.650″ N, 104°21′22.057″ E). For comparison, we selected another two adjacent villages, namely, Hewan village and Yangwa village (35°46′41.541″ N, 104°0′37.443″ E; 35°45′54.661″ N, 104°1′28.117″ E), located in Yuzhong County of Lanzhou City as control areas, which are 100 km away from Baiyin City and characterized by relatively low levels of heavy metal pollution. The two selected regions have similar levels of socioeconomic development and residents with similar lifestyles and dietary habits.

2.2. Collection of soil samples and heavy metal analysis

Soil samples were collected in April 2021 from the contaminated and control areas to assess the levels of heavy metal pollution. A total of 13 sampling points were selected in this study (B1–B6, L1–L7), with B1–B6 located in the field in the vicinity of Minqin village and Shuanghe village (Figure 1A) and L1–L7 located in the field near Yangwa village and Hewan village (Figure 1B). At each sampling point, areas of approximately 10 × 10 meters were randomly selected in the fields, and five subsampling sites were set up in each selected field using a five-point sampling method. After removing gravel and impurities at the surface, soil from five subsampling points (at 20 cm

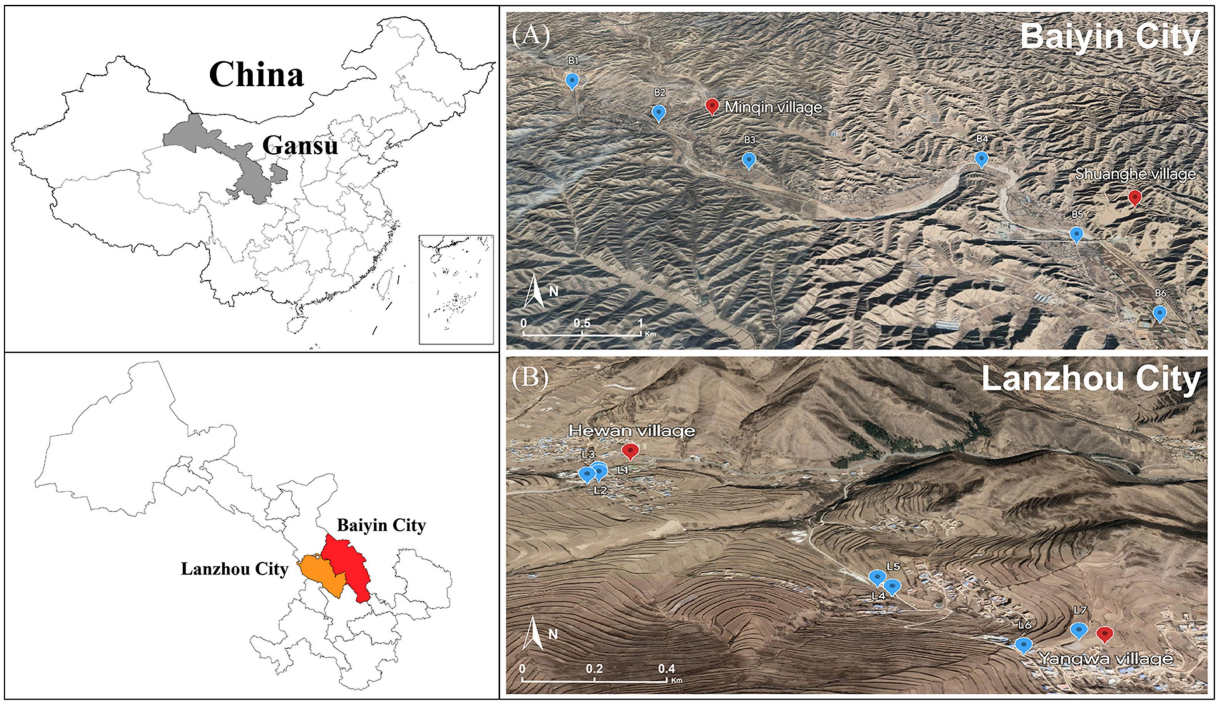

FIGURE 1
Location of sampling points in the contaminated **(A)** and control areas **(B)**.

depths) was collected using a sterile wooden spatula and thoroughly mixed into a composite sample. A total of 13 samples were collected. The samples were sent to the laboratory on the same day. To determine the heavy metal content in soil, each soil sample was first air-dried at room temperature, and then biological debris, plant roots, leaves, and stones were removed, followed by sieving through a 200-mesh nylon sieve. Finally, each sample was thoroughly mixed and stored in a polyethylene bag for further analysis. Each sample of approximately 0.5 g was digested using a microwave digestion system (Sartorius, PB-10, Germany). Then, the content of heavy metals (Mn, Sb, Cu, Cd, Zn, Hg, Pb, Mo, Co, and Ni) was measured using inductively coupled plasma–mass spectrometry (ICP–MS, Agilent, United States). Quality assurance/control procedures were conducted using standard reference materials (Chinese Academy of Measurement Science) with each batch of samples (one blank and one standard).

2.3. The collection of oral buccal mucosa and blood samples

In this study, a total of 137 subjects were enrolled for the collection of both buccal mucosa and blood samples. Among these, 92 subjects were from Baiyin City (i.e., Minqin and Shuanghe villages), and the remaining 45 were from Yuzhong County (i.e., Hewan and Yangwa villages). Subjects were further divided into two groups according to heavy metal exposure: (1) the exposure group ($n = 92$), comprised of residents residing in Baiyin District; and (2) the control group ($n = 45$), comprised of residents residing in Yuzhong District. The enrolled subjects had an average age of 60.03 ± 6.47 years (mean ± SD; range 42–72 years old). All participants fulfilled the following four criteria: (i) subjects signed informed consent and had not used any antibiotics for at least 3 months prior to sampling; (ii) subjects had no oral diseases, such as halitosis, chronic xerostomia, untreated cavitated caries lesions, abscesses, cancer, or candidiasis; (iii) subjects who reported being ill or unwell on the day of sampling were excluded; and (iv) subjects had at least 24 teeth. Prior to sample collection, the participants were restrained from drinking or eating and were asked to wash their mouth with drinking water 30 min before samples were taken. Then, using a sterile cotton-wool swab, we scraped the buccal mucosa on the left and right sides of their mouths for 10 s. After oral sampling, all samples were preserved immediately at −80°C until subsequent processing in the laboratory.

To investigate the association between the concentration of heavy metals in the blood and the composition of the buccal mucosa microbiota, blood samples were collected from the peripheral veins of some of the enrolled research subjects ($n = 79$). We collected 15 mL of heparinized venous blood, removed 2 mL of whole blood, and stored it at −80°C. The contents of heavy metals in blood were measured using an inductively coupled-mass spectrometer (ICP–MS, Elan DRC-II ICP–MS, PerkinElmer Sciex, United States). Survey subjects agreed to informed consent, and the study was approved by the Ethical Committees of the Public Health School of Lanzhou University.

2.4. DNA extraction, sequencing and bioinformatic analyses

DNA was extracted from each buccal mucosa sample using an E.Z.N.A. Soil DNA Kit (Omega Bio-Tek, Norcross, GA, United States) following the manufacturer's instructions, and its concentration and

purity were assessed on a 1% agarose gel. The hypervariable region V3–V4 of the bacterial 16S rRNA gene were amplified with primer pairs 338F (5′-ACTCCTACGGGAGGCAGCAG-3′) and 806R (5′-GGACTACHVGGGTWTCTAAT-3′) by an ABI GeneAmp® 9700 PCR thermocycler (ABI, CA, United States). Thermocycling conditions consisted of 3 min at 95°C followed by 30 amplification cycles of 30 s denaturation at 95°C, 30 s annealing at 55°C, 72°C for 45 s, and a final extension of 72°C for 10 min. All amplification reactions were performed in a total volume of 20 μL containing 4 μL of 5× FastPfu Buffer, 2 μL of 2.5 mM dNTPs, 0.8 μL of both the forward and reverse primers, 10 ng of template DNA, and 0.4 μL of FastPfu DNA Polymerase. To mitigate individual PCR biases, each sample was amplified in triplicate and pooled together. The amplicon quality of the PCR products was assessed on a 2% agarose gel, followed by purification with an AxyPrep Gel Extraction Kit (Axygen Biosciences, United States). Purified amplicons were combined at equimolar concentrations and paired-end sequenced (2 × 300 bp) on an Illumina MiSeq platform (Illumina, United States) at the Majorbio Bio-pharm Technology Co., Ltd. (Shanghai, China) according to standard protocols. Raw sequencing data of the bacterial 16S rRNA gene have been deposited in the NCBI Sequence Read Archive under BioProject accession number PRJNA979792. The resulting sequences were processed using the QIIME pipeline (Caporaso et al., 2010). Briefly, low-quality sequences were trimmed with Cutadapt and quality-filtered. Paired-end reads were assembled using FLASH version 1.2.11 (Magoč and Salzberg, 2011). USEARCH was used to remove chimeric sequences based on the UCHIME algorithm (Edgar et al., 2011), and the remaining sequences were allocated to operational taxonomic units (OTUs) with 97% similarity using the UPARSE pipeline. OTUs with fewer than two sequences were eliminated, and their representative sequences were assigned to taxonomic lineages using the RDP classifier version 2.2 (Wang et al., 2007) against the SILVA database (version 138) using confidence threshold of 0.7.

2.5. Construction and analysis of the bacterial molecular ecological network of the buccal mucosa

The bacterial molecular ecological networks (MENs) of the buccal mucosa were constructed using an online tool called the Molecular Ecosystem Network Analysis Pipeline (MENAP; Feng et al., 2022).[1] In the process of network construction, OTUs with a frequency of less than 10% were discarded. Based on the SparCC method with the default parameters, the filtered OTU table was utilized to calculate pairwise correlation (Friedman and Alm, 2012). Based on random matrix theory (RMT), the appropriate cut-off value was selected as a threshold and combined with a significance level of *p*-value adjusted using the Benjamini-Hochberg FDR correction method less than 0.05 to filter out unrelated associations in the matrix. The IDIRECT method was used to remove unreliable and indirect associations from the network (Xiao et al., 2022). After networks were built, the analysis of network properties [e.g., nodes, links, average degree (avgK), average path distance (GD), average clustering coefficient (avgCC), connectedness (Con), and modularity], and randomization were carried out using the default parameters (Deng et al., 2012). Network modules were then determined by using greedy modularity optimization. In this study, a total of three networks were constructed. Among them, networks with sample sizes of 92 and 45 were employed for the comparison between the exposure ($n = 92$) and control ($n = 45$) groups. Additionally, to investigate the impact of blood heavy metals on network structure, a network with a sample size of 79 was utilized to calculate the correlation between module-based eigenvalues and the concentration of heavy metals in blood. Furthermore, the functions of the modules were predicted by PICRUSt (Douglas et al., 2020) and the Kyoto Encyclopaedia of Genes and Genomes (KEGG) database (Kanehisa et al., 2017) in terms of metabolic pathways. All obtained networks were visualized using Gephi 0.9.7[2] and Cytoscape 3.9.1.[3]

2.6. Statistical analyses

Prior to analyses, the OTU table was subsequently rarefied to the lowest number of sequences (28367) found within an individual sample. Our resampled dataset included a total of 2,315 bacterial OTUs. We first calculated the α diversity index (i.e., Sobs, Shannon–Wiener, Simpson, ACE and Chao1 indices) for each buccal mucosa sample using the QIIME pipeline and then tested the differences between the exposure and control groups using the Wilcoxon rank-sum test. Principal coordinate analysis (PCoA) was then performed at OTU level to investigate the dissimilarities in bacterial community composition between the groups based on both weighted and unweighted UniFrac algorithms, and statistical significance was assessed by analysis of similarities (ANOSIM). We also compared the relative abundance of dominant bacterial taxa at both the phylum and genus levels (phyla with relative abundance above 1% and genera with relative abundance above 3% were considered dominant) between the groups using the Wilcoxon rank-sum test, and their *p* values were adjusted by using the false discovery rate. To identify the taxa most likely to account for the variations between exposure and control samples, we employed linear discriminant analysis effect size (LEfSe) analysis. An LDA score of greater than 3.5 was established as the threshold to identify discriminative taxa (from phylum to species). The Spearman correlation between the genera and the concentrations of heavy metals in blood was analyzed and visualized to further investigate whether the genera exhibiting differences between the exposed and control groups were correlated with the concentrations of heavy metals in blood. To assess the functional differences in terms of metabolic pathways between the microbial communities of the exposure and control groups, we used PICRUSt2[4] based on the SILVA database of 16S rRNA sequences (Langille et al., 2013) and the Kyoto Encyclopaedia of Genes and Genomes (KEGG) database (Kanehisa et al., 2017) to predict microbial functional genes. The Wilcoxon rank-sum test was used for comparison of the KEGG pathway abundances between the two groups. All above analyses were

1 http://mem.rcees.ac.cn:8081

2 https://gephi.org/

3 https://cytoscape.org/

4 https://github.com/picrust/picrust2

conducted by using SPSS (version 26.0; IBM SPSS Inc., United States) and R (version 4.2.2; http://cran.r-project.org/).

3. Results and discussion

3.1. The heavy metal pollution of the study area

To assess whether there are differences in metal pollution levels between the contaminated and control areas, the concentrations of heavy metals in the soil and the blood of the subjects in the two areas were compared using the Wilcoxon rank-sum test. In the ploughed soil of the contaminated area, our results showed that the mean values of seven metals (Mo, Cd, Sb, Cu, Hg, Pb, and Zn) were substantially higher than those of the control area (all $p < 0.05$), whereas the levels of Co, Ni, and Mn were similar between the two areas (all $p > 0.05$; Supplementary Table S1). The concentrations of four metals (Zn, Hg, Cd and Pb) in the blood of subjects living in contaminated areas were significantly higher than those in the control area (all $p < 0.05$; Supplementary Table S2).

3.2. Bacterial diversity of buccal mucosa

The rarefaction curves stabilized, indicating that the sequencing depth was sufficient to reflect the bacterial diversity in the majority of samples (Figure 2A). The bacterial Sobs, Chao1 and ACE indices of the exposure group were significantly higher than those of the control group (all $p < 0.001$), whereas we did not observe significant differences between the two groups for the Shannon–Wiener and Simpson indices (both $p > 0.05$; Figures 2B–F). The bacterial community structure of the buccal mucosa samples was analyzed using principal coordinate analysis (PCoA), which is based on both weighted and unweighted UniFrac distances, to see whether there were significant differences between the exposure and control groups. The first and second principal components together explained 45.51% and 22.28% of the total variation in bacterial communities based on weighted and unweighted UniFrac distances, respectively (Figures 2G,H). Our results revealed significant differences in bacterial community composition between the two groups (ANOSIM $R > 0.257$, both $p = 0.001$), although their distributions were found to partially overlap.

3.3. Bacterial community structure of buccal mucosa

The dominant bacterial phyla observed in the exposure and control groups were Firmicutes (45.41% vs. 60.45%), Actinobacteriota (31.75% vs. 15.54%), Proteobacteria (13.19% vs. 9.74%), Fusobacteriota (5.00% vs. 4.98%), Bacteroidota (2.50% vs. 6.30%), and Patescibacteria (1.74% vs. 2.16%; Figure 3A). The relative abundances of Actinobacteriota and Proteobacteria were significantly higher in the exposure group than in the control group (Wilcoxon rank-sum test, both $p < 0.01$), whereas the relative abundances of Firmicutes and Bacteroidota appeared to be significantly higher in the control group (both $p < 0.001$; Figure 3B). Moreover, the dominant bacterial genera in the control group were *Streptococcus* (41.64%), *Gemella* (7.45%), *Rothia* (4.72%), *Actinomyces* (4.71%), *Rhodococcus* (4.18%), *Neisseria* (3.53%), and *Prevotella* (3.34%), while the exposure

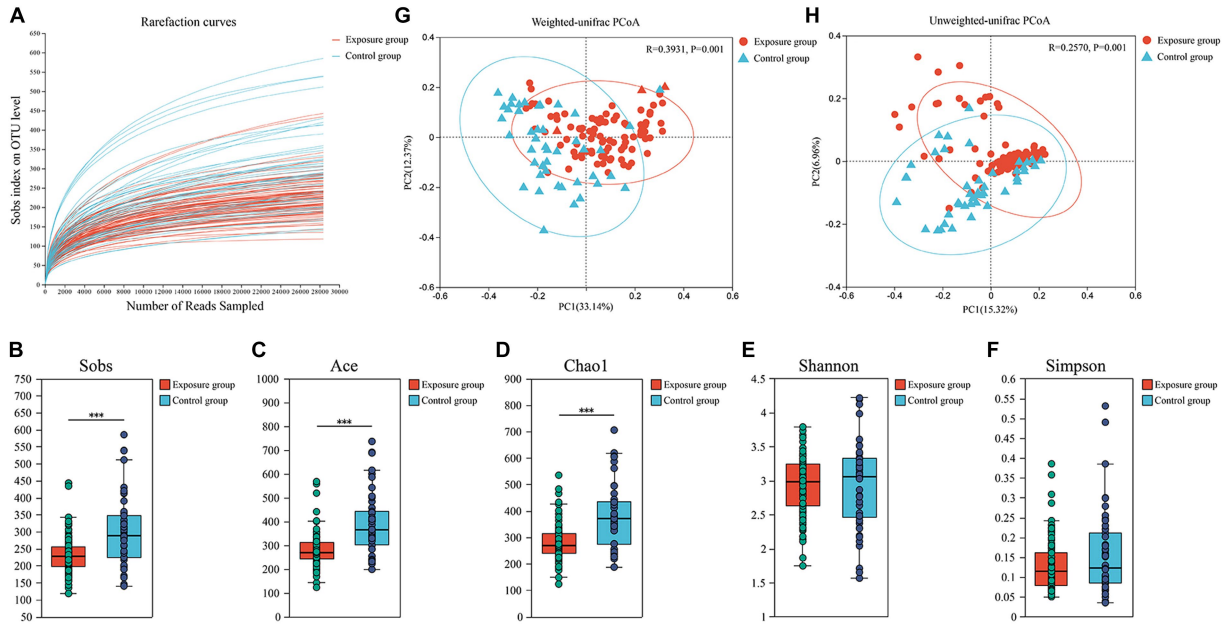

FIGURE 2
Analysis of α-diversity and principal coordinate analysis of buccal mucosal bacterial communities. **(A)** Rarefaction curves for the bacterial community dataset. The flat curve indicated that the sequence number used for analyses was adequate. **(B–F)** Differences in bacterial α diversity indices between the exposure and control groups. Significant differences were determined by using the Wilcoxon rank-sum test. $*p \leq 0.05$; $**p \leq 0.01$; $***p \leq 0.001$. **(G,H)** Principal coordinate analysis (PCoA) of bacterial community dissimilarities based on the weighted **(G)** and unweighted **(H)** UniFrac distances. Significant differences in bacterial β diversity between the exposure and control groups were determined by using ANOSIM statistics.

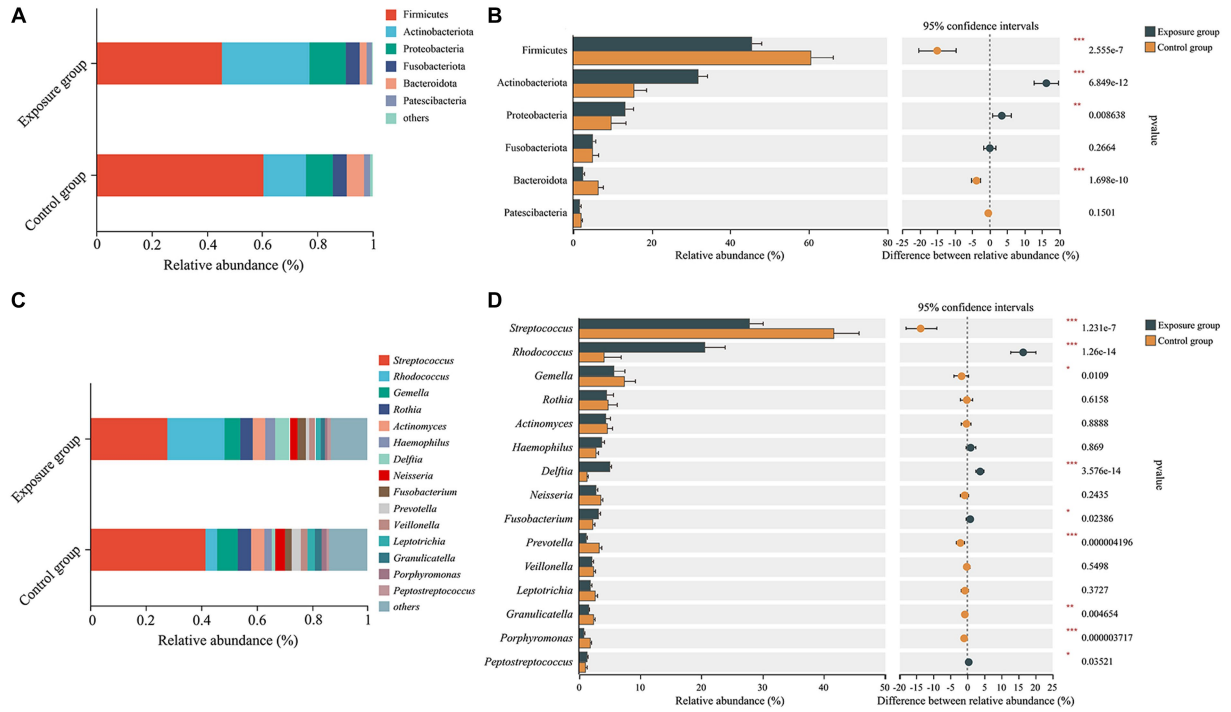

FIGURE 3
The bacterial community composition of the exposure and control groups and the correlations between bacterial community composition and blood heavy metal levels. Compositional differences in bacterial communities of the buccal mucosa at the phylum **(A,B)** and genus **(C,D)** levels. The *p*-value was calculated using the Wilcoxon rank-sum test and adjusted by using the false discovery rate. *$p < 0.05$; **$p < 0.01$; ***$p < 0.001$.

group exhibited dominant genera including *Streptococcus* (27.86%), *Rhodococcus* (20.57%), *Gemella* (5.71%), *Delftia* (5.09%), *Rothia* (4.53%), *Actinomyces* (4.40%), *Haemophilus* (3.70%), and *Fusobacterium* (3.13%; Figure 3C). Among the aforementioned dominant genera, the relative abundances of *Streptococcus*, *Gemella*, and *Prevotella* were significantly higher in the control group than in the exposure group (all $p < 0.05$), whereas those of *Rhodococcus*, *Delftia*, and *Fusobacterium* were significantly higher in the exposure group (all $p < 0.05$; Figure 3D). No significant differences were found in the relative abundance of *Rothia*, *Actinomyces*, *Haemophilus*, and *Neisseria* between the two groups. Furthermore, bacteria of the genera *Granulicatella* and *Porphyromonas* were significantly enriched in the control group (both $p < 0.001$), while *Peptostreptococcus* exhibited significant enrichment in the exposure group ($p < 0.05$).

We further used Spearman's correlation to evaluate the responses of the relative abundance of bacterial genera to concentrations of heavy metals in the blood (Figure 4). Our results showed that the relative abundances of *Rhodococcus* and *Delftia* were positively correlated with the concentrations of Cd and Pb, whereas those of *Granulicatella*, *Streptococcus*, *Neisseria*, *Gemella*, *Haemophilus*, and *Porphyromonas* exhibited negative associations with the concentration of Cd. *Porphyromonas* exhibited not only a negative correlation with Cd but also negative correlations with Hg and Pb. Moreover, the relative abundance of *Peptostreptococcus* was found to be positively correlated with the amount of Zn, and those of *Gemella* and *Abiotrophia* showed positive correlations with the content of Mo. There were no significant associations observed between the relative abundances of *Prevotella*, *Leptotrichia*, *Fusobacterium*, *Rothia*, *Actinomyces*, *norank_f_Saccharimonadaceae*, and *Veillonella* with the concentrations of any heavy metals in the blood.

A portion of the bacteria at the species level are presented in Supplementary Figure S1. We found that the relative abundances of *Rhodococcus erythropolis*, *Delftia tsuruhatensis*, and *Streptococcus anginosus* in the exposure group were significantly higher than those in the control group. The relative abundances of *Streptococcus gordonii*, *S. gordonii*, *S. mutans*, and *Porphyromonas gingivalis* were enriched in the exposed group, although the difference was not significant compared to the control group.

Linear discriminant analysis effect size (LEfSe) analysis was used to identify taxa effect size. The circles that radiate outwards from the center of the branch diagram represent the various levels of classification, from phylum to species (Supplementary Figure S2). These results showed significant enrichment of *Corynebacteriales*, *Rhodococcus*, *Nocardiaceae*, Actinobacteriota, and *Actinobacteria* in the exposure group. We also found that *Streptococcus*, *Bacilli*, Firmicutes, *Lactobacillales*, and *Streptococcaceae*, were more abundant in the control group than in the exposure group (Supplementary Figure S3). Furthermore, Firmicutes, which is thought to be the most prevalent phylum of bacteria in the buccal mucosa (Wang S. et al., 2022), was significantly decreased in the exposure group. However, the cladogram for this phylum suggests that *Streptococcus*, *Gemella*, and *Granulicatella* were primarily accountable for this difference, and other genera belonging to the Firmicutes phylum did not show a preference for metal exposure.

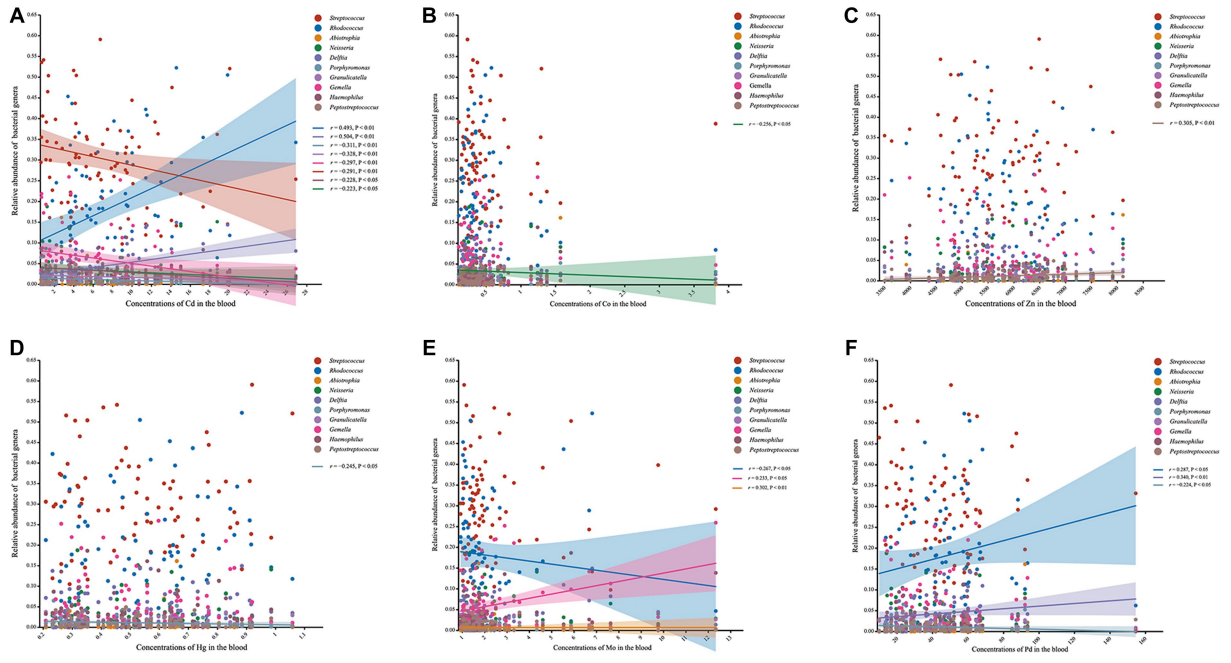

FIGURE 4
Scatter plots presenting the correlation between the genera and the concentrations of heavy metals in blood. **(A)** Scatter plot of the correlation between the genera and Cd. **(B)** Scatter plot of the correlation between the genera and Co. **(C)** Scatter plot of the correlation between the genera and Zn. **(D)** Scatter plot of the correlation between the genera and Hg. **(E)** Scatter plot of the correlation between the genera and Mo. **(F)** Scatter plot of the correlation between the genera and Pd.

3.4. Functional predictions of buccal mucosal bacterial communities

We predicted the functions of buccal mucosal bacterial communities based on the KEGG pathway database and then tested their functional differences in terms of metabolic pathways between the exposure and control groups (Figure 5). Overall, the two groups showed obvious functional differences, with a greater number of upregulated genes than downregulated genes (43 vs. 1 at KEGG level 2 and 258 vs. 64 at KEGG level 3). Specifically, predictions based on the KEGG level 2 pathway revealed that the top five upregulated genes in terms of fold change were involved in substance dependence, xenobiotic biodegradation and metabolism, lipid metabolism and catabolism, excretory system, and cancer: specific types were upregulated in the exposure group (Wilcoxon rank-sum test, all $p < 0.05$; Figure 5A), while sensory system-related genes were upregulated in the control group ($p < 0.05$). For the KEGG level 3 pathway, the top five upregulated genes in terms of fold change observed in the exposure group were involved in hematopoietic cell lineage, steroid degradation, caffeine metabolism, steroid biosynthesis and cAMP signaling pathway (Wilcoxon rank-sum test, all $p < 0.05$; Figure 5B). In contrast, the upregulated genes in the control group were involved in biosynthesis of enediyne antibiotics, isoflavonoid biosynthesis, aldosterone-regulated sodium reabsorption, endocrine and other factor-regulated calcium reabsorption, and insulin secretion (all $p < 0.05$).

3.5. Patterns of bacterial co-occurrence networks

We constructed molecular ecological networks (MENs) to compare the interaction and co-occurrence pattern of buccal mucosal bacterial communities between the exposure and control groups (Figure 6; Table 1). The network of the exposure group produced 66 nodes and 56 edges, while the network of the control group included 123 nodes and 135 edges (Table 1). For the network edges of the two groups, the proportion of positive interactions was much higher than that of negative interactions (98.21% vs. 1.79% in the exposure group, and 91.85% vs. 9.15% in the control group). To ascertain whether the networks of the two groups differ from random networks, we compared the empirical network with the random network generated using the Maslov-Sneppen procedure by rewiring the same number of nodes and edges to the corresponding empirical network (Zhou et al., 2011). The values of average clustering coefficient (avgCC), average path distance (GD), and modularity in both networks appeared to be significantly different from random ones (Supplementary Table S3), indicating nonrandom patterns of co-occurrence network.

Network topological properties revealed that degree distributions conformed to the power-law model (both $R^2 > 0.941$; Table 1), indicating the scale-free property of the two networks. The empirical networks exhibited higher average clustering coefficients compared to their corresponding random networks, which suggested the small-world property of the two networks (Deng et al., 2012). Modularity

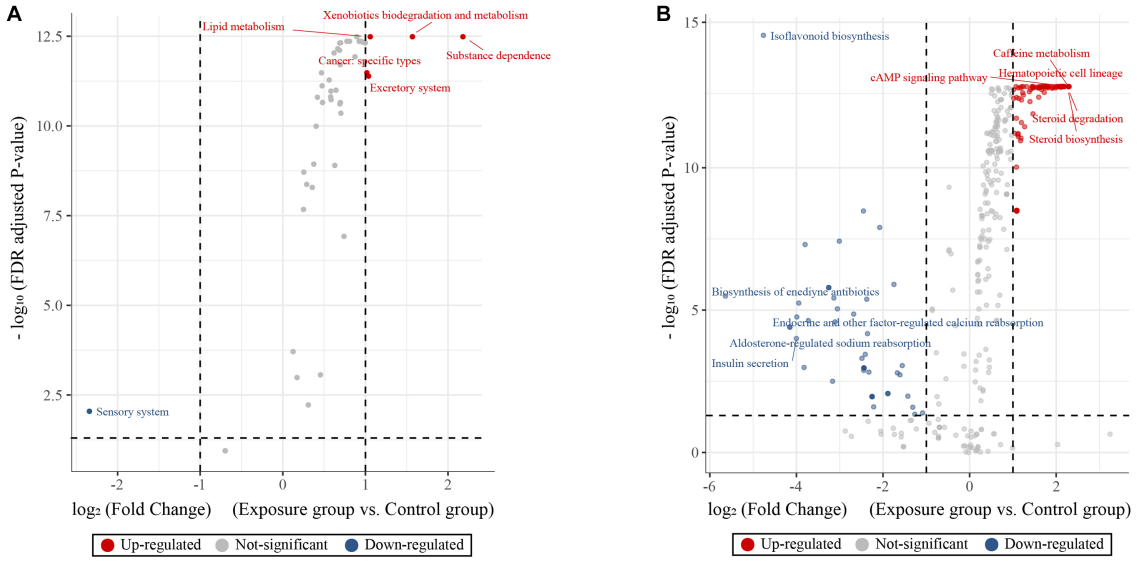

FIGURE 5
KEGG pathway volcano to predict differences in metabolic pathways of microbial communities. Volcano plot showing the predictive functional differences between the exposure and control groups based on the KEGG metabolic pathway at the second **(A)** and third **(B)** levels (fold change > 1 and adjusted *p*-value < 0.05). The red, blue and gray circles indicate upregulated, downregulated and insignificantly changed genes, respectively.

was utilized as a quantitative measure to evaluate the degree to which a network is organized into delimited modules. The modularity values for the exposure group (0.848) and the control group (0.793) were higher than for the corresponding random network (0.799 and 0.728), indicating that the two networks are modular (Newman, 2006; Deng et al., 2012). There were 6 and 9 modules (with >4 nodes) observed in the exposure and control groups, respectively (Figures 6C,D). Not only is the number of modules in the exposure group reduced compared to the control group pattern, but there are also fewer nodes and links within each module. These results suggested that the two networks possessed scale-free, small-world, and modular properties.

The network nodes of the exposure and control groups were mostly affiliated with 8 different bacterial phyla (Figure 7A). Among these, the relative abundances of Firmicutes, Fusobacteriota, and Synerqistota were higher in the network of the exposure group than in that of the control group. In contrast, there was a higher relative abundance of Bacteroidota, Proteobacteria, Actinobacteriota, Patescibacteria, and Spirochaetota in the network of the control group. A total of 73 nodes were unshared by the two networks (Figure 7B), indicating that most buccal mucosal bacterial species had unique niches in both networks (Qi et al., 2019). Therefore, these results indicated that the taxonomic composition of nodes was very different between the two networks.

We then determined the network topological roles of bacterial OTUs according to their locations in their respective modules and the extent to which they are connected to OTUs in other modules (Guimerà and Nunes Amaral, 2005). Specifically, the nodes were divided into four categories based on the indicators of within-module connectivity (Zi) and among-module connectivity (Pi): peripherals ($Zi \leq 2.5$, $Pi \leq 0.62$), connectors ($Zi \leq 2{,}5$, $Pi \geq 0.62$), module hubs ($Zi \geq 2.5$, $Pi \leq 0.62$), and network hubs ($Zi \geq 2.5$, $Pi \geq 0.62$; Guimerà and Nunes Amaral, 2005; Zhou et al., 2011; Figure 8).

Our results showed that none of the nodes within networks of the exposure and control groups were classified as network hubs, and all nodes within the network of the exposure group were peripherals with most of them (i.e., 92%) having no connections with nodes in other modules ($Pi = 0$). In contrast, approximately 4% of nodes within the network of the control groups were generalists (Olesen et al., 2007), with 1.6% being module hubs and 2.4% being connectors. Notably, module hubs and connectors, which are commonly thought to play an important role in the topological nature of co-occurrence networks, are considered keystone taxa (Li et al., 2017). The five keystone taxa detected in the network of the control group were affiliated with the species *Filifactor alocis* (OTU201), *Schaalia odontolytica* (OTU2018), *Prevotella salivae* (OTU367), *Solobacterium moorei* (OTU2014), and *Streptococcus vestibularis* (OTU339). Interestingly, among them, only OTU339 and OTU2018, belonging to the species *Streptococcus vestibularis* and *Schaalia odontolytica*, represented dominant taxa in the buccal mucosal bacterial community. The relative abundances of OTU339 and OTU2018 were 3.06% and 1.97%, respectively. However, the remaining three OTUs belonging to the species *Filifactor alocis*, *Prevotella salivae* and *Solobacterium moorei* only accounted for very low relative abundance in bacterial communities (averages of 0.58%, 0.13%, and 0.20%, respectively).

3.6. Correlations between network modules and the concentrations of heavy metals in the blood

We further tested the responses of network modules to intraexposure (i.e., the heavy metals in blood) using a subdataset that included 79 subjects. The topological properties of the empirical network are shown in Supplementary Table S4. There were obvious differences in both the average clustering coefficient (avgCC) and

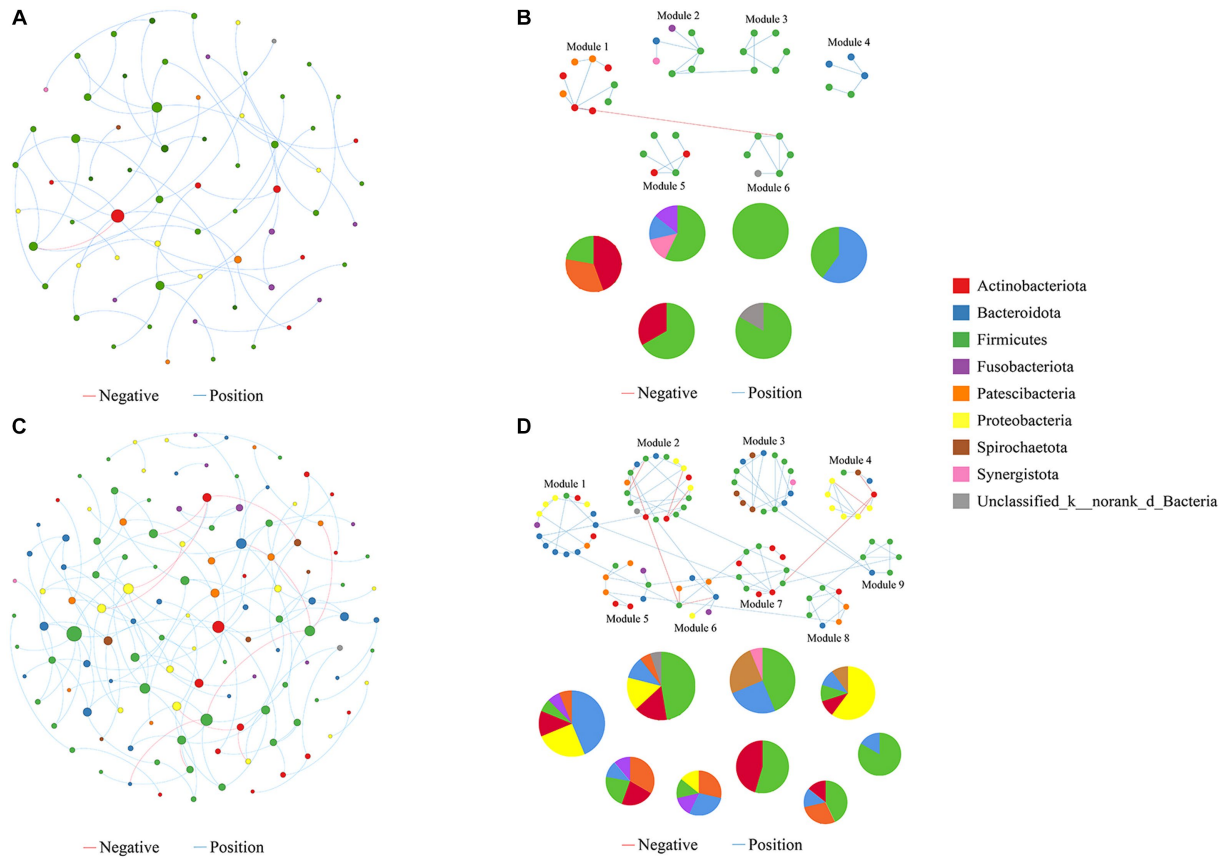

FIGURE 6
Molecular ecological networks were built on the basis of correlation among bacterial OTUs. The networks for the exposure **(A)** and control groups **(B)** are displayed. Node sizes are proportional to the number of connections. Panels **(C,D)** present the network modules determined by the fast greedy modularity optimization method (only showing nodes larger than 4) for the exposure and control groups, respectively, as well as their taxonomic composition at the phylum level. Each node represents a bacterial OTU and is colored by its phylum-level taxonomic affiliation. Red lines represent negative interactions among bacterial OTUs, whereas blue lines represent positive interactions.

average path distance (GD) between the empirical and random networks (Supplementary Table S5). The empirical network had 112 nodes and 101 edges (average degree of 1.804 and average path distance of 5.537). For the network edges, the proportion of positive interactions was higher than that of negative interactions (94.06% vs. 5.94%; Supplementary Figure S4). There were 9 modules (with >4 nodes) observed in the network (Figure 9A). After modules were determined, we further used eigengene analysis to reveal the higher order organizations in the network structure (Langfelder and Horvath, 2007). Our results indicated that many sets of modules eigengenes were closely correlated with each other and were clustered together as supergroups, such as #3 and #7 and #1, #4 and #5 (Figure 9C). More importantly, we observed significant correlations between several modules and the concentrations of heavy metals in the blood (Figure 9D). Specifically, the contents of Cd and Pb were significantly and negatively correlated with module #2 (both $p \leq 0.02$) and positively correlated with module #5 (both $p \leq 0.03$). Module #7 was positively correlated with the concentration of Sb in the blood ($p = 0.02$), and module #4 was negatively correlated with that of Hg ($p = 0.04$). Collectively, these results suggest that different network modules respond differently to the concentrations of heavy metals in the blood, and changes in heavy metal content may have a significant impact on members of certain modules (such as #2, #4, #5, and #7).

3.7. Functional predictions of network modules

We used the PICRUSt pipeline to predict the bacterial gene functions for the main network modules based on KEGG metabolic pathways (Figure 9B). The predominant functions were those related to metabolism and the processing of genetic information. Our results further showed that genes related to amino acid metabolism, carbohydrate metabolism, metabolism of cofactors and vitamins, metabolism of other amino acids, and replication and repair were richest in the categories of the level 2 KEGG pathway (Supplementary Figure S5). Interestingly, some functions were unique to individual modules, such as chemical structure transformation maps, which were unique to module 3 and module 9; substance dependence, which was unique to module 5 and module 9; and the circulatory system, which was detected only in module 9. Additionally, we also calculated the correlations between the contents of heavy metals in the blood and the relative abundance of the level 2 KEGG pathway of some network modules (i.e., #2, #4, #5, and #7; Supplementary Figure S6). Our results showed that among the gene functions that were associated with the contents of heavy metals, the strongest positive correlation between Cd and Pb was cell motility, and the most negative correlations were glycan biosynthesis and

TABLE 1 Topological properties of the empirical and 100 random MENs of microbial communities in the exposure and control groups; n.a denotes no data available in the random algorithm.

Network indices	Exposure group	Control group	Exposure group	Control group
	Empirical		Random (mean ± SD)	
Total nodes	66	123	n.a	n.a
Total links	56	135	n.a	n.a
RMT cut-off	0.45	0.45	n.a	n.a
R square of power-law	0.992	0.941	n.a	n.a
Average degree (avgK)	1.697	2.195	n.a	n.a
Average clustering coefficient (avgCC)	0.075	0.072	0 ± 0.005	0 ± 0.002
Average path distance (GD)	3.021	6.838	4.611 ± 0.928	5.814 ± 0.331
Geodesic efficiency (E)	0.460	0.199	0.321 ± 0.05	0.218 ± 0.009
Harmonic geodesic distance (HD)	2.174	5.027	3.188 ± 0.49	4.589 ± 0.199
Centralization of degree (CD)	0.082	0.048	0.082 ± 0	0.048 ± 0
Centralization of betweenness (CB)	0.058	0.246	0.16 ± 0.063	0.194 ± 0.048
Centralization of stress centrality (CS)	0.058	0.523	0.004 ± 0.002	0.004 ± 0.002
Centralization of eigenvector centrality (CE)	0.920	0.934	0.921 ± 0.015	0.89 ± 0.027
Centralization of closeness centrality (CCL)	0.006	0.015	0.014 ± 0.004	0.019 ± 0.004
Density (D)	0.026	0.018	0.026 ± 0	0.018 ± 0
Reciprocity	1	1	1 ± 0	1 ± 0
Transitivity (Trans)	0.146	0.065	0.014 ± 0.021	0.014 ± 0.012
Connectedness (Con)	0.136	0.675	0.311 ± 0.088	0.753 ± 0.065
Efficiency	0.887	0.984	0.999 ± 0.001	0.998 ± 0
Hierarchy	0	0	0.026 ± 0	0.018 ± 0
Lubness	1	1	0.142 ± 0.045	0.085 ± 0.018
Modularity	0.848 (17)	0.793 (18)	0.799 ± 0.018	0.725 ± 0.014

metabolism and the digestive system. The strongest positive correlation with Sb was in the digestive system, and the strongest negative correlation with Hg was in cancer: specific types.

4. Discussion

The oral cavity, as the beginning of the digestive tract, contains a complex population of microbes (Lamont et al., 2018; Zhang Y. et al., 2018). As part of the microbial community, the microbes of the buccal mucosa play an important role in human health (Du et al., 2020; Jung and Jang, 2022), but the impact of the environment, diet, and lifestyle habits on its composition is still poorly understood. MiSeq 16S rRNA gene sequencing was performed in this study on buccal mucosal samples from a total of 137 residents living in two villages. In summary, we found differences in microbial diversity, community composition, and co-occurrence patterns between the two groups.

Microbiota analysis showed that the structure and abundance of the buccal mucosal bacteria were significantly different between the exposure and control groups. The Sobs, Ace, and Chao1 indices in the control group are significantly higher than those in the exposure group, indicating that the species richness of buccal mucosal bacteria in residents living in the contaminated area was diminished. However, the Shannon and Simpson indices show no significant differences between the two groups. We speculate that this is because, even though the number of species has decreased in the exposure group, the relative abundance distribution of species remains stable between the two groups, and there are no significant dominant species. According to the PCoA based on the weighted and unweighted UniFrac distance analysis, the microbiota distribution varied significantly between the two groups (both $p = 0.001$). These results were consistent with previous studies showing that metal exposure can alter the composition of the oral bacterial spectrum (Eshed et al., 2012; Espinosa-Cristóbal et al., 2013; Khan et al., 2013), abundance, and diversity (Youravong et al., 2011; Davis et al., 2020). In terms of the composition of the microbiota, Firmicutes, Actinobacteriota, Proteobacteria, Fusobacteriota, and Bacteroidota were the dominant phyla. This is consistent with the dominant phyla of the oral microbiome identified by the Human Microbiome Project (HMP), indicating the reliability of the results (Human Microbiome Project Consortium, 2012). Firmicutes was the most abundant phylum in the buccal mucosa, although the relative abundance in the exposed group was significantly lower than that in the control group. At the genus level, we found that *Rhodococcus*, *Delftia*, *Fusobacterium*, and *Peptostreptococcus* were significantly enriched in the exposure group, whereas the relative abundances of *Streptococcus*, *Gemella*, *Prevotella*,

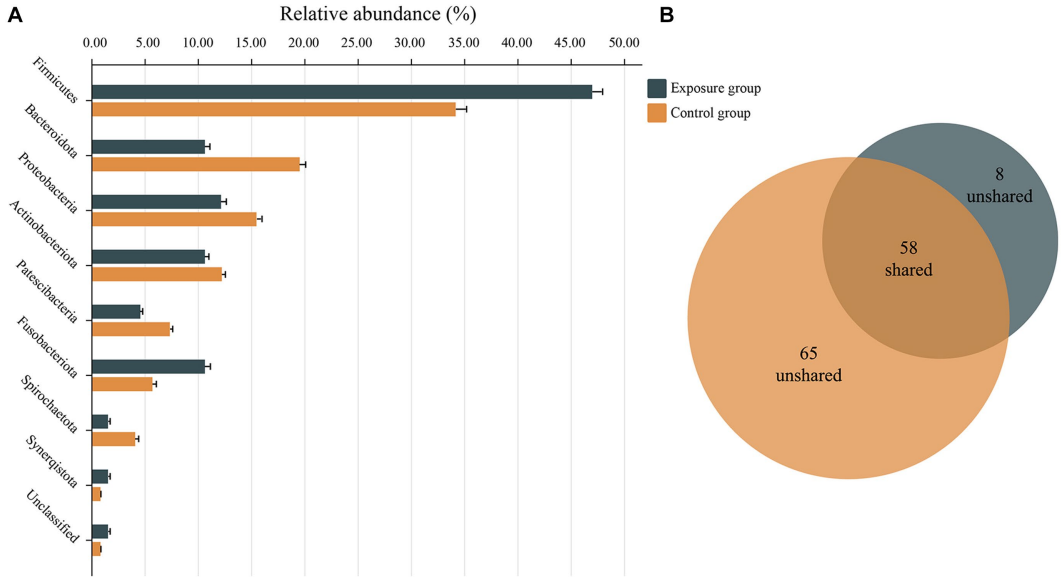

FIGURE 7
Relative abundances of different nodes in networks of the exposure and control groups. **(A)** Relative abundances of nodes belonging to different phyla categories in networks of exposure and control groups. **(B)** Venn charts showing the number of nodes shared and not shared by the networks of the exposure and control groups.

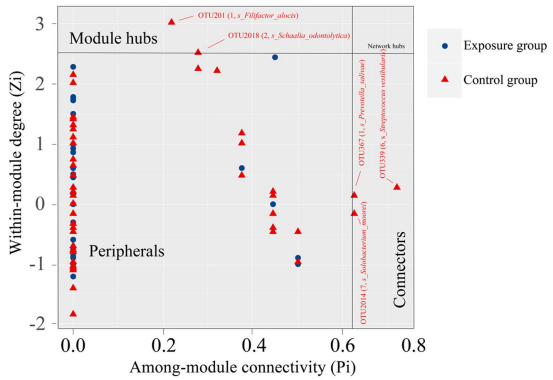

FIGURE 8
Z-P plot showing the topological roles of bacterial OTUs in the networks of the exposure and control groups. Each dot represents a bacterial OTU, and the ZP scatter plot was used to estimate the topological role of each OTU. The module hubs and connectors are labeled with OTU IDs, and in parentheses are the module IDs and species name.

Granulicatella, and *Porphyromonas* were significantly reduced in that group. This result confirmed the idea that the variation in bacterial abundance may be associated with metal exposure and that exogenous factors control which bacteria may settle, grow, and develop in the dominant population (Sedghi et al., 2021; Akimbekov et al., 2022). Correlation analysis showed that the majority of genera that exhibited a significant increase in relative abundance in the exposed group had positive correlations with the concentration of heavy metals in the blood, such as between *Rhodococcus* and *Delftia* with Cd and Pb. Conversely, in the control group, most genera with a significant increase in relative abundance were negatively correlated with the concentration of heavy metals in blood such as Cd with *Streptococcus*, *Porphyromonas*, and *Granulicatella*. Therefore, we speculated that long-term residence in areas contaminated with heavy metals leads to heavy metal accumulation in the body and further affects the microbial community structure of the buccal mucosa.

Oral lichen planus (OLP) is considered to be a chronic inflammatory disease associated with the buccal mucosa (Jung and Jang, 2022), and although the mechanism and cause of OLP are not yet explained, studies have found that the bacteria that settle on the surface of the buccal mucosa are related to OLP (Choi et al., 2016; He et al., 2017). In their study of the composition of the bacteria in the buccal mucosa of OLP patients and healthy controls, Hijazi et al. found that although there were no significant differences in the bacterial diversity between the two groups, alpha diversity decreased as the severity of OLP increased (Hijazi et al., 2020). Additionally, studies have shown that people with OLP have a more diverse microbiota in their buccal mucosa than healthy controls (He et al., 2017; Baek and Choi, 2018). In summary, although some studies report that the bacterial composition of healthy controls was similar to that of OLP patients (Hijazi et al., 2020), most of the studies on the microbial composition of the buccal mucosa have found that the bacterial structure of OLP patients can be distinguished from that of healthy controls (Du et al., 2020; Wang et al., 2020). In a previous study, a total of 19 different genera were found to have significant differences in abundance between OLP patients and healthy controls, with a significant increase in *Fusobacterium*, *Leptotrichia*, and *Lautropia* in patients, while *Streptococcus* was lower compared to the healthy control group (He et al., 2017). We created a combinatorial marker panel composed of four genera (*Fusobacterium*, *Leptotrichia*, *Lautropia*, and *Streptococcus*) and employed random forest analysis to investigate whether these genera could differentiate between the exposed and control groups (Supplementary Figure S7A). In the receiver-operating characteristic (ROC) curve, this result highlights

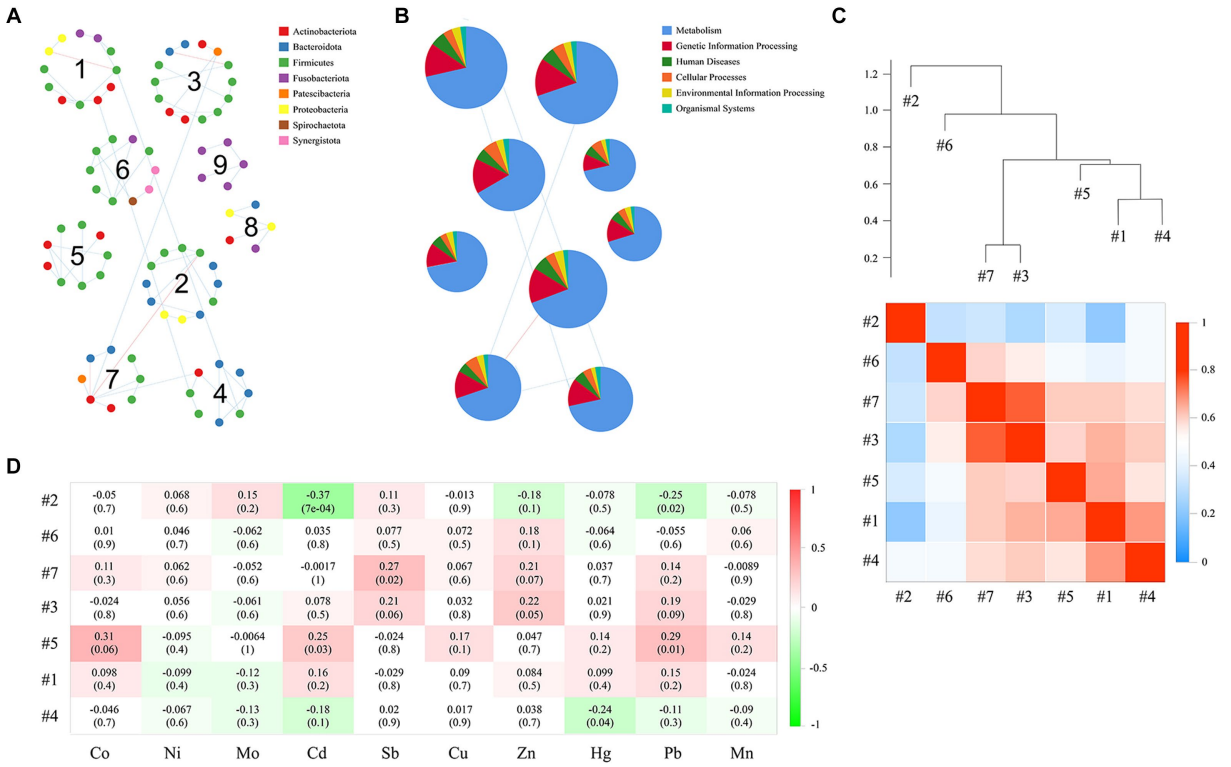

FIGURE 9
Correlation between modules, as well as the correlation of each module with the concentrations of heavy metals in the blood. Panel **(A)** presents the network module determined by the fast greedy modularity optimization method (only showing nodes larger than 4), as well as their taxonomic composition at the phylum level. Each node represents a bacterial OTU and is colored by its phylum-level taxonomic affiliation. Red lines represent negative interactions among bacterial OTUs, whereas blue lines represent positive interactions. **(B)** Relative abundance of KEGG categories of each network module. **(C)** Showing the correlations and heatmap of module eigengenes. The hierarchical clustering in the upper part is based on the Pearson correlations between module eigengenes, and the coefficient values (*r*) are shown in the lower part of the figure. **(D)** The Pearson correlations between module eigengenes and the content of heavy metals in blood. *r* in different colors, and the right side of the legend is the color range of different *r* values. The numbers represent the correlation coefficient (*r*) and significance (*P*) in parentheses.

the diagnostic potential of the combinatorial marker panel (AUC = 0.81, 95%CI: 0.73–0.89). It is reported that *Streptococcus* was closely associated with the development of oral cancer, and the relative abundances of *Streptococcus anginosus* and *S. gordonii* were significantly enriched in the buccal mucosa in patients with oral squamous cell carcinoma (OSCC; Karpiński, 2019). Moreover, *Streptococcus* (including *S. salivarius*, *S. mutans*, *S. milleri/anginosus*, and *S. mitis*) is alpha-hemolytic and opportunistic pathogenic (Nobbs et al., 2009). In this study, we found that the abundance of *S. anginosus* increased significantly in the exposure group, and that of *S. gordonii* and *S. mutans* increased but not significantly. However, in the ROC analysis, the combinatorial marker panel composed of *S. anginosus*, *S. gordonii*, and *S. mutans* cannot accurately distinguish between the exposure group and control group (AUC = 0.58, 95%CI: 0.48–0.868; Supplementary Figure S7B). Thus, our findings reveal that people who live in different environments have different microbial communities in the buccal mucosa and that living in areas contaminated with heavy metals may increase the risk of several diseases, including oral lichen planus.

PICRUSt analysis was used to predict the function of bacterial communities. In this study, there were significant differences in the metabolic function of buccal mucosal bacteria in the two groups, with most functions being upregulated in the exposure group. Metal ions may improve the adaptability of bacteria to different environments by regulating the function of bacterial cells in terms of substance dependence, xenobiotic biodegradation and metabolism, lipid metabolism, the excretory system, and the sensory system. According to findings from a previous study, during succession under the impact of the environment, microbes can develop adaptive mechanisms (Zhu et al., 2019). Due to the limitations of PICRUSt functional predictions (Langille et al., 2013), this study is only a preliminary prediction of bacterial function, and further verification should be carried out in future studies using methods such as metagenomics to better understand the function of buccal mucosal bacteria from different populations.

Based on high-throughput 16S rRNA sequencing data, we constructed microbial networks in this study. Most previous studies only analyzed the community composition, abundance, and diversity of oral microbes (Dong et al., 2021; Zhang et al., 2023), but the interactions between microbial species are critical to ecosystem stability. Therefore, microbial networks, as a new approach to analyzing the interactions between microbiota populations, can help us better understand the changes between the exposure and control groups.

Through bacterial molecular ecological network analysis, we observed that the network of the control group exhibited a greater number of interacting microbial species compared to the exposed group. In general, more interactive bacteria are present in the network, suggesting that there is more metabolism and information exchange between species, which allows the network work more efficiently (Faust and Raes, 2012). Modularity is one of the key topological features of network structures (Newman, 2006) and nodes in the same module usually have similar functions, metabolic pathways, niches, or phenotypic features (Qin et al., 2012; Layeghifard et al., 2017; Lurgi et al., 2019). In this study, both the number of modules and nodes within each module were found to be lower in the network of the exposure group than in the network of the control group, which means that the microbial network of the control group has a higher complexity and ecological diversity, and the interactions between microbes are more complex and tighter. Furthermore, a higher average connectivity implies a network of greater complexity (Qi et al., 2019). The average degree values for the exposure and control groups were 1.697 and 2.195, respectively. All of the aforementioned results indicated that exposure to heavy metals would reduce the complexity of the buccal mucosal bacterial network.

Keystone taxa were believed to play an important role in the network, making it more stable and ordered (Qi et al., 2019). Studies have shown that keystone taxa are important for the stability of ecosystems, and their extinction may lead to the fragmentation of the entire microbiome (Lupatini et al., 2014). In the network of the control group, we found 5 keystone taxa, while in the exposure group all nodes were identified as peripherals. In addition, the role of microbial species changed in the network of the exposure group compared to the control group. For example, module hubs in the network of the control group (OTU201 and OTU2018) and connectors (OTU367, OTU2014, and OTU339) were converted to peripherals in the exposure group. Shifts in the roles of these keystone taxa may lead to instability of the exposure group network and a weakening of the ability to suppress the growth of pathogens (such as *S. anginosus*, *S. gordonii*, and *P. gingivalis*). Interestingly, of the keystone taxa found in the control group, *Filifactoralocis*, *Prevotella salivae*, and *Solobacterium moorei* together accounted for less than 1% of the total relative abundance. These findings suggest that these relatively low-abundance bacteria occupy a very important place in the ecological network and therefore may exert a greater influence on microbial structure and function than some bacteria with relatively high abundances, despite the fact that their presence can have either beneficial or detrimental effects on humans and human activities (Zhang S. et al., 2018; Qi et al., 2019). Furthermore, we did not identify any keystone taxa in the network of the exposure group, indicating that heavy metal exposure would alter the initial structure of the network, causing the loss of the activities of taxa that were in key positions before and thereby making the entire network more vulnerable to damage. We also found that the concentrations of Cd, Pb, Sb, and Hg in blood were correlated with the microbial network structure of the buccal mucosa. Previous studies have shown that heavy metal ions, especially divalent ions such as lead and cadmium, affect the growth and vitality of oral bacterial communities (Youravong et al., 2011; Breton et al., 2013; Steiger et al., 2020). Thus, we speculate that Cd, Pb, Sb, and Hg in the blood are the main drivers of the bacterial network and may adversely affect the stability of the microbial network of the buccal mucosa in residents with long-term exposure to heavy metals.

5. Conclusion

(1) Long-term exposure to multiple metals perturbs normal buccal mucosal bacterial communities in inhabitants of contaminated areas and may increase their risk of developing a variety of diseases, including OLP.
(2) The concentrations of heavy metals (Pb, Cd, Hg, and Mo) in the blood are associated with the growth of *Rhodococcus*, *Delftia*, *Porphyromonas*, and *Gemella*.
(3) Long-term exposure to metals, reduces the complexity and stability of the microbial network of the buccal mucosa.
(4) As the main drivers of the network, Pb, Cd, Hg, and Mo in the blood can adversely affect the microbial network of the buccal mucosa in residents with long-term exposure to heavy metals.
(5) Some low-abundance bacteria may exert a greater influence on microbial structure than some bacteria with a relatively high abundance.

Data availability statement

The datasets presented in this study can be found in online repositories. The names of the repository/repositories and accession number(s) can be found at: https://www.ncbi.nlm.nih.gov/, PRJNA979792.

Ethics statement

The studies involving humans were approved by Ethical Committees of the Public Health School of Lanzhou University. The studies were conducted in accordance with the local legislation and institutional requirements. The participants provided their written informed consent to participate in this study.

Author contributions

SP: Data curation, Software, Writing – original draft. LF: Writing – review & editing. YZ: Data curation, Investigation, Methodology, Writing – review & editing. JLiu: Investigation, Methodology, Software, Writing – review & editing. JLi: Data curation, Software, Writing – review & editing. QZ: Data curation, Software, Writing – review & editing. XL: Conceptualization, Writing – review & editing. BL: Conceptualization, Writing – review & editing. HL: Conceptualization, Writing – review & editing. WH: Data curation, Methodology, Software, Writing – review & editing. JN: Conceptualization, Investigation, Writing – review & editing. TT: Conceptualization, Investigation, Writing – original draft. YR: Conceptualization, Investigation, Writing – review & editing.

Funding

The author(s) declare financial support was received for the research, authorship, and/or publication of this article. We are grateful for financial support from the National Natural Science Foundation of China (nos. 32001125 and 81872578), the Fundamental Research Funds for the Central Universities (lzujbky-2021-24), and the Science and Technology Program of Lanzhou, China (no. 2022-2-108).

Conflict of interest

The authors declare that the research was conducted in the absence of any commercial or financial relationships that could be construed as a potential conflict of interest.

Publisher's note

All claims expressed in this article are solely those of the authors and do not necessarily represent those of their affiliated organizations, or those of the publisher, the editors and the reviewers. Any product that may be evaluated in this article, or claim that may be made by its manufacturer, is not guaranteed or endorsed by the publisher.

Supplementary material

The Supplementary material for this article can be found online at: https://www.frontiersin.org/articles/10.3389/fmicb.2023.1264619/full#supplementary-material

References

Ahamed, M., and Siddiqui, M. K. (2007). Environmental lead toxicity and nutritional factors. *Clin. Nutr.* 26, 400–408. doi: 10.1016/j.clnu.2007.03.010

Akimbekov, N. S., Digel, I., Yerezhepov, A. Y., Shardarbek, R. S., Wu, X., and Zha, J. (2022). Nutritional factors influencing microbiota-mediated colonization resistance of the oral cavity: A literature review. *Front. Nutr.* 9:1029324. doi: 10.3389/fnut.2022.1029324

Azimi, A., Azari, A., Rezakazemi, M., and Ansarpour, M. (2017). Removal of heavy metals from industrial wastewaters: A review. *ChemBioEng Rev* 4, 37–59. doi: 10.1002/cben.201600010

Baek, K., and Choi, Y. (2018). The microbiology of oral lichen planus: is microbial infection the cause of oral lichen planus? *Mol. Oral Microbiol.* 33, 22–28. doi: 10.1111/omi.12197

Breton, J., Massart, S., Vandamme, P., De Brandt, E., Pot, B., and Foligné, B. (2013). Ecotoxicology inside the gut: impact of heavy metals on the mouse microbiome. *BMC Pharmacol. Toxicol.* 14:62. doi: 10.1186/2050-6511-14-62

Caporaso, J. G., Kuczynski, J., Stombaugh, J., Bittinger, K., Bushman, F. D., Costello, E. K., et al. (2010). QIIME allows analysis of high-throughput community sequencing data. *Nat. Methods* 7, 335–336. doi: 10.1038/nmeth.f.303

Chen, J., Liu, K., Sun, X., Shi, X., Zhao, G., and Yang, Z. (2022). Microbiome landscape of lesions and adjacent normal mucosal areas in oral lichen planus patient. *Front. Microbiol.* 13:992065. doi: 10.3389/fmicb.2022.992065

Chen, L., Zhou, M., Wang, J., Zhang, Z., Duan, C., Wang, X., et al. (2022). A global meta-analysis of heavy metal(loid)s pollution in soils near copper mines: evaluation of pollution level and probabilistic health risks. *Sci. Total Environ.* 835:155441. doi: 10.1016/j.scitotenv.2022.155441

Choi, Y. S., Kim, Y., Yoon, H.-J., Baek, K. J., Alam, J., Park, H. K., et al. (2016). The presence of bacteria within tissue provides insights into the pathogenesis of oral lichen planus. *Sci. Rep.* 6:29186. doi: 10.1038/srep29186

Curtis, M. A., Diaz, P. I., and Van Dyke, T. E. (2020). The role of the microbiota in periodontal disease. *Periodontol. 2000* 2000, 14–25. doi: 10.1111/prd.12296

Davis, E., Bakulski, K. M., Goodrich, J. M., Peterson, K. E., Marazita, M. L., and Foxman, B. (2020). Low levels of salivary metals, oral microbiome composition and dental decay. *Sci. Rep.* 10:14640. doi: 10.1038/s41598-020-71495-9

Deng, Y., Jiang, Y.-H., Yang, Y., He, Z., Luo, F., and Zhou, J. (2012). Molecular ecological network analyses. *BMC Bioinformatics* 13:113. doi: 10.1186/1471-2105-13-113

Dong, K., Wu, K., Zheng, T., Yue, J., Wang, W., Luo, R., et al. (2021). Comparative study of Oral Bacteria and Fungi microbiota in Tibetan and Chinese Han living at different altitude. *Tohoku J. Exp. Med.* 254, 129–139. doi: 10.1620/tjem.254.129

Douglas, G. M., Maffei, V. J., Zaneveld, J. R., Yurgel, S. N., Brown, J. R., Taylor, C. M., et al. (2020). PICRUSt2 for prediction of metagenome functions. *Nat. Biotechnol.* 38, 685–688. doi: 10.1038/s41587-020-0548-6

Driscoll, C. T., Mason, R. P., Chan, H. M., Jacob, D. J., and Pirrone, N. (2013). Mercury as a global pollutant: sources, pathways, and effects. *Environ. Sci. Technol.* 47, 4967–4983. doi: 10.1021/es305071v

Du, G., Wang, Y., Chen, J., Deng, Y., Han, X., and Tang, G. (2020). Potential association between *Fusobacterium nucleatum* enrichment on oral mucosal surface and oral lichen planus. *Oral Dis.* 26, 122–130. doi: 10.1111/odi.13232

Edgar, R. C., Haas, B. J., Clemente, J. C., Quince, C., and Knight, R. (2011). UCHIME improves sensitivity and speed of chimera detection. *Bioinformatics* 27, 2194–2200. doi: 10.1093/bioinformatics/btr381

Eshed, M., Lellouche, J., Matalon, S., Gedanken, A., and Banin, E. (2012). Sonochemical coatings of ZnO and CuO nanoparticles inhibit *Streptococcus mutans* biofilm formation on teeth model. *Langmuir* 28, 12288–12295. doi: 10.1021/la301432a

Espinosa-Cristóbal, L. F., Martínez-Castañón, G. A., Téllez-Déctor, E. J., Niño-Martínez, N., Zavala-Alonso, N. V., and Loyola-Rodríguez, J. P. (2013). Adherence inhibition of *Streptococcus mutans* on dental enamel surface using silver nanoparticles. *Mater. Sci. Eng. C* 33, 2197–2202. doi: 10.1016/j.msec.2013.01.039

Faust, K., and Raes, J. (2012). Microbial interactions: from networks to models. *Nat. Rev. Microbiol.* 10, 538–550. doi: 10.1038/nrmicro2832

Feng, K., Peng, X., Zhang, Z., Gu, S., He, Q., Shen, W., et al. (2022). iNAP: an integrated network analysis pipeline for microbiome studies. *iMeta* 1:e13. doi: 10.1002/imt2.13

Friedman, J., and Alm, E. J. (2012). Inferring correlation networks from genomic survey data. *PLoS Comput. Biol.* 8:e1002687. doi: 10.1371/journal.pcbi.1002687

Gao, L., Xu, T., Huang, G., Jiang, S., Gu, Y., and Chen, F. (2018). Oral microbiomes: more and more importance in oral cavity and whole body. *Protein Cell* 9, 488–500. doi: 10.1007/s13238-018-0548-1

García-Pérez, J., Pérez-Abad, N., Lope, V., Castelló, A., Pollán, M., González-Sánchez, M., et al. (2016). Breast and prostate cancer mortality and industrial pollution. *Environ. Pollut.* 214, 394–399. doi: 10.1016/j.envpol.2016.04.027

Ghnaya, T., Mnassri, M., Ghabriche, R., Wali, M., Poschenrieder, C., Lutts, S., et al. (2015). Nodulation by *Sinorhizobium meliloti* originated from a mining soil alleviates cd toxicity and increases cd-phytoextraction in *Medicago sativa* L. *Front. Plant Sci.* 6:863. doi: 10.3389/fpls.2015.00863

Guimerà, R., and Nunes Amaral, L. A. (2005). Functional cartography of complex metabolic networks. *Nature* 433, 895–900. doi: 10.1038/nature03288

Gupta, N., Yadav, V. K., Gacem, A., Al-Dossari, M., Yadav, K. K., Abd El-Gawaad, N. S., et al. (2022). Deleterious effect of air pollution on human microbial community and bacterial Flora: A short review. *Int. J. Environ. Res. Public Health* 19:15494. doi: 10.3390/ijerph192315494

Hajishengallis, G., and Lamont, R. J. (2021). Polymicrobial communities in periodontal disease: their quasi-organismal nature and dialogue with the host. *Periodontol. 2000* 2000, 210–230. doi: 10.1111/prd.12371

He, Y., Gong, D., Shi, C., Shao, F., Shi, J., and Fei, J. (2017). Dysbiosis of oral buccal mucosa microbiota in patients with oral lichen planus. *Oral Dis.* 23, 674–682. doi: 10.1111/odi.12657

Hijazi, K., Morrison, R. W., Mukhopadhya, I., Martin, B., Gemmell, M., Shaw, S., et al. (2020). Oral bacterial diversity is inversely correlated with mucosal inflammation. *Oral Dis.* 26, 1566–1575. doi: 10.1111/odi.13420

Human Microbiome Project Consortium (2012). Structure, function and diversity of the healthy human microbiome. *Nature* 486, 207–214. doi: 10.1038/nature11234

Irfan, M., Delgado, R. Z. R., and Frias-Lopez, J. (2020). The Oral Microbiome and Cancer. *Front Immunol* 11:591088. doi: 10.3389/fimmu.2020.591088

Jung, W., and Jang, S. (2022). Oral microbiome research on Oral lichen planus: current findings and perspectives. *Biology* 11:723. doi: 10.3390/biology11050723

Kanehisa, M., Furumichi, M., Tanabe, M., Sato, Y., and Morishima, K. (2017). KEGG: new perspectives on genomes, pathways, diseases and drugs. *Nucleic Acids Res.* 45, D353–D361. doi: 10.1093/nar/gkw1092

Karpiński, T. (2019). Role of Oral Microbiota in Cancer Development. *Microorganisms* 7:20. doi: 10.3390/microorganisms7010020

Khan, S. T., Ahamed, M., Alhadlaq, H. A., Musarrat, J., and Al-Khedhairy, A. (2013). Comparative effectiveness of NiCl2, Ni- and NiO-NPs in controlling oral bacterial

growth and biofilm formation on oral surfaces. *Arch. Oral Biol.* 58, 1804–1811. doi: 10.1016/j.archoralbio.2013.09.011

Kumar, A., Kumar, A. M. M. S. C. P., Chaturvedi, A. K., Shabnam, A. A., Subrahmanyam, G., Mondal, R., et al. (2020). Lead toxicity: health hazards, influence on food chain, and sustainable remediation approaches. *Int. J. Environ. Res. Public Health* 17:2179. doi: 10.3390/ijerph17072179

Lamont, R. J., Koo, H., and Hajishengallis, G. (2018). The oral microbiota: dynamic communities and host interactions. *Nat. Rev. Microbiol.* 16, 745–759. doi: 10.1038/s41579-018-0089-x

Langfelder, P., and Horvath, S. (2007). Eigengene networks for studying the relationships between co-expression modules. *BMC Syst. Biol.* 1:54. doi: 10.1186/1752-0509-1-54

Langille, M. G. I., Zaneveld, J., Caporaso, J. G., McDonald, D., Knights, D., Reyes, J. A., et al. (2013). Predictive functional profiling of microbial communities using 16S rRNA marker gene sequences. *Nat. Biotechnol.* 31, 814–821. doi: 10.1038/nbt.2676

Layeghifard, M., Hwang, D. M., and Guttman, D. S. (2017). Disentangling interactions in the microbiome: A network perspective. *Trends Microbiol.* 25, 217–228. doi: 10.1016/j.tim.2016.11.008

Li, Z., Ma, Z., van der Kuijp, T. J., Yuan, Z., and Huang, L. (2014). A review of soil heavy metal pollution from mines in China: pollution and health risk assessment. *Sci. Total Environ.* 468–469, 843–853. doi: 10.1016/j.scitotenv.2013.08.090

Li, X., Meng, D., Li, J., Yin, H., Liu, H., Liu, X., et al. (2017). Response of soil microbial communities and microbial interactions to long-term heavy metal contamination. *Environ. Pollut.* 231, 908–917. doi: 10.1016/j.envpol.2017.08.057

Li, Y., Wang, Y., Gou, X., Su, Y., and And Wang, G. (2006). Risk assessment of heavy metals in soils and vegetables around non-ferrous metals mining and smelting sites, Baiyin, China. *J. Environ. Sci.* 18, 1124–1134. doi: 10.1016/S1001-0742(06)60050-8

Liu, X., Song, Q., Tang, Y., Li, W., Xu, J., Wu, J., et al. (2013). Human health risk assessment of heavy metals in soil–vegetable system: A multi-medium analysis. *Sci. Total Environ.* 463–464, 530–540. doi: 10.1016/j.scitotenv.2013.06.064

Lu, Y., Li, Z., and Peng, X. (2023). Regulatory effects of oral microbe on intestinal microbiota and the illness. *Front. Cell. Infect. Microbiol.* 13:1093967. doi: 10.3389/fcimb.2023.1093967

Lupatini, M., Suleiman, A. K. A., Jacques, R. J. S., Antoniolli, Z. I., de Siqueira Ferreira, A., Kuramae, E. E., et al. (2014). Network topology reveals high connectance levels and few key microbial genera within soils. *Front. Environ. Sci.* 2:10. doi: 10.3389/fenvs.2014.00010

Lurgi, M., Thomas, T., Wemheuer, B., Webster, N. S., and Montoya, J. M. (2019). Modularity and predicted functions of the global sponge-microbiome network. *Nat. Commun.* 10:992. doi: 10.1038/s41467-019-08925-4

Magoč, T., and Salzberg, S. L. (2011). FLASH: fast length adjustment of short reads to improve genome assemblies. *Bioinformatics* 27, 2957–2963. doi: 10.1093/bioinformatics/btr507

Matović, V., Buha, A., Đukić-Ćosić, D., and Bulat, Z. (2015). Insight into the oxidative stress induced by lead and/or cadmium in blood, liver and kidneys. *Food Chem. Toxicol.* 78, 130–140. doi: 10.1016/j.fct.2015.02.011

Nakajima, M., Arimatsu, K., Kato, T., Matsuda, Y., Minagawa, T., Takahashi, N., et al. (2015). Oral Administration of *P. gingivalis* induces Dysbiosis of gut microbiota and impaired barrier function leading to dissemination of Enterobacteria to the liver. *PloS One* 10:e0134234. doi: 10.1371/journal.pone.0134234

Newman, M. E. J. (2006). Modularity and community structure in networks. *Proc. Natl. Acad. Sci.* 103, 8577–8582. doi: 10.1073/pnas.0601602103

Nobbs, A. H., Lamont, R. J., and Jenkinson, H. F. (2009). Streptococcus adherence and colonization. *Microbiol. Mol. Biol. Rev.* 73, 407–450. doi: 10.1128/MMBR.00014-09

Olesen, J. M., Bascompte, J., Dupont, Y. L., and Jordano, P. (2007). The modularity of pollination networks. *Proc. Natl. Acad. Sci.* 104, 19891–19896. doi: 10.1073/pnas.0706375104

Qi, G., Ma, G., Chen, S., Lin, C., and Zhao, X. (2019). Microbial network and soil properties are changed in bacterial wilt-susceptible soil. *Appl. Environ. Microbiol.* 85:e00162. doi: 10.1128/AEM.00162-19

Qin, J., Li, Y., Cai, Z., Li, S., Zhu, J., Zhang, F., et al. (2012). A metagenome-wide association study of gut microbiota in type 2 diabetes. *Nature* 490, 55–60. doi: 10.1038/nature11450

Sedghi, L., DiMassa, V., Harrington, A., Lynch, S. V., and Kapila, Y. L. (2021). The oral microbiome: role of key organisms and complex networks in oral health and disease. *Periodontol. 2000* 2000, 107–131. doi: 10.1111/prd.12393

Shao, M., and Zhu, Y. (2020). Long-term metal exposure changes gut microbiota of residents surrounding a mining and smelting area. *Sci. Rep.* 10:4453. doi: 10.1038/s41598-020-61143-7

Shi, J., Du, P., Luo, H., Wu, H., Zhang, Y., Chen, J., et al. (2022). Soil contamination with cadmium and potential risk around various mines in China during 2000–2020. *J. Environ. Manage.* 310:114509. doi: 10.1016/j.jenvman.2022.114509

Steiger, E. L., Muelli, J. R., Braissant, O., Waltimo, T., and Astasov-Frauenhoffer, M. (2020). Effect of divalent ions on cariogenic biofilm formation. *BMC Microbiol.* 20:287. doi: 10.1186/s12866-020-01973-7

Sudhakara, P., Gupta, A., Bhardwaj, A., and Wilson, A. (2018). Oral Dysbiotic communities and their implications in systemic diseases. *Dent. J.* 6:10. doi: 10.3390/dj6020010

Thomas, A. M., Gleber-Netto, F. O., Fernandes, G. R., Amorim, M., Barbosa, L. F., Francisco, A. L. N., et al. (2014). Alcohol and tobacco consumption affects bacterial richness in oral cavity mucosa biofilms. *BMC Microbiol.* 14:250. doi: 10.1186/s12866-014-0250-2

Wade, W. G. (2013). The oral microbiome in health and disease. *Pharmacol. Res.* 69, 137–143. doi: 10.1016/j.phrs.2012.11.006

Wang, Q., Garrity, G. M., Tiedje, J. M., and Cole, J. R. (2007). Naïve Bayesian classifier for rapid assignment of rRNA sequences into the new bacterial taxonomy. *Appl. Environ. Microbiol.* 73, 5261–5267. doi: 10.1128/AEM.00062-07

Wang, T., Ishikawa, T., Sasaki, M., and Chiba, T. (2022). Oral and gut microbial Dysbiosis and non-alcoholic fatty liver disease: the central role of *Porphyromonas gingivalis*. *Front. Med.* 9:822190. doi: 10.3389/fmed.2022.822190

Wang, S., Song, F., Gu, H., Wei, X., Zhang, K., Zhou, Y., et al. (2022). Comparative evaluation of the salivary and buccal mucosal microbiota by 16S rRNA sequencing for forensic investigations. *Front. Microbiol.* 13:777882. doi: 10.3389/fmicb.2022.777882

Wang, X., Zhao, Z., Tang, N., Zhao, Y., Xu, J., Li, L., et al. (2020). Microbial community analysis of saliva and biopsies in patients with Oral lichen planus. *Front. Microbiol.* 11:629. doi: 10.3389/fmicb.2020.00629

Xia, S., Song, Z., Jeyakumar, P., Shaheen, S. M., Rinklebe, J., Ok, Y. S., et al. (2019). A critical review on bioremediation technologies for Cr(VI)-contaminated soils and wastewater. *Crit. Rev. Environ. Sci. Technol.* 49, 1027–1078. doi: 10.1080/10643389.2018.1564526

Xiao, N., Zhou, A., Kempher, M. L., Zhou, B. Y., Shi, Z. J., Yuan, M., et al. (2022). Disentangling direct from indirect relationships in association networks. *Proc. Natl. Acad. Sci.* 119:e2109995119. doi: 10.1073/pnas.2109995119

Youravong, N., Carlen, A., Teanpaisan, R., and Dahlén, G. (2011). Metal-ion susceptibility of oral bacterial species. *Lett. Appl. Microbiol.* 53, 324–328. doi: 10.1111/j.1472-765X.2011.03110.x

Yue, B., Li, W.-J., Chang, G.-H., and Gao, T. (2020). Distribution characteristics of some heavy metal elements in the polluted soil in Baiyin Dongdagou. *IOP Conf Ser Earth Environ Sci* 568:012041. doi: 10.1088/1755-1315/568/1/012041

Zhang, W., Guo, R., Yang, Y., Ding, J., and Zhang, Y. (2016). Long-term effect of heavy-metal pollution on diversity of gastrointestinal microbial community of *Bufo raddei*. *Toxicol. Lett.* 258, 192–197. doi: 10.1016/j.toxlet.2016.07.003

Zhang, L., Liu, Y., Zheng, H. J., and Zhang, C. P. (2020). The Oral Microbiota May Have Influence on Oral Cancer. *Front Cell Infect Microbiol* 9:00479. doi: 10.3389/fcimb.2019.00476

Zhang, W., Qi, T., Yao, L., Wang, W., Yu, F., Yan, Y., et al. (2023). Influence of environmental factors on salivary microbiota and their metabolic pathway: next-generation sequencing approach. *Microb. Ecol.* 85, 317–329. doi: 10.1007/s00248-021-01951-0

Zhang, Y., Wang, X., Li, H., Ni, C., Du, Z., and Yan, F. (2018). Human oral microbiota and its modulation for oral health. *Biomed. Pharmacother.* 99, 883–893. doi: 10.1016/j.biopha.2018.01.146

Zhang, Q., Wang, S., Nan, Z., Li, Y., and Zang, F. (2018). Accumulation, fractionation, and risk assessment of mercury and arsenic in the soil-wheat system from the wastewater-irrigated soil in Baiyin, Northwest China. *Environ. Sci. Pollut. Res.* 25, 14856–14867. doi: 10.1007/s11356-018-1641-y

Zhang, S., Zhou, Z., Li, Y., and Meng, F. (2018). Deciphering the core fouling-causing microbiota in a membrane bioreactor: low abundance but important roles. *Chemosphere* 195, 108–118. doi: 10.1016/j.chemosphere.2017.12.067

Zhao, X., He, B., Wu, H., Zheng, G., Ma, X., Liang, J., et al. (2020). A comprehensive investigation of hazardous elements contamination in mining and smelting-impacted soils and sediments. *Ecotoxicol. Environ. Saf.* 192:110320. doi: 10.1016/j.ecoenv.2020.110320

Zhou, J., Deng, Y., Luo, F., He, Z., and Yang, Y. (2011). Phylogenetic molecular ecological network of soil microbial communities in response to elevated CO2. *MBio* 2:e00122. doi: 10.1128/mBio.00122-11

Zhu, L., Zhao, Y., Zhang, W., Zhou, H., Chen, X., Li, Y., et al. (2019). Roles of bacterial community in the transformation of organic nitrogen toward enhanced bioavailability during composting with different wastes. *Bioresour. Technol.* 285:121326. doi: 10.1016/j.biortech.2019.121326

frontiers | Frontiers in Microbiology

TYPE Original Research
PUBLISHED 08 December 2023
DOI 10.3389/fmicb.2023.1294402

Check for updates

OPEN ACCESS

EDITED BY
Hao Li,
Jining Medical University, China

REVIEWED BY
Alfonso Méndez-Bravo,
National Autonomous University of Mexico, Mexico
Da-Le Guo,
Chengdu University of Traditional Chinese Medicine, China

*CORRESPONDENCE
Jian Xie
✉ Xiejian@zmu.edu.cn
Yuqi He
✉ HYQJEFF@foxmail.com

RECEIVED 14 September 2023
ACCEPTED 13 November 2023
PUBLISHED 08 December 2023

CITATION
Zhao Y, Ji X, Liu X, Qin L, Tan D, Wu D, Bai C, Yang J, Xie J and He Y (2023) Age-dependent dendrobine biosynthesis in *Dendrobium nobile*: insights into endophytic fungal interactions. *Front. Microbiol.* 14:1294402. doi: 10.3389/fmicb.2023.1294402

COPYRIGHT
© 2023 Zhao, Ji, Liu, Qin, Tan, Wu, Bai, Yang, Xie and He. This is an open-access article distributed under the terms of the Creative Commons Attribution License (CC BY). The use, distribution or reproduction in other forums is permitted, provided the original author(s) and the copyright owner(s) are credited and that the original publication in this journal is cited, in accordance with accepted academic practice. No use, distribution or reproduction is permitted which does not comply with these terms.

Age-dependent dendrobine biosynthesis in *Dendrobium nobile*: insights into endophytic fungal interactions

Yongxia Zhao[1,2,3], Xiaolong Ji[1,2,3], Xiaoqi Liu[1,2,3], Lin Qin[1,2,3], Daopeng Tan[1,2,3], Di Wu[1,2,3], Chaojun Bai[4], Jiyong Yang[5], Jian Xie[1,2,3]* and Yuqi He[1,2,3]*

[1]Guizhou Engineering Research Center of Industrial Key-Technology for Dendrobium nobile, Engineering Research Center of Pharmaceutical Orchid Plant Breeding, High Efficiency Application in Guizhou Province, Zunyi Medical University, Zunyi, China, [2]Key Laboratory of Basic Pharmacology of Ministry of Education, Joint International Research Laboratory of Ethnomedicine of Ministry of Education, Zunyi Medical University, Zunyi, China, [3]2011 Cooperative Inovational Center for Guizhou Traditional Chinese Medicine and Ethnic Medicine, Zunyi Medical University, Zunyi, China, [4]Guangxi Shenli Pharmaceutical Co., Ltd., Yulin, China, [5]Chishui Xintian Chinese Medicine Industry Development Co., Ltd., Zunyi, China

Introduction: *Dendrobium nobile (D. nobile)*, a valued Chinese herb known for its diverse pharmacological effects, owes much of its potency to the bioactive compound dendrobine. However, dendrobine content varies significantly with plant age, and the mechanisms governing this variation remain unclear. This study delves into the potential role of endophytic fungi in shaping host-microbe interactions and influencing plant metabolism.

Methods: Using RNA-seq, we examined the transcriptomes of 1-year-old, 2-year-old, and 3-year-old *D. nobile* samples and through a comprehensive analysis of endophytic fungal communities and host gene expression in *D. nobile* stems of varying ages, we aim to identify associations between specific fungal taxa and host genes.

Results: The results revealing 192 differentially expressed host genes. These genes exhibited a gradual decrease in expression levels as the plants aged, mirroring dendrobine content changes. They were enriched in 32 biological pathways, including phagosome, fatty acid degradation, alpha-linolenic acid metabolism, and plant hormone signal transduction. Furthermore, a significant shift in the composition of the fungal community within *D. nobile* stems was observed along the age gradient. *Olipidium*, *Hannaella*, and *Plectospherella* dominated in 1-year-old plants, while *Strelitziana* and *Trichomerium* prevailed in 2-year-old plants. Conversely, 3-year-old plants exhibited additional enrichment of endophytic fungi, including the genus *Rhizopus*. Two gene expression modules (mediumpurple3 and darkorange) correlated significantly with dominant endophytic fungi abundance and dendrobine accumulation. Key genes involved in dendrobine synthesis were found associated with plant hormone synthesis.

Discussion: This study suggests that the interplay between different endophytic fungi and the hormone signaling system in *D. nobile* likely regulates dendrobine biosynthesis, with specific endophytes potentially triggering hormone signaling cascades that ultimately influence dendrobine synthesis.

KEYWORDS

***Dendrobium nobile*, endophytic fungi, transcriptomic analysis, dendrobine, age-dependent accumulation**

1 Introduction

Dendrobium nobile (*D. nobile*) is a precious medicinal herb found in the Danxia landform of Chishui City, Guizhou Province, China. It possesses a rich repertoire of bioactive compounds with notable antioxidant, anti-tumor, and immunomodulatory properties (Teixeira and Ng, 2017). *D. nobile* is considered a rare and valuable resource in Chinese herbal medicine, primarily obtained through wild-simulated cultivation. In its natural habitat, *D. nobile* thrives in clusters on Danxia rocks. Each cluster of *D. nobile* plants produces new stems and leaves every year, while the stems from previous years continue to grow. As a result, a cluster of Dendrobium plants may contain stems of 1-year-old, 2-year-old, 3-year-old and older ages. Interestingly, only the 1-year-old stems have leaves, while the older stems are leafless, and most of the 3-year-old stems produce new shoots at the nodes. Therefore, the age of the Dendrobium stems can be distinguished by these features. The chemical composition and content of Chinese herbs vary with different ages, and *D. nobile* is no exception (Lu et al., 2022).

However, the morphology and chemistry of plants are determined by a combination of gene expression and environmental factors. Environmental factors include not only light, humidity, temperature, etc., but also the microbial community within the plant, which is called endophyte and plays an important role in the plant's successional trajectory (Clay and Holah, 1999; Afkhami and Strauss, 2016), the balance between insects and plants, plant reproduction, and the accumulation of plant metabolites (Harrison et al., 2021). Interactions between symbiotic or parasitic microorganisms and their host plants are essential for maintaining plant homeostasis (Ma et al., 2021). Research in this area has entered a phase of rapid development, but our understanding of its microbe-hosts is still limited.

The main bioactive constituents of *D. nobile* are alkaloids, with dendrobine being a prominent compound regulated by the Pharmacopeia. Transcriptome analyzes have indicated that dendrobine is derived from the terpenoid-forming and indole pathways of the mevalonate pathway (MVA), the methylerythritol phosphate pathway (MEP), or the shikimate pathway (Wang et al., 2020). However, the details of these biosynthetic pathways to synthesize alkaloids are not well studied. We found that the content of dendrobine was closely related to the age of *D. nobile* and reached a maximum in the youngest 1-year-old plants. Moreover, we observed that the community and abundance of endophytes in 1-year-old *D. nobile* were significantly different from those in older plants. It has also been reported that some endophytic fungi can positively promote the accumulation of fatty acid metabolites in *D. nobile* by infestation and colonization (Zhao et al., 2023). Therefore, we hypothesize that endophyte colonization in 1-year-old *D. nobile* is closely related to the high content of dendrobine alkaloids. By performing transcriptome analysis on *D. nobile* samples of different ages, we identified a number of changes, including changes in some genes associated with the dendrobine synthesis pathway as well as changes in genes in other related pathways.

To validate this hypothesis, we conducted an extensive analysis of the endophytic fungal communities inhabiting *D. nobile* plants of varying ages and investigated their correlation with dendrobine content. Employing high-throughput sequencing technology, we identified and quantified the endophytic fungi residing within the stems of *D. nobile* plants. Subsequently, we performed a comprehensive analysis to determine the relationship between the relative abundance of specific fungal taxa and the levels of dendrobine present. Our findings not only shed new light on the intricate involvement of endophytic fungi in the regulation of dendrobine synthesis and accumulation in *D. nobile* but also hold significant implications for the cultivation and utilization of this invaluable medicinal plant.

2 Materials and methods

2.1 Sample collection

D. nobile stems of three age groups (1-year-old, 2-year-old and 3-year-old) in six biological replicates were collected from wild-simulated cultivation on Danxia rocks in ChiYan base in Chishui city, Guizhou (N 28°30′2″, E 105°55′48″) by using systematic sampling methods (Figure 1A). After the roots and leaves had been removed, the stems were divided into two parts: one part, containing 200 mg of each sample, was disinfected in the following way. First, the samples were immersed in 20 mL of 75% alcohol for 45 s. Second, after removing the alcohol, the samples were immersed in 20 mL of 0.1% mercuric chloride for 5 min. Finally, the samples were rinsed with sterile water three times to remove the remaining mercuric chloride. All of the stems were then sent to Novogene for the sequencing of the internal transcribed spacer (ITS) with −80°C stored process. The other part of fresh *D. nobile* stems was flash-frozen in liquid nitrogen and transported on dry ice to Novogene for RNA extraction and subsequent experiments.

2.2 DNA extraction and sequencing of endophytic fungi

To characterize the endophytic fungal community in *D. nobile* stems of different ages, we employed the CTAB/SDS method for total genomic DNA extraction from each sample. The ITS genes were then amplified in specific regions using designated primers (Forward: GGAAGTAAAAGTCGTAACAAGG; Reverse: GCTGCGTTCTTCA TCGATGC) along with respective barcodes. Subsequently, we conducted library construction and sequencing on an Illumina NovaSeq platform, generating 250 bp paired-end reads following amplification, purification, and library construction as briefly outlined below: Amplification protocol: 98°C (1 min) → (98°C (10 s) → 50°C (30 s) → 72°C (30 s) (30 cycles)) → 72°C (5 min). The PCR products were homogenously combined and then subjected to purification using the Qiagen Gel Extraction Kit (Qiagen, Germany). For library preparation, we employed the NEBNext® Ultra™ II DNA Library Prep Kit (Cat No. E7645). Subsequently, the library's quality was assessed utilizing the Qubit@ 2.0 Fluorometer (Thermo Scientific) and the Agilent Bioanalyzer 2,100 system.

2.3 Transcriptome sequencing

To profile the transcriptomes of 18 stems from *D. nobile* of varying ages, we initiated the process by extracting total RNA from the plant samples. Subsequently, mRNA was isolated from the total RNA pool using poly-T oligo-attached magnetic beads. Prior to this, we employed the RNA Nano 6,000 Assay Kit on the Bioanalyzer 2,100 system to evaluate RNA integrity. Of paramount importance was the

10.3389/fmicb.2023.1294402

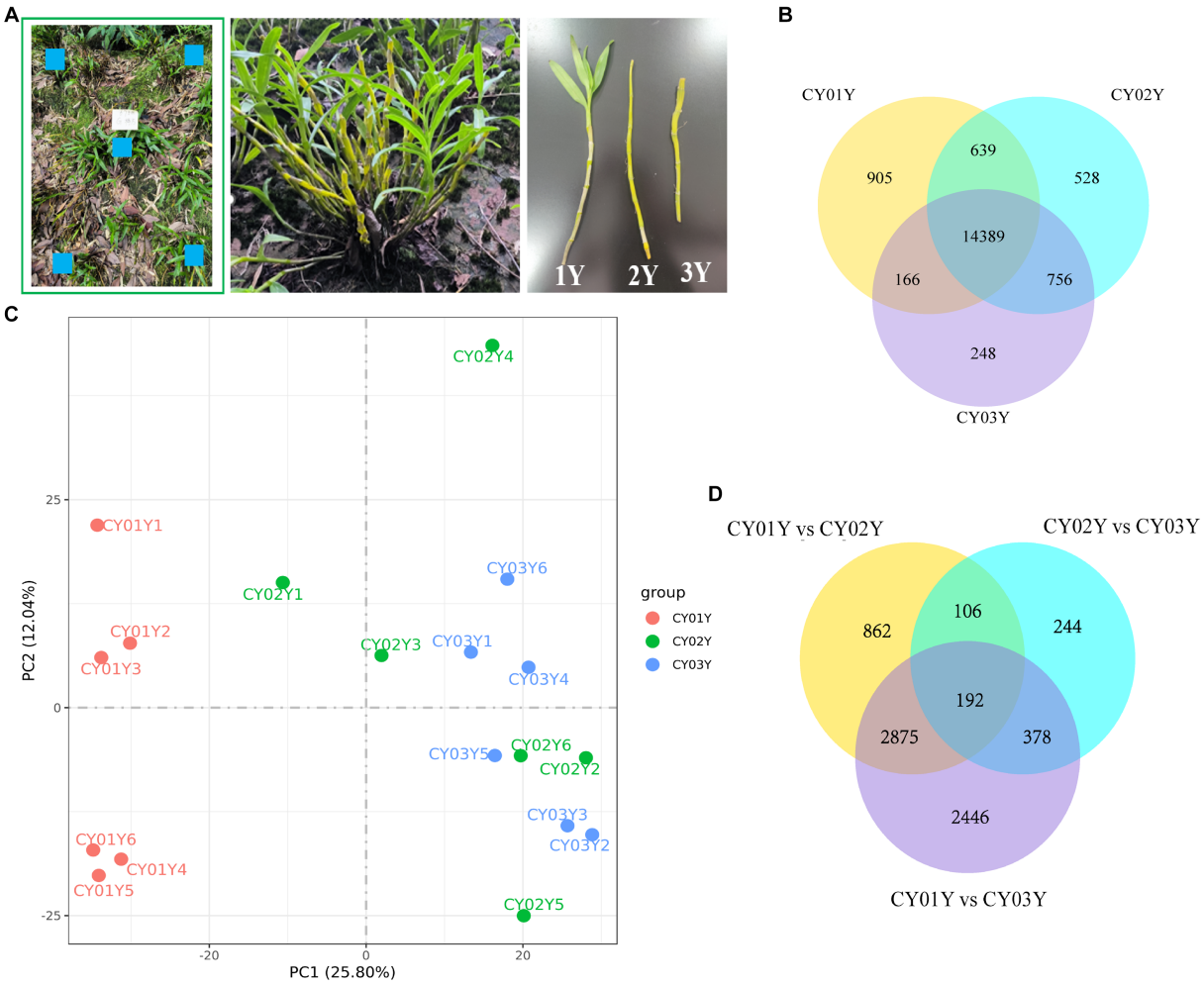

FIGURE 1
Samples collection and transcriptomic landscape of *D. nobile* stems along the years axis. **(A)** Schematic diagram of sampling, using a five-point systematic sampling method, with samples of one-, two-, and three-year old plants taken from the same cluster. **(B)** Co-expression Venn diagram of *D. nobile* with different ages, showing that there are 14,389 co-expressed genes in the stems of *D. nobile* of different ages. At the same time, there are 905 genes uniquely expressed in 1-year-old plants, 528 genes in 2-year-old plants and 248 genes in 3-year-old plants. **(C)** Principal component analysis (PCA) of the samples, showing that the samples of the CY01Y group are clustered together, while the samples of the CY02Y and CY03Y groups are merged together. Thus, the differences between the CY02Y and CY03Y groups are smaller, while the differences with the CY01Y group are larger. **(D)** Venn diagram for differential expression, showing that differential genes were more abundant between CY01Y and CY02Y as well as CY03Y, whereas the difference between CY02Y and CY03Y was the smallest and the number of differential genes was the least.

initiation of first strand cDNA synthesis, where a combination of random hexamer primers and M-MuLV Reverse Transcriptase (RNase H-) played a crucial role. Following this, DNA Polymerase I and RNase H were enlisted to synthesize the second strand of cDNA. The pivotal step in this process was library construction. Here, the AMPure XP system (Beckman Coulter, Beverly, United States) was utilized to meticulously purify and select cDNA fragments falling within the 370 ~ 420 bp range. Finally, the library preparations were subjected to sequencing on an Illumina Novaseq platform.

2.4 Data analysis of ASVs of endophytic fungi

The 18 samples were sequenced on the Illumina NovaSeq platform. We processed the raw reads by removing the barcodes and primer sequences according to barcode sequences. Paired-end reads were merged using FLASH.[1] To obtain high-quality Clean Tags, we used the fastp (Version 0.20.0) software to filter out low-quality reads. The Vsearch (Version 2.15.0) was used to detect the chimeric sequences, and then the chimeric sequences were removed to obtain the Effective Tags. ASVs Denoise and species annotation was realized in the QIIME2 software (Version QIIME2-202006), and then ASVs with abundance less than 5 were filtered out. The ASVs absolute abundance was normalized using a standard of sequence number corresponding to the sample with the least sequences. Subsequent analysis of alpha diversity and beta diversity were all performed based on the normalized data and calculated in QIIME2. Principal Coordinate Analysis (PCoA) was performed with QIIME2 package, ade4 package and ggplot2 package in R software (Version 3.5.3). To

1 Version 1.2.11, http://ccb.jhu.edu/software/FLASH/

identify the significantly different taxa at each taxonomic level (Phylum, Class, Order, Family, Genus, Species), T-test analysis was performed using R software (Version 3.5.3).

2.5 Data analysis of RNA-Seq

Clean data (clean reads) in fastq format was first processed by fastp software to remove adapter, poly-N and low-quality reads. The high-quality clean data was then analyzed for Q20, Q30 and GC content. Hisat2 v2.0.5 and StringTie (v1.3.3b) were adopted to map reads to the reference genome and predict novel transcripts. The number of reads mapped to each gene was counted using Feature Counts v1.5.0-p3. Finally, the FPKM (fragments per kilobase of transcript per million mapped reads) of each gene was calculated. FPKM provides a normalized measure of gene expression, factoring in sequencing depth and gene length, and is widely adopted for estimating gene expression levels. Differential expression analysis was performed between two groups, each consisting of two biological replicates per condition, using the DESeq2 R package (1.20.0). DESeq2 employs statistical routines based on the negative binomial distribution to determine differential expression in digital gene expression data. The resulting *p*-values were adjusted using the Benjamini and Hochberg's approach to control the false discovery rate. Genes with an adjusted *p*-value of <=0.05, as determined by DESeq2, were identified as differentially expressed. Gene Ontology (GO) enrichment analysis of differentially expressed genes was implemented by the clusterProfiler R package, then to test the statistical enrichment of differentially expressed genes in KEGG pathways.[2] Eventually, WGCNA (Weighted correlation network analysis) was performed through the R package WGCNA.

3 Results

3.1 Different transcriptomic landscapes in developmental gradients along the year axis

In this study, we examined the *Dendrobium nobile* stems (Figure 1A) from three distinct age groups: 1-year-old seedlings with leaves (CY01Y), 2-year-old bare stems without leaves (CY02Y), and 3-year-old stems that have sprouted (CY03Y). We conducted both a transcriptomics experiment and an endogenous fungi analysis. Gene expression in the stems of all 18 samples (with six biological replicates per age group) was assessed, and it is noteworthy that all samples exhibited comparable read counts (averaging 42,895,882, 41,514,350, and 44,681,382 clean reads, respectively). Additionally, all samples maintained an average quality score exceeding 30 phred (Supplementary Table S1).

The co-expression Venn diagram (Figure 1B) demonstrated that 905 genes were uniquely expressed in 1-year-old plants, 528 genes in 2-year-old plants, and 248 genes in 3-year-old plants. Moreover, a substantial overlap of 14,389 genes was observed across all three age groups. Principal component analysis (PCA) and differential gene analysis (Figures 1C,D) further illustrated the high degree of transcriptomic similarity between 2- and 3-year-old plants when compared to the 1-year-old plants.

To examine gene expression disparities, read counts from the 18 samples underwent DESeq2 analysis. Our analysis identified 4,035 differentially expressed genes between 1-year-old and 2-year-old plants, 5,891 differentially expressed genes between 1-year-old and 3-year-old plants, and 920 differentially expressed genes between 2-year-old and 3-year-old plants at $p < 0.05$ (Figure 2). Among them gene, 2,132 (52.8%) were up-regulated and 1,903 (47.2%) were down-regulated in annual and biennial *D. nobile* (Figure 2A). Similarly, the expression of 3,624 (61.5%) genes was up-regulated and 2,267 (38.5%) genes were down-regulated in one-year plants as compared to three-year plants (Figure 2B). However, fewer differential genes were identified between 2-year and 3-year plants, with only 748 (81.3%) genes up-regulated and 172 (18.7%) genes down-regulated in expression (Figure 2C). A Venn diagram of the commonly expressed differential genes between the different years of *D. nobile* stems revealed 192 common differential genes in the three sets of samples (Figure 1D).

For a deeper understanding of the functional distinctions among differentially expressed genes, we conducted Gene Ontology (GO) term enrichment analysis. Twenty-five genes were annotated to 154 biological processes, encompassing external encapsulating structure organization, cell wall organization, glucan metabolic processes, carboxylic acid metabolic processes, and others. Three genes were annotated to 16 cellular components including cell wall, external encapsulating structure, apoplast extracellular region, etc. Notably, differential genes were predominantly localized in the cell wall and organelles within the cytoplasm. Furthermore, 44 genes were annotated to 93 molecular functions, such as GTPase activity, heme binding, tetrapyrrole binding, transferase activity, enzyme inhibitor activity, glucosyltransferase activity, and others (Supplementary Table S2). Among the top 30 annotated GO terms, molecular function accounted for 53 percent while biological processes accounted for 47 percent (Figure 2D). Analyzing the 192 screened genes (Supplementary Table S3) through heatmap clustering, we observed that 166 genes exhibited a gradual decrease in expression year by year, while only 10 genes displayed a gradual increase in expression with age. The highest expression was observed in the 2-year-old plants, consistent with another 16 genes (Supplementary Figure S1). Subsequently, KEGG enrichment analysis of the three groups of differential genes revealed that group A differential genes were predominantly enriched in 32 biological pathways, including Phagosome, Phenylpropanoid biosynthesis, Phenylalanine metabolism, Fatty acid degradation, alpha-Linolenic acid metabolism, Plant hormone signal transduction, Sesquiterpenoid and triterpenoid biosynthesis, Biosynthesis of unsaturated fatty acids, and others (Figure 2E).

3.2 Endophytic fungal community composition in the stems shifts along the age axis

In this study, we thoroughly examined the distribution of endophytic fungal taxa in *D. nobile* stems across different age groups through internal transcribed spacer sequencing, complemented by a

2 http://www.genome.jp/kegg/

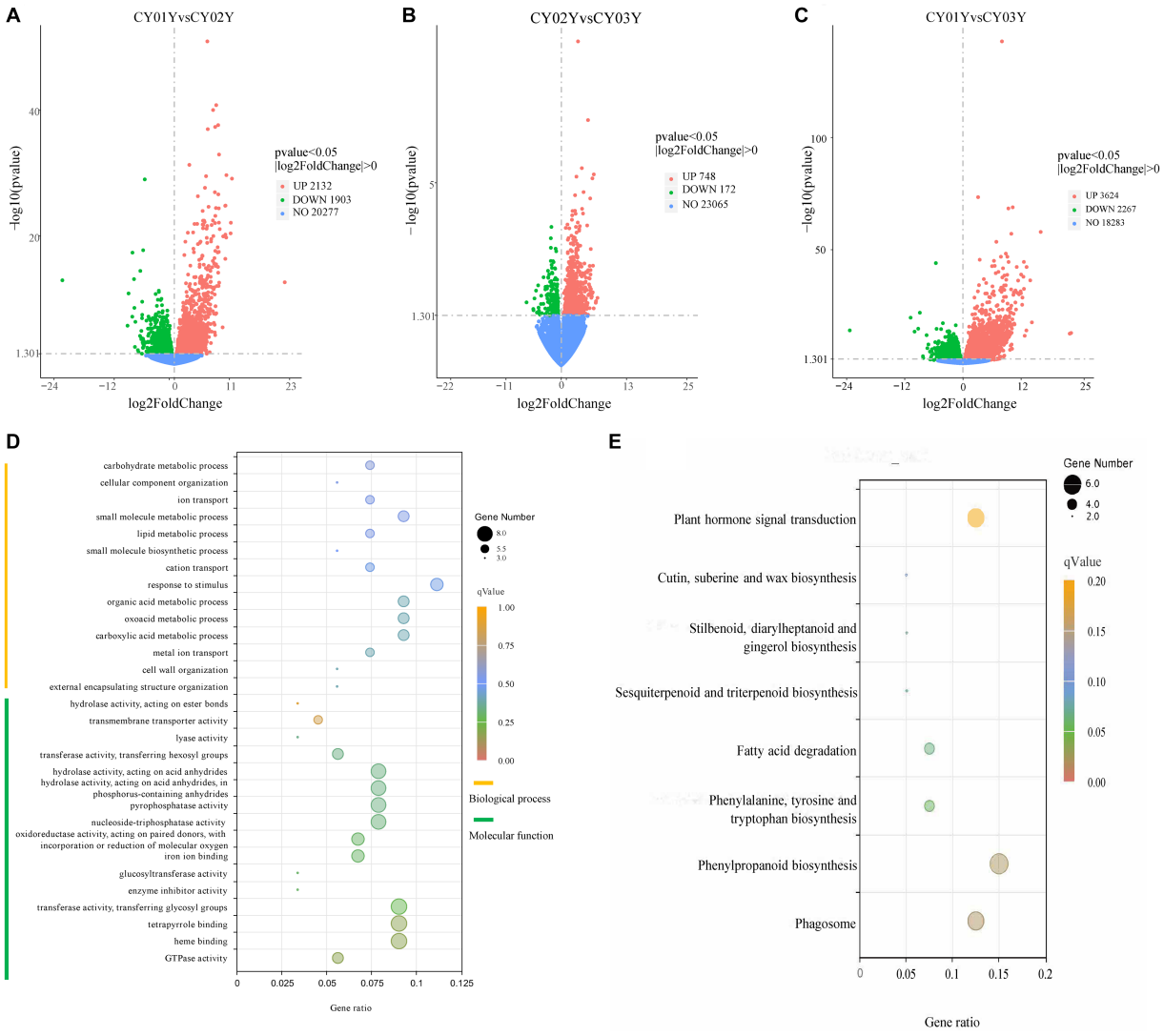

FIGURE 2
Screening of differentially expressed genes and Gene Ontology (GO) term enrichment analysis and KEGG enrichment. **(A)** The volcano plot for CY01Y and CY02Y comparisons. **(B)** The volcano plot for CY02Y and CY03Y comparisons. **(C)** The volcano plot for CY01Y and CY03Y comparisons. The horizontal coordinates in the plot indicate the fold change of gene expression in the two groups of treatment (log2FoldChange), and the vertical coordinates indicate the significance level of the difference in gene expression in the two groups of treatment (−log10pvalue). Up-regulated genes are indicated by red dots, and down-regulated genes are indicated by green dots. **(D)** The top 30 GO terms of 192 common differential genes. **(E)** KEGG enrichment of the 166 genes decreased in expression year by year.

detailed analysis of the fungal microbiomes (Methods). The systematic sampling approach (Figure 1A) was validated by rarefaction analysis, affirming the sequencing depth was sufficient to capture the majority of endophytic fungal members in all 18 stem samples (Supplementary Figure S2). A total of 1.72 million Effective Tags underwent analysis using QIIME2, leading to the identification of 1,817 Amplicon Sequence Variants (ASVs) at a 100% identity level. The overall analysis demonstrated discernible distinctions among the three age groups (Figures 3A, 4A2).

Principal Co-ordinates Analysis (PCoA) (Figure 3B) and Nonmetric Multidimensional Scaling (NMDS) (Figure 3C) of the 1,817 most abundant ASVs based on unweighted UniFrac and nonphylogenetic Bray-Curtis metrics (Adonis p value =0.001) unveiled a notable shift in fungal community composition within *D. nobile* stems across the age gradient. Both PCoA and NMDS plots highlighted distinct clustering based on age groups (CY01Y, CY02Y, or CY03Y). Alpha diversity metrics, including Chao1, observed OTUs, Shannon, and Simpson indices, indicated a balanced overall biodiversity of endophytic fungi across all samples (Figure 5).

We further investigated taxonomic differences in abundance among the endophytic microbiomes of CY01Y, CY02Y, and CY03Y plants using phyloseq. Eight phyla and 20 classes, orders, and genera were selected for analysis at different taxonomic ranks. Among them, 20 highly abundant ASVs exhibited significant differences between CY01Y, CY02Y, and CY03Y (Figure 4). Ternary plots and abundance accumulation diagrams of endophytic fungi in *D. nobile* stems across different ages were generated to visualize dominant taxa variations (Figure 4). Ascomycota exhibited the highest abundance in all samples, with significant enrichment in 2-year-old and 3-year-old *D. nobile* stems. Basidiomycota displayed a similar trend.

10.3389/fmicb.2023.1294402

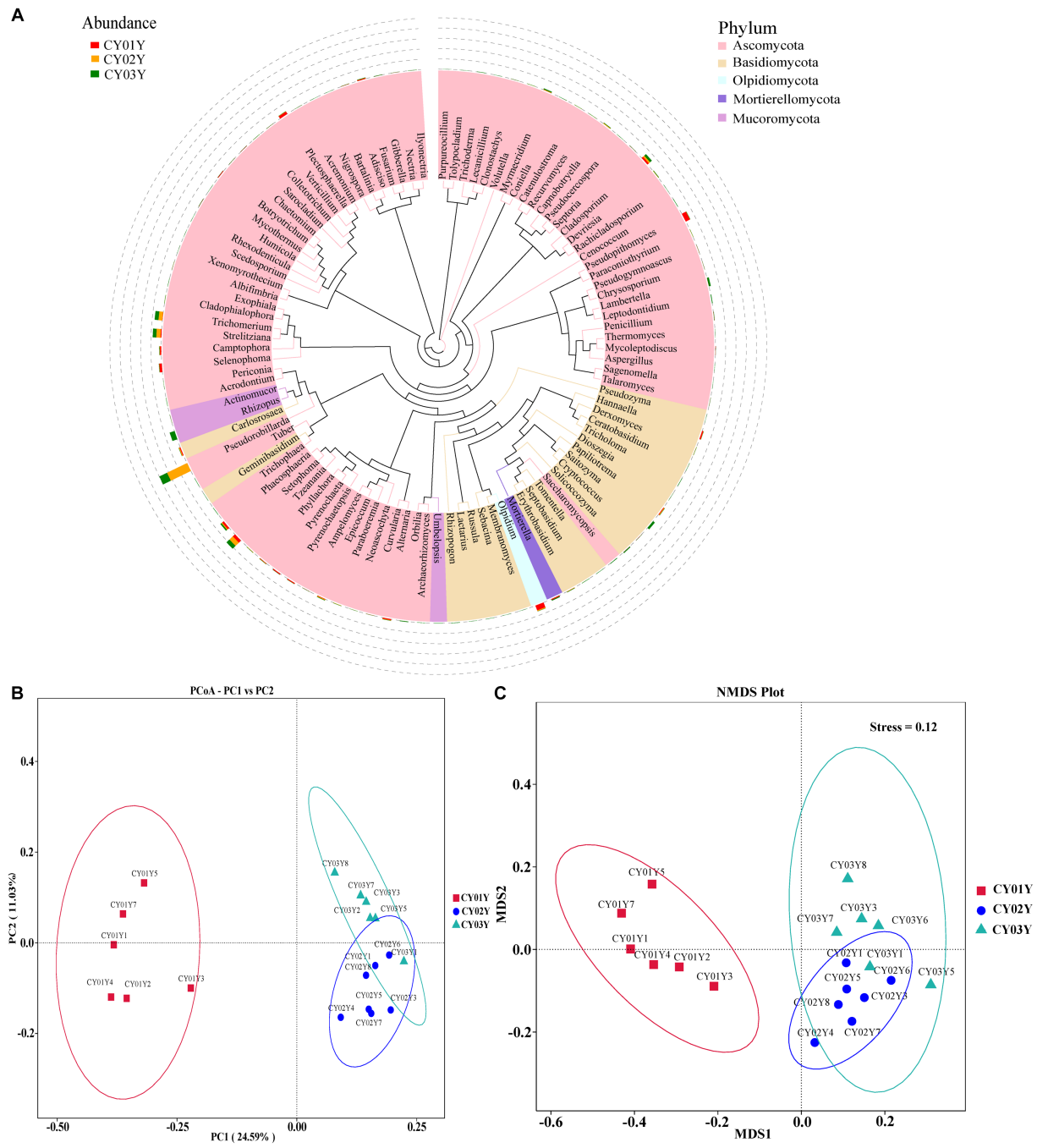

FIGURE 3
Endophytic fungal community composition outline in the stems of *D. nobile*. **(A)** Top 100 genera in species evolutionary trees at genus level. The colors of the branches and sectors indicate different phyla, and the stacked bar graphs on the exterior of the sector ring indicate information on the distribution of abundance of the genera in different samples. **(B)** Principal Co-ordinates Analysis (PCoA) of the 1,817 most abundant ASVs with unweighted UniFrac. **(C)** Nonmetric Multidimensional Scaling (NMDS) of the 1,817 most abundant ASVs with unweighted UniFrac. The samples were clustered based on different ages (CY01Y, CY02Y or CY03Y).

Mucoromycota were particularly abundant in 3-year-old samples, whereas Mortierellomycota were nearly absent in 2-year-old samples (Figures 4A1,A2).

At the genus level, *Pseudorobillarda* showed significant enrichment in 2-year-old and 3-year-old *D. nobile* stems, with markedly higher abundance in the 2-year-old plants compared to the 3-year-old ones. Conversely, *Pseudopithomyces* was enriched exclusively in 1-year-old samples and absent in 2- and 3-year-old samples. Several fungi were specifically enriched in 1-year-old samples, including *Pyrenochaeta*, *Plectosphaerella*, *Selenophoma*, *Olpidium*, and *Hannaella*, while no fungi were specifically enriched in 2-year-old stems. Three genera, *Rhizopus*, *Lambertella*, and *Saccharomycopsis*, exhibited higher abundance in 3-year-old samples compared to the other groups (Figures 4E1,E2). The T-test

10.3389/fmicb.2023.1294402

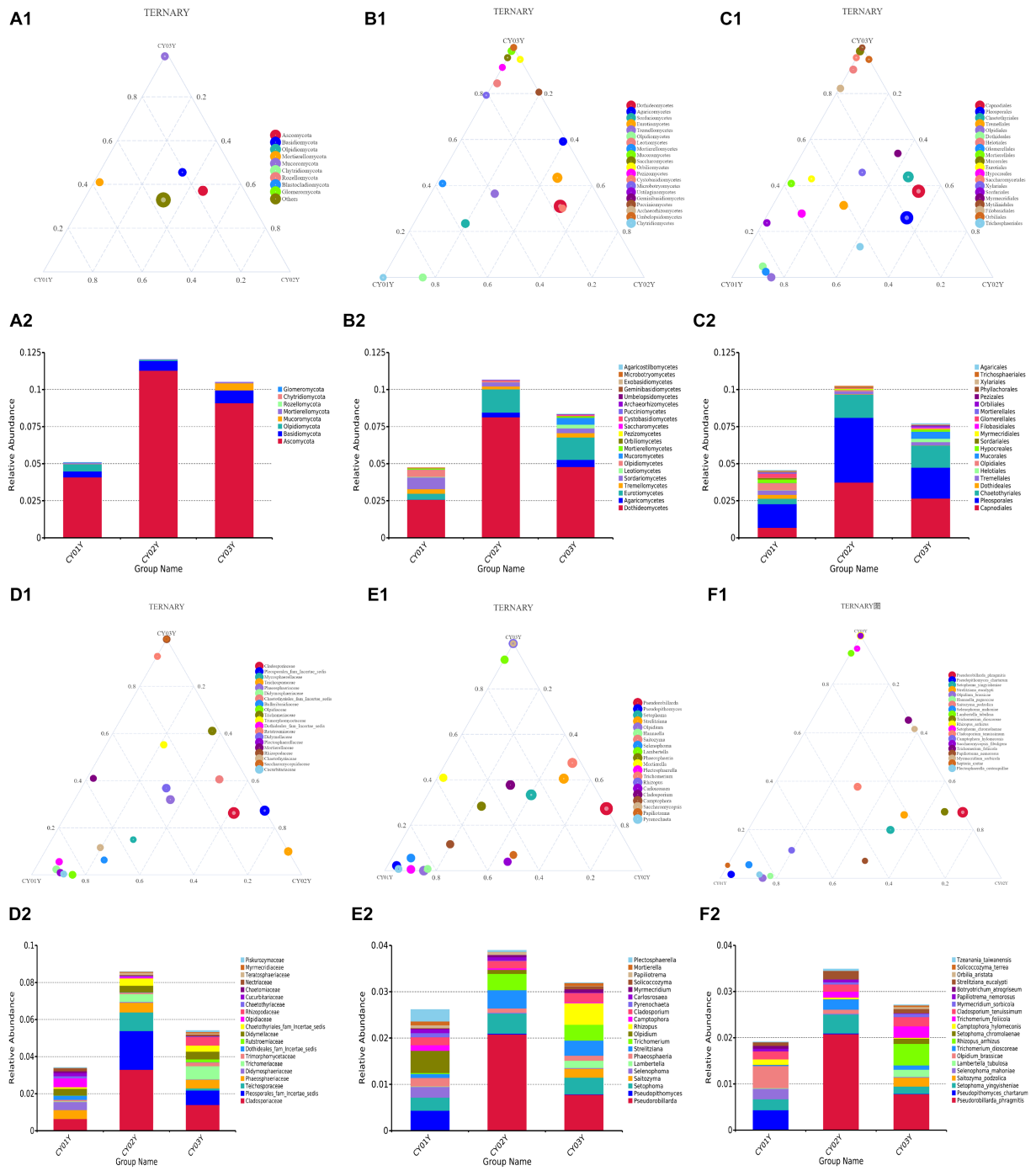

FIGURE 4
The ternaryplots and relative abundance accumulation diagram of endophytic fungi in *D. nobile* at different levels of categorization. **(A1)** The ternaryplot at the phylum level. **(A2)** The relative abundance accumulation diagram at the phylum level. **(B1)** The ternaryplot at the class level with top 20 classes. **(B2)** The relative abundance accumulation diagram at the class level. **(C1)** The ternaryplot at the order level with top 20 orders. **(C2)** The relative abundance accumulation diagram at the order level. **(D1)** The ternaryplot at the family level with top 20 families. **(D2)** The relative abundance accumulation diagram at the family level. **(E1)** The ternaryplot at the genus level with top 20 genus. **(E2)** The relative abundance accumulation diagram at the genus level. **(F1)** The ternaryplot at the species level with top 20 species. **(F2)** The relative abundance accumulation diagram at the species level.

results demonstrated higher similarity in endophytic fungi between 2-year-old and 3-year-old plants, while 1-year-old plants exhibited greater dissimilarity, aligning with the differences observed between 2-year-old and 3-year-old plants. Fungal genera significantly enriched in annuals were *Olipidium*, *Hannaella*, and *Plectospherella*, whereas endophytic fungi *Strelitziana* and *Trichomerium* were most enriched in biennials. Perennials were enriched in endophytes, including *Rhizopus*, with only a single addition compared to the biennials, while the rest remained consistent (Figure 6).

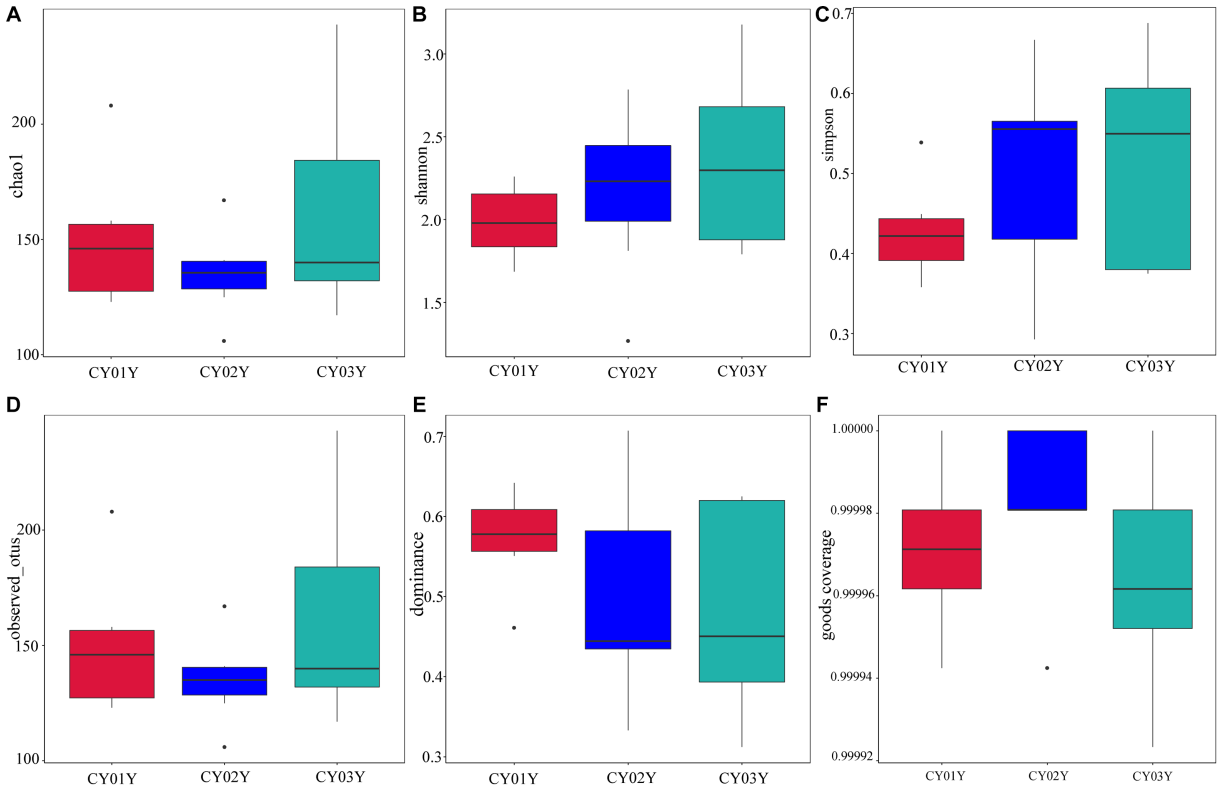

FIGURE 5
Species alpha diversity of stem-endophytic fungi in *D. nobile*. **(A)** The Chao 1 index of the endophytic fungi and Tukey's test showed no significant difference ($p > 0.05$), indicating that the number of species in stems is similar at different ages. **(B)** The Shannon index of endophytic fungi. **(C)** The Simpson diversity index showed no significant difference between them ($p > 0.05$). **(D)** The observed OTUs of endophytic fungi in *Dendrobium nobile*. **(E)** Dominance of different samples, the indices are all less than 1, indicating that the community has good species uniformity. **(F)** Good coverage index shows the higher sequencing coverage.

To probe into the relationships between stem genotype and age-dependent fungal ASVs in endophytic fungi, we constructed a co-abundance network. In line with PCA data, endophytic fungal ASVs exhibited intricate networks, providing insights into interactions between fungal communities at different age states. Notably, distinctive differences were observed in the community structures of microbes associated with 1-year-old stems versus those associated with 2- or 3-year-old stems. For microbes linked with 1-year-old stems, Spearman correlation analysis identified 17 species with a correlation above a threshold of 0.2 ($p < 0.01$; Figure 7A). Positive correlations were observed, such as *Pseudopithomyces* with *Pyrenochaeta*, *Phaeosphaeria*, and *Setophoma*, as well as *Septoria* with *Trichomerium* and *Fusarium*. Additionally, there were pairwise correlations between *Albifimbria* and *Myrmecridium*, *Lambertella* and *Mycoleptodiscus*, and *Botryotrichum* and *Solicoccozyma*. However, *Phyllachora* exhibited a negative correlation with *Papiliotrema*. For microbes associated with 2-year-old stems, Spearman correlation analysis revealed 16 taxa with a correlation above a threshold of 0.2 ($p < 0.01$; Figure 7B). Positive correlations were observed among *Pyrenochaetopsis*, *Carlosrosaea*, and *Hannaella*; *Phyllachora*, *Phaeosphaeria*, and *Setophoma*; and *Olpidium*, *Plectosphaerella*, and *Papiliotrema*. Additionally, there was a positive correlation between *Alternaria* and *Catenulostroma*, as well as *Epicoccum* with *Pseudorobillarda*, *Camptophora*, and *Cladosporium*. Furthermore, *Camptophora* showed a positive correlation with *Trichomerium*, while *Alternaria* showed a positive correlation with *Catenulostroma*. Thirteen species exhibited significant Spearman correlation with 3-year-old stems (Spearman >0.2, $p < 0.05$; Figure 7C). Among them, nine taxa (*Tomentella*, *Trichoderma*, *Mortierella*, *Tomentella*, *Saitozyma*, *Solicoccozyma*, *Cenococcum*, *Penicillium*) positively correlated with each other. The other two taxa groups *Pseudopithomyces* and *Epicoccum*, *Fusarium* and *Capnobotryella* also positively correlated.

3.3 Association of the stem transcriptome and endophytic fungi across different ages

The stem RNA-sequencing (RNA-seq) reads and microbial amplicon reads underwent stringent filtering to establish significant correlations of the factors ages, genes, and fungi between the datasets, thereby associating gene expression with fungi ASV abundance. Utilizing WGCNA analysis on all genes in the unigenes of the RNA-Seq data, 24 modules were delineated (weighting factor $\beta = 10$ and Height of Clustering of module eigengenes was 0.3). Among these, 16,441 genes were enriched in 23 modules, while 34 genes were not enriched in these modules and were cataloged as gray modules, resulting in a total of 24 modules (Supplementary Table S5; Figure 8A). The distribution of genes within each module is illustrated in Figure 8B.

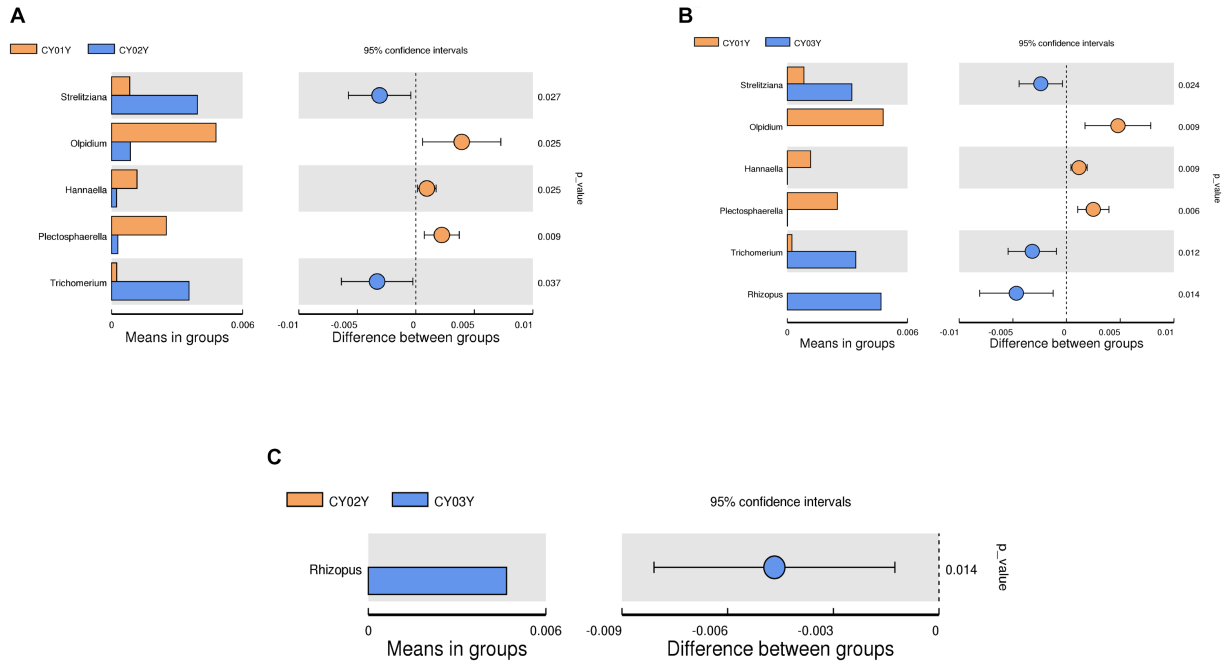

FIGURE 6
T-test of endophytic fungi in *D. nobile* at different ages at genus level. Each bar in the figure represents the mean value in each group for genera with significant differences in abundance between groups. The right panel shows the confidence level of intergroup differences. The leftmost endpoint of each circle in the figure represents the lower limit of the 95% confidence interval of the difference in means, and the rightmost endpoint of the circle represents the upper limit of the 95% confidence interval of the difference in means. The center of the circle represents the difference in means, and the circle color represents the value of p of the significance test for between-group differences for the corresponding differential taxa. **(A)** T-test of CY01Y and CY02Y. **(B)** T-test of CY01Y and CY03Y. **(C)** T-test of CY02Y and CY03Y.

Pearson correlation coefficients and environmental factors were computed for the Module Eigengenes (MEs) of all modules to identify modules associated with environmental factors (Figure 8C). The mediumpurple3 module exhibited a significant correlation with the endophytic fungal genera *Olpidium* ($R = 0.58$, $p = 0.01$), *Hannaella* ($R = 0.72$, $p = 8e\text{-}04$), and *Plectosphaerella* ($R = 0.43$, $p = 0.07$). Similarly, the darkorange module demonstrated a significant correlation with the endophytic fungal genera *Olpidium* ($R = 0.73$, $p = 5e\text{-}04$), *Hannaella* ($R = 0.65$, $p = 0.004$), and *Plectosphaerella* ($R = 0.86$, $p = 5e\text{-}06$). Additionally, the greenyellow module exhibited a significant correlation with the endophytic fungal genera *Strelitziana* ($R = 0.63$, $p = 0.005$) and *Trichomerium* ($R = 0.64$, $p = 0.005$), while showing a significantly lower correlation with the endophytic fungal genus *Rhizopus* (Figure 8C).

Subsequently, module membership (MM) was assessed to determine the correlation between genes and specific modules. Correlation analyzes were conducted between the Gene Significance (GS) of significantly different endophytic fungi and the MM of each modular gene to ascertain if the MM valus closely aligned with these endophytes, as well as dendrobine content. The outcomes revealed that in the darkorange module, the correlation coefficient between GS for *Olpidium*, *Hannaella*, and *Plectosphaerella* and MM was the highest. The correlation coefficients were $cor = 0.71$, $p = 2e\text{-}160$; $cor = 0.57$, $p = 9.9e\text{-}91$; $cor = 0.83$, $p < 1e\text{-}200$. Furthermore, in the greenyellow module, the correlation coefficients between the GS for endophytic fungi *Strelitziana* and *Trichomerium* and MM were the highest ($cor = 0.52$, $p = 3.7e\text{-}25$; $cor = 0.47$, $p = 3e\text{-}20$; Figure 9B).

To elucidate hub genes associated with the predominant endophytic fungi in 1-year-old *D. nobile* stems, the mediumpurple3 and darkorange modules were filtered based on Gene Significance (GS) and Module Membership (MM) values with a threshold of 3. The selected genes were then imported into Cytoscape, and the top 10 hub genes were identified using the cytoHubba plugin (Figures 8D,E). Among these genes, KFK09_024202 is a cell wall structural protein gene, KFK09_000278 is a CRIB domain-containing protein gene, KFK09_002541 is an mRNA of laccase-3, KFK09_000072 is an mRNA of probable polygalacturonase, KFK09_012583 is a HIP41 ARATH Heavy metal-associated isoprenylated plant protein gene, KFK09_002946 is a TOR1 ARATH Microtubule-associated protein gene, KFK09_021863 is a PMI11_ARATH Pectinesterase inhibitor coding mRNA, and KFK09_021567 is a KATAM_ORYSJ Xyloglucan galactosyltransferase gene (Figure 10).

For an in-depth analysis of the association of the greenyellow module with dominant endophytic fungi in 2- and 3-year-old *D. nobile*, 10 hub genes in the greenyellow module were selected based on GS and MM values, with a focus on $MM > 0.8$ and $GS > 0.2$. These hub genes exhibited significantly higher expression in 2- and 3-year-old plants compared to 1-year-old plants. Additionally, they exhibited a consistent trend of expression with the endophytic fungi *Trichomerium* and *Strelitziana* in *D. nobile* stems (Figure 11).

Consequently, it can be inferred that the gene expression modules significantly associated with the dominant endophytes of *D. nobile* are the mediumpurple3 and darkorange modules, correlating with different plant ages. The predominant fungi in young 1-year-old stems belong to the genera *Olpidium*, *Hannaella*, and *Plectosphaerella*,

10.3389/fmicb.2023.1294402

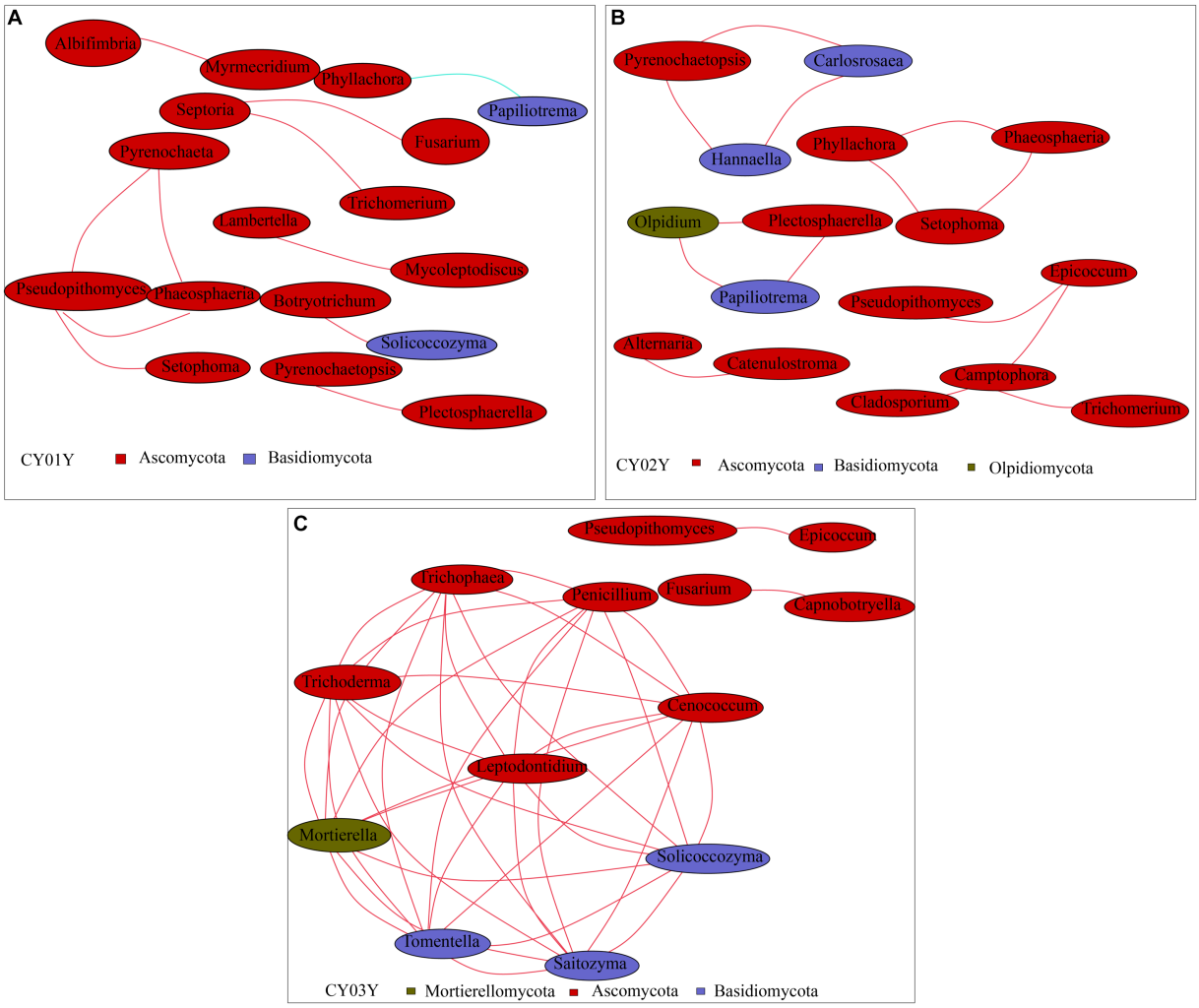

FIGURE 7
Co-occurrence network of age-associated ASVs selected. Different nodes represent different genera, node size represents the average relative abundance of the genus, nodes of the same phylum are of the same color (as shown in the legend), the thickness of the lines between the nodes is positively correlated with the absolute value of the correlation coefficient of the species interactions, and the color of the lines corresponds to the positive and negative correlation (red positive correlation, blue negative correlation). **(A)** Co-occurrence network of CY01Y. **(B)** Co-occurrence network of CY02Y. **(C)** Co-occurrence network of CY03Y. The key parameters in Network Diagram such as Network Diameter (ND), Modularity Degree (MD), Clustering Coefficient (CC), Graph Density (GD), Average Degree (AD). Average Path Length (APL) are shown in Supplementary Table 4.

exhibiting positive correlations with the mediumpurple3 and darkorange modules. Conversely, the dominant endophytic fungi expressed in older 2- and 3-year-old stems pertain to *Trichomerium* and *Strelitziana* species, and are significantly and positively correlated with the greenyellow module.

3.4 Age-dependent changes in the stem transcriptome and endophytic fungi are synchronized with properties of synthetic dendrobine in plants

Furthermore, we investigated whether the decline in dendrobine content with age is associated with age-specific transcriptome characterization in interaction with endophytic fungi. The 1-year-old stems of *D. nobile* exhibited the highest accumulation of dendrobine (Figure 9A). Through WGCNA analysis of the transcriptomes of Dendrobium stems of three different ages, we identified four modules - mediumpurple3 ($R = 0.78$, $p = 2e\text{-}04$), darkorange ($R = 0.75$, $p = 3e\text{-}04$), honeydew1 ($R = 0.61$, $p = 0.008$), and yellow ($R = 0.64$, $p = 0.004$) - that demonstrated a significant positive correlation with dendrobine content. In contrast, the greenyellow module ($R = -0.97$, $p = 7e\text{-}11$) displayed a significant negative correlation with dendrobine content. Subsequently, we conducted a correlation analysis between the GS of dendrobine content and MM of genes in each module to examine their relationship with dendrobine content. The highest correlation coefficients between GS of dendrobine content and MM were observed in the greenyellow, followed by the mediumpurple3 and darkorange modules, with correlation coefficients of cor = 0.94, $p = 2.6e\text{-}161$; cor = 0.77, $p = 1e\text{-}200$; and cor = 0.66, $p = 3.3e\text{-}131$ (Figure 9B). Given its significant negative correlation with dendrobine, the greenyellow module was not further analyzed.

The mediumpurple3 and darkorange modules were then subjected to GO functional enrichment. The mediumpurple3 module was

10.3389/fmicb.2023.1294402

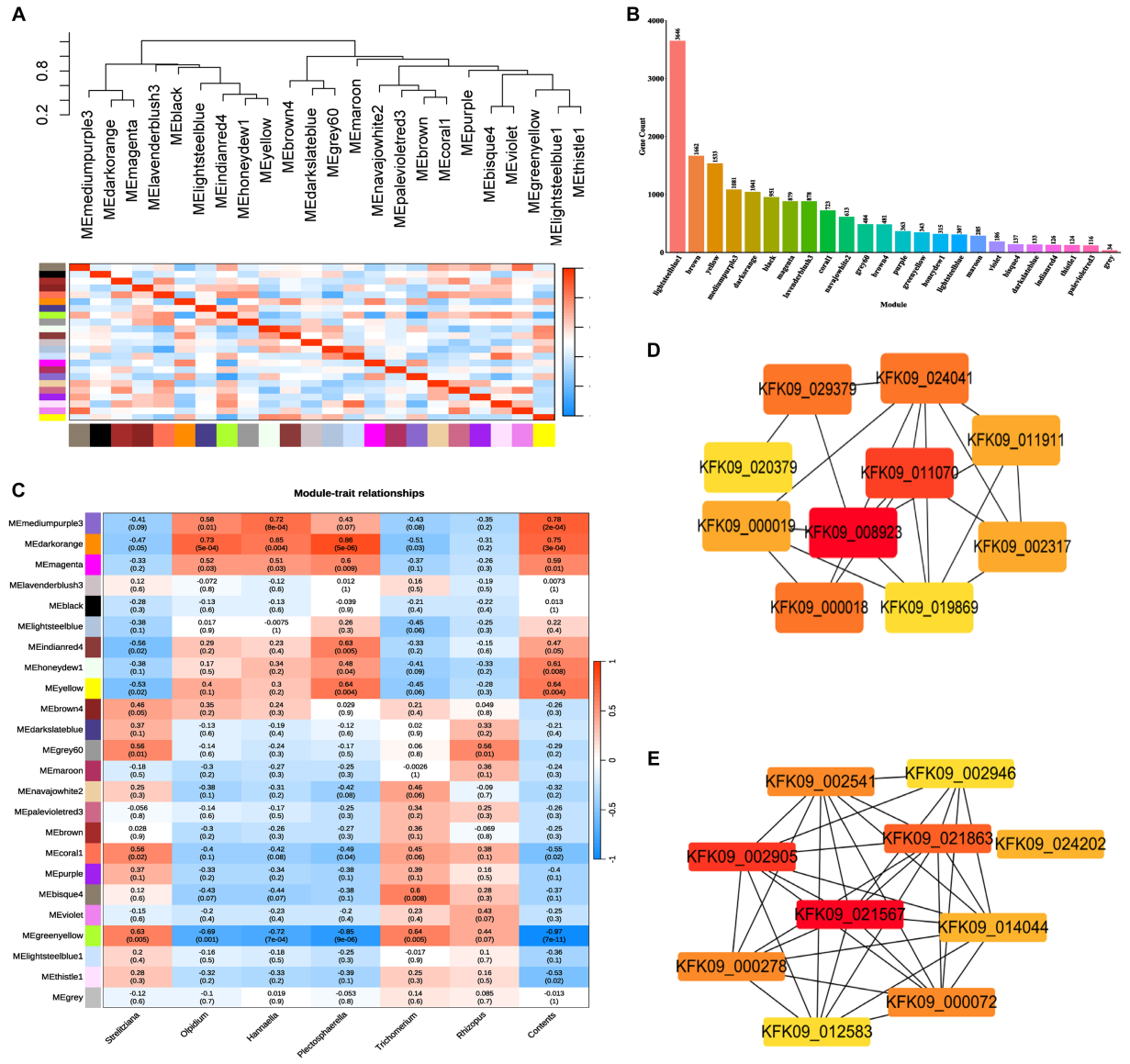

FIGURE 8
WGCNA analysis of all genes in the unigenes of the RNA-Seq data (weighting factor β = 10 and Height of Clustering of module eigengenes was 0.3). **(A)** Clustering dendrogram of all 18 samples. **(B)** Histogram of the number of genes in each module. **(C)** Pearson correlation coefficients between the 24 modules and dominant endophytic fungi and the contents of dendrobine. **(D)** The hub genes interaction network in cytoscape filtered by cytoHubba of mediumpurple3 module. **(E)** The hub genes interaction network in cytoscape filtered by cytoHubba of darkorange module.

primarily enriched for processes related to carbohydrate metabolism and transferase activity, while the darkorange module exhibited enrichment in processes associated with transferase activity and oxidoreductase activity (Supplementary Figure S3). However, only a few genes in the modules related to endophytic fungi showed significant enrichment in GO functions. This indicates that dissimilarity in gene expression does not always correspond to functional diversity.

Specifically, among the hub genes identified in these modules, only KFK09_002541, KFK09_000072, and KFK09_021863 were enriched in GO functional categories related to oxidation–reduction processes, carbohydrate metabolism, and enzyme inhibitor activity. Notably, no significant direct correlation with the dendrobine synthesis pathway was observed. Since alkaloid synthesis has been reported to correlate with the phytohormone pathway (Yan et al., 2019), we also examined four differential genes enriched in phytohormone signaling at different age gradients (gene-KFK09_020743, gene-KFK09_019829, gene-KFK09_027936, gene-KFK09_016712) categorized in the mediumpurple3 module. While these genes were not selected as core genes by WGCNA, they were listed as hub genes due to their functional significance (Figure 9C).

In addition, it's crucial to consider the reported changes in the expression of genes involved in the dendrobine synthesis pathway. The MVA pathway and the MEP pathway are the most documented biogenic pathways for dendrobine synthesis (Gong et al., 2021). Our data mining identified relevant genes in the MVA pathway, including acetoacetyl-CoA thiolase (AACT), 3-hydroxy-3-methylglutaryl-CoA synthase (HMGS), mevalonate kinase (MK), phosphomevalonate

10.3389/fmicb.2023.1294402

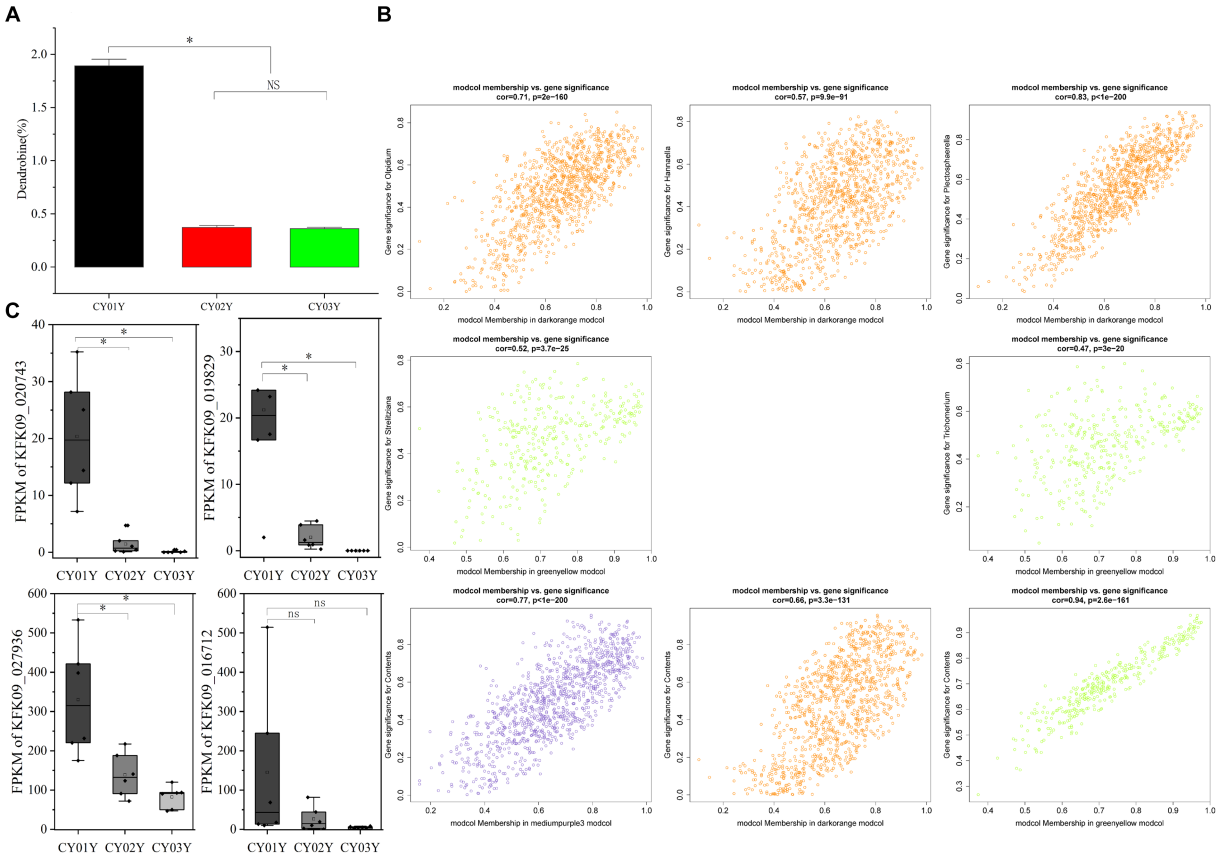

FIGURE 9
Dendrobine content and relationship with endophytic fungi and the plant transcriptome. **(A)** Contents of dendrobine along the timeline. **(B)** Module Membership vs. Gene Significance of darkorange, greenyellow and mediumpurple3 modules. **(C)** The expression of four differential genes enriched in phytohormone signaling (*$p < 0.05$).

kinase (PMK), mevalonate diphosphate decarboxylase (MVD), farnesyl diphosphate synthase (FPPS), and others. Genes that displayed a similar trend to dendrobine content included the HMGR genes KFK09_028710, KFK09_013183, KFK09_010477, as well as the PMK genes KFK09_023365, KFK09_015471, the IDI gene KFK09_008671, and some of the TPS genes KFK09_027207, KFK09_023284, KFK09_011873, and KFK09_006206 (Figure 12). Although none of the relevant genes in the MVA pathway were enriched in the mediumpurple3 and darkorange modules, their significance should not be overlooked. This suggests that the variation in dendrobine content across different years cannot be attributed solely to any one pathway. Furthermore, the subsequent biological processes involved in the formation of dendrobine from the terpene skeleton remain unclear (Chen et al., 2021), indicating that genetic changes in the MVA pathway and MEP pathway do not constitute the sole correlation with dendrobine synthesis.

4 Discussion

Since ancestral plants settled on land 450 million years ago, they have been interacting with microorganisms to form a "holobiont" (Hassani et al., 2018). These ubiquitous interactions between microbial communities and their host plants often shape host phenotypes and regulate metabolite synthesis (Sharma et al., 2021). Plants have evolved the ability to produce a large number of unique metabolites, and this metabolic diversification is likely driven by the need to adapt to different environments (Chae et al., 2014). One of the key environmental factors affecting plant health and adaptability is the host microbiota (Bulgarelli et al., 2012). Recent studies reveal an additional role for the plant-specialized metabolite camalexin in facilitating host-inter-root microbial interactions (Huang et al., 2019). However, how the microbial-host maintains homeostasis after perturbation remains poorly understood (Ma et al., 2021). Thus, the interaction between endophytic fungi and host has attracted wide attention, because they are a group of symbiotic fungi that colonize plant tissues and organs without causing apparent disease (Clay, 2004), but have the ability to reshape plant characteristics (Yan et al., 2019). There are two sides to every story. Endophytic fungi can provide various benefits to the host plant, such as promoting growth (Koberl et al., 2013; Shan et al., 2021), enhancing stress tolerance, inducing resistance (Ma et al., 2021) and producing bioactive compounds (Ancheeva et al., 2020). However, they also have negative effects on the host plant, conversion of endophytes from symbiotic to parasitic state (Thrall et al., 2007). Therefore, the interaction between endophytic fungi and host plant is complex and dynamic, and needs to be explored and understood in depth at different levels and scales.

10.3389/fmicb.2023.1294402

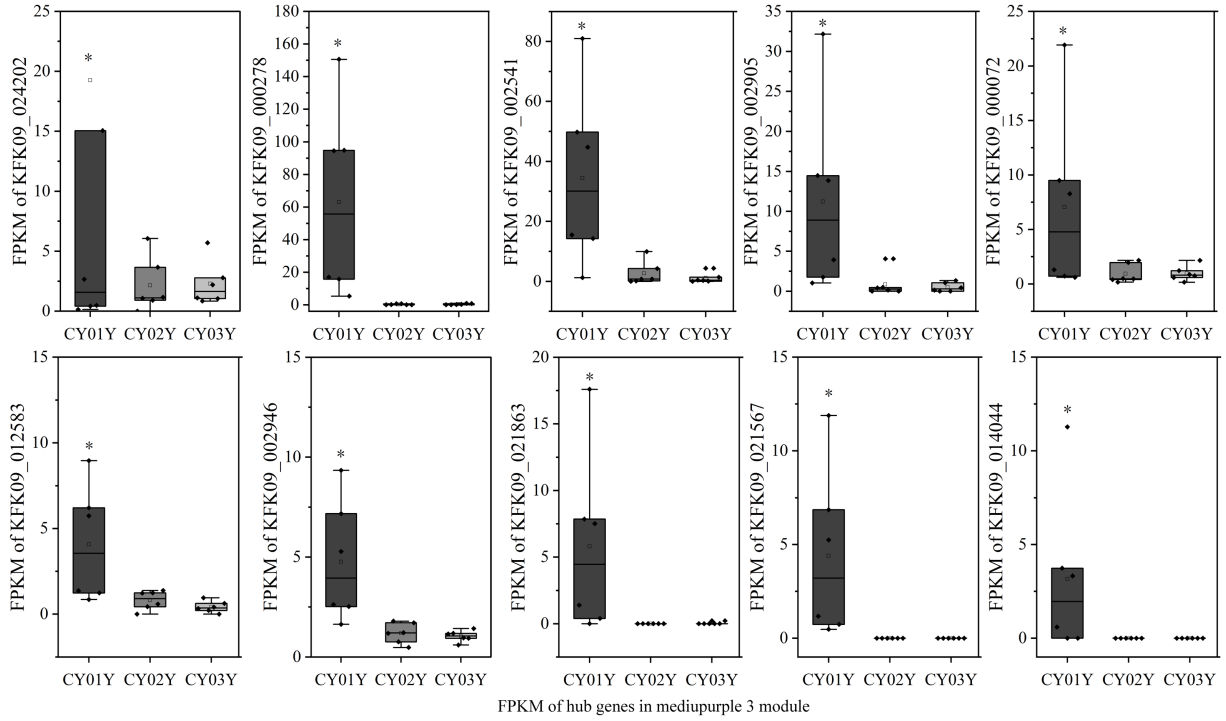

FIGURE 10
The expression graph of 10 genes in the mediumpurple3 module. The diagram showed the gene expression is significantly higher in annuals than in 2- and 3-year olds (*$p < 0.05$).

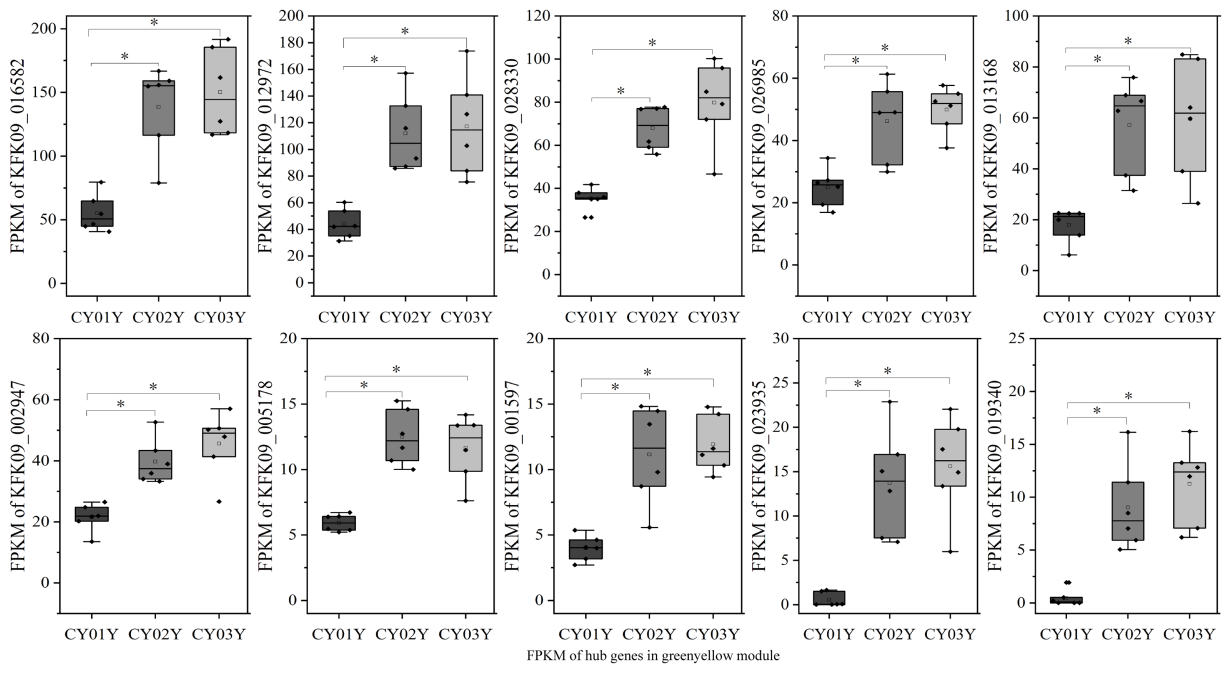

FIGURE 11
The expression graph of 10 genes in the greenyellow module. The graph shows that the expression of genes increases with the age of the plant (*$p<0.05$).

Dendrobium nobile is a traditional Chinese medicinal herb with various pharmacological effects, mainly derived from its main active ingredient, dendrobine. However, the content of dendrobine in *D. nobile* varies greatly with the age of the plant, and the underlying mechanism is still unclear (Gong et al., 2021). In this study, we observed significant shifts in the composition and abundance of

10.3389/fmicb.2023.1294402

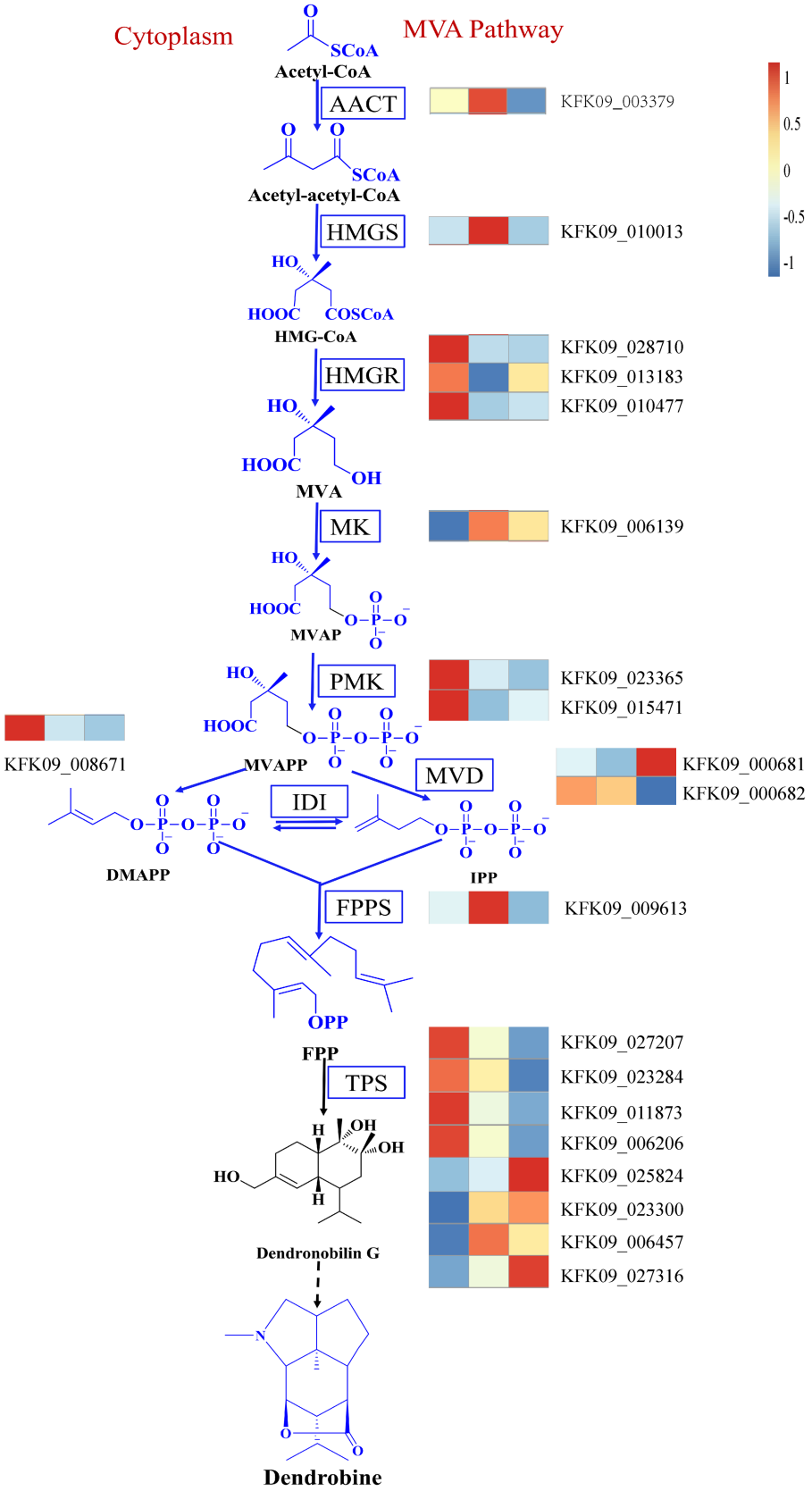

FIGURE 12
The MVA pathway of dendrobine and changes in key genes of the pathway. AACT, Acetoacetyl-CoA thiolase; HMGS, 3-hydroxy-3-methylglutaryl-coenzymeA synthase; HMGR, HMG-CoA reductase; MK, Mevalonate kinase. PMK, Phosphomevalonate kinase; MVD, Mevalonate diphosphate decarboxylase; IDI, Isopentenyl diphosphate isomerase; FPPS, Farnesyl diphosphate synthase; TPS, Terpenoid synthase.

endophytic fungi in the stems of *D. nobile* along the age axis, which correlated strongly with changes in the stem transcriptome. These findings are consistent with those of other studies on plants (Liu et al., 2017). Based on these observations, we hypothesized that age-dependent changes in the stem transcriptomes might be responsible for the observed variations in endophytic fungi. Several fungal genera, such as *Olpidium*, *Hannaella*, *Plectosphaerella*, *Strelitziana* and *Trichomerium*, were associated with different transcriptomic modules and dendrobine content. Meanwhile, some genes in plant hormone signaling and alkaloid biosynthesis pathways were differentially expressed among different ages and correlated with endophytic fungi and dendrobine content. Our results suggest that endophytic fungi may play an important role in regulating the stem transcriptome and dendrobine synthesis in *D. nobile* along the age gradient.

The co-occurrence network analysis revealed that the endophytic fungal community in the stems of *D. nobile* had a modularly structured according to different age groups. For instance, the 1-year-old *D. nobile* had a unique fungal community and corresponding transcriptomic module, which showed the highest correlation with *Olpidium*, *Hannaella*, and *Plectosphaerella* at the genus level compared to all other samples. *Olpidium* is known to act as a vector for plant viruses, infecting many plants with a wide range of hosts (Lay et al., 2018). At the level of species, there are *Olpidium brassicae* and *Olpidium virulentus* in the stems. *O. brassicae* and other *Olpidium* species sometimes form a large part of the fungal community in other plant roots or rhizospheres (Tkacz et al., 2015). Hannaella, which is a basidiomycetous yeast genus belonging to the order Tremellales, phylum Basidiomycota, had the highest abundance in *Alpinia zerumbet* (Yan et al., 2022) and *Salvia miltiorrhiza* (Chen et al., 2018). There are *Hannaella pagnoccae*, *Hannaella sinensis*, *Hannaella oryzae*, *Hannaella surugaensis*, *Hannaella luteola* and other species in our samples, and they all have been described in the *Hannaella* genus. Widespread on the leaf surfaces of various plants, including rice, wheat, and fruit trees (Han et al., 2017). *H. oryzae* was thought to play an important role in plant growth promotion and biocontrol as an important phyllosphere inhabiting yeast (Li Q. et al., 2021). The genus *Plectosphaerella* is the largest genus in the family Plectosphaerellaceae. Some species are plant pathogens, whereas others are soil-borne (Zhang et al., 2019). In the stem of *D. nobile*, several species were detected including *Plectosphaerella oratosquillae*, *Plectosphaerella oratosquillae* and *Plectosphaerella alismatis*. Most species of *Plectosphaerella* are pathogens causing large losses in agriculture reportedly (Yang et al., 2021). Therefore, according to the analysis, *Hannaella* is one of the endophytes instructive by subsequent studies. Moreover, module greenyellow had a significantly high correlation with fungus *Strelitziana*, *Trichomerium* in comparison with the 1-year ages. *Strelitziana* was found to be the dominant genus in plant biomass in muscadine grape skins (Sun et al., 2021) and *Pinus massoniana* (Chen et al., 2023), whereas *Trichomerium* was low in abundance in muscadine grape skins but played an important role in *Pinus massoniana*. Further investigation is needed to understand their effect on the host.

Recent evidence suggests that stress and defense response signaling play a role in the production of plant metabolites (SMs) (Isah, 2019). Fungal endophytes, as a phylogenetically and functionally diverse group, can interact with plants in various ways (Chen et al., 2022). Plants adjust their metabolism to environmental conditions, in part through the recognition of a wide array of self and non-self molecules. Among them, endophytes are a provider of the non-self molecules (Bjornson et al., 2021). Differences in endophytic fungal species and abundance must necessarily induce a direct response to host transcription. The transcriptional landscape of *D. nobile* is significantly different along the ages axis with distinct endophytes, but the analysis of the transcriptional landscape is complicated due to the numerous influencing factors. An interesting syndrome came to light through the differential expression analysis of ASV as well as the module analysis of WGCNA. The following genes specificity was summarized in mediumpurple3 module and varied significantly among samples, and correlated with plant hormone metabolism. Plant hormones are a key signaling mechanism for plants to respond to external abiotic factors, and then regulate plant morphology, growth, and synthesis of secondary metabolites (Blazquez et al., 2020). They can also mediate the interaction between plants and microorganisms, either positively or negatively (Kou et al., 2021). In our study, we found that some genes involved in plant hormone signaling, such as NPR1, SAUR, AUX/IAA and ARF, were differentially expressed among different ages and correlated with endophytic fungi and dendrobine content. NPR1 (gene-KFK09_020743) is a key node in signaling downstream from Salicylic acid (SA). It activates defense gene transcription under pathogen challenge (An and Mou, 2011). Auxin plays a crucial role in the process from embryogenesis to senescence in plants, much of which is achieved through the regulation of auxin response genes. As the largest family of early auxin response genes, gene KFK09_019829 (small auxin upregulated RNA (SAUR)) plays an key role in plant growth and development (Li et al., 2021). Auxin-responsive protein IAA (AUX/IAA) Aux/IAA proteins are short-lived nuclear proteins comprising several highly conserved domains that are encoded by the auxin early response gene family (Luo et al., 2018). We designed primers for these four key genes for RT-PCR and obtained the same trend of changes as RNA-seq (Supplementary Figure S4). Further elaboration, they all are the key regulatory nodes of different plant hormones.

Alkaloids, a diverse group of nitrogen-containing secondary metabolites, exhibit a range of biological activities and pharmacological effects (Bhambhani et al., 2021). Among these alkaloids, dendrobine plays a crucial role in *Dendrobium nobile*, displaying antioxidant properties (Hsu et al., 2022) and hepatoprotective effects (Zhou et al., 2020). Despite its significance, the biosynthesis of dendrobine remains poorly understood, although it is hypothesized to involve two major pathways: the mevalonate (MVA) pathway and the methylerythritol phosphate (MEP) pathway (Gong et al., 2021). The MVA pathway generates isopentenyl diphosphate (IPP) and dimethylallyl diphosphate (DMAPP), which serve as precursors for terpenoids. On the other hand, the MEP pathway produces 1-deoxy-D-xylulose-5-phosphate (DXP), a precursor for plastidial terpenoids. Both pathways converge at geranyl diphosphate (GPP), which is subsequently converted to dendrobine by terpene synthases (TPS) and other enzymes. In our study, we observed differential expression of genes involved in alkaloid biosynthesis pathways, such as HMGR, PMK, IDI and TPS, were differentially expressed among different ages and correlated with endophytic fungi and dendrobine content. HMGR, a key enzyme in the MVA pathway, catalyzes the conversion of 3-hydroxy-3-methylglutaryl-CoA (HMG-CoA) to mevalonate (MVA). PMK, an enzyme in the MVA pathway, catalyzes the phosphorylation of mevalonate to mevalonate-5-phosphate (MVP). IDI is an enzyme that

catalyzes the interconversion of IPP and DMAPP. TPS is a family of enzymes that catalyze the formation of various terpenoids from GPP or other prenyl diphosphates. The differential expression of these genes suggests that *D. nobile* exhibits varying capacities for alkaloid biosynthesis at different ages, influenced by the composition and abundance of the endophytic fungal community.

5 Conclusion

Our study provides novel insights into the interaction between endophytic fungi and the host plant, *D. nobile,* along the age gradient. Our results suggest that endophytic fungi may influence the transcriptome of the stem and the synthesis of dendrobine in *D. nobile* by modulating plant hormone signaling and alkaloid biosynthesis pathways. Additionally, we have identified specific fungal genera and gene modules that are associated with dendrobine content. These findings have potential implications for enhancing the quality and yield of *D. nobile* through targeted manipulation of the endophytic fungal community or host plant gene expression. However, it is important to acknowledge the limitations and uncertainties of our study, which should be addressed in future research. Firstly, our sampling was limited to the stems of *D. nobile* at three different ages, which may not fully represent the entire life cycle of the plant, although these ages are typically harvested within 3 years. It would be valuable to expand the sampling to include a broader range of ages and other tissues, such as roots and flowers, to obtain a more comprehensive understanding of the dynamics of the endophytic fungal community and transcriptome in *D. nobile*. Secondly, we solely employed ITS sequencing to identify the endophytic fungi in the stems of *D. nobile*, which may not capture the complete diversity and functionality of the fungal community. It would be beneficial to incorporate other molecular markers or metagenomic approaches to unveil the functional genes and metabolic pathways of the endophytic fungi in *D. nobile*.

Data availability statement

The data presented in the study are deposited in the NCBI repository, BioProject ID: PRJNA1040334, SRA: SRR26830466, https://submit.ncbi.nlm.nih.gov/subs/bioproject/SUB13972852/overview.

Author contributions

YZ: Data curation, Writing – original draft. XJ: Validation, Writing – original draft. XL: Validation, Writing – original draft. LQ: Data curation, Writing – review & editing. DT: Methodology, Writing – review & editing. DW: Validation, Writing – review & editing. CB: Resources, Writing – review & editing. JY: Resources, Writing – review & editing. JX: Supervision, Writing – review & editing. YH: Conceptualization, Funding acquisition, Visualization, Writing – review & editing.

Funding

The author(s) declare financial support was received for the research, authorship, and/or publication of this article. This research was funded by the National Nature Science Foundation of China (82160812), Guizhou Engineering Research Center of Industrial Key-technology for *Dendrobium nobile* [QJJ(2022)048, QJJ(2022)006], the Department of Science and Technology of Guizhou Province [QKHZC (2021)420, QKHZC (2023)261].

Acknowledgments

We would like to thank Guangxi Shenli Pharmaceutical Co., Ltd. and Chishui Xintian Chinese Medicine Industry Development Co., Ltd. for providing *Dendrobium nobile*.

Conflict of interest

CB was employed by Guangxi Shenli Pharmaceutical Co., Ltd. JY was employed by Chishui Xintian Chinese Medicine Industry Development Co., Ltd.

The remaining authors declare that the research was conducted in the absence of any commercial or financial relationships that could be construed as a potential conflict of interest.

Publisher's note

All claims expressed in this article are solely those of the authors and do not necessarily represent those of their affiliated organizations, or those of the publisher, the editors and the reviewers. Any product that may be evaluated in this article, or claim that may be made by its manufacturer, is not guaranteed or endorsed by the publisher.

Supplementary material

The Supplementary material for this article can be found online at: https://www.frontiersin.org/articles/10.3389/fmicb.2023.1294402/full#supplementary-material

References

Afkhami, M. E., and Strauss, S. Y. (2016). Native fungal endophytes suppress an exotic dominant and increase plant diversity over small and large spatial scales. *Ecology (Durham)* 97, 1159–1169. doi: 10.1890/15-1166.1

An, C., and Mou, Z. (2011). Salicylic acid and its function in plant immunity. *J. Integr. Plant Biol.* 53, 412–428. doi: 10.1111/j.1744-7909.2011.01043.x

Ancheeva, E., Daletos, G., and Proksch, P. (2020). Bioactive secondary metabolites from endophytic fungi. *Curr. Med. Chem.* 27, 1836–1854. doi: 10.2174/0929867326666190916144709

Bhambhani, S., Kondhare, K. R., and Giri, A. P. (2021). Diversity in chemical structures and biological properties of plant alkaloids. *Molecules* 26:374. doi: 10.3390/molecules26113374

Bjornson, M., Pimprikar, P., Nürnberger, T., and Zipfel, C. (2021). The transcriptional landscape of arabidopsis thaliana pattern-triggered immunity. *Nature Plants* 7, 579–586. doi: 10.1038/s41477-021-00874-5

Blazquez, M. A., Nelson, D. C., and Weijers, D. (2020). Evolution of plant hormone response pathways. *Annu. Rev. Plant Biol.* 71, 327–353. doi: 10.1146/annurev-arplant-050718-100309

Bulgarelli, D., Rott, M., Schlaeppi, K., Van Themaat, V. L., Ahmadinejad, N., Assenza, F., et al. (2012). Revealing structure and assembly cues for arabidopsis root-inhabiting bacterial microbiota. *Nature* 488, 91–95. doi: 10.1038/nature11336

Chae, L., Kim, T., Nilo-Poyanco, R., and Rhee, S. Y. (2014). Genomic signatures of specialized metabolism in plants. *Science* 344, 510–513. doi: 10.1126/science.1252076

Chen, X., Li, Q., Xu, X., Ding, G., Guo, S., and Li, B. (2021). Effects of the endophytic fungus mf23 on dendrobium nobile lindl. In an artificial primary environment. *Acs Omega* 6, 10047–10053. doi: 10.1021/acsomega.0c06325

Chen, K. H., Liao, H. L., Arnold, A. E., Korotkin, H. B., Wu, S. H., Matheny, P. B., et al. (2022). Comparative transcriptomics of fungal endophytes in co-culture with their moss hostdicranum scoparium reveals fungal trophic lability and moss unchanged to slightly increased growth rates. *New Phytol.* 234, 1832–1847. doi: 10.1111/nph.18078

Chen, H., Wu, H., Yan, B., Zhao, H., Liu, F., Zhang, H., et al. (2018). Core microbiome of medicinal plant salvia miltiorrhiza seed: a rich reservoir of beneficial microbes for secondary metabolism? *Int. J. Mol. Sci.* 19:672. doi: 10.3390/ijms19030672

Chen, H., Zhang, L., Huang, Z., Wu, Z., Tan, M., Zhang, X., et al. (2023). Effect of anoxic atmosphere on the physicochemical and pelletization properties of pinus massoniana sawdust during storage. *Int. J. Environ. Res. Public Health* 20:791. doi: 10.3390/ijerph20010791

Clay, K. (2004). Fungi and the food of the gods. *Nature* 427, 401–402. doi: 10.1038/427401a

Clay, K., and Holah, J. (1999). Fungal endophyte symbiosis and plant diversity in successional fields. *Science* 285, 1742–1744. doi: 10.1126/science.285.5434.1742

Gong, D. Y., Chen, X. Y., Guo, S. X., Wang, B. C., and Li, B. (2021). Recent advances and new insights in biosynthesis of dendrobine and sesquiterpenes. *Appl. Microbiol. Biotechnol.* 105, 6597–6606. doi: 10.1007/s00253-021-11534-1

Han, L., Li, Z., Guo, X., Tan, J., He, S., Cui, X. L., et al. (2017). *Hannaella dianchiensis* sp. Nov., a basidiomycetous yeast species isolated from lake water. *Int. J. Syst. Evol. Microbiol.* 67, 2014–2018. doi: 10.1099/ijsem.0.001908

Harrison, J. G., Beltran, L. P., Buerkle, C. A., Cook, D., Gardner, D. R., Parchman, T. L., et al. (2021). A suite of rare microbes interacts with a dominant, heritable, fungal endophyte to influence plant trait expression. *ISME J.* 15, 2763–2778. doi: 10.1038/s41396-021-00964-4

Hassani, M. A., Durán, P., and Hacquard, S. (2018). Microbial interactions within the plant holobiont. *Microbiome* 6:58. doi: 10.1186/s40168-018-0445-0

Hsu, W. H., Chung, C. P., Wang, Y. Y., Kuo, Y. H., Yeh, C. H., Lee, I. J., et al. (2022). Dendrobium nobile protects retinal cells from uv-induced oxidative stress damage via nrf2/ho-1 and mapk pathways. *J. Ethnopharmacol.* 288:114886. doi: 10.1016/j.jep.2021.114886

Huang, A. C., Jiang, T., Liu, Y., Bai, Y., Reed, J., Qu, B., et al. (2019). A specialized metabolic network selectively modulatesarabidopsis root microbiota. *Science* 364:6389. doi: 10.1126/science.aau6389

Isah, T. (2019). Stress and defense responses in plant secondary metabolites production. *Biol. Res.* 52:39. doi: 10.1186/s40659-019-0246-3

Koberl, M., Schmidt, R., Ramadan, E. M., Bauer, R., and Berg, G. (2013). The microbiome of medicinal plants: diversity and importance for plant growth, quality and health. *Front. Microbiol.* 4:400. doi: 10.3389/fmicb.2013.00400

Kou, M., Bastías, D. A., Christensen, M. J., Zhong, R., Nan, Z., and Zhang, X. X. (2021). The plant salicylic acid signalling pathway regulates the infection of a biotrophic pathogen in grasses associated with an epichloë endophyte. *J. Fungi* 7:633. doi: 10.3390/jof7080633

Lay, C., Hamel, C., and St-Arnaud, M. (2018). Taxonomy and pathogenicity of olpidium brassicae and its allied species. *Fungal Biol.* 122, 837–846. doi: 10.1016/j.funbio.2018.04.012

Li, M., Chen, R., Gu, H., Cheng, D., Guo, X., Shi, C., et al. (2021). Grape small auxin upregulated rna (saur) 041 is a candidate regulator of berry size in grape. *Int. J. Mol. Sci.* 22:11818. doi: 10.3390/ijms222111818

Li, Q., Li, L., Feng, H., Tu, W., Bao, Z., Xiong, C., et al. (2021). Characterization of the complete mitochondrial genome of basidiomycete yeast hannaella oryzae: intron evolution, gene rearrangement, and its phylogeny. *Front. Microbiol.* 12:567. doi: 10.3389/fmicb.2021.646567

Liu, T., Greenslade, A., and Yang, S. (2017). Levels of rhizome endophytic fungi fluctuate in Paris polyphylla var. Yunnanensi s as plants age. *Plant Divers.* 39, 60–64. doi: 10.1016/j.pld.2016.11.006

Lu, A. J., Jiang, Y., Wu, J., Tan, D. P., Qin, L., Lu, Y. L., et al. (2022). Opposite trends of glycosides and alkaloids indendrobium nobile of different age based on uplc-q/tof-ms combined with multivariate statistical analyses. *Phytochem. Anal.* 33, 619–634. doi: 10.1002/pca.3115

Luo, J., Zhou, J., and Zhang, J. (2018). Aux/iaa gene family in plants: molecular structure, regulation, and function. *Int. J. Mol. Sci.* 19:259. doi: 10.3390/ijms19010259

Ma, K., Niu, Y., Jia, Y., Ordon, J., Copeland, C., Emonet, A., et al. (2021). Coordination of microbe–host homeostasis by crosstalk with plant innate immunity. *Nat. Plants* 7, 814–825. doi: 10.1038/s41477-021-00920-2

Shan, T., Zhou, L., Li, B., Chen, X., Guo, S., Wang, A., et al. (2021). The plant growth-promoting fungus mf23 (mycena sp.) increases production of dendrobium officinale (orchidaceae) by affecting nitrogen uptake and nh 4 + assimilation. Front. *Plant Sci.* 12:693561. doi: 10.3389/fpls.2021.693561

Sharma, H., Rai, A. K., Dahiya, D., Chettri, R., and Nigam, P. S. (2021). Exploring endophytes for in vitro synthesis of bioactive compounds similar to metabolites produced in vivo by host plants. *Aims Microbiol.* 7, 175–199. doi: 10.3934/microbiol.2021012

Sun, D., Qu, J., Huang, Y., Lu, J., and Yin, L. (2021). Analysis of microbial community diversity of muscadine grape skins. *Food Res. Int.* 145:110417. doi: 10.1016/j.foodres.2021.110417

Teixeira, D. S. J., and Ng, T. B. (2017). The medicinal and pharmaceutical importance of dendrobium species. *Appl. Microbiol. Biotechnol.* 101, 2227–2239. doi: 10.1007/s00253-017-8169-9

Thrall, P. H., Hochberg, M. E., Burdon, J. J., and Bever, J. D. (2007). Coevolution of symbiotic mutualists and parasites in a community context. *Trends Ecol. Evol.* 22, 120–126. doi: 10.1016/j.tree.2006.11.007

Tkacz, A., Cheema, J., Chandra, G., Grant, A., and Poole, P. S. (2015). Stability and succession of the rhizosphere microbiota depends upon plant type and soil composition. *ISME J.* 9, 2349–2359. doi: 10.1038/ismej.2015.41

Wang, Z., Zhao, M., Cui, H., Li, J., and Wang, M. (2020). Transcriptomic landscape of medicinal dendrobium reveals genes associated with the biosynthesis of bioactive components. *Front. Plant Sci.* 11:391. doi: 10.3389/fpls.2020.00391

Yan, K., Pei, Z., Meng, L., Zheng, Y., Wang, L., Feng, R., et al. (2022). Determination of community structure and diversity of seed-vectored endophytic fungi in alpinia zerumbet. *Front. Microbiol.* 13:864. doi: 10.3389/fmicb.2022.814864

Yan, L., Zhu, J., Zhao, X., Shi, J., Jiang, C., and Shao, D. (2019). Beneficial effects of endophytic fungi colonization on plants. *Appl. Microbiol. Biotechnol.* 2019:713. doi: 10.1007/s00253-019-09713-2

Yang, X. Q., Ma, S. Y., Peng, Z. X., Wang, Z. Q., Qiao, M., and Yu, Z. (2021). Diversity of plectosphaerella within aquatic plants from Southwest China, with p. *Endophytica* and p. *Sichuanensis* spp. *Mycokeys* 80, 57–75. doi: 10.3897/mycokeys.80.64624

Zhang, Z., Chen, W., Zou, X., Han, Y., Huang, J., Liang, X. Q., et al. (2019). Phylogeny and taxonomy of two new plectosphaerella (plectosphaerellaceae, glomerellales) species from China. *Mycokeys* 57, 47–60. doi: 10.3897/mycokeys.57.36628

Zhao, Y., Qin, L., Tan, D., Wu, D., Wu, X., Fan, Q., et al. (2023). Fatty acid metabolites of dendrobium nobile were positively correlated with representative endophytic fungi at altitude. *Front. Microbiol.* 14:956. doi: 10.3389/fmicb.2023.1128956

Zhou, J., Zhang, Y., Li, S., Zhou, Q., Lu, Y., Shi, J., et al. (2020). *Dendrobium nobile* lindl. Alkaloids-mediated protection against ccl4-induced liver mitochondrial oxidative damage is dependent on the activation of nrf2 signaling pathway. *Biomed. Pharmacother.* 129:110351. doi: 10.1016/j.biopha.2020.110351

frontiers | Frontiers in Microbiology

TYPE Original Research
PUBLISHED 24 January 2024
DOI 10.3389/fmicb.2024.1331023

Check for updates

OPEN ACCESS

EDITED BY
Zhenlin Han,
University of Hawaii at Manoa, United States

REVIEWED BY
Rekha Arya,
Sungkyunkwan University, Republic of Korea
Sahana Vasudevan,
Institute for Stem Cell Science and Regenerative Medicine (inStem), India

*CORRESPONDENCE
Chuhua Tang
✉ tch306@126.com

†These authors have contributed equally to this work and share first authorship

RECEIVED 31 October 2023
ACCEPTED 04 January 2024
PUBLISHED 24 January 2024

CITATION
Zhu D, Qiao P, Zhou Q, Sun H, Xin B, Wu B and Tang C (2024) Effect of 15 days −6° head-down bed rest on microbial communities of supragingival plaque in young men.
Front. Microbiol. 15:1331023.
doi: 10.3389/fmicb.2024.1331023

COPYRIGHT
© 2024 Zhu, Qiao, Zhou, Sun, Xin, Wu and Tang. This is an open-access article distributed under the terms of the Creative Commons Attribution License (CC BY). The use, distribution or reproduction in other forums is permitted, provided the original author(s) and the copyright owner(s) are credited and that the original publication in this journal is cited, in accordance with accepted academic practice. No use, distribution or reproduction is permitted which does not comply with these terms.

Effect of 15 days −6° head-down bed rest on microbial communities of supragingival plaque in young men

Di Zhu[1,2†], Pengyan Qiao[2†], Qian Zhou[2], Hui Sun[1,2], Bingmu Xin[3], Bin Wu[4] and Chuhua Tang[1,2*]

[1]306th Clinical College of PLA, The Fifth Clinical College, Anhui Medical University, Beijing, China, [2]Department of Stomatology, PLA Strategic Support Force Medical Center, Beijing, China, [3]Engineering Research Center of Human Circadian Rhythm and Sleep, Space Science and Technology Institute, Shenzhen, China, [4]China Astronaut Research and Training Center, Beijing, China

Introduction: The microgravity environment astronauts experience during spaceflight can lead to an increased risk of oral diseases and possible changes in oral microecology. In this study, we aimed to assess changes in the microbial community of supragingival plaques to explore the effects of spaceflight microgravity environment on oral microecology.

Methods: Sixteen healthy male volunteers were recruited, and supragingival plaque samples were collected under −6° head-down bed rest (HDBR) at five-time points: day 1 before HDBR; days 5, 10, and 15 of HDBR; and day 6 of recovery. Bacterial genomic DNA was sequenced using gene sequencing technology with 16S ribosomal ribonucleic acid V3–V4 hypervariable region amplification and the obtained data were analyzed bioinformatically.

Results: Alpha diversity analysis showed a significant increase in species richness in supragingival plaque samples on day 15 of HDBR compared with that at pre-HDBR. Beta diversity analysis revealed that the community composition differed among the groups. Species distribution showed that, compared with those at pre-HDBR, the relative abundances of *Corynebacterium* and *Aggregatibacter* increased significantly during HDBR, while those of *Veillonella*, *Streptococcus*, and *Lautropia* decreased significantly. Moreover, compared with those at pre-HDBR, the relative abundance of *Leptotrichia* increased significantly on day 6 of recovery, whereas the relative abundances of *Porphyromonas* and *Streptococcus* decreased significantly. Network analysis showed that the interaction relationship between the dominant genera became simpler during HDBR, and the positive and negative correlations between them showed dynamic changes. Phylogenetic investigation of communities by reconstruction of unobserved states analysis showed that the amino acid metabolism function of plaque microorganisms was more enriched during HDBR.

Discussion: In summary, in a 15-day simulated microgravity environment, the diversity, species distribution, interaction relationship, and metabolic function of the supragingival plaque microbial community changed, which suggests that microgravity may affect the oral microecosystem by changing the balance of supragingival plaque microbial communities and further leading to the occurrence and development of oral diseases.

KEYWORDS

head-down bed rest, microgravity, supragingival plaque, microbial community, 16S rRNA high-throughput sequencing

1 Introduction

With the continuous exploration of space fields by humans, an increasing number of manned space missions have been successfully performed, and the construction of commercial spaceports is ongoing (Grenon et al., 2012). However, during space flights, the microgravity environment experienced by astronauts can affect human health and safety, including the musculoskeletal, hematopoietic, endocrine, and digestive systems (White and Averner, 2001; Graebe et al., 2004; Grimm et al., 2016).

Oral health is closely related to general health. The oral cavity is the gateway for pathogens to invade the human body and is a reservoir for infection-associated microorganisms that play a role in the spread of disease (Johnston and Dietlein, 1977). Oral dysbiosis can promote the development of oral diseases such as periodontal disease and caries, and may also affect systemic health by migration and colonization of pathogens, bacteremia, stimulating the body's inflammatory response and autoimmunity (Atarashi et al., 2017; Aarabi et al., 2018; Kwun et al., 2020). Therefore, oral health maintenance and monitoring of microbial communities are important for astronauts. According to a report, pain caused by pulpitis or gingivitis in astronauts during air flight may seriously affect their work efficiency (Brown et al., 1977). Astronauts experience increased dental calculus and gingival inflammation during space flights (Brown et al., 1976). In 1978, a Russian astronaut developed toothache symptoms during the last 2 weeks of a 96-day flight on Salyut 6; however, no emergency plans were made (Ball and Evans, 2001). A case of dental caries was reported in a medical incident at the Space Station MIR, which was treated with temporary fillings (Gontcharov et al., 2005). Rai (2009) confirmed through an 8-h−6° head-down-tilt bed rest experiment in 20 volunteers that a microgravity environment can cause toothache symptoms in healthy volunteers during tooth occlusion. Meanwhile, the results of space flight and simulation experiments showed that microgravity conditions could change the growth, morphology, virulence, antibiotic resistance, and secondary metabolism of microorganisms (Klaus and Howard, 2006; Wilson et al., 2007; Huang et al., 2018); change cellular interactions with the host (Foster et al., 2013); and cause negative effects on the immune system (Crucian et al., 2015). During life on the space station, astronauts' normal microflora composition changes significantly, which results in their bodies becoming less resistant to the source of infection (Ilyin, 2005).

Microbial factors are key factors leading to oral infectious diseases such as periodontal disease and caries. Plaque biofilms are thought to initiate the development and progression of periodontal disease (Marsh, 2012). Plaque accumulation at the gingival margin may cause chronic inflammation in periodontal tissues. Disruption of the homeostatic relationship between the plaque bacteria and the host can initiate and promote periodontal disease progression (Zhang et al., 2020). A close relationship exists between the stimulatory activity of Toll-like receptors (TLR)2 and TLR4 in supragingival plaques and the periodontal status (Yoshioka et al., 2008). By counting the number of plaque microorganism clones over 2 years in 24 participants, it was found that the stability of plaque microbial composition may be a good predictor of periodontal health (Kumar et al., 2006). Furthermore, plaque microorganisms mediate the development of caries. Bacterial microorganisms in the community produce acids to erode hard dental tissues, resulting in their demineralization and, ultimately, the formation of cavities. The accumulation of supragingival plaque biofilms on teeth is usually the first manifestation of caries (Bowen, 2016). Generally, a dynamic balance exists between plaque microbes and the host, and changes in health status alter the composition of substances released by the bacteria and correspondingly alter host responses (Darveau et al., 1997).

In a previous study, our group found that the structure of salivary microbial communities in young men in the 15-day head-down bedridden state changed significantly, and differences were observed in species distribution (Sun et al., 2022). However, microbial structures can vary across different microecological sites within the oral cavity (Yang et al., 2021). Compared to saliva, plaque microbiota accumulates on non-detached teeth surfaces, which provides them with more time to develop into uniform and complex communities (Shi et al., 2018). Simultaneously, teeth have non-shedding surfaces suitable for microbial growth, which are key ecological determinants contributing to the persistence of supragingival plaque (Marsh, 2003). Various microorganisms in the plaque community interact to form complex biological networks that provide ideal sites for microbial growth and reproduction. At present, the research on the microbial community of human oral cavity in microgravity environment mainly focuses on saliva samples, while the research on supragingival plaque is very limited. Therefore, studying the microbial community structure of supragingival plaque is crucial.

The −6° head-down bed rest model is considered a well-established model for simulating the physiological effects of microgravity in astronaut spaceflight (Pavy-Le Traon et al., 2007; Hargens and Vico, 2016). In 2015, the International Academy of Astronautics (IAA) has organized a team to study and publish a standardized guideline of bed-rest studies in the spaceflight context (Sundblad et al., 2016), which clearly proposes the use of −6° head-tilt to simulate microgravity. This experiment was performed under the guidance of this guideline.

Early scientists used culture-based methods to collect supragingival plaque samples from astronauts before and after space flights and found that their microbial counts were altered (Brown et al., 1974, 1976; Johnston and Dietlein, 1977). However, due to the limitation of experimental techniques, the previously investigated microbial species are limited to a few culturable species. Meanwhile, their findings were limited to changes in the counts of specific microorganisms. These do not reflect the overall changes in the microbial community of astronauts' supragingival plaque in the spaceflight microgravity environment, and do not report the co-occurring relationship between oral flora and predictions of microbial metabolic function. High-throughput sequencing technologies can provide new means to comprehensively understand the overall changes in the microbial community of supragingival plaques (Jagathrakshakan et al., 2015; Al-Hebshi et al., 2019). In addition, previous studies on microgravity have been limited to surveys before and after the flight or before and after simulation experiments and have not explored changes in plaque microflora at multiple time points during flight or experiments. Here, we used the −6° head-down bed rest method to simulate the microgravity environment and used 16S ribosomal ribonucleic acid (rRNA) gene sequencing technology based on the Illumina MiSeq platform to assess the changes in the microbial community of supragingival plaques at multiple time points and provide a basis for achieving

precise microbiological prevention and treatment of space oral diseases in the future.

2 Materials and methods

2.1 Participants

The participants were openly recruited from the public for this study. The inclusion criteria were as follows: male; age 18–45 years; height 160–175 cm; weight 50–80 kg; physical health status. The exclusion criteria included dental caries, periodontal disease, other oral infectious diseases, smoking history, drug dependence history, mental and psychological disease history, and systemic disease history. After a physical examination and screening, 16 male participants were recruited, and none withdrew from the experiment. This study protocol conformed to the ethical principles of the Declaration of Helsinki and was approved by the Ethics Review Committee of the Space Science and Technology Institute (Shenzhen) (SISCJK202009001). All participants provided informed consent, signed an informed consent form, and received remuneration after the end of the experiment.

2.2 −6° head-down bed rest test

In this experiment, we used the −6° head-down bed rest (HDBR) method to simulate a microgravity environment in space. During the experiment, participants held the longitudinal axis of their body with a horizontal line at −6° head down. The experiment lasted for 28 days, including 7 days of adaptation pre-HDBR, 15 days of HDBR, and 6 days of recovery post-HDBR. Two participants were housed in the same room with beds separated by a movable curtain. Room temperature was maintained between 22°C and 26°C. The participants were provided oral hygiene education and training on the bass brushing method before the experiment. During HDBR, it was required that: (1) participants perform daily activities in bed, such as eating, bathing, and urinating; they could turn on their sides but not get up. (2) The participants woke up at 07:00 and retired at 22:30 every day. The schedule of the daily activities was strictly controlled. (3) Participants were provided a uniform diet according to nutritional standards by dietitians. No beverage, except pure water, was offered. (4) Specialists monitored the participants' physical conditions and physiological changes to ensure that their physical indicators were within normal limits. This experiment was grouped according to 5-time points: day 1 before HDBR (AP group), during HDBR: day 5 of HDBR (BP group), day 10 of HDBR (CP group), day 15 of HDBR (DP group), and day 6 of recovery (EP group).

2.3 Samples collection

Supragingival plaque samples were collected at 9 a.m. Participants were asked to rinse their mouths and remove food debris. Following moisture removal using cotton rolls, supragingival plaque samples were collected from the buccal, lingual, and interproximal surfaces of six teeth, including the maxillary and mandibular first molars, the right maxillary central incisor, and the left mandibular central incisor, using sterile dental probes. The samples were placed in 1.5 mL Eppendorf tubes containing 1 mL of pre-chilled phosphate buffered saline, transferred on an ice bath, and stored in a−80°C freezer.

2.4 DNA extraction and purification

Target deoxyribonucleic acid (DNA) sequences in the samples were obtained using the cetyltrimethylammonium bromide (CTAB) method, and the purity and concentration of the DNA were detected using 1% agarose gel electrophoresis. An appropriate amount of DNA and a certain amount of sterile water were mixed in a centrifuge tube to dilute the sample to 1 ng/μl. Diluted genomic DNA was used as a template for PCR amplification using forward primer 341F and reverse primer 806R for the 16S rRNA V3–V4 region. PCR reactions used 15 μL Phusion® High-Fidelity PCR Master Mix (New England Biolabs, Ipswich, MA, USA), 2 μL forward and reverse primers and approximately 10 ng of template DNA. Thermal cycling consisted of initial denaturation at 98°C for 1 min, followed by 30 cycles of denaturation at 98°C for 10 s, annealing at 50°C for 30 s, and elongation at 72°C for 30 s. Finally, denaturation was performed at 72°C for 5 min. Samples were mixed equally with different tags and mixed thoroughly, and PCR amplification products were detected by 2% agarose gel electrophoresis. Target bands were tapped to obtain the recovered products. The products recovered by tapping were purified using the GeneJET Gel Extraction Kit (Qiagen, Hilden, Germany).

2.5 Sequencing and data analysis

Library construction was performed using a TruSeq® DNA polymerase chain reaction (PCR)-free sample preparation kit (Illumina, CA, USA). A Qubit fluorometer (Thermo Fisher, Carlsbad, CA, USA) and quantitative-PCR (Q-PCR) analysis were used to evaluate library quality. After the library was qualified, it was processed for sequencing using the Illumina NovaSeq platform (Nevogene, Beijing, China). Each data sample was split from the offboard data according to the barcode and PCR amplification primer sequences, and the sequencing reads of each sample were spliced, controlled, and filtered using FLASH (v1.2.7) after truncating the barcode and primer sequences to obtain clean tags (Magoč and Salzberg, 2011; Bokulich et al., 2013). The quality control process was completed according to the method described by Qiime (v1.9.1) (Caporaso et al., 2010; Poncheewin et al., 2019), and effective tags were obtained (Rognes et al., 2016). All effective tags were clustered using Uparse software (v7.0.1001) to cluster sequences into operational taxonomic units (OTUs) based on the similarity between sequences with 97% consistency (Haas et al., 2011). With SILVA based on the Mothur algorithm, the database performs species annotation analysis of OTUs sequences (setting a threshold of 0.8–1) to obtain the microbial community composition of each sample at different taxonomic levels (Edgar, 2013; Quast et al., 2013).[1] Species accumulation curves were plotted using the R software (v2.15.3). Observed species, Chao1, ACE, Shannon, Simpson, and good coverage indices were calculated using

1 http://www.arb-silva.de/

the Qiime software based on species annotation. Fast multiple sequence alignment was performed using the MUSCLE software (v3.8.31) to obtain phylogenic relationships for representative sequences of all OTUs (Edgar, 2004). Principal coordinate analysis (PCoA) was performed by calculating the UniFrac distances using Qiime software, using phylogenetic relationships among OTUs (Lozupone et al., 2011). An unweighted pair-group method with an arithmetic mean (UPGMA) sample cluster tree was constructed. Multidimensional data were visualized by performing non-metric multidimensional scaling (NMDS) analysis based on the Bray-Curtis distance (Lozupone et al., 2007). The corresponding images were drawn using R software. Analysis of dissimilarities (ADONIS), analysis of similarities (ANOSIM), and analysis of molecular variance (AMOVA) were used to test the significance of the differences in community structure among the groups (Roewer et al., 1996; Chapman and Underwood, 1999; Anderson, 2001). Statistical analyses were performed using the SPSS software (v21.0.0.0). To determine whether species diversity and relative abundance differed among groups, we performed normality tests using the Shapiro–Wilk method, one-way analysis of variance (ANOVA), and Tukey multiple tests if a normal distribution was met; otherwise, the Friedman rank sum test and Dunn's multiple tests were used. GraphPad Prism (v8.0.1) and R software were used for mapping. Network relationships among the genera were plotted using Spearman's correlation coefficient and Graphviz software (v2.38.0). Significantly different metabolic pathways were identified by the phylogenetic investigation of communities by reconstruction of unobserved states (PICRUSt). Differences in metabolic function between groups were analyzed using a paired sample t-test. Statistical significance was set at $p < 0.05$.

3 Results

3.1 Sequencing data processing

The raw data and quality control results for all samples after being subjected to double-end sequencing on the Illumina NovaSeq platform are shown in Supplementary Table 1. Raw off-machine data yielded an average of 87,621 sequences per sample. After splicing and filtering low-quality and short-length sequences, chimeras were removed, and an average of 50,627 high-quality sequences with an average length of 418 bp were obtained. A total of 3,948,939 high-quality valid sequences were obtained for subsequent analysis.

3.2 OTUs clustering and species annotation

OTUs clustering analysis was performed on valid sequence data from supragingival plaque samples according to 97% concordance to analyze the composition and distribution of species in the supragingival plaque samples (Supplementary Figure 1). The clustering results showed that 4,941 OTUs were obtained, and 4,080 (82.57%) were annotated to the database. The OTUs at each level represented 2 bacterial boundaries, 29 phyla, 44 classes, 96 orders, 176 families, 379 genera, and 412 species. A Venn diagram showed that 1,436, 1843, 1787, 2,918, and 1833 OTUs were identified in the AP, BP, CP, DP, and EP groups, respectively, after 97% consistency treatment. Five groups of overlapping regions, i.e., 560 OTUs, were shared by the five groups (Figure 1A). Analyzing five groups of unique OTUs, we found 332, 343, 286, 986, and 521 unique OTUs in the AP, BP, CP, DP, and EP groups, respectively. The number of unique OTUs in the DP group was significantly higher than in the AP group. The results of the cumulative box plot of species indicated that the sample size in this experiment was sufficient to meet the analytical requirements for species richness (Figure 1B).

3.3 Alpha diversity analysis

Alpha diversity reflects species complexity within the sample community, and the results of each index are presented as box plots (Figure 2). The Chao1 index was used to estimate the number of species contained in the supragingival plaque samples, i.e., species richness. The results showed that the number of species in the samples showed an increasing trend with an increase in the-6° head-down bed rest experimental time compared to the AP group. The DP group had the largest number of species, which was significantly different from the AP, BP, and CP groups ($p < 0.05$). The number of species in the EP group did not differ significantly from those in the other four groups. The observed species index also showed that, at the same sequencing depth, the highest number of species was found in the DP group, which was significantly different from that in the AP group ($p < 0.05$). The Shannon index results showed no statistical difference in species diversity during HDBR compared with the AP group. Although species diversity in the EP group decreased significantly compared with the DP group ($p < 0.05$), it was not statistically different from that in the AP group. The above results showed that alpha diversity differed among the samples, with the DP group having the highest species richness.

3.4 Beta diversity analysis

Beta diversity analysis was performed to determine whether microgravity altered the microbial community structure. PCoA and NMDS analyses showed that the EP group was distinct from the other four groups in different directions, and the community structure was quite different (Figures 3A,B). The beta diversity index heatmap and UPGMA cluster analysis showed that the community structures of the AP and EP groups were quite different from those of the other four groups; however, the structures of the three groups during HDBR were similar (Figures 3C,D). To further verify the correctness of the above results, we also performed tests for differences between the groups (Table 1). These results showed that the community structures of the AP and EP groups were significantly different from those of the other four groups of samples under a simulated microgravity environment ($p < 0.05$).

3.5 Species distribution

According to the species annotation results, 28 phyla were identified in the five groups of supragingival plaques at the phylum level. Columnar accumulation plots of the relative abundance of species drawn from the top 10 phyla with the maximum abundance were selected (Figure 4A). Among them, there were six dominant

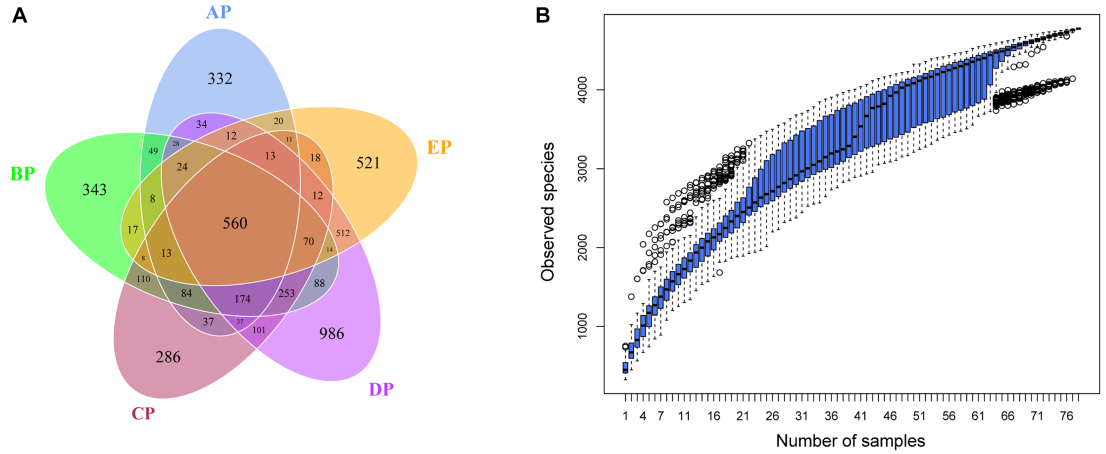

FIGURE 1
(A) Venn diagram of supragingival plaque samples. The numbers in the overlapping part of the circle represent the number of OTUs common to the group, and the numbers in the non-overlapping part represent the number of OTUs unique to the group. **(B)** Box plot of species accumulation in the supragingival plaque samples.

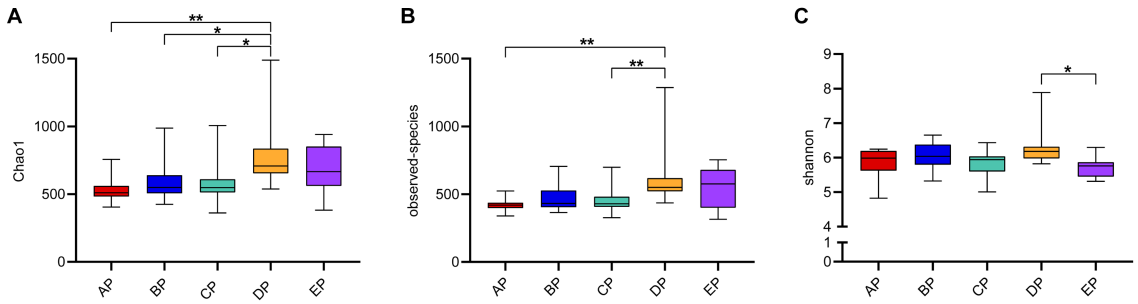

FIGURE 2
Box plot of Alpha diversity index of the supragingival plaque samples. The graphs show the Chao1 index **(A)**, observed species index **(B)**, and Shannon index **(C)**, respectively. The color boxes in the figure represent the middle 50% distribution interval of the group of data, and the upper and lower boundaries of the boxes are the upper and lower quartiles of the data, respectively; the middle line is the median. *$p < 0.05$, **$p < 0.01$.

phyla (mean relative abundance >1%): Fusobacteria, Bacteroidetes, Proteobacteria, Actinobacteria, Firmicutes, and Spirochaetes according to their relative abundances from high to low, and the total abundance of the dominant phyla was 94.74%. Statistical analysis of differences in the relative abundance of dominant phyla revealed that compared to the AP group, Actinobacteria were significantly increased in the CP group ($p < 0.05$), whereas Firmicutes were significantly decreased in the CP ($p < 0.01$) and DP groups ($p < 0.05$); Actinobacteria were significantly decreased in the EP group compared with the CP group ($p < 0.05$) (Figure 4B).

In total, 379 genera were identified. Columnar accumulation plots of the relative abundance of the species were drawn for the top 10 most abundant genera (Figure 4C). There were 15 dominant genera with a total abundance of 80.10%. Statistical analysis of differences in the relative abundance of dominant genera revealed that compared with the AP group, *Aggregatibacter* were significantly increased ($p < 0.01$) and *Lautropia* were significantly decreased ($p < 0.05$) in the BP group; *Corynebacterium* ($p < 0.05$) and *Aggregatibacter* ($p < 0.01$) were significantly increased, *Veillonella* and *Lautropia* were significantly decreased ($p < 0.05$) in the CP group; *Streptococcus* were significantly decreased ($p < 0.01$) in the DP group; and *Leptotrichia* were significantly increased ($p < 0.05$), *Porphyromonas* ($p < 0.05$), and *Streptococcus* ($p < 0.01$) were significantly decreased in the EP group. Compared with the BP group, the EP group showed a significant increase in *Leptotrichia* ($p < 0.05$) and a significant decrease in *Fusobacterium* ($p < 0.05$) and *Porphyromonas* ($p < 0.01$). Compared to the CP group, the EP group showed a significant increase in *Leptotrichia* ($p < 0.05$) and *Veillonella* ($p < 0.01$) and a significant decrease in *Corynebacterium*, *Porphyromonas*, and *Aggregatibacter* ($p < 0.01$) (Figure 4D).

3.6 Genus-level species phylogenetic tree

Representative sequences of the top 100 dominant and abundant genera in the supragingival plaque microorganisms were analyzed, and the microbial communities in all samples were mainly composed of Firmicutes, Proteobacteria, Actinobacteria, Bacteroidetes, and Fusobacteria. *Veillonella* in Firmicutes; *Neisseria* in Proteobacteria; *Corynebacterium* in Actinobacteria; *unidentified Prevotellaceae*,

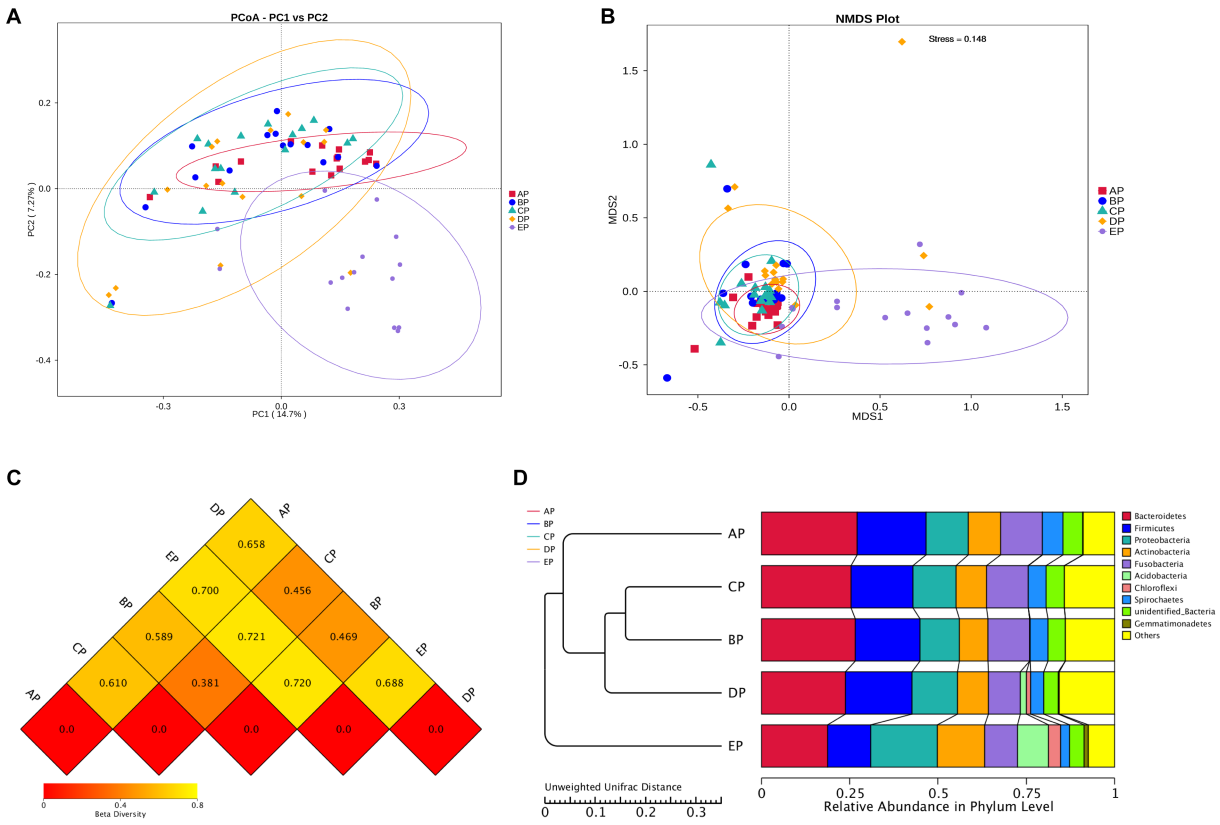

FIGURE 3
Beta diversity index plots of the supragingival plaque samples. **(A)** Two-dimensional principal coordinate analysis based on the Unweighted Unifrac distance. Horizontal coordinate, main component PC1; vertical coordinate, main component PC2. **(B)** Non-metric multidimensional scaling (NMDS) analysis based on the Bray-Curtis distance: Stress is less than 0.2, indicating that NMDS can accurately reflect the degree of dissimilarity among samples. **(C)** Heat map of the Beta diversity index. The numbers are the dissimilarity coefficients of the two groups. The reference values at the bottom right are the Beta diversity index values and the color shades correspondingly. **(D)** Unweighted pair-group method with arithmetic mean clustering tree.

TABLE 1 **Dissimilarity analysis of supragingival plaque samples between groups.**

Group	Anosim		Adonis		Amova	
	R	*p*	*R2*	*p*	Fs	*p*
AP-BP	0.1012	0.016	0.06707	0.017	1.33637	0.094
AP-CP	0.1364	0.003	0.07504	0.003	1.80369	0.011
AP-DP	0.1304	0.005	0.07517	0.004	2.58057	<0.001
AP-EP	0.1746	0.001	0.08985	0.006	3.68565	<0.001
BP-CP	0.02656	0.219	0.05628	0.07	0.673817	0.905
BP-DP	0.00344	0.378	0.04035	0.204	1.04837	0.34
BP-EP	0.1966	0.001	0.09544	0.002	4.06971	<0.001
CP-DP	0.08408	0.036	0.06574	0.012	1.14806	0.253
CP-EP	0.2694	0.002	0.11565	0.003	4.83831	<0.001
DP-EP	0.1492	0.001	0.07624	0.004	4.29182	<0.001

Anosim analysis and Adonis analysis based on Bray-Curtis distance; Amova analysis based on Unifrac distance. In Anosim analysis, $R > 0$ indicates significant differences between groups, and $R < 0$ indicates that intra-group differences are greater than inter-group differences. In Adonis analysis, a larger value of R2 indicates a higher degree of explanation of differences by group. In Amova analysis, Fs is the F-test value. The reliability of the above statistical analyses were expressed as p values, and $p < 0.05$ indicated that the statistical differences were significant.

Capnocytophaga, *Prevotella*, and *Porphyromonas* in Bacteroidetes; and *Leptotrichia* and *Fusobacterium* in Fusobacteria contributed more to the species composition (Figure 5).

3.7 Network analysis

Network relationship diagrams demonstrate the interaction relationships among microbial genera in different states. The interactions among microorganisms in the five groups of supragingival plaque samples were obtained by calculating the Spearman correlation coefficient for all samples and removing the filtering conditions, which were visualized using a network diagram (Supplementary Figure 2). The connections among the nodes represent a significant correlation among the genera. The AP group contained 64 nodes and 180 connectors, the BP group contained 82 nodes and 264 connectors, the CP group contained 70 nodes and 182 connectors, the DP group contained 98 nodes and 577 connectors, and the EP group contained 78 nodes and 266 connectors. It can be seen that the correlation of genera became progressively more complex in all samples during HDBR and did not return to pre-HDBR levels in the EP group. Furthermore, we analyzed the interactive relationships among the 15 dominant

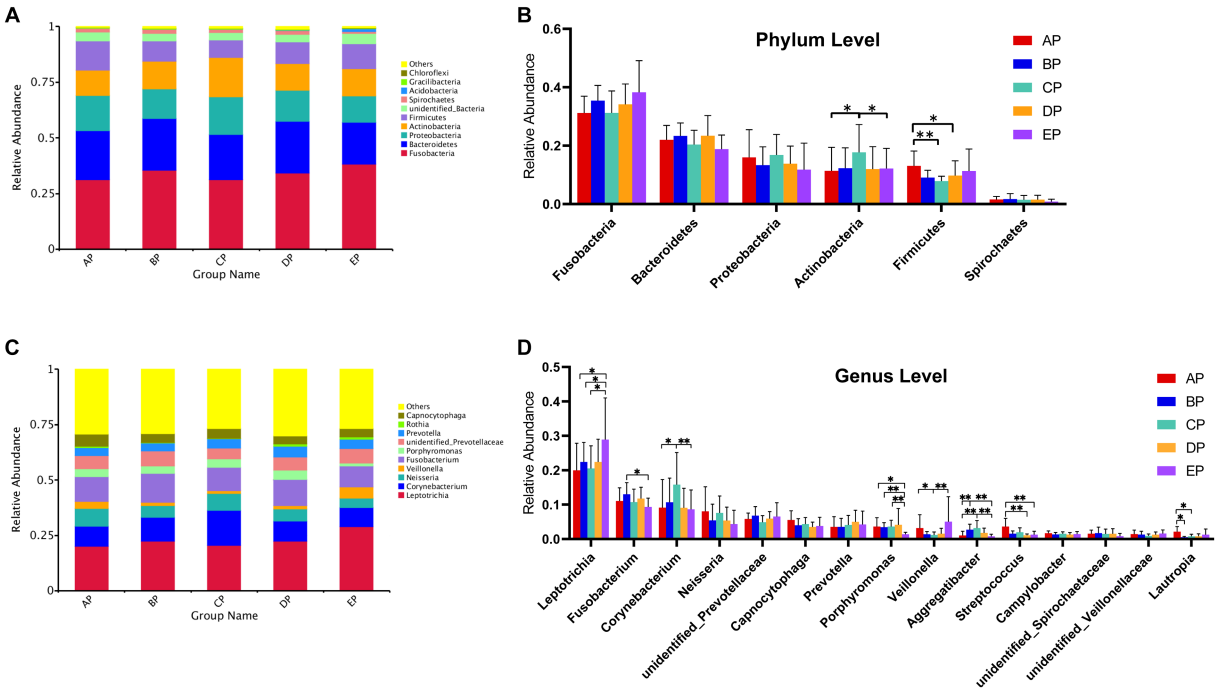

FIGURE 4
(A) Columnar accumulation plot for the top 10 phyla in relative abundance. **(B)** Differential analysis of the dominant phyla. **(C)** Columnar accumulation plot for the top 10 genera in relative abundance. **(D)** Differential analysis of the dominant genera. Others represent the sum of relative abundance of all species other than the first 10 species in the graph. *$p < 0.05$; **$p < 0.01$.

genera (Supplementary Figure 3). There were 17 pairs of interrelationships in the AP group, 13 in the BP group, 16 in the CP group, 5 in the DP group, and 16 in the EP group. With these data, we found that the interrelationship between the dominant genera became simpler during HDBR. Simultaneously, the positive and negative correlations between the dominant genera changed dynamically, and the specific correlation coefficient values are listed in Table 2. No correlation was observed between Porphyromonas, Prevotella, and an unidentified Spirochaet*aceae* in the AP group, whereas a positive correlation emerged in the DP group. *Neisseria* showed a positive correlation with *Capnocytophaga* in both the AP and EP groups; however, this was not observed during the experimental period. *Fusobacterium* and *unidentified Prevotellaceae* showed negative correlations in the AP group and positive correlations in the CP group. These results indicated that the correlations among the microbial communities changed under simulated microgravity conditions.

3.8 PICRUSt functional prediction

The Kyoto Encyclopedia of Genes and Genomes (KEGG) database was used to analyze functional genes. Based on the annotation results of the database, the top 10 functional information of each grouping in terms of maximum abundance at each annotation level was selected to generate a functional relative abundance histogram (Figures 6A,B). The main functional gene categories were the same for all groups. According to the functional annotation and abundance information of the samples in the database, the top 35 abundant functions and their abundance information in each sample were selected to draw a heatmap, and clustering was performed based on the functional difference level (Figures 6C,D). Differences between the groups were analyzed based on the annotation results (Figure 6E).

The results of the first annotation hierarchy showed that the KEGG pathways for supragingival plaque microbes were mainly focused on metabolic and genetic information processing. Compared to the AP group, no significant difference was observed in gene function during HDBR; however, the metabolic function was more abundant, and the genetic information processing function decreased significantly in the EP group.

The second annotation hierarchy results showed that the top 10 major functional gene categories in relative abundance were the same for the five groups of samples, including membrane transport, carbohydrate metabolism, amino acid metabolism, replication and repair, and translation. Among them, the most abundant membrane transport function did not differ among the five groups; however, compared with the AP group, carbohydrate metabolism function was richer in the EP group, and amino acid metabolism function was richer in the BP, DP, and EP groups, although replication and repair function and translation function decreased in the EP group.

4 Discussion

Dysbiosis of the oral microbiota can lead to the development of several oral diseases. Therefore, exploring how changes in

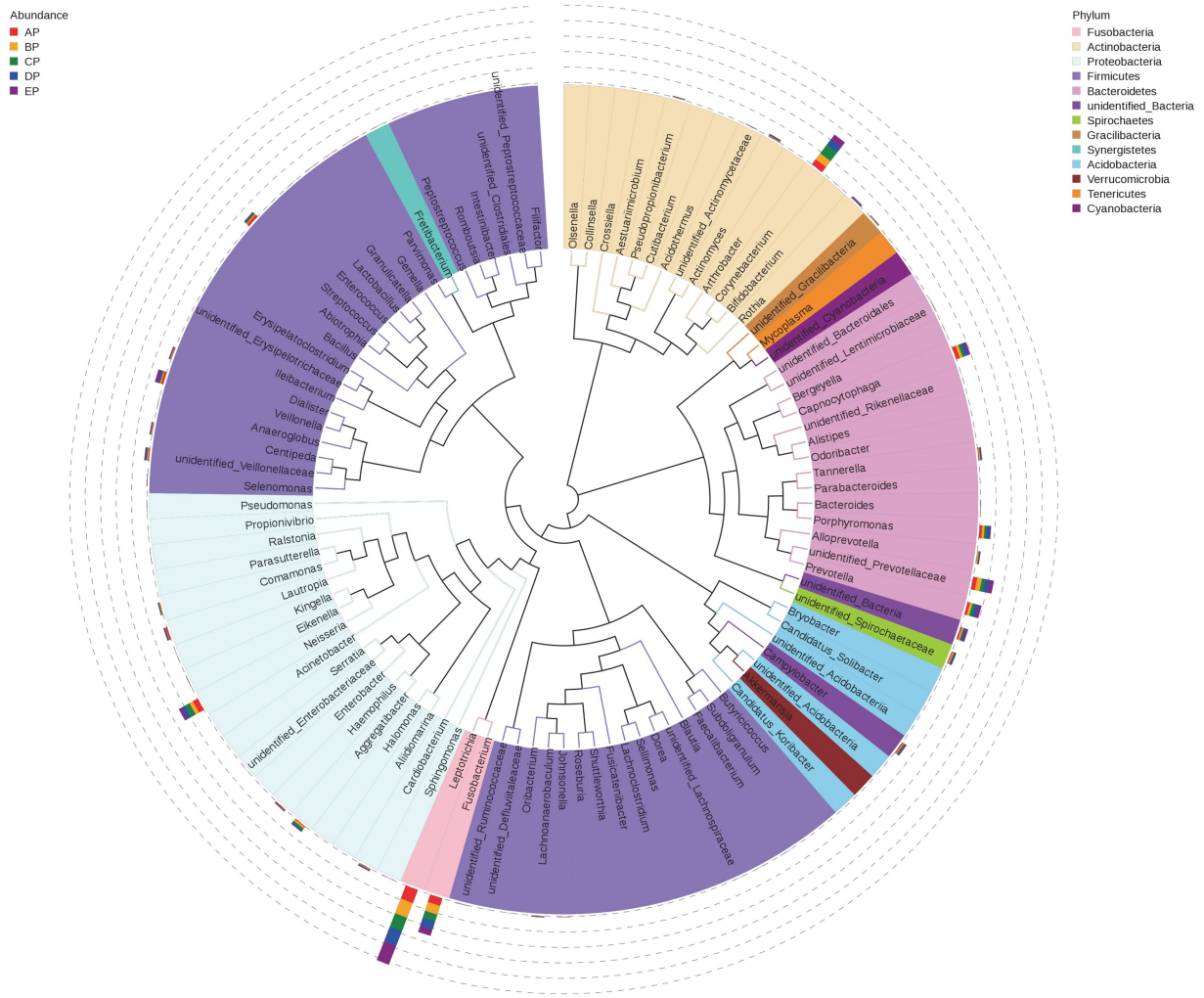

FIGURE 5
Phylogenetic tree of species at the genus level for supragingival plaque samples. The outer bar shows information on the abundance distribution of the genera in each of the five groups of samples, as shown in the left panel note. The colors of the branches and sectors indicate their corresponding phylum, as shown in the right panel note. The innermost tree structure refers to the OTU phylogenetic tree: each branch represents a species, and the length of the branch is the evolutionary distance between two species, i.e., the degree of species difference.

environmental factors can cause changes in the oral microbiota is crucial.

When clustering OTUs, we found a significant increase in the number of unique OTUs in the supragingival plaque microbial community on day 15 of HDBR compared to pre-HDBR. Meanwhile, Chao1 and the observed species indices showed a significant increase in species richness on day 15 of HDBR. This suggests that the number of species in the microbial community of the supragingival plaque increases under simulated microgravity. Ilyin (2005) collected oral microorganisms from astronauts at the Salyut and Mir orbital stations and found that the number of opportunistic pathogens increased during spaceflight, particularly the massive invasion of *Actinomyces_naeslundii*, *Prevotella_melaninogenica*, and *Fusobacterium_nucleatum* as well as bacterial species capable of maintaining the persistence of inflammation, but declined to preflight levels on day 14 after the return. Urbaniak et al. (2020) used 16S rRNA gene sequencing to analyze salivary microbes in 10 astronauts during missions of 2–9 months and observed that species richness increased significantly during space flight, but declined to preflight levels 6 months after returning to Earth. These studies are consistent with our experimental results, showing that the species richness of microorganisms increases significantly in microgravity environments. However, in this study, species richness did not return to pre-HDBR levels on day 6 of recovery, which may be because we did not observe species richness sufficiently long after HDBR. The Shannon index reflects the diversity of species, i.e., the combination of richness and evenness. The results showed no differential changes in microbial diversity during HDBR compared to pre-HDBR. Species diversity showed a significant decrease on day 6 of recovery compared to that during HDBR; however, considering no differences compared to pre-HDBR, we believe that species diversity returned to pre-HDBR levels on day 6 of recovery. Beta diversity analysis revealed significant differences in the structure of the supragingival plaque microbial community before and during HDBR and in the recovery state. Our group previously used 16S rRNA gene sequencing to

10.3389/fmicb.2024.1331023

TABLE 2 Correlations among the dominant genera in five groups.

Dominant genera		*R*				
		AP	BP	CP	DP	EP
Leptotrichia	*Fusobacterium*	−0.67	–	–	–	–
	Neisseria	−0.66	–	−0.67	–	–
	unidentified_Prevotellaceae	0.71	–	–	–	–
	unidentified_Bacteria	0.79	–	–	–	–
	unidentified_Veillonellaceae	0.73	–	–	–	0.66
	Lautropia	−0.66	–	–	–	–
Fusobacterium	*Corynebacterium*	–	–	−0.69	–	−0.60
	unidentified_Prevotellaceae	−0.63	–	0.64	–	–
	Porphyromonas	–	–	–	–	0.66
	unidentified_Veillonellaceae	−0.61	–	–	–	–
Corynebacterium	*Capnocytophaga*	–	0.75	–	–	–
	Prevotella	–	−0.70	−0.66	–	−0.65
	Porphyromonas	–	–	−0.62	–	–
	unidentified_Spirochaetaceae	–	–	−0.64	–	–
Neisseria	*unidentified_Prevotellaceae*	−0.84	−0.78	−0.66	–	–
	Capnocytophaga	0.63	–	–	–	0.85
	Prevotella	–	–	−0.71	–	−0.76
	Streptococcus	–	0.69	–	–	0.62
	Campylobacter	–	−0.60	–	–	–
	unidentified_Spirochaetaceae	–	–	–	–	−0.68
	unidentified_Veillonellaceae	−0.86	–	–	–	–
	Lautropia	0.72	–	–	–	–
unidentified_Prevotellaceae	*Capnocytophaga*	–	–	−0.66	–	–
	Prevotella	–	–	0.81	–	–
	unidentified_Bacteria	0.68	–	–	–	–
	Streptococcus	–	−0.83	–	–	–
	Campylobacter	–	0.80	–	–	–
	unidentified_Spirochaetaceae	–	–	0.65	–	–
	unidentified_Veillonellaceae	0.71	0.66	0.61	0.61	–
	Lautropia	−0.65	–	–	–	–
Capnocytophaga	*Prevotella*	–	–	−0.61	–	−0.75
	Aggregatibacter	–	–	0.62	–	–
	unidentified_Spirochaetaceae	–	–	−0.69	–	−0.60
	unidentified_Veillonellaceae	−0.71	–	–	–	–
	Lautropia	–	–	–	–	0.75
Prevotella	*Porphyromonas*	–	–	–	0.75	–
	unidentified_Spirochaetaceae	0.82	–	0.82	0.87	0.74
	Lautropia	–	–	–	–	−0.65
Porphyromonas	*unidentified_Spirochaetaceae*	–	–	–	0.76	–
Veillonella	*Campylobacter*	–	0.67	–	–	–
unidentified_Bacteria	*Aggregatibacter*	–	−0.84	–	–	−0.64
	unidentified_Veillonellaceae	0.62	0.61	–	–	–
Streptococcus	*Campylobacter*	–	−0.73	–	−0.65	–
	unidentified_Spirochaetaceae	–	−0.67	–	–	–
	unidentified_Veillonellaceae	–	−0.77	–	–	–
	Lautropia	0.78	–	–	–	–
Campylobacter	*unidentified_Veillonellaceae*	–	0.68	–	–	0.61
unidentified_Veillonellaceae	*Lautropia*	−0.69	–	–	–	–

Spearman's correlation coefficient is expressed by *R* value, and the table only shows data with correlation coefficient $|R| > 0.6$ and $p < 0.05$ between two dominant genera.

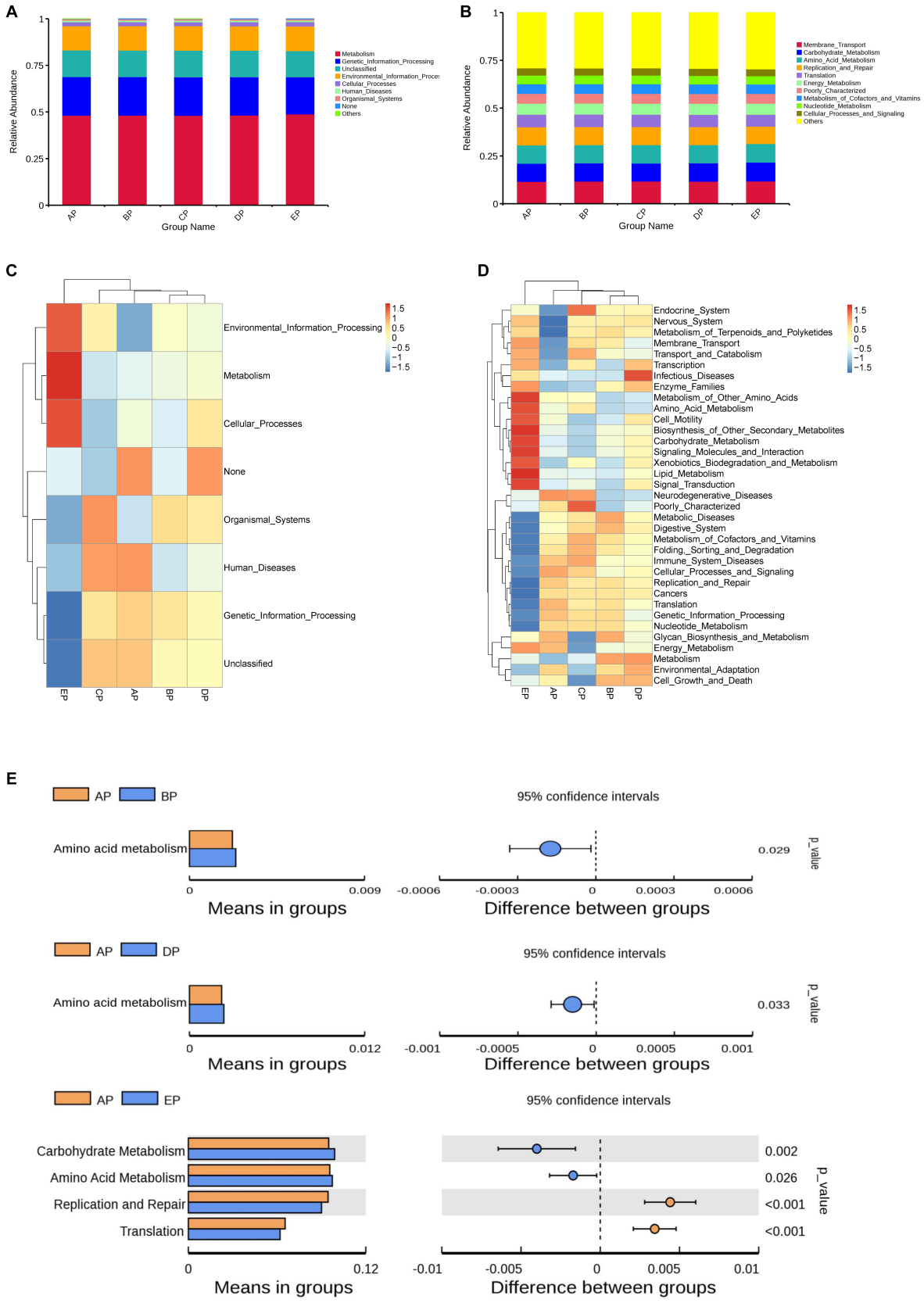

FIGURE 6
Functional genes of the samples were analyzed using the KEGG database. **(A,B)** Histograms of functional relative abundance at the first and second annotation levels. Others indicate the sum of relative abundance of all pathways other than metabolic pathways in the graph. **(C,D)** Heatmap of the top 35 functional genes in terms of relative abundance; the reference values on the top right are the correspondence between relative abundance and

(Continued)

FIGURE 6 (Continued)
color shades. **(E)** Analysis of differences in functional genes based on the *t*-test. Each bar in the figure indicates the mean value of functional genes with significant differences in abundance between groups in each group, respectively. The right side shows the confidence level of the difference between groups, the leftmost point of each circle in the figure indicates the lower limit of the 95% confidence interval of the mean difference, and the rightmost point of the circle indicates the upper limit of the 95% confidence interval of the mean difference. The center of the circle represents the difference of means. The group represented by the color of the circle is the group with the highest mean. The rightmost point of the displayed results indicates the value of *p* of the intergroup significance test corresponding to the difference species.

examine saliva samples from volunteers under simulated microgravity conditions and found that the structure of the microbial community during HDBR differed from that before HDBR (Sun et al., 2022). However, Sun et al. (2022) did not observe differences in the abundance of salivary microbial communities during HDBR compared to before HDBR. This suggests that the microbial community changes in the free state saliva and adherent state supragingival plaque in the oral cavity are different in microgravity environments. This further demonstrates the necessity of exploring the changes in different oral microniches under simulated microgravity environments.

Species distribution was analyzed among the different groups, and we observed that the relative abundance of supragingival plaque microorganisms differed at different time points. The relative abundances of *Corynebacterium* and *Aggregatibacter* increased significantly during HDBR compared to pre-HDBR, and both declined to pre-HDBR levels on day 6 of recovery. One study found that *Corynebacterium* plays a critical role in plaque formation and underlies plaque structure and community interactions (Schoilew et al., 2019). Metagenomic sequence analysis showed that *Corynebacterium* is a key taxon of supragingival plaques, constituting a hedgehog-like structure and providing a structural backbone for the aggregation of other bacteria (e.g., *Streptococcus* and *Porphyromonas*), thereby forming a polymicrobial complex (Mark Welch et al., 2016; Fakhruddin et al., 2019). Chen et al. (2021) collected oropharyngeal samples from four healthy volunteers in a 180-day ground-simulated space-enclosed environment and found *Corynebacterium* as the dominant genus, whose relative abundance increased significantly throughout the experiment. In this study, a significant increase in the relative abundance of *Corynebacterium* during HDBR may have facilitated the aggregation of more pathogenic microorganisms. *Aggregatibacter* is gram-negative bacilli that is integral to healthy oral microbial communities; however, in conditions such as trauma or mucosal damage, it invades healthy tissues, causing infection. Members of this genus identified in our analysis were *Aggregatibacter segnis* and *Aggregatibacter actinomycetemcomitans*. *A. actinomycetemcomitans* is a well-known human periodontal pathogen (Fine et al., 2019). *A. actinomycetemcomitans* can produce various virulence factors, such as leukotoxins and cell expansion lethal toxins, destroy the local immunity of the host, and help periodontal pathogens evade host immunity, leading to the occurrence and development of periodontal disease (Shenker et al., 1999; Kachlany, 2010). Simultaneously, *A. segnis* has been suggested to have adhesiveness to the cellular structure and coexists with other bacteria, causing supragingival calculus formation (Baris et al., 2017).

In contrast, the relative abundances of *Veillonella, Lautropia,* and *Streptococcus* decreased significantly during HDBR compared to pre-HDBR. On day 6 of recovery, the relative abundances of *Veillonella* and *Lautropia* increased to pre-HDBR levels, whereas the relative abundance of *Streptococcus* remained different from that of pre-HDBR. Evidence exists that *Veillonella* lacks glycolytic capacity, relies solely on lactic acid and other organic acids as energy sources, produces lower pKa acids, and may increase the pH, suggesting that *Veillonella* may have beneficial effects on the oral environment (Gross et al., 2010). Quantitative data suggest a reduction in the frequency index of isolation of *Veillonella* gingival crevicular fluid of astronauts on day 1 after space flight (Volozhin et al., 2001). Similarly, *Lautropia* is a normal oral cavity colonizer and is the dominant genus in healthy oral environments (Ikeda et al., 2020; Fragkioudakis et al., 2021). Individuals with periodontal disease have been observed to exhibit a decrease in the content of *Lautropia* (Shaddox et al., 2012). *Streptococcus* species consists of numerous opportunistic pathogens associated with dental caries. Cheng et al. (2014) found that simulating microgravity conditions can change the structure of *Streptococcus mutans* biofilms and the distribution of extracellular polysaccharides and improve the acid resistance of *S. mutans*. Brown et al. (1974) detected a significant increase in *S. mutans* counts in the dental plaque of three astronauts during a 56-day simulated space laboratory mission. Because of limited experimental conditions, they only examined quantitative changes in species.

Furthermore, a significant increase was observed in the relative abundance of *Leptotrichia* and a significant decrease in the relative abundance of *Porphyromonas* on day 6 of recovery compared to pre-HDBR and during HDBR. *Leptotrichia* is highly glycolytic and ferments a variety of monosaccharides and disaccharides into lactic acid (Birkeland and Hofstad, 1985; Thompson and Pikis, 2012). This implies that *Leptotrichia* may be involved in the development of dental caries and may have cariogenic potential. As an opportunistic pathogen, *Leptotrichia* is associated with infections, particularly in immunocompromised hosts (Eribe and Olsen, 2008; Eribe and Olsen, 2017). Moreover, Brown et al. (1976) found that 4 days after the end of a 59-day space laboratory mission, the number of *Leptotrichia* in the plaque of major aircrew increased significantly compared with that before the flight, which is consistent with our findings. *Porphyromonas* are genetically a highly heterogeneous group, and some species in this group, such as *P. pasteri* and *P. catoniae,* can be used as potential oral health markers (Crielaard et al., 2011; Yasunaga et al., 2017). However, other species, such as *P. gingivalis* and *P. endodontalis,* are closely related to the occurrence and development of oral diseases (Hajishengallis et al., 2012). The primary colonizing habitat of *P. gingivalis* in a normal oral environment is the sulcus (Reinhardt et al., 1989). However, the flow of crevicular fluid in microgravity environments may lead to the translocation of microorganisms. Shi et al. (2016) found through a rotating cell culture system that simulated microgravity promotes the growth of *P. gingivalis* and alters its gene expression.

Network analysis showed that the interaction relationships between the 15 dominant genera in the supragingival plaque

microbial community became simpler during HDBR than during pre-HDBR; however, new correlations emerged. We observed no correlation between *Porphyromonas* and *Prevotella* pre-HDBR or between *Porphyromonas* and *unidentified Spirochaetaceae*; however, a positive correlation was observed on day 15 of HDBR. The co-aggregation between *gingivalis* and *Prevotella_oris* has been proposed as a factor that promotes the advancement of periodontitis (Sato and Nakazawa, 2014). Simultaneously, *P. intermedia* exerted a synergistic effect with *P. gingivalis W83* and exacerbated the virulence of *P. gingivalis* by regulating the expression of its virulence factors (Zhang et al., 2019). Moreover, a synergistic growth relationship was observed between *P. gingivalis* and *T. denticola* (Huang et al., 2011). *P. gingivalis* produces isobutyric acid, which promotes the growth of *T. denticola* (Grenier, 1992). *T. denticola* produces succinic acid found in the phospholipids and lipids on the cell envelope of *P. gingivalis* (Lev, 1979). Therefore, we believe that alterations in the interactions between microbes may disrupt the balance of the oral microbial community structure and increase the risk of opportunistic infections. The impact of the interactions between these microbes should not be underestimated.

We also explored the alterations in microbial gene function in supragingival plaques under simulated microgravity. We found that amino acid metabolism was more abundant in the supragingival plaque microbes during HDBR, and this alteration persisted until day 6 of recovery. Current studies suggest that a complex regulatory network exists for amino acid metabolism and that acidic, basic, aromatic, and sulfur-containing amino acid metabolites produced by oral microorganisms through amino acid metabolism may negatively affect the host and exert pro-inflammatory and cytotoxic effects (Barbour et al., 2022). Moreover, environmental factors can alter the metabolic properties of certain bacteria, such as *Porphyromonas gingivalis*, *Prevotella intermedia*, and *Veillonella*, allowing them to exert different pathogenicity (Li et al., 2022). Therefore, we believe that the metabolic balance between microorganisms and their hosts plays an important role in maintaining a stable state of the body. The gene function of supragingival plaque microorganisms changed under the influence of a simulated microgravity environment, and this change persisted during the recovery period, which may lead to disturbances in oral microecology.

Overall, this study combined high-throughput sequencing technology with simulated microgravity experiments to comprehensively analyze the gene sequences of supragingival plaque microorganisms. We chose multiple time points to investigate changes in the microbial community under simulated microgravity conditions. Moreover, we explored the functions of the microbial genome to provide new insights for future studies. In the future, we will combine microbiome changes with laboratory findings to conduct metabolomic studies of supragingival plaque microorganisms in a broader population, further establish disease metabolic regulatory networks, lay the foundation for establishing *in vivo* and *ex vivo* research targets for the effects of microgravity environments on oral supragingival plaque microorganisms, and deeply explore the relationship between oral dysbiosis and immune disorders and systemic changes in the microgravity environment, providing a theoretical basis for the prevention and treatment of oral aerospace diseases.

5 Conclusion

This experimental study showed that a simulated microgravity environment with a 15-day −6° head-down bed rest would have an effect on the supragingival plaque microbial community in young men. In this state, the richness of the plaque microbial communities was significantly altered, and the community composition differed between the groups. Simultaneously, the relative abundance and functional genes of the microorganisms changed. Some of these changes persisted until the end of the experiment. This suggests that the simulated microgravity environment may affect the oral ecosystem by changing the balance of the supragingival plaque microbial community, leading to infectious diseases. Astronauts need to focus on oral hygiene care during and after spaceflight, either through a balanced diet or supplementation with specific probiotics to maintain a balanced microbial community.

Data availability statement

The original contributions presented in the study are publicly available. This data can be found here: [https://www.ncbi.nlm.nih.gov/, PRJNA1003027].

Ethics statement

The studies involving humans were approved by the Ethics Review Committee of the Space Science and Technology Institute (Shenzhen). The studies were conducted in accordance with the local legislation and institutional requirements. The participants provided their written informed consent to participate in this study.

Author contributions

DZ: Formal analysis, Validation, Writing – original draft, Writing – review & editing. PQ: Conceptualization, Investigation, Writing – review & editing. QZ: Conceptualization, Investigation. HS: Formal analysis. BX: Methodology, Resources. BW: Methodology, Resources. CT: Conceptualization, Project administration, Supervision, Writing – review & editing.

Funding

The author(s) declare that no financial support was received for the research, authorship, and/or publication of this article.

Acknowledgments

We sincerely thank all volunteers who provided samples. We thank the Space Science and Technology Institute (Shenzhen) for providing the experimental conditions. We thank Novogene Company Limited (Beijing) for sequencing the data from this study. All members of our team are thanked for their efforts to successfully complete this study.

Conflict of interest

The authors declare that the research was conducted in the absence of any commercial or financial relationships that could be construed as a potential conflict of interest.

Publisher's note

All claims expressed in this article are solely those of the authors and do not necessarily represent those of their affiliated organizations, or those of the publisher, the editors and the reviewers. Any product that may be evaluated in this article, or claim that may be made by its manufacturer, is not guaranteed or endorsed by the publisher.

Supplementary material

The Supplementary material for this article can be found online at: https://www.frontiersin.org/articles/10.3389/fmicb.2024.1331023/full#supplementary-material

References

Aarabi, G., Heydecke, G., and Seedorf, U. (2018). Roles of Oral infections in the Pathomechanism of atherosclerosis. *Int. J. Mol. Sci.* 19:1978. doi: 10.3390/ijms19071978

Al-Hebshi, N. N., Baraniya, D., Chen, T., Hill, J., Puri, S., Tellez, M., et al. (2019). Metagenome sequencing-based strain-level and functional characterization of supragingival microbiome associated with dental caries in children. *J. Oral Microbiol.* 11:1557986. doi: 10.1080/20002297.2018.1557986

Anderson, M. J. (2001). A new method for non-parametric multivariate analysis of variance. *Austral Ecol.* 26, 32–46. doi: 10.1111/j.1442-9993.2001.01070.pp.x

Atarashi, K., Suda, W., Luo, C., Kawaguchi, T., Motoo, I., Narushima, S., et al. (2017). Ectopic colonization of oral bacteria in the intestine drives TH1 cell induction and inflammation. *Science* 358, 359–365. doi: 10.1126/science.aan4526

Ball, J. R., and Evans, C. H. (2001). *Safe passage: astronaut care for exploration missions*. Washington, DC: National Academies Press.

Barbour, A., Elebyary, O., Fine, N., Oveisi, M., and Glogauer, M. (2022). Metabolites of the oral microbiome: important mediators of multikingdom interactions. *FEMS Microbiol. Rev.* 46:fuab039. doi: 10.1093/femsre/fuab039

Baris, O., Demir, T., and Gulluce, M. (2017). Investigation of in vitro mineral forming bacterial isolates from supragingival calculus. *Niger. J. Clin. Pract.* 20, 1571–1575. doi: 10.4103/1119-3077.187316

Birkeland, N. K., and Hofstad, T. (1985). Oligosaccharides obtained by partial hydrolysis of lipopolysaccharides from *Leptotrichia buccalis*. *Scand. J. Dent. Res.* 93, 432–435. doi: 10.1111/j.1600-0722.1985.tb01335.x

Bokulich, N. A., Subramanian, S., Faith, J. J., Gevers, D., Gordon, J. I., Knight, R., et al. (2013). Quality-filtering vastly improves diversity estimates from Illumina amplicon sequencing. *Nat. Methods* 10, 57–59. doi: 10.1038/nmeth.2276

Bowen, W. H. (2016). Dental caries – not just holes in teeth! A perspective. *Mol Oral Microbiol* 31, 228–233. doi: 10.1111/omi.12132

Brown, L. R., Frome, W. J., Handler, S. F., Wheatcroft, M. G., and Rider, L. J. (1977). *Skylab oral health studies*. Washington, DC: NASA.

Brown, L. R., Fromme, W. J., Handler, S. F., Wheatcroft, M. G., and Johnston, D. A. (1976). Effect of Skylab missions on clinical and microbiologic aspects of oral health. *J. Am. Dent. Assoc.* 93, 357–363. doi: 10.14219/jada.archive.1976.0502

Brown, L. R., Wheatcroft, M. G., Frome, W. J., and Rider, L. J. (1974). Effects of a simulated Skylab mission on the oral health of astronauts. *J. Dent. Res.* 53, 1268–1275. doi: 10.1177/00220345740530053201

Caporaso, J. G., Kuczynski, J., Stombaugh, J., Bittinger, K., Bushman, F. D., Costello, E. K., et al. (2010). QIIME allows analysis of high-throughput community sequencing data. *Nat. Methods* 7, 335–336. doi: 10.1038/nmeth.f.303

Chapman, M. G., and Underwood, A. J. (1999). Ecological patterns in multivariate assemblages: information and interpretation of negative values in ANOSIM tests. *Mar. Ecol. Prog. Ser.* 180, 257–265. doi: 10.3354/meps180257

Chen, Y., Xu, C., Zhong, C., Lyu, Z., Liu, J., Chen, Z., et al. (2021). Temporal characteristics of the oropharyngeal and nasal microbiota structure in crewmembers stayed 180 days in the controlled ecological life support system. *Front. Microbiol.* 11:617696. doi: 10.3389/fmicb.2020.617696

Cheng, X., Xu, X., Chen, J., Zhou, X., Cheng, L., Li, M., et al. (2014). Effects of simulated microgravity on *Streptococcus mutans* physiology and biofilm structure. *FEMS Microbiol. Lett.* 359, 94–101. doi: 10.1111/1574-6968.12573

Crielaard, W., Zaura, E., Schuller, A. A., Huse, S. M., Montijn, R. C., and Keijser, B. J. (2011). Exploring the oral microbiota of children at various developmental stages of their dentition in the relation to their oral health. *BMC Med. Genet.* 4:22. doi: 10.1186/1755-8794-4-22

Crucian, B., Stowe, R. P., Mehta, S., Quiriarte, H., Pierson, D., and Sams, C. (2015). Alterations in adaptive immunity persist during long-duration spaceflight. *NPJ Microgravity* 1:15013. doi: 10.1038/npjmgrav.2015.13

Darveau, R. P., Tanner, A., and Page, R. C. (1997). The microbial challenge in periodontitis. *Periodontol* 2000, 12–32. doi: 10.1111/j.1600-0757.1997.tb00190.x

Edgar, R. C. (2004). MUSCLE: multiple sequence alignment with high accuracy and high throughput. *Nucleic Acids Res.* 32, 1792–1797. doi: 10.1093/nar/gkh340

Edgar, R. C. (2013). UPARSE: highly accurate OTU sequences from microbial amplicon reads. *Nat. Methods* 10, 996–998. doi: 10.1038/nmeth.2604

Eribe, E. R., and Olsen, I. (2008). Leptotrichia species in human infections. *Anaerobe* 14, 131–137. doi: 10.1016/j.anaerobe.2008.04.004

Eribe, E. R. K., and Olsen, I. (2017). Leptotrichia species in human infections II. *J. Oral Microbiol.* 9:1368848. doi: 10.1080/20002297.2017.1368848

Fakhruddin, K. S., Ngo, H. C., and Samaranayake, L. P. (2019). Cariogenic microbiome and microbiota of the early primary dentition: a contemporary overview. *Oral Dis.* 25, 982–995. doi: 10.1111/odi.12932

Fine, D. H., Patil, A. G., and Velusamy, S. K. (2019). *Aggregatibacter actinomycetemcomitans* (Aa) under the radar: myths and misunderstandings of aa and its role in aggressive periodontitis. *Front. Immunol.* 10:728. doi: 10.3389/fimmu.2019.00728

Foster, J. S., Khodadad, C. L., Ahrendt, S. R., and Parrish, M. L. (2013). Impact of simulated microgravity on the normal developmental time line of an animal-bacteria symbiosis. *Sci. Rep.* 3:1340. doi: 10.1038/srep01340

Fragkioudakis, I., Riggio, M. P., and Apatzidou, D. A. (2021). Understanding the microbial components of periodontal diseases and periodontal treatment-induced microbiological shifts. *J. Med. Microbiol.* 70. doi: 10.1099/jmm.0.001247

Gontcharov, I. B., Kovachevich, I. V., Pool, S. L., Navinkov, O. L., Barratt, M. R., Bogomolov, V. V., et al. (2005). In-flight medical incidents in the NASA-Mir program. *Aviat. Space Environ. Med.* 76, 692–696.

Graebe, A., Schuck, E. L., Lensing, P., Putcha, L., and Derendorf, H. (2004). Physiological, pharmacokinetic, and pharmacodynamic changes in space. *J. Clin. Pharmacol.* 44, 837–853. doi: 10.1177/0091270004267193

Grenier, D. (1992). Nutritional interactions between two suspected periodontopathogens, Treponema denticola and *Porphyromonas gingivalis*. *Infect. Immun.* 60, 5298–5301. doi: 10.1128/iai.60.12.5298-5301.1992

Grenon, S. M., Saary, J., Gray, G., Vanderploeg, J. M., and Hughes-Fulford, M. (2012). Can I take a space flight? Considerations for doctors. *BMJ* 345:e8124. doi: 10.1136/bmj.e8124

Grimm, D., Grosse, J., Wehland, M., Mann, V., Reseland, J. E., Sundaresan, A., et al. (2016). The impact of microgravity on bone in humans. *Bone* 87, 44–56. doi: 10.1016/j.bone.2015.12.057

Gross, E. L., Leys, E. J., Gasparovich, S. R., Firestone, N. D., Schwartzbaum, J. A., Janies, D. A., et al. (2010). Bacterial 16S sequence analysis of severe caries in young permanent teeth. *J. Clin. Microbiol.* 48, 4121–4128. doi: 10.1128/JCM.01232-10

Haas, B. J., Gevers, D., Earl, A. M., Feldgarden, M., Ward, D. V., Giannoukos, G., et al. (2011). Chimeric 16S rRNA sequence formation and detection in sanger and 454-pyrosequenced PCR amplicons. *Genome Res.* 21, 494–504. doi: 10.1101/gr.112730.110

Hajishengallis, G., Darveau, R. P., and Curtis, M. A. (2012). The keystone-pathogen hypothesis. *Nat. Rev. Microbiol.* 10, 717–725. doi: 10.1038/nrmicro2873

Hargens, A. R., and Vico, L. (2016). Long-duration bed rest as an analog to microgravity. *J. Appl. Physiol.* 120, 891–903. doi: 10.1152/japplphysiol.00935.2015

Huang, R., Li, M., and Gregory, R. L. (2011). Bacterial interactions in dental biofilm. *Virulence* 2, 435–444. doi: 10.4161/viru.2.5.16140

Huang, B., Li, D. G., Huang, Y., and Liu, C. T. (2018). Effects of spaceflight and simulated microgravity on microbial growth and secondary metabolism. *Mil. Med. Res.* 5:18. doi: 10.1186/s40779-018-0162-9

Ikeda, E., Shiba, T., Ikeda, Y., Suda, W., Nakasato, A., Takeuchi, Y., et al. (2020). Japanese subgingival microbiota in health vs disease and their roles in predicted functions associated with periodontitis. *Odontology* 108, 280–291. doi: 10.1007/s10266-019-00452-4

Ilyin, V. K. (2005). Microbiological status of cosmonauts during orbital spaceflights on Salyut and Mir orbital stations. *Acta Astronaut.* 56, 839–850. doi: 10.1016/j.actaastro.2005.01.009

Jagathrakshakan, S. N., Sethumadhava, R. J., Mehta, D. T., and Ramanathan, A. (2015). 16S rRNA gene-based metagenomic analysis identifies a novel bacterial co-prevalence pattern in dental caries. *Eur. J. Dent.* 9, 127–132. doi: 10.4103/1305-7456.149661

Johnston, R. S., and Dietlein, L. F. (1977). *Biomedical results from Skylab*. Washington, DC: NASA.

Kachlany, S. C. (2010). *Aggregatibacter actinomycetemcomitans* leukotoxin: from threat to therapy. *J. Dent. Res.* 89, 561–570. doi: 10.1177/0022034510363682

Klaus, D. M., and Howard, H. N. (2006). Antibiotic efficacy and microbial virulence during space flight. *Trends Biotechnol.* 24, 131–136. doi: 10.1016/j.tibtech.2006.01.008

Kumar, P. S., Leys, E. J., Bryk, J. M., Martinez, F. J., Moeschberger, M. L., and Griffen, A. L. (2006). Changes in periodontal health status are associated with bacterial community shifts as assessed by quantitative 16S cloning and sequencing. *J. Clin. Microbiol.* 44, 3665–3673. doi: 10.1128/JCM.00317-06

Kwun, J.-S., Kang, S.-H., Lee, H.-J., Park, H.-K., Lee, W.-J., Yoon, C.-H., et al. (2020). Comparison of thrombus, gut, and oral microbiomes in Korean patients with ST-elevation myocardial infarction: a case-control study. *Exp. Mol. Med.* 52, 2069–2079. doi: 10.1038/s12276-020-00543-1

Lev, M. (1979). Sphingolipid biosynthesis and vitamin K metabolism in *Bacteroides melaninogenicus*. *Am. J. Clin. Nutr.* 32, 179–186. doi: 10.1093/ajcn/32.1.179

Li, Y. C., Zhang, S. W., and Pan, Y. P. (2022). Effects of oral bacterial metabolites on systemic diseases. *Zhonghua Kou Qiang Yi Xue Za Zhi* 57, 648–653. doi: 10.3760/cma.j.cn112144-20220325-00132

Lozupone, C. A., Hamady, M., Kelley, S. T., and Knight, R. (2007). Quantitative and qualitative beta diversity measures lead to different insights into factors that structure microbial communities. *Appl. Environ. Microbiol.* 73, 1576–1585. doi: 10.1128/AEM.01996-06

Lozupone, C., Lladser, M. E., Knights, D., Stombaugh, J., and Knight, R. (2011). UniFrac: an effective distance metric for microbial community comparison. *ISME J.* 5, 169–172. doi: 10.1038/ismej.2010.133

Magoč, T., and Salzberg, S. L. (2011). FLASH: fast length adjustment of short reads to improve genome assemblies. *Bioinformatics* 27, 2957–2963. doi: 10.1093/bioinformatics/btr507

Mark Welch, J. L., Rossetti, B. J., Rieken, C. W., Dewhirst, F. E., and Borisy, G. G. (2016). Biogeography of a human oral microbiome at the micron scale. *Proc. Natl. Acad. Sci. U. S. A.* 113, E791–E800. doi: 10.1073/pnas.1522149113

Marsh, P. D. (2003). Are dental diseases examples of ecological catastrophes? *Microbiology* 149, 279–294. doi: 10.1099/mic.0.26082-0

Marsh, P. D. (2012). Contemporary perspective on plaque control. *Br. Dent. J.* 212, 601–606. doi: 10.1038/sj.bdj.2012.524

Pavy-Le Traon, A., Heer, M., Narici, M. V., Rittweger, J., and Vernikos, J. (2007). From space to earth: advances in human physiology from 20 years of bed rest studies (1986-2006). *Eur. J. Appl. Physiol.* 101, 143–194. doi: 10.1007/s00421-007-0474-z

Poncheewin, W., Hermes, G. D. A., van Dam, J. C. J., Koehorst, J. J., Smidt, H., and Schaap, P. J. (2019). NG-tax 2.0: a semantic framework for high-throughput amplicon analysis. *Front. Genet.* 10:1366. doi: 10.3389/fgene.2019.01366

Quast, C., Pruesse, E., Yilmaz, P., Gerken, J., Schweer, T., Yarza, P., et al. (2013). The SILVA ribosomal RNA gene database project: improved data processing and web-based tools. *Nucleic Acids Res.* 41, D590–D596. doi: 10.1093/nar/gks1219

Rai, D. B. (2009). Human oral cavity in simulated microgravity: new prospects. *Adv. Med. Dent. Sci.* 3, 35–39.

Reinhardt, R. A., McDonald, T. L., Bolton, R. W., DuBois, L. M., and Kaldahl, W. B. (1989). IgG subclasses in gingival crevicular fluid from active versus stable periodontal sites. *J. Periodontol.* 60, 44–50. doi: 10.1902/jop.1989.60.1.44

Roewer, L., Kayser, M., Dieltjes, P., Nagy, M., Bakker, E., Krawczak, M., et al. (1996). Analysis of molecular variance (AMOVA) of Y-chromosome-specific microsatellites in two closely related human populations. *Hum. Mol. Genet.* 5, 1029–1033. doi: 10.1093/hmg/5.7.1029

Rognes, T., Flouri, T., Nichols, B., Quince, C., and Mahé, F. (2016). VSEARCH: a versatile open source tool for metagenomics. *PeerJ* 4:e2584. doi: 10.7717/peerj.2584

Sato, T., and Nakazawa, F. (2014). Coaggregation between Prevotella oris and *Porphyromonas gingivalis*. *J. Microbiol. Immunol. Infect.* 47, 182–186. doi: 10.1016/j.jmii.2012.09.005

Schoilew, K., Ueffing, H., Dalpke, A., Wolff, B., Frese, C., Wolff, D., et al. (2019). Bacterial biofilm composition in healthy subjects with and without caries experience. *J. Oral Microbiol.* 11:1633194. doi: 10.1080/20002297.2019.1633194

Shaddox, L. M., Huang, H., Lin, T., Hou, W., Harrison, P. L., Aukhil, I., et al. (2012). Microbiological characterization in children with aggressive periodontitis. *J. Dent. Res.* 91, 927–933. doi: 10.1177/0022034512456039

Shenker, B. J., McKay, T., Datar, S., Miller, M., Chowhan, R., and Demuth, D. (1999). *Actinobacillus actinomycetemcomitans* immunosuppressive protein is a member of the family of cytolethal distending toxins capable of causing a G2 arrest in human T cells. *J. Immunol.* 162, 4773–4780. doi: 10.4049/jimmunol.162.8.4773

Shi, X., Lu, Y., Tang, C., and Niu, Z. (2016). Effect of simulated microgravity on *Porphyromonas gingivalis* strain ATCC33277 growth and gene expression. *Int. J. Clin. Exp. Pathol.* 9, 3143–3151.

Shi, W., Tian, J., Xu, H., Zhou, Q., and Qin, M. (2018). Distinctions and associations between the microbiota of saliva and supragingival plaque of permanent and deciduous teeth. *PLoS One* 13:e0200337. doi: 10.1371/journal.pone.0200337

Sun, H., Zhou, Q., Qiao, P., Zhu, D., Xin, B., Wu, B., et al. (2022). Short-term head-down bed rest microgravity simulation alters salivary microbiome in young healthy men. *Front. Microbiol.* 13:1056637. doi: 10.3389/fmicb.2022.1056637

Sundblad, P., Orlov, O., Angerer, O., Larina, I., and Cromwell, R. (2016). Standardization of bed rest studies in the spaceflight context. *J. Appl. Physiol.* 121, 348–349. doi: 10.1152/japplphysiol.00089.2016

Thompson, J., and Pikis, A. (2012). Metabolism of sugars by genetically diverse species of oral Leptotrichia. *Mol Oral Microbiol* 27, 34–44. doi: 10.1111/j.2041-1014.2011.00627.x

Urbaniak, C., Lorenzi, H., Thissen, J., Jaing, C., Crucian, B., Sams, C., et al. (2020). The influence of spaceflight on the astronaut salivary microbiome and the search for a microbiome biomarker for viral reactivation. *Microbiome* 8:56. doi: 10.1186/s40168-020-00830-z

Volozhin, A. I., Tsarev, V. N., Malneva, N. S., Sashkina, T. I., and Saldusova, I. V. (2001). Interaction peculiarities between microbial cenosis and local immunity of periodontium of humans under extreme conditions. *Acta Astronaut.* 49, 53–57. doi: 10.1016/s0094-5765(00)00128-4

White, R. J., and Averner, M. (2001). Humans in space. *Nature* 409, 1115–1118. doi: 10.1038/35059243

Wilson, J. W., Ott, C. M., zu Bentrup, K. H., Ramamurthy, R., Quick, L., Porwollik, S., et al. (2007). Space flight alters bacterial gene expression and virulence and reveals a role for global regulator Hfq. *Proc. Natl. Acad. Sci. U. S. A.* 104, 16299–16304. doi: 10.1073/pnas.0707155104

Yang, X., He, L., Yan, S., Chen, X., and Que, G. (2021). The impact of caries status on supragingival plaque and salivary microbiome in children with mixed dentition: a cross-sectional survey. *BMC Oral Health* 21:319. doi: 10.1186/s12903-021-01683-0

Yasunaga, H., Takeshita, T., Shibata, Y., Furuta, M., Shimazaki, Y., Akifusa, S., et al. (2017). Exploration of bacterial species associated with the salivary microbiome of individuals with a low susceptibility to dental caries. *Clin. Oral Investig.* 21, 2399–2406. doi: 10.1007/s00784-016-2035-5

Yoshioka, H., Yoshimura, A., Kaneko, T., Golenbock, D. T., and Hara, Y. (2008). Analysis of the activity to induce toll-like receptor (TLR)2- and TLR4-mediated stimulation of supragingival plaque. *J. Periodontol.* 79, 920–928. doi: 10.1902/jop.2008.070516

Zhang, Y., Shi, W., Song, Y., and Wang, J. (2019). Metatranscriptomic analysis of an in vitro biofilm model reveals strain-specific interactions among multiple bacterial species. *J. Oral Microbiol.* 11:1599670. doi: 10.1080/20002297.2019.1599670

Zhang, S., Yu, N., and Arce, R. M. (2020). Periodontal inflammation: integrating genes and dysbiosis. *Periodontol.* 82, 129–142. doi: 10.1111/prd.12267

frontiers | Frontiers in Microbiology

TYPE Original Research
PUBLISHED 24 January 2024
DOI 10.3389/fmicb.2023.1336345

Check for updates

OPEN ACCESS

EDITED BY
Zhenlin Han,
University of Hawaii at Manoa, United States

REVIEWED BY
Vipin Rana,
University of Maryland, College Park, United States
Haijian Huang,
Ningbo University, China

*CORRESPONDENCE
Dong Chu
✉ chinachudong@qau.edu.cn

RECEIVED 10 November 2023
ACCEPTED 26 December 2023
PUBLISHED 24 January 2024

CITATION
Yang K, Zhang H-Y, Wang P, Jin G-X and Chu D (2024) Both symbionts and environmental factors contribute to shape the microbiota in a pest insect, *Sogatella furcifera*.
Front. Microbiol. 14:1336345.
doi: 10.3389/fmicb.2023.1336345

COPYRIGHT
© 2024 Yang, Zhang, Wang, Jin and Chu. This is an open-access article distributed under the terms of the Creative Commons Attribution License (CC BY). The use, distribution or reproduction in other forums is permitted, provided the original author(s) and the copyright owner(s) are credited and that the original publication in this journal is cited, in accordance with accepted academic practice. No use, distribution or reproduction is permitted which does not comply with these terms.

Both symbionts and environmental factors contribute to shape the microbiota in a pest insect, *Sogatella furcifera*

Kun Yang[1,2], Hua-Yue Zhang[1,2], Peng Wang[1,2], Gui-Xiu Jin[3] and Dong Chu[1,2]*

[1]Shandong Engineering Research Center for Environment-friendly Agricultural Pest Management, College of Plant Health and Medicine, Qingdao Agricultural University, Qingdao, China, [2]Shandong Province Centre for Bioinvasions and Eco-security, Qingdao, China, [3]Linyi Academy of Agricultural Sciences, Linyi, China

Introduction: Bacterial symbionts are prevalent in arthropods globally and play a vital role in the fitness and resistance of hosts. While several symbiont infections have been identified in the white-backed planthopper Sogatella furcifera, the impact of environmental factors on the microbiota within *S. furcifera* remains elusive.

Methods: In this study, a total of 142 S. furcifera individuals from 18 populations were collected from 14 locations across six countries (China, Thailand, Myanmar, Cambodia, Vietnam, and Laos) analyzed with 2bRAD-M sequencing, to examine the effects of symbionts on the microbiota in the *S. furcifera* population, as well as the vital effects of environmental factors on the bacterial communities.

Results and discussion: Based on the results, in *S. furcifera*, the presence of symbionts Wolbachia and Cardinium negatively influenced the abundance of other bacteria, including Enterobacter, Acinetobacter, and Lysinibacillus, while Wolbachia infection significantly decreased the diversity of the microbial community. Moreover, several environmental factors, including longitude, latitude, temperature, and precipitation, affected the abundance of symbionts and microbiota diversity in *S. furcifera*. These results collectively highlight the vital role of Wolbachia in *S. furcifera* microbiota, as well as the intricate effects of environmental factors on the bacterial communities of *S. furcifera*.

KEYWORDS

***Sogatella furcifera*, *Wolbachia*, *Cardinium*, 2bRAD-M sequencing, environmental factors**

1 Introduction

As a significant pest in China and South Asia, the white-backed planthopper (WBPH), scientifically referred to as *Sogatella furcifera* (Hemiptera: Delphacidae), causes substantial losses on agricultural fields, particularly rice paddies (Savary et al., 2012; Huang and Qin, 2018). *S. furcifera* causes damage by sucking phloem sap from rice plants and transmitting viruses, including the southern rice black-streaked dwarf virus, to rice hosts (Zhou et al., 2008, 2018). Over the past decade, the frequency of *S. furcifera* outbreaks has dramatically increased, making it a destructive pest in rice production (Hu et al., 2015; Wang et al., 2018). With its high adaptability, long-distance migratory abilities, and the development of resistance to existing pesticides, managing *S. furcifera* outbreaks has become increasingly challenging

(Wang et al., 2019). Coupled with the growing problem of pesticide residue, there is an urgent need to develop novel and efficient methods to mitigate the damage elicited by pest insects, including *S. furcifera*.

Microbial communities, especially bacteria, including endosymbionts, play a vital role in the development, fitness, fecundity, and resistance of host arthropods (Douglas, 2009; McFall-Ngai et al., 2013). These symbiotic bacteria fall into two categories: primary symbionts (obligate symbionts) and secondary symbionts (facultative symbionts), residing predominantly in bacteriocytes within hosts and exerting complex influences on host arthropods (Werren et al., 2008; Zeng et al., 2018; Yang et al., 2022). The former is essential for the development and survival of host invertebrates. For instance, the symbiont *Portiera* provides essential amino acids (EAA) and B vitamins to whitefly hosts (Wang et al., 2022), whilst the symbiont *Buchnera* supplies aphid hosts with various nutritional elements and protects them from heat stress (Dunbar et al., 2007; Douglas, 2009).

Wolbachia, the most renowned symbiont in invertebrates, was first discovered in mosquitoes in 1924 (Hertig and Wolbach, 1924). Interestingly, it can infect at least 66% of all arthropod species (Werren, 1997; Miao et al., 2020). In filarial nematodes, *Wolbachia* is regarded as an obligate mutualist, essential for the development and fertility of host nematodes (Taylor et al., 2005; Wasala et al., 2019). Previously considered reproductive parasitism in invertebrates, capable of manipulating host reproduction through phenomena such as cytoplasmic incompatibility, feminization, parthenogenesis, and male-killing (Werren et al., 2008), recent studies have established the benefits conferred by *Wolbachia* (Zug and Hammerstein, 2015). Another study corroborated the influence of *Wolbachia* on microbial communities in small planthoppers (Duan et al., 2020). However, the intricate interaction between *Wolbachia* and the bacterial community in arthropods warrants further investigations.

Microbial communities, including symbionts in arthropods, are influenced by various biotic and abiotic factors. For example, high temperatures significantly influence symbiont titer and the diversity of the bacterial community in whiteflies (Yang et al., 2022). Similarly, the diet of invertebrate hosts significantly impacts the structure of microbial communities (Santo Domingo et al., 1998; Colman et al., 2012), and both temperature and humidity affect bacterial communities (Behar et al., 2008). Furthermore, earlier research has documented the crucial impact of host genetic backgrounds on microbiota (Suzuki et al., 2019; Gupta and Nair, 2020). Interestingly, the presence of symbionts exerts a significant influence on microbial communities. Symbionts occupy a relatively large space and engage in competition with other bacteria for nutrients. According to a prior study, *Spiroplasma* infection significantly decreases the titer of *Wolbachia* in the same host (Goto et al., 2006). Additionally, endosymbionts such as *Wolbachia* and *Cardinium* can lower the microbiome diversity of the host *Sogatella furcifera* (Li et al., 2022). The complex effects of symbionts on the microbiota of *S. furcifera* require further investigation.

2bRAD-M sequencing is a novel method that is efficient in detecting low-biomass microbiomes at the species level with high fidelity (Sun et al., 2022). In recent years, the damage caused by *S. furcifera* has drammatically rapidly, particularly in Asia and China. However, the complex interactions between the bacterial community of *S. furcifera,* including bacterial symbionts and environmental factors, remain poorly understood. Moreover, the potential application of symbionts in the biocontrol of *S. furcifera* is an area that warrants exploration. In this study, 18 *S. furcifera* populations sourced from six Asian countries were subjected to 2bRAD-M sequencing in order to unravel the vital factors contributing to shaping microbial communities in *S. furcifera*. Moreover, this comprehensive study explored the effects of symbionts and environmental factors on bacterial communities.

2 Materials and methods

2.1 Collection of *Sogatella furcifera* populations in China and South Asia

To determine the relationships among symbionts, bacterial communities in *S. furcifera,* and environmental factors, a total of 142 *S. furcifera* individuals from 18 populations were collected from 14 locations across six countries (China, Thailand, Myanmar, Cambodia, Vietnam, and Laos) analyzed in this study. Each *S. furcifera* population comprised at least six independent samples. All *S. furcifera* samples were preserved in 100% alcohol and subsequently dispatched for 2bRAD-M sequencing. Information about the samples is detailed in Table 1 and Supplementary Table S1, wherein each replicate represents an independent *S. furcifera* adult.

2.2 DNA extraction and 2bRAD-M sequencing

Bacterial communities in *S. furcifera* were analyzed using the 2bRAD-M sequencing methods. 2bRAD-M sequencing and library construction were performed by Qingdao OE Biotech Co., Ltd. (Qingdao, China), following previously established protocols (Wang et al., 2012) with marginal modifications. Briefly, the DNA (100 ng) from each sample was digested using 4 U of the BcgI enzyme (NEB) at 37°C for 3 h. Next, the resulting DNA fragments were ligated with specific adaptors. A mix of 5 μL of digested DNA and 10 μL of ligation master mix, containing 0.2 μM of each adaptor and 800 U of T4 DNA ligase (NEB), underwent a ligation reaction at 4°C for 12 h.

Following ligation, the products were PCR amplified, and the resulting DNA was subjected to electrophoresis on an 8% polyacrylamide gel. An approximately 100-bp band was excised, and the DNA fragments were then diffused in DEPC water at 4°C for 12 h. A PCR test was conducted using primers bearing platform-specific barcodes to introduce sample-specific barcodes. Each PCR sample, totaling 20 μL, contained 25-ng of gel-extracted PCR product, 0.2 μM each of forward and reverse primers, 0.3 mM dNTP mix, 0.4 U Phusion high-fidelity DNA polymerase (NEB), and 1 × Phusion HF buffer. After PCR amplification and electrophoresis, the PCR products were purified using the QIAquick PCR purification kit (50) (Qiagen) and sequenced on the Illumina Nova PE150 platform.

2.3 Data analysis of 2bRAD-M sequencing results

To conduct the 2bRAD-M analysis, microbial genome data from the NCBI database, consisting of 173,165 species of fungi, bacteria, and archaea, were employed. Restriction enzymes of 16 type 2B were utilized to fragment the samples, and Perl scripts were

10.3389/fmicb.2023.1336345

TABLE 1 Collection information of *Sogatella furcifera* populations used in this experiment.

Population name	Collection location	Longitude	Latitude	Elevation	Collection date	Replicates	Host plants
VE	Vientiane, Laos	N18.215171	E102.502263		2014.3.18	12	Rice
SA	Sawakeexay Village,Hinhoun District,Khammvean Province. Laos	N17.724459	E104.567768	130	2014.3.20	8	Rice
1 M	Rangoon, Myanmar	N16.78333	E96.16667	15		8	Rice
2 M	Rangoon, Myanmar	N16.78333	E96.16667	15		8	Rice
CH	Changmai-Mangkok, Thailand	N16.487457	E99.485583	53	2014.5.14	7	Rice
RO	Royal university of agriculture, Cambodia	N11.513352	E104.901175	12	2014.3.24	6	Rice
KO	KomReurk,district,Siem Reap city,Siew Reap province, Cambodia	N13.336719	E103.661119	7	2014.3.27	6	Rice
LU	Luong Ninh commune,Quang Ninh district,Quang Ninh province, Vietnam	N17.428303	E106.633235	10	2014.4.17	6	Rice
LO	Los son commune,Phu loo district,Hue province, Vietnam	N16.331932	E107.750584	1.4	2014.4.18	8	Rice
BS	Baoshan, Yunnan Province, China	N25.057464	E99.163658	1699.9	2014.6.26	8	Rice
CX	Chuxiong, Yunnan Province, China	N25.086440	E101.467300	1812.8	2014.6.26	8	Rice
FN	Funing, Yunnan Province, China	N23.625847	E105.630900	680	2014.6.10	8	Rice
GM	Gengma, Yunnan Province, China	N23.538747	E99.397175	1,116	2014.7.10	8	Rice
JY	Jiyang, Jinan, Shandong Province, China	N36.972935	E117.21142	21		8	Rice
MH	Menghai, Yunnan Province, China	N21.966323	E100.449572	1,230	2014.5.15	8	Rice
TC	Tancheng, Linyi, Shandong Province, China	N34.61354	E118.36712	47		6	Rice
YT	Yutai, Jining, Shandong Province, China	N35	E116.65	35		7	Rice
ZY	Zhaoyang, Yunnan Province, China	N27.320429	E103.706542	1907	2014.7.10	12	Rice

One replicate in Table 1. Means an independent female adult sequenced by 2bRAD-M in this experiment.

used in this process. Thereafter, the RefSeq (GCF) number was used to assign 2bRAD-M tags with microbial genome information, including taxonomic data. Unique 2bRAD tags occurring only once in every GCF were selected as species-specific 2bRAD-M markers, forming a reference database. A detection threshold of 0.0001 (0.01%) relative abundance was set as the default (Franzosa et al., 2018).

To calculate the relative abundance of each bacterium, 2bRAD tags from all samples, post-quality control, were mapped against the 2bRAD marker database containing tags unique to the 26,163 microbial species using a built-in Perl script. To mitigate false positives in species identification, a G score was calculated for each identified species within a given sample. This score, derived from a harmonic means of read coverage of 2bRAD markers belonging to a species and the total number of possible 2bRAD markers for this species, was employed identify species while minimizing errors. A threshold G score of 5 was set to prevent false-positive microbial species discovery (Sun et al., 2022).

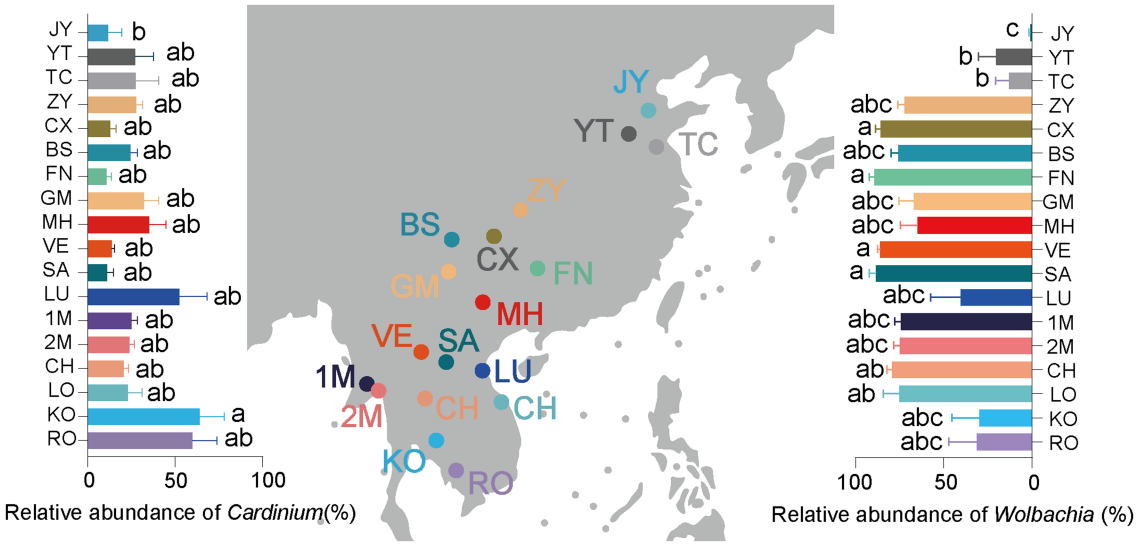

FIGURE 1
Relative infection abundance of *Cardinium* (left panel), *Wolbachia* (right panel) and collection sites (middle panel) of *Sogatella furcifera* across 18 geographical locations by 2bRAD-M sequencing. As the symbiont infection data do not follow a normal distribution, the difference of *Wolbachia* abundance in various *S. furcifera* populations was analyzed by Kruskal–Wallis test and Dunn's test with Bonferroni correction for multiple comparisons by SPSS 21.0, different letters represent significant difference.

$$\text{G score}_{\text{species i}} = \sqrt{S_i \times t_i}$$

S: the number of reads assigned to all 2bRAD markers belonging to species *i* within a sample.

T: number of all 2bRAD markers of species i that have been sequenced within a sample.

The average read coverage of all 2bRAD markers for each species was computed to represent the number of individuals of a species present within a sample at a given sequencing depth. The relative abundance of a species was then calculated as the ratio of the number of microbial individuals belonging to that species against the total number of individuals from known species detected within a sample.

$$\textit{Relative abundance}_{\textit{species i}} = \frac{S_i / T_i}{\sum_{i=1}^{n} S_i / T_i}$$

S: the number of reads assigned to all 2bRAD markers of species *i* within a sample.

T: the number of all theoretical 2bRAD markers of species *i*.

Additionally, five environmental factors, namely annual mean temperature, annual precipitation, longitude, latitude, and altitude, were analyzed in the study. Data for these factors were downloaded from the WorldClim website.[1] The impacts of climate and geographical factors on diversity and abundance indexes and symbiont infections were described using two structural equation models (SEM) with Satorra-Bentler correction. To limit heteroscedasticity, the log value of the "precipitation" values was used in the SEMs. SEM models were deemed acceptable when p value >0.05 and CFI > 0.95, after systematically excluding redundant pathways based on a lower AIC value. To standardize each parameter and eliminate variance, SEM coefficients were estimated through standardized transformation. Prior to analysis, data on *Cardinium* abundance (shown in Figure 1 left panel), *Wolbachia* abundance (shown in Figure 1 right panel), and microbial diversities of samples (shown in Figure 2) underwent normality testing using the Kolmogorov–Smirnov test and Levene's test to assess the homogeneity of group variances. Data exhibiting a normal distribution were analyzed using one-way ANOVA with post-hoc Tukey HSD. In cases where the *Cardinium* abundance, *Wolbachia* abundance, and diversity data did not conform to normal distribution, they were analyzed using the Kruskal-Wallis test and Dunn's test with Bonferroni correction for multiple comparisons. All statistical analyzes were conducted using SPSS 21.0. PCoA plots illustrating Bray-Curtis intersample distances and classification probabilities were generated using QIIME software (Caporaso et al., 2010). Pearson correlation analysis, performed using SPSS 21.0, was used to explore the relationships between different symbionts and diversity indexes. Furthermore, all graphical representations were generated using GraphPad Prism 9.0.0.

3 Results

3.1 Composition of bacterial communities in different *Sogatella furcifera* populations

In the current study, a total of 18 *S. furcifera* populations were analyzed, comprising 9 populations from China and 9 populations from the South Asian region. The predominant bacterial symbionts identified in all *S. furcifera* populations were *Wolbachia* and *Cardinium*.

1 https://worldclim.org/

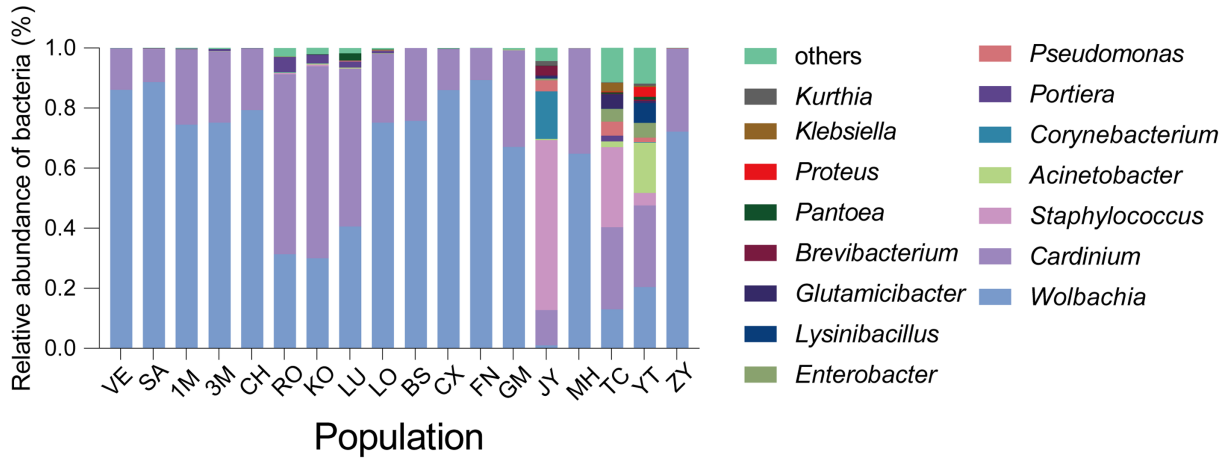

FIGURE 2
The abundance of microbial communities of *Sogatella furcifera* across 18 populations collected in Asia based on 2bRAD-M sequencing results. The relative abundance of top 15 abundant bacteria at the genus level was shown with different populations.

Interestingly, the former was the most abundant bacteria in nearly all *S. furcifera* populations, being present in every *S. furcifera* sample. Notably, the relative abundance of *Wolbachia* exceeded 80% in two Chinese populations, specifically CS (85.95 ± 2.92%, Mean ± SEM) and FN (89.26 ± 3.01%, Mean ± SEM), as well as in all Laos populations, including VE (86.02 ± 1.57%, Mean ± SEM) and SA (86.02 ± 3.58%, Mean ± SEM). Nevertheless, significant variations in *Wolbachia* abundance were observed among different populations. Meanwhile, 3 *S. furcifera* populations from China (JY, YT, and TC) exhibited the lowest *Wolbachia* abundance, significantly lower than the *Wolbachia*-abundant populations such as FN, VE, and SA (Figure 1 right panel). *Cardinium* emerged as the second most abundant bacterium in *S. furcifera* (Figure 1 left panel). In several South Asia populations, including KO (63.88 ± 14.38%, Mean ± SEM), RO (59.96 ± 14.04%, Mean ± SEM), and LU (52.50 ± 15.74%, Mean ± SEM) as well as one Chinese population, YT (27.18 ± 10.38%, Mean ± SEM) *Cardinium* was the dominant symbiont, with its abundance in the KO population being significantly higher than that in the JY population (11.72 ± 7.78%, Mean ± SEM) ($p < 0.05$, Kruskal-Wallis test). Besides, *Wolbachia* abundance was less than 1% in the JY population, while *Cardinium* abundance was the highest (56.59 ± 11.90%, Mean ± SEM). Additionally, the primary symbiont *Portiera*, typically associated with whiteflies, was also detected in several *S. furcifera* populations, including TC, KO, VE, etc. (Figure 3). Principal Component Analysis was conducted to explore differences among bacterial communities of all *S. furcifera* populations, revealing distinct microbial communities in *S. furcifera* individuals from FN and JY populations compared to other samples (Supplementary Figure S1).

3.2 Microbial diversities of different geographical *Sogatella furcifera* populations

To elucidate variations in microbial communities among different *S. furcifera* populations, alpha diversity indices, including Shannon, Simpson, and Chao1, were calculated for each *S. furcifera* population. Considering that the three alpha indices of all populations did not follow a normal distribution, the Kruskal–Wallis test, and Dunn's test with Bonferroni correction for multiple comparisons were adopted (Figure 2). Intriguingly, populations with low *Wolbachia* abundance exhibited higher alpha diversities in bacterial communities compared to those with high *Wolbachia* abundance. Specifically, populations with low *Wolbachia* abundance, such as JY, TC, and YT, displayed significantly higher Shannon and Simpson indices compared to populations with high *Wolbachia* abundance, including VE, SA, CX, and FN (Figure 2). The UPGMA hierarchical cluster diagram of different *Sogatella furcifera* populations with 2bRAD-M sequencing data was shown (Supplementary Figure S2), and the phylogenetic tree of different *Sogatella furcifera* populations with 2bRAD sequencing results was constructed (Supplementary Figure S3).

3.3 Influence of *Wolbachia* and *Cardinium* on other bacteria and microbial diversities of *Sogatella furcifera*

Pearson analysis was used to assess the correlations between symbionts and other bacteria in *S. furcifera*. As illustrated in Figure 4A, the presence of *Wolbachia* negatively impacted the abundance of various bacteria, encompassing *Enterobacter*, *Acinetobacter*, and *Lysinibacillus*. Notably, *Wolbachia* significantly and negatively influenced the abundance of *Portiera* in *S. furcifera* ($r = -0.518$, $p < 0.05$, Pearson analysis). While the abundance of *Wolbachia* was negatively correlated with that of *Cardinium*, the correlation was not statistically significant ($r = -0.451$, $p = 0.06$, Pearson analysis). Consistently, *Cardinium* significantly positively influenced the abundance of *Pseudomonas* ($r = -0.804$, $p < 0.001$, Pearson analysis) and that of various other bacteria, albeit the correlation was not statistically significant (Figure 4B).

Noteworthily, Pearson analysis exposed that the presence of *Wolbachia* significantly and negatively affected the three diversity

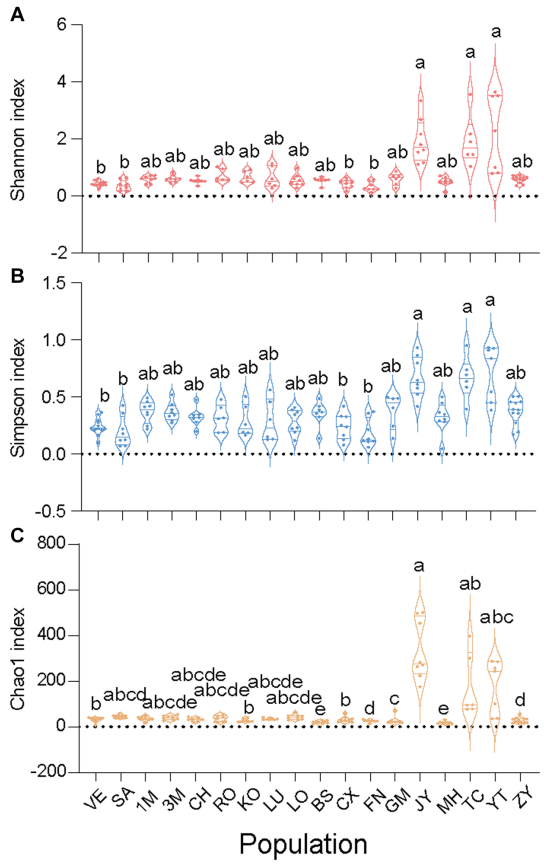

FIGURE 3
Alpha diversities of all 18 *Sogatella furcifera* MED populations collected in Asia. The Shannon index **(A)**, Simpson index **(B)** and Chao1 index **(C)** were present based on 2bRAD-M sequencing results, respectively. As the diversity data do not follow a normal distribution, they were analyzed by Kruskal–Wallis test and Dunn's test with Bonferroni correction for multiple comparisons by SPSS 21.0, different letters represent significant difference.

indexes of *S. furcifera*, namely the Shannon index ($r = -0.834$, $p < 0.001$, Pearson analysis), Simpson index ($r = -775$, $p < 0.001$, Pearson analysis), and Chao1 index ($r = -0.750$, $p < 0.001$, Pearson analysis) (Figure 5). *Cardinium* infection also had a negative impact on the diversity indexes, although the correlations were not significant (Supplementary Figure S4).

3.4 Effects of environmental factors on bacterial abundance, including symbionts in *Sogatella furcifera*

The effects of five environmental factors (annual mean temperature, annual precipitation, latitude, longitude, and altitude) on *S. furcifera* microbiota were determined through Pearson analysis. While both *Wolbachia* and *Cardinium* abundance in *S. furcifera* increased with annual mean temperature, there was no significant correlation between temperature and the abundance of these two symbionts. Notwithstanding, temperature had a significantly negative impact on the abundance of numerous bacteria, such as *Enterobacter*, *Lysinibacillus,* and *Acinetobacter* (Figure 6A). Precipitation had a significant positive influence on *Wolbachia* abundance ($r = 0.489$, $p < 0.05$, Pearson analysis) (Figure 6B). Latitude was significantly and positively correlated with the abundance of many bacteria and was negatively correlated with that of *Cardinium* and *Wolbachia*, although the difference was not significant for the latter (Figure 6C). On the other hand, longitude was significantly and negatively correlated with the abundance of *Wolbachia* ($r = 0.750$, $p < 0.001$, Pearson analysis) and positively correlated with the abundance of other bacteria in *S. furcifera* (Figure 6D). Finally, altitude did not significantly affect bacterial abundance in *S. furcifera* (Supplementary Figure S5).

SEM analysis validated the significant influence of precipitation on *Wolbachia* abundance ($r = 0.400$, $z = 1.967$,

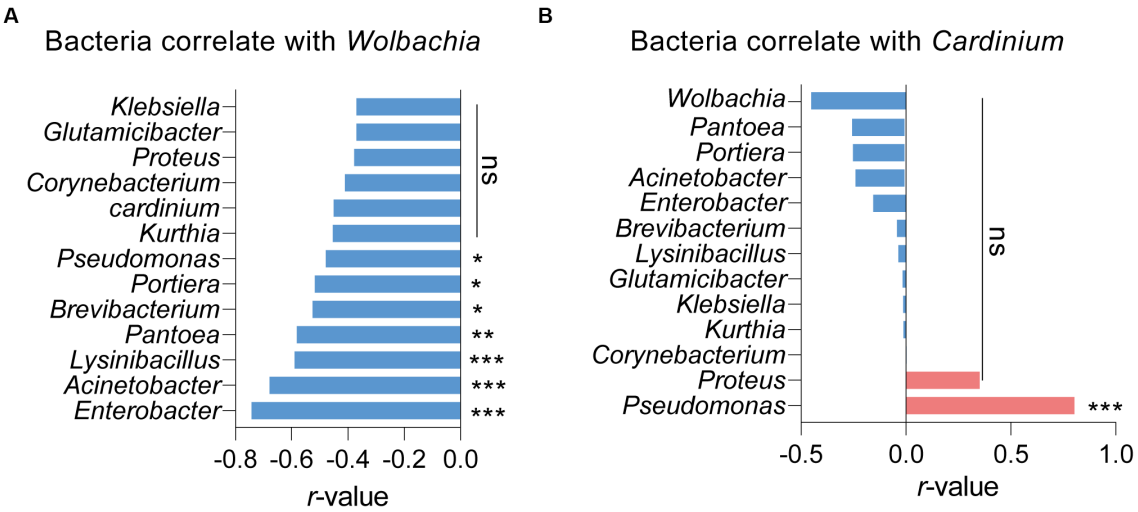

FIGURE 4
Relationships between the proportions of other main 13 bacteria and the proportions of *Wolbachia* **(A)** or the proportions of *Cardinium* **(B)** among all 18 *Sogatella furcifera* populations by Pearson correlation analysis (SPSS 21.0) based on 2bRAD-M sequencing results. *r*-values and *p* values of each linear regression plots are provided. "ns" means no significant; asterisks indicate significant difference the two compared group, *p<0.05; **p<0.01; ***p<0.001.

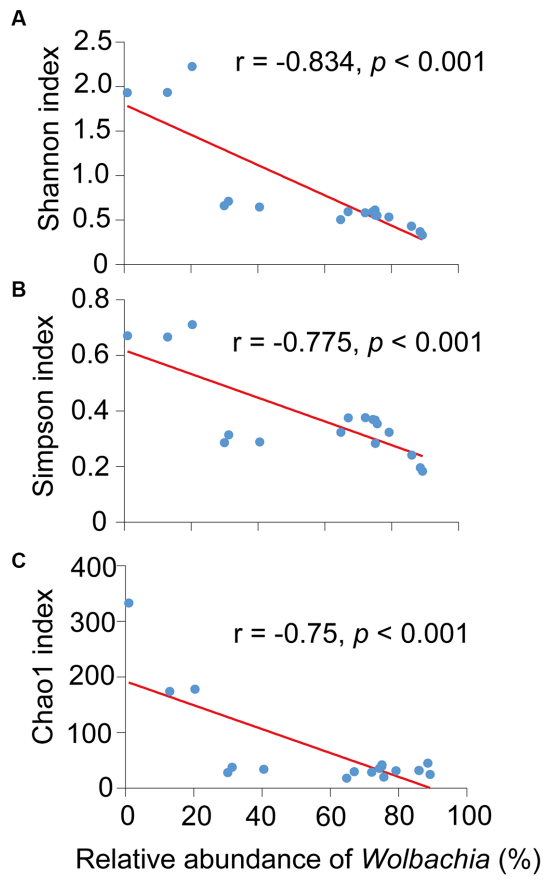

FIGURE 5
Relationships between the abundance of *Wolbachia* and the Shannon diversity index **(A)**, Simpson index **(B)** and Chao1 index **(C)** among all 18 *Sogatella furcifera* populations by Pearson correlation analysis (SPSS 21.0) based on 2bRAD-M sequencing results. *r*-values and *p* values of each linear regression plots are provided.

$p < 0.05$, SEM) and the negative effect of latitude on *Cardinium* abundance ($r = -3.021$, $z = -2.498$, $p < 0.05$, SEM). In contrast to Pearson analysis, SEM analysis revealed a significant negative correlation between *Wolbachia* and *Cardinium* ($r = -0.87$, $z = -2.785$, $p < 0.01$, SEM). Lastly, temperature had a numerically positive effect on *Wolbachia* abundance and a negative effect on *Cardinium* abundance (Figure 7).

3.5 Influence of environmental factors on microbial diversities in *S. furcifera*

Furthermore, the effects of environmental factors on microbiota diversity in *S. furcifera* were explored. According to Pearson analysis, both latitude and longitude exerted a positive influence on all three diversity indexes (Shannon, Simpson, and Chao1 indexes) of bacterial communities in *S. furcifera*, whereas altitude had a marginal negative effect on microbiota diversity (Figure 8). In contrast, SEM analysis identified that altitude negatively impacted the Shannon index ($r = -0.806$, $z = -2.096$, $p < 0.05$, SEM), which differed from the results of Pearson analysis (Figure 8G). SEM analysis uncovered that temperature had a negative influence on both the Shannon index ($r = -1.879$, $z = -2.527$, $p < 0.05$, SEM) and Simpson index ($r = -3.189$, $z = -3.493$, $p < 0.001$, SEM) (Figure 9).

4 Discussion

Symbiotic bacteria play a critical role in the biology, ecology, and evolution of hosts, and various environmental factors significantly impact bacterial communities in invertebrate hosts. Herein, the effects of symbionts on the microbiota in *S. furcifera* populations and the significant effects of environmental factors on bacterial communities in *S. furcifera* were analyzed. Our findings revealed that the presence of symbionts *Wolbachia* and *Cardinium* in *S. furcifera* negatively influenced the abundance of numerous other bacteria. Additionally, *Wolbachia* infection significantly reduced the diversity of microbial communities in *S. furcifera*. Several environmental factors, including longitude, latitude, temperature, and precipitation, were found to impact the abundance of symbionts and the microbial diversity in *S. furcifera*.

In the current study, the bacterial community composition in *S. furcifera* was abundant, primarily consisting of two dominant symbionts, namely *Wolbachia* and *Cardinium* (Figure 3). These results are consistent with the findings of previous studies on *S. furcifera* microbiota (Li et al., 2020, 2021, 2022). Notably, the presence of a primary symbiont, *Portiera*, in the *S. furcifera* microbiota, with significant infection rates was noted in various populations such as RO ($5.03 \pm 10.38\%$, Mean ± SEM) and KO ($2.73 \pm 1.40\%$, Mean ± SEM) (Figure 3). The horizontal transmission of symbionts between different arthropod species has been well-documented (Werren et al., 2008; Zhang et al., 2016). Research has established that horizontal transmission can occur between different phloem sap-feeding insect species, accounting for the presence of *Portiera* within *S. furcifera* (Gonella et al., 2015). Previous studies confirmed a vital influence of genetic backgroud on the microbiome in invertebrates (Suzuki et al., 2019; Gupta and Nair, 2020), however, no direct relationship between *S. furcifera* genetic phylogenetic tree and UPGMA hierarchical cluster diagram of microbiome in *S. furcifera* discovered (Supplementary Figures S2, S3).

Interactions among different bacteria, especially symbionts, are complex in arthropods. Specifically, the presence of one symbiont generally influences the infection patterns of other symbionts (Evans and Armstrong, 2006; Zhao et al., 2018; Fromont et al., 2019; Duan et al., 2020). This phenomenon is not surprising, given that symbionts are primarily restricted to bacteriocytes and reproductive tissues within invertebrate hosts, leading to competition for limited nutrition and space (Engel and Moran, 2013; Douglas, 2015; Yang et al., 2019). For example, in *Laodelphax striatellus, Wolbachia* infection negatively affects the abundance of 154 other bacterial genera within hosts (Duan et al., 2020). Conflicting interactions between symbionts, such as *Cardinium* and *Hamiltonella* in whiteflies, have been observed (Zhao et al., 2018), while other bacteria in honeybees decrease the development rate of the primary symbiont *Paenibacillus larvae* (Evans and Armstrong, 2006). Comparable results were obtained in our study; *Wolbachia* negatively influenced the abundance of 13 primary genera of bacteria, while *Cardinium* negatively influenced the abundance of 11 other genera (Figure 4). This observation suggests a competitive relationship among

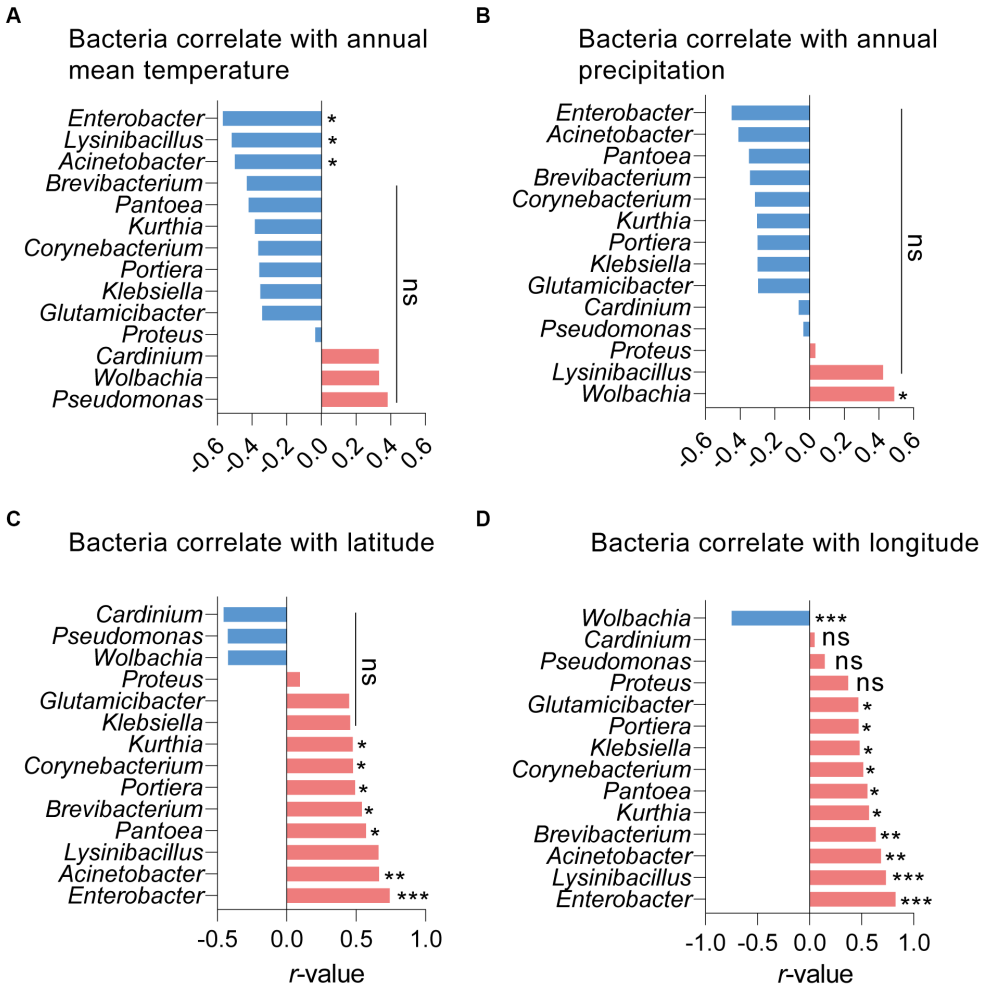

FIGURE 6
Relationships between the proportions of main 14 bacteria and the annual mean temperature **(A)**, annual precipitation **(B)**, latitude **(C)** and longitude **(D)** among all 18 *Sogatella furcifera* populations by Pearson correlation analysis (SPSS 21.0) based on 2bRAD-M sequencing results. *r*-values and *p* values of each linear regression plots are provided. "ns" means no significant; asterisks indicate significant difference the two compared group, **p*<0.05; ***p*<0.01; ****p*<0.001.

bacteria in *S. furcifera*. However, *Cardinium* infection was positively correlated with the abundance of *Pseudomonas* and *Proteus*, indicating a cooperative interaction between *Cardinium* and these two bacteria (Figure 4B). Similar interactions have been described in other studies. For example, the presence of *Wolbachia* in the fruit fly *Drosophila neotestacea* promotes the infection of *Spiroplasma* (Fromont et al., 2019). In *Laodelphax striatellus, Wolbachia* infection increases the abundance of other bacteria, such as *Spiroplasma* and *Ralstonia* (Duan et al., 2020). These complex interactions among bacteria, especially symbionts, necessitate further exploration.

Symbiont plays a pivotal role in shaping the microbial community of invertebrates and invariably influences the host's microbiota structure. Symbiont infections frequently lead to a reduction in bacterial diversities in arthropod hosts (Duan et al., 2020; Li et al., 2020, 2022). In the present study, *Wolbachia* infection significantly decreased the diversity of the bacterial community in *S. furcifera* (Figure 5). This finding is in line with the result of previous studies in *Aedes aegypti*, wherein the presence of *Wolbachia* reduced the diversity of resident bacteria in mosquitoes (Audsley et al., 2018). Similar reductions in microbial diversities have been observed in the small brown planthopper *Laodelphax striatellus* (Zhang et al., 2020) and *Drosophila melanogaster* (Ye et al., 2017). These studies collectively underscore the negative influence of symbionts on the bacterial communities of arthropods.

The influence of environmental factors on arthropod microbial communities has been explored in previous research. Studies on global invertebrates indicated that temperature significantly affects the occurrence of *Wolbachia* and *Cardinium* infections in host arthropods (Charlesworth et al., 2019). Similar temperature effects on symbionts were corroborated in other studies (Corbin et al., 2016). However, in this study, the impact of temperature on symbionts (*Cardinium* and *Wolbachia*) was not significant in *S. furcifera* (Figures 6A, 7), suggesting weak temperature effects on symbiont infections in *S. furcifera*. Other environmental factors also influence symbiont infections in hosts. For example, in the spider mite *Tetranychus truncatus*, *Wolbachia* infection was significantly influenced by annual mean temperatures, whereas the rates of *Cardinium* and *Spiroplasma* infections were correlated with altitude (Zhu et al., 2018). Additionally,

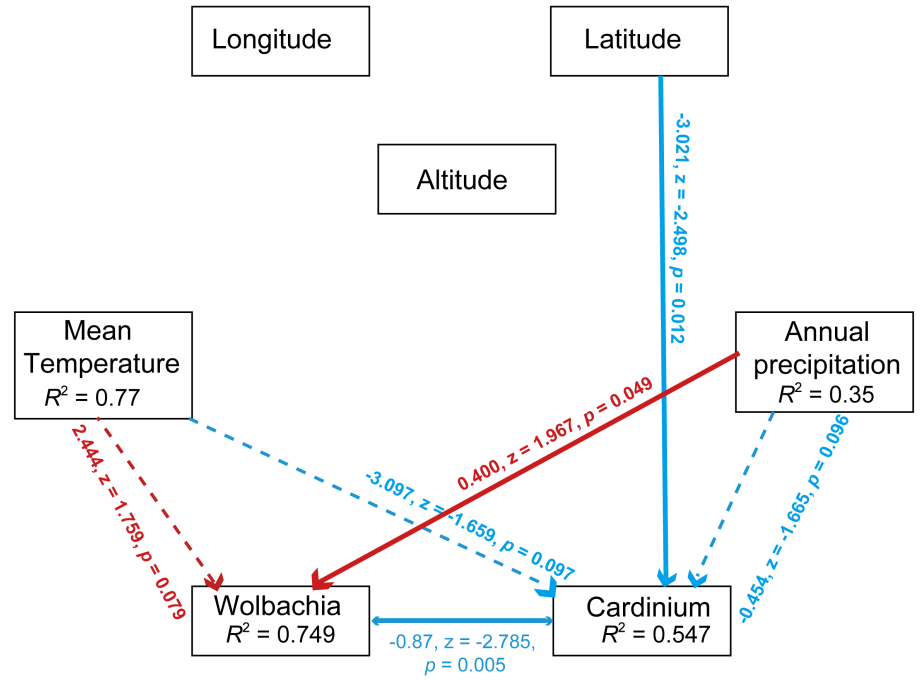

FIGURE 7
Path diagram for the structural equation model (SEM) for environmental factors (including annual mean temperature, annual precipitation, longitude, altitued and latitude) and symbionts' abundance (including *Wolbachia* and *Cardinium*). Statistically significant negative paths are indicated by blue arrows, while positive paths are indicated by red arrows. The *r* values in each box indicate the amount of variation in that variable explained by the input arrows. Numbers next to arrows are unstandardized slopes.

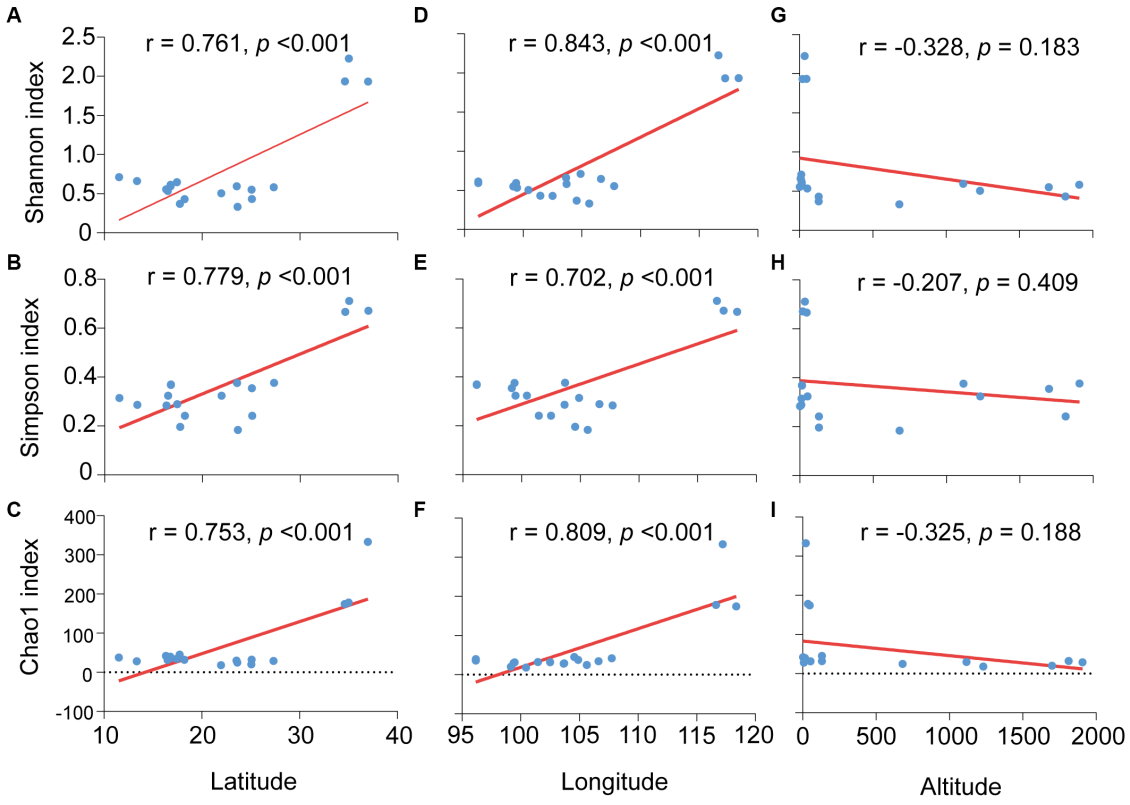

FIGURE 8
Relationships between the microbiota diversity indexes and environmental factors in *Sogatella furcifera*. The relationships between latitude and Shannon diversity index **(A)**, Simpson index **(B)** and Chao1 index **(C)**, between longitude and Shannon diversity index **(D)**, Simpson index **(E)** and Chao1 index **(F)**, between altitude and Shannon diversity index **(G)**, Simpson index **(H)** and Chao1 index **(I)** were shown, respectively, all analysis were used by Pearson correlation analysis (SPSS 21.0) based on 2bRAD-M sequencing results. *r*-values and *p* values of each linear regression plots are provided.

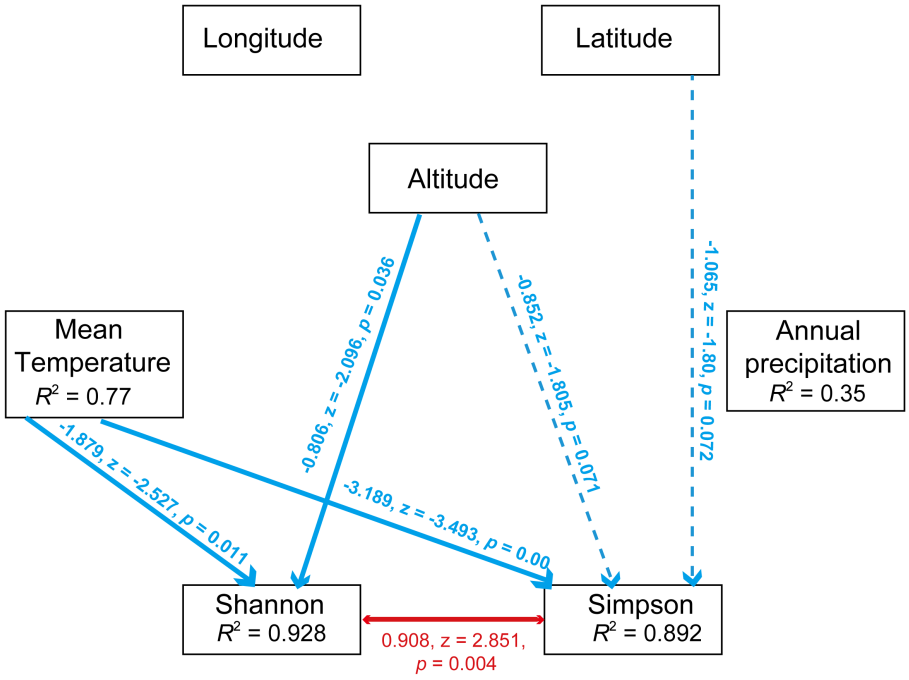

FIGURE 9
Path diagram for the structural equation model (SEM) for environmental factors (including annual mean temperature, annual precipitation, longitude, altitude and latitude) and diversity indexes (including Shannon index and Simpson index). Statistically significant negative paths are indicated by blue arrows, while positive paths are indicated by red arrows. The r values in each box indicate the amount of variation in that variable explained by the input arrows. Numbers next to arrows are unstandardized slopes.

bacterial communities were significantly affected by geographical distances in stoneflies (Zhu et al., 2022). Herein, the abundance of numerous bacteria in *S. furcifera* were affected by environmental factors, with *Wolbachia* abundance significantly influenced by precipitation and longitude and *Cardinium* abundance not significantly affected by the environment (Figure 6 and Supplementary Figure S3). The differential impact of the environment on *Wolbachia* and *Cardinium* requires further exploration.

In summary, our 2bRAD-M sequencing analysis of 18 *S. furcifera* populations offers a novel and comprehensive perspective of the relationship between bacterial community structure, environmental factors, and symbionts in Asian *S. furcifera* populations. Our observations provide credible evidence that the *Wolbachia* and *Cardinium* symbionts within host whiteflies influence each other and negatively impact the abundance of other bacteria. Importantly, *Wolbachia's* presence negatively affected microbial diversity, with both symbiont and microbiota diversities being significantly influenced by various environmental factors. However, further studies are necessary to elucidate the mechanisms by which environmental factors influence the diversity of bacterial communities in different *S. furcifera* populations across global ecological timescales.

Data availability statement

The original contributions presented in the study are publicly available. This data can be found here: NCBI, PRJNA1055281.

Ethics statement

The manuscript presents research on animals that do not require ethical approval for their study.

Author contributions

KY: Conceptualization, Data curation, Funding acquisition, Investigation, Methodology, Writing – original draft, Writing – review & editing. H-YZ: Investigation, Methodology, Validation, Writing – review & editing. PW: Supervision, Writing – original draft. G-XJ: Formal analysis, Validation, Conceptualization, Writing – original draft, Writing – review & editing. DC: Conceptualization, Formal analysis, Funding acquisition, Supervision, Validation, Writing – original draft, Writing – review & editing.

Funding

The author(s) declare financial support was received for the research, authorship, and/or publication of this article. This research was supported by the Taishan Scholar Foundation of Shandong Province of China (tstp20221135), and Shandong Modern Agricultural Technology & Industry System (SDAIT-17-07), and the Qingdao Agricultural University High-level Talent Fund (663–1121025).

Acknowledgments

We are grateful to Aidong Chen (Agriculture Environment and Resources Institute, Yunnan Academy of Agricultural Sciences, Kunming 650205, China) for providing the insect samples.

Conflict of interest

The authors declare that the research was conducted in the absence of any commercial or financial relationships that could be construed as a potential conflict of interest.

Publisher's note

All claims expressed in this article are solely those of the authors and do not necessarily represent those of their affiliated organizations, or those of the publisher, the editors and the reviewers. Any product that may be evaluated in this article, or claim that may be made by its manufacturer, is not guaranteed or endorsed by the publisher.

Supplementary material

The Supplementary material for this article can be found online at: https://www.frontiersin.org/articles/10.3389/fmicb.2023.1336345/full#supplementary-material

References

Audsley, M. D., Seleznev, A., Joubert, D. A., Woolfit, M., O'Neill, S. L., and McGraw, E. A. (2018). *Wolb-achia* infection alters the relative abundance of resident bacteria in adult *Aedes aegypti* m-osquitoes, but not larvae. *Mol. Ecol.* 27, 297–309. doi: 10.1111/mec.14436

Behar, A., Yuval, B., and Jurkevitch, E. (2008). Community structure of the Mediterranean fruit fly microbiota: seasonal and spatial sources of variation. *Isr. J. Ecol. Evol.* 54, 181–191. doi: 10.1080/15659801.2008.10639612

Caporaso, J. G., Kuczynski, J., Stombaugh, J., Bittinger, K., Bushman, F. D., Costello, E. K., et al. (2010). QIIME allows analysis of high-throughput community sequencing data. *Nat. Methods* 7, 335–336. doi: 10.1038/nmeth.f.303

Charlesworth, J., Weinert, L. A., Araujo, J. E. V., and Welch, J. J. (2019). *Wolbachia*, *Cardinium* and climate: an analysis of global data. *Biol. Lett.* 15:20190273. doi: 10.1098/rsbl.2019.0273

Colman, D. R., Toolson, E. C., and Takacs-Vesbach, C. D. (2012). Do diet and taxonomy influence insect gut bacterial communities? *Mol. Ecol.* 21, 5124–5137. doi: 10.1111/j.1365-294X.2012.05752.x

Corbin, C., Heyworth, E. R., Ferrari, J., and Hurst, G. D. D. (2016). Heritable symbionts in a world of varying temperature. *Heredity* 118, 10–20. doi: 10.1038/hdy.2016.71

Douglas, A. E. (2009). The microbial dimension in insect nutritional ecology. *Funct. Ecol.* 23, 38–47. doi: 10.1111/j.1365-2435.2008.01442.x

Douglas, A. E. (2015). Multiorganismal insects: diversity and function of resident microorganims. *Annu. Rev. Entomol.* 60, 17–34. doi: 10.1146/annurev-ento-010814-020822

Duan, X. Z., Sun, J. T., Wang, L. T., Shu, X. H., Guo, Y., Keiichiro, M., et al. (2020). Recent infection by *Wolbachia* alters microbial communities in wild *Laodelphax striatellus* populations. *Microbiome* 8:104. doi: 10.1186/s40168-020-00878-x

Dunbar, H. E., Wilson, A. C., Ferguson, N. R., and Moran, N. A. (2007). Aphid thermal tolerance is gov-erned by a point mutation in bacterial symbionts. *PLoS Biol.* 5:e96. doi: 10.1371/journal.pbio.0050096

Engel, P., and Moran, N. A. (2013). The gut microbiota of insects-diversity in structure and functi-on. *FEMS Microbiol. Rev.* 37, 699–735. doi: 10.1111/1574-6976.12025

Evans, J. D., and Armstrong, T. N. (2006). Antagonistic interactions between honey bee bacterial sy-mbionts and implications for disease. *BMC Ecol.* 6:4. doi: 10.1186/1472-6785-6-4

Franzosa, E. A., McIver, L. J., Rahnavard, G., Thompson, L. R., Schirmer, M., Weingart, G., et al. (2018). Species-level function-al profiling of metagenomes and metatranscriptomes. *Nat. Methods* 15, 962–968. doi: 10.1038/s41592-018-0176-y

Fromont, C., Adair, K. L., and Douglas, A. E. (2019). Correlation and causation between the microbio-me, *Wolbachia* and host functional traits in natural populations of drosophilid flies. *Mol. Ecol.* 28, 1826–1841. doi: 10.1111/mec.15041

Gonella, E., Pajoro, M., Marzorati, M., Crotti, E., Mandrioli, M., Pontini, M., et al. (2015). Plant-mediated interspecific horizontal transmission of an intracellular symbiont in insects. *Sci. Rep.* 5:15811. doi: 10.1038/srep15811

Goto, S., Anbutsu, H., and Fukatsu, T. (2006). Asymmetrical interactions between *Wolbachia* and *Spiroplasma* endosymbionts coexisting in the same insect host. *Appl. Environ. Microbiol.* 72, 4805–4810. doi: 10.1128/AEM.00416-06

Gupta, A., and Nair, S. (2020). Dynamics of insect-microbiome interaction influence host and microbial symbiont. *Front. Microbiol.* 11:1357. doi: 10.3389/fmicb.2020.01357

Hertig, M., and Wolbach, S. B. (1924). Studies on rickettsia-like microorganisms in insects. *J. Med. Res.* 44, 329–374.7.

Hu, S. J., Liu, X. F., Fu, D. Y., Huang, W., Wang, X. Y., Liu, X. J., et al. (2015). Projecting distribution of the overwintering population of *Sogatella furcifera* (Hemiptera: Delphacidae), in Yunn-an, China with analysis on key influencing climatic factors. *J. Insect Sci.* 15:148. doi: 10.1093/jisesa/iev131

Huang, Y. X., and Qin, D. Z. (2018). First mitogenome for the tribe Saccharosydnini (Hemiptera: D-elphacidae: Delphacinae) and the phylogeny of three predominant rice planthoppers. *Eur. J. Entomol.* 115:242. doi: 10.14411/eje.2018.023

Li, F., Li, P., Hua, H., Hou, M., and Wang, F. (2020). Diversity, tissue localization, and infection pa-ttern of bacterial symbionts of the white-backed blanthopper, *Sogatella furcifera* (Hemiptera: Delphacidae). *Microb. Ecol.* 79, 720–730. doi: 10.1007/s00248-019-01433-4

Li, T. P., Zha, S. S., Zhou, C. Y., Xia, X., Hoffmann, A. A., and Hong, X. Y. (2021). Two newly introduced *Wolbachia* endosymbionts induce cell host differences in competitiveness and metabolic re-sponses. *Appl. Environ. Microbiol.* 87:e0147921. doi: 10.1128/AEM.01479-21

Li, T. P., Zhou, C. Y., Wang, M. K., Zha, S. S., Chen, J., Bing, X. L., et al. (2022). Endosymbionts reduce microbiome diversity and modify host metabolism and fecundity in the planthopper *Sogatella furcifera*. *Msystems* 7:e0151621. doi: 10.1128/msystems.01516-21

McFall-Ngai, M., Hadfield, M. G., Bosch, T. C. G., Carey, H. V., Domazet-Lošo, T., Douglas, A. E., et al. (2013). Animals in a bacterial world, a new imperative for the life sciences. *Proc. Natl. Acad. Sci. U. S. A.* 110, 3229–3236. doi: 10.1073/pnas.1218525110

Miao, Y.-H., Xiao, J.-H., and Huang, D.-W. (2020). Distribution and evolution of the bacteriophage WO and its antagonism with *Wolbachia*. *Front. Microbiol.* 11:595629. doi: 10.3389/fmicb.2020.595629

Santo Domingo, J. W., Kaufman, M. G., Klug, M. J., Holben, W. E., Harris, D., and Tiedje, J. M. (1998). In-fluence of diet on the structure and function of the bacterial hindgut community of cricke-ts. *Mol. Ecol.* 7, 761–767. doi: 10.1046/j.1365-294x.1998.00390.x

Savary, S., Horgan, F., Willocquet, L., and Heong, K. L. (2012). A review of principles for sustainab-le pest management in rice. *Crop Prot.* 32, 54–63. doi: 10.1016/j.cropro.2011.10.012

Sun, Z., Huang, S., Zhu, P., Tzehau, L., Zhao, H., Lv, J., et al. (2022). Species-resolved sequencing of low-biomass or degraded microbiomes using 2bRAD-M. *Genome Biol.* 23:36. doi: 10.1186/s13059-021-02576-9

Suzuki, T. A., Phifer-Rixey, M., Mack, K. L., Sheehan, M. J., Lin, D., Bi, K., et al. (2019). Host genetic determinants of the gut microbiota of wild mice. *Mol. Ecol.* 28, 3197–3207. doi: 10.1111/mec.15139

Taylor, M. J., Bandi, C., and Hoerauf, A. (2005). *Wolbachia* bacterial endosymbionts of filarial nem-atodes. *Adv. Parasitol.* 60, 245–284. doi: 10.1016/S0065-308X(05)60004-8

Wang, Y. B., Li, C., Yan, J. Y., Wang, T. Y., Yao, Y. L., Ren, F. R., et al. (2022). Autophagy regulates whitefly-symbiont metabolic interactions. *Appl. Environ. Microbiol.* 88:e0208921. doi: 10.1128/AEM.02089-21

Wang, S., Meyer, E., McKay, J., and Matz, M. V. (2012). 2b-RAD: a simple and flexible method for genome-wide genotyping. *Nat. Methods* 9, 808–810. doi: 10.1038/nmeth.2023

Wang, Z., Yang, H., Zhou, C., Yang, W. G., Jin, D.-C., and Long, G.-Y. (2019). Molecular cloning, expr-ession, and functional analysis of the chitin synthase 1 gene and its two alternative splici-ng variants in the white-backed planthopper, *Sogatella furcifera* (Hemiptera: Delphacidae). *Sci. Rep.* 9:1087. doi: 10.1038/s41598-018-37488-5

Wang, Z., Zhou, C., Long, G. Y., Yang, H., and Jin, D. C. (2018). Sublethal effects of buprofezin on d-evelopment, reproduction, and chitin synthase 1 gene (*SfCHS1*) expression in the white-bac-ked planthopper, *Sogatella furcifera* (Hemiptera: Delphacidae). *J. Asia Pac. Entomol.* 21, 585–591. doi: 10.1016/j.aspen.2018.03.009

Wasala, S. K., Brown, A. M. V., Kang, J., Howe, D. N. K., Peetz, A. B., Zasada, I. A., et al. (2019). Variable abundance and distribution of *Wolbachia* and *Cardinium* endosymbionts in plantp-arasitic nematode field populations. *Front. Microbiol.* 10:964. doi: 10.3389/fmicb.2019.00964

Werren, J. H. (1997). Biology of wolbachia. *Annu. Rev. Entomol.* 42, 587–609. doi: 10.1146/annurev.ento.42.1.587

Werren, J. H., Baldo, L., and Clark, M. E. (2008). *Wolbachia*: master manipulators of invertebrate bio-logy. *Nat. Rev. Microbiol.* 6, 741–751. doi: 10.1038/nrmicro1969

Yang, K., Qin, P.-H., Yuan, M.-Y., Chen, L., Zhang, Y.-J., and Chu, D. (2022). Infection density pattern of *Cardinium* affects the responses of bacterial communities in an invasive whitefly under heat conditions. *Insect Sci.* 30, 1149–1164. doi: 10.1111/1744-7917.13141

Yang, K., Xie, K., Zhu, Y. X., Huo, S. M., Hoffmann, A. A., and Hong, X. Y. (2019). *Wolbachia* dominate *Spiroplasma* in the co–infected spider mite *Tetranychus truncatus*. *Insect Mol. Biol.* 29, 19–37. doi: 10.1111/imb.12607

Ye, Y. H., Seleznev, A., Flores, H. A., Woolfit, M., and McGraw, E. A. (2017). Gut microbiota in *Droso-phila* melanogaster interacts with *Wolbachia* but does not contribute to *Wolbachia*-mediated antiviral protection. *J. Invertebr. Pathol.* 143, 18–25. doi: 10.1016/j.jip.2016.11.011

Zeng, Z., Fu, Y., Guo, D. Y., Wu, Y. X., Ajayi, O. E., and Wu, Q. F. (2018). Bacterial endosymbiont *Cardi-nium* cSfur genome sequence provides insights for understanding the symbiotic relationshi-p in *Sogatella furcifera* host. *BMC Genomics* 19:688. doi: 10.1186/s12864-018-5078-y

Zhang, Y. K., Chen, Y. T., Yang, K., and Hong, X. Y. (2016). A review of prevalence and phylogeny of the bacterial symbiont *Cardinium* in mites (subclass: Acari). *Syst. Appl. Acarol.* 21, 978–990. doi: 10.11158/saa.21.7.11

Zhang, X., Li, T. P., Zhou, C. Y., Zhao, D. S., Zhu, Y. X., Bing, X. L., et al. (2020). A-ntibiotic exposure perturbs the bacterial community in the small brown planthopper Laodelphax striatellus. *Insect Sci.* 27, 895–907. doi: 10.1111/1744-7917.12675

Zhao, D. X., Hoffmann, A. A., Zhang, Z. C., Niu, H. T., and Guo, H. F. (2018). Interactions between facult-ative symbionts *Hamiltonella* and *Cardinium* in *Bemisia tabaci* (Hemiptera: Aleyrodoidea): cooperation or conflict? *J. Econ. Entomol.* 111, 2660–2666. doi: 10.1093/jee/toy261

Zhou, G. H., Wen, J. J., Cai, D. J., Xu, D. L., and Zhang, S. G. (2008). Southern rice black-streaked dwarf virus: a new proposed *Fijivirus* species in the family *Reoviridae*. *Chin. Sci. Bull.* 53, 3677–3685. doi: 10.1007/s11434-008-0467-2

Zhou, C., Yang, H., Wang, Z., Long, G.-Y., and Jin, D.-C. (2018). Comparative transcriptome analysis of *Sogatella furcifera* (Horváth) exposed to different insecticides. *Sci. Rep.* 8:8773. doi: 10.1038/s41598-018-27062-4

Zhu, Y. X., Huo, Q. B., Wen, T., Wang, X. Y., Zhao, M. Y., and Du, Y. Z. (2022). Mechanisms of fungal c-ommunity assembly in wild stoneflies moderated by host characteristics and local environ-ment. *NPJ Biofilms Microb.* 8:31. doi: 10.1038/s41522-022-00298-9

Zhu, Y. X., Song, Y. L., Zhang, Y. K., Hoffmann, A. A., Zhou, J. C., Sun, J. T., et al. (2018). Incidence of facultative bacterial endosymbionts in spider mites associated with local environments and host plants. *Appl. Environ. Microbiol.* 84, e02546–e02517. doi: 10.1128/AEM.02546-17

Zug, R., and Hammerstein, P. (2015). Bad guys turned nice? A critical assessment of *Wolbachia* mutualisms in arthropod hosts. *Biol. Rev.* 90, 89–111. doi: 10.1111/brv.12098

frontiers | Frontiers in Microbiology

TYPE Original Research
PUBLISHED 01 March 2024
DOI 10.3389/fmicb.2024.1295696

Check for updates

OPEN ACCESS

EDITED BY
Ruichang Gao,
Jiangsu University, China

REVIEWED BY
Dao-Feng Zhang,
Hohai University, China
Xingzhou Tian,
Guizhou University, China

*CORRESPONDENCE
Yu-Qin Zhang
✉ yzhang@imb.pumc.edu.cn
Binghuo Zhang
✉ binghuozh@126.com

†These authors share first authorship

RECEIVED 17 September 2023
ACCEPTED 21 February 2024
PUBLISHED 01 March 2024

CITATION
Xiao Y, Du M, Deng Y, Deng Q, Wang X, Yang Y, Zhang B and Zhang Y-Q (2024) Modulation of growth, microcystin production, and algal-bacterial interactions of the bloom-forming algae *Microcystis aeruginosa* by a novel bacterium recovered from its phycosphere.
Front. Microbiol. 15:1295696.
doi: 10.3389/fmicb.2024.1295696

COPYRIGHT
© 2024 Xiao, Du, Deng, Deng, Wang, Yang, Zhang and Zhang. This is an open-access article distributed under the terms of the Creative Commons Attribution License (CC BY). The use, distribution or reproduction in other forums is permitted, provided the original author(s) and the copyright owner(s) are credited and that the original publication in this journal is cited, in accordance with accepted academic practice. No use, distribution or reproduction is permitted which does not comply with these terms.

Modulation of growth, microcystin production, and algal-bacterial interactions of the bloom-forming algae *Microcystis aeruginosa* by a novel bacterium recovered from its phycosphere

Yao Xiao[1†], Mijia Du[1†], Yang Deng[2†], Qinglin Deng[1], Xin Wang[1], Yiwen Yang[1], Binghuo Zhang[1*] and Yu-Qin Zhang[2*]

[1]College of Pharmacy and Life Science, Jiujiang University, Jiujiang, China, [2]Institute of Medicinal Biotechnology, Chinese Academy of Medical Sciences & Peking Union Medical College, Beijing, China

Harmful algal blooms (HABs) in natural waters are of escalating global concern due to their detrimental impact on environmental health. Emerging evidence indicates that algae-bacteria symbionts can affect HAB features, though much about this interplay remains largely unexplored. The current study isolated a new species of *Mucilaginibacter* (type strain JXJ CY 39^T) from culture biomass of the bloom-causing *Microcystis aeruginosa* FACHB-905 (Maf) from Lake Dianchi, China. Strain JXJ CY 39^T was an aerobic, Gram-stain-negative rod bacterium that grew at 5–38°C, pH 4.0–11.0, and 0–3.0% NaCl. Taxonomic evaluation proposed a new species, with *Mucilaginibacter lacusdianchii* sp. nov., as the species epithet. Experimental results revealed that strain JXJ CY 39^T spurred the growth of Maf by supplying soluble phosphorus and nitrogen during cultivation, despite the unavailability of soluble phosphorus and nitrogen. Additionally, by producing the plant hormone indole-3-acetate, strain JXJ CY 39^T possibly impacted Maf's functionality. Results from co-culture experiments with other strains from Maf biomass showed possible effects of strain JXJ CY 39^T on the relationship between Maf and other cohabiting bacteria, as well as microcystin toxin production characteristics. Although Maf could foster the growth of strain JXJ CY 39^T by supplying organic carbon, the strain's growth could be regulated via specific chemical compounds based on antibiotic assays. Community composition analysis disclosed that this *Mucilaginibacter* strain positively affected Maf's growth and modified densities and types of bacteria linked to Maf. Overall, these results suggest that the interactions between important HAB-causing organisms and their attached bacteria are complex, dynamic, and may influence the growth characteristics of algae.

KEYWORDS

***Mucilaginibacter lacusdianchii*, harmful algal bloom, bacterial symbiont, genome, algal-bacterial interactions**

Highlights

- Harmful algal blooms (HABs) are persistent environmental problems caused by algae.
- A novel bacterium (JXJ CY 39^T) was isolated and characterized from the phycosphereof an HAB-alga (Maf).
- JXJ CY 39^T modulated the growth and microcystin production of Maf.
- JXJ CY 39^T also influenced the attached bacterial assemblages of Maf.
- Bacterial symbionts of HAB-algae should be more carefully considered in treatments.

1 Introduction

Various types of algae cause harmful algal blooms (HABs), which pose an accelerating concern in both oceans and freshwater worldwide owing to their expansion in recent times, primarily due to global climate changes such as warming trends (Glibert et al., 2005). These HABs impair water ecosystems considerably, including posing threats to environment and human health by producing potent toxins (Grattan et al., 2016).

Distinct exudates from different algal species exhibit different chemical characteristics that result in the coexistence of varying bacterial partners with specific algae (Yang et al., 2017), leading to extremely diverse and complex interactions (Shao et al., 2014) that can include nutrient exchange, signal transduction, and gene transfer (Kouzuma and Watanabe, 2015). Among these, nutrient exchange is considered the most common type of interactions (Kouzuma and Watanabe, 2015) and is frequently the basis of algal–bacterial mutualisms (Cooper and Smith, 2015). Specifically, algae provide attached bacteria with a safer habitat and protection from grazing, in addition to dissolved organic matter compounds like polysaccharides, while attached bacteria provide algae with various nutrients like bio-available P, N, CO_2, microelements, and vitamins (Yang and Xiao, 2011). The mutualisms between algae and attached bacteria are consequently highly mediated by the provisioning of nutrients from bacteria that may be able to initiate and maintain symbiotic relationships (Cooper and Smith, 2015). Importantly, the various interactions that have co-evolved between algae and their attached bacteria (Kouzuma and Watanabe, 2015; Cirri and Pohnert, 2019) have significant, but distinct impacts on the occurrence, duration and decline of algal blooms (Shao et al., 2014; Zhang et al., 2019). Consequently, the importance of attached bacteria must be considered when identifying treatments to control and mitigate HABs.

Microcystis aeruginosa is a common group of bloom-inducing Cyanobacteria, leading source of hepatotoxic microcystins (MCs) specifically produced in freshwater (Dawson, 1998; Park et al., 2009). Among over 270 different MC compounds (Lin et al., 2021), MC-LR (contains leucine and arginine) is the most prevalent in both natural water blooms and *M. aeruginosa* cultures in laboratory (Vasconcelos et al., 1996; Liu et al., 2012). *M. aeruginosa* can also secrete extracellular mucilage primarily composed of polysaccharides that provide habitats for bacteria that attach to *Microcystis* colonies and interact with the algae (Dziallas and Grossart, 2011; Parveen et al., 2013). Many bacteria attached to *M. aeruginosa* extracellular matrices have been isolated and identified, including in the genera *Erythrobacter* (Zhao et al., 2011), *Gordonia, Burkholderia* (Zhao et al., 2012), *Sphingomonas* (Guo et al., 2020), *Pseudomonas* (Yang and Xiao, 2011), and numerous other taxa within the phyla *Actinobacteria*, *Bacteroidetes*, *Proteobacteria*, and *Deinococcus-Thermus* (Berg et al., 2009; Guo et al., 2020). Indeed, many of these bacterial taxa have evolved with their algal hosts (Ramanan et al., 2016).

In this study, a bacterium JXJ CY 39^T was purified from the attached bacterial community of algal *M. aeruginosa* FACHB-905 (Maf), which was previously obtained from Lake Dianchi. Lake Dianchi is the largest lake on the Yunnan-Guizhou plateau and is one of the most seriously pollution-impacted eutrophic freshwater lakes in China. Cyanobacterial blooms primarily dominated by *M. aeruginosa* have gradually became a common phenomenon in Lake Dianchi since the 1980's due to increasing dumping of various wastes into the lake (Liu, 1999). Indeed, HABs occurred almost yearly from 1990 to 2010. Polyphasic taxonomic study revealed that JXJ CY 39^T represents a novel species of *Mucilaginibacter*, belonging to *Bacteroidota* which are the most common phylum attached to *Microcystis* HABs (Ndlela et al., 2018). The genus *Mucilaginibacter*, a large group in *Bacteroidota*, was first described by Pankratov et al. (2007) and later emended by Urai et al. (2008), Baik et al. (2010), and Chen et al. (2014). *Mucilaginibacter* currently comprises 80 species with validly published names[1] (List of Prokaryotic names with Standing in Nomenclature; December 9, 2023). Here, the interactions between Maf and its attached bacteria, including strain JXJ CY 39^T, were investigated with co-culture experiments to understand if and how Maf controls the growth of strain JXJ CY 39^T and vice-a-versa. Moreover, the bacterial communities associated with Maf that was co-cultured with and without strain JXJ CY 39^T were compared over 35 days with 16S rRNA gene amplicon sequence analysis. Taken together, these experiments were used to more comprehensively understand the interactions among Maf, JXJ CY 39^T, and other Maf-attached bacteria. The new insights reported here is to inform the treatment of HABs via consideration of their commensal bacteria.

2 Materials and methods

2.1 Polyphasic taxonomy study on strain JXJ CY 39^T

2.1.1 Isolation of the microorganisms

Algal *Microcystis aeruginosa* FACHB-905 (Maf) was obtained from Lake Dianchi, China, and subsequently incubated in our lab as described previously (Zhang et al., 2016c). Bacteria, including strain JXJ CY 39^T and other eight attached strains, were isolated from the culture biomass of Maf using International Streptomyces Project 2 (ISP 2) agar medium according to the described procedure (Xiao et al., 2022a). Isolated bacteria were preserved at 4.0°C using ISP 2 slants and − 80.0°C using glycerol suspensions (30–50%, v/v). Then we tried to purify Maf on BG11 (Blue-Green Medium) agar plate (Allen, 1968) to get rid of the culturable bacteria attached to the Maf. The purified-Maf was confirmed when no bacterial colony was formed

1 https://lpsn.dsmz.de/genus/mucilaginibacter

by inoculation of the Maf onto newly prepared ISP 2 agar and nutrient agar, respectively. Purified-Maf was cultured using BG11 liquid medium at 25.0°C under illumination of 30 μmol photon/m^2/s with a 12 h: 12 h light: dark cycle. In the subsequent experiments, the purified-Maf culture-system without supplement with other attached bacteria served as a basal control group.

2.1.2 Morphological and physiological characterization of strain JXJ CY 39^T

Bacterial cellular morphology was observed with transmission electron microscopy (TEM; JEM-2100, JEOL) after growing on ISP 2 agar medium at 28.0°C for four days. Gram stains were conducted using standard procedures. Catalase activity was evaluated from bubble production after addition of a drop of 3% (*v*/*v*) H_2O_2 on cell biomass. Growth at different temperatures (5, 10, 15, 20, 26, 28, 30, 32, 35, 38, 41, and 45°C), pH (2.0–12.0 in 1.0 intervals), and NaCl concentrations (0–10.0% *w*/*v*, in 1% intervals) was conducted using ISP 2 agar medium as the basal growth medium. Hydrolysis of starch and Tween (20, 40, and 80) tests were performed according to methods described by Dong and Cai (2001). Other physiological and biochemical characteristics were determined using API systems.

2.1.3 Chemotaxonomic characteristics

Cellular biomass subjected to chemical analysis was obtained from pure cultures grown on ISP 2 agar medium at 28.0°C for four days. Cellular fatty acids were analyzed using the MIDI System (Sherlock version 6.1; MIDI database: TSBA6). Polar lipids were extracted and analyzed by two-dimensional thin-layer chromatography (Minnikin et al., 1979). Further, respiratory quinones were extracted as described by Collins et al. (1977) and analyzed with HPLC (Tamaoka et al., 1983).

2.1.4 Phylogenetic and genome sequence analysis

Genomic DNA was prepared by using Rapid Bacterial Genomic DNA Isolation Kit (Sangon Biotech, Shanghai, China), and subsequently, the 16S rRNA gene sequences were obtained as described previously (Zhang et al., 2016b), and compared against those in the EzBioCloud Database. Phylogenetic trees were reconstructed using neighbor-joining (Saitou and Nei, 1987), maximum-parsimony (Fitch, 1971), and Maximum-Likelihood (Felsenstein, 1981) algorithms in MEGA version 11 (Tamura et al., 2021). The topologies of the phylogenetic trees were evaluated with bootstrap analysis of 1,000 replicates (Felsenstein, 1985).

Whole genome sequencing was conducted on the Illumina HiSeq 4000 platform at Sangon Biotech (Shanghai, China). Sequence read quality was evaluated with FastQC (v.0.11.2) and then trimmed of adapters and low-quality sequence regions with Trimmomatic (v.0.36) (Bolger et al., 2014). The resultant sequence reads were assembled with SPAdes (v.3.5.0) (Bankevich et al., 2012). Gaps in assembled contigs were filled using GapFiller (v.1.11) (Boetzer and Pirovano, 2012) and corrected with PrinSeS-G (v.1.0.0) (Massouras et al., 2010). Genes were predicted using the Prokka annotation program (v.1.10) (Seemann, 2014). Repeat sequences were determined using RepeatModeler (v.2.0.2) and RepeatMasker (v.4.1.0). CRISPR prediction and analysis was conducted with CRT (v.1.2) (Bland et al., 2007). Genomic annotations were further analyzed by searches with the NCBI BLAST+ program (v.2.2.28) using default parameters. The digital DNA–DNA hybridization (dDDH) and average nucleotide identity (ANI) values between the genome of strain JXJ CY 39^T and those of other *Mucilaginibacter* type strains were calculated using the Genome-to-Genome Distance Calculator (GGDC version 3.0) (Meier-Kolthoff et al., 2013) and the JspeciesWS (JSWS) portal, respectively. The genomes of other type strains were downloaded from the NCBI genome database.[2] DNA G + C% contents were calculated from genomic sequences. To construct a robust core gene phylogeny, a phylogenomic tree based on the concatenation of protein sequences from strain JXJ CY 39^T and the type strains of *Mucilaginibacter* was inferred with the EasyCGTree software package[3] (Xue et al., 2021). Evolutionary distances were calculated with IQ-TREE (v.1.6.1) (Nguyen et al., 2015).

2.2 Co-culture of Maf and the attached bacteria

Eight other bacterial strains (Table 1) isolated from Maf cultures were used in the co-culture experiments in addition to strain JXJ CY 39^T. Purified Maf (about 1.0×10^6 CFU mL^{-1}) was inoculated with attached bacteria in (i) binary culture systems (BCSs) that comprised Maf and an individual bacterium at a final cellular density of 1×10^6 CFU mL^{-1} and (ii) ternary culture systems (TCSs) comprising Maf and strain JXJ CY 39^T in addition to another bacterium, with final cellular densities of both strains at 1×10^6 CFU mL^{-1}. Here, the purified Maf was cultured without supplement with additional bacteria, which served as the control. Both treatments (BCS and TCS) and controls included triplicate replicates. BCSs, TCSs, and controls were sampled at 5 and 10 days of cultivation. The bacterial cellular densities were determined using spread plate techniques based on the different features of the colors and morphologies of the colonies. Chlorophyll a (chl-*a*), extracellular microcystin LR (E-MC-LR), and intracellular microcystin LR (I-MC-LR) concentrations were measured using previously described methods (Zhang et al., 2015).

2.3 Nitrogen fixation and dissolution of unavailable phosphate

Nitrogen fixation ability was determined as previously described (Xiao et al., 2022b). The ability to dissolve insoluble phosphorus was evaluated using methods described by Zhang et al. (2016b). Both $Ca_3(PO_4)_2$ (Damao Chemical Reagent Company, Tianjin, China) and phytin (Aladdin, Shanghai, China) were used as insoluble phosphorus sources at dosages of 1 g L^{-1}. After growing on ISP2 agar plates at 28°C for 3 days, the cell mass of strain JXJ CY 39^T was collected and suspended using sterile tap-water, and the cellular suspension was served as the inoculum of nitrogen-free, $Ca_3(PO_4)_2$ and phytin media.

2 https://www.ncbi.nlm.nih.gov/genome/

3 https://github.com/zdf1987/EasyCGTree4

TABLE 1 The information of other 8 attached bacteria to Maf.

Strain no.	16S rRNA gene accession no.	The most related type strain	16S rRNA gene accession number of the type strain	Similarity (%)
JXJ CY 05	MZ708736	*Brevibacterium epidermidis* NBRC 14811^T	BCSJ01000023	99.8
JXJ CY 11	OQ181347	*Pseudomonas oleovorans* ATCC 8062^T	DQ842018	99.5
JXJ CY 16	OQ162229	*Agrococcus terreus* DNG5^T	FJ423764	99.7
JXJ CY 18	MZ708737	*Methylorubrum thiocyanatum* DSM 11490^T	AB175646	99.1
JXJ CY 28	MZ541062	*Sphingomonas abaci* C42^T	AJ575817	99.6
JXJ CY 31	MZ708738	*Deinococcus wulumuqiensis* R12^T	APCS01000185	99.9
JXJ CY 37	OQ162230	*Mycolicibacterium monacense* DSM 44395^T	MVIA01000076	99.8
JXJ CY 57	MZ708739	*Pseudomonas toyotomiensis* DSM 26169^T	AB453701	99.9

2.4 Co-culture of Maf and JXJ CY 39^T in media with limited availability of N and P

Superfluous available nitrogen and phosphorus in eutrophic water are the critical element triggering cyanobacterial blooms. To assess nutrient provisioning activities, Maf at a density of 3×10^5 CFU mL^{-1} and strain JXJ CY 39^T at a density of 1×10^6 CFU mL^{-1} were co-cultured using modified BG11 media, where K_2HPO_4 (Damao Chemical Reagent Company, Tianjin, China) was replaced by $Ca_3(PO_4)_2$ or $NaNO_3$ (Damao Chemical Reagent Company, Tianjin, China) was removed to represent nitrogen-free media. Controls included purified Maf at a density of 3×10^5 CFU mL^{-1} and strain JXJ CY 39^T at a density of about 1×10^6 CFU mL^{-1} that were grown in modified BG11 media, respectively. Co-cultures and controls were all established in triplicate replicates. Bacterial cellular densities and the concentrations of chl-*a*, I-MC-LR, and E-MC-LR were examined as described above on days 7 and 14 for cultures in nitrogen-free medium and on days 9 and 18 for cultures in $Ca_3(PO_4)_2$ medium. The inoculation of Maf into modified BG11 media was also added 1.86 mg L^{-1} of K_2HPO_4 into $Ca_3(PO_4)_2$ medium and 71.4 mg L^{-1} of $NaNO_3$ into nitrogen-free medium. The inoculum of strain JXJ CY 39^T was prepared as described above.

2.5 Influences of Maf metabolites on the growth of attached bacteria

To assess the influence of Maf metabolites on attached bacteria, Maf cultures (5 L, final cell density of ~2.5×10^7 CFU mL^{-1}) were distilled at 50°C under reduced pressure to remove water. The resultant condensates were extracted using mixture solvents comprising water: methanol: ethanol: ethyl acetate (1,1:1:1, *v*/*v*) and extracts were separated by medium pressure liquid chromatography with a C_{18} column (YMC, ODS-AQ, 50 μm) using stepwise elution of mixed solvents (methanol/water, 0/10 → 1/9 → 2/8 → 3/7 → 4/6 → 5/5 → 6/4 → 7/3 → 8/2 → 9/1 → 10/0, *v*/*v*). The resultant eluents were combined into four fractions based on HPLC detection results and were designated as fractions I, II, III, and IV, with quantities of 12.5, 1.75, 0.2, and 0.9 g, respectively. Fractions I, II, and III were water-soluble, while fraction IV was fat-soluble. Only fraction III contained MC-LR at a amount of about 6.2 mg, based on HPLC analyses. The inhibitory activities of these fractions on attached bacteria were investigated using the paper disk method, as previously described (Zhang et al., 2016a). The dosages of fractions I, II, and IV were 4 mg per disk, while disks with fraction III contained 4 μg MC-LR. Total Maf extracts were dissolved with deionized water and solutions were evaluated with antibacterial activities at 4 mg per disk.

2.6 Influence of strain JXJ CY 39^T on the growth of non-culturable Maf-attached bacteria

To assess the influences of strain JXJ CY 39^T and Maf on other Maf-attached bacteria, Maf and strain JXJ CY 39^T at a density of 1×10^6 CFU mL^{-1} were co-cultured in BG11 medium as described above, followed by sampling at days 5, 10, 15 and 35 of cultivation (corresponding to sample IDs M39_1, M39_2, M39_3, and M39_4, respectively). Purified Maf cultures without strain JXJ CY 39^T were sampled at days 5, 10, 15, and 35 of cultivation and were considered the controls (C_1, C_2, C_3, and C_4). All of these samples were spread onto ISP2 plates and incubated at 28.0°C for 7 days to examine whether they were axenic. The V3–V4 hypervariable regions of 16S rRNA genes were amplified using the universal primers 338F (5′-ACTCCTACGGGAGGCAGCA-3′) and 806R (5′-GGACTACHVGGGTWTCTAAT-3′). The amplicons were sequenced on the Illumina MiSeq platform (Illumina, San Diego, USA) using standard protocols. Sequences were analyzed using the QIIME2 software package (2019.4) and by comparison of sequences to the Greengenes database (DeSantis et al., 2006). In addition, samples were inoculated onto ISP2 plates and cultured at 28.0°C for 5 to 7 days to assess the presence of viable strain JXJ CY 39^T.

2.7 Statistics

Data were expressed as means ± standard deviations ($n = 3$). Comparisons of cellular densities, and concentrations of chl-*a* and MC-LR between co-cultures of Maf-bacteria and pure cultures of Maf or bacteria were performed using analysis of variance (ANOVA) followed by Tukey's pairwise comparisons. Significance was set at p values of 0.05.

3 Results and discussion

3.1 Taxonomic study of strain JXJ CY 39^T

3.1.1 Morphological and physiological characteristics

Strain JXJ CY 39^T was aerobic, Gram-negative, and rod-shaped (0.5–0.8 × 0.9–2.0 μm) (Supplementary Figure S1). Its colonies were pale pink, smooth, convex, circular, and wet in appearance after 4–5 days of cultivation on IPS 2 agar plates. Growth occurred at 5.0–38.0°C, pH 4.0–11.0, and 0–3.0% NaCl, with optimal growth at 28.0°C, pH 7.0–8.0, and 0% NaCl. Strain JXJ CY 39^T was positive for catalase, oxidase, nitrate reduction, hydrolysis of starch, and Tween 40 and 80 tests, but negative for Tween 20. Additional phenotypic characteristics are shown in Table 2, along with the species description.

3.1.2 Chemotaxonomy

The major cellular fatty acids of strain JXJ CY 39^T were iso-$C_{15:0}$ (45.0%) and $C_{16:1}\omega7c/_{16:1}\omega6c$ (30.3%) (Supplementary Table S1) and the predominant menaquinone was MK-7, while the polar lipids comprised phosphatidylethanolamine (PE), unidentified aminophosphoglycolipid (APGL), unidentified aminoglycolipids (AGL), unidentified phospholipid (PL), and unidentified polar lipids (L1-3) (Supplementary Figure S2). The above characteristics were similar to the chemotaxonomic profile of *M. robiniae* F39- 2^T (Won et al., 2022) and *M. aquatilis* HME9299^T (Kang et al., 2021).

3.1.3 Molecular phylogenetic analysis

A nearly complete 16S rRNA gene sequence (1,509 bp length; GenBank accession MT674523) of strain JXJ CY 39^T exhibited close similarities with *Mucilaginibacter robiniae* F39-2^T (97.02%), *Mucilaginibacter aquatilis* HME9299^T (96.69%), *M. galii* PP-F2F-G47^T (96.50%), *M. straminoryzae* RS28^T (96.10%), and *M. polytrichastri* DSM 26907^T (96.05%), respectively, and < 96% similarities with other *Mucilaginibacter* spp. and these strains formed a distinct clade within the *Mucilaginibacter* lineage in the phylogenetic trees of 16S rRNA gene sequences (Supplementary Figures S3–S5), which was recapitulated in the Maximum-Likelihood core gene phylogenomic tree (Supplementary Figure S6). The dDDH and ANI values between strain JXJ CY 39^T and its phylogenetic neighbors were 18.8–19.9% and 70.43–73.95%, respectively. These values are all much lower than the generally accepted species threshold values (Chun et al., 2018). Therefore, based on the phenotypic, genotypic and phylogenetic properties, strain JXJ CY 39^T represents a novel species of the genus *Mucilaginibacter*, for which the name *Mucilaginibacter lacusdianchii* sp. nov. is proposed.

3.2 Genomic characteristics

The genome of strain JXJ CY 39^T was sequenced and submitted to GenBank under the accession ID WSRW00000000. The genome of strain JXJ CY39^T contains six contigs, with a total length of 5,070,224 bp and an N_{50} length of 1,554,798 bp. The genomic characteristics of the closest reference strains *M. robiniae* F39- 2^T (Won et al., 2022) and *M. aquatilis* HME9299^T (Kang et al., 2021) were included in Table 2.

In the genome of strain JXJ CY 39^T, some genes or gene clusters have been identified that are likely to enhance symbiotic interactions with the Maf (Supplementary Tables S2, S3). GO database annotation of genes indicated that strain JXJ CY 39^T encoded 19 gene clusters related to symbiotic interactions, immune responses, and their regulation (Supplementary Table S2); 3 gene clusters related to plant growth hormone synthesis (e.g., of indole-3-acetic acid, auxin, and polyamine); 13 gene clusters related to the synthesis of various vitamins (e.g., B_1, B_2, B_6, B_{12}, K_2, and biotin) and their derivatives; 4 genes related to ATP-binding cassette (ABC) transporter complexes; 8 genes related to protein secretion; over 26 gene clusters encoding various glycosidases; 76 genes related to carbohydrate catabolism; 44 genes related to phosphatases activity; 185 genes related to organic acid biosynthesis; 22 genes related to organic acid transport; 11 genes related to nodulation; 6 genes related to nitrogen fixation; 3 genes related to catalase activity; and 14 genes related to peroxidases; 7 genes related to carotenoid biosynthetic process (Supplementary Table S3).

The interconnected evolutionary histories of Cyanobacteria and bacteria have led to the formation of various interactions between the two, including through nutrient exchange, signal transduction, gene transfer, and inhibition (Kouzuma and Watanabe, 2015; Cirri and Pohnert, 2019). For example, protein secretion systems and ATP-binding cassette (ABC) transporters are involved in the exchange of substances and signal transduction between cyanobacteria and their attached bacteria (Zhu et al., 2021). Consequently, the above genomic data for strain JXJ CY 39^T suggest the potential for exchange of substances and signal transduction between the bacteria and Maf, prompting follow-on experiments to evaluate the presence of such interactions.

3.3 Co-culture growth of Maf and strain JXJ CY 39^T

The chl-*a* concentrations of the control increased from 0.092 mg L^{-1} to 0.555 and 1.149 mg L^{-1} after 5 and 10 days of cultivation, respectively. Six of the attached bacteria in the BCSs did not influence the growth of Maf after 5 days of cultivation ($p > 0.05$). The exceptions were strains JXJ CY 11, 37, and 57 that resulted in decreased chl-*a* concentrations of 26.1, 11.6, and 24.6% ($p < 0.01$), respectively (Figure 1A). After 5 days of cultivation, the chl-*a* concentration of TCS with strains JXJ CY 57 + 39 was 0.466 mg L^{-1} or 16.1% lower ($p < 0.01$) than that of the control. The chl-*a* concentration of TCS with strains JXJ CY 11 + 39 was not different from that of the control ($p > 0.05$), while the chl-*a* concentrations of the other six TCSs were 0.580–0.678 mg L^{-1} or 4.5–22.1% higher ($p < 0.05$, $p < 0.01$) than that of the control (Figure 1A). Moreover, all chl-*a* concentrations of TCSs were 6.7–34.7% higher ($p < 0.05$, $p < 0.01$) than those of related

10.3389/fmicb.2024.1295696

TABLE 2 Differential characteristics of strain JXJ CY 39^T and the closest type strains.

Characteristic	1	2	3
Isolation source	*M. aeruginosa*	Flower	Freshwater
Colony color	Pale pink	Pale orange	Pale pink
Cell size (μm)	0.5–0.7 × 1.0–2.0	0.7–0.8 × 1.5–2.5	0.5–0.7 × 1.1–1.8
Growth at (°C)	5–38 (28)	10–28	10–37 (30)
pH range for growth	4–11	6–8	6–8
Tolerance of NaCl (%, w/v)	0–3	0	0–2
Nitrate reduction	+	–	–
Starch hydrolysis	+	–	–
Assimilation of:			
D-Glucose	(+)	–	+
N-Acetyl-glucosamine	–	–	+
D-Mannose	(+)	–	+
L-Arabinose	–	–	+
Maltose	–	–	+
Acid production:			
L-Arabinose	–	–	+
D-Xylose	–	–	+
D-Galactose	–	–	+
D-Glucose	(+)	–	+
D-Fructose	–	–	+
D-mannose	(+)	–	+
L-Rhamnose	–	–	+
D-Cellobiose	–	–	+
D-Maltose	(+)	–	+
D-Melibiose	–	–	+
D-Sucrose	–	–	+
D-Trehalose	–	–	+
D-Raffinose	–	–	+
Enzyme activity (API ZYM):			
Cystine arylamidase	+	+	–
Trypsin	+	–	–
α-Mannosidase	+	–	–
α-Fucosidase	+	–	–
Genomic characteristics			
CheckM completeness	98.1%	98.1%	98.1%
CheckM contamination	1.9%	1.9%	1.19%
CheckM strain heterogeneity	0.0	0.0	0.0
5S count	1	3	1
16s count	1	3	1
23S count	1	3	1
tRNA count	18	19	19
Contig count	24	2	10
N50 contigs	1,543,143 bp	4,896,009 bp	729,309 bp
Longest contig	1,553,743 bp	4,896,009 bp	988,577 bp
Scaffold count	24	2	10
N50 scaffolds	1,543,143 bp	4,896,009 bp	729,309 bp
Longest scaffold	1,553,743 bp	4,896,009 bp	988,577 bp
Genome size	5,064,077 bp	4,984,039 bp	4,330,477 bp
Protein count	4,424	4,370	3,759
Coding density	89.24%	88.57%	90.70%
GC percentage	42.09%	41.39%	41.63%
Ambiguous bases	11	0	0
GTDB representative	GCA_009770985.1	GCA_012849215.1	GCA_009755275.1

1, JXJ CY 39^T; 2, *M. robiniae* F39- 2^T (Won et al., 2022); 3, *M. aquatilis* HME9299^T (Kang et al., 2021). +, positive; –, negative; (+), weak positive. All of these strains are rod-shaped; positive for catalase, oxidase, acid and alkaline phosphatase, lipase C4,8, α-Galactosidase and β-Glucosidase; negative for α-Chymotrypsin and β-Glucuronidase.

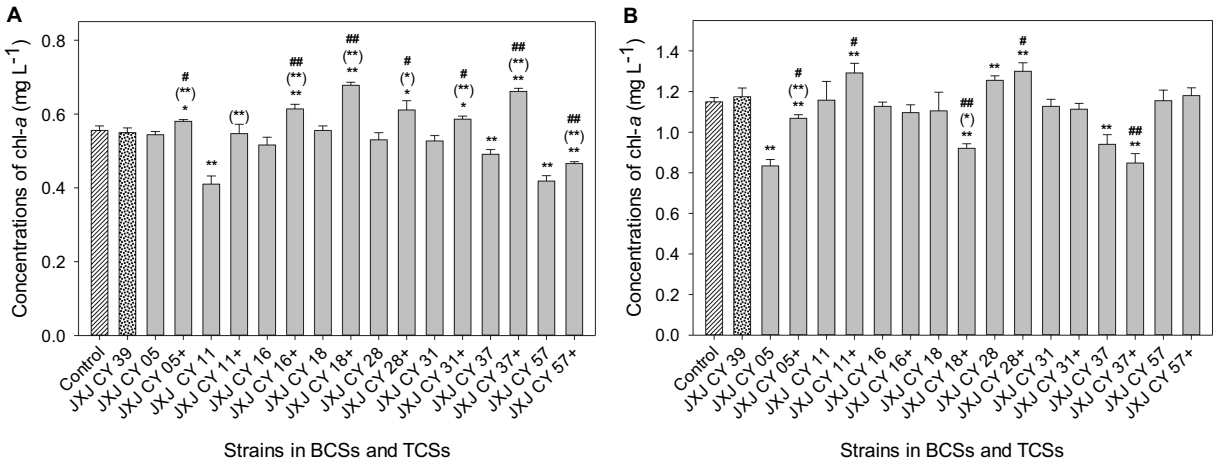

FIGURE 1
Influence of BCSs and TCSs on Maf growth. **(A,B)** Represent samples collected at 5 and 10 days of cultivation, respectively. +, indicates addition of strain JXJ CY 39^T in the culture. Error bars indicate standard deviation based on measurements of three replicates. * and ** indicate statistically significant differences in measurements between control cultures and BCS (or TCS) at $p < 0.05$ and $p < 0.01$, respectively. (*) and (**) indicate statistically significant differences in measurements between relevant BCSs and TCSs at $p < 0.05$ and $p < 0.01$, respectively. # and ## indicate statistically significant differences between measurements of BCS with JXJ CY 39^T cultures and relevant TCSs at $p < 0.05$ and $p < 0.01$, respectively.

BCSs after 5 days of cultivation, while six of the chl-*a* concentrations of TCSs were 5.6–23.4% higher ($p < 0.05$, $p < 0.01$) than that of BCS with JXJ CY 39^T (Figure 1A).

After 10 days of culture, the chl-*a* concentrations of BCSs with strain JXJ CY 05 and 37 were 0.834, and 0.940 mg L^{-1}, representing 27.4 and 18.2% lower ($p < 0.01$) than that of the control, respectively (Figure 1B). However, the chl-*a* concentration of BCS with JXJ CY 28 was 1.26 mg L^{-1} or 9.2% higher ($p < 0.01$) than that of the control (Figure 1B). In addition, the chl-*a* concentrations of TCSs with strains JXJ 05 + 39, 18 + 39, and 37 + 39 were 1.069, 0.921, and 0.848 mg L^{-1} after 10 days of cultivation, representing 7.0, 19.9, and 26.2% lower ($p < 0.01$) than that of the control. While, the chl-*a* concentrations of TCSs with strains JXJ CY 11 + 39 and 28 + 39 were 1.292 and 1.300 mg L^{-1} after 10 days of cultivation, representing 12.4 and 13.1% higher ($p < 0.01$) than that of the control, respectively. The chl-*a* concentrations of TCSs with strains JXJ CY 05 + 39 and 18 + 39 were 28.1% higher ($p < 0.01$) and 16.7% lower ($p < 0.05$) than those of the relevant BCSs, respectively.

The chl-*a* concentrations of TCSs with strains JXJ CY 05 + 39, 18 + 39, and 37 + 39 were 9.0, 21.6, and 27.8% lower ($p < 0.05$, $p < 0.01$) than that of the BCS with strain JXJ CY 39^T, respectively; while the chl-*a* concentrations of TCSs with strains JXJ CY 11 + 39 and 28 + 39 were 10.0 and 10.7% higher ($p < 0.05$) than that of BCS with JXJ CY 39^T, respectively. These data indicate that various strains may have distinct effects on Maf growth and that all adherent bacteria probably affect the interactions between Maf and other adherent bacteria, corroborating our previous research (Xiao et al., 2022c).

Algal–bacterial mutualisms are largely mediated by nutrition provisioning from bacteria (Cooper and Smith, 2015). Further, algal growth can be promoted by plant hormones, like indole-3-acetic acid (IAA) (Cirri and Pohnert, 2019; Hoke et al., 2021) and auxin (Seyedsayamdost et al., 2011). In addition, *Microcystis* requires vitamin B_{12} for methionine biosynthesis and many other vitamins for growth including B_1 and B_7 (Hoke et al., 2021). Gene annotations (Supplementary Table S3) indicated that strain JXJ CY 39^T could potentially provide Maf with plant growth hormones and various vitamins. Such mutualistic behaviors are likely the reason that the chl-*a* concentrations of some co-cultures were higher than those of the controls grown in BG11 medium (Figure 1). Kim et al. (2019) also reported that attached bacteria can promote Maf growth by decomposing H_2O_2 under aerobic growth conditions. Strain JXJ CY 39^T encodes catalases (Table 2; Supplementary Table S3) and peroxidases (Supplementary Table S3). Consequently, the decomposition of H_2O_2 produced by Maf could be another mechanism by which strain JXJ CY 39^T promotes the growth of Maf. Attached bacteria could provide *Microcystis* with complementary carotenoid molecules (Pérez-Carrascal et al., 2021). Carotenoids play an important role in protecting chlorophyll molecules against photo-oxidative damage (Young, 1991). Strain JXJ CY 39^T has 7 genes related to carotenoid biosynthetic process, indicating that this strain can also potentially protect chlorophyll molecules of Maf against photo-oxidative damage and promote the photosynthetic efficiency of the algae, which is probably another reason of JXJ CY 39^T potentially promoting the growth of Maf.

Interactions between algae and attached bacteria are dynamic and can be initiated and ended in response to environmental and developmental cues (Cooper and Smith, 2015). Such dynamism was apparent from the influences of attached bacteria on Maf growth. For example, the influences of attached bacteria on Maf growth in BCSs with strains JXJ 05, 11, 28, and 57, and in TCSs with strains 05 + 39, 11 + 39, 16 + 39, 18 + 39, 31 + 39, 37 + 39, and 57 + 39 changed with cultivation time (Figure 1). Almost the similar phenomena were also observed in previous studies (Zhang et al., 2016b,c, 2017; Xiao et al., 2022a,b,c).

Cellular densities of attached bacteria increased significantly ($p < 0.05$) after 5 days of cultivation (Table 3), except for those of strains JXJ CY 16, 18, 28, and 31 in BCSs, and strain JXJ CY 39^T in TCSs with JXJ CY 05 + 39 and 37 + 39, and strains JXJ CY 28 and 31 in TCSs. The cellular densities then significantly decreased ($p < 0.01$) with culture time. Further, strain JXJ CY 31 was even not detected on day

TABLE 3 Cell densities of nine strains in BCS and TCS.

Strains	Cell densities (CFU mL^{-1})					
	BCS		TCS		JXJ CY 39 in TCS	
	Day 5	Day 10	Day 5	Day 10	Day 5	Day 10
JXJ CY 39	$1.38 \pm 0.17 \times 10^{6}$*	0				
JXJ CY 05	$1.01 \pm 0.11 \times 10^{7}$**	$8.33 \pm 0.85 \times 10^{5}$**	$9.03 \pm 0.51 \times 10^{6}$**##	$1.11 \pm 0.15 \times 10^{5}$**##	$1.02 \pm 0.13 \times 10^{6}$#	0**
JXJ CY 11	$1.82 \pm 0.21 \times 10^{7}$**	$3.77 \pm 0.49 \times 10^{6}$**	$4.62 \pm 0.38 \times 10^{7}$**##	$2.19 \pm 0.32 \times 10^{7}$**##	$1.19 \pm 0.12 \times 10^{6}$*	0**
JXJ CY 16	$5.27 \pm 0.76 \times 10^{5}$**	$7.33 \pm 1.53 \times 10^{2}$**	$3.57 \pm 0.45 \times 10^{6}$**##	$1.39 \pm 0.14 \times 10^{4}$**##	$2.37 \pm 0.61 \times 10^{6}$*	0**
JXJ CY 18	$1.11 \pm 0.10 \times 10^{6}$	$1.59 \pm 0.18 \times 10^{4}$**	$2.01 \pm 0.22 \times 10^{6}$**##	$2.73 \pm 0.32 \times 10^{4}$**##	$1.43 \pm 0.15 \times 10^{6}$**	0**
JXJ CY 28	$5.57 \pm 0.72 \times 10^{4}$**	$1.82 \pm 0.14 \times 10^{4}$**	$1.82 \pm 0.17 \times 10^{5}$**##	$4.83 \pm 0.35 \times 10^{4}$**##	$1.62 \pm 0.11 \times 10^{6}$**	0**
JXJ CY 31	$1.02 \pm 0.13 \times 10^{5}$**	0**	0**##	0	$2.83 \pm 0.26 \times 10^{6}$**##	0**
JXJ CY 37	$3.73 \pm 0.61 \times 10^{7}$**	$1.11 \pm 0.18 \times 10^{6}$**	$4.15 \pm 0.33 \times 10^{6}$**##	$3.37 \pm 0.15 \times 10^{5}$**##	$8.77 \pm 0.86 \times 10^{5}$#	0**
JXJ CY 57	$3.03 \pm 0.20 \times 10^{7}$**	$1.39 \pm 0.15 \times 10^{7}$**	$3.86 \pm 0.17 \times 10^{7}$**##	$1.83 \pm 0.16 \times 10^{6}$**##	$1.85 \pm 0.18 \times 10^{6}$**#	0**

* and ** indicate statistically significant differences of measurements between days 0 and 5 or days 5 and 10 of cultivation in BCSs (or TCSs) at $p < 0.05$ and $p < 0.01$, respectively. # and ## indicate statistically significant differences between measurements from relevant BCSs and TCSs at $p < 0.05$ and $p < 0.01$, respectively.

10 of BCS cultivation nor on days 5 and 10 of cultivation in TCS, while strain JXJ CY 39^{T} was not detected in both BCS and TCSs on the day 10 of cultivation. The cellular densities of the other eight bacteria in TCSs were significantly influenced ($p < 0.01$) by cultivation with strain JXJ CY 39^{T} on both days 5 and 10 of cultivation. However, the cellular densities of JXJ CY 39^{T} in TCSs were only influenced by cultivation with strains JXJ CY 05, 16, 31, 37, and 57 on day 5 of cultivation ($p < 0.005$, $p < 0.001$), but were not influenced by cultivation with any of the other eight strains on day 10 of cultivation ($p > 0.05$). Thus, the influences of Maf on attached bacteria likely varies with bacterial strain and cultivation duration. Moreover, all attached bacteria would likely influence the interactions between Maf and other bacterial taxa. These results are consistent with those from our previous study (Xiao et al., 2022c), and also reflect the dynamic interactions between algae and attached bacteria.

BG11 medium is a synthetic medium that lacks sufficient organic carbon sources, such that heterotrophic attached bacteria will not grow due to insufficient carbon and energy sources. Dissolved organic carbon secreted by *M. aeruginosa* (Casamatta and Wickstrom, 2000) can be used by bacteria for growth. A previous study showed that bacteria attached to *Microcystis* cells encode higher relative abundances of carbon degradation genes and β-glucosidase activity to enable the use of organic carbon secreted by *Microcystis* (Yang et al., 2021). Annotation of the strain JXJ CY 39^{T} genome revealed the presence of many genes that would enable use of dissolved organic carbon secreted by Maf (Supplementary Table S3). This likely explains why the attached bacteria grew during the first five days despite the organic carbon-deficient medium used for cultivation.

The analysis of metagenomes, metatranscriptomes and metaproteomes on natural water bloom samples play important roles in the recognition of interactions in phytoplankton communities (Kazamia et al., 2016). However, these technologies can only let us know the overall metabolic capability and ecological state of a community (Kazamia et al., 2016), and many aspects of these interactions, especially specific interactions of the microbes within, are still unknown (Grossart and Simon, 2007; Kazamia et al., 2016; Zhang et al., 2019) because of most of these studies were performed under non-axenic conditions (Grossart and Simon, 2007; Zhang et al., 2019). Specific interactions can only probably be understood through physiological experiments using defined systems such as co-cultures of known and well-characterized partners in the laboratory, which can shed light on the interactions at the molecular and cellular levels (Kazamia et al., 2016). In this study, we have removed other culturable heterotrophic bacteria from Maf, and then inoculated the specific pure cultures of these isolated attached bacteria back to Maf, which can eliminate the distractions of other unknown culturable heterotrophic bacteria on the specific interactions, and let us know more about the interactions between Maf and its attached bacteria like mentioned above and below.

3.4 Influences of co-cultures on MC-LR concentrations

The E-MC-LR concentrations of the control were 37.6 and 172.2 μg mg^{-1} chl-*a* on days 5 and 10 of cultivation, respectively. The E-MC-LR concentrations of BCSs with strains JXJ CY 37 and 57, in addition to TCS with strains JXJ CY 57 + 39 on day 5 of cultivation were 44.0, 42.9, and 43.5 μg mg^{-1} chl-*a*, respectively, representing 17.0, 14.1 and 15.6% higher ($p < 0.05$) values compared to controls, respectively. However, the E-MC-LR concentrations of the other seven BCSs did not significantly differ from the control, while the E-MC-LR concentrations of the other seven TCSs were 11.3–30.5% lower ($p < 0.05$, $p < 0.01$) than that of the control (Figure 2A). Moreover, the E-MC-LR concentrations of the six TCSs were 11.4–28.2% lower ($p < 0.05$, $p < 0.01$) than those of the relevant BCSs (Figure 2A). The E-MC-LR concentrations of the TCSs were 7.6–27.6% lower ($p < 0.05$, $p < 0.01$) than that of BCS with strain JXJ CY 39, with the exception of TCS with strain JXJ CY 57 + 39 that was 20.4% higher ($p < 0.01$) (Figure 2A).

After day 10 of cultivation, the E-MC-LR concentrations of BCSs with strains JXJ CY 11, 18, 28, and 57 were 19.7, 23.6, 31.8, and 40.5% lower ($p < 0.01$) than that of the control, respectively; while the E-MC-LR concentrations of BCSs with strains JXJ CY 05, 16, 31, 37, and 39 were 60.8, 24.8, 29.7, 51.3, and 27.9% higher ($p < 0.01$) than that of the control, respectively (Figure 2B). At

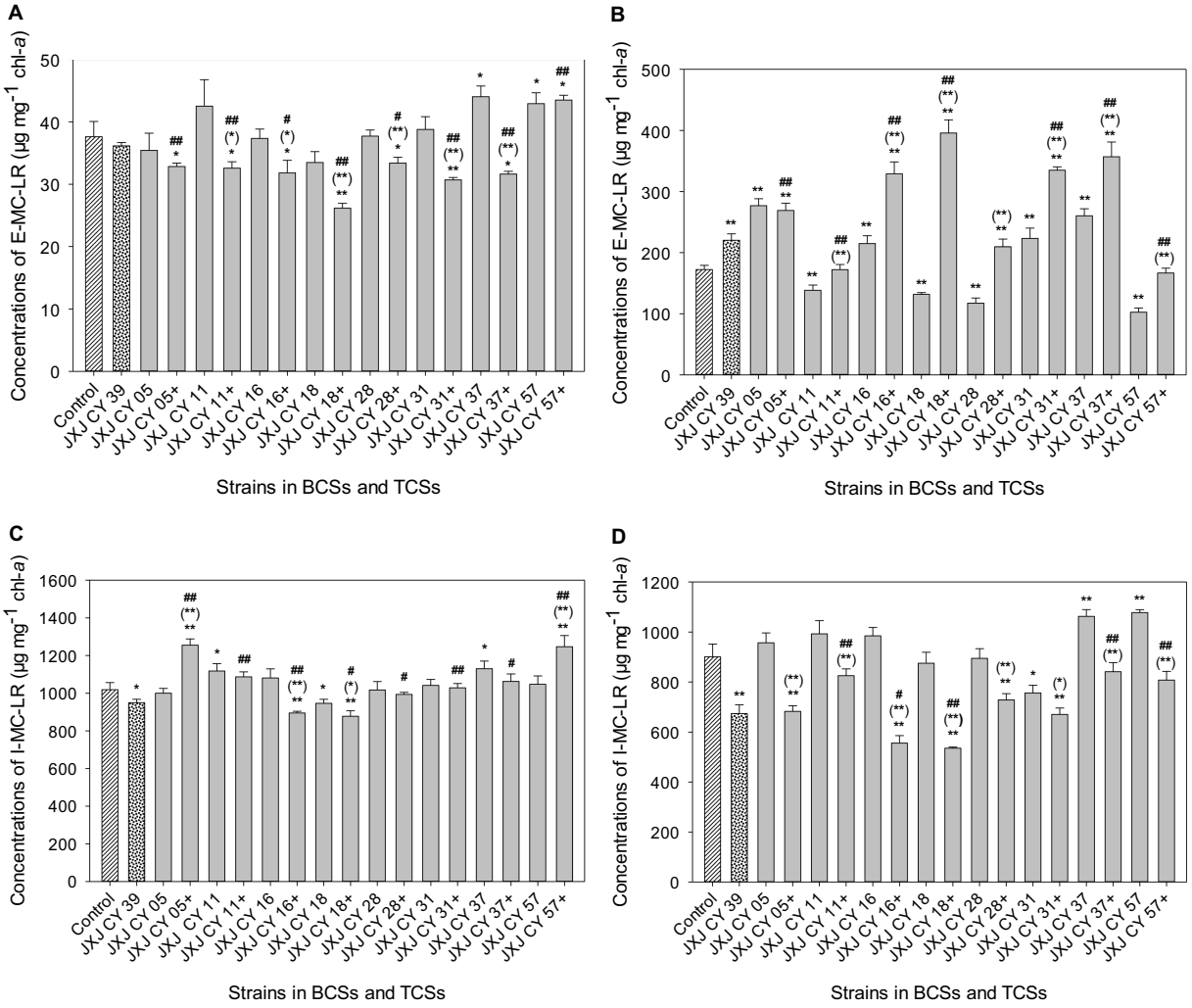

FIGURE 2
Influence of BCSs and TCSs on E-MC-LR and I-MC-LR concentrations in Maf cultures. **(A,C)** Represent samples collected at 5 day of cultivation. **(B,D)** Represent samples collected at 10 day of cultivation. + indicates strain JXJ CY 39^T was included in the co-culture. Error bars indicate standard deviations for measurements from three replicates. * and ** indicate statistically significant differences of measurements between control cultures and BCSs (or TCSs) at $p < 0.05$ and $p < 0.01$, respectively. (*) and (**) indicate statistically significant differences between measurements from relevant BCSs and TCSs at $p < 0.05$ and $p < 0.01$, respectively. # and ## indicate statistically significant differences between measurements of BCS with JXJ CY 39^T and relevant TCSs at $p < 0.05$ and $p < 0.01$, respectively.

10 days of cultivation, the E-MC-LR concentrations of the six TCSs were 21.7–129.8% higher ($p < 0.05$, $p < 0.01$) than the control, with the exception of TCSs containing strains JXJ CY 11 + 39 and 57 + 39 (Figure 2B). The E-MC-LR concentrations of the seven TCSs were 24.4–200.9% higher ($p < 0.01$) than those of relevant BCSs, with the exception of the TCS with strains JXJ CY 05 + 39 (Figure 2B). The E-MC-LR concentrations of TCSs with strains JXJ CY 11 + 39 and 57 + 39 were 21.9–24.3% lower ($p < 0.01$) than that of BCS with strain JXJ CY 39, while the E-MC-LR concentrations of the other TCSs were 22.2–79.7% higher ($p < 0.05$) than that of BCS with strain JXJ CY 39, with the exception of the TCS with strain JXJ CY 28 + 39 (Figure 2B). Thus, the different strains exerted different and dynamic influences on the E-MC-LR concentrations of Maf. Moreover, the results suggest that the addition of any strain into a BCS with one attached bacterium would likely influence the E-MC-LR concentrations of Maf. These results are consistent with previous study (Xiao et al., 2022c).

The I-MC-LR concentrations of the controls were 1,019.0 and 900.8 μg mg^{-1} chl-*a* on days 5 and 10 of cultivation, respectively (Figures 2C, D). On day 5 of cultivation, the I-MC-LR concentrations of BCSs with strains JXJ CY 11 and 37 were 1,117.8, and 1,130.7 μg mg^{-1} chl-*a*, representing 9.7 and 11.0% higher ($p < 0.05$) than that of the control, respectively. In addition, the I-MC-LR concentrations of BCSs with strains JXJ CY 18 and 39 were 946.9 and 950.1 μg mg^{-1} chl-*a*, respectively, representing 7.1 and 6.8% lower ($p < 0.05$) than that of the control, respectively (Figure 2C). After 5 days of culture, the I-MC-LR concentrations of TCSs with strains JXJ CY 05 + 39 and 57 + 39 were 25.4 and 19.1% higher ($p < 0.01$) than those of relevant BCSs, respectively. In addition, the I-MC-LR concentrations of TCSs with strains JXJ CY 16 + 39 and 18 + 39 were 17.2 and 7.2% lower ($p < 0.05$, $p < 0.01$) than those of the related BCSs, respectively. The I-MC-LR concentrations of TCSs were 4.6–32.1% higher ($p < 0.05$, $p < 0.01$) than that of BCS with JXJ CY 39, with the exception of TCSs with strains JXJ CY 16 + 39 and 18 + 39 that

TABLE 4 Influences of limited available N on the growths of Maf and JXJ CY 39^T.

Groups	Targets	On day 7	On day 14
a	Chl-*a* (mg L^{-1})	0.371 ± 0.013	0.176 ± 0.008$^{(**)}$
	E-MC-LR (μg mg^{-1} chl-*a*)	98.4 ± 3.8	339.4 ± 23.9$^{(**)}$
	I-MC-LR (μg mg^{-1} chl-*a*)	968.2 ± 42.6	1162.2 ± 39.2$^{(**)}$
b	Chl-*a* (mg L^{-1})	0.564 ± 0.026**	0.463 ± 0.013**$^{(**)}$
	E-MC-LR (μg mg^{-1} chl-*a*)	45.3 ± 0.9**	159.8 ± 5.7**$^{(**)}$
	I-MC-LR (μg mg^{-1} chl-*a*)	942.1 ± 27.5	965.5 ± 31.8**
	Cell densities of JXJ CY 39^T (CFU mL^{-1})	2.93 ± 0.31 × 10$^{6\#\#}$	3.27 ± 0.47 × 10$^{6\#\#}$
c	Cell densities of JXJ CY 39^T (CFU mL^{-1})	9.07 ± 0.50 × 10^4	2.03 ± 0.25 × 10$^{4(**)}$

a, Maf cultured with no strain JXJ CY 39^T; b, Maf cocultured with strain JXJ CY 39^T; c, strain JXJ CY 39^T cultured with no Maf. *, ** indicate the significant differences between a and b at the level of $p < 0.05$, $p < 0.01$, respectively, at the same culture time. (**) indicated the significant differences between day 7 and day 14. ## indicate the significant differences between b and c at the level of $p < 0.05$, $p < 0.01$, respectively, at the same culture time.

exhibited 5.8 and 7.6% lower ($p < 0.01$, $p < 0.05$) than that of BCS with strain JXJ CY 39, respectively (Figure 2C).

On day 10 of cultivation, the I-MC-LR concentrations of BCSs with strains JXJ CY 39 and 31 were 25.2 and 16.0% lower ($p < 0.01$, $p < 0.05$) than the control, respectively, and the I-MC-LR concentrations of BCSs with strains JXJ CY 37 and 57 were 18.0 and 19.6% higher ($p < 0.01$) than the control (Figure 2D), respectively. On day 10 of cultivation, the I-MC-LR concentrations of the TCSs were 11.4–43.5% lower ($p < 0.05$, $p < 0.01$) than those of the related BCSs, and 19.1–40.6% lower ($p < 0.01$) than the control, with the exception of TCSs with strains JXJ CY 11 + 39, 37 + 39, and 57 + 39 that were not different from the control ($p > 0.05$) (Figure 2D). The I-MC-LR concentrations of TCSs with strains JXJ CY 16 + 39 and 18 + 39, in addition to TCSs with strains JXJ CY 11 + 39, 37 + 39, and 57 + 39 were 17.5–20.6% lower ($p < 0.05$, $p < 0.01$) and 19.9–24.9% higher ($p < 0.01$) than that of the BCS with strain JXJ CY 39 (Figure 2D), respectively. While the I-MC-LR concentrations of the TCSs with JXJ 05 + 39 on day10 of cultivation was 24.2% lower ($p > 0.01$) than the control (Figure 2D) in contrast to that of TCSs with JXJ 05 + 39 on day 5 of cultivation, which was 23.2% higher ($p > 0.01$) than the control (Figure 2C). These data indicate that different strains probably exert different and dynamic influences on the I-MC-LR concentrations of Maf. Moreover, the addition of any strain into a BCS with one attached bacterium would also likely influence the I-MC-LR concentrations of Maf. These results are consistent with our previous study (Xiao et al., 2022c).

3.5 Capacity for nitrogen fixation and phosphate acquisition

Cellular densities of strain JXJ CY 39^T initially increased from 1 × 10^5 CFU mL^{-1} to 3.9 × 10^6 CFU mL^{-1} after 2 days of cultivation in nitrogen-free medium, indicating that this strain could convert N_2 into NH_3 to support its growth, which was consistent with annotation of the strain JXJ CY 39^T genome with the GO database (Supplementary Table S3). After 2 days of co-cultivation, the concentrations of available phosphorus increased by 10.41 ± 0.44 mg L^{-1} for $Ca_3(PO_4)_2$ and 5.68 ± 0.24 mg L^{-1} for phytin, indicating that strain JXJ CY 39^T can dissolve insoluble inorganic and organic phosphate, and release dissoluble phosphorus, consistent with the genomic analyses (Supplementary Table S3). Therefore, strain JXJ CY 39^T can potentially provide Maf with available N and P when available N and P are limited in the environment.

3.6 Influences of limited P and N availability on Maf and JXJ CY 39^T growth

In nitrogen-deficient medium, the color of Maf cultured without JXJ CY39^T turned green gradually during the first 7 days, and turned yellow quickly during the second 7 days. Consequently, chl-*a* concentrations of Maf cultured without JXJ CY39^T increased to 0.371 mg L^{-1} on day 7 from 0.030 mg L^{-1} on day 0, and then decreased to 0.176 mg L^{-1} on day 14 (Table 4). However, in nitrogen-deficient medium, the color of Maf co-cultured with JXJ CY39^T turned green more quickly during the first 7 days, and turned yellow more slowly during the second 7 days. Consequently, chl-*a* concentrations of Maf co-cultured with JXJ CY39^T increased to 0.564 mg L^{-1} on day 7, which was 52.0% higher ($p < 0.01$) than that of the control, and then decreased to 0.463 mg L^{-1} on day 14, which was 163.1% higher ($p < 0.01$) than that of the control (Table 4).

As mentioned above, the inoculation of Maf cultured in BG11 imported 71.4 mg L^{-1} of $NaNO_3$ into nitrogen-free medium, in addition to 0.321 mg L^{-1} of N as NH_4^+ in the ferric ammonium citrate. Additionally, degradation of phycobiliproteins of *Microcystis* can expand biomass by about 50% (Wang et al., 2021). These available nitrogen sources were the reasons of the growth of Maf cultured without JXJ CY39^T during the first 7 days in nitrogen-free medium. However, exhausting these available nitrogen sources resulted in mass mortality of Maf, which was the main reason that the color of Maf cultured without JXJ CY39^T turned yellow quickly during the second 7 days.

Ammonia is a key component involved in aquatic environment microbial interactions (Cirri and Pohnert, 2019), and can dissolve in water easily and form $NH_3{\cdot}H_2O$, which further ionizes and produces NH_4^+. *Microcystis* prefer ammonium (NH_4^+) because of its attached bacteria often lacking functional genes that mediate nitrification (Yang et al., 2021). Therefore, strain JXJ CY39^T can provide Maf with NH_4^+ since it can convert N_2 into NH_3, which was the main reason that Maf co-cultured with JXJ CY39^T expand more biomass during the first 7 days, and exhaust lesser biomass during the second 7 days (Table 4). Therefore, strain JXJ CY 39^T can provide Maf with available N when available N is limited. It is consistent with those of other co-cultures with other attached bacteria and Maf (Xiao et al., 2022a,b,c).

TABLE 5 Influences of limited available P on the growths of Maf and JXJ CY 39^T.

Groups	Targets	On day 9	On day 18
a	Chl-*a* (mg L^{-1})	0.639 ± 0.032	0.985 ± 0.017$^{(**)}$
	E-MC-LR (μg mg^{-1} chl-*a*)	16.0 ± 0.9	56.1 ± 2.5$^{(**)}$
	I-MC-LR (μg mg^{-1} chl-*a*)	1133.0 ± 26.9	1949.6 ± 17.6$^{(**)}$
b	Chl-*a* (mg L^{-1})	0.745 ± 0.008**	1.163 ± 0.022**$^{(**)}$
	E-MC-LR (μg mg^{-1} chl-*a*)	19.6 ± 0.8**	47.9 ± 6.2$^{(**)}$
	I-MC-LR (μg mg^{-1} chl-*a*)	1022.3 ± 40.6*	1713.1 ± 22.8**$^{(**)}$
	Cell densities of JXJ CY 39^T (CFU mL^{-1})	7.27 ± 0.71 × 10$^{4\#\#}$	1.46 ± 0.11 × 10$^{5\#\#(**)}$
c	Cell densities of JXJ CY 39^T (CFU mL^{-1})	1.43 ± 0.25 × 10^4	1.77 ± 0.42 × 10$^{3(**)}$

a, Maf cultured with no strain JXJ CY 39^T; b, Maf cocultured with strain JXJ CY 39^T; c, strain JXJ CY 39^T cultured with no Maf. *, ** indicate the significant differences between a and b at the level of $p < 0.05$, $p < 0.01$, respectively, at the same culture time. (**) indicated the significant differences between day 9 and day 18. ## indicate the significant differences between b and c at the level of $p < 0.05$, $p < 0.01$, respectively, at the same culture time.

In nitrogen-deficient medium, strain JXJ CY39^T also influenced the synthesis of MC-LR (Table 4). The E-MC-LR concentrations of Maf co-cultured with JXJ CY39^T were 45.3 and 159.8 μg mg^{-1} chl-*a*, which were 54.0, and 52.9% lower ($p < 0.01$) than those of the controls. The I-MC-LR concentration of Maf co-cultured with strain JXJ CY39^T was 1,162.2 μg mg^{-1} chl-*a* on day 14 of cultivation, which was 16.9% lower ($p < 0.01$) than that of the control. Similar phenomena were also found in previous studies (Xiao et al., 2022a,b).

In $Ca_3(PO_4)_2$ medium, the color of Maf cultured without strain JXJ CY39^T turned green gradually during the test time. Consequently, the chl-*a* concentrations increased to 0.639, and 0.985 mg L^{-1} after 9 and 18 days of culturation (Table 5), respectively. However, the color of Maf co-cultured with strain JXJ CY39^T turned greener during the test time, and the chl-*a* concentrations increased to 0.745, and 1.163 mg L^{-1} after 9 and 18 days of culturation, which were 16.6, and 18.1% higher ($p < 0.01$) than those of the controls (Table 5), respectively.

As mention above, the inoculation of Maf cultured in BG11 imported 1.86 mg L^{-1} of K_2HPO_4 into $Ca_3(PO_4)_2$ medium. And $Ca_3(PO_4)_2$ is slightly soluble in water and breaks down into Ca^{2+} and PO_4^{3+}. Therefore, dissoluble phosphorus is the key element that restricts the growth of Maf in $Ca_3(PO_4)_2$ medium, in spite of the uptake of PO_4^{3+} by Maf would result in more $Ca_3(PO_4)_2$ being dissolved. These were the reasons that Maf cultured without strain JXJ CY39^T turned green more slowly. Secreting phosphatases and organic acids are two of the important mechanisms that microbes degrade insoluble phosphorus into dissoluble phosphorus. Therefore, strain JXJ CY39^T can facilitate the dissolving of $Ca_3(PO_4)_2$ since it has abundant genes related to phosphatase activity, and organic acid biosynthetic process and transmembrane transport (Supplementary Table S3), which would relieve the restriction of lacking dissoluble phosphorus on the growth of Maf in $Ca_3(PO_4)_2$ medium. This was the main reason that Maf co-cultured with strain JXJ CY39^T expanded more biomass than Maf cultured without strain JXJ CY39^T in $Ca_3(PO_4)_2$ medium (Table 5). These results were consistent with previous studied of co-culture of other phosphate-solubilizing attached bacteria and *Microcystis* (Xiao et al., 2022a,b,c).

Strain JXJ CY39^T also significantly influenced MC-LR synthesis of Maf in $Ca_3(PO_4)_2$ medium (Table 5). The E-MC-LR concentration of Maf co-cultured with strain JXJ CY39^T was 19.6 μg mg^{-1} chl-*a* on day 9 of cultivation, which was 22.5% higher ($p < 0.01$) than that of the control. The I-MC-LR concentrations of Maf cultured with strain JXJ CY39^T were 1,022.3 and 1,713.1 μg mg^{-1} chl-*a* on days 9 and 18 of cultivation, representing 9.8 and 12.1% lower ($p < 0.05$, $p < 0.01$) than those of the controls, respectively. Similar phenomena were also found in previous studies (Xiao et al., 2022a,b).

The cellular densities of strain JXJ CY39^T cultured without Maf decreased with the cultivation time ($p < 0.01$) in media with both $Ca_3(PO_4)_2$ and nitrogen limitation (Tables 4, 5). However, the cellular densities of strain JXJ CY39^T co-cultured with Maf in available nitrogen-deficient medium increased to 2.93 × 10^6 CFU mL^{-1} after 7 days of cultivation, and maintained about 3 × 10^6 CFU mL^{-1}during the next 7 days, which were over 32–161-fold higher ($p < 0.01$) than those cultured without Maf in nitrogen-deficient medium (Table 4). Further, the cellular densities of strain JXJ CY39^T co-cultured with Maf in $Ca_3(PO_4)_2$ medium were 7.27 × 10^4 and 1.46 × 10^5 CFU mL^{-1} on days 9 and 18 of cultivation, which were over 5- and 82-fold increases in densities when cultured without Maf in $Ca_3(PO_4)_2$ medium (Table 5). As described above, strain JXJ CY39^T would disappear from cultures after co-culture with Maf in BG11 medium for 10 days or more. Thus, these results suggested that Maf could adjust interactions with strain JXJ CY39^T when available N and P are limited, and further certified that the interactions between algae and attached bacteria are dynamic and can be initiated and ended in response to environmental change.

3.7 Inhibition of attached bacteria by Maf metabolites

Plate-based antibacterial assays (Supplementary Figure S7) revealed that Maf extracts exhibited obvious inhibitory activities on strains JXJ CY 31, 37, and 39, in addition to weak (strains JXJ CY 16 and 28) or no inhibitory activities on other attached bacterial strains. Fraction IV represented the fat-soluble component and did not exhibit inhibitory activity against any of the nine attached bacteria. Fraction II exhibited the strongest inhibitory activity, followed by fraction I. Fraction III contained MC-LR at a concentration of 4 μg per disk and exhibited no or very weak inhibitory activities on any of the nine attached bacteria.

Co-culture analyses (Table 3) revealed that the cell densities of some strains increased at 5 days of cultivation and then decreased at day 10 of cultivation. The reason for this difference was likely because antibacterial compounds secreted by Maf did not achieve concentrations high enough to inhibit bacterial growth after 5 days of cultivation, but did after 10 days of cultivation. However, the cell

densities of strains JXJ CY 05, 11, 16, 18, 28, and 57 significantly decreased ($p < 0.01$) after day 10 of cultivation and even day 5 of cultivation, despite that Maf extracts exhibited no or very weak inhibitory activities on these bacteria grown on plates. It is possible that the synthesis of specific antibacterial compounds required the induction of these bacteria or alternatively that some antibacterial compounds lost their antibacterial activities during chemical extraction and isolation.

Healthy macroalgae can control their attached bacteria to avoid excessive bacterial growth and further competition for nutrients (Kouzuma and Watanabe, 2015). Specifically, healthy *M. aeruginosa* can apparently control their attached bacteria to avoid competition for nutrients (Zhang et al., 2016b,c; Xiao et al., 2022a,b,c). Likewise, extracts from *M. aeruginosa* exhibited inhibitory activities on some of their attached bacteria (Casamatta and Wickstrom, 2000) and many other bacterial taxa including *Escherichia coli* (Ostensvik et al., 1998; Valdor and Aboal, 2007), *Streptoverticillium* (Valdor and Aboal, 2007), *Bacillus subtilis*, *B. cereus*, and *Aeromonas hydrophila* (Ostensvik et al., 1998). Microcystins including MC-LR, MC-RR, and MC-YR were also evaluated for antibacterial activity. Ostensvik et al. (1998) observed that MCs did not exhibit any inhibitory activities against *E. coli*, *Bacillus subtilis*, *B. cereus*, and *Aeromonas hydrophila* at a concentration of 1–8 μg mL^{-1}, while Valdor and Aboal (2007) observed that MC-YR inhibited *Streptoverticillium* at a 12.5 μg mL^{-1}, while MC-RR and MC-LR inhibited *Streptoverticillium* at a 25 μg mL^{-1}, and MC-LR inhibited *E. coli* at a 5 μg mL^{-1}. Nevertheless, it has remained unclear whether MCs are the specific chemicals by which Maf control their attached bacteria.

MC-LR accounts for over 57% of the MCs produced in *M. aeruginosa* laboratory cultures (Liu et al., 2012) and 45.5–99.8% of the MCs in HAB-impacted natural waters (Vasconcelos et al., 1996). The results of this study showed that E-MC-LR, I-MC-LR, and total MC-LR concentrations were 0.017–0.37, 0.44–1.25, and 0.46–1.36 μg mL^{-1}, respectively. Thus, the concentrations of E-MC-LR and even the total MCs from both environmental samples and laboratory culture samples are a small fraction of the concentrations used in previous studies. Consequently, MCs may not be the specific chemicals secreted by Maf that control their attached bacteria. These results were further verified with antibacterial assays (Supplementary Figure S7). Fraction III contained MC-LR at a concentration of 4 μg per disk and exhibited no or very weak inhibitory activities on bacterial strains, while fractions I and II, and especially fraction II, exerted stronger and more broad-spectrum antibacterial activity. Consequently, fraction II likely contains one of the main chemicals that Maf uses to specifically control their attached bacteria.

Co-culture experiments (Table 3) revealed that strain JXJ CY 39^T disappeared when co-cultured with Maf in BG11 medium. However, the cellular density of strain JXJ CY 39^T on day 18 of cultivation in $Ca_3(PO_4)_2$ medium was 200% of that on day 9 of cultivation (Table 5). Thus, the concentrations of antibacterial components in Maf cultures did not increase with cultivation time although chl-*a* concentrations increased by 56.2%. Only enough strain JXJ CY 39^T biomass can provide Maf with enough available P in $Ca_3(PO_4)_2$ medium, probably partially explaining why the cell density of strain JXJ CY 39^T increased after 18 days of cultivation. Thus, Maf was apparently able to adjust the synthesis and secretion of specific antibacterial components based on their nutritional requirements. And this further proved that the interactions between algae and attached bacteria are dynamic and can be initiated and ended in response to environmental change.

3.8 Influence of strain JXJ CY 39^T on the growth of non-culturable Maf-attached bacteria

No bacteria grew on ISP2 plates after incubation at 28.0°C for 7 days, indicating that strain JXJ CY 39^T in the samples had died, and the control cultures remained axenic during the experiments. Community compositional analyses of eight samples of purified Maf co-cultured with strain JXJ CY 39^T and purified Maf cultured without strain JXJ CY 39^T from days 5, 10, 15, and 35 yielded 820,153 high-quality, partial 16S rRNA gene sequences without singletons, representing 379 amplicon sequence variants (ASVs). Each sample only contained a few unique ASVs (Supplementary Figure S8). Bacterial intra-sample (alpha) diversity was estimated by rarefaction analysis (Supplementary Figure S9) and by calculating the Shannon and Simpson diversity indices, in addition to the observed number of ASVs (Figure 3A). Rarefaction analyses with the Shannon index indicated that the sequencing efforts recovered nearly all diversity expected in these samples. The community diversity of purified Maf co-cultured with strain JXJ CY 39^T was higher than that of purified Maf cultured without strain JXJ CY 39^T.

ASVs were taxonomically classified using the latest version of the Ribosomal Database Project (RDP) database to assess bacterial taxonomic compositional changes across time in cultures of Maf with and without strain JXJ CY 39^T. Differences between culture conditions were evident. In the control groups, there were 159, 150, 134, 154 ASVs detected in purified Maf cultured without strain JXJ CY 39^T at days 5, 10, 15, 35 of the culture periods, respectively. While in the experimental groups, higher number of ASVs were detected in bacterial communities, with 183, 178, 217 and 157 ASVs detected in purified Maf co-cultured with strain JXJ CY 39^T on day 5, 10, 15, 35, respectively. A total of 9 phyla, 22 orders, and 28 genera were identified in culture samples of purified Maf co-cultured with strain JXJ CY 39^T, while 7 phyla, 20 orders, and 27 genera were identified in culture samples of Maf cultured without strain JXJ CY 39^T. The relative abundances of Maf cultured without strain JXJ CY 39^T were over 98.35% in all samples. Bacteria belonging to several phyla were also detected including *Proteobacteria*, *Bacteroidetes*, *Actinobacteria*, *Firmicutes*, and *Verrucomicrobia* on day 5 of cultivation; *Proteobacteria*, *Bacteroidetes*, *Actinobacteria*, *Firmicutes*, *Verrucomicrobia*, and *Deinococcus-Thermus* on day 10 of cultivation; *Proteobacteria*, *Bacteroidetes*, and *Firmicutes* on day 15 of cultivation; and *Proteobacteria*, *Firmicutes*, *Bacteroidetes*, and *Actinobacteria* on day 35 of cultivation. The relative abundances these phyla ranged between 0.0028–0.05%, except for *Proteobacteria* on day 35 of cultivation, that exhibited relative abundances of 1.59%. Thus, the relative abundances of non-culturable attached bacteria of Maf changed with cultivation time, while the *Proteobacteria*, *Bacteroidetes*, and *Firmicutes,* and especially *Proteobacteria,* were the most common phyla associated with *Microcystis* and were maintained at relatively high abundances. Specifically, on day 5 and 10 of the culture periods, the relative abundance of ASVs belonging to the genus *Dubosiella* was 0.003%, whereas on days 15 and 35 of the culture periods, it dropped to 0%.

10.3389/fmicb.2024.1295696

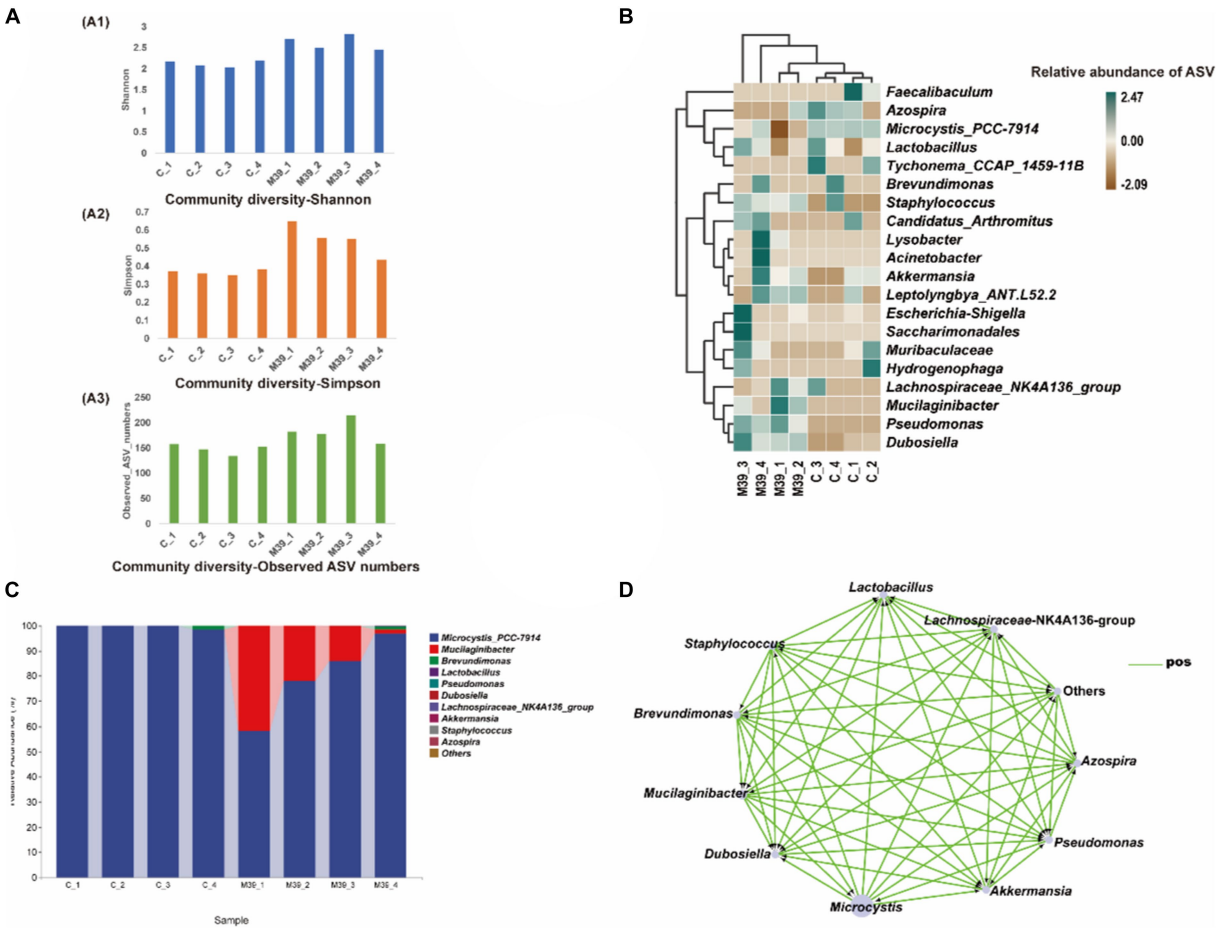

FIGURE 3
Analysis of bacterial community in samples of purified Maf co-cultured with and without strain JXJ CY 39^T on days 5, 10, 15, and 35. **(A)** Amplicon sequence variant (ASV) richness and diversity indices of culture communities assessed with Shannon diversity, Simpson diversity, and total ASV number indices. **(B)** Heatmap analysis of enriched bacterial taxa in these culture samples. **(C)** The relative abundances of the bacterial community at the genus taxon level in purified Maf co-cultured with or without strain JXJ CY 39^T on days 5, 10, 15, and 35. The relative abundances of the most abundant genera are shown. **(D)** Co-occurrence network visualization of dominant genera in the communities. Each node represents a dominant genus and each edge represents two correlated genera based on absolute Spearman's correlations >0.5 and with a $p < 0.05$. The edge length is based on Bray-Curtis distances and the node size reflects the relative abundances of genera. C_1, C_2, C_3, and C_4 indicate cultures of Maf without JXJ CY 39^T collected on days 5, 10, 15, and 35 of cultivation, respectively. M39_1, M39_2, M39_3, and M39_4 indicate co-cultures of JXJ CY 39^T and Maf collected on days 5, 10, 15, and 35 of cultivation, respectively.

Similarly, the abundance of ASVs belonging to the genus *Akkermansia* decreased from 0.007% on days 5, and 10 of culture to 0% on days 15, and 35 of culture. On the other hand, the relative abundance of ASVs belonging to the genus *Lactobacillus* was absent (0%) on day 5 of culture, increased to 0.011% on day 10 of culture, 0.026% on day 15 of culture, and decreased to 0.012% on day 35 of the culture period.

The relative abundances of Maf co-cultured with strain JXJ CY 39^T were 58.20, 77.94, 85.96, and 96.87% on days 5, 10, 15, and 35 of cultivation, respectively. The relative abundances of strain JXJ CY 39^T co-cultured with Maf were 41.72, 21.94, 13.85, and 1.59% on days 5, 10, 15, and 35 of cultivation, respectively. Thus, the relative abundances of Maf increased with cultivation time, in contrast to those of strain JXJ CY 39^T. The relative abundances of strain JXJ CY 39^T quickly decreased, indicating that its fraction of the community decreased with culture time. In addition, many other bacteria from various phyla were detected in the co-culture samples. *Proteobacteria*, *Firmicutes*, and *Verrucomicrobia* were detected on day 5 of cultivation, while *Actinobacteria* appeared on day 10 of cultivation along with the three abovementioned phyla. The *Epsilonbacteraeota*, and *Patescibacteria* likewise appeared on day 15 of cultivation in addition to the four above phyla, while *Deinococcus-Thermus* appeared on day 35 of cultivation alongside concomitant disappearances of *Epsilonbacteraeota* and *Patescibacteria*. The relative abundances of these phyla ranged between 0.0017–0.075%, except for *Proteobacteria* on day 35 of cultivation that exhibited a relative abundance of 1.45%. Notably, the *Epsilonbacteraeota* and *Patescibacteria* were detected in co-cultures of Maf and strain JXJ CY 39^T, unlike Maf cultured without strain JXJ CY 39^T.

Linear discriminant analysis (LDA) of effect size (LEfSe) analysis can be used to identify significant enrichment of bacteria among samples (Segata et al., 2011). A cladogram was constructed for LEfSe analysis (Figure 3B) that showed the most differentially abundant bacterial taxa (with default logarithmic, LDA, values >3.0) related to the two groups of samples. The bacterial taxa enriched in culture

samples of purified Maf co-cultured with strain JXJ CY 39^T were *Mucilaginibacter*, *Dubosiella*, and *Pseudomonas* (Figure 3B). As expected, *Microcystis* was most abundant in culture samples of purified Maf cultured without JXJ CY 39^T. A total of 16 genera were detected only in co-cultures of purified Maf and strain JXJ CY 39^T, including *Acidovorax*, *Acinetobacter*, *Aquabacterium*, *Arenimonas*, *Bacteroides*, *Bifidobacterium*, *Bosea*, *Chujaibacter*, *Helicobacter*, *Jeotgalicoccus*, *Lysobacter*, *Oscillibacter*, *Pseudomonas*, *Sphingomonas*, *Sporosarcina*, and *Truepera*. In addition, a total of 13 genera were found only in the control groups, including *Alloprevotella*, *Azonexus*, *Blautia*, *Bradyrhizobium*, *Cellulomonas*, *Devosia*, *Enterorhabdus*, *Faecalibaculum*, *Lawsonella*, *Muribaculum*, *Quadrisphaera*, *Romboutsia*, and *Thermus*. The relative abundances of the 11 most abundant genera across all culture samples were specifically investigated (Figure 3C). *Brevundimonas* was detected in co-culture samples of Maf and strain JXJ CY 39^T at day 15 (0.004%), and their relative abundances increased at day 35 (1.401%). In contrast, *Brevundimonas* was not detected in the samples of purified Maf cultured without JXJ CY 39^T until day 35 (1.577%). In addition, the relative abundances of *Dubosiella* in co-cultures of purified Maf and strain JXJ CY 39^T (0.0098, 0.0111, 0.0182, and 0.0087%; on days 5, 10, 15, and 35, respectively) were all higher than in cultures without JXJ CY 39^T (0.0028, 0.0031, 0, and 0%, respectively).

Co-occurrence network analysis was used to identify correlations between genera among samples (Figure 3D). Specifically, the relative abundances of the 11 most dominant genera in cultures with purified Maf co-cultured with and without strain JXJ CY 39^T were compared at days 5, 10, 15, and 35 of cultivation. *Mucilaginibacter* (e.g., like strain JXJ CY 39^T), *Brevundimonas,* and *Pseudomonas* relative abundances were positively associated with Maf growth and Maf was positively correlated to the relative abundances of *Akkermansia*, *Azospira*, *Dubosiella*, *Lactobacillus*, and *Staphylococcus*. Consistently, the chl-*a* concentrations in some co-cultures of purified Maf and strain JXJ CY 39^T were higher than control values in BG11 medium. In addition, strains JXJ CY 11 and 57 belonged to the genus *Pseudomonas*. On day 5 of cultivation, the I-MC-LR concentration of BCS with strain JXJ CY 11 were 9.7% higher ($p < 0.05$) than that of the control. On day 10 of cultivation, the I-MC-LR concentration of BCS with strain JXJ CY 57 were 19.6% higher ($p < 0.01$) than that of the control. Thus, *Mucilaginibacter* and *Pseudomonas* may positively influence the growth of Maf, consistent with the co-occurrence network analyses. Thus, co-culture with strain JXJ CY 39^T may also influence the growth of other attached bacteria of Maf.

3.9 Description of *Mucilaginibacter lacusdianchii* sp. nov.

Mucilaginibacter lacusdianchii sp. nov. (la.cus.di.a'n.chii L. gen. n. *lacus*, of a lake; N.L. gen. n. *dianchii*, of Dianchi; N.L. gen. n. *lacusdianchii*, of Dianchi lake).

Strain JXJ CY 39^T is aerobic, Gram-negative, rod-shaped (0.7–1.0 × 0.9–2.0 μm) and grows well on ISP2 medium. The pH, NaCl content (*w*/*v*), and temperature ranges for growth are 4.0–11.0, 0–3.0%, and 5–38°C, respectively, with optimal growth at pH 7.0–8.0, 0% NaCl, and 28.0°C, respectively. The strain is positive for catalase, oxidase, nitrate reduction, hydrolysis of starch, Tween 40 and 80, and negative for Tween 20 hydrolysis. The major cellular fatty acids were iso-$C_{15:0}$ and $C_{16:1}\omega7c/_{16:1}\omega6c$. The predominant respiratory quinone is MK-7. The polar lipids are phosphatidylethanolamine (PE), unidentified aminophosphoglycolipid (APGL), unidentified aminoglycolipids (AGL), an unidentified phospholipid (PL), and unidentified polar lipids (L1-3).

The type strain, JXJ CY 39^T (= KCTC 72617^T = CGMCC 1.17449^T), was isolated from the culture biomass of *Microcystis aeruginosa* FACHB-905 collected from Lake Dianchi in the Yunnan province of southwestern China. The genome has a G + C content of 42.1%. The GenBank accession numbers for the 16S rRNA gene sequence and draft genome sequence of strain JXJ CY 39^T are MT674523 and WSRW00000000, respectively.

4 Conclusion

A novel species (type strain JXJ CY 39^T) of the genus *Mucilaginibacter* was discovered from the phycosphere of Maf and we established *Mucilaginibacter lacusdianchii* sp. nov. based on the polyphasic taxonomic study. The interplay between the Maf-associated bacteria and their host is intricate and fluctuates with time. Additional research is necessary to determine if manipulating these microbial interactions could serve as a viable strategy for controlling Harmful Algal Blooms (HABs).

Data availability statement

The datasets presented in this study can be found in online repositories. The names of the repository/repositories and accession number(s) can be found in the article/Supplementary material.

Author contributions

YX: Data curation, Investigation, Validation, Writing – original draft, Writing – review & editing. MD: Investigation, Validation, Writing – original draft, Writing – review & editing. YD: Data curation, Validation, Visualization, Writing – original draft, Writing – review & editing. QD: Investigation, Validation, Data curation, Resources, Writing – review & editing. XW: Investigation, Validation, Data curation, Writing – review & editing. YY: Investigation, Validation, Writing – review & editing. BZ: Conceptualization, Funding acquisition, Supervision, Validation, Writing – original draft, Writing – review & editing. Y-QZ: Conceptualization, Formal analysis, Funding acquisition, Methodology, Supervision, Validation, Writing – original draft, Writing – review & editing.

Funding

The author(s) declare financial support was received for the research, authorship, and/or publication of this article. The National Natural Science Foundation of China (32360028; 32170021) supported to catty out the experiments, the Program of Jiujiang University (201511) supported to collect samples and data, and the Beijing Natural Science Foundation (5212018) supported to analyze the data.

Acknowledgments

We thank LetPub (www.letpub.com) for linguistic assistance and pre-submission expert review.

Conflict of interest

The authors declare that the research was conducted in the absence of any commercial or financial relationships that could be construed as a potential conflict of interest.

The author(s) declared that they were an editorial board member of Frontiers, at the time of submission. This had no impact on the peer review process and the final decision.

Publisher's note

All claims expressed in this article are solely those of the authors and do not necessarily represent those of their affiliated organizations, or those of the publisher, the editors and the reviewers. Any product that may be evaluated in this article, or claim that may be made by its manufacturer, is not guaranteed or endorsed by the publisher.

Supplementary material

The Supplementary material for this article can be found online at: https://www.frontiersin.org/articles/10.3389/fmicb.2024.1295696/full#supplementary-material

References

Allen, M. M. (1968). Simple conditions for growth of unicellular blue-green algae on plates. *J. Phycol.* 4, 1–4. doi: 10.1111/j.1529-8817.1968.tb04667.x

Baik, K. S., Park, S. C., Kim, E. M., Lim, C. H., and Seong, C. N. (2010). *Mucilaginibacter rigui* sp. nov., isolated from wetland freshwater, and emended description of the genus *Mucilaginibacter*. *Int. J. Syst. Evol. Microbiol.* 60, 134–139. doi: 10.1099/ijs.0.011130-0

Bankevich, A., Nurk, S., Antipov, D., Gurevich, A. A., Dvorkin, M., Kulikov, A. S., et al. (2012). SPAdes: a new genome assembly algorithm and its applications to single-cell sequencing. *J. Comput. Biol.* 19, 455–477. doi: 10.1089/cmb.2012.0021

Berg, K. A., Lyra, C., Sivonen, K., Paulin, L., Suomalainen, S., Tuomi, P., et al. (2009). High diversity of cultivable heterotrophic bacteria in association with cyanobacterial water blooms. *ISME J.* 3, 314–325. doi: 10.1038/ismej.2008.110

Bland, C., Ramsey, T. L., Sabree, F., Lowe, M., Brown, K., Kyrpides, N. C., et al. (2007). CRISPR recognition tool (CRT): a tool for automatic detection of clustered regularly interspaced palindromic repeats. *BMC Bioinformatics* 8:209. doi: 10.1186/1471-2105-8-209

Boetzer, M., and Pirovano, W. (2012). Toward almost closed genomes with GapFiller. *Genome Biol.* 13:R56. doi: 10.1186/gb-2012-13-6-r56

Bolger, A. M., Lohse, M., and Usadel, B. (2014). Trimmomatic: a flexible trimmer for Illumina sequence data. *Bioinformatics* 30, 2114–2120. doi: 10.1093/bioinformatics/btu170

Casamatta, D. A., and Wickstrom, C. E. (2000). Sensitivity of two disjunct bacterioplankton communities to exudates from the cyanobacterium *Microcystis aeruginosa* kützing. *Microb. Ecol.* 40, 64–73. doi: 10.1007/s002480000035

Chen, X., Zhao, R., Tian, Y., Kong, B., Li, X., Chen, Z., et al. (2014). *Mucilaginibacter polytrichastri* sp. nov., isolated from a moss (*Polytrichastrum formosum*), and emended description of the genus *Mucilaginibacter*. *Int. J. Syst. Evol. Microbiol.* 64, 1395–1400. doi: 10.1099/ijs.0.055335-0

Chun, J., Oren, A., Ventosa, A., Christensen, H., Arahal, D. R., da Costa, M. S., et al. (2018). Proposed minimal standards for the use of genome data for the taxonomy of prokaryotes. *Int. J. Syst. Evol. Microbiol.* 68, 461–466. doi: 10.1099/ijsem.0.002516

Cirri, E., and Pohnert, G. (2019). Algae–bacteria interactions that balance the planktonic microbiome. *New Phytol.* 223, 100–106. doi: 10.1111/nph.15765

Collins, M. D., Pirouz, T., Goodfellow, M., and Minnikin, D. E. (1977). Distribution of menaquinones in actinomycetes and corynebacteria. *J. Gen. Microbiol.* 100, 221–230. doi: 10.1099/00221287-100-2-221

Cooper, M. B., and Smith, A. G. (2015). Exploring mutualistic interactions between microalgae and bacteria in the omics age. *Curr. Opin. Plant Biol.* 26, 147–153. doi: 10.1016/j.pbi.2015.07.003

Dawson, R. M. (1998). The toxicology of microcystins. *Toxicon* 36, 953–962. doi: 10.1016/s0041-0101(97)00102-5

DeSantis, T. Z., Hugenholtz, P., Larsen, N., Rojas, M., Brodie, E. L., Keller, K., et al. (2006). Greengenes, a chimera-checked 16S rRNA gene database and workbench compatible with ARB. *Appl. Environ. Microbiol.* 72, 5069–5072. doi: 10.1128/AEM.03006-05

Dong, X., and Cai, M. (2001). *Manual of systematic identification of common bacteria*. Science Press: Beijing, pp. 349–389.

Dziallas, C., and Grossart, H. P. (2011). Temperature and biotic factors influence bacterial communities associated with the cyanobacterium *Microcystis* sp. *Environ. Microbiol.* 13, 1632–1641. doi: 10.1111/j.1462-2920.2011.02479.x

Felsenstein, J. (1981). Evolutionary trees from DNA sequences: a maximum likelihood approach. *J. Mol. Evol.* 17, 368–376. doi: 10.1007/bf01734359

Felsenstein, J. (1985). Confidence limits on phylogenies: an approach using the bootstrap. *Evolution* 39, 783–791. doi: 10.1111/j.1558-5646.1985.tb00420.x

Fitch, W. M. (1971). Toward defining the course of evolution: minimum change for a specific tree topology. *Syst. Biol.* 20, 406–416. doi: 10.1093/sysbio/20.4.406

Glibert, P. M., Anderson, D. M., Gentien, P., Granéli, E., and Sellner, K. G. (2005). The global, complex phenomena of harmful algal blooms. *Oceanography* 18, 136–147. doi: 10.5670/oceanog.2005.49

Grattan, L. M., Holobaugh, S., and Morris, J. G. Jr. (2016). Harmful algal blooms and public health. *Harmful Algae* 57, 2–8. doi: 10.1016/j.hal.2016.05.003

Grossart, H. P., and Simon, M. (2007). Interactions of planktonic algae and bacteria: effects on algal growth and organic matter dynamics. *Aquat. Microb. Ecol.* 47, 163–176. doi: 10.3354/ame047163

Guo, Q., Xiong, S., Xiao, Y., Xu, C., and Zhang, B. (2020). The diversity and phosphate solubilization activity of *Microcystis aeruginosa*-associated bacteria. *J. Jiangxi Norm. Univ. Nat. Sci. Ed.* 44, 76–81. doi: 10.16357/j.cnki.issn1000-5862.2020.01.13

Hoke, A. K., Reynoso, G., Smith, M. R., Gardner, M. I., Lockwood, D. J., Gilbert, N. E., et al. (2021). Genomic signatures of Lake Erie bacteria suggest interaction in the *Microcystis* phycosphere. *PLoS One* 16:e0257017. doi: 10.1371/journal.pone.0257017

Kang, H., Kim, H., Bae, S., and Joh, K. (2021). *Mucilaginibacter aquatilis* sp. nov., *Mucilaginibacter arboris* sp. nov., and *Mucilaginibacter ginkgonis* sp. nov., novel bacteria isolated from freshwater and tree bark. *Int. J. Syst. Evol. Microbiol.* 71:004755. doi: 10.1099/ijsem.0.004755

Kazamia, E., Helliwell, K. E., Purton, S., and Smith, A. G. (2016). How mutualisms arise in phytoplankton communities: building eco-evolutionary principles for aquatic microbes. *Ecol. Lett.* 19, 810–822. doi: 10.1111/ele.12615

Kim, M., Shin, B., Lee, J., Park, H. Y., and Park, W. (2019). Culture-independent and culture-dependent analyses of the bacterial community in the phycosphere of cyanobloom-forming *Microcystis aeruginosa*. *Sci. Rep.* 9:20416. doi: 10.1038/s41598-019-56882-1

Kouzuma, A., and Watanabe, K. (2015). Exploring the potential of algae/bacteria interactions. *Curr. Opin. Biotechnol.* 33, 125–129. doi: 10.1016/j.copbio.2015.02.007

Lin, W., Hung, T. C., Kurobe, T., Wang, Y., and Yang, P. (2021). Microcystin-induced immunotoxicity in fishes: a scoping review. *Toxins (Basel)* 13:765. doi: 10.3390/toxins13110765

Liu, L. P. (1999). Characteristics of blue algal bloom in Dianchi Lake and analysis on its cause. *Res. Environ. Sci.* 12, 36–37.

Liu, Y., Gao, B., Yue, Q., Guan, Y., Wang, Y., and Huang, L. (2012). Influences of two antibiotic contaminants on the production, release and toxicity of microcystins. *Ecotoxicol. Environ. Saf.* 77, 79–87. doi: 10.1016/j.ecoenv.2011.10.027

Massouras, A., Hens, K., Gubelmann, C., Uplekar, S., Decouttere, F., Rougemont, J., et al. (2010). Primer-initiated sequence synthesis to detect and assemble structural variants. *Nat. Methods* 7, 485–486. doi: 10.1038/nmeth.f.308

Meier-Kolthoff, J. P., Auch, A. F., Klenk, H. P., and Göker, M. (2013). Genome sequence-based species delimitation with confidence intervals and improved distance functions. *BMC Bioinformatics* 14:60. doi: 10.1186/1471-2105-14-60

Minnikin, D. E., Collins, M. D., and Goodfellow, M. (1979). Fatty acid and polar lipid composition in the classification of *Cellulomonas*, *Oerskovia* and related taxa. *J. Appl. Bacteriol.* 47, 87–95. doi: 10.1111/j.1365-2672.1979.tb01172.x

Ndlela, L. L., Oberholster, P. J., Van Wyk, J. H., and Cheng, P. (2018). Bacteria as biological control agents of freshwater cyanobacteria: is it feasible beyond the laboratory? *Appl. Microbiol. Biotechnol.* 102, 9911–9923. doi: 10.1007/s00253-018-9391-9

Nguyen, L. T., Schmidt, H. A., von Haeseler, A., and Minh, B. Q. (2015). IQ-TREE: a fast and effective stochastic algorithm for estimating maximum-likelihood phylogenies. *Mol. Biol. Evol.* 32, 268–274. doi: 10.1093/molbev/msu300

Ostensvik, O., Skulberg, O., Underdal, B., and Hormazabal, V. (1998). Antibacterial properties of extracts from selected planktonic freshwater cyanobacteria – a comparative study of bacterial bioassays. *J. Appl. Microbiol.* 84, 1117–1124. doi: 10.1046/j.1365-2672.1998.00449.x

Pankratov, T. A., Tindall, B. J., Liesack, W., and Dedysh, S. N. (2007). *Mucilaginibacter paludis* gen. Nov., sp. nov. and *Mucilaginibacter gracilis* sp. nov., pectin-, xylan- and laminarin-degrading members of the family *Sphingobacteriaceae* from acidic *Sphagnum* peat bog. *Int. J. Syst. Evol. Microbiol.* 57, 2349–2354. doi: 10.1099/ijs.0.65100-0

Park, M. H., Chung, I. M., Ahmad, A., Kim, B. H., and Hwang, S. J. (2009). Growth inhibition of unicellular and colonial *Microcystis* strains (*Cyanophyceae*) by compounds isolated from rice (*Oryza sativa*) hulls. *Aquat. Bot.* 90, 309–314. doi: 10.1016/j.aquabot.2008.11.007

Parveen, B., Ravet, V., Djediat, C., Mary, I., Quiblier, C., Debroas, D., et al. (2013). Bacterial communities associated with *Microcystis* colonies differ from free-living communities living in the same ecosystem. *Environ. Microbiol. Rep.* 5, 716–724. doi: 10.1111/1758-2229.12071

Pérez-Carrascal, O. M., Tromas, N., Terrat, Y., Moreno, E., Giani, A., Marques, L. C. B., et al. (2021). Single-colony sequencing reveals microbe-by-microbiome phylosymbiosis between the cyanobacterium *Microcystis* and its associated bacteria. *Microbiome* 9:194. doi: 10.1186/s40168-021-01140-8

Ramanan, R., Kim, B. H., Cho, D. H., Oh, H. M., and Kim, H. S. (2016). Algae–bacteria interactions: evolution, ecology and emerging applications. *Biotechnol. Adv.* 34, 14–29. doi: 10.1016/j.biotechadv.2015.12.003

Saitou, N., and Nei, M. (1987). The neighbor-joining method: a new method for reconstructing phylogenetic trees. *Mol. Biol. Evol.* 4, 406–425. doi: 10.1093/oxfordjournals.molbev.a040454

Seemann, T. (2014). Prokka: rapid prokaryotic genome annotation. *Bioinformatics* 30, 2068–2069. doi: 10.1093/bioinformatics/btu153

Segata, N., Izard, J., Waldron, L., Gevers, D., Miropolsky, L., Garrett, W. S., et al. (2011). Metagenomic biomarker discovery and explanation. *Genome Biol.* 12:R60. doi: 10.1186/gb-2011-12-6-r60

Seyedsayamdost, M. R., Case, R. J., Kolter, R., and Clardy, J. (2011). The Jekyll-and-Hyde chemistry of *Phaeobacter gallaeciensis*. *Nat. Chem.* 3, 331–335. doi: 10.1038/nchem.1002

Shao, K., Zhang, L., Wang, Y., Yao, X., Tang, X., Qin, B., et al. (2014). The responses of the taxa composition of particle-attached bacterial community to the decomposition of *Microcystis* blooms. *Sci. Total Environ.* 488-489, 236–242. doi: 10.1016/j.scitotenv.2014.04.101

Tamaoka, J., Katayama-Fujimura, Y., and Kuraishi, H. (1983). Analysis of bacterial menaquinone mixtures by high performance liquid chromatography. *J. Appl. Bacteriol.* 54, 31–36. doi: 10.1111/j.1365-2672.1983.tb01297.x

Tamura, K., Stecher, G., and Kumar, S. (2021). MEGA11: molecular evolutionary genetics analysis version 11. *Mol. Biol. Evol.* 38, 3022–3027. doi: 10.1093/molbev/msab120

Urai, M., Aizawa, T., Nakagawa, Y., Nakajima, M., and Sunairi, M. (2008). *Mucilaginibacter kameinonensis* sp., nov., isolated from garden soil. *Int. J. Syst. Evol. Microbiol.* 58, 2046–2050. doi: 10.1099/ijs.0.65777-0

Valdor, R., and Aboal, M. (2007). Effects of living cyanobacteria, cyanobacterial extracts and pure microcystins on growth and ultrastructure of microalgae and bacteria. *Toxicon* 49, 769–779. doi: 10.1016/j.toxicon.2006.11.025

Vasconcelos, V. M., Sivonen, K., Evans, W. R., Carmichael, W. W., and Namikoshi, M. (1996). Hepatotoxic microcystin diversity in cyanobacterial blooms collected in portuguese freshwaters. *Water Res.* 30, 2377–2384. doi: 10.1016/0043-1354(96)00152-2

Wang, J., Wagner, N. D., Fulton, J. M., and Scott, J. T. (2021). Diazotrophs modulate phycobiliproteins and nitrogen stoichiometry differently than other cyanobacteria in response to light and nitrogen availability. *Limnol. Oceanogr.* 66, 2333–2345. doi: 10.1002/lno.11757

Won, M., Weon, H., Heo, J., Lee, D., Han, B., Hong, S., et al. (2022). *Ferruginibacter albus* sp. nov., isolated from a mountain soil, and *Mucilaginibacter robiniae* sp. nov., isolated from a black locust ffower, *Robinia pseudoacacia*. *Int. J. Syst. Evol. Microbiol.* 72:005556. doi: 10.1099/ijsem.0.005556

Xiao, Y., Chen, J., Chen, M., Deng, S., Xiong, Z., Tian, B., et al. (2022b). *Mycolicibacterium lacusdiani* sp. nov., an attached bacterium of *Microcystis aeruginosa*. *Front. Microbiol.* 13:861291. doi: 10.3389/fmicb.2022.861291

Xiao, Y., Chen, M., Chen, J., Mao, L., Peng, Y., Gui, S., et al. (2022a). *Microbacterium kunmingensis* sp. nov., an attached bacterium of *Microcystis aeruginosa*. *J. Antibiot.* 75, 662–670. doi: 10.1038/s41429-022-00568-w

Xiao, Y., Wang, L., Wang, X., Chen, M., Chen, J., Tian, B., et al. (2022c). *Nocardioides lacusdianchii* sp. nov., an attached bacterium of *Microcystis aeruginosa*. *Antonie Van Leeuwenhoek* 115, 141–153. doi: 10.1007/s10482-021-01690-9

Xue, H., Zhang, D., Xu, L., Wang, X., Zhang, A., Huang, J., et al. (2021). *Actirhodobacter atriluteus* gen. Nov., sp. nov., isolated from the surface water of the Yellow Sea. *Antonie Van Leeuwenhoek* 114, 1059–1068. doi: 10.1007/s10482-021-01576

Yang, L., Cao, X., Chen, X., Deng, Q., Wan, L., Li, X., et al. (2021). Community composition and functional genes explain different ecological roles of heterotrophic bacteria attached to two bloom-forming cyanobacterial genera. *Sci. Total Environ.* 758:143850. doi: 10.1016/j.scitotenv.2020.143850

Yang, C., Wang, Q., Simon, P. N., Liu, J., Liu, L., Dai, X., et al. (2017). Distinct network interactions in particle-associated and free-living bacterial communities during a *Microcystis aeruginosa* bloom in a plateau lake. *Front. Microbiol.* 8:1202. doi: 10.3389/fmicb.2017.01202

Yang, L., and Xiao, L. (2011). *Outburst, jeopardize and control of cyanobacterial bloom in lakes*. Science Press, Beijing, pp. 71–212.

Young, A. J. (1991). The photoprotective role of carotenoids in higher plants. *Physiol. Plantarum* 83, 702–708. doi: 10.1111/j.1399-3054.1991.tb02490.x

Zhang, B., Chen, W., Li, H., Zhou, E., Hu, W., Duan, Y., et al. (2015). An antialgal compound produced by *Streptomyces jiujiangensis* JXJ 0074^{T}. *Appl. Microbiol. Biotechnol.* 99, 7673–7683. doi: 10.1007/s00253-015-6584-3

Zhang, B., Ding, Z., Li, H., Mou, X., Zhang, Y., Yang, J., et al. (2016a). Algicidal activity of *Streptomyces eurocidicus* JXJ-0089 metabolites and their effects on *Microcystis* physiology. *Appl. Environ. Microbiol.* 82, 5132–5143. doi: 10.1128/AEM.01198-16

Zhang, B., Salam, N., Cheng, J., Li, H., Yang, J., Zha, D., et al. (2017). *Microbacterium lacusdiani* sp. nov., a phosphate-solubilizing novel actinobacterium isolated from mucilaginous sheath of *Microcystis*. *J. Antibiot.* 70, 147–151. doi: 10.1038/ja.2016.125

Zhang, B., Salam, N., Cheng, J., Li, H., Yang, J., Zha, D., et al. (2016c). *Modestobacter lacusdianchii* sp. nov., a phosphate-solubilizing actinobacterium with ability to promote *Microcystis* growth. *PLoS One* 11:e0161069. doi: 10.1371/journal.pone.0161069

Zhang, B., Salam, N., Cheng, J., Xiao, M., Li, H., Yang, J., et al. (2016b). *Citricoccus lacusdiani* sp. nov., an actinobacterium promoting *Microcystis* growth with limited soluble phosphorus. *Antonie Van Leeuwenhoek* 109, 1457–1465. doi: 10.1007/s10482-016-0745-y

Zhang, J., Zhang, W., Wang, H., Chen, J., and Shen, H. (2019). Progress in the relationships between *Microcystis* and aquatic bacteria. *Acta Hydrobiol. Sin.* 43, 448–456. doi: 10.7541/2019.055

Zhao, G., Du, J., Jia, Y., Lv, Y., Han, G., and Tian, X. (2012). The importance of bacteria in promoting algal growth in eutrophic lakes with limited available phosphorus. *Ecol. Eng.* 42, 107–111. doi: 10.1016/j.ecoleng.2012.02.007

Zhao, J., Li, J., Guan, Z., Xu, L., Pan, C., and Li, P. (2011). Effect of an attached bacterium of alkaline phosphatase producting on the growth of *Microcystis aeruginosa*. *J. Lake Sci.* 23, 49–55. doi: 10.18307/2011.0108

Zhu, C., Zhang, J., Wang, X., Yang, Y., Chen, N., Lu, Z., et al. (2021). Responses of cyanobacterial aggregate microbial communities to algal blooms. *Water Res.* 196:117014. doi: 10.1016/j.watres.2021.117014

frontiers | Frontiers in Microbiology

TYPE Original Research
PUBLISHED 06 March 2024
DOI 10.3389/fmicb.2024.1307677

Check for updates

OPEN ACCESS

EDITED BY
Zhenlin Han,
University of Hawai'i at Mānoa, United States

REVIEWED BY
Agnieszka Kuźniar,
The John Paul II Catholic University of Lublin, Poland
Sakineh Abbasi,
Institut National de Recherche pour l'Agriculture, l'Alimentation et l'Environnement (INRAE), France

*CORRESPONDENCE
Haizhu Zhang
✉ hzningjing@163.com
BaoShun Su
✉ 461631589@qq.com

RECEIVED 05 October 2023
ACCEPTED 14 February 2024
PUBLISHED 06 March 2024

CITATION
Xie Q, Xu H, Wen R, Wang L, Yang Y and Zhang H (2024) Integrated management of fruit trees and *Bletilla striata*: implications for soil nutrient profiles and microbial community structures.
Front. Microbiol. 15:1307677.
doi: 10.3389/fmicb.2024.1307677

COPYRIGHT
© 2024 Xie, Xu, Wen, Wang, Yang and Zhang. This is an open-access article distributed under the terms of the Creative Commons Attribution License (CC BY). The use, distribution or reproduction in other forums is permitted, provided the original author(s) and the copyright owner(s) are credited and that the original publication in this journal is cited, in accordance with accepted academic practice. No use, distribution or reproduction is permitted which does not comply with these terms.

Integrated management of fruit trees and *Bletilla striata*: implications for soil nutrient profiles and microbial community structures

Qiufeng Xie[1,2], Huimei Xu[1,2], Rouyuan Wen[1,2], Le Wang[1], Yan Yang[1], Haizhu Zhang[1,2]* and BaoShun Su[3]*

[1]College of Pharmaceutical Science, Dali University, Dali, China, [2]Western Yunnan Traditional Chinese Medicine and Ethnic Drug Engineering Center, College of Pharmacy, Dali University, Dali, China, [3]Dali Lin Yun Biotechnology Development Co., Ltd., Dali, China

Introduction: Forest medicinal compound systems in agroforestry ecosystems represent a multi-layered cultivation approach that utilizes forest resources efficiently. However, research on how these systems affect soil nutrients and microbial communities is limited.

Methods: This study compared the soil chemical properties and microbial communities of *Bletilla striata* (C) grown alone versus in agroforestry systems with apple (PB), pear (LB), and peach trees (TB), aiming to understand the impact of these systems on soil health and microbial diversity.

Results: Soil in the GAB systems showed increased levels of essential nutrients but lower pH and ammonium nitrogen levels compared to the control. Significant improvements in organic matter, total phosphorus, and total potassium were observed in TB, PB, and LB systems, respectively. The bacterial diversity increased in GAB systems, with significant changes in microbial phyla indicative of a healthier soil ecosystem. The correlation between soil properties and bacterial communities was stronger than with fungal communities.

Discussion: Integrating *B. striata* with fruit trees enhances soil nutrients and microbial diversity but may lead to soil acidification. Adjustments such as using controlled-release fertilizers and soil amendments like lime could mitigate negative impacts, improving soil health in GAB systems.

KEYWORDS

agroforestry integration, rhizosphere soil, soil physicochemical properties, microbial community, *Bletilla striata*

1 Introduction

Bletilla striata, initially recorded in the "Shennong's Classic of Materia Medica," is also referred to as the windbell orchid, windbell *Bletilla*, and Wulan (in China). It is generally known as a species under the *Bletilla* genus of the Orchidaceae family. Its tuber is frequently used for medicinal purposes (Sun B. et al., 2022; Zhu et al., 2023). The primary components include polysaccharides, phenanthrenes, phenanthroquinones,

bibenzyls, triterpenes, lignans, and organic acids, showcasing a range of biological activities such as anti-inflammatory (Jiang et al., 2019; Zhang C. et al., 2021), antifibrotic (Jiang et al., 2023), anti-tumor (Liu et al., 2022), and immune-regulatory effects (Gong et al., 2023), thereby highlighting its significant medicinal value. Furthermore, due to the vivid and diverse colors of *B. striata* flowers, their prolonged blooming period, and strong adaptability, they have commendable applications in horticulture. With the escalating market demand for *B. striata*, its large-scale production has become prominent (Han et al., 2023). In situations where forest resources are limited, singular cultivation practices often do not maximize the utilization of light, water, and soil resources within the same three-dimensional space. A monotonous plant community structure can lead to population degradation, continuous cropping barriers, allelopathic suppression, and other challenges, resulting in a weakened ecological function of the cultivated area (Zhang H. et al., 2020; Yang et al., 2023). In light of these challenges, it is imperative to adopt effective technical strategies to enhance the economic benefits farmers gain from cultivating *B. striata*, further promoting its sustainable development.

The forestry-medicated intercropping system seamlessly integrates the understorey space, forest canopy shading, and unique climatic and soil characteristics, leading to a notable enhancement in forest land productivity and economic yield. This approach not only bolsters the ecological diversity and soil health of the forested region but also fortifies the stability of the forestry-medicated ecosystem. With the growing emphasis on combined cultivation methods, forestry-medicated intercropping has gradually been recognized as a mainstream cultivation strategy. Such a system not only fosters the efficient utilization of plant resources and space but also plays a pivotal role in the continuous improvement of the soil environment. Its immense potential to enhance ecological diversity, optimize the ecological environment, and offer a myriad of ecosystem services hints at its broad application prospects (Mortimer et al., 2018; Wolz and DeLucia, 2018; Zhang et al., 2018). Several instances of forestry-medicated composite systems have been documented; for example, Verma et al. (2013) discerned that a combined management system of forestry and medicinals facilitated the accumulation of active medicinal components in mint. Research by Sujatha and Bhat (2010) revealed that intercropping vanilla orchids in betel nut gardens augments soil pH, quick-acting soil nutrient content, and economic returns per unit area. In recent years, an increasing number of scholars have opined that studies on crop growth, development, and yield formation should pivot back to the rhizosphere (Philippot et al., 2013). The forestry-medicated intercropping pattern has been proven to safeguard the soil, enrich soil organic matter (OM) and nutrients, amplify biodiversity, bolster ecosystem stability, disrupt pest life cycles, and thereby curtail reliance on chemical pesticides (Wang et al., 2020). While rational forest land combined management can enhance soil fertility (Li B. et al., 2022), not all underforest-combined operations achieve synergistic benefits. For instance, Cardoso et al. (2003) found that the phosphorus content in soil from single-cropped coffee was higher than in its intercropped counterpart. Currently, research on *B. striata* primarily focuses on its intercropping with *Phyllostachys pubescens*. After intercropping *B. striata* with *P. pubescens*, the soil organic carbon (SOC), available nitrogen (AN), and available phosphorus (AP) significantly surged, enhancing microbial abundance. Additionally, there was a significant increase in the total phenol and flavonoid content in *B. striata* (Deng et al., 2023). Intercropping *B. striata* augments soil quality and medicinal material standards.

While some studies have delved into alterations in soil microbial traits induced by forestry-medicinal intercropping (Lin et al., 2012), detailed investigations into shifts in the soil microbial community resulting from the combined management of *B. striata* with fruit trees remain uncharted territory. Therefore, a comprehensive understanding of the soil microbial communities within these *B. striata* agroforestry-based (GAB) systems could be instrumental in the design and management of forestry-medicinal intercropping systems. In this study, we embarked on assessing the changes occurring within bacterial and fungal microbiomes in the context of *B. striata* intercropped with a diversity of fruit trees. We postulate that forestry-medicinal intercropping can significantly modulate the physicochemical properties of the soil, influence the diversity of its microbial communities, and induce shifts in the structure of these communities. The primary objectives of this research are twofold: to analyze variations in the structure of soil microbial communities under different *B. striata*-fruit tree intercropping paradigms using high-throughput sequencing techniques. To elucidate the correlations between these microbial community structures and soil environmental factors under various *B. striata*-fruit tree combined management scenarios, thereby offering theoretical underpinning for the scientific establishment of *B. striata* forestry-medicinal intercropping models.

2 Materials and methods

2.1 Experimental materials and site description

The research site is located in Dacheng Village, Wase Town, Dali City, Yunnan Province, at the Dali Linyun Tourist Garden in Fengweiqing (100°29′19″E, 25°90′67″N; altitude 2,332 m). The field soil is yellow soil, and the garden has been continuously cropping *B. striata* for 3 years. This region is characterized by a North subtropical highland monsoon climate, with mild weather, no extreme heat or severe cold, minimal wind frost, and spring-like conditions throughout the year. The average annual temperature is 15.4°C, with an average annual rainfall of 510 mm.

Peach trees (*Prunus persica*), Pear trees (*Pyrus sorotina*), and Apple trees (*Malus pumila* Mill.) are intercropped with *B. striata*. The experimental design includes four treatments: (1) Peach trees – *B. striata* intercropping (TB); (2) Pear trees – *B. striata* intercropping (LB); (3) Apple trees – *B. striata* intercropping (PB); (4) Solo cultivation of *B. striata* (C). The field experiment employs a completely randomized design, with three replicates for each treatment (each plot being 100 m^2). The agroforestry compound planting garden was established in August 2014, and *B. striata* was planted in April 2019. The planting densities for different treatments are as shown in **Figure 1**. All crops are irrigated by drip irrigation, and the cultivation process is managed routinely.

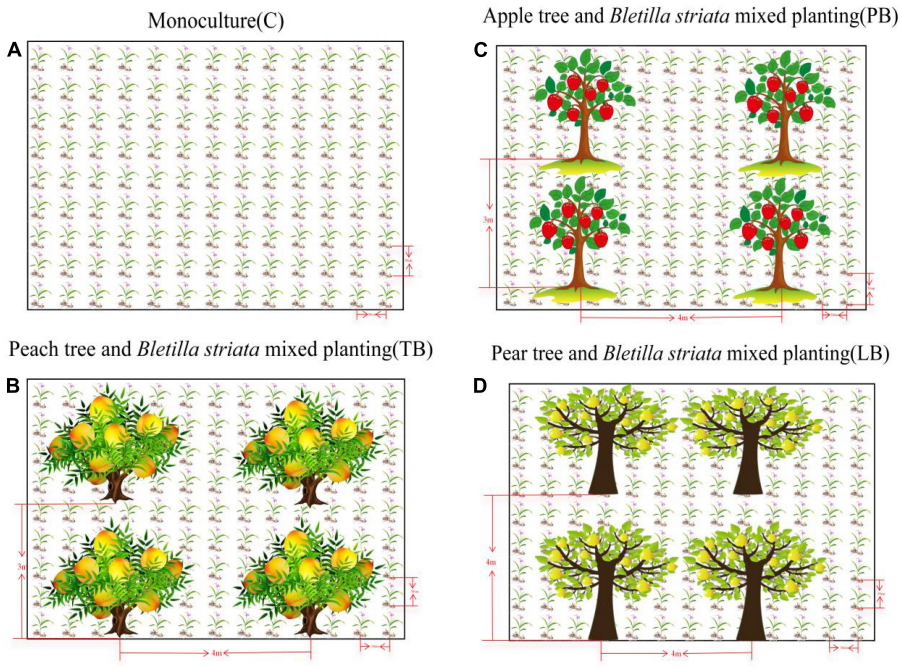

FIGURE 1
Schematic representation of *Bletilla striata* cultivation patterns. **(A)** Monoculture of *B. striata* (C); **(B)** *B. striata* intercropped with Peach trees (TB); **(C)** *B. striata* intercropped with Apple trees (PB); **(D)** *B. striata* intercropped with Pear trees (LB).

In October 2022, soil from the rhizosphere of *B. striata* in each plot was collected. Five soil sub-samples were randomly collected from each plot, mixed to form one root sample, and repeated three times. After removing debris such as stones and residual roots, the soil samples were sealed in pre-prepared sterile bags, quickly transported back to the laboratory in ice boxes, and sieved through a 2 mm soil sieve. The samples were then mixed evenly and divided into two portions. One portion was stored in a −80°C freezer for DNA extraction, and the other portion was air-dried for analysis of soil physicochemical properties.

2.2 Determination of soil physicochemical properties

The rhizosphere soil was air-dried at 25°C, subsequently ground, and then sieved through a 0.84 mm mesh. Parameters such as soil pH, OM, total nitrogen (TN), total phosphorus (TP), total potassium (TK), AN, readily available phosphorus (AP), available potassium (AK), NH_4^+-N, and nitrate nitrogen (NO_3^--N) were measured. The soil pH was determined using a PHS-3C pH meter (Shanghai Scientific Instrument Co. Ltd., Shanghai, China), Precisely weigh 10.00 g of soil sample and place it in a 50 ml centrifuge tube. Add 25 ml of distilled water, shake vigorously for 2 min, and let it stand for 30 min to measure the pH. The determination of OM, TN, TP, TK, AN, AP, AK, NH_4^+-N, and NO_3^--N was carried out following the methods described in the third edition of "Soil Agrochemical Analysis," edited by Bao (2000). The book, published by the China Agricultural Press in 2000, is widely regarded as an authoritative source in the fields of soil science and agriculture. We chose to follow its methods because they are not only widely applied in Chinese soil analysis practices but also align with internationally accepted standards in their fundamental principles and procedural steps. Despite differences in specific chemicals and equipment used, by incorporating modern measurement technology from the LD-GT1 Intelligent Soil Nutrient Analyzer (Shandong Lainde Intelligent Technology Co., Ltd., Shandong, China), we were able to execute these methods with greater efficiency and accuracy. Additionally, the LD-GT1 employs advanced sensing technology and automated processes for the effective quantification of OM content in soil, a methodology whose accuracy has been corroborated through scholarly research and practical application (Pu et al., 2022). The determination of OM was carried out using the potassium dichromate dilution hot colorimetric method. The procedure is as follows: initially, a bag of soil OM extraction agent powder was placed in a 500 ml plastic bottle, and distilled water was added up to the marked line to prepare the soil OM extraction solution. Subsequently, 4.0 g of air-dried soil sample was weighed and added to the extraction bottle, followed by the addition of 20 ml of the aforementioned extraction agent. The mixture was thoroughly shaken and agitated for 5 min before filtration. The resultant filtrate served as the test solution for OM. The determination of AN employed the alkali digestion distillation method. Precisely, 1.0 g of air-dried soil sample was placed in a 100 ml conical flask, followed by the sequential addition of 25 ml distilled water, 12 drops of hydrolysis agent, 2 drops of stabilizer, and 1.0 g of reductant (a mixture of ferrous sulfate and zinc powder in a 5:1 ratio). The conical flask was immediately sealed and connected to an absorption bottle containing distilled water (with 3 drops of absorbent) via a distillation tube. The flask was then placed on an asbestos net and heated with an alcohol lamp, causing the mixture to boil and sustain distillation for 7 min. After cooling,

the liquid in the absorption bottle was transferred to a 100 ml volumetric flask, and the apparatus was rinsed with distilled water before being brought up to volume. The resulting solution was the test solution for AN. The determinations of NH_4^+-N, NO_3^--N, AP, and AK in the soil were conducted respectively using the Nessler's reagent colorimetric method, nitrate test powder method, molybdenum blue colorimetric method, and tetraphenylborate sodium turbidimetric method. A bag of combined soil extraction agent powder was added to a 500 ml volumetric flask and brought up to volume with distilled water to prepare the soil extraction agent. Then, 1.0 g of air-dried soil sample was weighed and added to an extraction bottle along with 20 ml of soil extraction agent and an appropriate amount of soil decolorizing agent. After vigorous shaking for 3 min and subsequent filtration, the filtrate obtained served as the test solution for NH_4^+-N, NO_3^--N, AP, and AK. Furthermore, the contents of TN, TP, and TK in the soil were determined using the Kjeldahl distillation method, acid dissolution-antimony molybdenum colorimetric method, and perchloric acid-nitric acid digestion method, respectively. Similarly, a bag of combined soil extraction agent powder was added to a 500 ml volumetric flask and made up to volume with distilled water. Subsequently, 1.0 g of air-dried soil sample was placed in a Kjeldahl flask, moistened with 10 drops of water, followed by the sequential addition of 0.2 g of TN reductant, 4 ml of concentrated sulfuric acid, and 10 drops of soil TN oxidant. After heating, the contents of the Kjeldahl flask were transferred to a 100 ml volumetric flask and made up to volume with distilled water. Finally, 20 ml of the clear supernatant was transferred to another 100 ml volumetric flask, to which 1.6 ml of TN regulator (1:1 NaOH solution) was added, and then brought up to volume with distilled water and filtered. The resultant filtrate served as the test solution for TN, TP, and TK. During all determinations, 2 ml of distilled water, 2 ml of soil extraction solution (containing 1 drop of soil standard reserve solution), and 2 ml of soil test solution were used as the blank, standard, and test solutions, respectively. These samples were placed in three separate test tubes, followed by the addition of respective soil testing reagents. After thorough mixing and standing, the solutions were transferred to cuvettes for the determination of nutrient contents.

2.3 Soil DNA extraction, PCR amplification, and sequencing

Weigh 0.5 g of fresh soil and extract DNA from the samples using the CTAB method, repeating the process three times. The DNA amplification products are then detected using the Agilent 5400 automatic capillary electrophoresis system to assess the quality and concentration of DNA. Subsequently, an appropriate amount of sample DNA is taken in a centrifuge tube and diluted with sterile water to 1 ng/μl. PCR amplification of the bacterial V3–V4 region is performed using primers 341F (5′-CCTAYGGGRBGCASCAG-3′) and 806R (5′-GGACTACNNGGGTATCTAAT-3′); and for fungal ITS fragments, primers ITS1-1F-F (5′-CTTGGTCATTTAGAGGAAGTAA-3′) and ITS1-1F-R (5′-GCTGCGTTCTTCATCGATGC-3′) are used. The reaction system includes 10 ng of gDNA template, 15 μl of Phusion Master Mix (2×), 0.2 μl of each upstream and downstream primer (1 μM), and ddH_2O added up to 30 μl. The amplification program is as follows: initial denaturation at 98°C for 1 min; followed by 30 cycles of 98°C denaturation for 10 s, 50°C annealing for 30 s, 72°C extension for 30 s; and a final extension at 72°C for 5 min. The PCR products are extracted from a 2% agarose gel and purified and quantified using the Qiagen gel recovery kit (Qiagen, Germantown, MD, USA) along with Qubit fluorometric quantitation and Q-PCR methods. High-throughput sequencing is conducted using the Illumina NovaSeq6000 platform.

2.4 Sequencing data processing

Based on Barcode and PCR amplification primer sequences, individual sample data were extracted from the initial sequencing output. Following the removal of Barcode and primer sequences, FLASH (v1.2.11[1]) was employed to assemble reads for each sample, yielding the primary Raw Tags data. These assembled Raw Tags then underwent rigorous filtration to derive high-quality Clean Tags data. Adhering to the Tags quality control process outlined by Qiime (V1.9.1[2]), the following steps were executed: (a) Tags Truncation: Raw Tags were truncated at the first low-quality base position when a predefined length (default value set to 3) of consecutive bases exhibited a quality threshold of ≤ 19; (b) Tags Length Filtering: following truncation, the resulting Tags dataset was further refined to exclude Tags with high-quality base lengths less than 75% of the total Tags length. After these procedures, the resultant Tags underwent chimera sequence removal. The Tags sequences were aligned with species annotation databases via VSEARCH[3] to detect chimeric sequences, which were subsequently removed to produce the final Effective Tags.

2.5 Statistical data analysis

Unless otherwise specified, data statistics and visualization were conducted using the R programming language and its associated packages. Based on the experimental design, the acquired OTU data was filtered, removing OTUs with a prevalence of less than 30% in soil samples. After standardizing the OTU table using the TMM (Trimmed Means of M) algorithm, the relative expression abundance of OTUs was calculated. The vegan package was employed to determine microbial α-diversity and β-diversity (utilizing the Shannon and Chao1 indices). One-way analysis of variance (ANOVA) and the least significant difference (LSD) method ($P < 0.05$) were performed using SPSS 21.0 (IBM, USA) to ascertain if the differences in diversity between samples based on α and β indices were statistically significant. The "ggplot2" package facilitated the principal coordinate analysis (PCoA) to assess the distribution trends of soil microbial communities under different treatments. Similarity analysis (ANOSIM) and permutationl multivariate analysis of variance (ADONIS) with 999 permutations were used to identify significant inter-sample group differences in β-diversity based on the Bray–Curtis distance

1 http://ccb.jhu.edu/software/FLASH/
2 http://qiime.org/scripts/split_libraries_fastq.html
3 https://github.com/torognes/vsearch/

matrix. Linear discriminant analysis Effect Size (LEfSe) was utilized to elucidate taxonomic features characterizing inter-treatment microbial species differences.[4] To simplify the LEfSe workflow, OTU table filtering was conducted, selecting only OTUs with a relative abundance of $P > 0.01\%$. The factorial Kruskal–Wallis sum-rank test ($\alpha = 0.05$) was employed to identify taxa with significant group inter-abundance differences. Subsequently, the effect size of each discriminative trait was calculated based on log LDA scores (threshold = 4.0). The Spearman rank correlation test was applied to determine correlations between module feature genes and soil properties. The "vegan" package was utilized for redundancy analysis (RDA) to explore the relationships between environmental factors, dominant microbes, and microbial functions. The Spearman rank correlation test further examined the explanatory power of environmental factors on microbial species and functionalities.[5]

3 Results

3.1 Effects of intercropping on soil physicochemical properties

In all orchard-*B. striata* integrated planting soil systems (LB, TB, and PB), levels of TN, AN, AP, and AK were significantly higher than in monoculture systems (C) (LSD, $P < 0.05$, Table 1). Compared to C, the content of TN, AN, AP, AK, and NO_3^--N in LB increased by 22.37%, 34.31%, 163.49%, 146.22%, and 63.90%, respectively. In PB, the levels of TN, AN, AP, and AK were elevated by 13.70%, 49.44%, 120.86%, and 147.12% in comparison to C. For TB, TN, AN, AP, AK, and NO_3^--N content increased by 6.85%, 64.91%, 161.71%, 106.53%, and 16.82% relative to C (Table 1). Among the different intercropping soil systems, the soil in LB showed the highest concentrations of TN, TK, AP, and AK. The soil in PB had the highest levels of TP and AK, while the soil in TB presented the maximum concentrations of OM, AN, and AP (Table 1). The soil pH values in the LB, PB, and TB systems were significantly different from C, all showing a marked reduction (Table 1).

3.2 Impact on *Bletilla striata* root microbial community diversity and structure under different compound modes

After high-throughput sequencing, approximately 832,533 quality 16s sequences and 818,986 quality ITS2 sequences were produced during the raw-read sequencing process. The average read lengths for bacteria and fungi were 415 and 246 bp, respectively. Using a 97% identity threshold, sequences from all samples were clustered into 9,150 bacterial OTUs and 3,499 fungal OTUs. Figure 2 illustrates the α-diversity indices of bacterial and fungal communities under different intercropping modes, measured based on the Shannon index, encompassing both community richness and evenness. For bacterial microbes, the order of Shannon diversity values was: TB > LB > PB > C. Compared to C, the Shannon diversity values of TB, LB, and PB were significantly elevated (LSD, $P < 0.05$, Figure 2A). The order for Chao1 diversity values was TB > LB > PB > C. In comparison to C, TB and LB exhibited significantly higher Chao1 diversity values (LSD, $P < 0.05$, Figure 2B), while no significant difference was observed between PB and C ($P > 0.05$, Figure 2B). For fungal microbes, the sequence of Shannon diversity values was: C > TB > LB > PB. When contrasted with C, no discernible differences in Shannon diversity indices for TB, LB, and PB were detected ($P > 0.05$, Figure 2C). The order for Chao1 diversity values was TB > C > LB > PB. Relative to C, no significant differences in Chao1 diversity indices were observed for TB, LB, and PB ($P > 0.05$, Figure 2D). However, the Chao1 diversity index for TB surpassed those of PB and LB ($P < 0.05$, Figure 2D).

Assessing microbial community differences among treatments using PCoA based on Bray–Curtis distances. Utilizing the PCoA based on Bray–Curtis distances, we evaluated microbial community distinctions across different treatments. In the context of bacterial microbial communities, clear separations were observed between TB, PB, LB, and C treatments. Notably, LB and PB showcased partial overlaps (Figure 3A). The PCoA results indicated that the first two axes account for 59.28% and 28.66% of the overall variance in bacterial microbial compositions, respectively. Regarding the fungal microbial communities, pronounced separations were discernible between TB, PB, and C, with TB partially overlapping with both C and LB (Figure 3B). The PCoA demonstrated that the first two axes elucidated 64.4% and 30.33% of the total variability in fungal microbial compositions, respectively. Results from ANOSIM revealed significant distinctions in both bacterial and fungal microbial communities between at least two treatments. Additionally, ADONIS results indicated a significant difference in bacterial microbial communities across a minimum of two treatments (Supplementary Table 1). Venn diagrams affirmed that variations in microbial compositions between different soil intercropping systems stemmed from changes in both unique and shared OTU compositions. Out of all identified OTUs in this research, 2,224 bacterial OTUs were common across all intercropping soil systems. Specifically, PB, LB, TB, and C had 593, 628, 877, and 552 unique OTUs, respectively (Figure 3C). For fungal communities, 746 OTUs were shared across all systems, while PB, LB, TB, and C exhibited 202, 323, 210, and 257 unique OTUs, respectively (Figure 3D).

3.3 Influence of combined management on soil microbial composition

Figure 4 presents the results of sequence analyses conducted at both the genus and phylum levels. For bacteria (Figures 4A, B and Supplementary Table 2), the most abundant phylum was Proteobacteria, constituting 38.56%, followed by Acidobacteriota (12.91%) and Firmicutes (12.99%). Among the dominant taxa,

4 https://cloud.oebiotech.com/

5 https://www.cloudtutu.com

10.3389/fmicb.2024.1307677

TABLE 1 Chemical properties of the soil in the *Bletilla striata* rhizosphere.

	C	LB	PB	TB	*P*-values	Significant
OM	167.7 ± 0.49b	167.07 ± 0.60b	164.49 ± 1.15c	185.04 ± 0.35a	0	***
TN	2.19 ± 0.02d	2.68 ± 0.04a	2.49 ± 0.02b	2.34 ± 0.03c	0	***
TP	0.84 ± 0.01b	0.76 ± 0.05b	1.09 ± 0.07a	0.66 ± 0.03c	0	***
TK	146.54 ± 4.23b	177.17 ± 7.96a	117.19 ± 5.28d	128.91 ± 2.54c	0	***
AN	143.7 ± 8.83d	193.01 ± 5.41c	214.74 ± 9.95b	236.97 ± 6.05a	0	***
AP	59 ± 1.69c	155.46 ± 1.19a	130.31 ± 1.99b	154.41 ± 1.18a	0	***
AK	196.93 ± 2.56c	484.89 ± 2.71a	486.65 ± 5.61a	406.72 ± 5.77b	0	***
NH_4^+-N	96.42 ± 2.31a	5.23 ± 0.98d	34.29 ± 2.32b	19.11 ± 1.15c	0	***
NO_3^--N	72.14 ± 1.25c	118.24 ± 1.50a	66.78 ± 1.33d	86.73 ± 2.48b	0	***
pH	6.8 ± 0.04a	5.69 ± 0.08b	5.44 ± 0.24b	5.69 ± 0.30b	0	***

Values are presented as mean ± SE ($n = 3$). Different lowercase letters indicate statistically significant differences among treatments ($P < 0.05$). The symbol "***" denotes significant differences at the ≤0.001 level. OM, organic matter; TN, total nitrogen; TP, total phosphorus; TK, total potassium; AN, available nitrogen; AP, rapidly available phosphorus; AK, readily available potassium; NH_4^+-N, ammonium nitrogen; NO_3^--N, nitrate nitrogen; C, monoculture of *B. striata*; LB, *B. striata* intercropped with Pear trees; PB, *B. striata* intercropped with Apple trees; TB, *B. striata* intercropped with Peach trees.

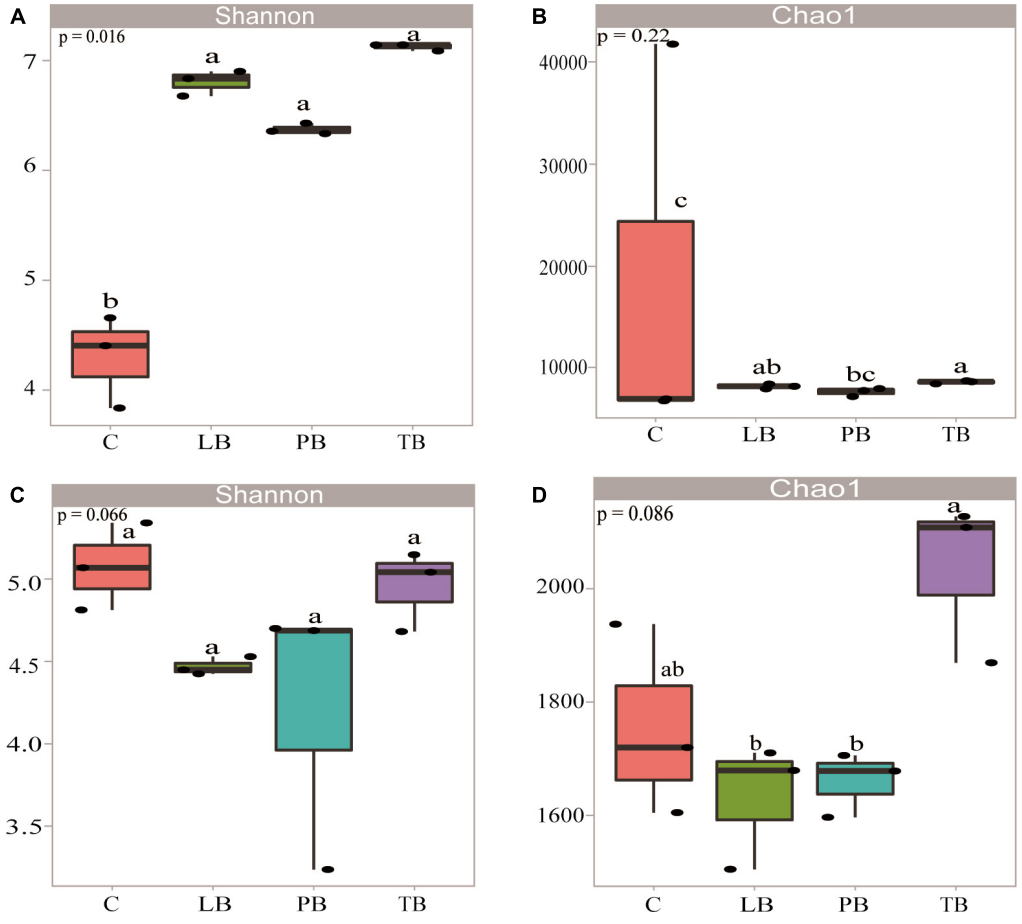

FIGURE 2
Diversity indices of *Bletilla striata*'s bacterial **(A,B)** and fungal **(C,D)** communities in different intercropping systems. **(A)** Bacterial Shannon diversity index; **(B)** bacterial Chao1 richness index; **(C)** fungal Shannon diversity index; **(D)** fungal Chao1 richness index. Lowercase letters on each box denote the least significant differences (LSD; $P < 0.05$) among treatments. C, monoculture of *B. striata*; LB, *B. striata* intercropped with Pear trees; PB, *B. striata* intercropped with Apple trees; TB, *B. striata* intercropped with Peach trees.

no significant variation in abundance was observed in PB's Myxococcota, Bacteroidota, Actinobacteria, Verrucomicrobiota, and Firmicutes; in TB's Gemmatimonadetes, Actinobacteria, Verrucomicrobiota, Actinobacteriota, Chloroflexi, and Firmicutes; and LB's Actinobacteriota, Chloroflexi, Actinobacteria, Verrucomicrobiota, and Acidobacteriota when compared

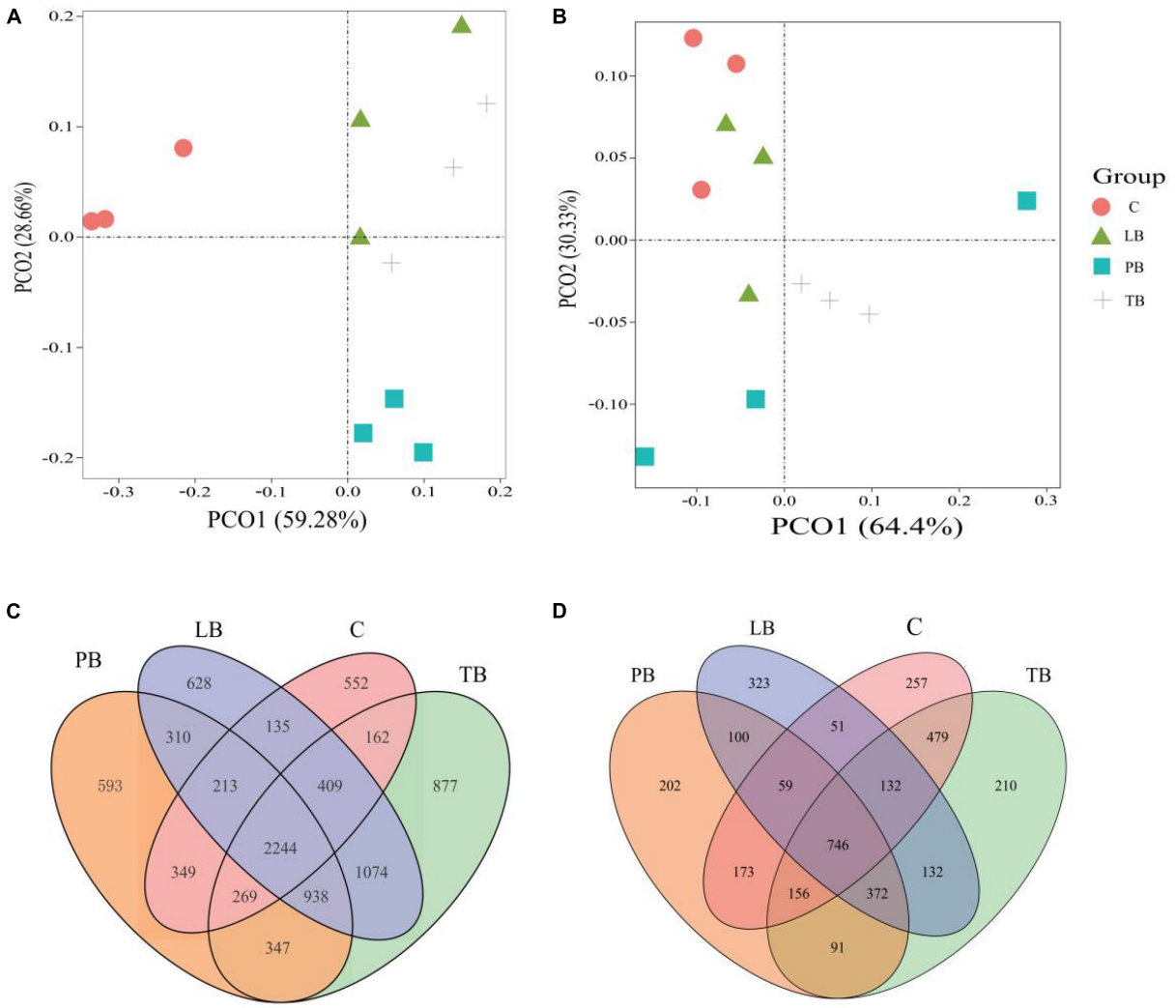

FIGURE 3
Microbial community diversity under different *Bletilla striata* integrated planting regimes. The principal coordinate analysis (PCoA) plot, based on the Bray–Curtis dissimilarity, illustrates the separation between soil bacterial **(A)** and fungal **(B)** communities across treatments. Venn diagrams display the number of operational taxonomic units (OTUs) for bacteria **(C)** and fungi **(D)** under each intercropping scheme. C, monoculture of *B. striata*; LB, *B. striata* intercropped with Pear trees; PB, *B. striata* intercropped with Apple trees; TB, *B. striata* intercropped with Peach trees.

to C (Figure 4A). A notable decline in the abundance of Proteobacteria was evident in PB, TB, and LB compared to C (Figure 4A). Contrarily, an elevated richness was discerned in TB's Myxococcota, Bacteroidota, and Acidobacteriota; in PB's Gemmatimonadetes, Actinobacteriota, Chloroflexi, and Acidobacteriota; and LB's Myxococcota, Bacteroidota, Gemmatimonadetes, and Firmicutes in contrast to C (Figure 4A). The most prevalent genera across different intercropping soils included *Pseudomonas* (9.92%), *Sphingomonas* (3.24%), *Pseudarthrobacter* (1.84%), *Bryobacter* (1.75%), *Bradyrhizobium* (1.36%), and *Gemmatimonas* (1.07%) (Figure 4B). In comparison to the monoculture system (C), the intercropping systems (PB, LB, TB) did not manifest significant shifts in the abundance of *Sphingomonas*, *Pseudarthrobacter*, *Bryobacter*, *Bradyrhizobium*, *Gemmatimonas*, or *Acidibacter*. In juxtaposition with C, TB, and LB showcased a higher abundance of *Haliangium*, whereas LB exhibited a heightened abundance of unidentified *Clostridiaceae*. Furthermore, when contrasted with C, an increased significance was noted in the "others" category across LB, TB, and PB. Conversely, a lower abundance of *Pseudomonas* was evident in PB, TB, and LB when juxtaposed with C.

Referring to fungi, Figures 4C, D and Supplementary Table 3 depict that Ascomycota was the most abundant phylum, making up 44.90% of the samples. It was closely followed by Basidiomycota (13.60%) and Mortierellomycota (5.18%). Among the prevalent taxa, the abundance of Basidiomycota, Mortierellomycota, Zoopagomycota, and Monoblepharomycota remained consistent across the three examined intercropping systems, showing no significant deviation when compared to the monoculture soil system (C) (Figure 4C). In contrast to C, the abundance of Ascomycota and Chytridiomycota in PB, Ascomycota in TB, and Chytridiomycota and Mucoromycota in LB was markedly reduced (Figure 4C). When compared to C, a significantly enhanced abundance of Basidiobolomycota in LB and Glomeromycota in PB was evident (Figure 4C). The most prevalent genera across different intercropping soil systems

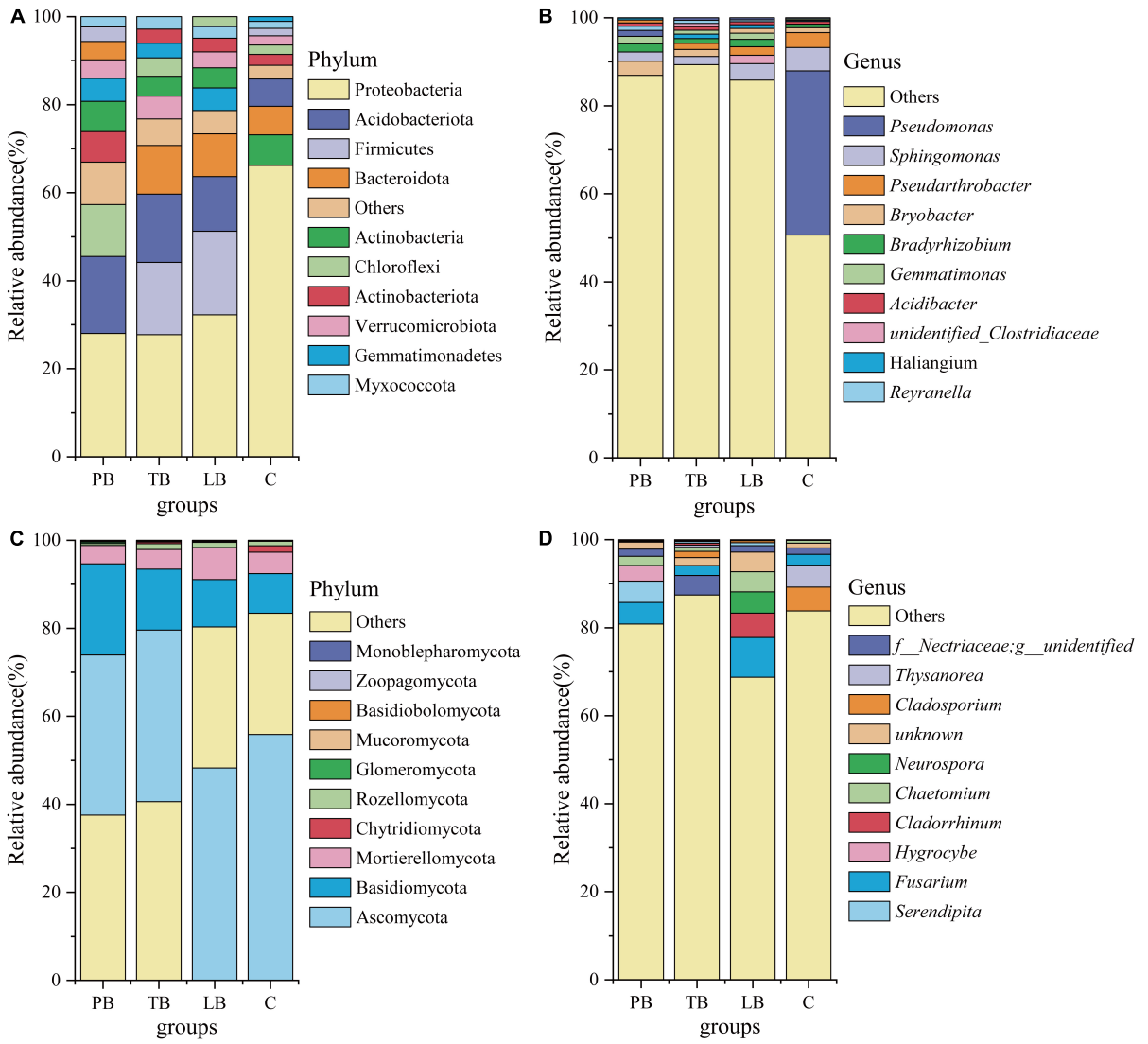

FIGURE 4
Relative abundance of soil microbial communities at the phylum and genus levels under different intercropping systems. **(A)** Bacterial phylum level; **(B)** bacterial genus level; **(C)** fungal phylum level; **(D)** fungal genus level. C, monoculture of *Bletilla striata*; LB, *B. striata* intercropped with Pear trees; PB, *B. striata* intercropped with Apple trees; TB, *B. striata* intercropped with Peach trees.

included *Fusarium* (4.67%), *Nectriaceae* (2.27%), *Chaetomium* (2.03%), *Cladosporium* (1.88%), *Cladorrhinum* (1.57%), *Serendipity* (1.49%), *Thysanorea* (1.37%), *Neurospora* (1.30%), and *Hygrocybe* (1.00%) (Figure 4D). In juxtaposition with the monoculture soil system (C), there was no notable variance in the abundance of *Serendipita*, *Hygrocybe*, and *Chaetomium* across PB, TB, and LB. When contrasted with C, a significant surge in abundance was observed for *Nectriaceae* in TB and *Cladorrhinum* and *Fusarium* in LB. Conversely, a notable decrease in the abundance of *Thysanorea* and *Cladosporium* was evident across PB, TB, and LB compared to C (Figure 4D).

The LEfSe was employed to discern the effects of various composite patterns on the composition of soil microbial communities. The analysis identified significant differences in the relative abundance of 23 bacterial taxa among the different composite soil systems. As shown in Figure 5A, 4 bacterial taxa in C, 6 in LB, 11 in PB, and 2 in TB were pinpointed as biomarkers. Furthermore, the LEfSe delineated that 33 fungal taxa have significant variations in their relative abundance across the different composite soil systems. Notably, the identified biomarkers included 19 fungal taxa in C, 8 in LB, and 6 in TB (Figure 5B).

3.4 Relationship between soil properties and soil microbial community

To elucidate the effects of climatic factors of different composite modes on fungal and bacterial communities, RDA was employed to correlate dominant species of fungi and bacteria with climatic factors of the composite modes. The results are presented in Figure 6. For bacteria, the RDA results revealed that the RDA1 and RDA2 axes accounted for 40.31% and 36.22% of the variation in the soil bacterial community, respectively, cumulating an overall

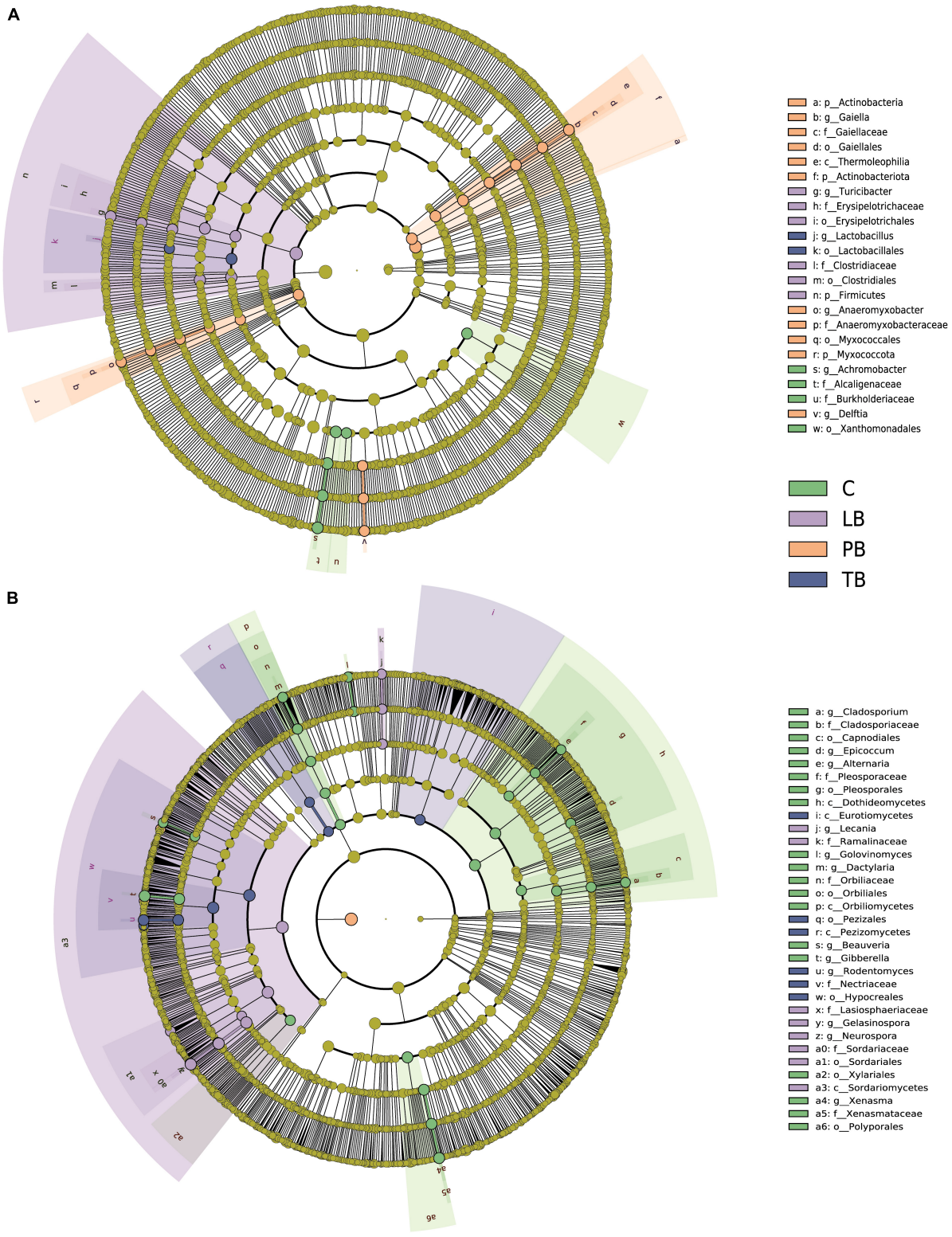

FIGURE 5
Cladogram from Linear discriminant analysis Effect Size (LEfSe) highlighting the significant discriminative bacterial **(A)** and fungal **(B)** taxa associated with different co-planting schemes (LDA >4). C, monoculture of *Bletilla striata*; LB, *B. striata* intercropped with Pear trees; PB, *B. striata* intercropped with Apple trees; TB, *B. striata* intercropped with Peach trees.

76.53% explanation rate (Figure 6A). pH and NH_4^+-N were closely associated with C; TP, TK, TN, and AK showed a close relation with LB and PB; while OM, AN, and AP were intimately correlated with TB. Projections of environmental factors onto the first and second ordination axes indicated that AN exhibited the most substantial impact on the bacterial community, followed by pH, OM, TN,

AK, AP, and NH_4^+-N ($P < 0.05$). TP, NO_3^--N, and TK showed no discernible impact on the bacterial community (**Figure 6A** and **Supplementary Table 4**). Concerning fungi, the RDA1 and RDA2 axes represented 35.66% and 28.07% of the variation in the soil fungal community, respectively, amounting to a total explanation rate of 63.73% (**Figure 6B**). TK, pH, NH_4^+-N, and TP were closely tied to both C and LB; TP, TN, and AK correlated strongly with PB; while AP, AN, and OM were linked with TB. Evaluations of environmental factors on the first and second ordination axes identified AN as having the most pronounced influence on the fungal community, trailed by OM, TP, pH, AK, AP, and NH_4^+-N ($P < 0.05$). Meanwhile, TN, NO_3^--N, and TK bore no significant effect on the fungal community (**Figure 6B** and **Supplementary Table 4**).

To delve deeper into the correlation between dominant microbial species in *B. striata* soil and environmental factors under various composite modes, a Spearman correlation test was conducted between dominant microbial species and environmental factors. For bacteria, as depicted in **Figure 6C**: Myxococcota was significantly negatively correlated with OM ($P < 0.01$). Gemmatimonadetes showed a positive correlation with TP ($P < 0.05$), a significant negative correlation with OM ($P < 0.01$), and a negative correlation with AN ($P < 0.05$). Actinobacteriota was strongly positively correlated with NH_4^+-N ($P \leq 0.001$), significantly positively correlated with pH ($P < 0.01$), and strongly negatively correlated with AP ($P \leq 0.001$). It also showed a significant negative correlation with AK and AN ($P < 0.01$). Chloroflexi exhibited strong positive correlations with NH_4^+-N and pH ($P \leq 0.001$), and strong negative correlations with AK, AN, and AP ($P \leq 0.001$). Bacteroidota was strongly positively correlated with TN ($P \leq 0.001$), positively correlated with AK ($P < 0.01$), and AP ($P < 0.05$), and significantly negatively correlated with NH_4^+-N and pH ($P < 0.01$). Firmicutes showed a positive correlation with TN ($P < 0.05$). Acidobacteriota exhibited a significant negative correlation with AN and OM ($P < 0.01$). Proteobacteria was significantly positively correlated with OM ($P < 0.01$) and positively correlated with AN ($P < 0.05$).

For fungi, as shown in **Figure 6D**: Monoblepharomycota positively correlated with OM ($P < 0.05$). Basidiobolomycota was strongly positively correlated with TP ($P \leq 0.001$) and negatively correlated with OM ($P < 0.05$). Mucoromycota displayed a significant positive correlation with pH ($P < 0.01$), negative correlations with TN and TP ($P < 0.05$), and a significant negative correlation with AK ($P < 0.01$). Glomeromycota showed positive correlations with NH_4^+-N and pH ($P < 0.05$), a negative correlation with AP ($P < 0.05$), and a significant negative correlation with AN ($P < 0.01$). Chytridiomycota positively correlated with AN ($P < 0.05$) and showed a significant positive correlation with OM ($P < 0.01$). Rozellomycota was strongly positively correlated with AK ($P \leq 0.001$), significantly positively correlated with AP and TN ($P < 0.01$), positively correlated with AN ($P < 0.05$), and showed a significant negative correlation with NH_4^+-N ($P < 0.01$) and negative correlation with pH ($P < 0.05$). Basidiomycota positively correlated with pH ($P < 0.05$) and negatively correlated with AN and AP ($P < 0.05$). Ascomycota demonstrated a significant positive correlation with AN ($P < 0.01$) and positively correlated with OM ($P < 0.05$). These findings indicate that different composite modes have distinct impacts on the relationship between the dominant microbial species in *B. striata* roots and environmental factors. *B. striata* under different composite modes affect related physicochemical properties in the soil, subsequently influencing the composition and distribution of the microbial community.

4 Discussion

4.1 Relationship between bacterial communities and environmental factors

Interplanting strategies effectively harness available arable land, moisture, nutrients, and thermophotonic resources, bolstering the crop diversity index. By leveraging interspecific competition and complementarity, these techniques enhance agricultural yield and efficiency (Dapaah et al., 2003). Concurrently, they amplify aboveground and belowground interspecific interactions in fields, augmenting, and modulating soil biodiversity. This in turn improves the microecological quality of the soil and alleviates obstacles associated with continuous cropping (Li et al., 2023). Existing studies underscore the pivotal role soil OM, nitrogen, and phosphorus play in uplifting crop yield and quality. The soil quality is predominantly influenced by soil OM affecting soil pH, moisture retention, and the concentration of soil nutrients, among other pedological traits (Ruthes et al., 2023). Intercropping can significantly shape the structure and diversity of soil microbial communities, elevating the count of beneficial microorganisms while suppressing pathogens. Such practices are instrumental in refining the soil environment and fortifying plant disease resistance (Li et al., 2014). Our findings reveal that, in comparison to the monocropping system, the silvo-medicinal intercropping management has a notable impact on soil nutrients, including OM, TN, TP, TK, AN, AP, AK, NH_4^+-N, and NO_3^--N, as well as on pH levels (**Table 1**). Specifically, in the TB system, there was an increase in OM, TN, AN, AP, AK, and NO_3^--N levels, with a concurrent reduction in TP, TK, NH_4^+-N levels, and pH values. In contrast, the PB system elevated the levels of TN, TP, AN, AP, and AK, but reduced OM, TK, and NO_3^--N levels, along with pH values. The LB system resulted in heightened levels of TN, TK, AP, AK, and NO_3^--N, but exhibited a decrease in NH_4^+-N levels and pH values. Generally, in the intercropping systems, the levels of TN, AK, AP, and AN consistently surged, while NH_4^+-N levels and pH values markedly dwindled. This could be attributed to the significant variations in the canopy type, litterfall, and root exudates of *B. striata* in different forest settings, thus triggering alterations in soil nutrients (Zhang Y. et al., 2021; Li X. et al., 2022). Notably, in a majority of ecological systems, over 90% of the nitrogen and phosphorus required by plants from the soil are sourced from the decomposition of litterfall (Lucas-Borja et al., 2019), which corroborates the findings of Zhang X. et al. (2020).

Although numerous studies have explored the effects of tree leaf litter on soil microbiota, research investigating the structure and functional response of soil microbes beneath fruit trees to the decomposition of *B. striata* leaf litter remains uncharted territory. The decomposition of leaves and fallen fruits under fruit trees plays a pivotal role in shaping the soil nutrient profile and microbial community structure. Moreover, distinct soil characteristics can induce shifts in soil microbial assemblies (Shi et al., 2016).

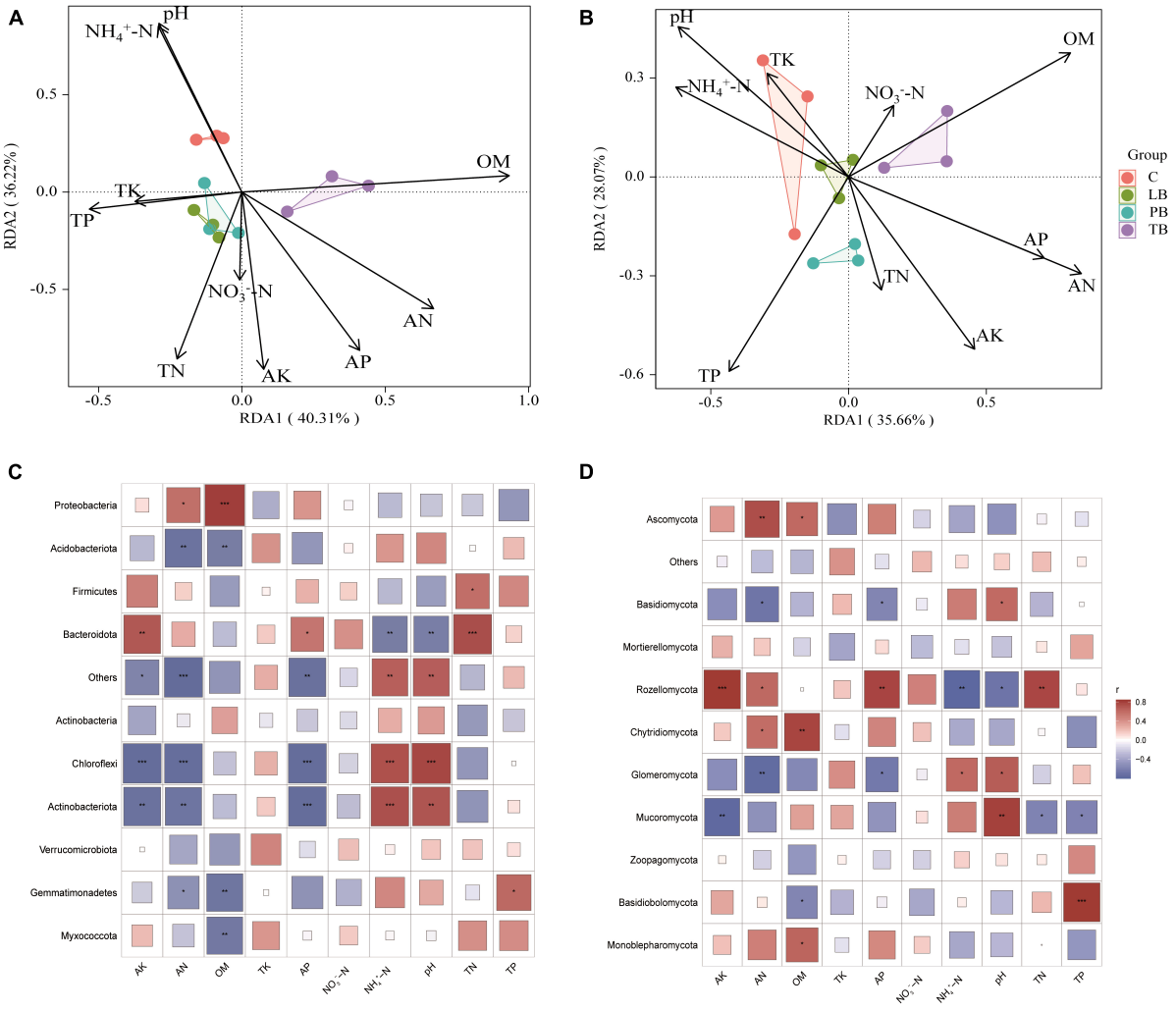

FIGURE 6
Redundancy analysis (RDA) of bacterial **(A)** and fungal **(B)** community compositions under orchard-*Bletilla strata* combined planting regimes. Statistical correlations between soil physicochemical properties and bacterial **(C)** and fungal **(D)** microbiota. OM, organic matter; TN, total nitrogen; TP, total phosphorus; TK, total potassium; AN, available nitrogen; AP, available phosphorus; AK, readily available potassium; NH_4^+-N, ammonium nitrogen; NO_3^--N, nitrate nitrogen; C, monoculture of *Bletilla striata*; LB, *B. striata* intercropped with Pear trees; PB, *B. striata* intercropped with Apple trees; TB, *B. striata* intercropped with Peach trees. *$P < 0.05$; **$P < 0.01$; and ***$P < 0.001$.

In the present study, the abundance of *Actinobacteriota* and *Chloroflexi* displayed a significant positive correlation with NH_4^+-N and pH, but a negative correlation with AN, AK, and AP. *Bacteroidota* showed a positive association with AK, AP, and TN, yet a negative relationship with NH_4^+-N and pH (Figure 6C). Meanwhile, Myxococcota negatively correlated with OM. Our survey identified Proteobacteria, Acidobacteriota, Firmicutes, Bacteroidota, Actinobacteria, Chloroflexi, and Actinobacteriota as dominant bacterial phyla in both intercropping and monocropping systems. These are common bacterial taxa found in soils, aligning with earlier research findings (Fierer and Jackson, 2006; Janssen, 2006). Among these, the soil bacterium Proteobacteria emerged as the predominant phylum across all intercropping patterns and is recognized as a primary functional bacterium responsible for decomposition and transformation. This observation is congruent with previously reported findings (Mander et al., 2012; Huang et al., 2016).In the context of our findings, the bacterial phyla Acidobacteriota, Firmicutes, Chloroflexi, Verrucomicrobiota, Gemmatimonadetes, and Myxococcota exhibited significantly higher abundances in LB, TB, and PB intercropping systems compared to monocropping (Figure 4). Within the PB system, the relative abundance of Bacteroidota was lower than in C, whereas in the TB and LB systems, the relative abundance of Actinobacteria was lower than in C (Supplementary Table 2).

Though Acidobacteriota is ubiquitous across various soil types, it exemplifies soils under acidic conditions and showcases diverse metabolic capabilities, particularly linked to OM decomposition (Jones et al., 2009; Kielak et al., 2016). This explains the decrease in soil pH in the rhizosphere of *B. striata* post-fruit tree intercropping. Firmicutes bacteria possess the capacity to ferment complex polysaccharides and other organic substances and play an instrumental role in beneficial plant-root interactions (Yutin and Galperin, 2013). This capability might be related to the synthesis of *B. striata* polysaccharides. Chloroflexi, on the other hand, aids in the decomposition of OM in the soil, contributing to organic carbon cycling and nitrogen cycling,

whilst interacting with other soil microbial communities, thus impacting soil structure and stability (Hug et al., 2013; Kielak et al., 2016). A salient feature of Myxococcota, one of the few known predatory bacteria, is its ability to prey on other bacteria or organic substances. These bacteria can form unique multicellular structures, enabling them to withstand unfavorable environmental conditions over extended periods. Furthermore, their presence is instrumental in maintaining soil structure and enhancing its mechanical stability (Shimkets, 1990; Reichenbach, 1999; Berleman and Kirby, 2009; Weissman and Müller, 2010). When comparing the relative abundance of dominant bacterial genera in different soil conditions, we observed that after intercropping, the abundance of *Pseudomonas*, *Sphingomonas*, and *Pseudarthrobacter* declined compared to monocultures. These bacteria are known to decompose OM and facilitate ecological restoration in soils (Stolz, 2009). In contrast, the abundance of *Bryobacter*, *Bradyrhizobium*, *Gemmatimonas*, *Acidibacter*, *Haliangium*, and *Reyranella* increased relative to monocultures. These bacterial genera play critical roles in decomposing OM, fixing atmospheric nitrogen, and enhancing soil fertility (Barns et al., 2007; Alippi et al., 2012). The findings indicate that soil conditions improved following the intercropping of *B. striata* with fruit trees, resulting in the suppression of *Pseudomonas*, *Sphingomonas*, and *Pseudarthrobacter* growth, and the promotion of *Bryobacter*, *Bradyrhizobium*, *Gemmatimonas*, *Acidibacter*, *Haliangium*, and *Reyranella* growth. Additionally, in this study, the genera labeled as "Others" and "Unidentified" accounted for over 50% and 6.8%, respectively, in both systems. This suggests that there remains a substantial number of unknown or rare bacteria in the soil under *B. striata* that require further identification and research.

4.2 Relationship between fungal communities and environmental factors

Previous studies have suggested that orchard intercropping can significantly increase microbial community diversity (Dahlstrom et al., 2020; Ding et al., 2021; Zhu et al., 2022). In contrast, other research has indicated that while intercropping reduces the number of soil microbes, it does not compromise their richness (Zhong et al., 2018). Such findings underscore the notion that the impact of intercropping on soil microbial diversity may vary depending on the specific plants involved in the intercrop. In our study, the indices related to fungi were generally higher in monocultures than in intercropping systems. This suggests that, over a certain period, the intercropping of fruit trees with *B. striata* leads to a decline in both the quantity and diversity of fungi. The significantly reduced fungal richness in PB and LB compared to monocultures could be attributed to the presence of acidic substances, such as malic and citric acids, in fallen apples and pears. As these fruits decompose in the soil, the resulting organic acids may acidify the soil (Gallinger et al., 2021), potentially contributing to the observed reduction in fungal numbers. Given that our sampling coincided with the period of apple and pear drop, further observations are needed to discern the impact of soil pH and microbial abundance changes.

Significantly, TB enhanced the Chao1 index of *B. striata* rhizosphere soil, suggesting that TB can effectively boost the fungal community diversity in *B. striata* root soil, playing a crucial role in enhancing the soil's ecological environment and microbial diversity. Additionally, dominant microbial communities in both intercropped and monocultured soils included beneficial microbes for plants, such as Basidiomycota, Ascomycota, Chytridiomycota, and Glomeromycota (Sommermann et al., 2018; Li Y. et al., 2022; Sun P. et al., 2022; Wang et al., 2022). These microbes facilitate OM recycling, decompose organic materials, and establish mycorrhizal symbiotic relationships with plants. Notably, in this study, Ascomycota emerged as the predominant fungal phylum capable of decomposing soil OM, promoting the cycling of key nutrients and enhancing soil fertility (Brakhage, 2013). Their abundance showed a significant positive correlation with AN and OM (**Figure 6D**).

Rozellomycota is understood to be a group of fungi predominantly characterized by their parasitic and symbiotic lifestyles. They potentially play pivotal roles in OM decomposition, soil structure formation, and interactions with other soil biota, such as establishing symbiotic relationships with plants (Jones et al., 2011). Their abundance exhibited a significant positive correlation with AK, AN, AP, and TN while showing a pronounced negative correlation with NH_4^+-N and pH (**Figure 6D**). *Mucoromycota*, on the other hand, can serve as biological pesticides, combating soil-borne pests and pathogenic microbes. They form endomycorrhizal symbiotic relationships with plants and participate in OM decomposition (Spatafora et al., 2016; Orchard et al., 2017). Their abundance is significantly positively correlated with pH but negatively associated with AK, TN, and TP (**Figure 6D**). *B. striata* is a shade-loving plant that is averse to strong sunlight. The results suggest that intercropping generates favorable impacts on soil nutrient levels and microbial community composition. Moreover, microbes appear to play an integral role in nutrient cycling. This insight aids in further evaluating the implications of intercropping fruit trees with *B. striata* on the physicochemical properties of soil.

5 Conclusion

The mixed planting of fruit trees and *B. striata* significantly elevates the levels of AN, AP, and AK in the soil, concurrently reducing NH_4^+-N content and pH values. Additionally, this integrated cultivation strategy modifies the soil microbial community, notably increasing the relative abundance of Acidobacteriota and Firmicutes phyla. A marked correlation exists between soil microbes and soil physicochemical properties, with NH_4^+-N and pH demonstrating significant relationships with both bacterial and fungal communities. Beyond the enhancement of the bacterial community structure within the soil, there is a noted rise in the relative abundance of beneficial bacterial and fungal groups linked primarily to disease prevention and nutrient cycling. In essence, the integration of *B. striata* with fruit trees can considerably augment soil nutrient levels, and refine the soil bacterial microbiome in terms of composition and diversity, albeit leading to soil acidification and depletion of NH_4^+-N. For such agroforestry systems, adopting measures like the application of controlled or slow-release nitrogen fertilizers and the addition of lime or wood ash can ameliorate soil pH. Comprehensive long-term analyses of these intercropping systems are requisite, with a focus on identifying the most advantageous planting patterns

for farmers. Such findings are expected to provide theoretical underpinnings for ensuing agricultural practices and research.

Data availability statement

The original contributions presented in the study are publicly available. This data can be found here: https://www.ncbi.nlm.nih.gov/genbank/, PRJNA1021261.

Author contributions

QX: Conceptualization, Formal analysis, Investigation, Software, Writing – original draft. HX: Formal analysis, Investigation, Writing – original draft. RW: Data curation, Formal analysis, Investigation, Writing – original draft. LW: Data curation, Formal analysis, Investigation, Writing – original draft. YY: Formal analysis, Software, Writing – original draft. HZ: Resources, Supervision, Validation, Writing – review & editing. BS: Resources, Validation, Writing – review and editing.

Funding

The author(s) declare financial support was received for the research, authorship, and/or publication of this article. This research was funded by the National Natural Science Foundation of China (81960696) and the key technology projects in Yunnan province of China (202307AC110003).

Conflict of interest

The authors declare that the research was conducted in the absence of any commercial or financial relationships that could be construed as a potential conflict of interest.

Publisher's note

All claims expressed in this article are solely those of the authors and do not necessarily represent those of their affiliated organizations, or those of the publisher, the editors and the reviewers. Any product that may be evaluated in this article, or claim that may be made by its manufacturer, is not guaranteed or endorsed by the publisher.

Supplementary material

The Supplementary Material for this article can be found online at: https://www.frontiersin.org/articles/10.3389/fmicb.2024.1307677/full#supplementary-material

References

Alippi, A. M., López, A. C., and Balatti, P. A. (2012). Diversity among agrobacteria isolated from diseased plants of blueberry (vaccinium corymbosum) in argentina. *Eur. J. Plant Pathol.* 134, 415–430. doi: 10.1007/s10658-012-0001-x

Bao, S. (2000). *Soil Agrochemical Analysis*, 3rd Edn. Beijing: China Agriculture Press Co., Ltd.

Barns, S. M., Cain, E. C., Sommerville, L., and Kuske, C. R. (2007). Acidobacteria phylum sequences in uranium-contaminated subsurface sediments greatly expand the known diversity within the phylum. *Appl. Environ. Microbiol.* 73, 3113–3116. doi: 10.1128/AEM.02012-06

Berleman, J. E., and Kirby, J. R. (2009). Deciphering the hunting strategy of a bacterial wolfpack. *FEMS Microbiol. Rev.* 33, 942–957. doi: 10.1111/j.1574-6976.2009.00185.x

Brakhage, A. A. (2013). Regulation of fungal secondary metabolism. *Nat. Rev. Microbiol.* 11, 21–32. doi: 10.1038/nrmicro2916

Cardoso, I. M., Janssen, B. H., Oenema, O., and Kuyper, T. W. (2003). Phosphorus pools in oxisols under shaded and unshaded coffee system on farmers' fields in brazil. *Agrofor. Syst.* 58, 55–64. doi: 10.1023/A:1025436908000

Dahlstrom, K. M., McRose, D. L., and Newman, D. K. (2020). Keystone metabolites of crop rhizosphere microbiomes. *Curr. Biol.* 30, R1131–R1137. doi: 10.1016/j.cub.2020.08.005

Dapaah, H. K., Asafu-Agyei, J. N., Ennin, S. A., and Yamoah, C. (2003). Yield stability of cassava, maize, soya bean and cowpea intercrops. *J. Agric. Sci.* 140, 73–82.

Deng, P., Yin, R., Wang, H., Chen, L., and Cao, X. (2023). Comparative analyses of functional traits based on metabolome and economic traits variation of bletilla striata: contribution of intercropping. *Front. Plant Sci.* 14:1147076. doi: 10.3389/fpls.2023.1147076

Ding, T., Yan, Z., Zhang, W., and Duan, T. (2021). Green manure crops affected soil chemical properties and fungal diversity and community of apple orchard in the loess plateau of china. *J. Soil Sci. Plant Nutr.* 21, 1089–1102. doi: 10.1007/s42729-021-00424-0

Fierer, N., and Jackson, R. B. (2006). Diversity and biogeography of soil bacterial communities. *Proc. Natl. Acad. Sci.* 103, 626–631. doi: 10.1073/pnas.0507535103

Gallinger, J., Zikeli, K., Zimmermann, M. R., Gorg, L. M., and Mithofer, A. (2021). Specialized 16srx phytoplasmas induce diverse morphological and physiological changes in their respective fruit crops. *PLoS Pathog.* 17:e1009459. doi: 10.1371/journal.ppat.1009459

Gong, S., Lv, R., Fan, Y., Shi, Y., and Zhang, M. (2023). The potential mechanism of bletilla striata in the treatment of ulcerative colitis determined through network pharmacology, molecular docking, and in vivo experimental verification. *Naunyn Schmiedebergs Arch. Pharmacol.* 396, 983–1000. doi: 10.1007/s00210-022-02370-9

Han, X., Song, Z., Liu, J., Zhang, Y., and Wu, M. (2023). Effects of different drying methods on the quality of bletilla striata scented tea. *Molecules* 28:2438.

Huang, J., Hu, B., Qi, K., Chen, W., and Pang, X. (2016). Effects of phosphorus addition on soil microbial biomass and community composition in a subalpine spruce plantation. *Eur. J. Soil Biol.* 72, 35–41.

Hug, L. A., Castelle, C. J., Wrighton, K. C., Thomas, B. C., and Sharon, I. (2013). Community genomic analyses constrain the distribution of metabolic traits across the chloroflexi phylum and indicate roles in sediment carbon cycling. *Microbiome* 1:22.

Janssen, P. H. (2006). Identifying the dominant soil bacterial taxa in libraries of 16s rrna and 16s rrna genes. *Appl. Environ. Microbiol.* 72, 1719–1728. doi: 10.1128/AEM.72.3.1719-1728.2006

Jiang, F., Li, M., Wang, H., Ding, B., and Zhang, C. (2019). Coelonin, an anti-inflammation active component of bletilla striata and its potential mechanism. *Int. J. Mol. Sci.* 20:4422.

Jiang, G., Wang, B., Wang, Y., Kong, H., and Wang, Y. (2023). Structural characteristics of a novel bletilla striata polysaccharide and its activities for the alleviation of liver fibrosis. *Carbohydr. Polym.* 313:120781.

Jones, M. D., Forn, I., Gadelha, C., Egan, M. J., and Bass, D. (2011). Discovery of novel intermediate forms redefines the fungal tree of life. *Nature* 474, 200–203.

Jones, R. T., Robeson, M. S., Lauber, C. L., Hamady, M., and Knight, R. (2009). A comprehensive survey of soil acidobacterial diversity using pyrosequencing and clone library analyses. *ISME J.* 3, 442–453. doi: 10.1038/ismej.2008.127

Kielak, A. M., Barreto, C. C., Kowalchuk, G. A., van Veen, J. A., and Kuramae, E. E. (2016). The ecology of acidobacteria: moving beyond genes and genomes. *Front. Microbiol.* 7:744. doi: 10.3389/fmicb.2016.00744

Li, B., Shen, X., Zhao, Y., Cong, P., and Wang, H. (2022). Sloping farmlands conversion to mixed forest improves soil carbon pool on the loess plateau. *Int. J. Environ. Res. Public Health* 19:5157.

Li, L., Tilman, D., Lambers, H., and Zhang, F. S. (2014). Plant diversity and overyielding: insights from belowground facilitation of intercropping in agriculture. *New Phytol.* 203, 63–69. doi: 10.1111/nph.12778

Li, M., Wei, Y., Yin, Y., Zhu, W., and Bai, X. (2023). Characteristics of soil physicochemical properties and microbial community of mulberry (morus alba l.) And alfalfa (medicago sativa l.) Intercropping system in northwest liaoning. *Microorganisms* 11:114.

Li, X., Chu, Y., Jia, Y., Yue, H., and Han, Z. (2022). Changes to bacterial communities and soil metabolites in an apple orchard as a legacy effect of different intercropping plants and soil management practices. *Front. Microbiol.* 13:956840. doi: 10.3389/fmicb.2022.956840

Li, Y., He, X., Yuan, H., and Lv, G. (2022). Differed growth stage dynamics of root-associated bacterial and fungal community structure associated with halophytic plant lycium ruthenicum. *Microorganisms* 10:1644.

Lin, H., Hong, T., Wu, C., Chen, H., and Chen, C. (2012). Monthly variation in litterfall and the amount of nutrients in an aleurites montana plantation. *For. Stud. China* 14, 30–35. doi: 10.1007/s11632-012-0109-2

Liu, C., Dai, K. Y., Ji, H. Y., Jia, X. Y., and Liu, A. J. (2022). Structural characterization of a low molecular weight bletilla striata polysaccharide and antitumor activity on h22 tumor-bearing mice. *Int. J. Biol. Macromol.* 205, 553–562. doi: 10.1016/j.ijbiomac.2022.02.073

Lucas-Borja, M. E., Hedo De Santiago, J., Yang, Y., Shen, Y., and Candel-Pérez, D. (2019). Nutrient, metal contents and microbiological properties of litter and soil along a tree age gradient in mediterranean forest ecosystems. *Sci. Total Environ.* 650, 749–758.

Mander, C., Wakelin, S., Young, S., Condron, L., and O'Callaghan, M. (2012). Incidence and diversity of phosphate-solubilising bacteria are linked to phosphorus status in grassland soils. *Soil Biol. Biochem.* 44, 93–101.

Mortimer, R., Saj, S., and David, C. (2018). Supporting and regulating ecosystem services in cacao agroforestry systems. *Agrofor. Syst.* 92, 1639–1657.

Orchard, S., Standish, R. J., Dickie, I. A., Renton, M., and Walker, C. (2017). Fine root endophytes under scrutiny: a review of the literature on arbuscule-producing fungi recently suggested to belong to the mucoromycotina. *Mycorrhiza* 27, 619–638.

Philippot, L., Raaijmakers, J. M., Lemanceau, P., and Van der Putten, W. H. (2013). Going back to the roots: the microbial ecology of the rhizosphere. *Nat. Rev. Microbiol.* 11, 789–799.

Pu, T., Liu, J., Dong, J., Qian, J., and Zhou, Z. (2022). Microbial community diversity and function analysis of aconitum carmichaelii debeaux in rhizosphere soil of farmlands in southwest china. *Front. Microbiol.* 13:1055638. doi: 10.3389/fmicb.2022.1055638

Reichenbach, H. (1999). The ecology of the myxobacteria. *Environ. Microbiol.* 1, 15–21.

Ruthes, B. E. S., Kaschuk, G., de Moraes, A., Lang, C. R., and Crestani, C. (2023). Soil microbial biomass, n nutrition index, and yield of maize cultivated under eucalyptus shade in integrated crop-livestock-forestry systems. *Int. J. Plant Prod.* 17, 323–335.

Shi, L., Zhang, H., Liu, T., Zhang, W., and Shao, Y. (2016). Consistent effects of canopy vs. Understory nitrogen addition on the soil exchangeable cations and microbial community in two contrasting forests. *Sci. Total Environ.* 553, 349–357.

Shimkets, L. J. (1990). Social and developmental biology of the myxobacteria. *Microbiol. Rev.* 54, 473–501.

Sommermann, L., Geistlinger, J., Wibberg, D., Deubel, A., and Zwanzig, J. (2018). Fungal community profiles in agricultural soils of a long-term field trial under different tillage, fertilization and crop rotation conditions analyzed by high-throughput its-amplicon sequencing. *PLoS One* 13:e195345. doi: 10.1371/journal.pone.0195345

Spatafora, J. W., Chang, Y., Benny, G. L., Lazarus, K., and Smith, M. E. (2016). A phylum-level phylogenetic classification of zygomycete fungi based on genome-scale data. *Mycologia* 108, 1028–1046.

Stolz, A. (2009). Molecular characteristics of xenobiotic-degrading sphingomonads. *Appl. Microbiol. Biotechnol.* 81, 793–811.

Sujatha, S., and Bhat, R. (2010). Response of vanilla (vanilla planifolia a.) Intercropped in arecanut to irrigation and nutrition in humid tropics of india. *Agric. Water Manage.* 97, 988–994.

Sun, B., Zhang, W., Liu, Y., Xue, M., and Qiu, L. (2022). A biomass based photonic crystal hydrogel made of bletilla striata polysaccharide. *Biosensors Basel* 12:841.

Sun, P., Wu, J., Lin, X., Wang, Y., and Zhu, J. (2022). Effect of ozonated water, mancozeb, and thiophanate-methyl on the phyllosphere microbial diversity of strawberry. *Front. Plant Sci.* 13:967797. doi: 10.3389/fpls.2022.967797

Verma, R. K., Chauhan, A., Verma, R. S., Rahman, L., and Bisht, A. (2013). Improving production potential and resources use efficiency of peppermint (mentha piperita l.) Intercropped with geranium (pelargonium graveolens l. Herit ex ait) under different plant density. *Ind. Crop. Prod.* 44, 577–582.

Wang, H. Y., Kang, C. Z., Zhang, W. J., Zhou, L. Y., and Wan, X. F. (2020). [Land use strategy of ecological agriculture of chinese materia medica in future development]. *Zhongguo Zhong Yao Za Zhi* 45, 1990–1995.

Wang, Q., Wang, C., Wei, Y., Yao, W., and Lei, Y. (2022). Soil microbes drive the flourishing growth of plants from leucocalocybe mongolica fairy ring. *Front. Microbiol.* 13:893370. doi: 10.3389/fmicb.2022.893370

Weissman, K. J., and Müller, R. (2010). Myxobacterial secondary metabolites: bioactivities and modes-of-action. *Nat. Prod. Rep.* 27, 1276–1295.

Wolz, K. J., and DeLucia, E. H. (2018). Alley cropping: global patterns of species composition and function. *Agric. Ecosyst. Environ.* 252, 61–68.

Yang, C., Shen, X., Shi, X., Cui, Z., and Nan, J. (2023). Impact of submerged macrophytes on growth and 2-mib release risk of pseudanabaena sp.: from field monitoringa to cultural experiments. *J. Hazard. Mater.* 442:130052.

Yutin, N., and Galperin, M. Y. (2013). A genomic update on clostridial phylogeny: gram-negative spore formers and other misplaced clostridia. *Environ. Microbiol.* 15, 2631–2641.

Zhang, C., Ning, D., Pan, J., Chen, C., and Gao, C. (2021). Anti-inflammatory effect fraction of bletilla striata and its protective effect on lps-induced acute lung injury. *Mediat. Inflamm.* 2021:6684120.

Zhang, H., Hua, Z. W., Liang, W. Z., Niu, Q. H., and Wang, X. (2020). The prevention of bio-organic fertilizer fermented from cow manure compost by bacillus sp. Xg-1 on watermelon continuous cropping barrier. *Int. J. Environ. Res. Public Health* 17:5714.

Zhang, S., Shen, T., Yang, Y., Li, Y. C., and Wan, Y. (2018). Controlled-release urea reduced nitrogen leaching and improved nitrogen use efficiency and yield of direct-seeded rice. *J. Environ. Manage.* 220, 191–197.

Zhang, X., Gao, G., Wu, Z., Wen, X., and Zhong, H. (2020). Responses of soil nutrients and microbial communities to intercropping medicinal plants in moso bamboo plantations in subtropical china. *Environ. Sci. Pollut. Res. Int.* 27, 2301–2310.

Zhang, Y., Han, M., Song, M., Tian, J., and Song, B. (2021). Intercropping with aromatic plants increased the soil organic matter content and changed the microbial community in a pear orchard. *Front. Microbiol.* 12:616932. doi: 10.3389/fmicb.2021.616932

Zhong, Z., Huang, X., Feng, D., Xing, S., and Weng, B. (2018). Long-term effects of legume mulching on soil chemical properties and bacterial community composition and structure. *Agric. Ecosyst. Environ.* 268, 24–33. doi: 10.1016/j.agee.2018.09.001

Zhu, L., He, J., Tian, Y., Li, X., and Li, Y. (2022). Intercropping wolfberry with gramineae plants improves productivity and soil quality. *Sci. Hortic.* 292:110632.

Zhu, Z., Liang, T., Dai, G., Zheng, J., and Dong, J. (2023). Extraction, structural-activity relationships, bioactivities, and application prospects of bletilla striata polysaccharides as ingredients for functional products: a review. *Int. J. Biol. Macromol.* 245:125407.

frontiers | Frontiers in Microbiology

TYPE Original Research
PUBLISHED 15 March 2024
DOI 10.3389/fmicb.2024.1294833

Check for updates

OPEN ACCESS

EDITED BY
Zhenlin Han,
University of Hawaii at Manoa, United States

REVIEWED BY
Xiangxiang Fu,
Nanjing Forestry University, China
Elisa Petrussa,
University of Udine, Italy
Tiantian Lin,
Leiden University, Netherlands

*CORRESPONDENCE
Honggang Sun
honggangsun@caf.ac.cn

RECEIVED 15 September 2023
ACCEPTED 08 February 2024
PUBLISHED 15 March 2024

CITATION
Wu C, Yang Y, Wang Y, Zhang W and Sun H (2024) Colonization of root endophytic fungus *Serendipita indica* improves drought tolerance of *Pinus taeda* seedlings by regulating metabolome and proteome. *Front. Microbiol.* 15:1294833. doi: 10.3389/fmicb.2024.1294833

COPYRIGHT
© 2024 Wu, Yang, Wang, Zhang and Sun. This is an open-access article distributed under the terms of the Creative Commons Attribution License (CC BY). The use, distribution or reproduction in other forums is permitted, provided the original author(s) and the copyright owner(s) are credited and that the original publication in this journal is cited, in accordance with accepted academic practice. No use, distribution or reproduction is permitted which does not comply with these terms.

Colonization of root endophytic fungus *Serendipita indica* improves drought tolerance of *Pinus taeda* seedlings by regulating metabolome and proteome

Chu Wu[1], Yujie Yang[1], Yun Wang[2], Wenying Zhang[3] and Honggang Sun[4]*

[1]College of Horticulture and Gardening, Yangtze University, Jingzhou, Hubei, China, [2]College of Life Sciences, Yangtze University, Jingzhou, Hubei, China, [3]College of Agricultural Sciences, Yangtze University, Jingzhou, Hubei, China, [4]Research Institute of Subtropical Forestry, Chinese Academy of Forestry, Hangzhou, China

Pinus taeda is an important forest tree species for plantations because of its rapid growth and high yield of oleoresins. Although *P. taeda* plantations distribute in warm and wet southern China, drought, sometime serious and long time, often occurs in the region. To explore drought tolerance of *P. taeda* and usage of beneficial microorganisms, *P. taeda* seedlings were planted in pots and were inoculated with root endophytic fungus *Serendipita indica* and finally were treated with drought stress for 53 d. Metabolome and proteome of their needles were analyzed. The results showed that *S. indica* inoculation of *P. taeda* seedlings under drought stress caused great changes in levels of some metabolites in their needles, especially some flavonoids and organic acids. Among them, the levels of eriocitrin, *trans*-aconitic acid, vitamin C, uric acid, alpha-ketoglutaric acid, vitamin A, stachydrine, coumalic acid, itaconic acid, calceolarioside B, 2-oxoglutaric acid, and citric acid were upregulated more than three times in inoculated seedlings under drought stress, compared to those of non-inoculated seedlings under drought stress. KEGG analysis showed that some pathways were enriched in inoculated seedlings under drought stress, such as flavonoid biosynthesis, ascorbate and aldarate metabolism, C5-branched dibasic acid metabolism. Proteome analysis revealed some specific differential proteins. Two proteins, namely, H9X056 and H9VDW5, only appeared in the needles of inoculated seedlings under drought stress. The protein H9VNE7 was upregulated more than 11.0 times as that of non-inoculated seedlings under drought stress. In addition, *S. indica* inoculation increased enrichment of water deficient-inducible proteins (such as LP3-1, LP3-2, LP3-3, and dehydrins) and those involved in ribosomal structures (such as A0A385JF23). Meanwhile, under drought stress, the inoculation caused great changes in biosynthesis and metabolism pathways, mainly including phenylpropanoid biosynthesis, cutin, suberine and wax biosynthesis, and 2-oxocarboxylic acid metabolism. In addition, there were positive relationships between accumulation of some metabolites and enrichment of proteins in *P. taeda* under drought stress. Altogether, our results showed great changes in metabolome and proteome in inoculated seedlings under drought stress and provided a guideline to further study functions of metabolites and proteins, especially those related to drought stress.

KEYWORDS

forest trees, drought stress, metabolome, proteome, beneficial microorganisms

1 Introduction

Loblolly pine (*Pinus taeda*) is native to the southeastern United States (US) and is an important forest tree species in the southern mixed pine-oak forest (Kricher and Morrison, 1998) and the Coastal Plain oak-pine forests (Keyser et al., 2016) in the southern and the southeastern US, respectively. The forest species is the most-planted forest tree species in North America and managed for wood production (Matallana-Ramirez et al., 2021; McKeand et al., 2021). There are approximately 25 million hectares of planted trees in US in 2011, of which loblolly pine represents 10 million hectares, making it the most-planted tree species in the country (Gonzalez-Benecke et al., 2017). Planted forests account for 22% of all forested area in the southeastern US (Gonzalez-Benecke et al., 2017), and they play a large role in meeting the nation's wood and fiber demand. Gonzalez-Benecke et al. (2017) predicted that an increase in productivity can be expected for a large majority of the planted loblolly pine stands in the southeastern US during 21th century. Because of its rapid growth and high oleoresins yield, loblolly pine was also introduced to other countries around the world. Terpenoid oleoresins can be converted into rosin and turpentine, which show wide and strong commercial uses such as adhesives, inks, emulsifiers, solvents, fragrances, and resins (da Silva Rodrigues-Corrêa et al., 2012). According to an estate in 2004, approximately 30,000 tons of pinenes were consumed only by the flavor and fragrance industry per year to produce a range of products (Swift, 2004); thus, such great requirement improves oleoresins production from *Pinus* species around the world. Since loblolly pine was introduced into China in thirties of last century, the forest tree species became more and more important for plantations along with slash pine (*Pinus elliottii*) in southern China, especially the valleys of the Yangtze River and Zhujiang River. Approximately 0.6 million of tons of resin was harvested each year in China, accounting for 60% of the global gum resin yield and about half of the worldwide turpentine trade (McConnell et al., 2021; Yi et al., 2021), most of which was harvested from loblolly pine and slash pine.

Along with other environmental factors, such as soil chemistry, annual average temperature, and incident radiation, water availability is one of the principal physical factors limiting primary productivity of terrestrial plants. Water availability was identified as the most influential single variable for estimating the net primary productivity of terrestrial ecosystems (Churkina et al., 1999). Thus, drought stress affects the net primary productivity of terrestrial ecosystems, especially forest ecosystems because of their important ecosystem system service functions. For *P. taeda* in a 35-year-old stand, oleoresin yield was closely associated with periods of calculated moderate soil water deficit and presumed growth (Lorio and Sommers, 1986). In such stand, moderate seasonal water deficits limited pine growth but did not limit photosynthesis and translocation of photosynthates and favor differentiation processes, such as oleoresin synthesis (Lorio and Sommers, 1986). However, serious and long-term drought certainly reduces both pine growth and oleoresin yield. In fact, drought stress is the principal cause of seedling mortality in pine forests of the southeastern US (Lorenz et al., 2006). Although annual precipitation is enough for growth and development of loblolly pine in southern and southwestern China, climate change often caused seasonal drought in some areas in this region. For example, persistent drought in 2006 summer caused pine death in large scale in Sichuan province, localized in southwestern China (Wang, 2012). From the autumn to the spring in 2009/2010 and 2011/2012, severe drought occurred in southwestern China, especially in Yunnan province (Sun et al., 2014). Such severe drought caused death of seedlings and saplings of *Pinus kesiya* var. *langbianensis* and *Pinus yunnanensis* in this province. Subsequently, severe drought occurred in Fujian province, located in southeastern China, in March–June of 2018 (He F. et al., 2022). In the summer of 2022, great reduction in precipitation occurred in the valley of the Yangtze River, which is the longest river in China with an average stream flow of 33,980 $m^3 \cdot s^{-1}$, resulting in flux break of few tributary rivers and partial occurrence of riverbed of the Yangtze River. According to data collected from 1952 to 2010, Um et al. (2022) confirmed that the propagation phenomenon of meteorological to hydrological and agricultural droughts occurred in the valley of the Yangtze River. The concurrent occurrence of drought and pine diseases accelerates pine death. For example, persistent summer drought triggered energy metabolism imbalance and entire wilt and even death of pine trees caused by *Bursaphelenchus xylophilus* in China (Wang, 2012). Therefore, under the background of climate change, forest ecosystems in the valley of the Yangtze River are under threat from severe droughts (Yin et al., 2021).

Plants use different mechanisms to survive under drought stress, including the five aspects: (1) soil water deficit avoidance (e.g., root exploration, water conservation, and phenology); (2) stress avoidance (e.g., osmotic adjustment and root-soil isolation); (3) damage avoidance (i.e., stress tolerance, e.g., leaf orientation, evaporative cooling, and root-to-shoot ratio); (4) damage tolerance (e.g., night-time recovery, heat shock proteins, and dehydrins); (5) unadapted (e.g., death, organ loss, and permanent damage) (Gilbert and Medina, 2016). During water deficient, plants synergistically use these mechanisms to survive, especially under severe drought stress. Facing drought stress, loblolly pine forest farm managers and tree physiologists have to find suitable ways to maintain survival, growth, and oleoresin yield of loblolly pine. The suitable ways include few aspects: (1) to clearly explore the genetic characteristics of loblolly pine (Lorenz et al., 2011; Wegrzyn et al., 2014; Perera et al., 2018; Caballero et al., 2021) and functions of genes and metabolites related to drought stress (González-Martínez et al., 2006; Lorenz et al., 2006; Talbot et al., 2017; Wu et al., 2023), further providing the base for genetic modification of loblolly pine; (2) based on genetic characteristics of loblolly pine, to breed new cultivars of loblolly pine with stronger drought tolerance (Zapata-Valenzuela et al., 2013; Matallana-Ramirez et al., 2021); (3) to take advantage of benefits from beneficial microbes, especially ectomycorrhizal fungi and root endophytic fungi under

drought stress (Piculell et al., 2019; Wu et al., 2019; Frank and Garcia, 2021).

Symbiosis between plants and microorganisms occurs wide in natural ecosystems, affects plant terrestrializations (Puginier et al., 2022), evolution (Batstone, 2022; van Galen et al., 2023), and tolerance to abiotic and biotic stress (Zeng et al., 2022), and widens the habitability ranges of plants (Muñoz and Carneiro, 2022). Among all the beneficial microorganisms symbiosing with plants, five families of microorganisms have been greatly paid on attentions, i.e., arbuscular mycorrhizal fungi (Kaur et al., 2022; Razak and Gange, 2023; Chen W. et al., 2023), ectomycorrhizal fungi (Karlsen-Ayala et al., 2022; Jörgensen et al., 2023; Xiao et al., 2023), root endophytic fungi (Manzur et al., 2022; Sun et al., 2022; Qin et al., 2023), dark septate fungi (Gaber et al., 2023; Wang et al., 2023; Chen S. et al., 2023), and plant growth-promoting rhizobacteria (PGPR) (Ahmad et al., 2022; Gowtham et al., 2022; Zhao et al., 2023). These beneficial microorganisms show strong effects on their plant hosts under drought stress (Ahmad et al., 2022; Gowtham et al., 2022; Zhao et al., 2023). In review of such functions, they are often used as components of biofilmed biofertilizers (Das et al., 2017; Kumar et al., 2021; Zahra et al., 2023). Biofilmed biofertilizers have emerged as a new improved inoculant technology to improve efficient nutrition uptake, strengthen management of pests and pathogenic microorganisms, and sustain soil fertility (Das et al., 2017). However, because of their life traits, i.e., obligate biotroph (Zuccaro et al., 2014), it is difficult to proliferate arbuscular mycorrhizal fungi on a large scale in short time. Ectomycorrhizal fungi, root endophytic fungi, and PGPR show their advantage in agricultural application because of their facultative biotroph. The root endophytic fungus *Serendipita indica* (i.e., formerly named as *Piriformospora indica*) can colonize in a wide range of plant hosts, such as *Arabidopsis thaliana* (Opitz et al., 2021), *Juglans regia* (Liu et al., 2021), *Oryza sativa* (Ghorbani et al., 2021), *Platycladus orientalis* (Wu et al., 2019), and tomato (*Solanum lycopersicum*) (De Rocchis et al., 2022), and shows strong effects on their plant hosts, especially improving plant nutrition uptake (Wu et al., 2019) and tolerance to drought stress (Liu et al., 2021; Boorboori and Zhang, 2022). However, it is unclear how *S. indica* regulates responses of plant hosts to drought stress in levels of metabolome and proteome, especially forest tree species. The related mechanisms are not still clear, such as the functions of effector proteins secreted by the fungus. Analysis of metabolome and proteome provides outline of changes in metabolites and proteins in plants under drought stress, and the related results also provide a guide for future research, especially the functions of small metabolites and unique proteins that accumulate to high levels in plants under drought stress.

As mentioned above, beneficial microorganisms show strong ability to improve plant tolerance to drought stress; however, related studies involved in loblolly pine are few, especially those involved in drought tolerance mechanisms. The root endophytic fungus *S. indica* can be used to improve plant tolerance to drought stress, as shown above. In the present study, *S. indica* was used to inoculate with loblolly pine seedlings, and untargeted metabolome and proteome of their needles were analyzed. Our aims are (1) to know changes in metabolome and proteome caused by inoculation of *S. indica* under drought stress and (2) to explore the related mechanisms that are involved in increased drought tolerance caused by *S. indica*.

2 Experimental materials and methods

2.1 Experimental materials

Seeds of loblolly pine (*Pinus taeda*) came from the Forest Farm of Maple Mountain in Jingdezhen, Jiangxi province, China. These seeds were sterilized and then sown in sterilized sand in big plastic pots. After these seeds were germinated, the pots were transferred to a growth chamber (light period: 16-h light/8-h dark; PPFD: 350 $\mu mol \cdot m^{-2} \cdot s^{-1}$; RH: 80%; temperature: 25°C). When pine seedlings grew with four true needles, they were transplanted into plastic pots (20 cm in diameter and 30 cm in height) containing sterilized cultivation substance (peat: vermiculite = 50: 50, pH ~ 7.0), three pine seedlings per pot. These pots were then transferred into a greenhouse with natural sunlight and controlled temperature (25°C) and relative humidity (~75%). Water was provided according to the moisture of the cultivation substance in the pots. After a month, half of these pots were inoculated with the root endophytic fungus *S. indica*.

Serendipita indica strain DSM 11827 was provided by Prof. Ralf Oelmüller (Faculty of Biological Science, Friedrich-Schiller-University Jena, Jena, Germany). The fungus was cultured on potato dextrose agar (PDA) in liquid culture at 180–200 rpm for 7 d (28°C). The hyphae were filtered, rinsed with sterile water three times, and then treated with filter paper. In total, 10 g of fresh hyphae was weighed and made into homogenate. The homogenate was then made to a suspension solution of 1 L, and the suspension solution was used for inoculation of loblolly pine seedlings.

2.2 Inoculation and drought stress treatment

When loblolly pine seedlings were inoculated with the suspension solution mentioned above, every pot was injected with 10 mL of the suspension solution at the center of a pot. After inoculation, all the pots with loblolly pine seedlings were cultivated in a glasshouse as mentioned above. After culture of 120 d, drought stress treatment was carried out: 30 pots with inoculated seedlings were divided into two groups, one was treated with drought stress, and another group was watered well; 30 pots with non-inoculated seedlings were also divided into two groups, one group treated with drought stress, and another group watered well. Therefore, four treatments were established, i.e., non-inoculated seedlings under well-watered condition (NI_W treatment), inoculated seedlings under well-watered condition (I_W treatment), non-inoculated seedlings under drought stress (NI_D treatment), and inoculated seedlings under drought stress (I_D treatment). These pots treated with drought stress were provided with 100 mL water once every week. According to the previous trial experiment, 100 mL of water for a pot could maintain approximately 53% field capacity. Well-watered seedlings were provided with enough water once every week at the same time. After drought stress treatment of 53 d, six pots were random chosen from every treatment, and a seedling was random chosen from a pot. Their needles of the six seedlings were harvested and then were rinsed with sterile water three times. The needles from the two random chosen seedlings were combined into a sample. Thus, three samples were harvested for each treatment, and total 12 samples harvested for all the four

treatments. These samples were immediately treated with liquid nitrogen and stored under −80°C for further analysis.

2.3 Examination of *Serendipita indica* infection

Twenty days after inoculation of *S. indica* with loblolly pine seedlings, *S. indica* infection was examined according to the method introduced by Xu et al. (2023).

2.4 Methods of untargeted metabolomic analysis

Needle tissues (100 mg) were individually grounded with liquid nitrogen, and the homogenate was resuspended with prechilled 80% methanol by well vortex. The samples were incubated on ice for 5 min and then were centrifuged at 15,000 *g* for 20 min (4°C). Some of supernatant was diluted to final concentration containing 53% methanol by LC–MS grade water. The samples were subsequently transferred to fresh Eppendorf tubes and then were centrifuged at 15000 g for 20 min (4°C). Finally, the supernatant was injected into the LC–MS/MS system analysis (Want et al., 2013). Subsequently, UHPLC–MS/MS analysis, data processing and metabolite identification, and data analysis were carried out according to the previous introduction (Wu et al., 2023).

2.5 Methods of untargeted proteome analysis

2.5.1 Extraction of total proteins in leaves of *Pinus taeda* seedlings

The sample was ground individually in liquid nitrogen and lysed with SDT lysis buffer (containing 100 mM NaCl) and 1/100 volume of DTT, followed by 5 min of ultrasonication on ice. After reacting at 95°C for 8–15 min and ice bath for 2 min, the lysate was centrifuged at 12,000 *g* for 15 min at 4°C. The supernatant was alkylated with sufficient IAM for 1 h at room temperature in the dark. Then, the samples were completely mixed with four times the volume of pre-cooled acetone by vortexing and incubated at-20°C for at least 2 h. The samples were then centrifuged at 12,000 *g* for 15 min at 4°C, and the precipitation was collected. After washing with 1 mL cold acetone, the pellet was dissolved by dissolution buffer (DB buffer).

2.5.2 Protein quality test

BSA standard protein solution was prepared according to the instructions of Bradford protein quantitative kit, with gradient concentration ranging from 0 to 0.5 g·L^{-1}. BSA standard protein solutions and sample solutions with different dilution multiples were added into 96-well plate to fill up the volume to 20 μL, respectively. Each gradient was repeated three times. The plate was added 180 μL G250 dye solution quickly and placed at room temperature for 5 min, and the absorbance at 595 nm was detected. The standard curve was drawn with the absorbance of standard protein solution, and the protein concentration of the sample was calculated. 20 μg of the protein sample was loaded to 12% SDS-PAGE gel electrophoresis, wherein the concentrated gel was performed at 80 V for 20 min, and the separation gel was performed at 120 V for 90 min. The gel was stained by Coomassie brilliant blue R-250 and decolored until the bands were visualized clearly.

2.5.3 Trypsin treatment

Trypsin treatment was carried out according to the method introduced by Zhang et al. (2016). Each protein sample was taken, and the volume was made up to 100 μL with DB lysis buffer (8 M Urea, 100 mM TEAB, pH 8.5), trypsin and 100 mM TEAB buffer were added, and the sample was mixed and digested at 37°C for 4 h. Then, trypsin and $CaCl_2$ were added digested overnight. Formic acid was mixed with digested sample, adjusted pH under 3, and centrifuged at 12,000 *g* for 5 min at room temperature. The supernatant was slowly loaded to the C18 desalting column, washed with washing buffer (0.1% formic acid, 3% acetonitrile) three times, and then added elution buffer (0.1% formic acid, 70% acetonitrile). The eluents of each sample were collected and lyophilized (Zhang et al., 2016).

2.5.4 Separation of fractions (high-depth quantification)

Mobile phases A (2% acetonitrile, adjusted pH to 10.0 using ammonium hydroxide) and B (98% acetonitrile, adjusted pH to 10.0 using ammonium hydroxide) were used to develop a gradient elution. The lyophilized powder was dissolved in solution A and centrifuged at 12,000 *g* for 10 min at room temperature. The sample was fractionated using a C18 column (Waters BEH C18, 4.6 × 250 mm, 5 μm) on a Rigol L3000 HPLC system, and the column oven was set as 45°C. The detail of elution gradient is shown in Supplementary Table S1. The eluates were monitored at UV 214nm, collected in a tube per minute, and combined into 10 fractions finally. All fractions were dried under vacuum and then reconstituted in 0.1% (v/v) formic acid (FA) in water.

2.5.5 LC–MS/MS analysis

UHPLC–MS/MS analyses were performed using an EASY-nLC™ 1,200 UHPLC-HFX system (Thermo Fisher, Germany) coupled with a Q Exactive™ HF-X mass spectrometer (Thermo Fisher, Germany) in Novogene Co., Ltd. (Beijing, China). First, mobile phase A (100% water, 0.1% formic acid) and B (80% acetonitrile, 0.1% formic acid) solutions were prepared. The lyophilized powder was dissolved in 10 μL of solution A and centrifuged at 14,000 *g* for 20 min at 4°C, and 1 μg of the supernatant was injected into a home-made C18 Nano-Trap column (4.5 cm × 75 μm, 3 μm). The temperature of the column oven was set to 55°C. Peptides were separated in a home-made analytical column (15 cm × 150 μm, 1.9 μm), using a linear gradient elution as listed in Supplementary Table S1. The separated peptides were analyzed by Q Exactive™ HF-X mass spectrometer, with ion source of Nanospray Flex™(ESI), spray voltage of 2.1 kV, and ion transport capillary temperature of 320°C. Full scan ranges from *m/z* 350 to 1,500 with resolution of 60,000 (at *m/z* 200), an automatic gain control (AGC) target value was 3×10^6, and a maximum ion injection time was 20 ms. The top 40 precursors of the highest abundant in the full scan were selected and fragmented by higher energy collisional dissociation (HCD) and analyzed in MS/MS, where resolution was 15,000 (at *m/z* 200), the automatic gain control (AGC) target value was 1×10^5, the maximum ion injection time was 45 ms, a normalized collision energy was set as 27%, an intensity threshold was 2.2×10^4,

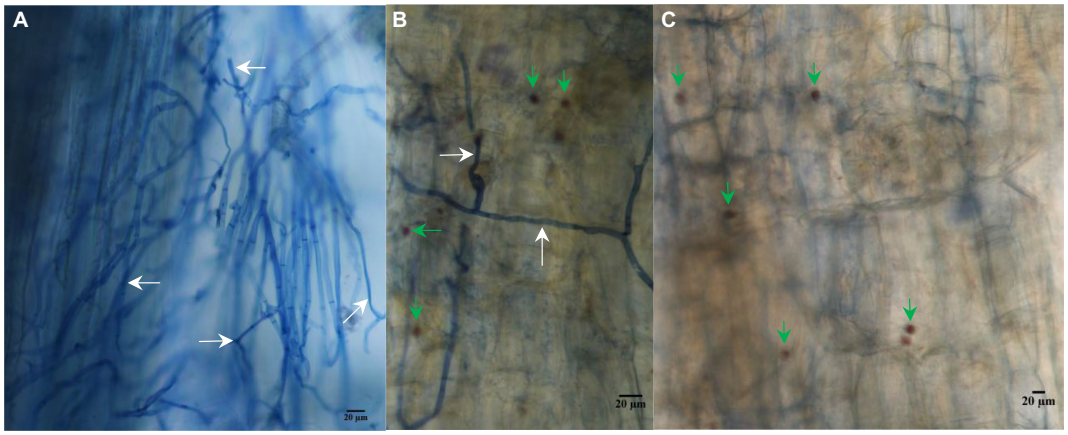

FIGURE 1
Infection of *Serendipita indica* in roots of *Pinus taeda* plants. **(A)** *S. serendipita* hyphae (shown by white arrows) on the roots of *Pinus taeda* plants. **(B)** Hyphae (shown by white arrows) and spores (shown by green arrows) of *Serendipita indica* on the root surface of *Pinus taeda* plants. **(C)** Spores (shown by green arrows) of *Serendipita indica* in the root cortex of *Pinus taeda* plants. Bar = 20 μm.

and the dynamic exclusion parameter was 20 s. The raw data of MS detection were named as ".raw."

2.5.6 Data analysis

At first, the identification and quantitation of protein were carried out. The resulting spectra were searched against *** database by the search engines: Proteome Discoverer (Thermo, HFX and 480) or MaxQuant (Bruker, Tims). The search parameters of Proteome Discoverer were set as follows: Mass tolerance for precursor ion was 10 ppm, and mass tolerance for product ion was 0.02 Da. Carbamidomethyl was specified as fixed modifications, and oxidation of methionine (M) was specified as dynamic modification and loss of methionine at the N-Terminal. A maximum of two missed cleavage sites were allowed. The search parameters of MaxQuant were set as follows: Mass tolerance for precursor ion was 20 ppm, and mass tolerance for product ion was 0.05 Da. Carbamidomethyl was specified as fixed modifications, oxidation of methionine (M) was specified as dynamic modification, and acetylation was specified as N-terminal modification. A maximum of two missed cleavage sites were allowed. To improve the quality of analysis results, the software PD or MaxQuant further filtered the retrieval results: Peptide spectrum matches (PSMs) with a credibility of more than 99% were identified PSMs. The identified protein contained at least one unique peptide. The identified PSMs and protein were retained and performed with FDR no more than 1.0%. The protein quantitation results were statistically analyzed by *t*-test. The proteins whose quantitation was significantly different between experimental and control groups ($p < 0.05$) and |log2FC| > * [FC > * or FC < * (fold change, FC)] were defined as differentially expressed proteins (DEPs).

Next, the functional analysis of proteins and DEPs was carried out. Gene Ontology (GO) and InterPro (IPR) functional analysis were conducted using the InterProScan program against the non-redundant protein database (including Pfam, PRINTS, ProDom, SMART, ProSite, PANTHER) (Jones et al., 2014), and the databases of Clusters of Orthologous Groups (COG) and Kyoto Encyclopedia of Genes and Genomes (KEGG) were used to analyze the protein families and pathways. DEPs were used for volcanic map analysis, cluster heat map analysis, and enrichment analysis of GO, IPR, and KEGG (Huang et al., 2009). The probable protein–protein interactions were predicted using the STRING-db server (Franceschini et al., 2013)[1].

2.6 Correlation analysis on metabolites–proteins

Correlation analysis was carried out based on Pearson's coefficients of correlation to measure the correlation extents among top 50 differential proteins and top 50 differential metabolites with significant differences in the four treatments. When Pearson's coefficients of correlation were less than 0, the correlation was negative, while when Pearson's coefficients of correlation were more than 0, the correlation was positive. Network figures showed the visualized relationships between these proteins and metabolites with significant differences. Top 10 differential proteins and top 5 differential metabolites were selected for visualized network figures. Differential metabolites were marked as yellow, and differential proteins were marked as blue. Lines showed their respective relationships: Red and blue lines showed positive and negative relationships between these differential metabolites and proteins, respectively.

3 Results

3.1 Colonization of *Serendipita indica* in roots of *Pinus taeda* seedlings

Just like its ability to colonize in roots of some plant species (Wu et al., 2019; Liu et al., 2021; De Rocchis et al., 2022), *S. indica* colonized in the roots of *P. taeda* seedlings (Figure 1). Its hyphae and spores were found on the root surface and cortex of *P. taeda* seedlings, as shown in Figures 1A,B, respectively.

1 http://string.embl.de/

3.2 Effects of *Serendipita indica* colonization on untargeted metabolome

3.2.1 Outline of differential metabolites under the four treatments

After examination of quality control and identification of differential metabolites (Supplementary material 1, including Supplementary Tables S2, S3), Venn maps were used to show that the four comparisons possessed different numbers of unique differential metabolites. Under positive ionization mode, 34, 33, 25, and 53 unique differential metabolites occurred in the four comparisons, i.e., I_W vs. NI_W, NI_D vs. NI_W, I_D vs. I_W, and I_D vs. NI_D, respectively (Figure 2A; Supplementary Table S4). Under negative ionization mode, 27, 21, 17, and 24 unique differential metabolites occurred in the four comparisons, respectively (Figure 2B; Supplementary Table S4). Combining the numbers of these unique differential metabolites under positive and negative ionization mode, it was found that the comparison, i.e., I_D vs. NI_D, possessed the greatest number of unique differential metabolites (77 metabolites), suggesting that inoculation of *S. indica* resulted in great changes in metabolites in *P. taeda* seedlings under drought stress. The two metabolites, i.e., gomisin D and vinorelbine tartrate, occurred in all the four comparisons under negative ionization mode, and the other four metabolites, i.e., arachidonic acid methyl ester, LPC 12:0, estriol, and 2-[amino (3-chloroanilino)methylene]malononitrile, occurred in all the four comparisons under positive ionization mode (Figure 2; Supplementary Table S4).

3.2.2 Hierarchical clustering analysis of all differential metabolites

Hierarchical clustering analysis was carried out on all the differential metabolites of the individual sample groups under positive (Supplementary Figure S1A) and negative (Supplementary Figure S1B) ionization mode. Under drought stress, *S. indica* inoculation resulted in great changes in metabolites levels in the needles of *P. taeda* seedlings. In detail, under positive ionization mode, some metabolites, such as taxifolin, hesperetin, indole-3-carboxylic acid, pteroside A, phenprobamate, 8-isoprostaglandin A2, celestolide, puerarin, demethylnobiletin, gardenin B, topotecan, stachydrine, uric acid, DL-panthenol, and vitamin A, showed higher levels in the needles of I_D seedlings, compared to their levels in the needles of NI_D seedlings (Supplementary Figure S2A). Under negative ionization mode, procyanidin B1, ixoside, nicotinamide adenine dinucleotide, toddalolactone, sibirioside A, hordatine A, tectoridin, tricin 5-*O*-hexoside, trifolirhizin, hesperetin 5-*O*-glucode, myricitrin, polydatin, calceolarioside B, artesunate, sattabacin, and casticin showed higher levels in the needles of I_D seedlings, compared to NI_D seedlings (Supplementary Figure S2B). Under positive ionization mode, the levels of methyl syringate, N-lauroylsarcosine, and corymboside increased in NI_D seedlings, increasing to 46.50, 34.45, and 23.03 time as those in NI_W seedlings, respectively (the file "NI_D.vs.NI_W_pos_Diff_order" in Supplementary Table S3). Under negative ionization mode, 8-iso-15-keto prostaglandin E2 increased to 39.50 times in NI_D seedlings as that in NI_W seedlings (the file "NI_D.vs._NI_W_neg_Diff_order" in Supplementary Table S3). Under positive ionization mode, eriocitrin, *trans*-aconitic acid, vitamin C, uric acid, alpha-ketoglutaric acid, vitamin A, stachydrine, and coumalic acid were upregulated more than three times in I_D seedlings, compared to their levels in NI_D seedlings (the file "I_D.vs.NI_D_pos_Diff_order" in Supplementary Table S3). Similarly, under negative ionization mode, itaconic acid, calceolarioside B, 2-oxoglutaric acid, and citric acid were upregulated more than three times in I_D seedlings, compared to their levels in NI_D seedlings (the file "I_D.vs.NI_D_neg_Diff_order" in Supplementary Table S3). Some of these differential metabolites showed close correlations (Supplementary material 2, including Supplementary Table S5), suggesting their synergetic roles in the needles of *P. taeda* seedlings under drought stress. All these results suggest that *S. indica* inoculation caused great differences in species and numbers of differential metabolites in *P. taeda* seedlings under drought stress.

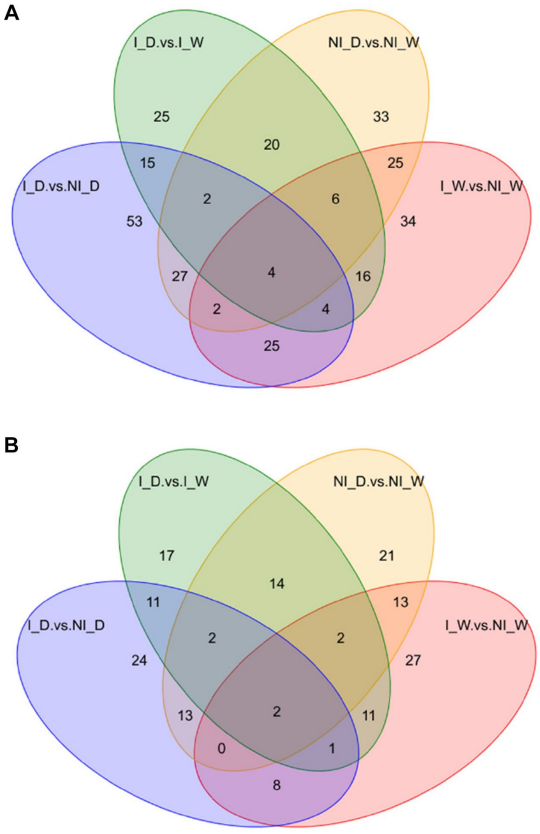

FIGURE 2
Venn diagram of differential metabolites under positive **(A)** and negative **(B)** ionization modes. I_W: inoculated seedlings under well-watered condition; NI_W: non-inoculated seedlings under well-watered condition; I_D: inoculated seedlings under drought stress; I_W: inoculated seedlings under well-watered condition; NI_D: non-inoculated seedlings under drought stress.

3.2.3 KEGG enrichment analysis

KEGG enrichment pathways are shown in Figure 3; Supplementary Figure S3; Supplementary Table S6. Under positive ionization mode, thiamine metabolism and lysine degradation were the most enriched in the comparison of I_W vs. NI_W (Figure 3A and the file "I_W.vs.NI_W_pos_kegg_enrichment" in Supplementary Table S6). In lysine degradation pathway, pipecolic acid and N6,N6,N6-trimethyl-L-lysine were enriched; in thiamine metabolism pathway, L-tyrosine and vitamin B1 were enriched (the file "I_W.vs.NI_W_pos_kegg_enrichment" in Supplementary Table S6). In the comparison, under

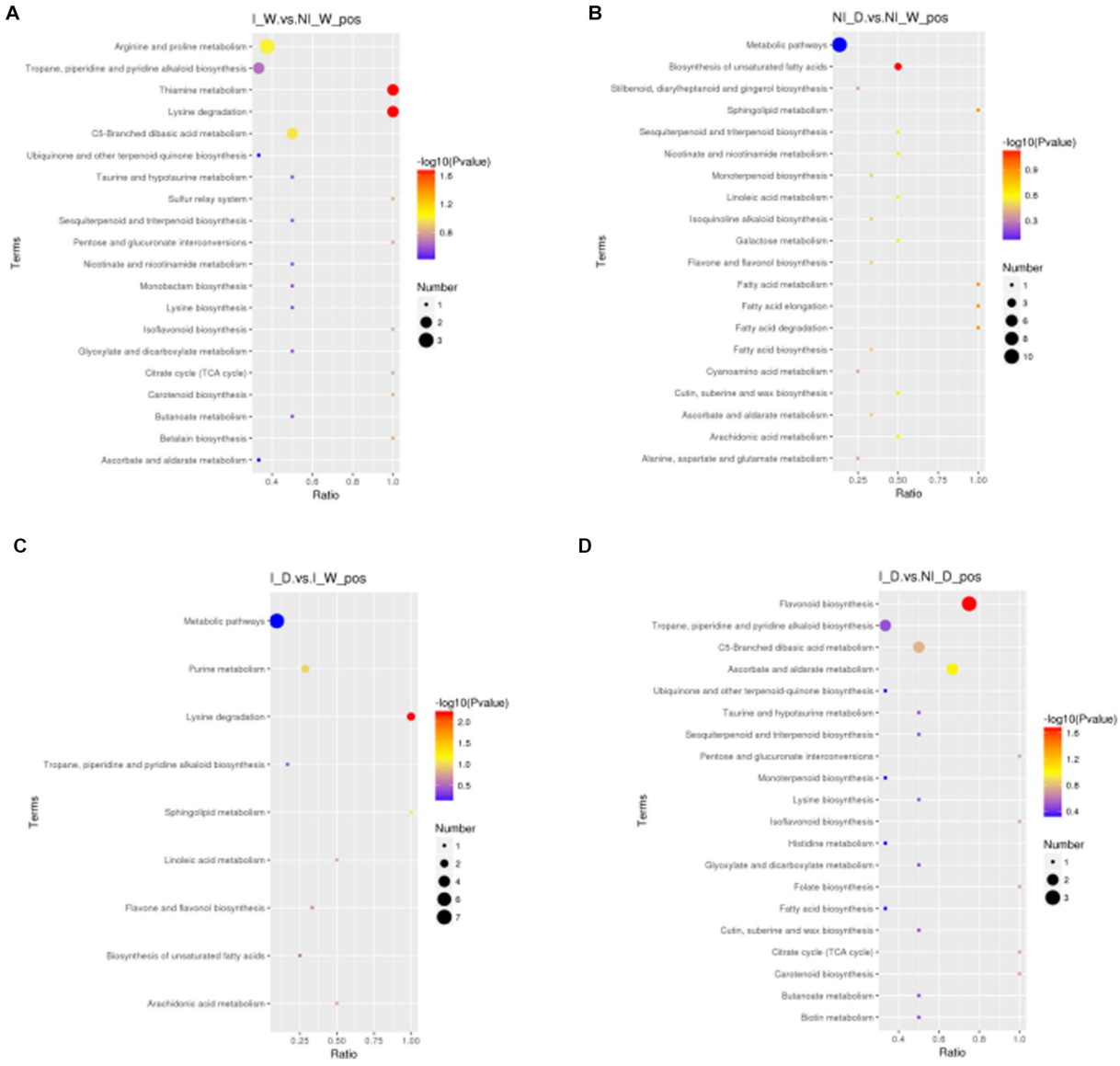

FIGURE 3
Metabolites enriched in KEGG pathways under positive ionization mode (top 20 pathways). In the small figures, horizontal axis represented the ratio of number of differential metabolites to the total numbers of metabolites identified in a pathway. The greater the ratio was, the higher the differential metabolites enriched in the pathway. The color of a circle represented value of *p* in geometric test. The size of a circle represented the number of differential metabolites in the corresponding pathway. **(A)** I_W vs. NI_W; **(B)** NI_D vs. NI_W; **(C)** I_D vs. I_W; **(D)** I_D vs. NI_D.I_W: inoculated seedlings under well-watered condition; NI_W: non-inoculated seedlings under well-watered condition; I_D: inoculated seedlings under drought stress; NI_D: non-inoculated seedlings under drought stress.

negative ionization mode, the two pathways, namely, porphyrin and chlorophyll metabolism and tyrosine metabolism, were the most enriched (Supplementary Figure S3A and the file "I_W.vs.NI_W_neg_kegg_enrichment" in Supplementary Table S6). In porphyrin and chlorophyll metabolism, pheophorbide A and L-threonine were enriched; in tyrosine metabolism, homovanillic acid and levodopa were enriched (the file "I_W.vs.NI_W_neg_kegg_enrichment" in Supplementary Table S6).

In the comparison of NI_D vs. NI_W, six pathways were the most enriched under positive ionization mode, i.e., biosynthesis of unsaturated fatty acids, fatty acid elongation, fatty acid degradation, sphingolipid metabolism, fatty acid metabolism, and galactose metabolism. In these pathways, arachidonic acid, palmitic acid, 4-D-hydroxysphinganine, and raffinose were enriched (Figure 3B and the file "NI_D.vs.NI_W_pos_kegg_enrichmen" in Supplementary Table S6). In the comparison, under negative ionization mode, pyruvate metabolism was the most enriched (Supplementary Figure S3B and the file "NI_D.vs.NI_W_neg_kegg_enrichmen" in Supplementary Table S6). In the pathway, fumaric acid was enriched (the file "NI_D.vs.NI_W_neg_kegg_enrichmen" in Supplementary Table S6).

In the comparison of I_D vs. I_W, lysine degradation, sphingolipid metabolism, and purine metabolism were the most enriched pathways under positive ionization mode, and some differential metabolites, i.e., pipecolic acid, N6,N6,N6-trimethyl-L-lysine, 4-D-hydroxysphinganine, uric acid, and hypoxanthine, were enriched (Figure 3C and the file "I_D.

vs.I_W_pos_kegg_enrichment" in Supplementary Table S6). In the comparison, under negative ionization mode, the three pathways, i.e., fructose and mannose metabolism, D-arginine and D-ornithine metabolism, and amino sugar and nucleotide sugar metabolism, were the most enriched (Supplementary Figure S3C and the file "I_D.vs.I_W_neg_kegg_enrichment" in Supplementary Table S6). In the three pathways, α-D-mannose 1-phosphate and L-ornithine were enriched (the file "I_D.vs.I_W_neg_kegg_enrichment" in Supplementary Table S6).

In the comparison of I_D vs. NI_D, the three pathways, i.e., flavonoid biosynthesis, ascorbate and aldarate metabolism, and C5-branched dibasic acid metabolism, were the most enriched under positive ionization mode (Figure 3D and the file "I_D.vs.NI_D_pos_kegg_enrichment" in Supplementary Table S6). In the three pathways, some differential metabolites were enriched, such as hesperetin, myricetin, taxifolin, alpha-ketoglutaric acid, vitamin C, and *trans*-aconitic acid (the file "I_D.vs.NI_D_pos_kegg_enrichment" in Supplementary Table S6). In the comparison, under negative ionization mode, the four pathways, i.e., thiamine metabolism, oxidative phosphorylation, phenylalanine, tyrosine, and tryptophan biosynthesis, and C5-branched dibasic acid metabolism, were the most enriched (Supplementary Figure S3D and the file "I_D.vs.NI_D_neg_kegg_enrichment" in Supplementary Table S6). Nicotinamide adenine dinucleotide, 5-dehydroquinic acid, and itaconic acid were enriched in these pathways under negative ionization mode (the file "I_D.vs.NI_D_neg_kegg_enrichment" in Supplementary Table S6).

3.3 Effects of *Serendipita indica* colonization on untargeted proteome

3.3.1 Analysis on differential proteins

After function annotation of proteins and quantitative analysis (shown in Supplementary material 3, including Supplementary Tables S7, S8), differential proteins were analyzed. Statistic results of differential protein analysis showed that 32 and 14 differential proteins with FC > 2.0 were up- and downregulated, respectively, in the comparison of I_W vs. NI_W; 16 and 19 proteins were up- and downregulated, respectively, in the comparison of NI_D vs. NI_W; 13 and 21 proteins were up- and downregulated, respectively, in the comparison of I_D vs. I_W; 14 and 7 proteins were up- and downregulated, respectively, in the comparison of I_D vs. NI_D (Table 1; Supplementary Table S9).

Volcano plots showed changes in FCs of differential proteins under different comparisons (Figure 4), suggesting that some proteins were greatly affected by the four different treatments. Some proteins were greatly upregulated in the comparison of I_W vs. NI_W. For example, six proteins, i.e., A0A385JF21, H9VK00, H9V5W8, Q06IN7, K7NJV0, and H9WJS5, only occurred in the needles of I_W seedlings, and FCs of other three proteins (H9VRU0, A0A3G6JFD6, and Q84KL6) were more than 3.0 (the file "I_W.vs.NI_W.diff_prot" in Supplementary Table S10). At the same time, some proteins were greatly downregulated, such as R4L654, H9XAU6, H9W9Y6, H9X0G1, and H9WTG5 (the file "I_W.vs.NI_W.diff_prot" in Supplementary Table S10).

In the comparison of NI_D vs. NI_W, five proteins, i.e., H9V821, A0A385JF21, H9V5W8, K7NJV0, and H9WW19, only occurred in the needles of NI_D seedlings, and FCs of H9VCA2 and O22430 were more than 3.0 (the file "NI_D.vs.NI_W.diff_prot" in Supplementary Table S10). At the same time, some proteins, such as H9WTS5, H9X1G6, H9XAC0, R4L654, H9VRX6, H9W9Y6, H9VZM7, and H9WTG5, were greatly downregulated (the file "NI_D.vs.NI_W.diff_prot" in Supplementary Table S10).

In the comparison of I_D vs. I_W, five proteins, i.e., H9V821, A0A3G6JA21, K7NMB8, H9WSD7, and H9WKX6, only occurred in the needles of I_D seedlings, and FCs of H9VNE7, Q41096, H9X0G1, and O22430 were more than 3.0 (the file "I_D.vs.I_W.diff_prot" in Supplementary Table S10). At the same time, some proteins were greatly downregulated, such as H9VNX9, H9WAU3, A0A023SGT4, H9VRU0, and H9X861 (the file "I_D.vs.I_W.diff_prot" in Supplementary Table S10).

In the comparison of I_D vs. NI_D, two proteins, i.e., H9X056 and H9VDW5, only occurred in the needles of I_D seedlings, and FCs of H9VNE7, A0A385JF23, and H9W5R1 were more than 11.0, 5.0, and 3.0, respectively (the file "I_D.vs.NI_D.diff_prot" in Supplementary Table S10). At the same time, some proteins were greatly downregulated, such as H9WD94, H9WLL7, H9X861, and H9VCA2 (the file "I_D.vs.NI_D.diff_prot" in Supplementary Table S10).

3.3.2 Analysis on enriched differential proteins

GO enrichment analysis showed that different treatments greatly affected enrichment of differential proteins in different GO terms (Figure 5). In the comparison of I_W vs. NI_W, the most enriched GO term was "metabolic process" in the section of "Biological process." In this GO term, 36 proteins were significantly regulated, with 28 and 8

TABLE 1 Statistic results of differential proteins.

Compared Samples	Num. of total quant.	Regulated type	FC > 1.2	FC > 1.3	FC > 1.5	FC > 2.0
I_W vs. NI_W	704	Upregulated	149	103	62	32
		Downregulated	66	53	35	14
NI_D vs. NI_W	701	Upregulated	64	51	32	16
		Downregulated	128	98	59	19
I_D vs. I_W	702	Upregulated	50	40	28	13
		Downregulated	114	87	48	21
I_D vs. NI_D	700	Upregulated	102	75	47	14
		Downregulated	24	17	13	7

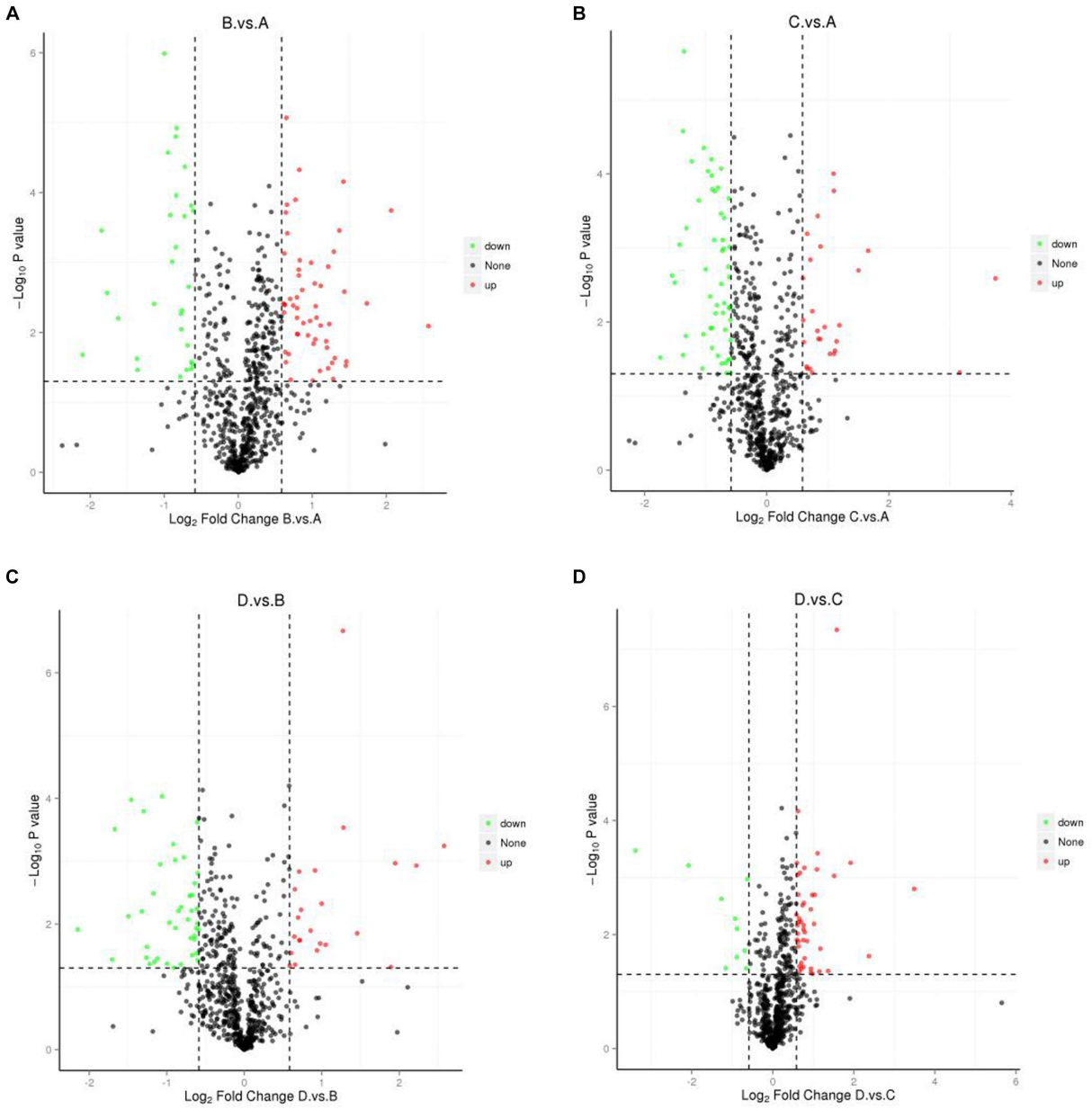

FIGURE 4
Volcano plots showing differential proteins. **(A)** I_W vs. NI_W; **(B)** NI_D vs. NI_W; **(C)** I_D vs. I_W; **(D)** I_D vs. NI_D. I_W: inoculated seedlings under well-watered condition; NI_W: non-inoculated seedlings under well-watered condition; I_D: inoculated seedlings under drought stress; NI_D: non-inoculated seedlings under drought stress.

proteins up- and downregulated, respectively (Figure 5A, the file "I_W.vs.NI_W.GO_Enrich.updown" in Supplementary Table S11). In the section of "Molecular Function," the GO term "structural constituent of ribosome" was the most enriched (Figure 5A). In the GO term, 12 and 3 proteins (including R4LC26, R4L654, and H9X6V5) were up- and downregulated, respectively (the file "I_W.vs.NI_W.GO_Enrich.updown" in Supplementary Table S11).

In the other three comparisons, the numbers of enriched GO terms were small (Figures 5B–D). In the comparison of I_D vs. NI_D, the most enriched GO term was "response to stress" (Figure 5D). In the GO term, 9 and 1 proteins were up- and downregulated (Figure 5D, the file "I_D.vs.NI_D.GO_Enrich.updown" in Supplementary Table S11). In the GO term "response to water," the two proteins (i.e., A0A2D1UKD2 and A0A023W8I6) were upregulated (Figure 5D, the file "I_D.vs.NI_D.GO_Enrich.updown" in Supplementary Table S11). Barplots of downregulated GO terms are shown in Supplementary Figure S4.

KEGG enrichment analysis is shown in Figure 6, and the top 20 enriched pathways were exhibited. In the comparison of I_W vs. NI_W, the most enriched pathways were monoterpenoid biosynthesis and biosynthesis of unsaturated fatty acids (Figure 6A). In the first pathway, the protein H9XB69 was enriched; in the second pathway, the two proteins, namely, H9W5R1 and H9V8G2, were enriched (the file "I_W.vs.NI_W.KEGG_Enrich" in Supplementary Table S12).

10.3389/fmicb.2024.1294833

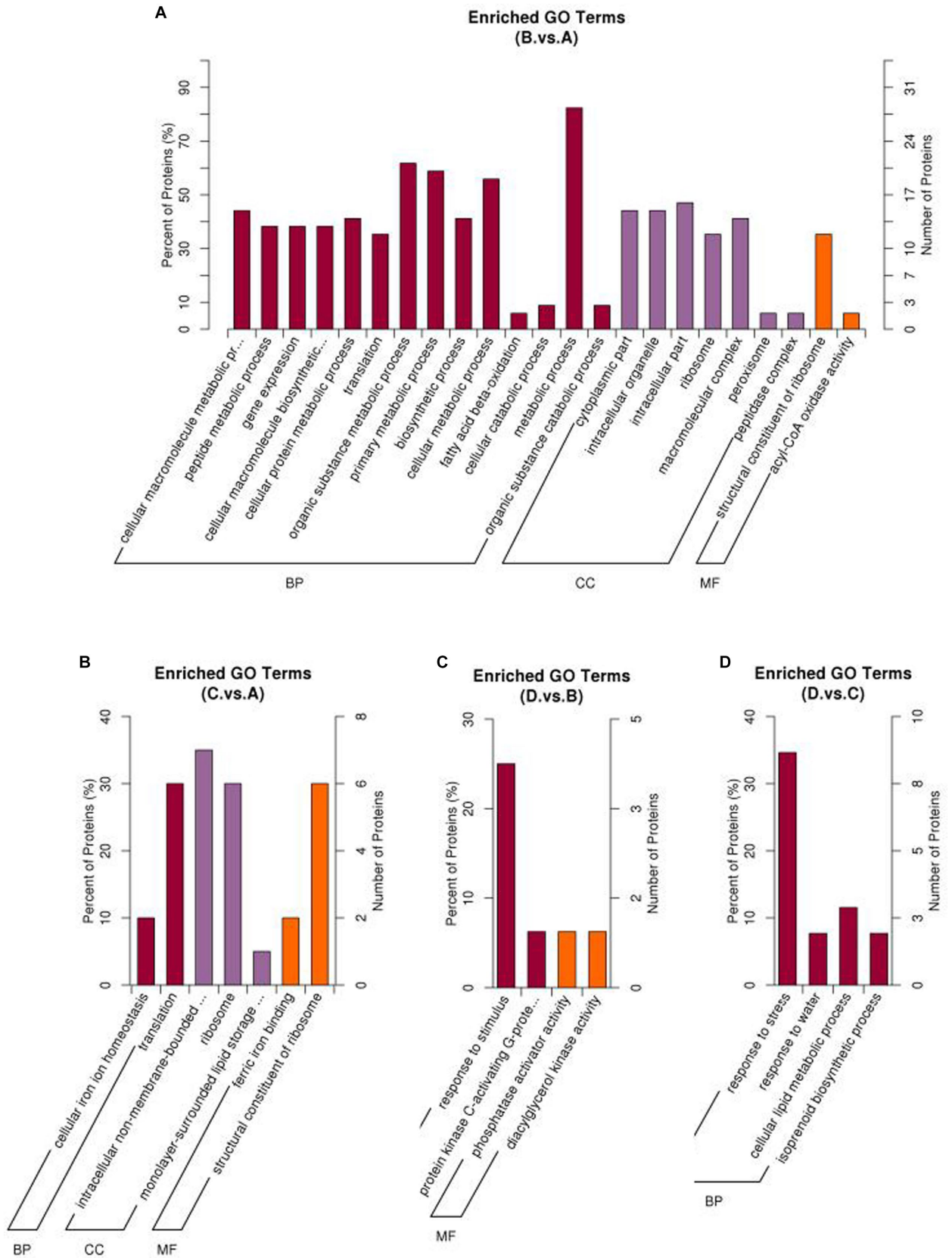

FIGURE 5
Percentage of upregulated proteins in different enriched GO terms under different comparisons. **(A)** I_W vs. NI_W; **(B)** NI_D vs. NI_W; **(C)** I_D vs. I_W; **(D)** I_D vs. NI_D. I_W: inoculated seedlings under well-watered condition; NI_W: non-inoculated seedlings under well-watered condition; I_D: inoculated seedlings under drought stress; NI_D: non-inoculated seedlings under drought stress.

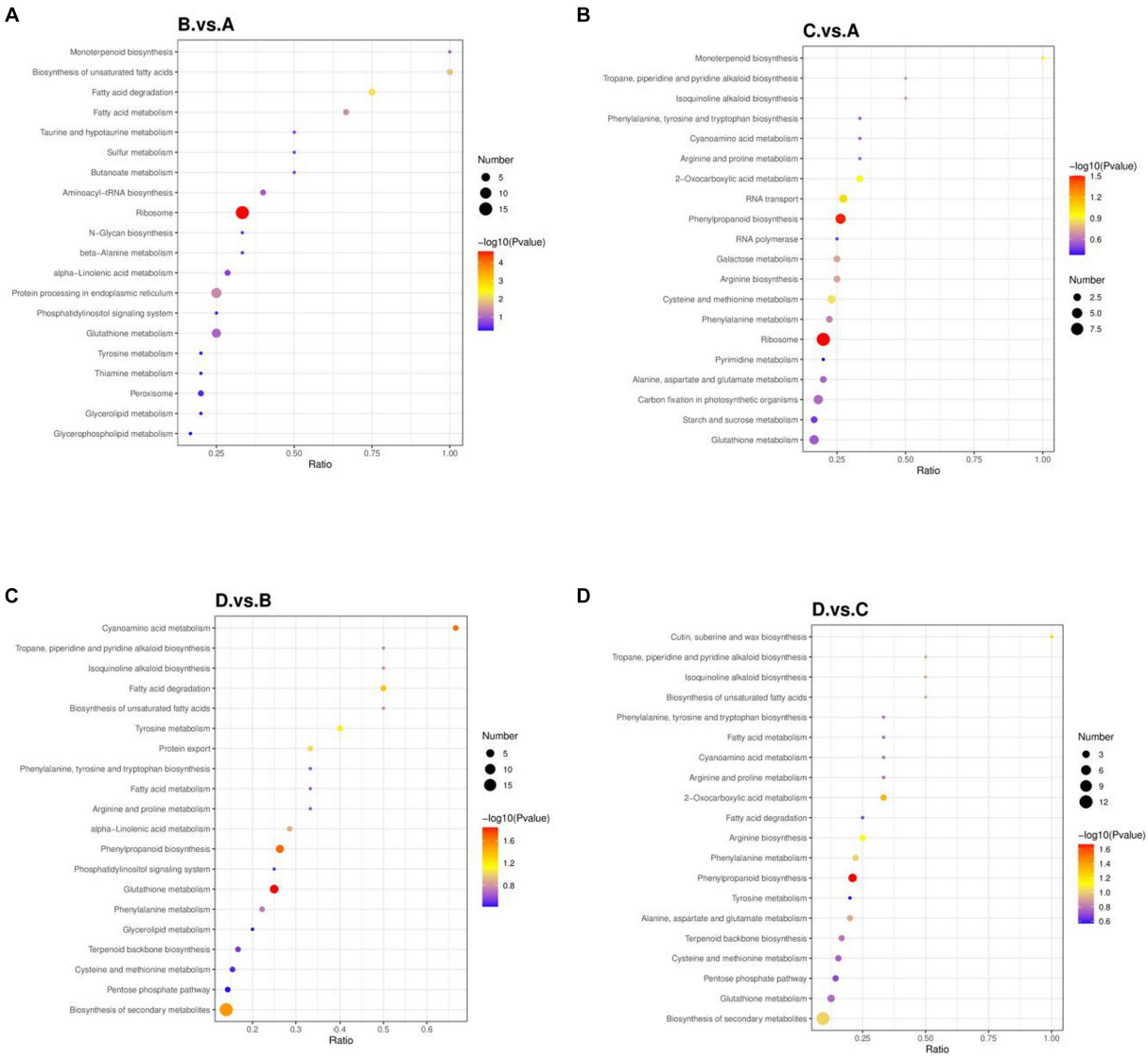

FIGURE 6
Bubble charts of KEGG pathways. **(A)** I_W vs. NI_W; **(B)** NI_D vs. NI_W; **(C)** I_D vs. I_W; **(D)** I_D vs. NI_D. In a bubble charts, *x* axis stands for the ratio of the number of differential proteins in a pathway to the total number of identified proteins in the pathway. The higher the ratio is, the higher the enriched differential proteins. The color of a round spot stands for value of *p* in the hypergeometric test. The color changes from blue to red. The smaller value of *p* is, the more reliable the hypergeometric test is, and the more significant the hypergeometric test is. The size of a round spot stands for the number of differential proteins in a pathway. The bigger the size of a round spot is, the more the number of differential proteins in a pathway is. I_W: inoculated seedlings under well-watered condition; NI_W: non-inoculated seedlings under well-watered condition; I_D: inoculated seedlings under drought stress; NI_D: non-inoculated seedlings under drought stress.

In addition, ribosome pathway contained the greatest number of differential proteins, and the next were protein processing in endoplasmic reticulum and glutathione metabolism (Figure 6A). In the comparison of NI_D vs. NI_W, the most enriched pathways were isoquinoline alkaloid biosynthesis and tropane, piperidine, and pyridine alkaloid biosynthesis, and the protein H9X056 was involved in both of the two pathways (Figure 6B, the file "NI_D.vs.NI_W.KEGG_Enrich" in Supplementary Table S12). In the comparison of I_D vs. I_W, cyanoamino acid metabolism was the most enriched pathway (Figure 6C). In this pathway, two proteins, namely, H9XB10 and H9W1J3, were identified (the file "I_D vs. I_W.KEGG_Enrich" in Supplementary Table S12). In addition, biosynthesis of secondary metabolites contained the greatest number of identified differential proteins, and the next were phenylpropanoid biosynthesis and glutathione metabolism (Figure 6C). In the comparison of I_D vs. NI_D, the most enriched pathway was cutin, suberine, and wax biosynthesis (Figure 6D). In this pathway, the protein H9WHC3 was identified (the file "I_D.vs.NI_D.KEGG_Enrich" in Supplementary Table S12). Biosynthesis of secondary metabolites contained the greatest number of identified differential proteins, and the next was phenylpropanoid biosynthesis (Figure 6D).

In aspect of structural domain enrichment, the four different treatments also affected the expression of differential proteins with different structural domains (Figure 7). In the comparison

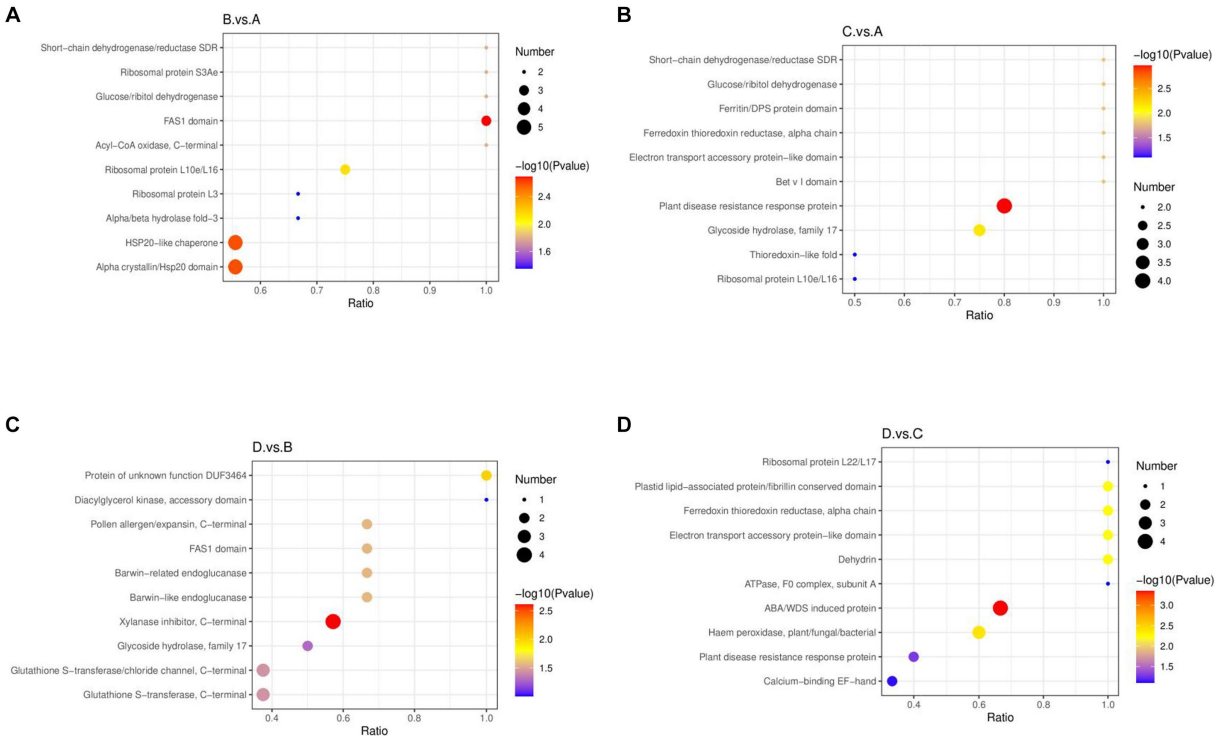

FIGURE 7
Bubble diagrams of enriched structural domains of differential proteins. **(A)** I_W vs. NI_W; **(B)** NI_D vs. NI_W; **(C)** I_D vs. I_W; **(D)** I_D vs. NI_D. In a bubble diagram, *x* axis stands for the ratio of the numbers of differential proteins with the responsive structural domain to the number of total number of identified proteins with the structural domain. The higher the ratio is, the more the number of differential proteins with the structural domain is. The color of a round spot stands for value of *p* in the hypergeometric test. The color changes from blue to red. The smaller value of *p* is, the more reliable the hypergeometric test is, and the more significant the hypergeometric test is. The size of a round spot stands for the number of proteins with the responsive structural domain. The bigger the size of a round spot is, the more the number of differential proteins with the structural domain is. I_W: inoculated seedlings under well-watered condition; NI_W: non-inoculated seedlings under well-watered condition; I_D: inoculated seedlings under drought stress; NI_D: non-inoculated seedlings under drought stress.

of I_W vs. NI_W, the proteins with the structural domains (short-chain dehydrogenase/reductase SDR, ribosomal protein S3Ae, glucose/ribitol dehydrogenase, FAS1 domain, and acyl-CoA oxidase) were enriched, and the two structural domains, such as HSP20-like chaperone and alpha crystallin/Hsp20 domain, contained the greatest numbers of identified differential proteins (Figure 7A, the file "I_W.vs.NI_W.IPR_Enrich.merge" in Supplementary Table S13). In the comparison of NI_D vs. NI_W, the proteins with these structural domains (short-chain dehydrogenase/reductase SDR, glucose/ribitol dehydrogenase, ferritin/DPS protein domain, ferredoxin thioredoxin reductase electron transport accessory protein-like domain, and bet v I domain) were enriched (Figure 7B), and the structural domain "plant disease resistance response protein" contained the greatest number of identified differential proteins (the file "NI_D.vs.NI_W.IPR_Enrich.merge" in Supplementary Table S13). In the comparison of I_D vs. I_W, the proteins with the two structural domains (protein of unknown function DUF3464 and diacylglycerol kinase, accessory domain) were enriched (Figure 7C). The structural domains, xylanase inhibitor (C-terminal), glutathione S-transferase/chloride channel (C-terminal), and glutathione S-transferase (C-terminal) contained more identified differential proteins (Figure 7C, the file "I_D.vs.I_W.IPR_Enrich.merge" in Supplementary Table S13). In the comparison of I_D vs. NI_D, the proteins with the structural domains, i.e., ribosomal protein L22/L17, plastid lipid-associated protein/fibrillin conserved domain, ferredoxin thioredoxin reductase (alpha chain), electron transport accessory protein-like domain, dehydrin, and ATPase (F0 complex, subunit A), were enriched (Figure 7D). In addition, the structural domain "ABA/WDS-induced protein" contained the greatest number of proteins (Q41087, Q41095, Q41096, and A0A023W8D4) (Figure 7D, the file "I_D.vs.NI_D.IPR_Enrich.merge" in Supplementary Table S13).

The analysis on subcellular localization showed that differential proteins mainly distributed in cytoplasm (31.71%), chloroplasts (17.07%), and nuclei (12.20%), in the comparison of I_W vs. NI_W, together occupying more 60% of the total number (Figure 8A). In chloroplasts, H9X1G6 and H9VZM7 are SHSP domain-containing proteins; in cytoplasm, most differential proteins were uncharacterized; and in nuclei, H9V4J8 and H9VFX4 are also SHSP domain-containing proteins (the file "I_W.vs.NI_W.Subcellular_diff" in Supplementary Table S14). In the comparison of NI_D vs. NI_W, most differential proteins also mainly distributed cytoplasm (22.22%), chloroplasts (22.22%), and nuclei (11.11%) (Figure 8B). In chloroplasts, H9VCA2 and H9VCA1 are two FeThred_A domain-containing proteins, and H9X1G6 and H9VZM7 are two SHSP domain-containing proteins; in cytoplasm, H9WKD5 and

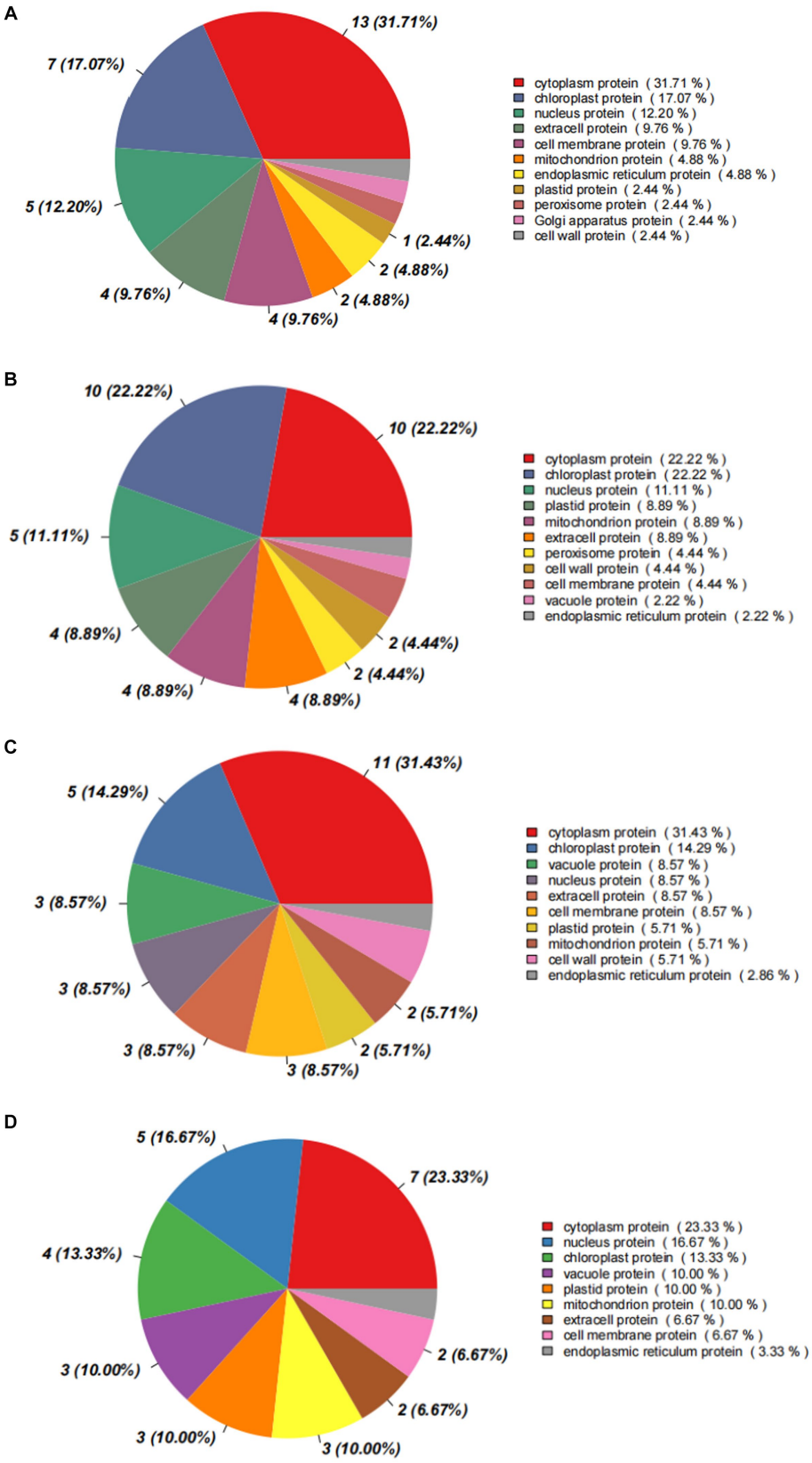

FIGURE 8
Statistic diagrams of subcellular localization of differential proteins. **(A)** I_W vs. NI_W; **(B)** NI_D vs. NI_W; **(C)** I_D vs. I_W; **(D)** I_D vs. NI_D. I_W: inoculated seedlings under well-watered condition; NI_W: non-inoculated seedlings under well-watered condition; I_D: inoculated seedlings under drought stress; NI_D: non-inoculated seedlings under drought stress.

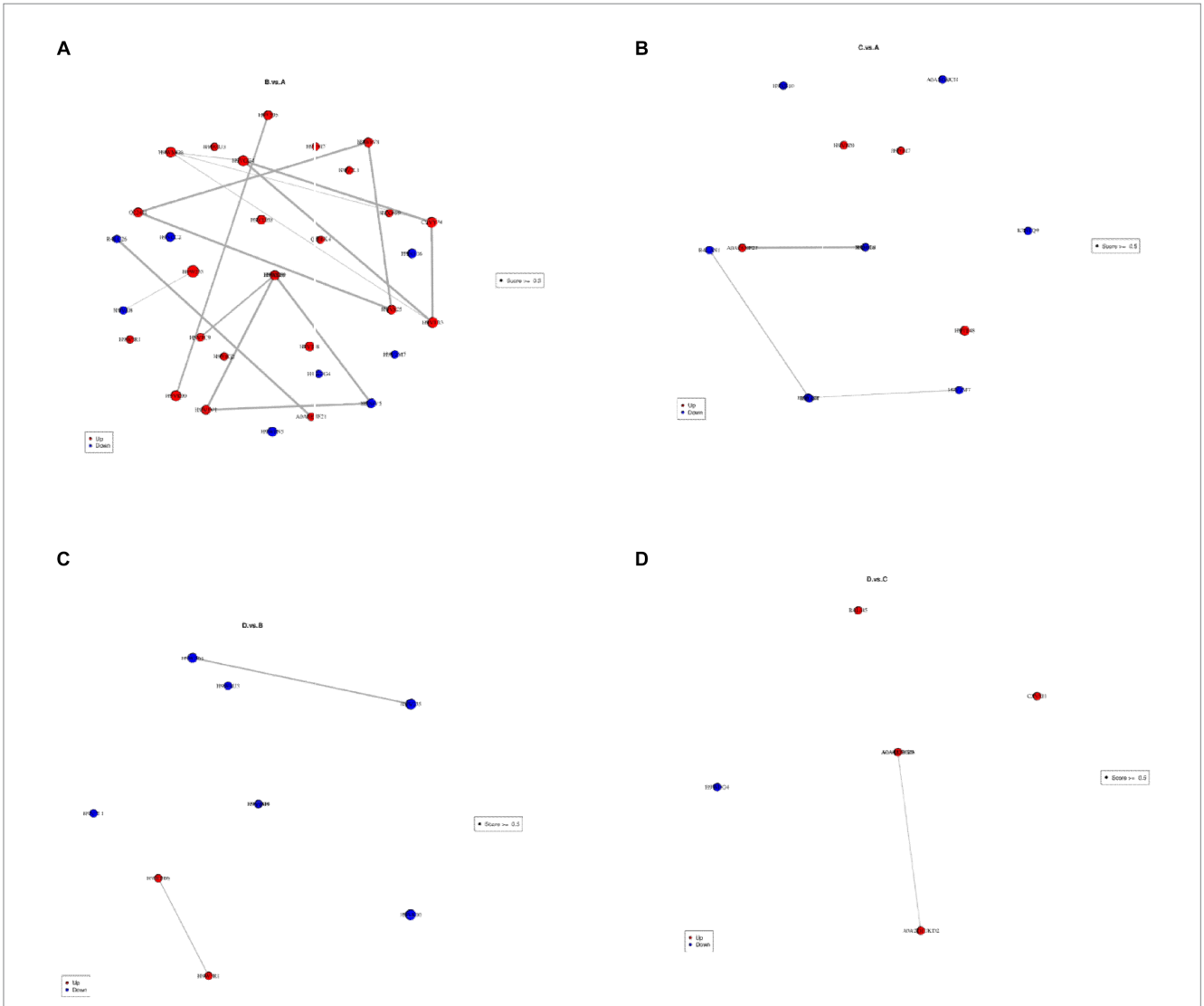

FIGURE 9
Analysis on interactions between differential proteins. In each diagram, each spot stands for a differential protein labeled with its name. **(A)**: I_W vs. NI_W; **(B)**: NI_D vs. NI_W; **(C)**: I_D vs. I_W; **(D)**: I_D vs. NI_D. I_W: inoculated seedlings under well-watered condition; NI_W: non-inoculated seedlings under well-watered condition; I_D: inoculated seedlings under drought stress; NI_D: non-inoculated seedlings under drought stress.

H9WFS7 are two Bet_v_1 domain-containing proteins; in nuclei, two proteins, namely, Q41095 and Q41096, are water deficit-inducible, encoded by the genes *lp3-3* and *lp3-2*, respectively (the file "NI_D.vs.NI_W.Subcellular_diff" in Supplementary Table S14). In the comparison of I_D vs. I_W, differential proteins mainly distributed in cytoplasm (31.43%), chloroplasts (4.29%), and vacuoles (8.57%) (Figure 8C). Some new proteins occurred in cytoplasm, chloroplasts, and vacuoles, such as H9W1G7 (SHSP domain-containing protein) in cytoplasm, A5HIY3 (thaumatin-like protein) in vacuoles, Q84KL6 (alpha-pine synthase) in chloroplasts, and O24314 and Q41096 (water deficit-inducible protein) in nuclei (the file "I_D.vs.I_W.Subcellular_diff" in Supplementary Table S14). In the comparison of I_D vs. NI_D, differential proteins also distributed in cytoplasm (23.33%), nuclei (16.67%), and chloroplasts (13.33%) (Figure 8D). More notably, four water deficit-inducible proteins, i.e., Q41087, Q41095, Q41096, and A0A023W8D4, occurred in nuclei (the file "I_D.vs.NI_D.Subcellular_diff" in Supplementary Table S14).

3.3.3 Interactions between differential proteins

To investigate the interactions between differential proteins, StringDB data bank[2] was used to analyze the interactions (Figure 9; Supplementary Table S15). Under the comparison of I_W vs. NI_W, strong interactions occurred between significantly upregulated proteins, such as the protein O22431 and the two proteins H9VX25 and H9W8V8, H9V595 and H9VK00, H9VGG4 and C3VYP4, H9VLB3 and C3VYP4, H9VX25 and H9W8V8, and H9WJV1 and H9WG89 (Figure 9A; Supplementary Table S15). In the comparison of NI_D vs. NI_W, weak interactions occurred between significantly downregulated proteins, such as H9W129 and H9VZM7, and R4LAN1 and R4L654 (Figure 9B; Supplementary Table S15). In the comparison of I_D vs. I_W, strong interactions occurred between

2 http://string-db.org/

significantly downregulated proteins, such as H9V4M9 and H9VGG4, and H9WN61 and H9W235; strong interaction occurred between significantly upregulated proteins, i.e., H9W5R1 and H9WBB6 (Figure 9C; Supplementary Table S15). In the comparison of I_D vs. NI_D, strong interaction only occurred between the significantly upregulated proteins, i.e., A0A023W8I6 and A0A2D1UKD2 (Figure 9D; Supplementary Table S15).

3.4 Correlations between differential metabolites and proteins

Correlations between differential metabolites and proteins were analyzed (Figure 10). In the comparison of I_W vs. NI_W, under positive ionization mode, the protein H9V5W8 was in significantly positive correlations to few metabolites, including targinine, LPE 18:2, 2,4-dihydroxyheptadec-16-3n-1-yl acetate, sedanolide, and N3,N4-dimethyl-L-arginine; the protein K7NMB8 was in significantly positive correlation to few metabolites, such as beta-caryophyllene, sclareolide, N-(9-oxodecyl)acetamide, sophoridine, and triacetonamine (Figure 10A and the file "I_W.vs.NI_W_pos_I_W.vs.NI_W_corr" in Supplementary Table S16). In addition, proline biosynthesis was in significantly positive correlations to some proteins, such as the three proteins, namely, A0A023SGT4, A0A385JF21, and A0A3G6JDK7, but in significantly negative correlations to some proteins, such as the four proteins H9V143, H9V4J8, H9V5X1, and H9VCC2 (the file "I_W.vs.NI_W_pos_I_W.vs.NI_W_corr" in Supplementary Table S16). Under negative ionization mode,

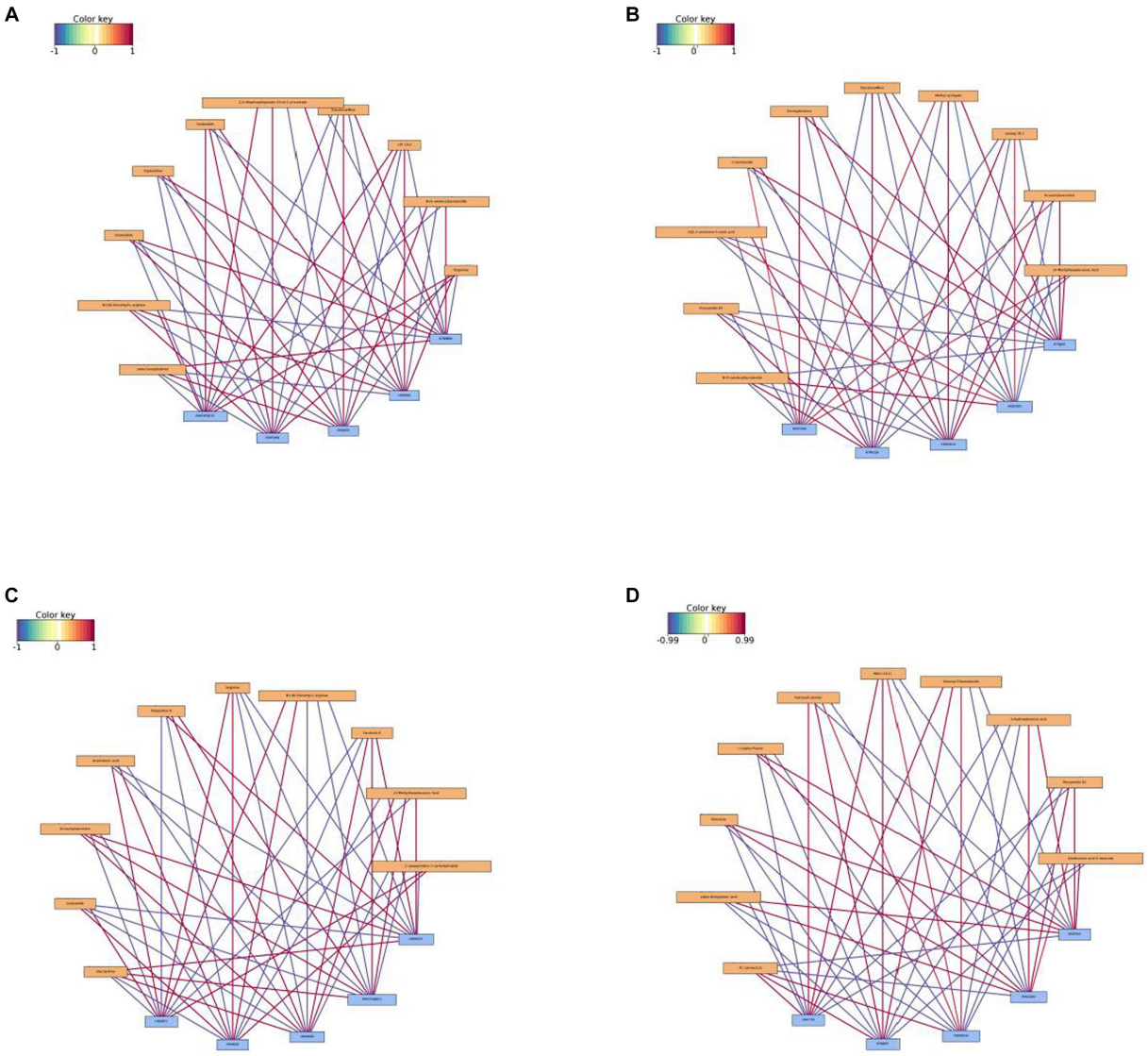

FIGURE 10
Network diagrams of correlation analysis under positive ionization mode. **(A)** I_W vs. NI_W; **(B)** NI_D vs. NI_W; **(C)** I_D vs. I_W; **(D)** I_D vs. NI_D. The top 10 differential proteins and the top 5 differential metabolites were used in correlation analysis. In a network diagram, yellow stands for a differential metabolite, and blue stands for a differential protein. Red line stands for positive correlation, and blue line stands for negative correlation. The deeper the color is, the bigger the correlation coefficient is. I_W: inoculated seedlings under well-watered condition; NI_W: non-inoculated seedlings under well-watered condition; I_D: inoculated seedlings under drought stress; NI_D: non-inoculated seedlings under drought stress.

gibberellic acid was in significantly positive correlations to the three proteins, i.e., A0A385JF21, H9V5W8, and H9VK00, but in significantly negative correlations to the two proteins, i.e., K7NMB8 and H9XBF0 (Supplementary Figure S5A and the file "I_W.vs.NI_W_neg_I_W.vs.NI_W_corr" in Supplementary Table S16). Salicylic acid *O*-glucoside was in significantly positive correlations to the four proteins, A0A385JF21, H9V5W8, H9VBI7, and H9VK00, but in significantly negative correlations to the three proteins, K7NMB8, H9V4J8, and H9XBF0 (Supplementary Figure S5A and the file "I_W.vs.NI_W_neg_I_W.vs.NI_W_corr" in Supplementary Table S16).

In the comparison of NI_D vs. NI_W under positive ionization mode, the metabolite methyl syringate was in significantly positive correlations to the three proteins, K7NJV0, H9WW19, and H9V5WB, but in significantly negative correlations to the two proteins, H9VDW5 and K7NLQ9; the metabolite N-lauroylsarcosine was in significantly positive correlations to the two proteins, K7NJV0 and H9WW19, but in significantly negative correlations to the two proteins, H9VDW5 and K7NLQ9 (Figure 10B and the file "NI_D.vs.NI_W_pos_NI_D.vs.NI_W_c" in Supplementary Table S16). In addition, vitamin C biosynthesis was in significantly positive correlations to the three proteins, A0A3G6J9T6, A0A3G6JA21, and A0A3G6JAC7, but in significantly negative correlations to the three proteins, A0A385JF21, B2CBS5, and H9V821 (the file "NI_D.vs.NI_W_pos_NI_D.vs.NI_W_c" in Supplementary Table S16). Under negative ionization mode, 4-coumaric acid was in significantly positive correlations to the three proteins, K7NJV0, H9WW19, and H9V5W8, but in significantly negative correlations to the two proteins, H9VDW5 and K7NLQ9 (Supplementary Figure S5B and the file "NI_D.vs.NI_W_neg_NI_D.vs.NI_W_c" in Supplementary Table S16). In addition, methyl jasmonate was in significantly positive correlations to the three proteins, A0A2D1UKD2, A0A385JEN6, and A0A3G6JA21, but in significantly negative correlations to the three proteins, A0A385JF21, H9V5W8, and H9V821 (the file "NI_D.vs.NI_W_neg_NI_D.vs.NI_W_c" in Supplementary Table S16).

In the comparison of I_D vs. I_W under positive ionization mode, both of stachydrine and N-lauroylsarcosine were in significantly positive correlations to the three proteins, H9WSD7, A0A3G6JA21, and H9WKX6, but in significantly negative correlations to the two proteins, H9VK00 and H9VRP1 (Figure 10C and the file "I_D.vs.I_W_pos_I_D.vs.I_W_corr" in Supplementary Table S16). The metabolite arachidonic acid just showed contrary correlations to these proteins (Figure 10C). Under negative ionization mode, L-ornithine was in significantly positive correlations to the two proteins, H9VRP1 and H9VK00, but in significantly negative correlations to the three proteins, H9WKX6, A0A3G6JA21, and H9WSD7; trifolirhizin was in significantly positive correlations to the three proteins, H9WSD7, A0A3G6JA21, and H9WKX6, but in significantly negative correlations to the two proteins, H9VRP1 and H9VK00 (Supplementary Figure S5C and the file "I_D.vs.I_W_neg_I_D.vs.I_W_corr" in Supplementary Table S16). In addition, methyl jasmonate was in significantly positive correlations to the three proteins, A0A023SGT4, A0A3G6JAC7, and A0A3G6JDJ9, but in significantly negative correlations to the three proteins, A0A023W8I6, A0A3G6JA21, and C3VXI1 (the file "I_D.vs.I_W_neg_I_D.vs.I_W_corr" in Supplementary Table S16).

In the comparison of I_D vs. NI_D under positive ionization mode, fatty acids PC (16:0e/2:0) and MAG (18:1) were in significantly positive correlations to the three proteins, H9V739, K7NJV0, and H9WDG4, but in significantly negative correlations to the two proteins, H9X056 and H9VDW5 (Figure 10D and the file "I_D.vs.NI_D_pos_I_D.vs.NI_D_cor" in Supplementary Table S16). The metabolite rotenone just showed the contrary correlations to these proteins (Figure 10D). In addition, vitamin C was in significantly positive correlations to the four proteins, A0A023W8D4, H9V6D7, A0A2D1UL07, and H9V5W8, but in significantly negative correlations to the three proteins, H9V739, H9VCA2, and H9VVX5 (the file "I_D.vs.NI_D_pos_I_D.vs.NI_D_cor" in Supplementary Table S16). Under negative ionization mode, the metabolites 4-coumaric acid and LPC18:0 were in significantly positive correlations to the three proteins, H9V739, K7NJV0, and H9WDG4, but in significantly negative correlations to the two proteins, H9X056 and H9VDW5 (Supplementary Figure S5B and the file "I_D.vs.NI_D_neg_I_D.vs.NI_D_cor" in Supplementary Table S16). The metabolite trifolirhizin just showed the contrary correlations to these proteins (Supplementary Figure S5D). In addition, the metabolite itaconic acid was in significantly positive correlations to the four proteins, A0A023W8I6, A0A023W8D4, C3VXI1, and C6ZG55, but in significantly negative correlations to the four proteins, H9V739, H9VCA2, H9VCR5, and H9WDG4 (the file "I_D.vs.NI_D_neg_I_D.vs.NI_D_cor" in Supplementary Table S16).

4 Discussion

As functions of symbiosis of mycorrhizal fungi (Chandrasekaran, 2022; Begum et al., 2023; Zou et al., 2023), plant growth-promoting rhizobacteria (PGPR) (Shankar and Prasad, 2023; Tanveer et al., 2023; Zhao et al., 2023), and dark septate endophytes (DSE) (Li et al., 2022; He C. et al., 2022; Liu et al., 2023) during drought stress, root endophytic fungi also play important roles in increasing tolerance to drought stress of their host plants (Azevedo et al., 2021; Manzur et al., 2022; Zuo et al., 2022). *S. indica* is also a root endophytic fungus, and it improves drought tolerance of their host plants, as described above. However, the related mechanisms are not clear. In this present study, combination of metabolomics and proteomics revealed the potential mechanisms.

4.1 *Serendipita indica*-induced drought tolerance by improving biosynthesis of flavonoids in *Pinus taeda*

Under drought stress, *S. indica* inoculation resulted in great changes in species and levels of flavonoids and their derivatives, such as taxifolin, hesperetin 5-*O*-glucode, puerarin, 5-demethylnobiletin, gardenin B, procyanidin B1, tectoridin, tricin, trifolirhizin, myricitrin, and eriocitrin (Supplementary Figures S1, S2; Supplementary Table S3). The metabolite eriocitrin (a dietary flavonoid) was the most enriched compound in the needles of I_D seedlings, increasing 4.86 times as that in the needles of NI_D seedlings, even more than the level of ascorbate (vitamin C, increasing 4.48 times as that in the needles of NI_D seedlings) (the file "I_D.vs.NI_D_pos_Diff_order" in Supplementary Table S3). Eriocitrin is an abundant flavonoid in lemons, which is known as a strong antioxidant agent (Kwon and Choi, 2020). Although it remain unclear about its functions in plants, especially under drought stress, the increased levels caused by *S. indica* inoculation with *P. taeda*

seedlings should be related to its strong ability to scavenge reactive oxygen species (ROS) as an antioxidant. Its accurate function should be focused on in plants under drought stress. *S. indica* inoculation increased the level of taxifolin under drought stress (Supplementary Figure S3A; Supplementary Table S3). Taxifolin, i.e., dihydroquercetin, is a unique bioactive flavonoid. However, it is not clear about its functions in plants, especially under drought stress. But at present, it was known well about functions of quercetin in plants (Singh et al., 2021). The metabolite facilitates several plant physiological processes, such as seed germination, pollen growth, antioxidant machinery, and photosynthesis, as well as induces proper plant growth and development. Quercetin level increased in leaves and flowers of St. John's wort (*Hypericum perforatum*) under drought stress (Gray et al., 2003). Since quercetin, a known flavonoid, acts as an antioxidant (Di Petrillo et al., 2022), it should be able to play an important role in scavenging ROS produced in plants under drought stress. More importantly, quercetin mediates ABA signaling (Singh et al., 2021); thus, the metabolite is involved in drought tolerance. Taxifolin is a derivative of quercetin; thus, its increased level caused by *S. indica* inoculation suggests that the metabolite might possess a more impalpable role in plants under drought stress, just like quercetin. In addition to taxifolin, the levels of two derivatives of quercetin increased in the needles of I_D seedlings, i.e., quercetin-3-O-beta-glucopyranosyl-6′-acetate ($C_{23}H_{22}O_{13}$, the file "I_D.vs.NI_D_neg_Diff_order" in Supplementary Table S3) and quercetin-3-ramnoside ($C_{21}H_{20}O_{11}$, the file "I_D.vs.NI_D_pos_Diff_order" in Supplementary Table S3), increasing 2.79 and 1.72 times, respectively. On the other hand, a report showed that the levels of some derivatives of quercetin reduced in the leaves of *Quercus pubescens* under drought stress, such as quercetin-3-O-glucose, quercetin pentose hexose, quercetin galloyl glucose, and quercetinhexose 1 (Saunier et al., 2022). Their levels reduced 36, 50, 45, and 33%, respectively. Altogether, the functions of quercetin derivatives are distinct from each other in plants under drought stress. Since the level of taxifolin increased in the needles of I_D seedlings, the increase should be useful for increased tolerance of *P. taeda* seedlings to drought stress.

S. indica inoculation also increased hesperetin level in the needles of *P. taeda* seedlings under drought stress (Supplementary Figure S3A), increasing 1.83 times, compared to its level in the needles of NI_D seedlings (the file "I_D.vs.NI_D_pos_Diff_order" in Supplementary Table S3). Hesperetin is a citrus flavonoid; however, no report showed its function in plants. Since it acts as an antioxidant in human cells (Famurewa et al., 2022), it is reasonable to speculate that it can scavenge free radicals in plants under drought stress or maybe it plays a specific role in plants under drought stress. Similarly, puerarin, an isoflavone, increased in the I_D seedlings (Supplementary Figure S3A), increasing 1.64 times as that in the needles of NI_D seedlings (the file "I_D.vs.NI_D_pos_Diff_order" in Supplementary Table S3). At present, it is not clear about its functions in plants under drought stress.

In the flavonoid biosynthesis pathway, the protein, H9WXL2, was enriched in the needles of I_D seedlings (the file "I_D.vs.NI_D.KEGG_Enrich" in Supplementary Table S12). H9WXL2 is NmrA domain-containing protein[3]. Those NmrA domain-containing proteins possess multiple functions in organisms. For example, in the soil-living protozoan, *Dictyostelium discoideum*, a protein with an NmrA-like domain, is required for cell differentiation and development (Núñez-Corcuera et al., 2008). In fungi, such proteins act as transcription repressors (Nichols et al., 2001; Zhao et al., 2010) and are involved in the post-translational modulation of the GATA-type transcription factor AreA, forming part of a system controlling nitrogen metabolite repression and stress resistance in various fungi (Stammers et al., 2001; Li et al., 2021). At present, it is not clear about the functions of NmrA domain-containing proteins in plants. Since *S. indica* inoculation improved H9WXL2 enrichment in needles of *P. taeda* seedlings under drought stress, the protein should possess its functions in *P. taeda* under drought stress. As mentioned above, the levels of many flavonoids increased in I_D seedlings, and H9WXL2 enrichment should be in positive correlation with these increased flavonoids.

4.2 *Serendipita indica*-induced drought tolerance by improving biosynthesis of organic acids in *Pinus taeda*

The levels of many organic acids increase in plants under drought stress and play important roles (Khosravi-Nejad et al., 2022; Ma et al., 2022; Wu et al., 2023). *S. indica* inoculation further increased biosynthesis of some organic acids in *P. taeda* seedlings under drought stress. In the needles of I_D seedlings, the levels of many organic acids are increased, compared to their levels in the needles of NI_D seedlings (the file "I_D.vs.NI_D_pos_Diff_order" in Supplementary Table S3). Out of them, *trans*-aconitic acid showed the highest increased level in I_D seedlings, 4.57 times as that of in NI_D seedlings (the file "I_D.vs.NI_D_pos_Diff_order" in Supplementary Table S3).

Trans-aconitic acid is a tricarboxylic acid and natural geometric isomer of *cis*-aconitic acid which is an intermediate in the citric acid cycle and with a well-defined role in energy metabolism. *Trans*-aconitic acid accumulated in surprisingly high concentrations in early-season forage grasses, such as *Hordeum leporinum* (3.5% of dry material), *Phalaris tuberosa* var. *stenoptera* (4.2% of dry material), and *Delphinium hesperium* (12.2% of dry leaves) (Burau and Stout, 1965). Burau and Stout (1965) speculated such high accumulation of *trans*-aconitic acid may be partially responsible for nutritional disorders, such as grass tetany (hypomagnesemia). As an allelochemical, *trans*-aconitic acid can reduce the germination and seed bank of weeds in the soil, and exogenous *trans*-aconitic acid applied in soil inhibits the growth and photosynthesis of *Glycine max* (Bortolo et al., 2018). It might be speculated that increased accumulation in the needles of I_D seedlings is related to inhibition of growth and photosynthesis. On the other hand, *trans*-aconitic acid acts as an inhibitor of glutamate decarboxylase (Endo and Kitahara, 1977), which catalyzes conversion of L-glutamate to aminobutanoate. This inhibition caused by the increased level of *trans*-aconitic acid might maintain well function of L-glutamate in I_D seedlings. *Trans*-aconitic acid is synthesized via potassium-dependent citrate dehydrase in maize (*Zea mays*), and its isozymes CD I and CD II are situated in mitochondria and cytosol, respectively (Brauer and Teel, 1982). It was reported that *trans*-aconitic biosynthesis by CD I is regulated

3 https://www.uniprot.org/uniprotkb/

by both citrate concentration and pH and that its biosynthesis by CD II is regulated by potassium (Brauer and Teel, 1982). Thus, the positive correlation between leaf potassium/citrate and *trans*-aconitic acid in maize was established. Therefore, increase in the level of *trans*-aconitic acid in the needles of I_D seedlings might suggest that high level of potassium ions/citrate occurred in these needles. Potassium ions possess strong physiological functions, especially under abiotic stress (Anil Kumar et al., 2022). The availability of potassium ions during drought stress increases the stomatal conductance with subsequent increase in water level (Oddo et al., 2020). Proline biosynthesis triggered by potassium ions has been found to be associated with osmotic adjustment and involved in scavenging ROS under drought stress (Jatav et al., 2012; Hasanuzzaman et al., 2018). Altogether, based the three aspects about *trans*-aconitic acid mentioned above, it is still difficult to explain the accurate function of *trans*-aconitic acid in inoculated *P. taeda* seedlings, and more experiments are necessary.

Next, to *trans*-aconitic acid, uric acid increased 4.22 times in the needles of I_D seedlings, compared to its level in NI_D seedlings (the file "I_D.vs.NI_D_pos_Diff_order" in Supplementary Table S3). Interestingly, uric acid deposits occurred in symbiotic marine algae when the marine algae symbiosed with *Aiptasia* sp. anemones (Clode et al., 2009), and uric acid deposits are likely to be associated with the nitrogen metabolism of the symbiosis. Exogenous application of uric acid enhanced the resistance of apple (*Malus×domestica* Borkh.) plants to salinity stress, and overexpression of MdNAT7 (nucleobase-ascorbate transporter, NAT) in apple plants enhanced uric acid concentrations and improved tolerance to salinity stress, compared with non-transgenic plants, while opposite phenotypes were observed for MdNAT7 RNAi plants (Sun et al., 2021). Therefore, it is possible to speculate that accumulation of uric acid in the needles of I_D seedlings might show two physiological functions to increase drought tolerance: scavenging ROS and involvement in nitrogen metabolism.

In the needles of I_D seedlings, the level of alpha-ketoglutaric acid increased to 3.93 times as that in NI_D seedlings (the file "I_D.vs.NI_D_pos_Diff_order" in Supplementary Table S3). The increase is helpful for improvement of drought tolerance of *P. taeda* seedlings, because foliar application of alpha-ketoglutarate improves drought resistance in soybean (*Glycine max*) (Gai et al., 2022). Exogenous alpha-ketoglutarate significantly increased proline concentrations in the leaves of the two soybean cultivars (drought resistant "Henong 51" and drought-sensitive "Henong43") (Gai et al., 2022). In needles of I_D seedlings, the level of coumalic acid increased to 3.23 times as that in NI_D seedlings (the file "I_D.vs.NI_D_pos_Diff_order" in Supplementary Table S3). Information about functions of coumalic acid in plants was known less; therefore, it is difficult to explain why *S. indica* inoculation increased the level of coumalic acid in the needles of *P. taeda* seedlings under drought stress.

Under drought stress, stachydrine increased to 3.26 times in the needles of inoculated seedlings as that in non-inoculated seedlings under drought stress (the file "I_D.vs.NI_D_pos_Diff_order" in Supplementary Table S3). Stachydrine (alias proline betaine) is an osmoprotectant that is at least as effective as glycine betaine and more effective than L-proline, for various strains of *Staphylococcus aureus*, *Staphylococcus epidermidis*, and *Staphylococcus saprophyticus* (Amin et al., 1995). It was reported that symbiosis between arbuscular mycorrhizal fungus *Glomus intraradices* and sugarcane plantlets (*Saccharum* spp. cv. Mex 69–290) increased the levels of proline and glycine betaine under drought stress (Spinoso-Castillo et al., 2023). Therefore, the increased level of stachydrine caused by *S. indica* inoculation is helpful for *P. taeda* seedlings under drought stress. Vitamin C increased in the needles of I_D seedlings, compared to those of NI_D seedlings (the file "I_D.vs.NI_D_pos_Diff_order" in Supplementary Table S3). Ascorbic acid (vitamin C) is a strong antioxidant and plays important roles in plants under abiotic stress.

Under negative ionization mode, itaconic acid was detected to increase to more than three times in I_D seedlings as that of NI_D seedlings (Supplementary Table S3). Itaconic acid and its derivatives possess functions via affecting plant growth and development. Exogenous application of the itaconic acid derivative, hexylitaconic acid (100 $mg \cdot L^{-1}$), promoted the growth of rice seedlings by 20–30%, indicating that the derivative shows plant growth-regulating activity (Isogai et al., 1984). However, the three derivative of itaconic acid, i.e., octyl itaconic acid, deoxysporothric acid, and epideoxysporothric acid, inhibited radicle and germ growth of the dicotyledon weeds *Eclipta prostrata* and *Veronica persica* at 400 $\mu g \cdot mL^{-1}$, and the growth inhibition rates were 49.7 and 18.4%, 81.7 and 24.6%, and 63.7 and 20.3%, respectively; their growth inhibition rates at 400 $\mu g \cdot mL^{-1}$ against the monocotyledon weeds *Eclipta crusgalli* and *Apostichopus japonicus* were 12.3 and 11.7%, 21.3 and 19.7%, and 9.8 and 20.2%, respectively (Cao et al., 2019). The mechanism underlying growth inhibition by these itaconic acid derivatives is not clear. A report showed that hexylitaconic acid exerts acetylcholinesterase inhibitory activity ($IC_{50} = 1.54\ \mu M$) (Kaaniche et al., 2019). Acetylcholine is a well-known neurotransmitter in the cholinergic nervous systems of vertebrates and insects and harbors positive effects on plant growth and development, especially under abiotic stress (Sugiyama and Tezuka, 2011; Qin et al., 2020, 2021; Su et al., 2020). Acetylcholinesterase is in charge of conversion of acetylcholine to choline and acetic acid. Thus, the abovementioned inhibitory effect of hexylitaconic acid on acetylcholinesterase might increase the level of acetylcholine, further maintaining acetylcholine function under drought stress. Maybe itaconic acid exerts such an effect to increase acetylcholine level in the needles of I_D seedlings, further maintaining physiological activity in their needles under drought stress. Anyway, such high accumulation of itaconic acid improves more research on its function in plants under drought stress. Furthermore, the metabolite itaconic acid was in significantly positive correlations to the four proteins, i.e., A0A023W8I6, A0A023W8D4, C3VXI1, and C6ZG55 (the file "I_D.vs.NI_D_neg_I_D.vs.NI_D_cor" in Supplementary Table S16). A0A023W8I6 is dehydrin 1 in *Pinus echinata* (Shortleaf pine), A0A023W8D4 is the protein LP3-3 in *Pinus elliottii*, C3VXI1 and C6ZG55 are large ribosomal subunit protein uL22c and 1-deoxy-D-xylulose-5-phosphate synthase in *P. taeda*, respectively (See Foot note text 2). Therefore, high accumulation of itaconic acid in the needles of I_D seedlings suggests that the metabolite might upregulate the expression of water deficient-inducible proteins (dehydrin 1 and LP3-3) and at the same time maintain the ribosomal function (the protein uL2cc) and carbohydrate conversion (1-deoxy-D-xylulose-5-phosphate synthase). In view of high accumulation of itaconic

acid in the needles of *P. taeda* seedlings under drought stress, it is necessary to explore its function in plants under drought stress.

4.3 *Serendipita indica*-induced drought tolerance by increasing levels of drought-related proteins in *Pinus taeda*

Serendipita indica inoculation caused different pattern changes in differential proteins in *P. taeda* seedlings under drought stress, compared to those in NI_D seedlings. Two aspects occurred in the pattern changes. First, in the comparison of NI_D vs. NI_W, there were five proteins (H9V821, A0A385JF21, H9V5W8, K7NJV0, and H9WW19) only occurring in the needles of NI_D seedlings (the file "NI_D.vs.NI_W.diff_prot" in Supplementary Table S10), but in the comparison of I_D vs. NI_D, there were two proteins (H9X056 and H9VDW5) only occurring in the needles of I_D seedlings (the file "I_D.vs.NI_D.diff_prot" in Supplementary Table S10). On the other hand, *S. indica* inoculation under drought stress did not increase FCs of H9V821, A0A385JF21, H9V5W8, K7NJV0, and H9WW19 (the file "NI_D.vs.NI_W.diff_prot" and the file "I_D.vs.NI_D.diff_prot" in Supplementary Table S10) but increased levels of two other proteins (H9X056 and H9VDW5). The results suggest that this inoculation changed adaptation mechanisms of *P. taeda* by upregulating levels of unique proteins under drought stress. Second, *S. indica* inoculation caused upregulation of 47 differential proteins in *P. taeda* seedlings under drought stress (the file "I_D.vs.NI_D.diff_prot" in Table S10), but 32 differential proteins were upregulated in non-inoculated seedlings (the file "NI_D.vs.NI_W.diff_prot" in Supplementary Table S10). Among the 79 differential proteins mentioned above, only two proteins were the same, i.e., H9V5W8 and Q41096. H9V5W8 is an uncharacterized protein, and Q41096 is a water deficit stress-inducible protein (LP3-2) (See Foot note text 3). These results suggest that *S. indica* inoculation caused significant changes in species and number of differential proteins in needles of *P. taeda* seedlings under drought stress. Interestingly, five differential proteins, i.e., H9WT28, H9X056, H9VCM7, H9VDW5, and K7NLQ9, did not occur in the NI_D seedlings but appeared in NI_W seedlings (the file "NI_D.vs.NI_W.diff_prot" in Supplementary Table S10), and two of the five proteins, i.e., H9X056 and H9VDW5, again occurred in I_D seedlings (the file "I_D.vs.NI_D.diff_prot" in Supplementary Table S10). The strange situation seems to indicate that better water situation occurred in I_D seedlings. H9X056 is an aspartate transaminase (the file "NI_D.vs.NI_W.diff_prot" and the file "I_D.vs.NI_D.diff_prot" in Supplementary Table S10). H9X056 catalyzes the reaction: L-aspartate +2-oxoglutarate = oxaloacetate + L-glutamate. In the reaction, the product L-glutamate is a very important and multifunctional amino acid (Forde and Lea, 2007; Liao et al., 2022). As an important neurotransmitter in plants, L-glutamate level increased in plants under drought stress (Wu et al., 2023). Thus, the increased level of H9X056 caused by *S. indica* inoculation under drought stress might improve L-glutamate biosynthesis to increase glutamate function. However, L-glutamate was not detected in the needles of I_D seedlings in positive or negative ionization mode (Supplementary Table S3). The result seems to indicate that L-glutamate was rapidly used up once its biosynthesis. H9VDW5 is a stress-response A/B barrel domain-containing protein (the file "NI_D.vs.NI_W.diff_prot" and the file "I_D.vs.NI_D.diff_prot" in Table S10). According to information from NCIB, the protein class occurs in microbes and plants, but little is known about their functions, especially under abiotic stress. In *Arabidopsis thaliana*, four genes encode stress-response A/B barrel domain-containing proteins, i.e., At5g22580, At2g31670, At1g51360, and At3g17210. At3g17210 encodes heat stable protein 1 (HS1)[4]. Such proteins harbor short chains of amino acids; thus, they maybe function as auxiliary proteins to exhibit enzyme protective effects against abiotic stress (Drira et al., 2023). In addition, under negative ionization mode, the metabolites 4-coumaric acid and LPC18:0 were in significantly negative correlations to H9X056 and H9VDW5 (Supplementary Figure S5D and the file "I_D.vs.NI_D_neg_I_D.vs.NI_D_cor" in Supplementary Table S16), suggesting that the enrichment of the two proteins might downregulate their levels. It is easy to understand why LPC18:0 might be downregulated by the two proteins because LPC18:0 is a saturated fatty acid. The increased levels of unsaturated fatty acids are more useful to maintain membrane fluidity of plant cells under drought stress. The significantly negative correlation between 4-coumaric acid and the two proteins suggests reduction of the metabolite in the needles of I_D seedlings. However, some other experiments showed that 4-coumaric acid accumulated in plants under drought stress (Arabsalehi et al., 2023; Oksana et al., 2023). Its reduced level may be related to difference in plant species because Arabsalehi et al. (2023) found decrease in level of quercetin, which often accumulated high levels in plants and played important physiological roles under drought stress (Gray et al., 2003; Singh et al., 2021). Therefore, reduction in the levels of 4-coumaric acid and LPC18:0 is reasonable in *P. taeda* seedlings under drought stress. At the same time, H9X056 and H9VDW5 were in significantly positive correlation with three metabolites, i.e., procyanidin B1, trifolirhizin, and tricin 5-*O*-hexoside (Supplementary Figure S5D). As mentioned, the three metabolites played important roles in plants under drought stress. Therefore, the two proteins showed strong effect on biosynthesis of these metabolites mentioned above.

In the comparison of I_D vs. NI_D, FCs of H9VNE7, A0A385JF23, and H9W5R1 were more than 11.0, 5.0, and 3.0, respectively (the file "I_D.vs.NI_D.diff_prot" in Supplementary Table S10), suggesting that the three proteins played important roles in *P. taeda* seedlings under drought stress. H9VNE7 is an uncharacterized protein in *P. taeda* (See Foot note text 3), and no information can be found about its function in NCBI. A0A385JF23 is ribosomal protein L5 in *P. taeda*. Its enrichment in the needles of I_D seedlings suggests its function in maintaining integrity of ribosome and normal protein biosynthesis under drought stress. H9W5R1is acyl-CoA oxidase C-terminal domain-containing protein in *P. taeda*. Acyl-CoA oxidase acts on CoA derivatives of fatty acids with chain lengths from 8 to 18. It catalyzes the first and rate-determining step of the peroxisomal beta-oxidation of fatty acids and a major producer of hydrogen peroxide (Nakajima et al., 2002; Chung et al., 2020). Its enrichment in the needles of I_D seedlings suggests increased fatty acid metabolisms and H_2O_2 production.

As mentioned above, vitamin C significantly increased in the needles of I_D seedlings, compared to that in NI_D seedlings. At the same time, vitamin C was in significantly positive correlations to the four proteins, i.e., A0A023W8D4, H9V6D7, A0A2D1UL07, and

4 https://www.arabidopsis.org/

H9V5W8 (the file "I_D.vs.NI_D_pos_I_D.vs.NI_D_cor" in Supplementary Table S16). A0A023W8D4 is water stress-inducible protein 3 (LP3-3) in *Pinus elliottii* (Slash pine), and H9V6D7, A0A2D1UL07, and H9V5W8 are dirigent protein, dehydrin 5, and uncharacterized protein in *P. taeda*, respectively (See Foot note text 3). Dirigent protein subfamily has an important function in phenol metabolism (Meng et al., 2023) and modulates cell wall metabolisms during abiotic stress (Paniagua et al., 2017). *ScDir*, a dirigent-like gene in sugarcane, responded to drought and salt stress (Guo et al., 2012). The protein ZmESBL, a dirigent family protein in maize, confers variation of Casparian strip thickness and salt tolerance in maize (Wang et al., 2022). Thus, H9V6D7 should have the same function in *P. taeda* under drought stress. Therefore, these proteins showed synergistic roles with vitamin C.

In addition, some function-known and water stress-related proteins were upregulated in I_D seedlings, such as A0A023W8I6 (dehydrin 1) and A0A2D1UL07 (dehydrin 5), compared to their levels in NI_D seedlings (the file "I_D.vs.NI_D.diff_prot" in Supplementary Table S10). These upregulated proteins increased drought tolerance of the inoculated seedlings. Furthermore, as mentioned above, four water deficit-inducible proteins, i.e., Q41087, Q41095, Q41096, and A0A023W8D4, occurred in nuclei (the file "I_D.vs.NI_D.Subcellular_diff" in Supplementary Table S14). Q41087, Q41096, and Q41095 are LP3-1, LP3-2, and LP3-3 in *P. taeda*, respectively; A0A023W8D4 is LP3-3 in *Pinus elliottii* (See Foot note text 3). LP3 paralogs in *P. taeda* belong to the abscisic acid and water stress-induced protein family and act as transcription factors for genes involved in hexose transport, and their levels were upregulated in *P. taeda* under drought stress (Lecoy et al., 2023). Therefore, our results about the subcellular localization of LP3 paralogs are reasonable. Since they act as transcription factors, their targeted genes are still not clear.

4.4 Changes in metabolism pathways caused by *Serendipita indica* inoculation in *Pinus taeda* under drought stress

As mentioned above, the levels of some metabolites were increased in the needles of I_W and I_D seedlings, suggesting the related biosynthesis pathways were strengthened. In the comparison of NI_D vs. NI_W seedlings, there were more differential proteins occurring in ribosome and phenylpropanoid biosynthesis pathway, with higher test reliability (Figure 6B), 9 and 5 differential proteins in the two pathways, respectively (the file "NI_D.vs.NI_W.KEGG_Enrich" in Supplementary Table S12). Nine differential proteins in ribosome pathway included R4LC26, H9VPZ0, H9VBV6, H9V5C5, H9WG89, C3VXI1, H9V4M9, H9WZ62, and R4L654 (the file "NI_D.vs.NI_W.KEGG_Enrich" in Supplementary Table S12). These proteins are structural constituents of ribosomes (See Foot note text 3). Out of them, R4LC26, C3VXI1, and R4L654 are involved in rRNA binding. The enrichment of these proteins under drought stress suggests that protein biosynthesis increases to maintain cell physiological functions. The phenylpropanoid biosynthesis pathway produces a great number of important organic compounds with an aromatic ring and a three-carbon propene tail, and they are synthesized by plants from the amino acids phenylalanine and tyrosine (Zhang and Stephanopoulos, 2016). Its general pathway begins from phenylalanine, which is converted to cinnamic acid by phenylalanine ammonia-lyase, and then many compounds were converted, such as coumarins, benzoic acids, anthocyanins, flavonoids, and stilbenes (Vanholme et al., 2019). In phenylpropanoid biosynthesis pathway, the five proteins, i.e., H9VFU4, H9VCR5, H9XAC0, H9WR60, and H9XB10, were enriched (the file "NI_D.vs.NI_W.KEGG_Enrich" in Supplementary Table S12). H9VFU4, H9XAC0, and H9WR60 are plant heme peroxidases and are involved in response to oxidative stress. Their enrichment is useful for scavenging of reactive oxygen species, and the related reaction products are used for biosynthesis of metabolites. H9VCR5 is a phenylalanine ammonia-lyase and is involved in cinnamic acid biosynthetic process. Cinnamic acid and its derivatives harbor antioxidant and antimicrobial activities (Sova, 2012), and *cis*-cinnamic acid is a natural plant growth-promoting metabolite (Steenackers et al., 2019). Thus, the increased levels of cinnamic acid and its derivatives caused by H9VCR5 enrichment are helpful for *P. taeda* seedlings under drought stress. H9XB10 is a glycoside hydrolase and is involved in carbohydrate metabolic process, i.e., hydrolyzing *O*-glycosyl compounds. Its products should be used in phenylpropanoid biosynthesis. Altogether, all the results suggest great changes in metabolism pathways in *P. taeda* caused by drought stress, compared with suitable water condition.

Similarly, some changes in metabolism pathways occurred were caused by *S. indica* inoculation under drought stress. In the comparison of I_D and NI_D seedlings, the first three KEGG enrichment pathways with lower *p*-values were phenylpropanoid biosynthesis, 2-oxocarboxylic acid metabolism, and cutin, suberine, and wax biosynthesis (Figure 6D and the file "I_D.vs.NI_D.KEGG_Enrich" in Supplementary Table S12). In the phenylpropanoid biosynthesis pathway, four proteins, i.e., H9WGR4, H9VCR5, H9XAC0, and H9WR60, were enriched (the file "I_D.vs.NI_D.KEGG_Enrich" in Supplementary Table S12). Out of them, H9WGR4 was a new face and is a plant heme peroxidase. Enrichment of the heme peroxidase suggests that *S. indica* inoculation increased response of *P. taeda* seedlings to oxidative stress under drought stress. As mentioned above, the three proteins, i.e., H9VCR5, H9XAC0, and H9WR60, were enriched in NI_D seedlings. The three proteins were also enriched in I_D seedlings, suggesting *S. indica* inoculation strengthened phenylpropanoid biosynthesis pathway to increase drought tolerance. In the 2-oxocarboxylic acid metabolism pathway, two proteins, i.e., H9VVX5 and H9X056, were enriched in I_D seedlings. H9VVX5 is an uncharacterized protein, and no information is known about its function. As mentioned above, H9X056 was only enriched in I_D seedlings. Its enrichment strengthened L-glutamate biosynthesis. In the cutin, suberine, and wax biosynthesis pathway, the protein, H9WHC3, was enriched (the file "I_D.vs.NI_D.KEGG_Enrich" in Supplementary Table S12). H9WHC3 is also an uncharacterized protein, and no information is known. Since it is involved in cutin, suberine, and wax biosynthesis, its enrichment is useful for plants to reduce water loss from I_D seedlings.

As mentioned above, it is known that *S. indica* inoculation improved two biosynthesis pathways, i.e., phenylpropanoid biosynthesis, and cutin, suberine, and wax biosynthesis, and strengthened a metabolism pathway, i.e., 2-oxocarboxylic acid metabolism, by upregulating the related proteins.

5 Conclusion

Our experimental results based on untargeted metabolome and proteome analysis showed inoculation of the root endophytic fungus *S. indica* with *P. taeda* improved biosynthesis of some flavonoids and

organic acids under drought stress. These metabolites showed their respective physiological functions in *P. taeda* under drought stress. At the same time, the inoculation increased enrichment of water deficient-inducible proteins (such as LP3-1, LP3-2, LP3-3, and dehydrins) and those proteins involved in ribosomal structures (such as A0A385JF23). Changes in biosynthesis and metabolism pathways caused by the inoculation mainly included phenylpropanoid biosynthesis, cutin, suberine, and wax biosynthesis, and 2-oxocarboxylic acid metabolism. In addition, there were positive relationships between accumulation of some metabolites and enrichment of proteins in *P. taeda* under drought stress. The results provided a strong base for breeding drought-tolerant cultivars of *P. taeda* under global climate change and future research, especially the functions of highly accumulated metabolites (such as itaconic acid) and unique proteins (such as water deficient-inducible proteins localized in the nucleus).

Data availability statement

The original contributions presented in the study are publicly available. This data can be found here: https://www.cncb.ac.cn under accession numbers: OMIX005953 for metabolome data and OMIX005954 for proteome data.

Author contributions

CW: Data curation, Funding acquisition, Investigation, Writing – original draft, Writing – review & editing. YY: Investigation, Methodology, Software, Writing – original draft, Writing – review & editing. YW: Data curation, Investigation, Methodology, Software, Writing – original draft, Writing – review & editing. WZ: Resources, Supervision, Writing – review & editing. HS: Funding acquisition, Project administration, Resources, Software, Writing – review & editing.

Funding

The author(s) declare financial support was received for the research, authorship, and/or publication of this article. This study was supported by the General Program of the National Natural Science Foundation of China (No. 31470635 and No. 31870378).

Acknowledgments

The authors thank Novogene Co. Ltd. for its technological support for metabolomics and proteomics analysis.

Conflict of interest

The authors declare that the research was conducted in the absence of any commercial or financial relationships that could be construed as a potential conflict of interest.

Publisher's note

All claims expressed in this article are solely those of the authors and do not necessarily represent those of their affiliated organizations, or those of the publisher, the editors and the reviewers. Any product that may be evaluated in this article, or claim that may be made by its manufacturer, is not guaranteed or endorsed by the publisher.

Supplementary material

The Supplementary material for this article can be found online at: https://www.frontiersin.org/articles/10.3389/fmicb.2024.1294833/full#supplementary-material

References

Ahmad, H. M., Fiaz, S., Hafeez, S., Zahra, S., Shah, A. N., Gul, B., et al. (2022). Plant growth-promoting rhizobacteria eliminate the effect of drought stress in plants: a review. *Front. Plant Sci.* 13:875774. doi: 10.3389/fpls.2022.875774

Amin, U. S., Lash, T. D., and Wilkinson, B. J. (1995). Proline betaine is a highly effective osmoprotectant for *Staphylococcus aureus*. *Arch. Microbiol.* 163, 138–142. doi: 10.1007/BF00381788

Anil Kumar, S., Kaniganti, S., Hima Kumari, P., Sudhakar Reddy, P., Suravajhala, P., et al. (2022). Functional and biotechnological cues of potassium homeostasis for stress tolerance and plant development. *Biotechnol. Genet. Eng. Rev.* 5, 1–44. doi: 10.1080/02648725.2022.2143317

Arabsalehi, F., Rahimmalek, M., Sabzalian, M. R., Ghanadian, M., Matkowski, A., and Szumny, A. (2023). Changes in polyphenolic composition, physiological characteristics, and yield-related traits of Moshgak (*Ducrosia anethifolia* Boiss.) populations in response to drought stress. *Protoplasma* 260, 967–985. doi: 10.1007/s00709-022-01828-0

Azevedo, R. P., Alves, N. M., Costa, I. A., Domingues, M. I. S., Bandória, N. A., de Figueiredo, U. J., et al. (2021). Endophytic fungi assures tropical forage grass growth by water stress tolerances. *Curr. Microbiol.* 78, 4060–4071. doi: 10.1007/s00284-021-02672-w

Batstone, R. T. (2022). Genomes within genomes: nested symbiosis and its implications for plant evolution. *New Phytol.* 234, 28–34. doi: 10.1111/nph.17847

Begum, N., Xiao, Y., Wang, L., Li, D., Irshad, A., and Zhao, T. (2023). Arbuscular mycorrhizal fungus *Rhizophagus irregularis* alleviates drought stress in soybean with overexpressing the GmSPL9d gene by promoting photosynthetic apparatus and regulating the antioxidant system. *Microbiol. Res.* 273:127398. doi: 10.1016/j.micres.2023.127398

Boorboori, M. R., and Zhang, H. Y. (2022). The role of *Serendipita indica* (*Piriformospora indica*) in improving plant resistance to drought and salinity stresses. *Biology* 11:952. doi: 10.3390/biology11070952

Bortolo, T. D. S. C., Marchiosi, R., Viganó, J., Siqueira-Soares, R. C., Ferro, A. P., Barreto, G. E., et al. (2018). *Trans*-aconitic acid inhibits the growth and photosynthesis of *Glycine max*. *Plant Physiol. Biochem.* 132, 490–496. doi: 10.1016/j.plaphy.2018.09.03

Brauer, D., and Teel, M. R. (1982). Metabolism of *trans*-aconitic acid in maize: II. Regulatory properties of two compartmented forms of citrate dehydrase. *Plant Physiol.* 70, 723–727. doi: 10.1104/pp.70.3.723

Burau, R., and Stout, P. R. (1965). *Trans*-aconitic acid in range grasses in early spring. *Science* 150, 766–767. doi: 10.1126/science.150.3697.766

Caballero, M., Lauer, E., Bennett, J., Zaman, S., McEvoy, S., Acosta, J., et al. (2021). Toward genomic selection in *Pinus taeda:* integrating resources to support array design in a complex conifer genome. *Appl. Plant. Sci.* 9:e11439. doi: 10.1002/aps3.11439

Cao, L., Yan, W., Gu, C., Wang, Z., Zhao, S., Kang, S., et al. (2019). New alkylitaconic acid derivatives from *Nodulisporium* sp. A21 and their auxin herbicidal activities on weed seeds. *J. Agric. Food Chem.* 67, 2811–2817. doi: 10.1021/acs.jafc.8b04996

Chandrasekaran, M. (2022). Arbuscular mycorrhizal fungi mediated alleviation of drought stress via non-enzymatic antioxidants: a meta-analysis. *Plants* 11:2448. doi: 10.3390/plants11192448

Chen, W., Ye, T., Sun, Q., Niu, T., and Zhang, J. (2023). Arbuscular mycorrhizal fungus alleviates anthracnose disease in tea seedlings. *Front. Plant Sci.* 13:1058092. doi: 10.3389/fpls.2022.1058092

Chen, S., Zhang, G., Liang, X., Wang, L., Li, Z., He, Y., et al. (2023). A dark septate endophyte improves cadmium tolerance of maize by modifying root morphology and promoting cadmium binding to the cell wall and phosphate. *J. Fungi.* 9:531. doi: 10.3390/jof9050531

Chung, H. L., Wangler, M. F., Marcogliese, P. C., Jo, J., Ravenscroft, T. A., Zuo, Z., et al. (2020). Loss-or gain-of-function mutations in ACOX1 cause axonal loss via different mechanisms. *Neuron* 106, 589–606.e6. doi: 10.1016/j.neuron.2020.02.021

Churkina, G., Running, S. W., and Schloss, A. L. (1999). Comparing global models of terrestrial net primary productivity (NPP): the importance of water availability. *Glob. Change Biol.* 5, 46–55. doi: 10.1046/j.1365-2486.1999.00006.x

Clode, P. L., Saunders, M., Maker, G., Ludwig, M., and Atkins, C. A. (2009). Uric acid deposits in symbiotic marine algae. *Plant Cell Environ.* 32, 170–177. doi: 10.1111/j.1365-3040.2008.01909.x

da Silva Rodrigues-Corrêa, K. C., de Lima, J. C., and Fett-Neto, A. G. (2012). Pine oleoresin: tapping green chemicals, biofuels, food protection, and carbon sequestration from multipurpose trees. *Food Energy Secur.* 1, 81–93. doi: 10.1002/fes3.13

Das, K., Rajawat, M. V. S., Saxena, A. K., and Prasanna, R. (2017). Development of *Mesorhizobium ciceri*-based bofilms and analyses of their antifungal and plant growth promoting activity in chickpea challenged by *fusarium* wilt. *Indian J. Microbiol.* 57, 48–59. doi: 10.1007/s12088-016-0610-8

De Rocchis, V., Jammer, A., Camehl, I., Franken, P., and Roitsch, T. (2022). Tomato growth promotion by the fungal endophytes S*erendipita indica* and S*erendipita herbamans* is associated with sucrose de-novo synthesis in roots and differential local and systemic effects on carbohydrate metabolisms and gene expression. *J. Plant Physiol.* 276:153755. doi: 10.1016/j.jplph.2022.153755

Di Petrillo, A., Orrù, G., Fais, A., and Fantini, M. C. (2022). Quercetin and its derivatives as antiviral potentials: a comprehensive review. *Phytother. Res.* 36, 266–278. doi: 10.1002/ptr.7309

Drira, M., Ghanmi, S., Zaidi, I., Brini, F., Miled, N., and Hanin, M. (2023). The heat-stable protein fraction from *Opuntia ficus-indica* seeds exhibits an enzyme protective effect against thermal denaturation and an antibacterial activity. *Biotechnol. Appl. Biochem.* 70, 593–602. doi: 10.1002/bab.2382

Endo, A., and Kitahara, N. (1977). *cis-and trans*-aconitic acids as inhibitors of glutamate decarboxylase. *Hoppe Seylers Z. Physiol. Chem.* 358, 1365–1368.

Famurewa, A. C., Renu, K., Eladl, M. A., Chakraborty, R., Myakala, H., El-Sherbiny, M., et al. (2022). Hesperidin and hesperetin against heavy metal toxicity: insight on the molecular mechanism of mitigation. *Biomed. Pharmacother.* 149:112914. doi: 10.1016/j.biopha.2022.112914

Forde, B. G., and Lea, P. J. (2007). Glutamate in plants: metabolism, regulation, and signalling. *J. Exp. Bot.* 58, 2339–2358. doi: 10.1093/jxb/erm121

Franceschini, A., Szklarczyk, D., Frankild, S., Kuhn, M., Simonovic, M., Roth, A., et al. (2013). STRING V9.1: protein-protein interaction networks, with increased coverage and integration. *Nucleic Acids Res.* 41, D808–D815. doi: 10.1093/nar/gks1094

Frank, H. E. R., and Garcia, K. (2021). Benefits provided by four ectomycorrhizal fungi to *Pinus taeda* under different external potassium availabilities. *Mycorrhiza* 31, 755–766. doi: 10.1007/s00572-021-01048-z

Gaber, D. A., Berthelot, C., Blaudez, D., Kovács, G. M., and Franken, P. (2023). Impact of dark septate endophytes on salt stress alleviation of tomato plants. *Front. Microbiol.* 14:1124879. doi: 10.3389/fmicb.2023.1124879

Gai, Z., Liu, J., Cai, L., Zhang, J., and Liu, L. (2022). Foliar application of alpha-ketoglutarate plus nitrogen improves drought resistance in soybean (*Glycine max* L. Merr.). *Sci. Rep.* 12:14421. doi: 10.1038/s41598-022-18660-4

Ghorbani, A., Tafteh, M., Roudbari, N., Pishkar, L., Zhang, W., and Wu, C. (2021). *Piriformospora indica* augments arsenic tolerance in rice (*Oryza sativa*) by immobilizing arsenic in roots and improving iron translocation to shoots. *Ecotoxicol. Environ. Saf.* 209:111793. doi: 10.1016/j.ecoenv.2020.111793

Gilbert, M. E., and Medina, V. (2016). Drought adaptation mechanisms should guide experimental design. *Trends Plant Sci.* 21, 639–647. doi: 10.1016/j.tplants.2016.03.003

Gonzalez-Benecke, C. A., Teskey, R. O., Dinon-Aldridge, H., and Martin, T. A. (2017). *Pinus taeda* forest growth predictions in the 21st century vary with site mean annual temperature and site quality. *Glob. Chang. Biol.* 23, 4689–4705. doi: 10.1111/gcb.13717

González-Martínez, S. C., Ersoz, E., Brown, G. R., Wheeler, N. C., and Neale, D. B. (2006). DNA sequence variation and selection of tag single-nucleotide polymorphisms at candidate genes for drought-stress response in *Pinus taeda* L. *Genetics* 172, 1915–1926. doi: 10.1534/genetics.105.047126

Gowtham, H. G., Singh, S. B., Shilpa, N., Aiyaz, M., Nataraj, K., Udayashankar, A. C., et al. (2022). Insight into recent progress and perspectives in improvement of antioxidant machinery upon PGPR augmentation in plants under drought stress: a review. *Antioxidants* 11:1763. doi: 10.3390/antiox11091763

Gray, D. E., Pallardy, S. G., Garrett, H. E., and Rottinghaus, G. E. (2003). Effect of acute drought stress and time of harvest on phytochemistry and dry weight of St. John's wort leaves and flowers. *Planta Med.* 69, 1024–1030. doi: 10.1055/s-2003-45150

Guo, J.-L., Xu, L.-P., Fang, J.-P., Su, Y.-C., Fu, H.-Y., Que, Y.-X., et al. (2012). A novel dirigent protein gene with highly stem-specific expression from sugarcane, response to drought, salt and oxidative stresses. *Plant Cell Rep.* 31, 1801–1812. doi: 10.1007/s00299-012-1293-1

Hasanuzzaman, M., Bhuyan, M. H. M., Nahar, K., Hossain, M. D., Mahmud, J., Hossen, M., et al. (2018). Potassium: a vital regulator of plant responses and tolerance to abiotic stresses. *Agronomy* 8:31. doi: 10.3390/agronomy8030031

He, C., Han, T., Tan, L., and Li, X. (2022). Effects of dark septate endophytes on the performance and soil microbia of *Lycium ruthenicum*under drought stress. *Front. Plant Sci.* 13:898378. doi: 10.3389/fpls.2022.898378

He, F., Lai, S., Chi, Y., Pan, H., Cao, R., and Bao, R. (2022). Variation characteristics of drought circulation in Fujian province from march to June 2018. *J. Arid. Meteorol.* 40, 22–29. doi: 10.11755/j.issn.1006-7639(2002)-01-0022

Huang, D. W., Sherman, B. T., and Lempicki, R. A. (2009). Bioinformatics enrichment tools: paths toward the comprehensive functional analysis of large gene lists. *Nucleic Acids Res.* 37, 1–13. doi: 10.1093/nar/gkn923

Isogai, A., Washizu, M., Kondo, K., Murakoshi, S., Suzuki, A., Akira, I., et al. (1984). Isolation and identification of (+)-hexylitaconic acid as a plant growth regulator. *Agric. Biol. Chem.* 48, 2607–2609. doi: 10.1080/00021369.1984.10866557

Jatav, K. S., Agarwal, R. M., Singh, R. P., and Shrivastava, M. (2012). Growth and yield responses of wheat (*Triticum aestivum* L) to suboptimal water supply and different potassium doses. *J. Funct. Environ. Bot.* 2, 39–51. doi: 10.5958/j.2231-1742.2.1.005

Jones, P., Binns, D., Chang, H.-Y., Fraser, M., Li, W., McAnulla, C., et al. (2014). Inter pro scan 5: genome-scale protein function classification. *Bioinformatics* 30, 1236–1240. doi: 10.1093/bioinformatics/btu031

Jörgensen, K., Clemmensen, K. E., Wallander, H., and Lindahl, B. D. (2023). Do ectomycorrhizal exploration types reflect mycelial foraging strategies? *New Phytol.* 237, 576–584. doi: 10.1111/nph.18566

Kaaniche, F., Hamed, A., Abdel-Razek, A. S., Wibberg, D., Abdissa, N., El Euch, I. Z., et al. (2019). Bioactive secondary metabolites from new endophytic fungus *Curvularia*. Sp isolated from *Rauwolfia macrophylla*. *PLoS One* 14:e0217627. doi: 10.1371/journal.pone.0217627

Karlsen-Ayala, E., Smith, M. E., Askey, B. C., and Gazis, R. (2022). Native ectomycorrhizal fungi from the endangered pine rocklands are superior symbionts to commercial inoculum for slash pine seedlings. *Mycorrhiza* 32, 465–480. doi: 10.1007/s00572-022-01092-3

Kaur, S., Campbell, B. J., and Suseela, V. (2022). Root metabolome of plant-arbuscular mycorrhizal symbiosis mirrors the mutualistic or parasitic mycorrhizal phenotype. *New Phytol.* 234, 672–687. doi: 10.1111/nph.17994

Keyser, PD, Fearer, T, and Harper, CA. (2016). *Managing oak forests in the eastern United States*. Boca Raton, CRC Press, 36–38.

Khosravi-Nejad, F., Khavari-Nejad, R. A., Moradi, F., and Najafi, F. (2022). Cytokinin and abscisic acid alleviate drought stress through changing organic acids profile, ion immolation, and fatty acid profile to improve yield of wheat (*Triticum aestivum* L.) cultivars. *Physiol. Mol. Biol. Plants* 28, 1119–1129. doi: 10.1007/s12298-022-01173-9

Kricher, JC, and Morrison, G. (1998). *Eastern forests--a field guide to birds, mammals, trees, flowers, and more*. New York, Houghton Mifflin, pp. 92.

Kumar, S., Diksha, S. S. S., and Kumar, R. (2021). Biofertilizers: An ecofriendly technology for nutrient recycling and environmental sustainability. *Curr. Res. Microb. Sci.* 3:100094. doi: 10.1016/j.crmicr.2021.100094

Kwon, E. Y., and Choi, M. S. (2020). Eriocitrin improves adiposity and related metabolic disorders in high-fat diet-induced obese mice. *J. Med. Food* 23, 233–241. doi: 10.1089/jmf.2019.4638

Lecoy, J., Ranade, S. S., and García-Gil, M. R. (2023). Analysis of the *ASR* and *LP3* homologous gene families reveal positive selection acting on *LP3-3* gene. *Gene* 850:146935. doi: 10.1016/j.gene.2022.146935

Li, C., Zhang, Q., Xia, Y., and Jin, K. (2021). MaNmrA, a negative transcription regulator in nitrogen catabolite repression pathway, contributes to nutrient utilization, stress resistance, and virulence in entomopathogenic fungus *Metarhizium acridum*. *Biology* 10:1167. doi: 10.3390/biology10111167

Li, X., Zhang, X., Xu, M., Ye, Q., Gao, H., and He, X. (2022). Improved tolerance of *Artemisia ordosica* to drought stress via dark septate endophyte (DSE) symbiosis. *J. Fungi.* 8:730. doi: 10.3390/jof8070730

Liao, H. S., Chung, Y. H., and Hsieh, M. H. (2022). Glutamate: a multifunctional amino acid in plants. *Plant Sci.* 318:111238. doi: 10.1016/j.plantsci.2022.11123

Liu, N., Jacquemyn, H., Liu, Q., Shao, S. C., Ding, G., and Xing, X. (2023). Effects of a dark septate fungal endophyte on the growth and physiological response of seedlings to drought in an epiphytic orchid. *Front. Microbiol.* 13:961172. doi: 10.3389/fmicb.2022.961172

Liu, B., Jing, D., Liu, F., Ma, H., Liu, X., and Peng, L. (2021). *Serendipita indica* alleviates drought stress responses in walnut (*Juglans regia* L.) seedlings by stimulating osmotic adjustment and antioxidant defense system. *Appl. Microbiol. Biotechnol.* 105, 8951–8968. doi: 10.1007/s00253-021-11653-9

Lorenz, W. W., Alba, R., Yu, Y. S., Bordeaux, J. M., Simões, M., and Dean, J. F. (2011). Microarray analysis and scale-free gene networks identify candidate regulators in drought-stressed roots of loblolly pine (*P. taeda* L.). *BMC Genomics* 12:264. doi: 10.1186/1471-2164-12-264

Lorenz, W. W., Sun, F., Liang, C., Kolychev, D., Wang, H., Zhao, X., et al. (2006). Water stress-responsive genes in loblolly pine (*Pinus taeda*) roots identified by

analyses of expressed sequence tag libraries. *Tree Physiol.* 26, 1–16. doi: 10.1093/treephys/26.1.1

Lorio, P. L. Jr., and Sommers, R. A. (1986). Evidence of competition for photosynthates between growth processes and oleoresin synthesis in *Pinus taeda* L. *Tree Physiol.* 2, 301–306. doi: 10.1093/treephys/2.1-2-3.301

Ma, W. F., Li, Y. B., Nai, G. J., Liang, G. P., Ma, Z. H., Chen, B. H., et al. (2022). Changes and response mechanism of sugar and organic acids in fruits under water deficit stress. *Peer J.* 10:e13691. doi: 10.7717/peerj.13691

Manzur, M. E., Garello, F. A., Omacini, M., Schnyder, H., Sutka, M. R., and García-Parisi, P. A. (2022). Endophytic fungi and drought tolerance: ecophysiological adjustment in shoot and root of an annual mesophytic host grass. *Funct. Plant Biol.* 49, 272–282. doi: 10.1071/FP21238

Matallana-Ramirez, L. P., Whetten, R. W., Sanchez, G. M., and Payn, K. G. (2021). Breeding for climate change resilience: a case study of loblolly pine (*Pinus taeda* L.) in North America. Front. *Plant Sci.* 12:606908. doi: 10.3389/fpls.2021.606908

McConnell, T. E., Silva, B. K. D., Sun, C. Y., and Tanger, S. M. (2021). Forest to mill timber price trends and volatility for Mississippi timber products. *For. Prod. J.* 71, 177–187. doi: 10.13073/FPJ-D-21-00010

McKeand, S. E., Payn, K. G., Heine, A. J., and Abt, R. C. (2021). Economic significance of continued improvement of loblolly pine genetics and its efficient deployment to landowners in the southern United States. *J. For.* 119, 62–72. doi: 10.1093/jofore/fvaa044

Meng, Q., Kim, S. J., Costa, M. A., Moinuddin, S. G. A., Celoy, R. M., Smith, C. A., et al. (2023). Dirigent protein subfamily function and structure in terrestrial plant phenol metabolism. *Methods Enzymol.* 683, 101–150. doi: 10.1016/bs.mie.2023.02.025

Muñoz, E., and Carneiro, J. (2022). Plant-microbe symbiosis widens the habitability range of the Daisyworld. *J. Theor. Biol.* 554:111275. doi: 10.1016/j.jtbi.2022.111275

Nakajima, Y., Miyahara, I., Hirotsu, K., Nishina, Y., Shiga, K., Setoyama, C., et al. (2002). Three-dimensional structure of the flavoenzyme acyl-CoA oxidase-II from rat liver, the peroxisomal counterpart of mitochondrial acyl-CoA dehydrogenase. *J. Biochem.* 131, 365–374. doi: 10.1093/oxfordjournals.jbchem.a003111

Nichols, C. E., Cocklin, S., Dodds, A., Ren, J., Lamb, H., Hawkins, A. R., et al. (2001). Expression, purification and crystallization of *aspergillus nidulans* NmrA, a negative regulatory protein involved in nitrogen-metabolite repression. *Acta Crystallogr. D Biol. Crystallogr.* 57, 1722–1725. doi: 10.1107/s090744490101410x

Núñez-Corcuera, B., Serafimidis, I., Arias-Palomo, E., Rivera-Calzada, A., and Suarez, T. (2008). A new protein carrying an NmrA-like domain is required for cell differentiation and development in *Dictyostelium discoideum*. *Dev. Biol.* 321, 331–342. doi: 10.1016/j.ydbio.2008.06.027

Oddo, E., Abbate, L., Inzerillo, S., Carimi, F., Motisi, A., Sajeva, M., et al. (2020). Water relations of two Sicilian grapevine cultivars in response to potassium availability and drought stress. *Plant Physiol. Biochem.* 148, 282–290. doi: 10.1016/j.plaphy.2020.01.025

Oksana, S., Marek, K., Marian, B., and Marek, Z. (2023). Cultivar-dependent and drought-induced modulation of secondary metabolites, adaptative defense in *Fagopyrum esculentum* L. *Physiol. Mol. Biol. Plants* 29, 1605–1618. doi: 10.1007/s12298-023-01376-8

Opitz, M. W., Daneshkhah, R., Lorenz, C., Ludwig, R., Steinkellner, S., and Wieczorek, K. (2021). *Serendipita indica* changes host sugar and defense status in *Arabidopsis thaliana*: cooperation or exploitation? *Planta* 253:74. doi: 10.1007/s00425-021-03587-3

Paniagua, C., Bilkova, A., Jackson, P., Dabravolski, S., Riber, W., Didi, V., et al. (2017). Dirigent proteins in plants: modulating cell wall metabolism during abiotic and biotic stress exposure. *J. Exp. Bot.* 68, 3287–3301. doi: 10.1093/jxb/erx141

Perera, D., Magbanua, Z. V., Thummasuwan, S., Mukherjee, D., Arick, M. 2nd, Chouvarine, P., et al. (2018). Exploring the loblolly pine (*Pinus taeda* L.) genome by BAC sequencing and cot analysis. *Gene* 663, 165–177. doi: 10.1016/j.gene.2018.04.024

Piculell, B. J., José Martínez-García, P., Nelson, C. D., and Hoeksema, J. D. (2019). Association mapping of ectomycorrhizal traits in loblolly pine (*Pinus taeda* L.). *Mol. Ecol.* 28, 2088–2099. doi: 10.1111/mec.15013

Puginier, C., Keller, J., and Delaux, P. M. (2022). Plant-microbe interactions that have impacted plant terrestrializations. *Plant Physiol.* 190, 72–84. doi: 10.1093/plphys/kiac258

Qin, C., Ahanger, M. A., Lin, B., Huang, Z., Zhou, J., Ahmed, N., et al. (2021). Comparative transcriptome analysis reveals the regulatory effects of acetylcholine on salt tolerance of *Nicotiana benthamiana*. *Phytochemistry* 181:112582. doi: 10.1016/j.phytochem.2020.112582

Qin, C., Ahanger, M. A., Zhou, J., Ahmed, N., Wei, C., Yuan, S., et al. (2020). Beneficial role of acetylcholine in chlorophyll metabolism and photosynthetic gas exchange in *Nicotiana benthamiana* seedlings under salinity stress. *Plant Biol.* 22, 357–365. doi: 10.1111/plb.13079

Qin, X., Xu, J., An, X., Yang, J., Wang, Y., Dou, M., et al. (2023). Insight of endophytic fungi promoting the growth and development of woody plants. *Crit. Rev. Biotechnol.* 44, 78–99. doi: 10.1080/07388551.2022.2129579

Razak, N. A., and Gange, A. C. (2023). Multitrophic interactions between arbuscular mycorrhizal fungi, foliar endophytic fungi and aphids. *Microb. Ecol.* 85, 146–156. doi: 10.1007/s00248-021-01937-y

Saunier, A., Greff, S., Blande, J. D., Lecareux, C., Baldy, V., Fernandez, C., et al. (2022). Amplified drought and seasonal cycle modulate *Quercus pubescens* leaf metabolome. *Meta* 12:307. doi: 10.3390/METABO12040307

Shankar, A., and Prasad, V. (2023). Potential of desiccation-tolerant plant growth-promoting rhizobacteria in growth augmentation of wheat (*Triticum aestivum* L.) under drought stress. *Front. Microbiol.* 14:1017167. doi: 10.3389/fmicb.2023.1017167

Singh, P., Arif, Y., Bajguz, A., and Hayat, S. (2021). The role of quercetin in plants. *Plant Physiol. Biochem.* 166, 10–19. doi: 10.1016/j.plaphy.2021.05.023

Sova, M. (2012). Antioxidant and antimicrobial activities of cinnamic acid derivatives. *Mini Rev. Med. Chem.* 12, 749–767. doi: 10.2174/138955712801264792

Spinoso-Castillo, J. L., Moreno-Hernández, M. D. R., Mancilla-Álvarez, E., Sánchez-Segura, L., Sánchez-Páez, R., and Bello-Bello, J. J. (2023). Arbuscular mycorrhizal symbiosis improves ex vitro acclimatization of sugarcane plantlets (*Saccharum* spp.) under drought stress conditions. *Plants* (Basel), 12:687. doi: 10.3390/plants12030687

Stammers, D. K., Ren, J., Leslie, K., Nichols, C. E., Lamb, H. K., Cocklin, S., et al. (2001). The structure of the negative transcriptional regulator NmrA reveals a structural superfamily which includes the short-chain dehydrogenase/reductases. *EMBO J.* 20, 6619–6626. doi: 10.1093/emboj/20.23.6619

Steenackers, W., El Houari, I., Baekelandt, A., Witvrouw, K., Dhondt, S., Leroux, O., et al. (2019). *cis*-cinnamic acid is a natural plant growth-promoting compound. *J. Exp. Bot.* 70, 6293–6304. doi: 10.1093/jxb/erz39

Su, Y., Qin, C., Begum, N., Ashraf, M., and Zhang, L. (2020). Acetylcholine ameliorates the adverse effects of cadmium stress through mediating growth, photosynthetic activity and subcellular distribution of cadmium in tobacco (*Nicotiana benthamiana*). *Ecotoxicol. Environ. Saf.* 198:110671. doi: 10.1016/j.ecoenv.2020.110671

Sugiyama, K., and Tezuka, T. (2011). Acetylcholine promotes the emergence and elongation of lateral roots of *Raphanus sativus*. *Plant Signal. Behav.* 6, 1545–1553. doi: 10.4161/psb.6.10.16876

Sun, R. T., Feng, X. C., Zhang, Z. Z., Zhou, N., Feng, H. D., Liu, Y. M., et al. (2022). Root endophytic fungi regulate changes in sugar and medicinal compositions of *Polygonum cuspidatum*. *Front. Plant Sci.* 13:818909. doi: 10.3389/fpls.2022.818909

Sun, G., Li, Z., and Feng, J. (2014). Relationship between atmospheric low-frequency oscillation and two severe drought events in Southwest China. *Plateau Meteorol.* 33, 1562–1567. doi: 10.7522/j.issn.1000-0534.2013.00166

Sun, T., Pei, T., Yang, L., Zhang, Z., Li, M., Liu, Y., et al. (2021). Exogenous application of xanthine and uric acid and nucleobase-ascorbate transporter MdNAT7 expression regulate salinity tolerance in apple. *BMC Plant Biol.* 21:52. doi: 10.1186/s12870-021-02831-y

Swift, K. A. D. (2004). Catalytic transformations of the major terpene feedstocks. *Top. Catal.* 27, 143–155. doi: 10.1023/B:TOCA.0000013549.60930.da

Talbot, B., Chen, T. W., Zimmerman, S., Joost, S., Eckert, A. J., Crow, T. M., et al. (2017). Combining genotype, phenotype, and environment to infer potential candidate genes. *J. Hered.* 108, 207–216. doi: 10.1093/jhered/esw077

Tanveer, S., Akhtar, N., Ilyas, N., Sayyed, R. Z., Fitriatin, B. N., Perveen, K., et al. (2023). Interactive effects of *pseudomonas putida* and salicylic acid for mitigating drought tolerance in canola (*Brassica napus* L.). *Heliyon* 9:e14193. doi: 10.1016/j.heliyon.2023.e14193

Um, M. J., Kim, Y., Jung, K., Lee, M., An, H., Min, I., et al. (2022). Evaluation of drought propagations with multiple indices in the Yangtze River basin. *J. Environ. Manag.* 317:115494. doi: 10.1016/j.jenvman.2022.115494

van Galen, L. G., Orlovich, D. A., Lord, J. M., Nilsen, A. R., Dutoit, L., and Larcombe, M. J. (2023). Correlated evolution in an ectomycorrhizal host-symbiont system. *New Phytol.* 238, 1215–1229. doi: 10.1111/nph.18802

Vanholme, B., Houari, I. E., and Boerjan, W. (2019). Bioactivity: phenylpropanoids' best kept secret. *Curr. Opin. Biotechnol.* 56, 156–162. doi: 10.1016/j.copbio.2018.11.012

Wang, F. (2012). Relationships between summer drought and strong typhoon events and pine wilt disease occurrence in eastern Asia. Chin. *J. Appl. Ecol.* 23, 1533–1544. doi: 10.13287/j.1001-9332.2012.0254

Wang, Y., Cao, Y., Liang, X., Zhuang, J., Wang, X., Qin, F., et al. (2022). A dirigent family protein confers variation of Casparian strip thickness and salt tolerance in maize. *Nat. Commun.* 13:2222. doi: 10.1038/s41467-022-29809-0

Wang, L., Li, Z., Zhang, G., Liang, X., Hu, L., Li, Y., et al. (2023). Dark septate endophyte *Exophiala pisciphila* promotes maize growth and alleviates cadmium toxicity. *Front. Microbiol.* 14:1165131. doi: 10.3389/fmicb.2023.1165131

Want, E. J., Masson, P., Michopoulos, F., Wilson, I. D., Theodoridis, G., Plumb, R. S., et al. (2013). Global metabolic profiling of animal and human tissues via UPLC-MS. *Nat. Protoc.* 8, 17–32. doi: 10.1038/nprot.2012.135

Wegrzyn, J. L., Liechty, J. D., Stevens, K. A., Wu, L.-S., Loopstra, C. A., Vasquez-Gross, H. A., et al. (2014). Unique features of the loblolly pine (*Pinus taeda* L.) megagenome revealed through sequence annotation. *Genetics* 196, 891–909. doi: 10.1534/genetics.113.159996

Wu, C., Wang, Y., and Sun, H. (2023). Targeted and untargeted metabolomics reveals deep analysis of drought stress responses in needles and roots of *Pinus taeda* seedlings. *Front. Plant Sci.* 13:1031466. doi: 10.3389/fpls.2022.1031466

Wu, C., Wei, Q., Deng, J., and Zhang, W. (2019). Changes in gas exchange, root growth, and biomass accumulation of *Platycladus orientalis* seedlings colonized by *Serendipita indica*. *J. For. Res.* 30, 1199–1207. doi: 10.1007/s11676-018-0712-8

Xiao, Y., Liu, C., Hu, N., Wang, B., Zheng, K., Zhao, Z., et al. (2023). Contributions of ectomycorrhizal fungi in a reclaimed poplar forest (*Populus yunnanensis*) in an abandoned metal mine tailings pond, Southwest China. *J. Hazard. Mater.* 448:130962. doi: 10.1016/j.jhazmat.2023.13096

Xu, Z. W., Pehlivan, N., Ghorbani, A., and Wu, C. (2023). Effects of *Azorhizobium caulinodans* and *Piriformospora indica* co-inoculation on growth and fruit quality of tomato (*Solanum lycopersicum* L.) under salt stress. *Horticulturae* 8:302. doi: 10.3390/horticulturae8040302

Yi, M., Jia, T., Dong, L. M., Zhang, L., Leng, C. H., Liu, S. Y., et al. (2021). Resin yield in *Pinus elliottii* Engelm. Is related to the resin flow rate, resin components and resin duct characteristics at three locations in southern China. *Ind. Crop. Prod.* 160:113141. doi: 10.1016/j.indcrop.2020.113141

Yin, J., Yuan, Z., and Li, T. (2021). The spatial-temporal variation characteristics of natural vegetation drought in the Yangtze River source region, China. *Int. J. Environ. Res. Public Health* 18:1613. doi: 10.3390/ijerph18041613

Zahra, S. T., Tariq, M., Abdullah, M., Azeem, F., and Ashraf, M. A. (2023). Dominance of *Bacillus* species in the wheat (*Triticum aestivum* L.) rhizosphere and their plant growth promoting potential under salt stress conditions. *Peer J.* 11:e14621. doi: 10.7717/peerj.14621

Zapata-Valenzuela, J., Whetten, R. W., Neale, D., McKeand, S., and Isik, F. (2013). Genomic estimated breeding values using genomic relationship matrices in a cloned population of loblolly pine. *G3* 3, 909–916. doi: 10.1534/g3.113.005975

Zeng, M., Hause, B., van Dam, N. M., Uthe, H., Hoffmann, P., Krajinski, F., et al. (2022). The mycorrhizal symbiosis alters the plant defence strategy in a model legume plant. *Plant Cell Environ.* 45, 3412–3428. doi: 10.1111/pce.14421

Zhang, H., Liu, T., Zhang, Z., Payne, S. H., Zhang, B., McDermott, J. E., et al. (2016). Integrated proteogenomic characterization of human high-grade serous ovarian cancer. *Cell* 166, 755–765. doi: 10.1016/j.cell.2016.05.069

Zhang, H. R., and Stephanopoulos, G. (2016). Co-culture engineering for microbial biosynthesis of 3-amino-benzoic acid in *Escherichia coli*. *Biotechnol. J.* 11, 981–987. doi: 10.1002/biot.201600013

Zhao, X., Hume, S. L., Johnson, C., Thompson, P., Huang, J., Gray, J., et al. (2010). The transcription repressor NmrA is subject to proteolysis by three *aspergillus nidulans* proteases. *Protein Sci.* 19, 1405–1419. doi: 10.1002/pro.421

Zhao, X., Yuan, X., Xing, Y., Dao, J., Zhao, D., Li, Y., et al. (2023). A meta-analysis on morphological, physiological and biochemical responses of plants with PGPR inoculation under drought stress. *Plant Cell Environ.* 46, 199–214. doi: 10.1111/pce.14466

Zou, Y. N., Qin, Q. Y., Ma, W. Y., Zhou, L. J., Wu, Q. S., Xu, Y. J., et al. (2023). Metabolomics reveals arbuscular mycorrhizal fungi-mediated tolerance of walnut to soil drought. *BMC Plant Biol.* 23:118. doi: 10.1186/s12870-023-04111-3

Zuccaro, A., Lahrmann, U., and Langen, G. (2014). Broad compatibility in fungal root symbioses. *Curr. Opin. Plant Biol.* 20, 135–145. doi: 10.1016/j.pbi.2014.05.013

Zuo, Y. L., Hu, Q. N., Qin, L., Liu, J. Q., and He, X. L. (2022). Species identity and combinations differ in their overall benefits to *Astragalus adsurgens* plants inoculated with single or multiple endophytic fungi under drought conditions. *Front. Plant Sci.* 13:933738. doi: 10.3389/fpls.2022.933738

frontiers | Frontiers in Microbiology

TYPE Original Research
PUBLISHED 18 March 2024
DOI 10.3389/fmicb.2024.1358137

Check for updates

OPEN ACCESS

EDITED BY
Zhenlin Han,
University of Hawaii at Manoa, United States

REVIEWED BY
Taihe Xiang,
Hangzhou Normal University, China
Sakineh Abbasi,
Institut National de recherche pour l'agriculture, l'alimentation et l'environnement (INRAE), France
Zexin Jin,
Taizhou University, China

*CORRESPONDENCE
Xiaofeng Liao
lxfnsd@163.com

†These authors have contributed equally to this work and share first authorship

RECEIVED 19 December 2023
ACCEPTED 06 March 2024
PUBLISHED 18 March 2024

CITATION
Tian F, Wang J, Ding F, Wang L, Yang Y, Bai X, Tan C and Liao X (2024) Comparative transcriptomics and proteomics analysis of the symbiotic germination of *Paphiopedilum barbigerum* with *Epulorhiza* sp. FQXY019. *Front. Microbiol.* 15:1358137. doi: 10.3389/fmicb.2024.1358137

COPYRIGHT
© 2024 Tian, Wang, Ding, Wang, Yang, Bai, Tan and Liao. This is an open-access article distributed under the terms of the Creative Commons Attribution License (CC BY). The use, distribution or reproduction in other forums is permitted, provided the original author(s) and the copyright owner(s) are credited and that the original publication in this journal is cited, in accordance with accepted academic practice. No use, distribution or reproduction is permitted which does not comply with these terms.

Comparative transcriptomics and proteomics analysis of the symbiotic germination of *Paphiopedilum barbigerum* with *Epulorhiza* sp. FQXY019

Fan Tian[1,2†], Juncai Wang[3†], Fangjun Ding[1,2], Lianhui Wang[1,2], Yanbing Yang[1,2], Xinxiang Bai[4], Chengjiang Tan[5] and Xiaofeng Liao[3*]

[1]Guizhou Academy of Forestry, Guiyang, Guizhou, China, [2]Key Laboratory for Biodiversity Conservation in the Karst Mountain Area of Southwestern China, National Forestry and Grassland Administration, Guiyang, Guizhou, China, [3]Guizhou Academy of Sciences, Guiyang, Guizhou, China, [4]College of Forestry, Guizhou University, Guiyang, Guizhou, China, [5]Guizhou Maolan National Nature Reserve Administration, Libo, Guizhou, China

Introduction: *Paphiopedilum barbigerum* is currently the rarest and most endangered species of orchids in China and has significant ornamental value. The mature seeds of *P. barbigerum* are difficult to germinate owing to the absence of an endosperm and are highly dependent on mycorrhizal fungi for germination and subsequent development. However, little is known about the regulation mechanisms of symbiosis and symbiotic germination of *P. barbigerum* seeds.

Methods: Herein, transcriptomics and proteomics were used to explore the changes in the *P. barbigerum* seeds after inoculation with (FQXY019 treatment group) or without (control group) *Epulorhiza* sp. FQXY019 at 90 days after germination.

Results: Transcriptome sequencing revealed that a total of 10,961 differentially expressed genes (DEGs; 2,599 upregulated and 8,402 downregulated) were identified in the control and FQXY019 treatment groups. These DEGs were mainly involved in carbohydrate, fatty acid, and amino acid metabolism. Furthermore, the expression levels of candidate DEGs related to nodulin, Ca^{2+} signaling, and plant lectins were significantly affected in *P. barbigerum* in the FQXY019 treatment groups. Subsequently, tandem mass tag-based quantitative proteomics was performed to recognize the differentially expressed proteins (DEPs), and a total of 537 DEPs (220 upregulated and 317 downregulated) were identified that were enriched in processes including photosynthesis, photosynthesis-antenna proteins, and fatty acid biosynthesis and metabolism.

Discussion: This study provides novel insight on the mechanisms underlying the *in vitro* seed germination and protocorm development of *P. barbigerum* by using a compatible fungal symbiont and will benefit the reintroduction and mycorrhizal symbiotic germination of endangered orchids.

KEYWORDS

***Paphiopedilum barbigerum*, mycorrhizal fungi, symbiotic germination, transcriptome, proteome**

1 Introduction

The *Orchidaceae* is one of the largest and most diverse families of flowering plants in the world, with >28,000 accepted species across 800 genera (Chao et al., 2014; Zhao et al., 2021). Orchids are considerably valuable from ecological, ornamental, medical, and evolutionary perspectives (Zhang et al., 2018; Yang et al., 2020). *Paphiopedilum* is one of the most primordial genera of Orchidaceae, which includes 107 species so far. Members of this genus have considerable horticultural value and development potential (Huang et al., 2016; Fang et al., 2021). The *Paphiopedilum* orchids are generally known as the Lady's slipper orchid owing to their slipper-shaped pouch (Tsai et al., 2020). They are extremely popular and highly valued in the horticulture market because of their unique flowers that have abundant colors, shapes, and sizes and long floral lifespan (Tsai et al., 2020; Fang et al., 2021). Unfortunately, members of this genus are endangered with their population severely declining in recent decades owing to the native habitat loss, rampant smuggling, and over-collection (Fang et al., 2021). To conserve these endangered species, the Convention on International Trade in Endangered Species of Wild Fauna and Flora (CITES) placed all *Paphiopedilum* species on the conservation list in 2017 to ban illegal trade (Yang et al., 2020). Furthermore, the mature *Paphiopedilum* seeds are very small, have few nutrient reserves, and lack an endosperm and are consequently difficult to germinate under natural conditions, making them particularly vulnerable to extinction (Zhang et al., 2018; Mujica et al., 2021). Therefore, the *Paphiopedilum* seed germination requires investigation, which is important for appropriately utilizing and conserving species resources.

The traditional propagation of *Paphiopedilum* orchids using an axillary bud division from the mother plant is unproductive and time-consuming (Chen et al., 2004). Many *Paphiopedilum* seeds form a compatible and symbiotic relationship with mycorrhizal or endophytic fungi that facilitates their germination in conditions of their natural habitat (Xu et al., 2020; Li Y. Y. et al., 2021). During this process, regarded as symbiotic germination, fungi and seeds form a nonphotosynthetic spherical body named a protocorm, which completely relies on mycorrhizal fungi for nourishment (Fang et al., 2021). Therefore, symbiotic germination can be used as an ordinary and efficient approach for promoting the germination and the large-scale propagation of *Paphiopedilum* (Chen et al., 2004). Several studies have found that mycorrhizal fungi can provide carbon and nitrogen sources, amino acids, and other nutrients as well as metabolic regulatory substances such as hormones for the seed germination of *Paphiopedilum* plants, whereas the plants provide carbohydrates for the mycorrhizal fungi (Fochi et al., 2017; Mujica et al., 2021; Zhao et al., 2021). Furthermore, the existence of compatible mycorrhizal fungi in *Paphiopedilum* seedlings enhances the adaptability of plants to the environment to increase plant survival and growth rate (Zhang et al., 2018). However, *Paphiopedilum* seedlings do not simply form a symbiotic relationship with any fungus, and germination can only happen when an appropriate fungus is present (Pujasatria et al., 2020), which includes *Tulasnellaceae*, *Ceratobasidiaceae*, *Serendipitaceae*, *Mycena*, *Helicogloea*, *Fusarium*, or other fungi (Xu and Guo, 1989; Kottke et al., 2010; Sebastián et al., 2014; Jiang et al., 2019). Understanding the interaction between *Paphiopedilum* and mycorrhizal fungi is a significant for generative reproduction, augmenting existing populations, and maintaining species diversity in orchids (Yang et al., 2020). Currently, research on the interaction between mycorrhiza and *Paphiopedilum* plants mainly includes promoting seed germination, growth and development, nutrient absorption, improving stress resistance of plants and the symbiotic relationship (Gao et al., 2022; Tian et al., 2023; Xu et al., 2023; Yang H. et al., 2023; Yang J. X. et al., 2023), whereas the molecular regulation mechanism of the interaction underlying the symbiotic relationship need further investigation.

In recent decades, understanding of the symbiotic interaction mechanism between mycorrhizal fungi and orchids has entered a new era with the development of next-generation sequencing and multi-omics technologies (Chen et al., 2018, 2022; Ahmad et al., 2022a). Multi-omics technology (i.e., transcriptomics, proteomics, and metabolomics) has become an effective method of exploring the orchid-fungus relationship (Balilashaki et al., 2019). For example, Fochi et al. (2017) used transcriptomics analysis to identify two functional ammonium transporters and several amino acid transporters involved in nitrogen uptake and transfer to host plants by the orchid mycorrhiza fungus *Tulasnella calospora*. Ghirardo et al. (2020) applied untargeted metabolomics to report that many metabolites, especially lipid compounds, were significantly altered during the symbiotic relationship between the Mediterranean orchid *Serapias vomeracea* and the basidiomycete *T. calospora*. In addition, Chen et al. (2018) used proteomic analysis to identify 42 proteins associated with antioxidant pathways, protein metabolism, and energy metabolism in *Phalaenopsis*. Hence, the multi-omics techniques are regarded as a promising approach for exploring the molecular mechanisms of the symbiotic relationship between mycorrhizal fungi and orchids.

Herein, we investigated the germination of *P. barbigerum,* a rare *Paphiopedilum* native to southwest China with high ornamental value, in the presence of a mycorrhizal fungus, *Epulorhiza* sp. FQXY019, which we had previously isolated and which progressed seed germination of *P. barbigerum* (Tian et al., 2022). Based on this, we integrated transcriptomics analyses with proteomic techniques to investigate the genes and proteins differentially expressed in the seed germination of *P. barbigerum* with and without Epulorhiza sp. FQXY019 inoculation. Thus, this study aimed to (1) reveal the transcriptional changes in the major metabolic pathways, and (2) investigate the differences in the proteomic profiles of *P. barbigerum* inoculated and uninoculated *Epulorhiza* sp. FQXY019. We hypothesized that: FQXY019 would induce the different biological and metabolic pathways of the *P. barbigerum* seed germination, and activate numerous responsive genes and proteins involved in molecular pathways at transcriptomic and proteomic level. The results will provide a theoretical basis for further elucidating the molecular regulation mechanism of the symbiotic relationship between orchids and mycorrhizal fungi as well as for the propagation and conservation of orchids.

2 Materials and methods

2.1 *Paphiopedilum barbigerum* seed collection and growth of the free-living mycelium

In January 2021, the mature and well-grown fruit capsules were collected from *P. barbigerum* plants in the greenhouse of the Institute of Biotechnology, Guizhou Academy of Forestry. Capsules were

desiccated at room temperature and stored in a glass vessel at 4°C until sowing. *Epulorhiza* sp. FQXY019 had been isolated from the mycorrhizal roots of *P. barbigerum* in our previous study (Tian et al., 2022). First, a layer of cellophane was placed onto 9 cm Petri dishes containing 30 mL potato dextrose agar (PDA) medium (200 g potato, 10 g agar, 20 g glucose, and 1 L distilled water). *Epulorhiza* sp. FQXY019 was then inoculated onto the cellophane. After 2 weeks of culture, the healthy mycelium of the fungus filled the Petri dishes and was used for the symbiotic seed germination assay.

2.2 Symbiotic and asymbiotic germination of *Paphiopedilum barbigerum* seeds

Capsules of *P. barbigerum* were surface sterilized in 70% ethanol for 30 s, and shook for 6 min in 0.1% mercuric chloride, before being washed five times with sterile distilled water (Tian et al., 2022). Subsequently, the fruit capsules were cut with a sterile scalpel and forceps, gently shaken, and approximately 100 seeds were evenly sown on *Epulorhiza* sp. FQXY019 mycelium for symbiotic germination testing as the FQXY019-treatment group. Symbiotic seed germination was obtained by placing surface-sterilized seeds directly on PDA culture medium without *Epulorhiza* sp. FQXY019 as the control group (CK). Each treatment had 30 plates, which represented three replicates. The average temperature of culture was 25/20°C (darkness/light), light intensity was 1,200 lux, and day/night photoperiod was 18/6 h (Meng et al., 2020; Tian et al., 2022). Symbiotic and asymbiotic plants were collected after culturing for 90 days. At this point, the seeds had germinated, and the seedlings had two or three leaves. Sampling (the whole seedling) was performed after 90 days of culture because we had previously found that the seeds of *P. barbigerum* inoculated with *Epulorhiza* sp. FQXY019 can further develop, and rooting occurred after 90 days of culture (Tian et al., 2022). The figures of plant growing with and without *Epulorhiza* sp. FQXY019 was showed in Supplementary Figure S1. Three biological replicates were collected for each experimental group. All samples were quickly flash-frozen in liquid nitrogen and stored at −80°C for further analysis.

2.3 RNA extraction, sequencing, and *de novo* assembly

Total RNA was extracted from approximately 200 mg of frozen *P. barbigerum* plant samples of each treatment using prechilled RNA extraction Kit (TIANGEN, No DP411, in China) following the manufacture's protocols (Ahmad et al., 2022a). The extracted RNA concentration and purity were assessed using a spectrophotometer (NanoDrop 2000, Thermo Fisher Scientific), and the integrity of RNA was assessed using an Agilent Bioanalyzer 2,100 system (Agilent Technologies, USA) (Mumtaz et al., 2022). Three separate libraries were prepared from three biological replicates per treatment. An RNA integrity number > 8.0 was selected to construct the sequencing library. cDNA libraries were constructed using the TruSeq™ RNA sample prep kit (Illumina, San Diego, USA) following the manufacturing specification after mRNA was isolated from total RNA using oligo (dT) magnetic beads and broken randomly into numerous fragments. Subsequently, sequencing was performed using an NovaSeq 6,000 platform by Beijing Biomarker Technologies Co., Ltd. To obtain high-quality clean reads, the remaining adapters, ploy-N, and low-quality value raw reads were eliminated (Ahmad et al., 2022a). High-quality clean reads were further *de novo* assembled using Trinity software. The unigenes were annotated in accordance with the NR, GO, KEGG, KOG, Pfam, SwissProt, TrEMBL, and eggNOG databases. The raw data of transcriptomics were available in the NCBI under accession PRJNA868469.

2.3.1 Differential expression genes and enrichment analysis

Gene expression levels were assessed using the fragments per kilobase per transcript per million mapped reads (FPKM). To consider the correlation of gene expression levels between control and treatment group samples, Pearson's correlation coefficient was evaluated. Screening standards for differentially expressed genes (DEGs) were $|\log2(\text{fold change, FC})| > 1$ and false discovery rates (FDR) < 0.01 (Li P. et al., 2021). DEGs were identified utilizing the DEseq R package. To deduce the supposed function of DEGs, we performed GO enrichment analysis and KEGG pathway analysis using the topGO R package and KOBAS software, respectively.

2.3.2 qRT-PCR validation

To confirmation the accuracy of RNA-seq data, 12 DEGs were randomly chosen for qRT-PCR validation. Primers were designed via Primer Premier version 5.0 and are listed in Supplementary Table S1. qRT-PCR was performed as reported by Li P. et al. (2021). The calculation method of $2^{-\Delta\Delta Ct}$ was employed for the relative expression level of genes. Three biological replicates were measured per gene, and actin was used as a reference gene.

2.4 Proteomic extraction and tandem mass tag quantification

Plant material protein isolation and Tandem Mass Tag (TMT) label-based proteome analyzes were conducted by Beijing Biomarker Technologies Co., Ltd. The proteins of *P. barbigerum* were extracted as described by Hao et al. (2017) and Zhu et al. (2021). Briefly, frozen samples were ground into a fine powder under liquid nitrogen. Then, the powder was transferred into a centrifuge tube and sonicated on ice three times in lysis buffer of 8 M urea, 2 mM EDTA, 10 mM dithiothreitol (DTT), and 1% protease inhibitor cocktail. The sediment was pelleted by centrifugation at 12,000 × *g* for 20 min. The protein in the supernatant was deposited with 15% precooled TCA buffer for 2 h at −20°C. The supernatant was removed, and then residual sediment was rinsed with cold acetone. Finally, the protein was redissolved in 8 M urea/100 mM tetraethylammonium bromide buffer (pH 8.0). The amount of protein in each sample was measured via the Bradford method and examined by sodium dodecyl sulfate polyacrylamide gel electrophoresis.

The protein sample was reduced with 10 mM DTT for 1 h at 37°C followed by an alkylation reaction at room temperature for 45 min by incubation in 40 mM iodoacetamide without light. Subsequently, the protein solution was diluted with 100 mM TEAB to a urea concentration of <2 M. Trypsin was added at a ratio of 1:50 (enzyme: protein, w/w) for the first digestion overnight and then was secondly digested for 4 h at a ratio of 1:100. After digestion, the protein samples were peptide desalted using a Strata X C18 SPE column and vacuum

dried. The peptide was reconstituted with 0.5 M TEAB in accordance with the manufacturer's protocol for the TMT kit (Thermo-Scientific, United States). Briefly, one unit of TMT reagent was reconstituted in acetonitrile. The peptide mixtures were incubated at room temperature for 2 h, and merged, desalted, and dried by vacuum centrifugation (Grosjean et al., 2022).

2.4.1 HPLC fractionation and LC–MS/MS analysis

The sample was fractionated and purified using high-pH reverse-phase HPLC via an Agilent Zorbax 300Extend-C18 column (250 × 4.6 mm, 5-mm particles). Peptides were divided into eighty fractions over 80 min using a 2–60% acetonitrile gradient in 10 mM ammonium bicarbonate (pH 10). Peptides were collected into 18 fractions and dried via vacuum centrifugation (Jian et al., 2020).

Peptide samples were redissolved in 0.1% formic acid (FA, buffer A) and then loaded onto an EASY-nLC 1,000 UPLC system (Thermo-Scientific, USA) equipped with an Agilent Zorbax 300Extend-C18 column as above. Peptides were eluted with a linear gradient from 7 to 26% solvent B (1% FA in 98% acetonitrile) for 22 min, 26 to 40% in 12 min and 40 to 80% in 3 min, then remaining at 80% for the last 3 min, at a flow rate of 400 nL/min. Target peptides were analyzed using mass spectrometry (MS/MS) with a Q Exactive™ Plus (Thermo-Scientific, USA) with a Nanospray Flex™ (NSI) source. The electrospray voltage applied was 2.4 kV. Full-scan MS spectra (m/z 400–1,500) were examined in an Orbitrap at a mass resolution of 60,000 at m/z 200. A data-dependent procedure was conducted with 15-s dynamic exclusion of one MS scan followed by 20 MS/MS scans. Automatic gain control (AGC) was set as 3e6. After the full scan, the top 40 intense precursor ions were chosen for MS2 analysis at a resolution of 17,500 at m/z 200. The MS2 activation type was higher-energy collisional dissociation, normalized collision energy was 30 eV; AGC was set as 5e4. The obtained MS/MS data were evaluated with the Maxquant search engine (v.1.5.2.8). Multiple *p* values were controlled to a FDR of 1%. Protein quantification analysis was conducted on at least two unique peptides, and protein confidence was set at a 95% confidence interval (Jian et al., 2020; Zhou et al., 2022).

2.4.2 Bioinformatics analysis

DEPs were identified using the thresholds of |log2(fold change, FC)| > 1 and *p*-value <0.05 in three biological replicates. The relative expression of the studied proteins was utilized to perform hierarchical clustering analysis by Cluster 3.0. GO functional annotation of the proteome was derived from the UniProt-GOA database using the Blast2GO program. DEPs were divided into three categories: BP, CC, and MF based on GO terms. The KEGG database was used to categorize these screened protein species via Blastx/Blastp 2.2.24 software. Then, the pathway enrichment of GO and KEGG of the DEPs was conducted using the Fisher' exact test, and pathways with a p-value <0.05 were considered significant (Peng et al., 2019; Yu et al., 2019).

3 Results

3.1 Transcriptome assembly

Three independent replicates of *P. barbigerum* in the control (CK) and FQXY019 treatment groups were analyzed via RNA-seq to reveal the potential symbiosis mechanism. The number of clean reads generated from a total of six libraries (three repeats per treatment) ranged from 22,375,505 to 24,054,439, with a GC content >47.86%; the percentage of Q20, Q30. and mapped ratio value was more than 97.77, 93.77, and 73%, respectively (Supplementary Table S2). After assembling the high-quality reads, the total number of transcripts and unigenes were 175,386 and 100,136 with a mean length of 1071.96 and 800.22 bp and an N50 length of 1842 and 1,577 bp, respectively (Supplementary Table S3). Overall, these results illustrated the high quality of the RNA-Seq data and practicability for further analysis.

All 40,742 unigenes were annotated via eight public databases, and 39,850 (97.81%), 30,367 (74.53%), 23,334 (57.27%), 20,217 (49.62%), 24,422 (59.94%), 20,781 (51.01%), 36,768 (90.25%), and 30,161 (74.03%) unigenes were successfully annotated to known proteins in the National Centre for Biotechnology Information (NCBI) non-redundant protein sequences (NR), Gene Ontology (GO), Kyoto Encyclopedia of Genes and Genomes (KEGG), eukaryotic Orthologous Groups (KOG), Protein family (Pfam), Swiss-prot protein Sequence (Swiss-Prot), TrEMBL, and Evolutionary Genealogy of Genes: Nonsupervised Orthologous Groups (eggNOG) databases, respectively (Supplementary Table S4). The homologous species distribution analysis showed that 29.49% of annotated unigenes were matched with *Dendrobium catenatum*, in the *Orchidaceae* family (Supplementary Figure S2). This result implied that some gene sequence results of *D. catenatum* could be used as reference in the further study of the molecular mechanism of the symbiotic germination of *P. barbigerum* seeds as *P. barbigerum* is a reference-free genome plant. In addition, since these two plants belong to different genera, many unknown functional genes may be present in *P. barbigerum* that are different from those in *D. catenatum* and need further exploration.

A correlation coefficient (R^2) of biological samples between 0.8 and 1 is a strong correlation relationship ($p < 0.05$), and when R^2 is <0.8, the correlation relationship between samples is low. In the case of the gene expression patterns in each treatment, the R^2 among the three replicates was >0.9, implying a remarkably high correlation (Figure 1A). Meanwhile, principal component analysis (PCA) suggested that the expression of gene clusters in the control and inoculation treatments was distinguishable, indicating a distinct responsive effect of *Epulorhiza* sp. FQXY019 inoculation on the gene expression patterns (Figure 1B).

3.2 Identification and enrichment analysis of DEGs

To identify DEGs in the two groups, we used a pairwise comparison. As shown in Figure 2, a total of 10,961 DEGs (2,599 upregulated and 8,402 downregulated) was identified in CK compared with expression in the FQXY019-treatment group (Supplementary Table S5). Subsequently, we annotated these DEGs using the GO database to investigate their functions. According to GO enrichment, a total of 6,828 DEGs were enriched to 57 GO terms, including 22, 20, and 15 terms in biological process (BP), cellular component (CC), and molecular function (MF), respectively (Figure 3A). Among them, the metabolic, cellular, and single-organism processes were the top three subcategories in BP; cell, cell part, and organelle were the top three subcategories in CC; and

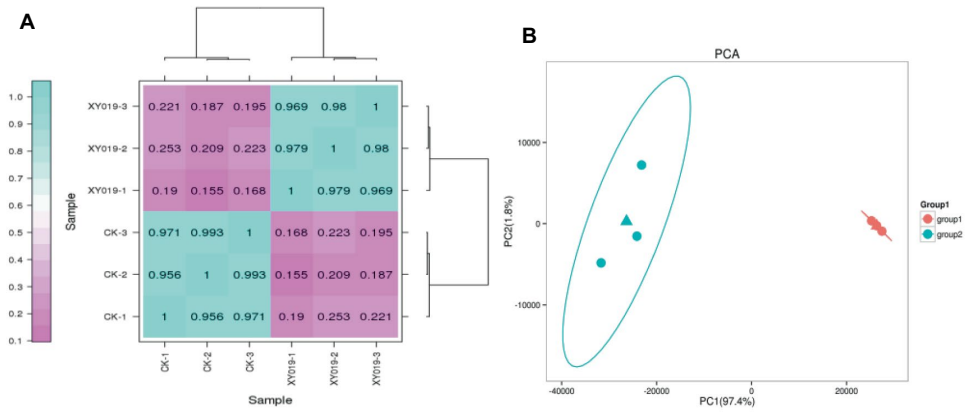

FIGURE 1
(A) Correlation analysis of the gene expression patterns in the FQXY019 treatment and CK groups. **(B)** Principal component analysis (PCA) of FPKM profiles in the FQXY019 treatment groups (group 1) and CK (group 2). The deeper the blue represents the stronger the positive correlation, and the deeper the purple the weaker the positive correlation **(A)**. The blue and orange triangles represent the average coordinates of the three groups **(B)**.

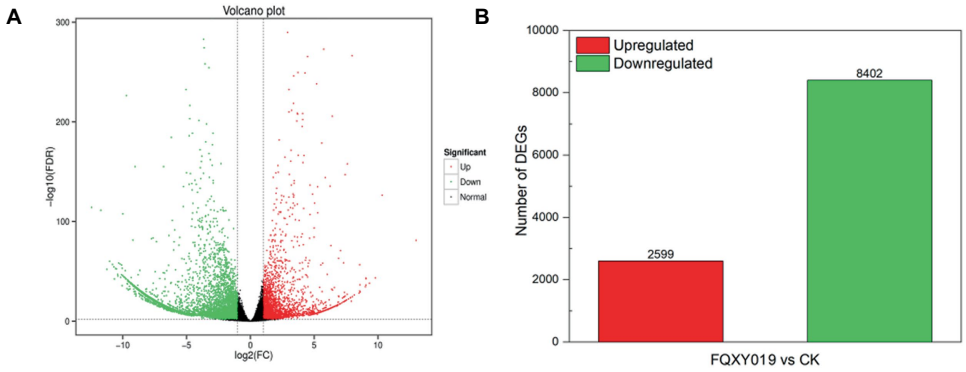

FIGURE 2
Differentially expressed genes (DEGs) for FQXY019 treatment groups vs. control (CK). **(A)** Volcano plot and **(B)** histogram; the number of up- and downregulated genes are represented by red and green, respectively.

binding, catalytic activity, and transporter activity were the top three subcategories in MF (Figure 3A). Therefore, the DEGs between the two treatment groups were mainly involved in these processes, revealing that inoculation had an effect on these pathways.

To reveal the biological functions and associated pathways of DEGs in *Epulorhiza* sp. FQXY019-induced symbiotic relationships, KEGG enrichment analysis was performed. Most DEGs were mainly annotated in metabolic pathways (Figures 3A–C; Supplementary Figure S3 and Supplementary Table S6), indicating that these pathways are important for symbiotic germination of *P. barbigerum* seeds. The top three most significant KEGG pathways were glycolysis/gluconeogenesis, starch and sucrose metabolism, and phenylpropanoid biosynthesis in upregulated DEGs in CK, compared with the FQXY019 treatment group (Figure 3B; Supplementary Figures S4–S6). The DEGs involved in glycolysis/gluconeogenesis, such as *PFK, PFP, PDC, PGAM*, etc. were significantly upregulated, but the DEGs (*FBA, PDHA, DLD, FBP*, etc.) were downregulated in the FQXY019 treatment. The DEGs (*ISA, WAXY, E 2.4.1.14, etc*) related to starch and sucrose metabolism were significantly upregulated and the DEGs (*GYG1, SUS, INV, ENPP1, etc*) were downregulated in the FQXY019 treatment. The genes (*CCR, 4CL, CAD, COMT*, etc.) of phenylpropanoid biosynthesis were significantly upregulated, and the genes (*4CL, HCT, CCR*, etc.) were significantly downregulated in the FQXY019 treatment relative to CK treatment (Supplementary Figures S4–S6). By contrast, the mannose type O-glycan biosynthesis, porphyrin and chlorophyl II metabolism, and fatty acid elongation pathways were ranked the top three significantly enriched pathways in downregulated DEGs in CK compared with that in the FQXY019 treatment group (Figure 3C; Supplementary Figures S7–S9). In addition, the largest number of upregulated DEGs was in amino acid biosynthesis, carbon metabolism, and plant hormone signal transduction, whereas the largest number of downregulated DEGs was in carbon metabolism and ribosome and amino acid biosynthesis. This suggests that the inoculation of FQXY019 affected the growth of seedlings by regulating metabolic pathways, including those of carbon and amino acid metabolism. In summary, these results imply that carbohydrate, fatty acid, and amino acid metabolism are the main physiological activity pathways used to maintain the stability of symbiotic relationships during the germination of *P. barbigerum* seeds.

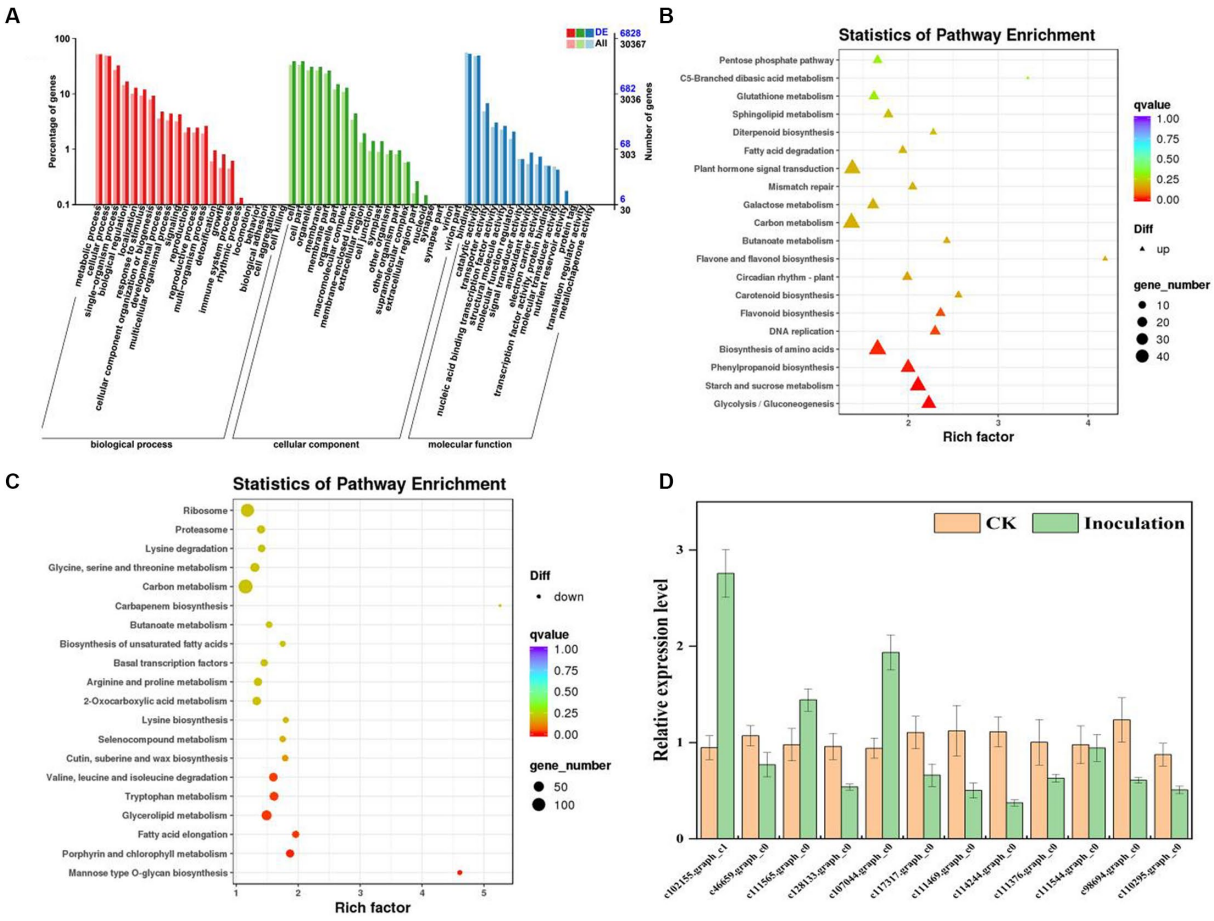

FIGURE 3
Graphical representation of significantly enriched pathways. **(A)** GO enrichment analysis of DEGs for FQXY019 treatment groups vs. CK. The bubble diagram shows the top 20 significant enriched pathways in the upregulated **(B)** and downregulated **(C)** DEGs for FQXY019 treatment groups vs. CK obtained via KEGG analysis. **(D)** qRT-PCR validation of DEG results. Values of qRT-PCR are mean ± SD (n = 3). Bars indicate SD. The detailed primer information is shown in Supplementary Table S1. The X-axis was the rich factor, which was the ratio of the DEG number to the total gene number in a certain pathway; the Y-axis represents the name of the pathway. The bubble size represents the number of DEGs involved. The bubble color indicates the enrichment degree of the pathway.

3.3 Validation of the DEG results via qRT-PCR analysis

To validate the reliability of the transcriptome results, we randomly selected 12 DEGs and examined them by qRT-PCR. According to the qRT-PCR analysis, the expression trends of 12 DEGs except in two DEGs (c46659.graph_c0 and c128133.graph_c0) were consistent with those obtained via transcriptome analysis (Figure 3D). The qRT-PCR results demonstrated that the transcriptome results were reliable and suitable for subsequent analysis.

3.4 Protein identification and comparison

To determine and identify up- or downregulated proteins in the *P. barbigerum* proteome inoculated with *Epulorhiza* sp. FQXY019 mycelium, we performed tandem mass tag (TMT) quantitative proteomic profiling of 90-day-old *P. barbigerum* seedlings in the CK and FQXY019 treatment groups, each with three biological replicates. After the combination of the two treatments of samples, 2,614 proteins were identified and quantified (Supplementary Table S10). Pairwise comparison of proteins with the criteria of a $|\log2(\text{fold change, FC})| > 1$ and a p-value <0.05 were screened as differentially expressed proteins (DEPs, Figure 4A). As shown in Figure 4B, 537 DEPs (220 upregulated and 317 downregulated) were detected in CK compared with the FQXY019 treatment group.

3.5 Hierarchical clustering and enrichment analysis of DEPs

We conducted a hierarchical clustering analysis of the DEPs in different treatments to explore the similarity between them. Each of the three replicates of the FQXY019 treatment groups and CK samples were clustered together independently and had high repeatability (Figure 4C). The protein abundance and the diversity of expression levels were markedly different between the FQXY019 treatment groups and the CK sample. PCA also showed similar results (Supplementary Figure S10).

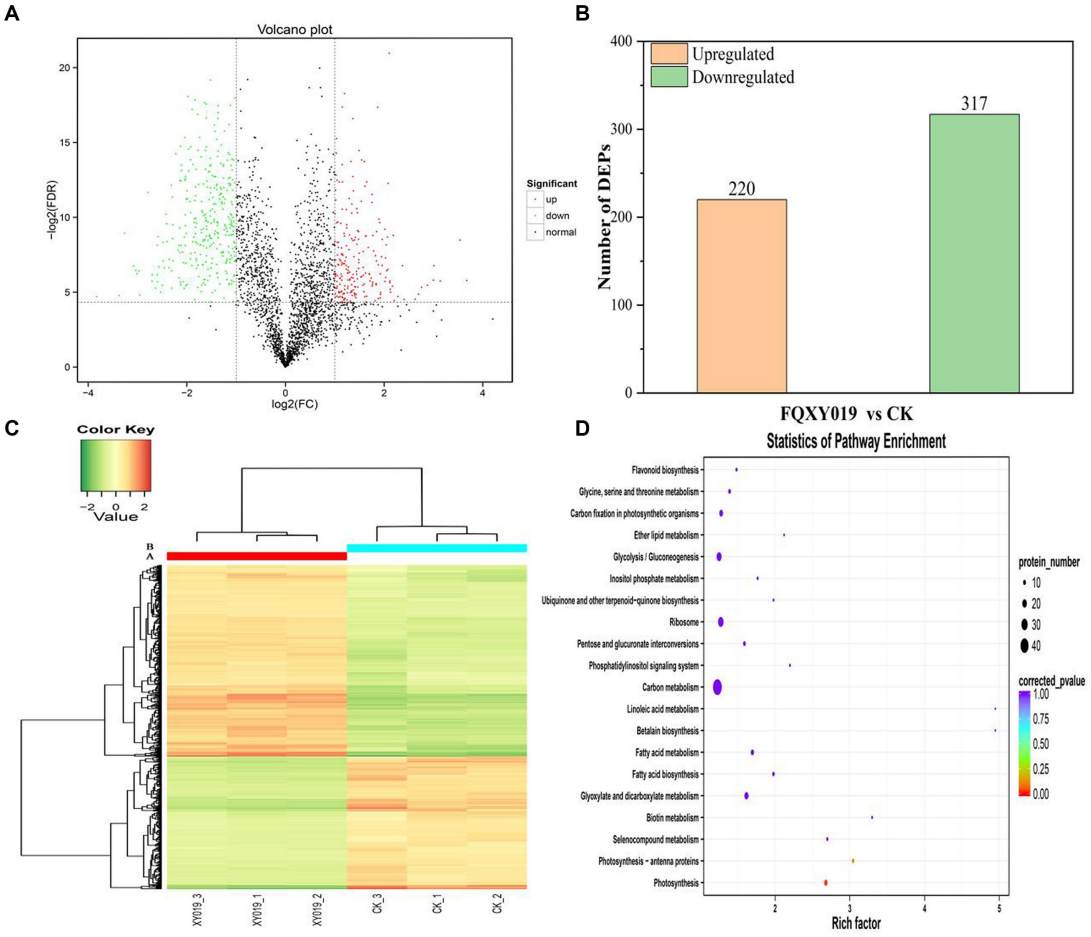

FIGURE 4
Differentially expressed proteins (DEPs) for FQXY019 treatment groups vs. control (CK). **(A)** Volcano plot and **(B)** histogram; the number of up- and downregulated genes are represented by red and green, respectively. **(C)** Hierarchical clustering analysis of the DEPs in different treatments. CK was the control treatment and FQXY019 was the inoculation treatment. Blue represents the CK, and red represents the FQXY019 treatment groups. **(D)** Bubble diagram showing the top 20 pathways with significant enrichment of DEPs for FQXY019 treatment groups and CK on KEGG pathway analysis. The X-axis was the rich factor, which was the ratio of the DEP number to the total protein number in a certain pathway; the Y-axis represents the name of the pathway. The bubble size represents the number of DEPs involved. The color of the circle represents *p*-value, which indicates the enrichment degree of the pathway.

3.6 Go and KEGG analysis of DEPs

To investigate the biological function of the DEPs, enrichment-based functional annotation was employed. GO functional annotation was performed on these DEPs, and 486 DEPs were successfully enriched into three categories including BP, CC, and MF. In the category of BP, the top three GO terms were metabolic process, cellular process, and single-organism process (Supplementary Figure S11a); the cell, cell part, and organelle were the largest subcategories in the CC category (Supplementary Figure S11b); and the top three GO terms were catalytic activity, binding, and structural molecule activity in MF analysis, respectively (Supplementary Figure S11c). Photosynthesis (BP), chloroplast thylakoid membrane (CC), and chlorophyl II binding (MF) were the most significantly enriched terms in these three processes (Supplementary Figure S11).

Proteins cannot accomplish their functions independently in an organism, and different proteins must coordinate with each other to achieve a series of biochemical reactions to conduct their biological functions. We therefore performed KEGG pathway enrichment analysis to help us understand how these DEPs were related to metabolism or signaling pathways and to reveal the biological functions and effect factors involved in the process. The DEPs were involved in 102 metabolic pathways, of which the top 20 pathways are shown in Figure 4D, including carbon metabolism, photosynthesis, amino acid biosynthesis, and fatty acid metabolism. Notably, the DEPs were primarily involved in metabolic pathways (Supplementary Figure S12); and the photosynthesis and photosynthesis-antenna proteins pathways were significantly enriched (Figures 4D, 5, 6). The DEPs (*PsaA, PsaD, PsaK, PsaF, etc*) related to photosynthesis I pathway and the DEPs (*PsbA, PsbO, PsbQ, Psb27, etc*) related to photosynthesis II pathway were significantly downregulated in the FQXY019 treatment compared with the CK treatment. The DEPs (*Lhca1, Lhca3, Lhcb1, Lhcb2*, etc.) involved in light-harvesting chlorophyl II protein complex pathway was significantly downregulated. These results indicating that

symbiosis with *Epulorhiza* sp. FQXY019 could affect seed germination and seedling growth via changing the photosynthesis of *P. barbigerum*.

4 Discussion

In this work, a combined transcriptomics, and proteomics analysis was performed to explore the symbiotic interaction of *P. barbigerum* inoculated and uninoculated *Epulorhiza* sp. FQXY019. Lots of DEGs were obtained using transcriptome sequencing during *P. barbigerum* seeds germination. The proteome changes, which were based on TMT labeling-based proteome quantification, also identified a large number of DEPs. Our study demonstrated that symbiosis induced substantial genes and proteins alterations, and regulate growth and development in *P. barbigerum* with FQXY019 (Figure 7). Several studies have proved that the beneficial relationship of carbon exchange in symbionts affects the nutritional balance between fungi and host plants (Li Y. Y. et al., 2021; Zhao et al., 2021). Fungi need to acquire carbohydrates from host plants, thereby regulating nutrient transport to play a dominant role in symbiosis (Vives-Peris et al., 2020). As they lack a mature endosperm, orchid seeds contain only a small amount of carbohydrates as a source of nutrients and need mycorrhizal fungi mycelium to obtain carbohydrates (Zhang et al., 2018; Zhao et al., 2021). However, to adapting to the environment and orchid metabolism, mycorrhizal fungi regulate their carbon and amino acid metabolism and improve their adaptability and survival competitiveness (Zhao et al., 2021).

4.1 Transcriptomic analysis

4.1.1 Expression of nodulin-related genes

Nodulation genes are mainly involved in the formation and structural maintenance of nodules, protection of nitrogen fixation activity, and metabolism of nitrogen fixation products in nodule plants, especially in the establishment of the relationship between orchids and mycorrhizal fungi and the development of protocorm symbionts (Zhang et al., 2022). However, these genes not only play a role in nodulation but also in other developmental stages of plants. Several studies reported that nodulation genes and their encoded proteins are activated and actively expressed after arbuscular mycorrhizal fungi infection in plants (Wang et al., 2016; Ghirardo et al., 2020). These genes belong to the phytocyanin family of type I, and the expression products of this family are characterized by binding to type I copper ions and participate in the electron transfer process of the plant–microorganism interaction, plant cell growth, and development (Denance et al., 2014). We identified 17 genes that encoded proteins with a plastocyanin-like domain, which were predicted to be phytocyanin family genes, and one gene that encoded

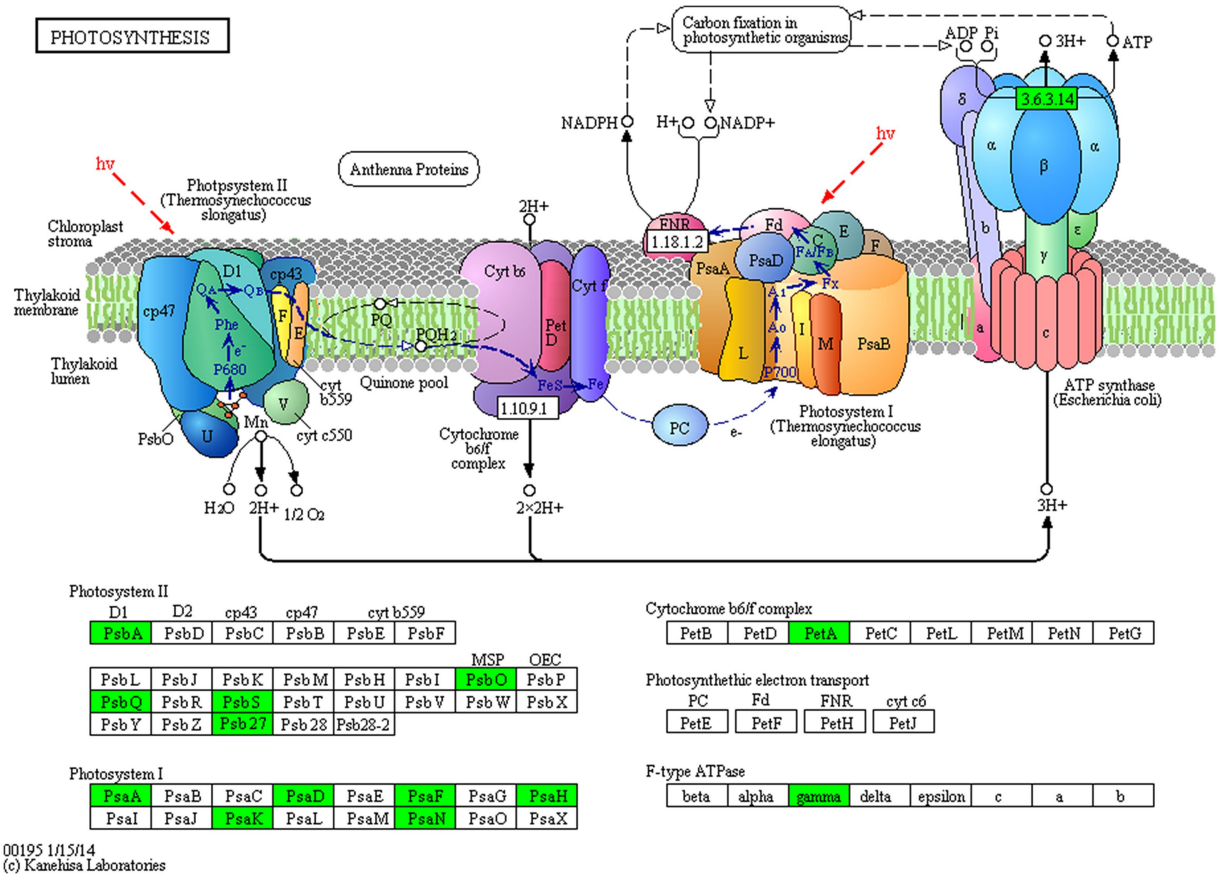

FIGURE 5
The expression levels of common DEPs in *P. barbigerum* involved in photosynthesis.

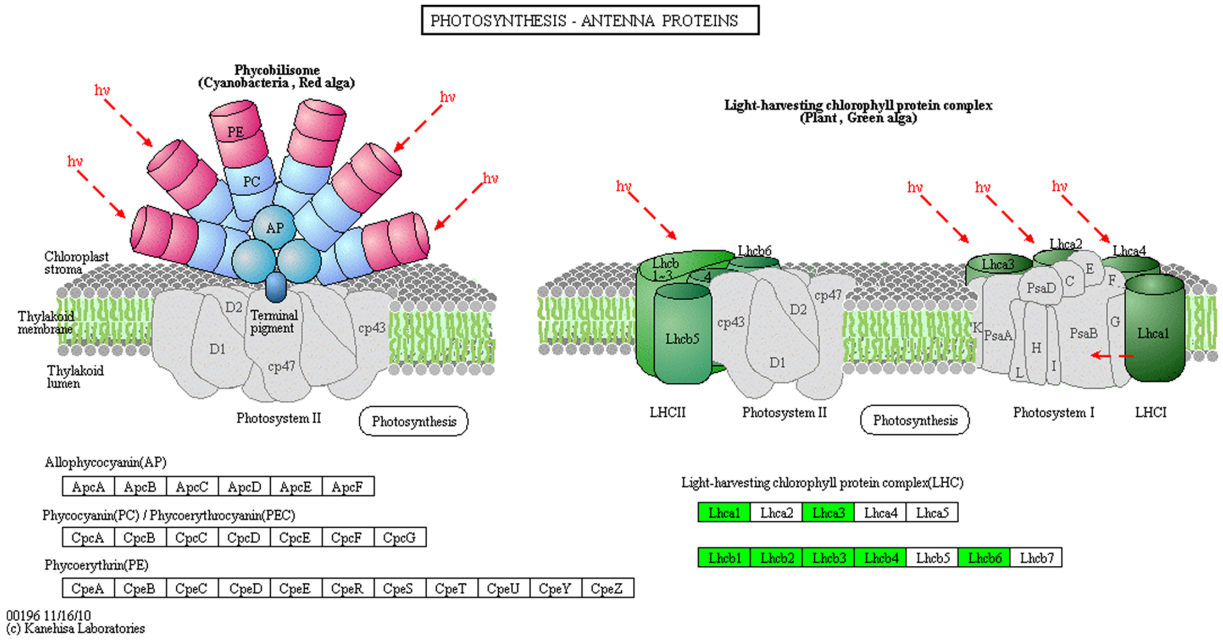

FIGURE 6
The expression levels of common DEPs in *P. barbigerum* related to photosynthesis-antenna proteins.

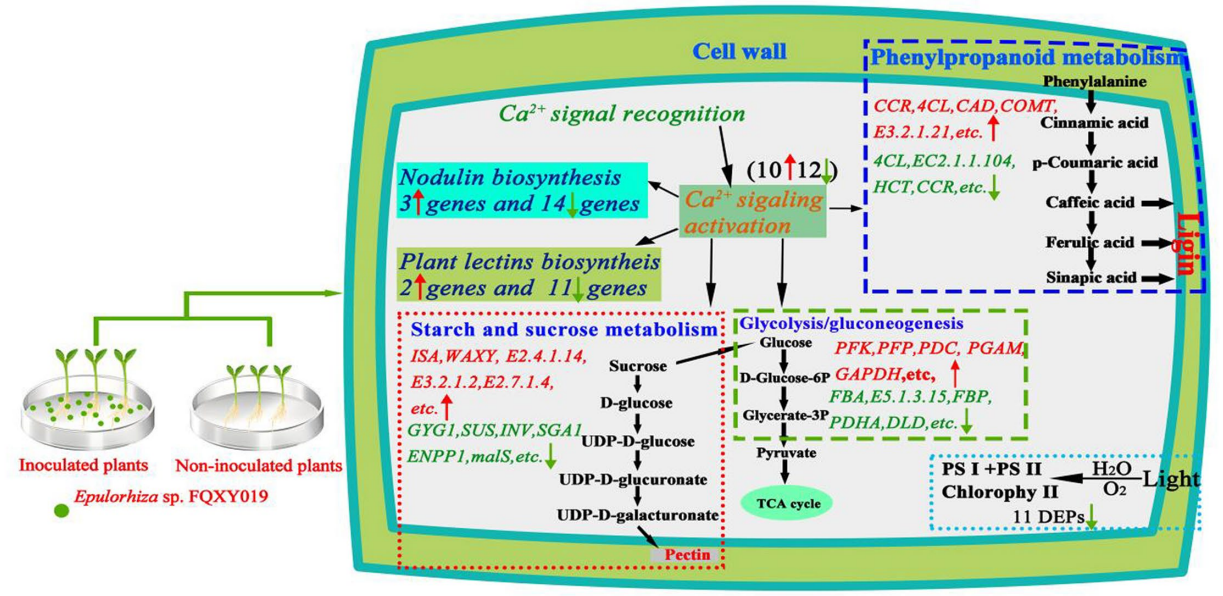

FIGURE 7
Schematic diagram of the potential mechanisms involved in the effect of *Epulorhiza* sp. FQXY019 symbiosis on the growth of *P. barbigerum*. Red and upward arrows indicate upregulated. Green and downward arrows indicate downregulated.

an early nodulation protein through screening the DEGs in CK compared with the FQXY019 treatment group (Supplementary Table S7). In a previous study, the effect of TaCLP1 (a gene encoding plastocyanin protein) on miRNA408 in wheat enhanced the resistance of wheat to stripe rust (Maunoury and Vaucheret, 2011). In addition, nodulin genes were found to be involved in the regulation of nodule formation in Arabidopsis, soybean, and other plants (Svistoonoff et al., 2010; Cheng et al., 2011; Gong et al., 2020). The induced expression of these genes indicated that inoculation could activate the expression of plastocyanin-like domain proteins, enhance the photosynthesis of seedlings, and accelerate seedling growth and development. These genes can also promote the formation of symbiotic nodules, which is beneficial to the uptake of nitrogen by the root system. In conclusion, the study of

plant-mycorrhizal fungi interactions involving these genes still needs further study.

4.1.2 Expression of Ca^{2+} signaling-related genes

Ca^{2+} signaling plays a crucial role in regulating the growth and development of plants, such as plant carbon and nitrogen metabolism and ion water transmembrane transport, and the defense response of plants to abiotic environmental stress (Zhang et al., 2022). Ca ions are enriched around the nucleus of root hair cells, which is considered as the earliest cellular response of plants after the establishment of symbiotic relationship (Zhu, 2016). Plant cells have evolved a series of Ca^{2+} responsive receptors, including calmodulin-like protein (CLPs), calcium-binding protein (CBPs), calcium-dependent protein kinases (CDPKs), and calcineurin B-like proteins (CBLs), which can recognize and transmit Ca^{2+} signaling to regulate various cellular activities (De Bang et al., 2021). In this study, numerous genes related to Ca^{2+} signaling were screened, including three DEGs encoding CLPs, eight DEGs encoding CBPs, nine DEGs encoding CDPKs, and one DEG encoding a CBLa (Supplementary Table S8). The protein genes regulated by Ca^{2+} signals are known to be closely related to the formation of arbuscular mycorrhizal symbionts in rice, and the signals generated by these genes can regulate fungal colonization in plant cells (Campos-Soriano et al., 2011). The roots of *Medicago truncatula* activate Ca^{2+} signals and induce the expression of nodule genes to promote root nodule formation after recognizing mycorrhizal factors (such as nodulation factors) released by arbuscular mycorrhizal fungi (Kosuta et al., 2018). In addition, many genes involved in Ca^{2+} signaling have been found in the mycorrhizal symbionts of other orchids. For example, five DEGs encoding CDPKs were reported in the mycorrhizal symbionts of *Epidendrum* (Zhao et al., 2021), and five DEGs encoding CBPs and two DEGs encoding CDPKs were also found in the mycorrhizal symbionts of *Cymbidium hybridum* (Zhao et al., 2014). Therefore, our results indicated that after inoculation with *Epulorhiza* sp. FQXY019, *P. barbigerum* can induce the expression of Ca^{2+} signaling-related genes, then transfer the signal from the upstream to the downstream gene expression in the root hair area, thus inducing the expression of orchid mycorrhizal symbiotic-related genes and the production of a variety of substances to identify fungi, digest mycelia, and establish an advantageous symbiotic relationship.

4.1.3 Expression of plant lectin-related genes

Plant lectins are a class of nonenzymatic proteins found in legumes that can agglutinate cells and precipitate monosaccharide or polysaccharide complexes (Kosuta et al., 2018; Ahmad et al., 2022b). Plant lectins play a crucial role in many signaling processes, for instance, signal transduction, plant defense, and immune response. Recent studies have reported that the specific recognition of plant symbiosis may be mediated by lectins, which can specifically bind carbohydrate complexes owing to their specific ability to bind monosaccharides and carbohydrate complexes, such as with mannitol-specific lectins (Houston et al., 2016; Andrade et al., 2019; Valadares et al., 2020). In this study, 13 DEGs were found to encode lectin-related proteins in the symbiotic mechanism of *P. barbigerum* between the FQXY019 treatment and CK group, six of which were downregulated DEGs that encoded mannose-specific lectin proteins (Supplementary Table S9). Our results were similar to previous studies. For example, significantly upregulated expression of mannose-specific lectin genes was found in several studies of orchid–fungi symbiotic relationships, such as between a *Cymbidium* hybrid and six different fungal strains (Reinhold-Hurek et al., 2015), *Platanthera sikkimensis, T. calospora* and *Epidendrum secundum* (Pujasatria et al., 2020). In addition, a mannose-specific lectin was reported to be involved in the establishment of the interaction with microorganisms during *Gastrodia elata* seed germination (Zeng et al., 2017). The induced expression of these genes indicates that they are one of the key factors for the establishment of symbiotic relationship between orchids and mycorrhizal fungi. Mycorrhizal fungi have faster growth and development than orchid plants and can quickly invade plant cells to establish a symbiotic relationship with plants (Dong et al., 2008; Xu et al., 2017). During this process, numerous plant lectin-related genes were induced and expressed, which played an important role in regulating and maintaining the interaction between orchids and mycorrhizal fungi.

4.2 Proteomic analysis

4.2.1 Deps related to photosynthesis and energy-associated metabolism

Although most orchids can obtain carbon via photosynthesis, they still need fungi to provide nutrients. Zhang et al. (2020) found that *Mycena* increased the expression of photosynthesis-related proteins, such as antenna proteins, in *Dendrobium officinale*, thereby enhancing the photosynthetic efficiency of *D. officinale*. In a study on the symbiotic relationship between *Oncidium sphacelatum* and *Ceratobasidium*, the expression of photosynthesis-related proteins in the green protocorm of *O. sphacelatum* was found to be upregulated, including that of ribulose diphosphate carboxylase and chlorophyl a-apolipoprotein A1 of photosystem I, which affected their own photosynthesis. However, in this study, we observed that the expression of 13 DEPs related to photosynthesis was greatly downregulated in the CK in comparison with that in the FQXY019 treatment groups (Supplementary Table S11). In addition, eight DEPs related to photosynthesis antenna proteins were markedly downregulated in the CK in comparison with that in the FQXY019 treatment groups (Supplementary Table S12). These resulted indicate that the photosynthesis of *P. barbigerum* was gradually changed during the symbiotic development with *Epulorhiza* sp. FQXY019. Thus, this enables the energy requirement of seeding germination to be met with adjustment of the seed germination rate to quickly enable growth of seedlings of *P. barbigerum*.

During plant seed germination, starch in the endosperm is gradually degraded as the main source of ATP, which provides a precursor for the biosynthetic and metabolic reactions in embryos (Zhao et al., 2021). Nevertheless, orchid seeds are very small and nutrient storage is limited, and seed germination and subsequent developments of orchids in nature mainly depend on the colonization of mycorrhizal fungi (Li Y. Y et al., 2021). After the mycorrhizal fungi colonize the orchid seeds, the mycelium passes through the seed coat and produces amylase to hydrolyze starch in the embryo, which promotes the growth of the embryo protoplasm and absorbs nutrients

from the surrounding environment to accelerate the further germination and growth of seeds (Pujasatria et al., 2020). In this study, transcriptomics showed that two pathways (starch and sucrose metabolism, and glycolysis/gluconeogenesis) related to energy metabolism were significantly enriched, involving a total of 72 DEGs, all of which were upregulated in the CK in comparison with the FQXY019 treatment groups (Supplementary Tables S13, S14). Interestingly, proteomics also showed that two pathways (pentose and glucuronate interconversions, and glycolysis/gluconeogenesis) related to energy metabolism were enriched and included a total of 31 DEPs, of which 20 DEPs were upregulated and 11 DEPs were downregulated in the CK in comparison with that in the FQXY019 treatment groups (Supplementary Tables S15, S16). These results demonstrated that the energy metabolism-related pathways in seeds of *P. barbigerum* rapidly changed after the seeds were infected by *Epulorhiza* sp. FQXY019, and the seeds germinated and formed seedlings. The energy metabolism pathways in seedlings also changed during the symbiotic development of seedlings and mycelium to meet the energy required for seedling growth, which is consistent with results from previous studies (Fochi et al., 2017).

4.2.2 Deps related to fatty acid metabolism

Orchid seeds are among the smallest seeds in nature, and they are naturally rich in fatty acids (Chen et al., 2018). Fatty acids can generate intermediate products of sugar metabolism via glyoxylate and dicarboxylate metabolism and other metabolic processes and then convert them into carbohydrates via gluconeogenesis, which can provide sufficient energy for seed germination by glycolysis and pentose phosphate pathway (Ghirardo et al., 2020). Therefore, in this study, the DEGs and DEPs involved in the fatty acid metabolism in *P. barbigerum* were analyzed. The transcriptomics analysis showed that a total of 11 upregulated DEGs involved in fatty acid degradation, and 16 and 8 of the downregulated DEGs involved in fatty acid elongation and biosynthesis of unsaturated fatty acids, respectively, in the CK in comparison with that the FQXY019 treatment groups (Supplementary Table S17). A total of 13 DEPs (seven upregulated and six downregulated DEPs) were involved in fatty acid biosynthesis and metabolism in proteomics in the CK in comparison to the FQXY019 treatment groups, respectively (Supplementary Table S18). In addition, we found that two DEPs (one upregulated and one downregulated DEP) were related to linoleic acid metabolism in the CK in comparison with that in the FQXY019 treatment groups (Supplementary Table S18). These results indicate that inoculation with *Epulorhiza* sp. FQXY019 can affect the synthesis, decomposition, and metabolism of fatty acids in seeds of *P. barbigerum* by invading into seeds, so that the fatty acids stored in embryos can be more efficiently used to pass through the early stage of germination. Chen et al. (2022) found that the colonization by fungi could change the metabolic pattern and improve the nutrient utilization efficiency of *D. officinale*, especially when lipid metabolism was activated. In addition, genes encoding key enzymes involved in fatty acid metabolism, such as acetyl-CoA binding protein and β-oxidation polyfunctional protein genes, were significantly upregulated. Overall, our results indicated that the *Epulorhiza* sp. FQXY019 can induce the expression of genes and proteins related to fatty acid metabolism in *P. barbigerum*, and that the carbohydrates produced by this process can provide energy resources for seed germination and seedling growth.

5 Conclusion

This study demonstrated that inoculation of *Epulorhiza* sp. FQXY019 boosted and changed the transcriptomic and proteomic profile of *P. barbigerum* seed germination. Based on transcriptional evidence, numerous DEGs were identified in the CK and FQXY019 treatment groups, which are mainly associated with sugar, fatty acid, and amino acid metabolic pathway The expression levels of candidate DEGs related to nodulin, Ca^{2+} signaling, and plant lectins were significantly affected in *P. barbigerum* with FQXY019 treatment. Additionally, a total of 537 DEPs were identified in proteomic analysis and were involved in carbon metabolism, amino acid biosynthesis, and fatty acid metabolism. We identified several candidate DEPs related to photosynthesis, energy metabolism, and fatty acid metabolic pathways. Collectively, the identified genes and proteins will provide insight into the specific mechanism underlying the fungal inoculation of *Paphiopedilum* orchid seeds and their subsequent germination, and will act as a constructive reference resource to improve the genetic improvement of *Paphiopedilum* orchids.

Data availability statement

The datasets presented in this study can be found in online repositories. The names of the repository/repositories and accession number(s) can be found in the article/Supplementary material.

Author contributions

FT: Writing – original draft, Software, Investigation, Data curation. JW: Writing – original draft, Software, Methodology, Investigation, Data curation. FD: Writing – review & editing. LW: Writing – review & editing. YY: Writing – review & editing. XB: Writing – review & editing. CT: Writing – review & editing. XL: Writing – review & editing.

Funding

The author(s) declare financial support was received for the research, authorship, and/or publication of this article. This research was supported by the National key wildlife protection subsidy project: *Paphiopedilum emersonii*, *P. barbigerum*, and other *Paphiopedilum* plants rescue and protection project. The Scientific Search Projects of Guizhou Forestry Bureau [2019] 02; Innovative Talent Team Project of Guizhou Academy of Sciences (2019–07); The Project of Science & Technology of Guizhou Province [grant number: Qiankehezhicheng [2017]2524]; The Capacity Improvement Project of State Key Laboratory of Southwest Karst Mountain Biodiversity Conservation of National Forestry and Grassland Administration [2019–000411–05-01-001641]; Scientific Search Projects of Guizhou Forestry Bureau [2022] 36.

Acknowledgments

We are grateful to English language and grammar by editors of NES (www.nesediting.com) greatly improved the manuscript.

Conflict of interest

The authors declare that the research was conducted in the absence of any commercial or financial relationships that could be construed as a potential conflict of interest.

Publisher's note

All claims expressed in this article are solely those of the authors and do not necessarily represent those of their affiliated organizations, or those of the publisher, the editors and the reviewers. Any product that may be evaluated in this article, or claim that may be made by its manufacturer, is not guaranteed or endorsed by the publisher.

Supplementary material

The Supplementary material for this article can be found online at: https://www.frontiersin.org/articles/10.3389/fmicb.2024.1358137/full#supplementary-material

References

Ahmad, S., Chen, J., Chen, G., Huang, J., Hao, Y., and Shi, X. (2022a). Transcriptional proposition for uniquely developed protocorm flowering in three orchid species: resources for innovative breeding. *Front. Plant Sci.* 13:942591. doi: 10.3389/fpls.2022.942591

Ahmad, S., Gao, J., Wei, Y., Lu, C., Zhu, G., and Yang, F. (2022b). The transcriptome profiling of flavonoids and bibenzyls reveals medicinal importance of rare orchid *Arundina graminifolia*. *Front. Plant Sci.* 13:1934. doi: 10.3389/fpls.2022.923000

Andrade, L. M., Peixoto-Junior, R. F., Ribeiro, R. V., Nóbile, P. M., Brito, M. S., and Marchiori, P. E. R. (2019). Biomass accumulation and cell wall structure of rice plants overexpressing a dirigent-jacalin of sugarcane (ShDJ) under varying conditions of water availability. *Front. Plant Sci.* 10:65. doi: 10.3389/fpls.2019.00065

Balilashaki, K., Zakizadeh, H., Olfati, J. A., Vahedi, M., Kumar, A., and Indracanti, M. (2019). Recent advances in *Phalaenopsis* orchid improvement using omics approaches. *Plant Tissue Cult. Biotechnol.* 29, 133–149. doi: 10.3329/ptcb.v29i1.41986

Campos-Soriano, L., Gómez-Ariza, J., Bonfante, P., and San, S. B. (2011). A rice calcium-dependent protein kinase is expressed in cortical root cells during the presymbiotic phase of the arbuscular mycorrhizal symbiosis. *BMC Plant Biol.* 11:90. doi: 10.1186/1471-2229-11-90

Chao, Y. T., Su, C. L., Jean, W. H., Chen, W. C., Chang, Y. C., and Shih, M. C. (2014). Identification and characterization of the microRNA transcriptome of a moth orchid *Phalaenopsis aphrodite*. *Plant Mol. Biol.* 84, 529–548. doi: 10.1007/s11103-013-0150-0

Chen, T. Y., Chen, J. T., and Chang, W. C. (2004). Plant regeneration through direct shoot bud formation from leaf cultures of *Paphiopedilum* orchids. *Plant Cell Tissue Organ Cult.* 76, 11–15. doi: 10.1023/A:1025858211320

Chen, J., Tang, Y., Kohler, A., Lebreton, A., Xing, Y., and Zhou, D. (2022). Comparative transcriptomics analysis of the symbiotic germination of *D. officinale* (*Orchidaceae*) with emphasis on plant cell wall modification and cell wall-degrading enzymes. Front. *Plant Sci.* 13:880600. doi: 10.3389/fpls.2022.880600

Chen, C., Zeng, L., and Ye, Q. (2018). Proteomic and biochemical changes during senescence of Phalaenopsis 'red dragon' petals. *Int. J. Mol. Sci.* 19:1317. doi: 10.3390/ijms19051317

Cheng, X. G., Wang, L., Wang, H., Yu, G. H., Bai, Y. L., and Liu, M. M. (2011). Specific expression of a novel nodulin gmN479 gene in the infected cells of soybean (glycine max) nodules. *Agric. Sci. China* 10, 1512–1524. doi: 10.1016/S1671-2927(11)60146-6

De Bang, T. C., Husted, S., Laursen, K. H., Persson, D. P., and Schjoerring, J. K. (2021). The molecular-physiological functions of mineral macronutrients and their consequences for deficiency symptoms in plants. *New Phytol.* 229, 2446–2469. doi: 10.1111/nph.17074

Denance, N., Szurek, B., and Noël, L. D. (2014). Emerging functions of nodulin-like proteins in non-nodulating plant species. *Plant Cell Physiol.* 55, 469–474. doi: 10.1093/pcp/pct198

Dong, F., Liu, H. X., Jin, H., and Luo, Y. B. (2008). Symbiosis between fungi and the hybrid cymbidium and its mycorrhizal microstructures. *For. Stud. China* 10, 41–44. doi: 10.1007/s11632-008-0002-1

Fang, L., Kong, X., Wen, Y., Li, J., Yin, Y., and Li, L. (2021). Characterization of embryo and protocorm development of *Paphiopedilum spicerianum*. *Plant Physiol. Biochem.* 167, 1024–1034. doi: 10.1016/j.plaphy.2021.09.001

Fochi, V., Chitarra, W., Kohler, A., Voyron, S., Singan, V. R., and Lindquist, E. A. (2017). Fungal and plant gene expression in the *Tulasnella calospora-Serapias vomeracea* symbiosis provides clues about nitrogen pathways in orchid mycorrhizas. *New Phytol.* 213, 365–379. doi: 10.1111/nph.14279

Gao, Y., Ji, J., Zhang, Y., Yang, N., and Zhang, M. (2022). Biochemical and transcriptomic analyses of the symbiotic interaction between *Cremastra appendiculata* and the mycorrhizal fungus *Coprinellus disseminatus*. *BMC Plant Biol.* 22:15. doi: 10.1186/s12870-021-03388-6

Ghirardo, A., Fochi, V., Lange, B., Witting, M., Schnitzler, J. P., Perotto, S., et al. (2020). Metabolomic adjustments in the orchid mycorrhizal fungus *Tulasnella calospora* during symbiosis with *Serapias vomeracea*. *New Phytol.* 228, 1939–1952. doi: 10.1111/nph.16812

Gong, Z., Xiong, L., Shi, H., Yang, S., Herrera-Estrella, L. R., and Xu, G. (2020). Plant abiotic stress response and nutrient use efficiency. *Sci. China Life Sci.* 63, 635–674. doi: 10.1007/s11427-020-1683-x

Grosjean, N., Le Jean, M., Armengaud, J., Schikora, A., Chalot, M., and Gross, E. M. (2022). Combined omics approaches reveal distinct responses between light and heavy rare earth elements in *Saccharomyces cerevisiae*. *J. Hazard. Mater.* 425:127830. doi: 10.1016/j.jhazmat.2021.127830

Hao, J., Guo, H., Shi, X., Wang, Y., Wan, Q., and Song, Y. B. (2017). Comparative proteomic analyses of two *Taxus* species (*Taxus x media* and *Taxus mairei*) reveals variations in the metabolisms associated with paclitaxel and other metabolites. *Plant Cell Physiol.* 58, 1878–1890. doi: 10.1093/pcp/pcx128

Houston, K., Tucker, M. R., Chowdhury, J., Shirley, N., and Little, A. (2016). The plant cell wall: a complex and dynamic structure as revealed by the responses of genes under stress conditions. *Front. Plant Sci.* 7:984. doi: 10.3389/fpls.2016.00984

Huang, J. Z., Lin, C. P., Cheng, T. C., Huang, Y. W., Tsai, Y. J., and Cheng, S. Y. (2016). The genome and transcriptome of *Phalaenopsis* yield insights into floral organ development and flowering regulation. *PeerJ* 4:e2017. doi: 10.7717/peerj.2017

Jian, M., Zhang, D., Wang, X., Wei, S., Zhao, Y., and Ding, Q. (2020). Differential expression pattern of the proteome in response to cadmium stress based on proteomics analysis of wheat roots. *BMC Genomics* 21:343. doi: 10.1186/s12864-020-6716-8

Jiang, J., Zhang, K., Cheng, S., Nie, Q., Zhou, S. X., and Chen, Q. (2019). *Fusarium oxysporum* KB-3 from *Bletilla striata*: an orchid mycorrhizal fungus. *Mycorrhiza* 29, 531–540. doi: 10.1007/s00572-019-00904-3

Kosuta, S., Chabaud, M., Lougnon, G., Gough, C., Dénarié, J., and Barker, D. G. (2018). A diffusible factor from arbuscular mycorrhizal fungi induces symbiosis-specific MtENOD 11 expression in roots of *Medicago truncatula*. *Plant Physiol.* 131, 952–962. doi: 10.1104/pp.011882

Kottke, I., Suárez, J. P., Herrera, P., Cruz, D., Bauer, R., and Haug, I. (2010). Atractiellomycetes belonging to the 'rust' lineage (*Pucciniomycotina*) form mycorrhizae with terrestrial and epiphytic Neotropical orchids. *Proc. Biol. Sci.* 277, 1289–1298. doi: 10.1098/rspb.2009.1884

Li, Y. Y., Boeraeve, M., Cho, Y. H., Jacquemyn, H., and Lee, Y. I. (2021). Mycorrhizal switching and the role of fungal abundance in seed germination in a fully mycoheterotrophic orchid, *Gastrodia confusoides*. *Front. Plant Sci.* 12:775290. doi: 10.3389/fpls.2021.775290

Li, P., Ruan, Z., Fei, Z., Yan, J., and Tang, G. (2021). Integrated transcriptome and metabolome analysis revealed that flavonoid biosynthesis may dominate the resistance of *Zanthoxylum bungeanum* against stem canker. *J. Agric. Food Chem.* 69, 6360–6378. doi: 10.1021/acs.jafc.1c00357

Maunoury, N., and Vaucheret, H. (2011). AGO1 and AGO2 act redundantly in miR408-mediated plantacyanin regulation. *PLoS One* 6:e28729. doi: 10.1371/journal.pone.0028729

Meng, X., Li, G., Gu, L., Sun, Y., Li, Z., and Liu, J. (2020). Comparative metabolomic and transcriptome analysis reveal distinct flavonoid biosynthesis regulation between petals of white and purple *Phalaenopsis amabilis*. *J. Plant Growth Regul.* 39, 823–840. doi: 10.1007/s00344-019-10025-y

Mujica, M. I., Cisternas, M., Claro, A., Simunovic, M., and Pérez, F. (2021). Nutrients and fungal identity affect the outcome of symbiotic germination in *Bipinnula fimbriata* (*Orchidaceae*). *Symbiosis* 83, 91–101. doi: 10.1007/s13199-020-00737-1

Mumtaz, M. A., Hao, Y., Mehmood, S., Shu, H., Zhou, Y., and Jin, W. (2022). Physiological and transcriptomic analysis provide molecular insight into 24-Epibrassinolide mediated Cr (VI)-toxicity tolerance in pepper plants. *Environ. Pollut.* 306:119375. doi: 10.1016/j.envpol.2022.119375

Peng, C., Chang, L., Yang, Q., Tong, Z., Wang, D., and Tan, Y. (2019). Comparative physiological and proteomic analyses of the chloroplasts in halophyte *Sesuvium portulacastrum* under differential salt conditions. *J. Plant Physiol.* 232, 141–150. doi: 10.1016/j.jplph.2018.10.028

Pujasatria, G. C., Miura, C., and Kaminaka, H. (2020). In vitro symbiotic germination: a revitalized heuristic approach for orchid species conservation. *Plants* 9:1742. doi: 10.3390/plants9121742

Reinhold-Hurek, B., Bünger, W., Burbano, C. S., Sabale, M., and Hurek, T. (2015). Roots shaping their microbiome: global hotspots for microbial activity. *Annu. Rev. Phytopathol.* 53, 403–424. doi: 10.1146/annurev-phyto-082712-102342

Sebastián, F., Vanesa, S., Eduardo, F., Graciela, T., and Silvana, S. (2014). Symbiotic seed germination and protocorm development of *aa achalensis Schltr.*, a terrestrial orchid endemic from Argentina. *Mycorrhiza* 24, 35–43. doi: 10.1007/s00572-013-0510-2

Svistoonoff, S., Sy, M. O., Diagne, N., Barker, D. G., Bogusz, D., and Franche, C. (2010). Infection-specific activation of the *Medicago truncatula* Enod11 early nodulin gene promoter during actinorhizal root nodulation. *Mol. Plant-Microbe Interact.* 23, 740–747. doi: 10.1094/MPMI-23-6-0740

Tian, F., Liao, X. F., Wang, L. H., Bai, X. X., Yang, Y. B., and Luo, Z. Q. (2022). Isolation and identification of beneficial orchid mycorrhizal fungi in *Paphiopedilum barbigerum* (Orchidaceae). *Plant Signal. Behav.* 17:2005882. doi: 10.1080/15592324.2021.2005882

Tian, F., Wang, J. C., Bai, X. X., Yang, Y. B., Huang, L., and Liao, X. F. (2023). Symbiotic seed germination and seedling growth of mycorrhizal fungi in *Paphiopedilum hirsutissimun* (Lindl.Ex hook.) stein from China. *Plant Signal. Behav.* 18:2293405. doi: 10.1080/15592324.2023.2293405

Tsai, C. C., Liao, P. C., Ko, Y. Z., Chen, C. H., and Chiang, Y. C. (2020). Phylogeny and historical biogeography of *Paphiopedilum Pfitzer* (*Orchidaceae*) based on nuclear and plastid DNA. *Front. Plant Sci.* 11:126. doi: 10.3389/fpls.2020.00126

Valadares, R. B. S., Perotto, S., Lucheta, A. R., Santos, E. C., Oliveira, R. M., and Lambais, M. R. (2020). Proteomic and transcriptomic analyses indicate metabolic changes and reduced defense responses in mycorrhizal roots of *Oeceoclades maculata* (*Orchidaceae*) collected in nature. *J. Fungi* 6:148. doi: 10.3390/jof6030148

Vives-Peris, V., De Ollas, C., Gómez-Cadenas, A., and Pérez-Clemente, R. M. (2020). Root exudates: from plant to rhizosphere and beyond. *Plant Cell Rep.* 39, 3–17. doi: 10.1007/s00299-019-02447-5

Wang, Y., Xu, L., Tang, M., Jiang, H., Chen, W., and Zhang, W. (2016). Functional and integrative analysis of the proteomic profile of radish root under Pb exposure. *Front. Plant Sci.* 7:1871. doi: 10.3389/fpls.2016.01871

Xu, X., Fang, L., Li, L., Ma, G., Wu, K., and Zeng, S. (2020). Abscisic acid inhi bits asymbiotic germination of immature seeds of *Paphiopedilum armeniacum*. *Int. J. Mol. Sci.* 21:9561. doi: 10.3390/ijms21249561

Xu, J. T., and Guo, S. X. (1989). Fungus associated with nutrition of seed germination of *Gastrodia elata-Mycena osmundicola* Lange. *Acta Mycol. Sin.* 8, 221–226. doi: 10.13346/j.mycosystema.1989.03.011

Xu, L., Tian, J. N., Wang, T., and Li, L. B. (2017). Symbiosis established between orchid and *Tulasnella* spp. Fungi. *J. Nucl. Agric. Sci.* 31, 876–883. doi: 10.11869/j.issn.100-8551.2017.05.0876

Xu, Z. X., Zhu, X. M., Yin, H., Li, B., Chen, X. J., Fan, X. L., et al. (2023). Symbiosis between *Dendrobium catenatum* protocorms and *Serendipita indica* involves the plant hypoxia response pathway. *Plant Physiol.* 192, 2554–2568. doi: 10.1093/plphys/kiad198

Yang, J. X., Dierckxsens, N., Bai, M. Z., and Guo, Y. Y. (2023). Multichromosomal mitochondrial genome of *Paphiopedilum micranthum*: compact and fragmented genome, and rampant intracellular gene transfer. *Int. J. Mol. Sci.* 24:3976. doi: 10.3390/ijms24043976

Yang, H., Li, N. Q., and Gao, J. Y. (2023). A novel method to produce massive seedlings via symbiotic seed germination in orchids. *Front. Plant Sci.* 14:1114105. doi: 10.3389/fpls.2023.1114105

Yang, W. K., Li, T. Q., Wu, S. M., Finnegan, P. M., and Gao, J. Y. (2020). Ex situ seed baiting to isolate germination-enhancing fungi for assisted colonization in *Paphiopedilum spicerianum*, a critically endangered orchid in China. *Glob. Ecol. Conserv.* 23:e01147. doi: 10.1016/j.gecco.2020.e01147

Yu, R., Jiang, Q., Bu, S., and Shi, G. (2019). Comparative proteomics analysis of peanut roots reveals differential mechanisms of cadmium detoxification and translocation between two cultivars differing in cadmium accumulation. *BMC Plant Biol.* 19, 137–135. doi: 10.1186/s12870-019-1739-5

Zeng, X., Li, Y., Ling, H., Liu, S., Liu, M., and Chen, J. (2017). Transcriptomic analyses reveal clathrin-mediated endocytosis involved in symbiotic seed germination of *Gastrodia elata*. *Bot. Stud.* 58:31. doi: 10.1186/s40529-017-0185-7

Zhang, J. Y., Qin, J. L., and Liu, J. (2020). Transcriptomic analysis of *Dendrobium officinale* photosynthesis promoted by Mycena sp. *Plant Physiol. J.* 56, 1408–1418. doi: 10.13592/j.cnki.ppj.2020.0202

Zhang, S., Yang, Y., Li, J., Qin, J., Zhang, W., and Huang, W. (2018). Physiological diversity of orchids. *Plant Divers.* 40, 196–208. doi: 10.1016/j.pld.2018.06.003

Zhang, H., Zhu, J., Gong, Z., and Zhu, J. K. (2022). Abiotic stress responses in plants. *Nat. Rev. Genet.* 23, 104–119. doi: 10.1038/s41576-021-00413-0

Zhao, D. K., Selosse, M. A., Wu, L., Luo, Y., Shao, S. C., and Ruan, Y. L. (2021). Orchid reintroduction based on seed germination-promoting mycorrhizal fungi derived from protocorms or seedlings. *Front. Plant Sci.* 12:701152. doi: 10.3389/fpls.2021.701152

Zhao, X., Zhang, J., Chen, C., Yang, J., Zhu, H., Liu, M., et al. (2014). Deep sequencing-based comparative transcriptional profiles of *Cymbidium hybridum* roots in response to mycorrhizal and non-mycorrhizal beneficial fungi. *BMC Genomics* 15:747. doi: 10.1186/1471-2164-15-747

Zhou, Z., Lin, B., Tan, J., Hao, P., Hua, S., and Deng, Z. (2022). Tandem mass tag-based quantitative proteomics reveals implication of a late embryogenesis abundant protein (BnLEA57) in seed oil accumulation in *Brassica napus* L. *Front. Plant Sci.* 13:907244. doi: 10.3389/fpls.2022.907244

Zhu, J. K. (2016). Abiotic stress signaling and responses in plants. *Cell* 167, 313–324. doi: 10.1016/j.cell.2016.08.029

Zhu, Y., Qiu, W., He, X., Wu, L., Bi, D., and Deng, Z. (2021). Integrative analysis of transcriptome and proteome provides insights into adaptation to cadmium stress in *sedum plumbizincicola*. *Ecotoxicol. Environ. Saf.* 230:113149. doi: 10.1016/j.ecoenv.2021.113149

10.3389/fmicb.2024.1358137

Glossary

AGC	Automatic gain control
BP	Biological process
CBL	Calcineurin B-like
CBP	Calcium-binding protein
CC	Cellular component
CDPK	Calcium-dependent protein kinases
CLP	Calmodulin-like protein
DEG	Differentially expressed genes
DEP	Differentially expressed proteins
FA	Formic acid
FDR	False discovery rates
GO	Gene Ontology
KEGG	Kyoto Encyclopedia of Genes and Genomes
MF	Molecular function
MS	Mass spectrometry
NCBI	National Centre for Biotechnology Information
PCA	Principal component analysis
PDA	Potato dextrose agar
TMT	Tandem mass tag

frontiers | Frontiers in Microbiology

TYPE Original Research
PUBLISHED 27 March 2024
DOI 10.3389/fmicb.2024.1289022

Check for updates

OPEN ACCESS

EDITED BY
Wei Hu,
Shandong University, China

REVIEWED BY
Busayo Joshua Babalola,
University of Georgia, United States
Shrivardhan Dheeman,
MVN University, India

*CORRESPONDENCE
Yutong Hu
✉ hyt@xjau.edu.cn

RECEIVED 05 September 2023
ACCEPTED 14 March 2024
PUBLISHED 27 March 2024

CITATION
Zhou X, Hu Y, Li H, Sheng J, Cheng J, Zhao T and Zhang Y (2024) Phosphorus addition increases stability and complexity of co-occurrence network of soil microbes in an artificial *Leymus chinensis* grassland. *Front. Microbiol.* 15:1289022. doi: 10.3389/fmicb.2024.1289022

COPYRIGHT
© 2024 Zhou, Hu, Li, Sheng, Cheng, Zhao and Zhang. This is an open-access article distributed under the terms of the Creative Commons Attribution License (CC BY). The use, distribution or reproduction in other forums is permitted, provided the original author(s) and the copyright owner(s) are credited and that the original publication in this journal is cited, in accordance with accepted academic practice. No use, distribution or reproduction is permitted which does not comply with these terms.

Phosphorus addition increases stability and complexity of co-occurrence network of soil microbes in an artificial *Leymus chinensis* grassland

Xiaoguo Zhou[1,2], Yutong Hu[1,2]*, Huijun Li[1,3,4], Jiandong Sheng[1,2], Junhui Cheng[1,2], Tingting Zhao[1,2] and Yuanmei Zhang[5]

[1]College of Resources and Environment, Xinjiang Agricultural University, Urumqi, China, [2]Xinjiang Key Laboratory of Soil and Plant Ecological Processes, Urumqi, China, [3]The Research Center of Soil and Water Conservation and Ecological Environment, Chinese Academy of Sciences and Ministry of Education, Yangling, China, [4]University of Chinese Academy of Sciences, Beijing, China, [5]College of Forestry and Landscape Architecture, Xinjiang Agricultural University, Urumqi, China

Introduction: Understanding the response of cross-domain co-occurrence networks of soil microorganisms to phosphorus stability and the resulting impacts is critical in ecosystems, but the underlying mechanism is unclear in artificial grassland ecosystems.

Methods: In this study, the effects of four phosphorus concentrations, P0 (0 kg P ha^{-1}), P1 (15.3 kg P ha^{-1}), P2 (30.6 kg P ha^{-1}), and P3 (45.9 kg P ha^{-1}), on the cross-domain co-occurrence network of bacteria and fungi were investigated in an artificial Leymus chinensis grassland in an arid region.

Results and discussion: The results of the present study showed that phosphorus addition significantly altered the stem number, biomass and plant height of the Leymus chinensis but had no significant effect on the soil bacterial or fungal alpha (ACE) diversity or beta diversity. The phosphorus treatments all increased the cross-domain co-occurrence network edge, node, proportion of positively correlated edges, edge density, average degree, proximity to centrality, and robustness and increased the complexity and stability of the bacterial-fungal cross-domain co-occurrence network after 3 years of continuous phosphorus addition. Among them, fungi (Ascomycota, Basidiomycota, Mortierellomycota and Glomeromycota) play important roles as keystone species in the co-occurrence network, and they are significantly associated with soil AN, AK and EC. Finally, the growth of Leymus chinensis was mainly due to the influence of the soil phosphorus content and AN. This study revealed the factors affecting the growth of Leymus chinense in artificial grasslands in arid areas and provided a theoretical basis for the construction of artificial grasslands.

KEYWORDS

phosphorus addition, *Leymus chinensis*, microbial community, cooccurrence network, keystone species

1 Introduction

Phosphorus (P) is a crucial mineral element necessary for the growth and development of plants within terrestrial ecosystems (Wang et al., 2017). However, the proportion of phosphorus in the soil that plants can directly absorb and utilize is very low (Heuer et al., 2017; Luo et al., 2019). Many studies have shown that the cooperation of bacteria and fungi can not only promote the absorption of phosphorus by plants but also play a key role in plant phosphorus uptake (Rashid et al., 2016; Anzuay et al., 2017; Ceci et al., 2018). Furthermore, climate change also has an important impact on the healthy growth of plants (Deveau et al., 2018). Microorganisms in the soil demonstrate a remarkable level of sensitivity to changes in their immediate surroundings. These alterations in the environment can directly or indirectly influence the range of species within the microbiome, as well as their diversity in terms of structure and function (Bragazza et al., 2012; Deveau et al., 2018; Guo et al., 2018). It has been shown that under phosphorus addition, there is a significant response from the microbial community (Li et al., 2015; Tian et al., 2015). The exact mechanism through which soil microorganisms interact in artificial grasslands under phosphorus addition conditions has not been determined. Therefore, it is important to explore the response of microbial co-occurrence networks to phosphorus addition and its effect on artificial grasslands to develop a rational fertilization program.

The community of microbial species in the soil environment is not only rich and diverse but also complex (Faust and Raes, 2012). Co-occurrence network analysis is a method for describing complex microbial community structures and can be used to visualize the relationships between microbial communities and reveal symbiotic relationships and influencing factors (Fuhrman, 2009; Zhou et al., 2010). This method has been used to explore microbial interactions in soil environments (Ma et al., 2018). For example, it has been shown that positive interactions in the bacterial-fungal mutualism network are enhanced and negative interactions are reduced after exogenous nutrient addition, which may be due to the fact that nutrient addition enriches the trophic structure of the community and eases competition (Banerjee et al., 2016a). This method can be used to calculate the influential keystone species in the network (Banerjee et al., 2016b). Each node in a co-occurring network can be assigned a role based on its topological attributes, where the topological characteristics are its connectivity within and between network modules. These keystone species are highly connected groups that have significant spatial and temporal effects on the stability, structure, and function of microbial communities (Banerjee et al., 2018; Wagg et al., 2019). These groups not only provide communities with greater biological connectivity but also serve as important indicators of community change. Co-occurrence network complexity can be assessed by correlation network scores such as those derived from connectivity and clustering elements that indicate connectivity among taxa (ASVs). The keystone species in microbial communities are highly important for ecosystems. One study revealed that the keystone species of the microbial community are correlated with soil health and quality (Liu et al., 2022). Notably, long-term fertilization can change the key groups in the co-occurrence network (Lin et al., 2019), and changes in keystone species may lead to changes in the structural and functional diversity of microbial communities (Herren and McMahon, 2018; Fan et al., 2019). For example, keystone species in the microbial community have been shown to be directly related to the rate of soil nitrogen mineralization and to regulate the divergent-convergent trajectory of residue chemistry (Yang et al., 2021; Wang et al., 2023a). Co-occurrence networks are widely used to study microbial community interactions and classify important microorganisms in the soil. However, most related studies have focused on analyzing bacteria and fungi as separate groups, failing to consider the interrelationships between them. Understanding the interactions between bacteria and fungi is crucial for a comprehensive understanding of ecosystem dynamics.

Leymus chinensis is a perennial C3 plant that has a strong ability to adapt to saline and drought conditions (Baoyin et al., 2014; Li et al., 2016). Grassland ecosystem protection and restoration have significant potential for managing and enhancing Xinjiang's grassland ecosystems. In arid regions, we investigated whether phosphorus supplementation affects the composition of soil microbial communities and keystone species, resulting in changes in the structure of the cross-domain bacteria–fungus co-occurrence network and influencing the growth of *Leymus chinensis*. We hypothesized that (1) P addition affects soil environmental factors and the growth of *Leymus chinensis*, (2) P addition changes the co-occurrence network structure, and (3) P addition affects the composition and diversity of keystone species.

2 Materials and methods

2.1 Study area

Our test site is located at the Sanping Experimental Base of Xinjiang Agricultural University, Urumqi, Xinjiang (87°35′25″E，43°93′31″N, altitude 580 m). Situated in the Eurasian hinterland, the region experiences a prototypical arid continental climate, with an average annual temperature measuring 7.2°C. The temperature can soar as high as 42°C or plummet to as low as −38°C. The area benefits from ample sunlight, with an annual accumulated temperature of approximately 3400°C and a sunshine duration of 2829.4 hours. Precipitation levels average 228.8 mm annually, and evaporation stands at 2647 mm, creating favourable conditions for the cultivation of diverse crops (Li et al., 2023). The tested soil is calcic soil, and the soil organic matter content is 8.12 $g{\cdot}kg^{-1}$. The content of available phosphorus was 11.22 $mg{\cdot}kg^{-1}$, available nitrogen was 26.75 $mg{\cdot}kg^{-1}$, available potassium was 164.25 $mg{\cdot}kg^{-1}$, and the pH value was 8.2.

2.2 Experimental design

Leymus chinensis (Zhongke No. 1) seeds were obtained from the Hutubi Experimental Station, which belongs to Xinjiang Jinfangyuan Grassland Ecotourism Development Co., Ltd. and were used as test material in this study. The experimental site was established in October 2019. The phosphorus gradient had four levels: P0 (0 kg P ha^{-1}), P1 (15.3 kg P ha^{-1}), P2 (30.6 kg P ha^{-1}), and P3 (45.9 kg P ha^{-1}). The fertilizer used was mono-ammonium phosphate, and the nitrogen treatment was unified at each of the four phosphorus levels (150 kg N ha^{-1}); the nitrogen fertilizer used was urea, and each year was divided into spring fertilization and autumn fertilization, of which 50%

nitrogen fertilizer was applied in spring and 40% phosphate fertilizer was applied, while the rest were applied in autumn. The plants were randomly distributed, each with an area of 5 m*4 m, and there was a 1 m isolation zone between them.

2.3 Sample collection

Soil samples were collected in the third year after *Leymus chinensis* construction (July 12, 2022). A soil auger (with a length of 20 cm and an inner diameter of 4 cm) was used to collect 0–20 cm of soil from each plot, for a total of five points in each plot. Then, the soil was mixed together evenly and partially loaded into 5 mL centrifuge tubes and placed into ice boxes. The samples were subsequently transported to the laboratory and stored at −80°C for DNA extraction. The other part was put into self-sealing bags, labeled for direct return to the laboratory to dry naturally and stored at room temperature for the determination of soil physicochemical properties. A 1 × 1 m square was used to select a representative *Leymus chinensis* plant with uniform growth in the plot, and each experimental treatment was repeated three times. The stem number of *Leymus chinensis* in each square was recorded, the plant height was measured, and then they were killed at 105°C for 30 min and finally dried at 70°C to a constant weight and the weight was recorded.

2.4 Index measurement

2.4.1 Soil physical and chemical property indices

At the College of Resources and Environment, Xinjiang Agricultural University, an analysis was conducted on the soil samples to examine their physical and chemical properties. These properties were determined in accordance with the guidelines outlined in the "Soil Agricultural Chemical Analysis" document (Bao, 2000). The values of pH and EC were measured using a potentiometry technique at a soil–water ratio of 1:5. The leaching of sodium bicarbonate and the molybdenum-antimony sulfate resistance colorimetric method were employed to determine the available phosphorus (AP) in the soil. The ammonium acetate extraction method coupled with flame photometry was utilized to determine the available potassium (AK) in the soil. The alkaline hydrolysis diffusion method was employed to determine the available nitrogen (AN), while the molybdenum antimony colorimetric method was used to determine the total phosphorus (TP) concentration. An elemental analyzer (EA3000) was used to determine the total carbon (TC) and total nitrogen (TN) in the soil.

2.4.2 Extraction of soil DNA

We used a TGuide S96 magnetic bead method DNA extraction kit (Tiangen Biochemical Technology (Beijing) Co., Ltd., model: DP812) to complete the extraction of soil nucleic acids according to the manufacturer's instructions, after which an enzyme labeling instrument (model: synergyHTX) was used to determine the concentration of nucleic acids. DNA samples from bacteria and fungi were analyzed using specific primer sets to amplify the target gene regions. For the bacterial 16S rRNA gene V3-V4 region, the primers 338F (5′-ACTCCTACGGGAGGCAGCA-3′) and 806R (5′-GGACT ACHVGGGTWTCTAAT-3′) were utilized (Quast et al., 2013). In the case of fungi, the region with high variability in the ITS gene was targeted using the primers ITS1F (5′-CTTGGTCATTTAGAG GAAGTAA-3′) and ITS2 (5′-GCTGCGTTCTTCATCGATGC-3′) to amplify the ITS1 region of the 18S rRNA gene (Koljalg et al., 2013). After amplification, the integrity of the PCR products was tested by electrophoresis with agarose at a concentration of 1.8%, and a sequencing library was established quantitatively and uniformly. The established library was first inspected and subsequently sequenced on an Illumina NovaSeq 6000.

2.4.3 Computational analysis

To preprocess the data, we employed Trimmomatic v0.33 software to filter the raw reads obtained from sequencing. Cutadapt 1.9.1 software was subsequently used to detect and eliminate primer sequences, resulting in clean reads devoid of any primer sequences. Then, paired-end sequence splicing was performed with Usearch v10 software to concatenate overlapping clean reads from each sample, and length filtration was applied based on the specific ranges in different regions. Finally, the final valid data (nonchimeric reads) were obtained by denoising and removing chimeric sequences using the dada2 method in QIIME2 2020.6 software (Callahan et al., 2016; Bolyen et al., 2019).

2.5 Data analysis

Univariate analysis of variance (LSD for multiple comparisons) was used for soil physicochemical property and microbial alpha diversity data. Beta diversity was analyzed by nonmetric multidimensional scaling (NMDS) with "vegan" in R and Bray–Curtis dissimilarity, and the differences in microbial communities under different phosphorus treatments were tested by ANOSIM. Correlations between keystone species at the phylum level abundance and soil physicochemical properties determined via redundancy analysis (RDA) (performed with Canoco software). Relationships between environmental factors and topological properties of the co-occurrence network were analyzed based on Pearson correlation-based analysis. In addition, we used the "relaimpo" package in R to evaluate the effects of soil physicochemical properties, microbial diversity and keystone species in the bacteria–fungus cross-domain co-occurrence network on the growth of *Leymus chinensis* (Jiao et al., 2019).

The relative abundances of bacteria and fungi were screened before conducting the ecological network analysis. To ensure the accuracy of the network analysis, only the top 0.1% of the bacterial and fungal taxa were chosen based on their relative abundance. Additionally, more than 60% of the soil samples were included in the network analysis (Yang et al., 2022). We analyzed the bacterial-fungal cross-domain co-occurrence network under different fertilization conditions. First, the "phyloseq" package in R was used to construct the data frame for bacterial and fungal ASVs, and the correlation between the ASVs of bacteria and fungi was calculated using the "ggClusterNet" software package (Spearman correlation was used, $R2 > 0.9$; $p < 0.05$) (Wen et al., 2022). The networks were evaluated by calculating their topological characteristics, including the number of edges, average degree, and average path length, Finally, visualization with Cytoscape 3.9.1. Robustness and natural connectivity are used to determine the stability of the network, and nodes are randomly removed from the constructed co-occurrence network to describe the

natural connectivity changes. Robustness was calculated by randomly removing network nodes (50% of nodes were removed) as the ratio between natural connectivity and nonremoval (Deng et al., 2012; Wang et al., 2023). Keystone species were identified as network hubs and module hubs based on the intramodular connectivity (Zi) and intermodular connectivity (Pi) of bacteria-fungi cross-domain co-occurrence networks. Connectors have Pi values higher than 0.62, while module hubs have Zi values greater than 2.5. Conversely, peripherals are characterized by Pi values less than 0.62 and Zi values less than 2.5 (Cong et al., 2015; Shi et al., 2020a).

3 Results

3.1 Effects of phosphorus on soil physicochemical properties, growth of *Leymus chinensis*

Phosphorus addition significantly increased soil nutrients at 0–20 cm in the artificial *Leymus chinensis* grassland (Table 1). Compared with P0, AP, AN and TP increased with the addition of phosphorus, increasing by 58.02%–137.61%, 2.45–22.47% and 0–24.32%, respectively. Phosphorus addition had no significant effect on the soil pH, EC, or TN ($p > 0.05$). Phosphorus significantly changed the growth of *Leymus chinensis* (Table 2). Compared with P0, phosphorus addition enhanced the number of stems, biomass, and plant height of *Leymus chinensis* in by 43.69%–54.96%, 10.20%–24.04%, and 12.38%–23.04%, respectively.

3.2 Effects of phosphorus treatments on the diversity of soil bacteria and fungi

Through high-throughput sequencing, 959,619 and 935,153 effective chimeric sequences were obtained for bacteria and fungi from 12 soil samples, respectively, among which 958,122 (99.84%) and 931,844 (99.65%) were high-quality sequences. The OUT dilution curve was used to reflect whether the test results covered all taxonomic groups, and the results of the dilution curve showed that the sequencing data covered all taxonomic groups (Figures 1A,B).

There was no significant effect ($p > 0.05$) on the bacterial or fungal abundance (ACE) or diversity (Simpson) after 3 years of continuous phosphorus addition (Table 3). The overall structure of the soil microbial communities was analyzed based on the Bray–Curtis variability (NMDS) method, which revealed differences in the structure of bacteria and fungi at different phosphorus concentrations; however, according to the ANOSIM test results, phosphorus did not significantly ($p > 0.05$) change the beta diversity of the bacterial and fungal communities (Figures 1C,D).

3.3 Effect of phosphorus addition on the bacterial-fungal cross-domain co-occurrence network

The complexity of the bacteria–fungi cross-domain co-occurrence network differed significantly under the addition of different levels of phosphorus (Figure 2; Table 4). The P0 co-occurrence network contained 592 edges among 11,846 nodes, and the percentage of positive edges was 52.11%. Edges, nodes and average degree were all greater than those of P0. An elevated topological metric can directly or indirectly indicate an increase in the stability and intricacy of the co-occurrence network or a decrease in its stability and complexity. Stability was also assessed by network robustness natural connectivity, which was highest at P3 (Figure 3A). By calculating the natural connectivity of the network through the randomized removal of nodes, it was observed that the network's natural connectivity decreased with an increasing number of removed nodes. The highest natural connectivity was achieved at P0 and increased as the concentration of phosphorus added increased (Figure 3B). Among the co-occurrence networks associated with different phosphorus concentrations, we found that the nodes associated with bacteria were much more abundant than those associated with fungi; moreover, the proportion of positively correlated edges first increased and then decreased, and that associated with P2 was the highest.

3.4 Relationships between soil physical and chemical properties, keystone species and network topological characteristics

By analyzing the importance of nodes in the dominant network, key nodes (network hubs, module hubs, and connectors) were identified (Figure 4). In this study, we found that keystone species

TABLE 1 Effects of different phosphorus concentrations on soil physical and chemical properties.

Treatment	pH	EC (μS cm^{-1})	AP (mg kg^{-1})	AN (mg kg^{-1})	AK (mg kg^{-1})
P0	8.04 ± 0.06a	223.30 ± 17.63a	15.34 ± 4.08c	46.10 ± 3.63c	171.91 ± 6.149b
P1	8.05 ± 0.02a	188.16 ± 11.98a	24.24 ± 2.93b	47.23 ± 2.49bc	197.63 ± 8.06a
P2	8.08 ± 0.02a	227.23 ± 37.08a	25.02 ± 1.00b	54.15 ± 4.02ab	190.15 ± 23.53ab
P3	8.09 ± 0.01a	199.07 ± 30.67a	36.45 ± 3.26a	56.46 ± 5.67a	177.56 ± 7.40ab

Treatment	TP (g kg^{-1})	TN (g kg^{-1})	TC (g kg^{-1})	C/N
P0	0.37 ± 0.00b	0.14 ± 0.02a	7.33 ± 0.60a	52.64 ± 5.47a
P1	0.37 ± 0.01b	0.14 ± 0.01a	6.89 ± 0.09ab	48.63 ± 2.93ab
P2	0.42 ± 0.01ab	0.15 ± 0.01a	6.50 ± 0.11b	43.75 ± 1.07b
P3	0.46 ± 0.06a	0.15 ± 0.01a	7.60 ± 0.55a	51.84 ± 5.10a

were mainly concentrated in module hubs. These species were found in 56 ASVs in the fungal kingdom, mainly *Ascomycota*, *Basidiomycota*, *Mortierellomycota*, and *Glomeromycotan*. At these taxa levels, we identified 50 keystone genera (Schedule 1). The relative abundance of keystone species increased under phosphorus-addition conditions compared with that under P0 conditions (Figure 5A). The RDA results revealed significant relationships between keystone species and EC ($p < 0.01$) and between AN and AK ($p < 0.5$) (Figure 5B).

TABLE 2 Effects of different phosphorus concentrations on the stem number, biomass and plant height of *Leymus chinensis*.

Treatment	Stem number (plant/m²)	Biomass (g/m²)	Plant height (cm)
P0	551.70 ± 11.14b	457.20 ± 15.29b	54.68 ± 1.20c
P1	792.75 ± 33.30a	503.85 ± 9.95ab	61.45 ± 0.73b
P2	810.47 ± 11.89a	559.97 ± 29.62a	62.18 ± 1.31b
P3	854.90 ± 12.08a	567.10 ± 21.09a	67.28 ± 1.61a

Soil physical and chemical properties and co-occurrence network topological characteristics were analyzed based on Pearson correlation, and the results showed that soil C/N pair network edges and centralization closeness, AN, pH, and TN pair robustness, and AK had a significant relationship with average path length and degree centrality, while TC had a significant relationship with centralization closeness (Figure 5C) (Schedule 2).

3.5 Effects of soil physical and chemical properties and network keystone species on the growth of *Leymus chinensis*

The effects of soil physicochemical properties, microbial diversity and keystone species in the bacterial-fungal cross-domain co-occurrence network on the growth of *Leymus chinensis* were analyzed using multiple regression models (Figure 6). The results showed that soil nutrients were the main factors affecting the growth of *Leymus chinensis* plants under the different phosphorus addition

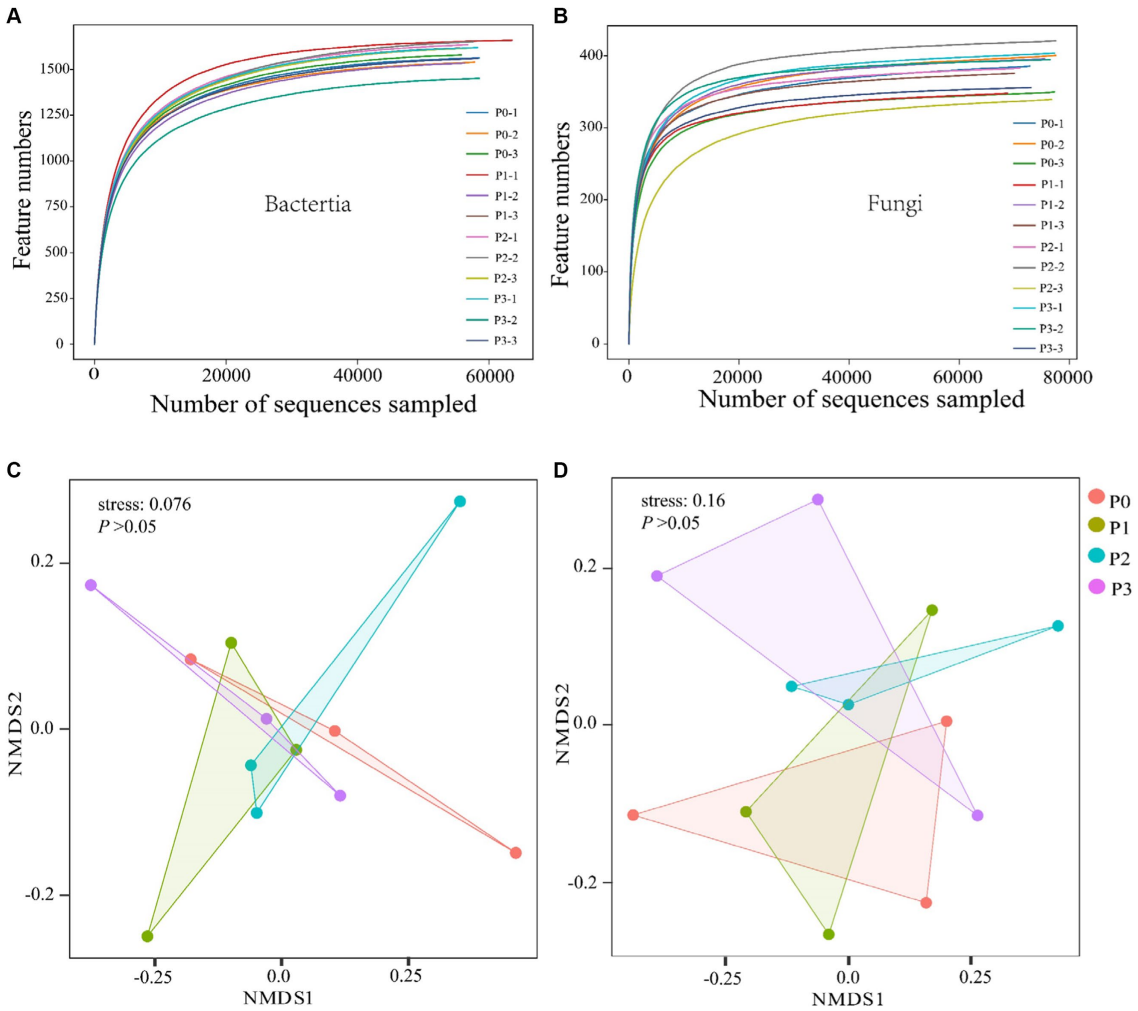

FIGURE 1
Analysis of soil bacterial and fungal diversity. **(A,B)** Show bacterial and fungal dilution curves. Nonmetric multidimensional scale (NMDS) analysis was conducted using the Bray–Curtis difference method. **(C,D)** Show the differences in bacterial and fungal microbial communities, respectively. ANOSIM was used to test the differences in microbial communities under different fertilization gradients.

10.3389/fmicb.2024.1289022

TABLE 3 Effects of different phosphorus concentrations on the alpha diversity of bacteria and fungi.

	Bacteria		Fungi	
Treatment	ACE	Simpson	ACE	Simpson
P0	1569.41 ± 18.96a	0.998 ± 0.000a	383.35 ± 26.86a	0.956 ± 0.012a
P1	1611.93 ± 60.33a	0.998 ± 0.000a	375.72 ± 23.98a	0.962 ± 0.018a
P2	1646.28 ± 18.83a	0.997 ± 0.001a	384.27 ± 39.91a	0.942 ± 0.043a
P3	1552.56 ± 85.05a	0.997 ± 0.000a	387.01 ± 26.39a	0.963 ± 0.004a

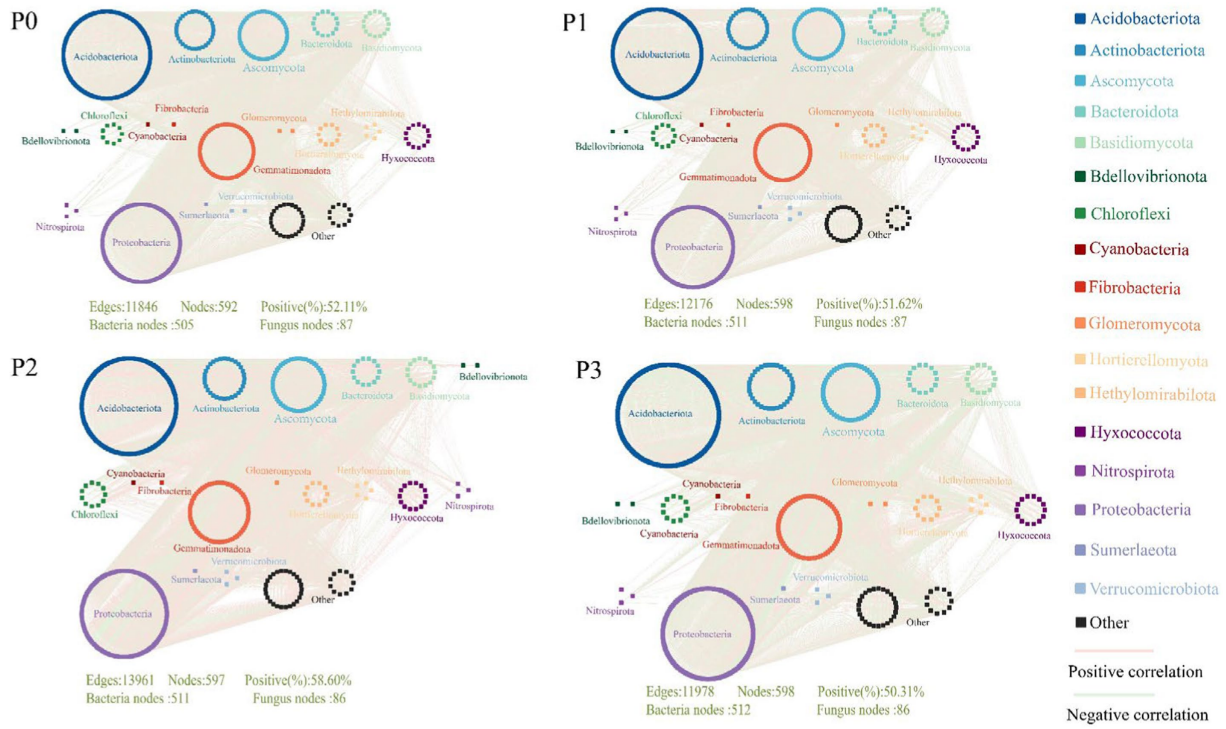

FIGURE 2
Cross-domain co-occurrence network of bacteria-fungi under different phosphorus level treatments.

gradients. For example, soil AP, TP and AN were the main variables affecting stem number, biomass and plant height. However, most of the keystone species in the co-occurrence network exhibited a negative correlation with the growth of *Leymus chinensis*. For example, the effects of Glomeromycotan on the stem number and biomass of *Leymus chinensis* were negatively correlated.

4 Discussion

4.1 Effects of phosphorus on soil physicochemical properties, *Leymus chinensis* growth and microbial diversity

The addition of phosphorus to grassland ecosystems can supplement the nutrients needed by plants, thereby improving soil fertility and productivity. The results of this study showed that pH, AP, AN, TP and TC increased with the addition of phosphorus (Table 1). These results are consistent with those of previous studies (Yu et al., 2009; Zhang et al., 2019; Jiang et al., 2022). These findings may be attributed to the concentration of phosphorus added and residual absorption by *Leymus chinensis* (Zhao et al., 2014; Shi et al., 2020b). In our study, phosphorus significantly affected the growth of *Leymus chinensis* (Table 2) because phosphorus is involved in many metabolic processes during plant growth, such as photosynthesis and other important life processes (Hasan et al., 2016; Li et al., 2016).

In our study, we examined how different levels of phosphorus affect the diversity of soil microbial communities in arid regions. We focused on engineered *Leymus chinensis* ecosystems and analyzed both alpha and beta diversity (Table 2) (Figures 1C,D). Changes in soil phosphorus content can directly or indirectly affect microbial species richness and diversity (DeForest and Scott, 2010; Luo et al., 2015). Our results showed that phosphorus addition did not significantly ($p > 0.05$) affect soil bacterial or fungal abundance (ACE) or diversity (Simpson), consistent with previous results, this is due to the strong buffering capacity of soils, where soil properties stabilize quickly after shorter nutrient additions, so exploring soil microbial changes in response to the environment requires long-term investigations (Xia et al., 2020; Ma et al., 2022). Changes in soil microbial richness may be directly or indirectly caused by changes in

10.3389/fmicb.2024.1289022

TABLE 4 Topological characteristics of the bacterial–fungal cross-domain co-occurrence network under phosphorus addition.

Network metrics	P0	P1	P2	P3
Edges	11,846	12,176	13,961	11,978
Num pos edges	6,173	6,285	8,181	6,026
Num neg edges	5,673	5,891	5,780	5,952
Positive (%)	52.11%	51.62%	58.60%	50.31%
Nodes	592	598	597	598
Bacteria nodes	505	511	511	512
Fungus nodes	87	87	86	86
Edge density	0.068	0.068	0.078	0.067
Average degree	40.02	40.72	46.77	40.06
Average path length	1.78	1.75	1.75	1.77
Degree centrality	0.30	0.21	0.26	0.29
Centralization betweenness	0.0053	0.0023	0.0039	0.0035
Centralization closeness	0.65	0.74	0.83	0.64

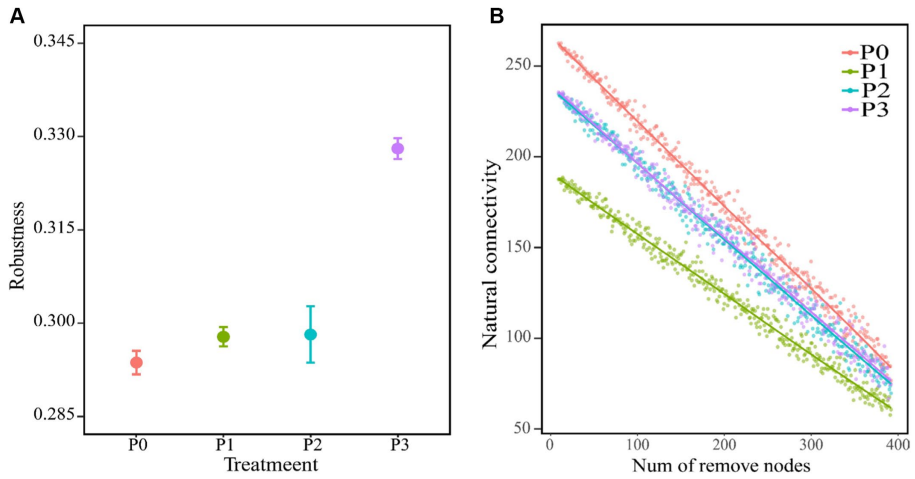

FIGURE 3
Co-occurring network stability. **(A)** Shows the robustness of the co-occurrence network (where 50% of the nodes are removed), with an average of ±SE and $n = 3$. **(B)** Is the change between the natural connectivity of the co-occurring network and the number of removed nodes.

environmental factors, such as pH (Gao et al., 2019; Wang et al., 2023b). P has no significant effect on soil pH for three consecutive years according to our results. The different phosphorus treatments had no significant effect on the microbial beta diversity ($p > 0.05$) (Figures 1C,D). It can be inferred that the response of the soil microbial community to phosphorus addition is low (Widdig et al., 2020), this because changes in soil microbial communities under phosphorus conditions are mainly due to nitrate dominance (Xia et al., 2020).

4.2 Effects of phosphorus addition on keystone species in co-occurrence networks

Co-occurrence network keystone species can have an enormous impact on other microorganisms and play an important role in maintaining ecosystem function (Berry and Widder, 2014; Ma et al., 2016; Banerjee et al., 2018). Keystone species richness in the co-occurrence network varies under different phosphorus conditions (Figure 5A), the fungal community structure under phosphorus conditions is affected by AN (Huang et al., 2016; Ai et al., 2018; Wu et al., 2023), which is consistent with our results. *Basidiomycota* and *Mortierellomycota* are closely related to soil pH, and phosphorus addition affects soil pH and thus abundance (Deng et al., 2021; Tarin et al., 2021). Some studies have shown that *Ascomycota* can promote soil nutrient cycling (Guo et al., 2020; Chang et al., 2022), this is in line with our findings that its abundance is positively correlated with soil nutrient content (Figure 5B). *Glomeromycotans* belong to a phylum of arbuscular mycorrhizal fungi that promote nutrient uptake (Spatafora et al., 2016; Wipf et al., 2019; Muneer et al., 2020). We speculate that the alteration of soil nutrients directly or indirectly promotes its mutually beneficial relationship with *Leymus chinensis*, thus affecting its richness.

10.3389/fmicb.2024.1289022

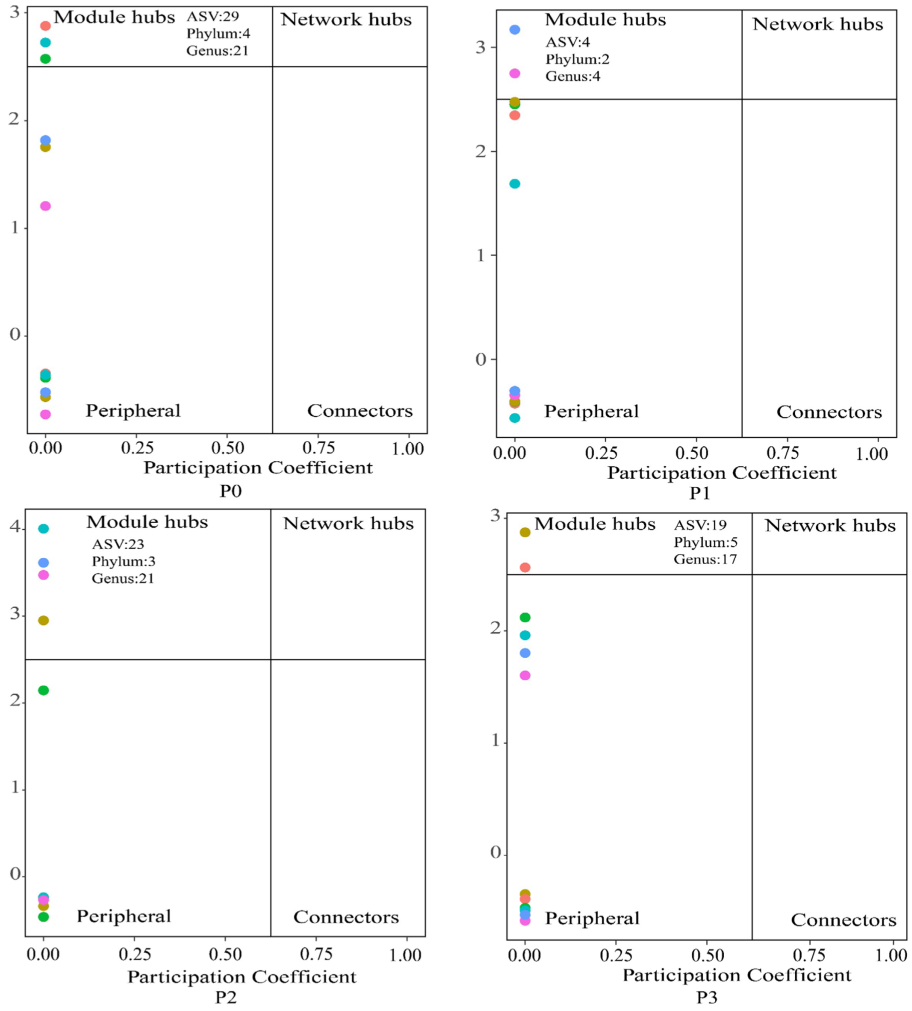

FIGURE 4
Effects of the addition of different phosphorus levels on the keystone species in the cooccurrence networks. Nodes are classified to identify keystone species in the network based on connectivity within a co-occurring network module (Zi) and connectivity between modules (Pi); connectors s: Pi > 0.62, module network hubs: Pi > 0.62, Zi > 2.5 and module hubs: Zi > 2.5 are identified as keystone species.

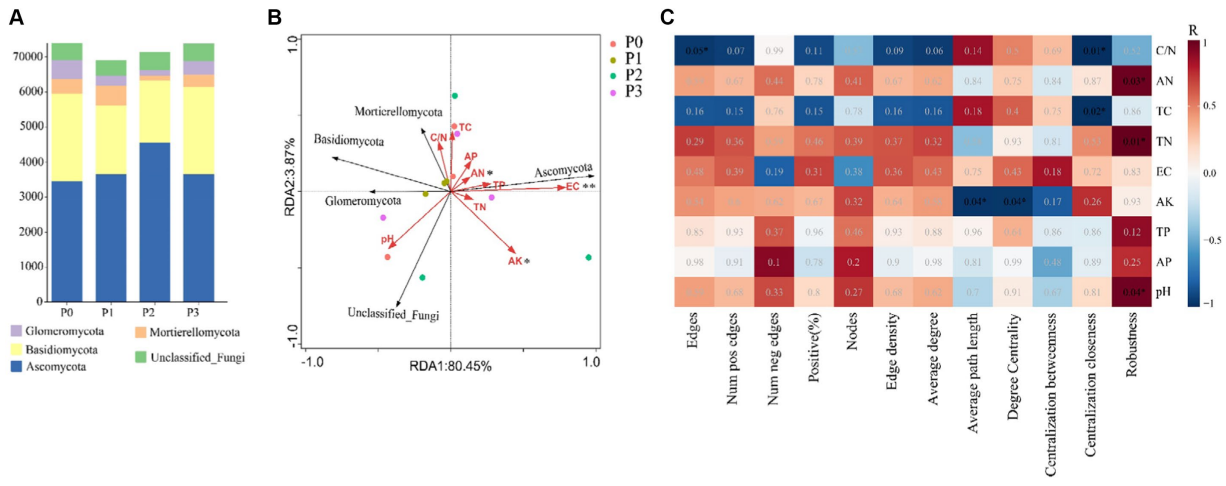

FIGURE 5
Keystone species abundance, keystone species and environmental factors and network topological characteristics and environmental factor relationships. **(A)** Is the relative richness at the key phylum level. **(B)** RDA of keystone species and environmental factors. **(C)** Based on the relationship between Pearson correlation environmental factors and cooccurrence network topological features. * Indicates that the significance level is $p < 0.05$, ** Indicates that the significance level is $p < 0.01$.

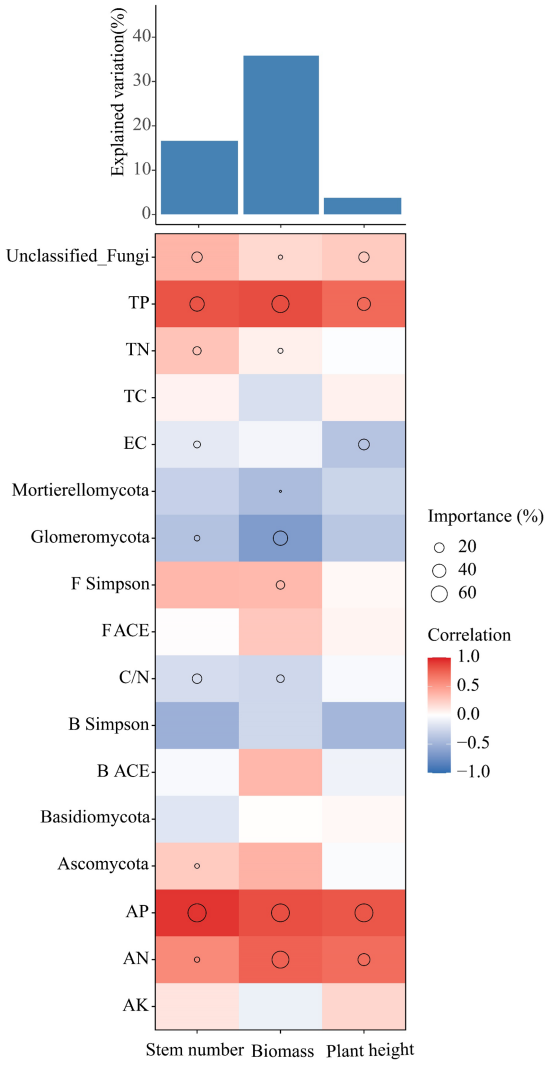

FIGURE 6
Analysis of soil physicochemical and microbial diversity and the contributions of keystone species in the co-occurrence network to the growth of *Leymus chinensis* based on correlation and optimal multiple regression models. The size of the circle indicates the significance of the variable, and the color represents Spearman's correlation.

4.3 Influence of phosphorus addition on the co-occurrence network

Microbial co-occurrence network analysis can be used not only to determine the interrelationships among groups but also to identify the keystone species that are closely related to the microbial community (Liu et al., 2013; Banerjee et al., 2016a,b). The results of this study showed that phosphorus treatment increased the stability and complexity of the bacteria–fungi co-occurrence networks. We hypothesize that this difference may be attributed to the increase in and accumulation of soil nutrients, which promote cooperation between microbial communities (Johnson, 2010; Trivedi et al., 2020; Lastovetsky et al., 2022). Among the keystone species in this study, *Glomeromycotan* is an arbuscular mycorrhizal fungus (AMF), and interactions between plants and AMF occur through the participation of many microorganisms that have positive effects on plant nutrient uptake. For example, the supply of phosphorus by AMF is facilitated by interactions with phosphorus-soluble bacteria. Phosphorus-soluble bacteria can move along AMF mycelia to reach organophosphorus patches that plants cannot reach (Zhang et al., 2014; Paul et al., 2017; Qian et al., 2019; Jiang et al., 2021). However, in our study, Glomeromycotan abundance was negatively correlated with the growth of *Leymus chinensis* (Figure 6). When Glomeromycotan plants form a symbiotic relationship with the root system of *Leymus chinensis*, they need to rely on the absorption of phosphorus and other nutrients and *Leymus chinensis* nutrient exchange to obtain carbon to maintain normal life activities, and when the phosphorus content in the soil increases, the symbiotic relationship between the two plants will increase (Williams et al., 2016; Qin et al., 2020). The reciprocal and antagonistic relationships between microbial community species can be represented by positive and negative correlation edges, respectively, in the co-occurrence network (Xu et al., 2017). Our study showed that P2 had the highest proportion of positively correlated edges (Table 3), possibly because the addition of phosphorus increased soil nutrients, thereby alleviating competition between microbial communities (Banerjee et al., 2016a,b). In addition, the keystone species in the co-occurrence network under different phosphorus levels were all fungi, which may be due to the long life cycle of fungi and the slow community replacement rate. In addition, changes in soil environmental factors caused by phosphorus addition had a relatively small impact on fungi, and the community had a high diffusion ability (Stegen et al., 2013; Zhou and Ning, 2017).

5 Conclusion

The use of microbial co-occurrence networks to determine the response of microbial communities to environmental changes is a novel approach. However, the response mechanism of microbial co-occurrence networks to phosphorus addition in artificial grassland ecosystems and the resulting impact systems are unclear. The results of the present study showed that phosphorus significantly affects the growth of *Leymus chinensis* but has no significant effect on soil bacterial or fungal alpha or beta diversity. The keystone species in the co-occurrence network exhibited significant relationships with AN, AK, and EC, and phosphorus enhanced the stability and complexity of the bacteria–fungi cross-domain co-occurrence network. The growth of artificial *Leymus chinensis* was mainly due to the soil phosphorus content and effects of AN. This study revealed the factors influencing the growth of *Leymus chinensis* in artificial grasslands in arid zones and provided a theoretical basis for the construction of artificial grasslands.

Data availability statement

The datasets presented in this study can be found in online repositories. The names of the repository/repositories and accession number(s) can be found in the article/supplementary material.

Author contributions

XZ: Methodology, Investigation, Conceptualization, Data curation, Writing – original draft. YH: Writing – review & editing, Project administration, Funding acquisition, Conceptualization. HL: Writing – original draft, Conceptualization. JS: Supervision, Methodology, Writing – review & editing. JC: Software, Data curation, Writing – review & editing. TZ: Data curation, Writing – original draft. YZ: Writing – original draft, Data curation.

Funding

The author(s) declare financial support was received for the research, authorship, and/or publication of this article. This work was funded by the Natural Science Foundation of Xinjiang Uygur Autonomous Region (2022D01A187) and the Natural Science Foundation of Xinjiang Uygur Autonomous Region (2019D01B19), the Postdoctoral Station of Grass Science, Xinjiang Agricultural University, and the Xinjiang Key Laboratory of Soil and Plant Ecological Processes.

Conflict of interest

The authors declare that the research was conducted in the absence of any commercial or financial relationships that could be construed as a potential conflict of interest.

Publisher's note

All claims expressed in this article are solely those of the authors and do not necessarily represent those of their affiliated organizations, or those of the publisher, the editors and the reviewers. Any product that may be evaluated in this article, or claim that may be made by its manufacturer, is not guaranteed or endorsed by the publisher.

Supplementary material

The Supplementary material for this article can be found online at: https://www.frontiersin.org/articles/10.3389/fmicb.2024.1289022/full#supplementary-material

References

Ai, C., Zhang, S., Zhang, X., Guo, D., Zhou, W., and Huang, S. (2018). Distinct responses of soil bacterial and fungal communities to changes in fertilization regime and crop rotation. *Geoderma* 319, 156–166. doi: 10.1016/j.geoderma.2018.01.010

Anzuay, M. S., Ciancio, M. G. R., Luduena, L. M., Angelini, J. G., Barros, G., Pastor, N., et al. (2017). Growth promotion of peanut (*Arachis hypogaea* L.) and maize (*Zea mays* L.) plants by single and mixed cultures of efficient phosphate solubilizing bacteria that are tolerant to abiotic stress and pesticides. *Microbiol. Res.* 199, 98–109. doi: 10.1016/j.micres.2017.03.006

Banerjee, S., Baah-Acheamfour, M., Carlyle, C. N., Bissett, A., Richardson, A. E., Siddique, T., et al. (2016a). Determinants of bacterial communities in Canadian agroforestry systems. *Environ. Microbiol.* 18, 1805–1816. doi: 10.1111/1462-2920.12986

Banerjee, S., Kirkby, C. A., Schmutter, D., Bissett, A., Kirkegaard, J. A., and Richardson, A. E. (2016b). Network analysis reveals functional redundancy and keystone taxa amongst bacterial and fungal communities during organic matter decomposition in an arable soil. *Soil Biol. Biochem.* 97, 188–198. doi: 10.1016/j.soilbio.2016.03.017

Banerjee, S., Schlaeppi, K., and van der Heijden, M. G. A. (2018). Keystone taxa as drivers of microbiome structure and functioning. *Nat. Rev. Microbiol.* 16, 567–576. doi: 10.1038/s41579-018-0024-1

Bao, S. (2000). *Soil agrochemical analysis. 3rd* Edn China Agricultural Press.

Baoyin, T., Li, F. Y., Bao, Q., Minggagud, H., and Zhong, Y. (2014). Effects of mowing regimes and climate variability on hay production of *Leymus chinensis* (Trin.) Tzvelev grassland in northern China. *Rangeland J.* 36:593. doi: 10.1071/rj13088

Berry, D., and Widder, S. (2014). Deciphering microbial interactions and detecting keystone species with co-occurrence networks. *Front. Microbiol.* 5:219. doi: 10.3389/fmicb.2014.00219

Bolyen, E., Rideout, J. R., Dillon, M. R., Bokulich, N. A., Abnet, C. C., Al-Ghalith, G. A., et al. (2019). Reproducible, interactive, scalable and extensible microbiome data science using QIIME 2. *Nat. Biotechnol.* 37, 852–857. doi: 10.1038/s41587-019-0209-9

Bragazza, L., Parisod, J., Buttler, A., and Bardgett, R. D. (2012). Biogeochemical plant–soil microbe feedback in response to climate warming in peatlands. *Nat. Clim. Chang.* 3, 273–277. doi: 10.1038/nclimate1781

Callahan, B. J., McMurdie, P. J., Rosen, M. J., Han, A. W., Johnson, A. J., and Holmes, S. P. (2016). DADA2: High-resolution sample inference from Illumina amplicon data. *Nat. Methods* 13, 581–583. doi: 10.1038/nmeth.3869

Ceci, A., Pinzari, F., Russo, F., Maggi, O., and Persiani, A. M. (2018). Saprotrophic soil fungi to improve phosphorus solubilisation and release: *In vitro* abilities of several species. *Ambio* 47, 30–40. doi: 10.1007/s13280-017-0972-0

Chang, Y., Chen, F., Zhu, Y., You, Y., Cheng, Y., and Ma, J. (2022). Influence of revegetation on soil microbial community and its assembly process in the open-pit mining area of the Loess Plateau, China. *Front. Microbiol.* 13:992816. doi: 10.3389/fmicb.2022.992816

Cong, J., Yang, Y., Liu, X., Lu, H., Liu, X., Zhou, J., et al. (2015). Analyses of soil microbial community compositions and functional genes reveal potential consequences of natural forest succession. *Sci. Rep.* 5:10007. doi: 10.1038/srep10007

DeForest, J. L., and Scott, L. G. (2010). Available organic soil phosphorus has an important influence on microbial community composition. *Soil Sci. Soc. Am. J.* 74, 2059–2066. doi: 10.2136/sssaj2009.0426

Deng, Y., Jiang, Y. H., Yang, Y., He, Z., Luo, F., and Zhou, J. (2012). Molecular ecological network analyses. *BMC Bioinformatics* 13:113. doi: 10.1186/1471-2105-13-113

Deng, Q., Zhang, T., Xie, D., and Yang, Y. (2021). Rhizosphere microbial communities are significantly affected by optimized phosphorus management in a slope farming system. *Front. Microbiol.* 12:739844. doi: 10.3389/fmicb.2021.739844

Deveau, A., Bonito, G., Uehling, J., Paoletti, M., Becker, M., Bindschedler, S., et al. (2018). Bacterial-fungal interactions: ecology, mechanisms and challenges. *FEMS Microbiol. Rev.* 42, 335–352. doi: 10.1093/femsre/fuy008

Fan, K., Delgado-Baquerizo, M., Guo, X., Wang, D., Wu, Y., Zhu, M., et al. (2019). Suppressed N fixation and diazotrophs after four decades of fertilization. *Microbiome* 7:143. doi: 10.1186/s40168-019-0757-8

Faust, K., and Raes, J. (2012). Microbial interactions: from networks to models. *Nat. Rev. Microbiol.* 10, 538–550. doi: 10.1038/nrmicro2832

Fuhrman, J. A. (2009). Microbial community structure and its functional implications. *Nature* 459, 193–199. doi: 10.1038/nature08058

Gao, G. F., Li, P. F., Zhong, J. X., Shen, Z. J., Chen, J., Li, Y. T., et al. (2019). *Spartina alterniflora* invasion alters soil bacterial communities and enhances soil N(2)O emissions by stimulating soil denitrification in mangrove wetland. *Sci. Total Environ.* 653:231. doi: 10.1016/j.scitotenv.2018.10.277

Guo, X., Feng, J., Shi, Z., Zhou, X., Yuan, M., Tao, X., et al. (2018). Climate warming leads to divergent succession of grassland microbial communities. *Nat. Clim. Chang.* 8, 813–818. doi: 10.1038/s41558-018-0254-2

Guo, Z., Wan, S., Hua, K., Yin, Y., Chu, H., Wang, D., et al. (2020). Fertilization regime has a greater effect on soil microbial community structure than crop rotation and growth stage in an agroecosystem. *Appl. Soil Ecol.* 149:103510. doi: 10.1016/j.apsoil.2020.103510

Hasan, M. M., Hasan, M. M., Teixeira da Silva, J. A., and Li, X. (2016). Regulation of phosphorus uptake and utilization: transitioning from current knowledge to practical strategies. *Cell. Mol. Biol. Lett.* 21:7. doi: 10.1186/s11658-016-0008-y

Herren, C. M., and McMahon, K. D. (2018). Keystone taxa predict compositional change in microbial communities. *Environ. Microbiol.* 20, 2207–2217. doi: 10.1111/1462-2920.14257

Heuer, S., Gaxiola, R., Schilling, R., Herrera-Estrella, L., Lopez-Arredondo, D., Wissuwa, M., et al. (2017). Improving phosphorus use efficiency: a complex trait with emerging opportunities. *Plant J.* 90, 868–885. doi: 10.1111/tpj.13423

Huang, J., Hu, B., Qi, K., Chen, W., Pang, X., Bao, W., et al. (2016). Effects of phosphorus addition on soil microbial biomass and community composition in a subalpine spruce plantation. *Eur. J. Soil Biol.* 72, 35–41. doi: 10.1016/j.ejsobi.2015.12.007

Jiang, Q., Madramootoo, C. A., and Qi, Z. (2022). Soil carbon and nitrous oxide dynamics in corn (*Zea mays* L.) production under different nitrogen, tillage and residue management practices. *Field Crop Res.* 277:108421. doi: 10.1016/j.fcr.2021.108421

Jiang, F., Zhang, L., Zhou, J., George, T. S., and Feng, G. (2021). Arbuscular mycorrhizal fungi enhance mineralisation of organic phosphorus by carrying bacteria along their extraradical hyphae. *New Phytol.* 230, 304–315. doi: 10.1111/nph.17081

Jiao, S., Xu, Y., Zhang, J., Hao, X., and Lu, Y. (2019). Core microbiota in agricultural soils and their potential associations with nutrient cycling. *mSystems* 4:e00313-18. doi: 10.1128/mSystems.00313-18

Johnson, N. C. (2010). Resource stoichiometry elucidates the structure and function of arbuscular mycorrhizas across scales. *New Phytol.* 185, 631–647. doi: 10.1111/j.1469-8137.2009.03110.x

Koljalg, U., Nilsson, R. H., Abarenkov, K., Tedersoo, L., Taylor, A. F., Bahram, M., et al. (2013). Towards a unified paradigm for sequence-based identification of fungi. *Mol. Ecol.* 22, 5271–5277. doi: 10.1111/mec.12481

Lastovetsky, O. A., Caruso, T., Brennan, F. P., Wall, D. P., McMahon, S., and Doyle, E. (2022). Evidence of a selective and bi-directional relationship between arbuscular mycorrhizal fungal and bacterial communities co-inhabiting plant roots. *Environ. Microbiol.* 24, 5378–5391. doi: 10.1111/1462-2920.16227

Li, J., Cooper, J. M., Lin, Z., Li, Y., Yang, X., and Zhao, B. (2015). Soil microbial community structure and function are significantly affected by long-term organic and mineral fertilization regimes in the North China Plain. *Appl. Soil Ecol.* 96, 75–87. doi: 10.1016/j.apsoil.2015.07.001

Li, H., Hu, Y., Liu, G., Sheng, J., Zhang, W., Zhao, H., et al. (2023). Responses of biomass accumulation and nutrient utilization along a phosphorus supply gradient in *Leymus chinensis*. *Sci. Rep.* 13:5660. doi: 10.1038/s41598-023-31402-4

Li, L., Yang, H., Ren, W., Liu, B., Cheng, D., Wu, X., et al. (2016). Physiological and biochemical characterization of sheepgrass (*Leymus chinensis*) reveals insights into photosynthetic apparatus coping with low-phosphate stress conditions. *Journal of Plant Biology* 59, 336–346. doi: 10.1007/s12374-016-0117-1

Lin, Y., Ye, G., Kuzyakov, Y., Liu, D., Fan, J., and Ding, W. (2019). Long-term manure application increases soil organic matter and aggregation, and alters microbial community structure and keystone taxa. *Soil Biol. Biochem.* 134, 187–196. doi: 10.1016/j.soilbio.2019.03.030

Liu, X., Liu, H., Ren, D., Liu, C., Zhang, Y., Wang, S., et al. (2022). Interlinkages between soil properties and keystone taxa under different tillage practices on the North China Plain. *Appl. Soil Ecol.* 178:104551. doi: 10.1016/j.apsoil.2022.104551

Liu, L., Zhang, T., Gilliam, F. S., Gundersen, P., Zhang, W., Chen, H., et al. (2013). Interactive effects of nitrogen and phosphorus on soil microbial communities in a tropical forest. *PLoS One* 8:e61188. doi: 10.1371/journal.pone.0061188

Luo, P., Han, X., Wang, Y., Han, M., Shi, H., Liu, N., et al. (2015). Influence of long-term fertilization on soil microbial biomass, dehydrogenase activity, and bacterial and fungal community structure in a brown soil of northeast China. *Ann. Microbiol.* 65, 533–542. doi: 10.1007/s13213-014-0889-9

Luo, B., Ma, P., Nie, Z., Zhang, X., He, X., Ding, X., et al. (2019). Metabolite profiling and genome-wide association studies reveal response mechanisms of phosphorus deficiency in maize seedling. *Plant J.* 97, 947–969. doi: 10.1111/tpj.14160

Ma, B., Wang, H., Dsouza, M., Lou, J., He, Y., Dai, Z., et al. (2016). Geographic patterns of co-occurrence network topological features for soil microbiota at continental scale in eastern China. *ISME J.* 10, 1891–1901. doi: 10.1038/ismej.2015.261

Ma, B., Zhao, K., Lv, X., Su, W., Dai, Z., Gilbert, J. A., et al. (2018). Genetic correlation network prediction of forest soil microbial functional organization. *ISME J.* 12, 2492–2505. doi: 10.1038/s41396-018-0232-8

Ma, X., Zhou, Z., Chen, J., Xu, H., Ma, S., Dippold, M. A., et al. (2022). Long-term nitrogen and phosphorus fertilization reveals that phosphorus limitation shapes the microbial community composition and functions in tropical montane forest soil. *Sci. Total Environ.* 854:158709. doi: 10.1016/j.scitotenv.2022.158709

Muneer, M. A., Wang, P., Zaib-un-Nisa, , Lin, C., and Ji, B. (2020). Potential role of common mycorrhizal networks in improving plant growth and soil physicochemical properties under varying nitrogen levels in a grassland ecosystem. *Glob. Ecol. Conserv.* 24:e01352. doi: 10.1016/j.gecco.2020.e01352

Paul, R., Singh, R. D., Patra, A. K., Biswas, D. R., Bhattacharyya, R., and Arunkumar, K. (2017). Phosphorus dynamics and solubilizing microorganisms in acid soils under different land uses of Lesser Himalayas of India. *Agrofor. Syst.* 92, 449–461. doi: 10.1007/s10457-017-0168-4

Qian, T., Yang, Q., Jun, D. C. F., Dong, F., and Zhou, Y. (2019). Transformation of phosphorus in sewage sludge biochar mediated by a phosphate-solubilizing microorganism. *Chem. Eng. J.* 359, 1573–1580. doi: 10.1016/j.cej.2018.11.015

Qin, Z., Zhang, H., Feng, G., Christie, P., Zhang, J., Li, X., et al. (2020). Soil phosphorus availability modifies the relationship between AM fungal diversity and mycorrhizal benefits to maize in an agricultural soil. *Soil Biol. Biochem.* 144:107790. doi: 10.1016/j.soilbio.2020.107790

Quast, C., Pruesse, E., Yilmaz, P., Gerken, J., Schweer, T., Yarza, P., et al. (2013). The SILVA ribosomal RNA gene database project: improved data processing and web-based tools. *Nucleic Acids Res.* 41, D590–D596. doi: 10.1093/nar/gks1219

Rashid, M. I., Mujawar, L. H., Shahzad, T., Almeelbi, T., Ismail, I. M., and Oves, M. (2016). Bacteria and fungi can contribute to nutrients bioavailability and aggregate formation in degraded soils. *Microbiol. Res.* 183, 26–41. doi: 10.1016/j.micres.2015.11.007

Shi, Y., Delgado-Baquerizo, M., Li, Y., Yang, Y., Zhu, Y. G., Penuelas, J., et al. (2020a). Abundance of kinless hubs within soil microbial networks are associated with high functional potential in agricultural ecosystems. *Environ. Int.* 142:105869. doi: 10.1016/j.envint.2020.105869

Shi, Y., Ziadi, N., Hamel, C., Bélanger, G., Abdi, D., Lajeunesse, J., et al. (2020b). Soil microbial biomass, activity and community structure as affected by mineral phosphorus fertilization in grasslands. *Appl. Soil Ecol.* 146:103391. doi: 10.1016/j.apsoil.2019.103391

Spatafora, J. W., Chang, Y., Benny, G. L., Lazarus, K., Smith, M. E., Berbee, M. L., et al. (2016). A phylum-level phylogenetic classification of zygomycete fungi based on genome-scale data. *Mycologia* 108, 1028–1046. doi: 10.3852/16-042

Stegen, J. C., Lin, X., Fredrickson, J. K., Chen, X., Kennedy, D. W., Murray, C. J., et al. (2013). Quantifying community assembly processes and identifying features that impose them. *ISME J.* 7, 2069–2079. doi: 10.1038/ismej.2013.93

Tarin, M. W. K., Fan, L., Xie, D., Tayyab, M., Rong, J., Chen, L., et al. (2021). Response of soil fungal diversity and community composition to varying levels of bamboo biochar in red soils. *Microorganisms* 9:1385. doi: 10.3390/microorganisms9071385

Tian, W., Wang, L., Li, Y., Zhuang, K., and Li, G. (2015). Responses of microbial activity, abundance, and community in wheat soil after three years of heavy fertilization with manure-based compost and inorganic nitrogen. *Agriculture, Ecosystems & Environment*, 213, 219–227. doi: 10.1016/j.agee.2015.08.009

Trivedi, P., Leach, J. E., Tringe, S. G., Sa, T., and Singh, B. K. (2020). Plant-microbiome interactions: from community assembly to plant health. *Nat. Rev. Microbiol.* 18, 607–621. doi: 10.1038/s41579-020-0412-1

Wagg, C., Schlaeppi, K., Banerjee, S., Kuramae, E. E., and van der Heijden, M. G. A. (2019). Fungal-bacterial diversity and microbiome complexity predict ecosystem functioning. *Nat. Commun.* 10:4841. doi: 10.1038/s41467-019-12798-y

Wang, Y., Dang, N., Feng, K., Wang, J., Jin, X., Yao, S., et al. (2023a). Grass-microbial inter-domain ecological networks associated with alpine grassland productivity. *Front. Microbiol.* 14:1109128. doi: 10.3389/fmicb.2023.1109128

Wang, X., Liang, C., Mao, J., Jiang, Y., Bian, Q., Liang, Y., et al. (2023). Microbial keystone taxa drive succession of plant residue chemistry. *ISME J.* 17, 748–757. doi: 10.1038/s41396-023-01384-2

Wang, D., Lv, S., Jiang, P., and Li, Y. (2017). Roles, regulation, and agricultural application of plant phosphate transporters. *Front. Plant Sci.* 8:817. doi: 10.3389/fpls.2017.00817

Wang, Y., Men, J., Zheng, T., Ma, Y., Li, W., Cernava, T., et al. (2023b). Impact of pyroxasulfone on sugarcane rhizosphere microbiome and functioning during field degradation. *J. Hazard. Mater.* 455:131608. doi: 10.1016/j.jhazmat.2023.131608

Wen, T., Xie, P., Yang, S., Niu, G., and Liu, X. (2022). ggClusterNet: An R package for microbiome network analysis and modularity-based multiple network layouts. *iMeta*, 1, doi: 10.1002/imt2.32

Widdig, M., Heintz-Buschart, A., Schleuss, P.-M., Guhr, A., Borer, E. T., Seabloom, E. W., et al. (2020). Effects of nitrogen and phosphorus addition on microbial community composition and element cycling in a grassland soil. *Soil Biol. Biochem.* 151:108041. doi: 10.1016/j.soilbio.2020.108041

Williams, A., Manoharan, L., Rosenstock, N. P., Olsson, P. A., and Hedlund, K. (2016). Long-term agricultural fertilization alters arbuscular mycorrhizal fungal community composition and barley (*Hordeum vulgare*) mycorrhizal carbon and phosphorus exchange. *New Phytol.* 213, 874–885. doi: 10.1111/nph.14196

Wipf, D., Krajinski, F., van Tuinen, D., Recorbet, G., and Courty, P. E. (2019). Trading on the arbuscular mycorrhiza market: from arbuscules to common mycorrhizal networks. *New Phytol.* 223, 1127–1142. doi: 10.1111/nph.15775

Wu, C., Yan, B., Wei, F., Wang, H., Gao, L., Ma, H., et al. (2023). Long-term application of nitrogen and phosphorus fertilizers changes the process of community construction by affecting keystone species of crop rhizosphere microorganisms. *Sci. Total Environ.* 897:165239. doi: 10.1016/j.scitotenv.2023.165239

Xia, Z., Yang, J., Sang, C., Wang, X., Sun, L., Jiang, P., et al. (2020). Phosphorus reduces negative effects of nitrogen addition on soil microbial communities and functions. *Microorganisms* 8:1828. doi: 10.3390/microorganisms8111828

Xu, F., Cai, T., Yang, X., and Sui, W. (2017). Soil fungal community variation by large-scale reclamation in Sanjiang plain, China. *Ann. Microbiol.* 67, 679–689. doi: 10.1007/s13213-017-1296-9

Yang, F., Chen, Q., Zhang, Q., Long, C., Jia, W., Cheng, X., et al. (2021). Keystone species affect the relationship between soil microbial diversity and ecosystem function under land use change in subtropical China. *Funct. Ecol.* 35, 1159–1170. doi: 10.1111/1365-2435.13769

Yang, Y., Shi, Y., Fang, J., Chu, H., and Adams, J. M. (2022). Soil microbial network complexity varies with ph as a continuum, not a threshold, across the North China plain. *Front. Microbiol.* 13:895687. doi: 10.3389/fmicb.2022.895687

Yu, Z.-Y., Zeng, D.-H., Jiang, F.-Q., and Zhao, Q. (2009). Responses of biomass to the addition of water, nitrogen and phosphorus in Keerqin sandy grassland, Inner Mongolia, China. *J. For. Res.* 20, 23–26. doi: 10.1007/s11676-009-0004-4

Zhang, L., Fan, J., Ding, X., He, X., Zhang, F., and Feng, G. (2014). Hyphosphere interactions between an arbuscular mycorrhizal fungus and a phosphate solubilizing bacterium promote phytate mineralization in soil. *Soil Biol. Biochem.* 74, 177–183. doi: 10.1016/j.soilbio.2014.03.004

Zhang, L., Shao, H., Wang, B., Zhang, L., and Qin, X. (2019). Effects of nitrogen and phosphorus on the production of carbon dioxide and nitrous oxide in salt-affected soils under different vegetation communities. *Atmos. Environ.* 204, 78–88. doi: 10.1016/j.atmosenv.2019.02.024

Zhao, S., Qiu, S., Cao, C., Zheng, C., Zhou, W., and He, P. (2014). Responses of soil properties, microbial community and crop yields to various rates of nitrogen fertilization in a wheat–maize cropping system in north-central China. *Agric. Ecosyst. Environ.* 194, 29–37. doi: 10.1016/j.agee.2014.05.006

Zhou, J. Z., and Ning, D. (2017). Stochastic community assembly: does it matter in microbial ecology? *Microbiol. Mol. Biol. Rev.* 81, e00002–e00017. doi: 10.1128/MMBR

Zhou, J., Deng, Y., Luo, F., He, Z., Tu, Q., and Zhi, X. (2010). Functional molecular ecological networks. *MBio* 1:1. doi: 10.1128/mBio.00169-10

frontiers | Frontiers in Microbiology

TYPE Original Research
PUBLISHED 28 March 2024
DOI 10.3389/fmicb.2024.1368215

Check for updates

OPEN ACCESS

EDITED BY
Zhenlin Han,
University of Hawaii at Manoa, United States

REVIEWED BY
Dirk Benndorf,
Otto von Guericke University Magdeburg, Germany
Hao Zhou,
Dalian University of Technology, China
Minmin Pan,
Helmholtz Association of German Research Centres (HZ), Germany

*CORRESPONDENCE
Yue-Qin Tang
✉ tangyq@scu.edu.cn

RECEIVED 10 January 2024
ACCEPTED 20 March 2024
PUBLISHED 28 March 2024

CITATION
Yao J, Zhang Q, Gou M and Tang Y-Q (2024) High synthetic cost-amino acids reduce member interactions of acetate-degrading methanogenic microbial community. *Front. Microbiol.* 15:1368215. doi: 10.3389/fmicb.2024.1368215

COPYRIGHT
© 2024 Yao, Zhang, Gou and Tang. This is an open-access article distributed under the terms of the Creative Commons Attribution License (CC BY). The use, distribution or reproduction in other forums is permitted, provided the original author(s) and the copyright owner(s) are credited and that the original publication in this journal is cited, in accordance with accepted academic practice. No use, distribution or reproduction is permitted which does not comply with these terms.

High synthetic cost-amino acids reduce member interactions of acetate-degrading methanogenic microbial community

Jian Yao[1,2], Quan Zhang[3], Min Gou[1,2] and Yue-Qin Tang[1,2]*

[1]College of Architecture and Environment, Sichuan University, Chengdu, Sichuan, China, [2]Sichuan Environmental Protection Key Laboratory of Organic Wastes Valorization, Chengdu, Sichuan, China, [3]SINOPEC (Dalian) Research Institute of Petroleum and Petrochemicals Co., Ltd., Dalian, Liaoning, China

Introduction: The cooperation among members of microbial communities based on the exchange of public goods such as 20 protein amino acids (AAs) has attracted widespread attention. However, little is known about how AAs availability affects interactions among members of complex microbial communities and the structure and function of a community.

Methods: To investigate this question, trace amounts of AAs combinations with different synthetic costs (low-cost, medium-cost, high-cost, and all 20 AAs) were supplemented separately to acetate-degrading thermophilic methanogenic reactors, and the differences in microbial community structure and co-occurring networks of main members were compared to a control reactor without AA supplementation.

Results: The structure of the microbial community and the interaction of community members were influenced by AAs supplementation and the AAs with different synthetic costs had different impacts. The number of nodes, links, positive links, and the average degree of nodes in the co-occurrence network of the microbial communities with AAs supplementation was significantly lower than that of the control without AAs supplementation, especially for all 20 AAs supplementation followed by the medium- and high-cost AAs supplementation. The average proportion of positive interactions of microbial members in the systems supplemented with low-cost, medium-cost, high-cost, all AAs, and the control group were 0.42, 0.38, 0.15, 0.4, and 0.45, respectively. In addition, the ecological functions of community members possibly changed with the supplementation of different cost AAs.

Discussion: These findings highlight the effects of AAs availability on the interactions among members of complex microbial communities, as well as on community function.

KEYWORDS

amino acid availability, acetate-degrading methanogenic microbial community, amino acid synthesis cost, microbiological interactions, microbial community structure

1 Introduction

Microorganisms in nature do not exist alone but often share a habitat with many other microorganisms. These microorganisms have very complex interactions with each other, which are critical for the stability of microbial community structure and ecological functions (Zengler and Zaramela, 2018). Currently, researchers have been trying to understand the interactions among individual microorganisms through mathematical modeling and construction of artificial laboratory floras, and one of the major research hotspots is the study of amino acid (AA) -based exchange cooperation of microorganisms.

As basic building blocks of proteins, AAs are essential for microorganisms. However, many studies have shown that many microorganisms that survive in AA-deficient environments are AA auxotrophic (Mee et al., 2014; Embree et al., 2015; Zhu et al., 2020). This means that the microorganisms in that habitat have to obtain AAs from the rest of the members and accordingly form an important symbiosis relationship. Mee et al. (2014) constructed 14 AA auxotrophs by using *Escherichia coli*. These auxotrophs were used to construct two-, three- and fourteen-member artificial microbial floras, and the differences among the structures of these microbial floras were measured after 400 generations. It has been shown that AAs with different synthetic costs lead to different floras structures and that high synthetic-cost AAs (methionine, lysine, isoleucine, arginine, tyrosine, and phenylalanine) result in stronger cooperation. D'Souza and Kost (2016) used *E. coli* evolutionary experiments to show that after 2000 generations of evolution, AA auxotrophs appeared in all lineages, and that these auxotrophs were more adaptive. These studies demonstrated that AA auxotroph in a habitat can form a solid cooperative relationship among members and this relationship is beneficial to the community stability.

A further question is whether this AA cooperation remains robust and how the community is affected if the concentration of AAs in the environment is changed. Hoek et al. (2016) used yeast to construct two AA auxotrophs (tryptophan and leucine), and the two were able to form a solid symbiosis without AA supplementation. However, with the increase of freely available AA in the environment, this pair of strains can exhibit obligatory symbiosis, facultative symbiosis, competition, parasitism, and competitive exclusion. This confirms that the availability of AAs can change the microbial interactions and thus affect the overall stability of the community. However, this study only considered the exchange of two AAs between two members, and it is still doubtful whether this conclusion can be generalized to natural microbial communities.

In order to investigate this issue, we enriched an acetate-degrading methanogenic microbial community by operating a thermophilic methanogenic reactor fed with acetate as the sole carbon source and without exogenous AA supplementation. The microorganisms in this reactor were found to lack the ability to synthesize some AAs by metagenomic and metatranscriptomic analysis. In addition, we found that the AAs synthesis strategies of members in communities were influenced by the synthetic energy cost of AA (Akashi and Gojobori, 2002; Yao et al., 2021). The work of Akashi and Gojobori (2002) converts metabolites in the AA synthesis pathway to ATP amounts and uses the sum of ATPs as synthesis costs of AAs. As energy metabolism strategies are more important for microorganisms in energy-limited anaerobic environments, therefore, in the present study, we classified 20 AAs into four groups (low-cost AA combinations, medium-cost AA combinations, high-cost AA combinations, and all AA combinations) according to their synthetic energy cost and supplemented them separately into four methanogenic reactors fed with acetate. The differences in the structure of communities as well as the member relationships were compared. The community structure and the co-occurrence network were significantly changed in these four reactors compared to the control reactor without AA addition.

2 Materials and methods

2.1 Reactor construction and operation

Seed sludge taken from a stably operating thermophilic methanogenic chemostat fed with acetate as the sole carbon source (Zeng et al., 2024) was used to inoculate five completely mixed continuous thermophilic methanogenic reactors with a working volume of 400 ml. The reactors were fed with synthetic wastewater [total organic carbon (TOC): 8 g/L] with acetate as the sole carbon source. Detailed concentrations of inorganic salt fractions, trace elements, and vitamins in the synthetic wastewater can be found in the study by Yao et al. (2021) and Zeng et al. (2024). The reactors were operated at a dilution rate of 0.1 d^{-1} with a hydraulic retention time (HRT) of 10 days at 55°C.

Reactors A, B, C, and D were supplied with low synthetic cost-, medium synthetic cost-, high synthetic cost-AAs, and all 20 AAs, separately, after 30 d-operation. Reactor E was used as a control without AA addition. The grouping of AAs fed to the reactors and the amounts of AAs added are shown in Table 1.

The biogas generated was collected using a drainage collection tank and the volume of biogas generated per day was counted based on the volume of water discharged. The gas components were analyzed using a gas chromatograph (GC-2014C, Shimadzu, Japan). The chromatographic column was C13X (Shimadzu, Japan, column temperature 50°C). Hydrogen was detected by a FID detector, and methane and carbon dioxide were detected by a TCD-L detector. An appropriate amount of fermentation broth was sampled and filtered through a 0.25 μm filter membrane. The filtrate was used for the measurement of the concentration of volatile fatty acids (VFAs) and TOC. VFAs were determined using a high performance liquid chromatograph (SCL-10AVP, Shimadzu, Japan) and TOC were determined using a TOC detector (TOC-VE, Shimadzu, Japan) (Zheng et al., 2019).

2.2 DNA extraction and 16S rRNA data analysis

During the stable operation phase of the reactors after AA supplementation, sludge samples were collected at six time points (39, 42, 48, 51, 55, and 61 days) in chronological order for DNA extraction to track changes in the microbial community structure in each reactor. DNA was extracted using the CTAB method (Yao et al., 2022). The V4-V5 variable region of 16S rRNA was amplified using the universal primers 515F (5′-GTGCCAGCMGCCGCGGTAA-3′) and 909R (5′-CCCCGYCAATTCMTTTRAGT-3′). Sequencing of these amplicons was done on the Illumina MiSeq platform and the raw data are available in NCBI Sequence Read Archive (SRA, BioProject ID: PRJNA1078993).

TABLE 1 The strategy of AAs addition.

Amino acids	Reactor_A	Reactor_B	Reactor_C	Reactor_D	Reactor_E
Glutamate	2*	0	0	2	0
Cysteine	2	0	0	2	0
Alanine	2	0	0	2	0
Glutamine	2	0	0	2	0
Aspartate	2	0	0	2	0
Proline	2	0	0	2	0
Asparagine·H_2O	0	2	0	2	0
Threonine	0	2	0	2	0
Glycine	0	2	0	2	0
Valine	0	2	0	2	0
Serine	0	2	0	2	0
Leucine	0	2	0	2	0
Arginine	0	2	0	2	0
Methionine	0	2	0	2	0
Lysine	0	0	2	2	0
Isoleucine	0	0	2	2	0
Tyrosine	0	0	2	2	0
Histidine	0	0	2	2	0
Phenylalanine	0	0	2	2	0
Tryptophan	0	0	2	2	0

*The unit of amino acid is μmol/day.

Analyses of microbial community species composition as well as beta diversity were done by the R package phyloseq (McMurdie and Holmes, 2013). Bray-Curtis distances among archaeal communities and among bacterial communities were calculated separately and sorted by non-metric multidimensional sorting (NMDS) to show the differences in microbial community structure among samples. The microbial co-occurrence network as well as the network characteristics analysis were conducted in iNAP (integrated Network Analysis Pipeline) (Feng et al., 2022). SparCC correlation (Friedman and Alm, 2012) was calculated using genus as the basic unit. The SparCC correlation at $r > 0.6$ and $p < 0.05$ were used for the network construction. The proportion of positive interactions for each genus in the network is defined as the value of the number of positive interactions of the genus/degree of the genus. The Greedy modularity optimization method was used to construct module separation of each network (Newman, 2004).The within-module connectivity (Z) and among-module connectivity (P) for each genus were computed and the keystones were determined accordingly (Olesen et al., 2006). The inter-group significance test in the boxplot was done by ANOVA and Tukey's multiple tests.

3 Results

3.1 Reactor performance

AA addition to the reactors was started after three HRTs of stable operation of each reactor (no accumulation of acetate and stable biogas production). The biogas yields of reactors A, B, C, and D with AA addition decreased gradually over the next 2 days, and the accumulation of acetate occurred, whereas reactor E without AA addition did not show such a phenomenon. However, over the next six days, biogas production of reactors A, B, C and D gradually recovered and acetate ceased to accumulate. All the reactors then remained in a stable operating condition for over three HRTs. These results suggests that the AA addition produced some perturbation on the microbial communities in reactors but did not lead to the collapse of the system. We summarized the daily production of biogas and the proportions of gas components in each reactor during the stabilization phase after reactor recovery and tested the differences among reactors by Tukey's test (Figure 1). When acetate is used as the carbon source, methane is produced through two pathways, one is that acetate can be converted to methane directedly by acetoclastic methanogens, and the other is that acetate is oxidized by syntrophic acetate-oxidizing bacteria (SAOB) to produce hydrogen and carbon dioxide which are later converted to methane by hydrogenotrophic methanogens (Schink, 1997; Yao et al., 2021). Thus, the biogas production as well as the biogas composition can reflect the activity of methanogens and bacteria in the microbial community. In terms of biogas production, reactors A and B supplemented with low-cost and medium-cost AAs, respectively, had significantly lower biogas yields than reactor C supplemented with high-cost AAs and the control reactor E. There was no significant difference among the biogas production of reactor D supplemented with all AAs and the other reactors. It is noteworthy that the proportion of methane in the biogas was significantly lower in the reactor supplemented with highly cost-AAs and all AAs than in the rest of the reactors, while the proportions of carbon dioxide and hydrogen were significantly higher than in the rest of the reactors.

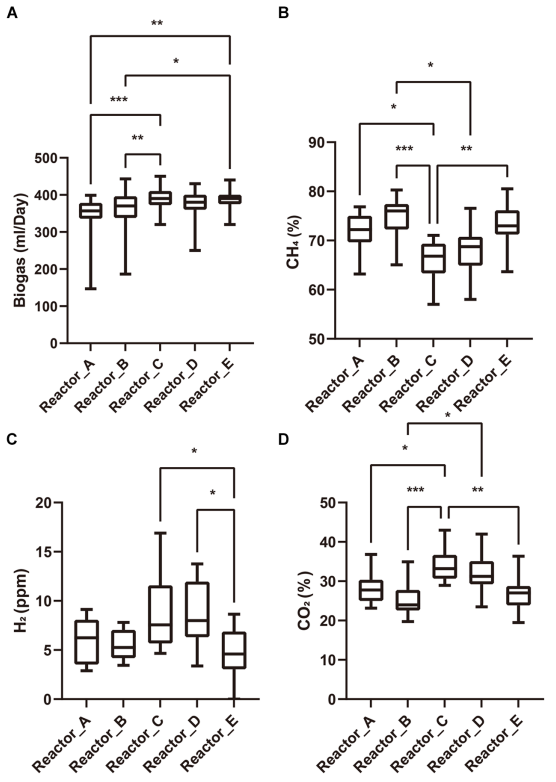

FIGURE 1
Biogas and its composition. **(A)** biogas production; **(B)** proportion of methane; **(C)** partial pressure of hydrogen; **(D)** proportion of carbon dioxide. "*": $p < 0.05$; "**": $p < 0.01$; "***": $p < 0.001$. The whiskers on a box plot indicate the range from the lowest to the highest value. Bottom to top of the box indicates 25th, 50th, and 75th percentile, respectively.

Differences in biogas composition among reactors supplemented with low- and medium-cost AAs and the control reactor were not significant. These differences in the biogas (yield and proportion of gas components) among the different experimental groups indicated that the AAs with different synthetic cost had different effects on the metabolism of the microbial community.

3.2 Microbial community structure and composition

The differences in microbial community structure in these five reactors are shown in Figures 2A,B. The effect of AA supplementation on the structure of the archaeal community was not significant, and the samples in each reactor did not show significant clustering. In addition, analysis of variance by permutation multivariate ANOVA also showed that there was no significant difference among the archaeal communities in different reactors (Supplementary Table S1). Distinctly, the bacterial communities in different reactors had different clustering patterns and were significantly different among reactors (Supplementary Table S1). According to PERMANOVA, the R2 and *p*-value among reactors A, B, C, D, and the control reactor E were 38%, 0.001; 34%, 0.001; 34%, 0.002; and 50%, 0.001, respectively. Significant differences in bacterial community structure were also observed among microbial communities supplemented with different AAs (such as reactor B and reactors A, C, and D).

Among the archaeal communities of all the reactors, the four main genera were methanogens including *Methanosarcina*, *Methanothermobacter*, *Candidatus*_Methanomethylicus, and *Methanomassiliicoccus* (Figure 2C). *Methanosarcina* was overwhelmingly dominant in the microbial community, with average relative abundances of 40.25, 40.2, 39.78, 38.45, and 41.03% in reactors A, B, C, D, and E, respectively. This was due to the fact that *Methanosarcina* is able to produce methane via both the acetate trophic pathway and the hydrogen trophic pathway and thus gains a stronger energetic advantage in acetate-fed methanogenic system. The dominant bacterial genera were mainly norank_f_Lentimicrobiaceae (an unidentified genus in the family Lentimicrobiaceae), norank_f_Ruminococcaceae (an unidentified genus in the family Ruminococcaceae), *Ureibacillus*, and *Acetomicrobium* (Figure 2D). However, the relative abundance of these bacterial genera in different reactors varied significantly. The mean relative abundance of *Ureibacillus* was 7.14, 6.04, and 14.36% in reactors A, C, and D, respectively, while it was only 0.92 and 1.46% in reactors B and E, respectively. Also with significant differences in relative abundance across reactors were *Coprothermobacter* (A, 0.70%; B, 2.52%; C, 0.90%; D, 0.60%; E, 1.06%), and *Rhodococcus* (A, 0.01%; B, 0.01%; C, 0.99%; D, 0.01%; E, 0.03%). The associated statistical tests are shown in Supplementary Table S2. Thus, the bacterial communities were more susceptible to AA supplementation than the methanogens.

3.3 Microbial co-occurrence network analysis

In order to investigate the changes in the interactions among members in the communities of five reactors under different AA supplementation conditions, SparCC correlation coefficients (Friedman and Alm, 2012) among the main genera of the microbial communities in the five reactors were calculated at the genus level and relationships with significance ($r > 0.6$, $p < 0.05$) were used for the construction of microbial coexistence networks (Supplementary Figure S1). The characteristics of the networks of community members in each reactor are shown in Table 2. The total nodes, total links, total positive links, and the average degree of nodes in the microbial co-occurrence networks of the four reactors with AAs supplementation were lower than those of the control reactor without AAs supplementation, especially for the reactor with all AAs supplementation followed by medium- and high-cost AAs supplementation. These may indicate that the supplementation of AAs reduced the interaction relationships among the microbial members. The AAs with different synthetic costs had different effects and AAs with low synthetic cost had the least effect.

To further compare the variability of members interactions in different reactors, we listed the total number of interactions and the proportion of positive interactions for genera (Figure 3). The mean proportions of positive correlations for genera in reactors A, B, C, D, and E were 0.42, 0.38, 0.15, 0.4, and 0.45, respectively. It can be seen that the proportion of positive correlations among genera in reactor C supplemented with high-cost AAs was significantly lower than that in the rest of the reactors (Figure 3A). In addition, the proportion of positive correlations among genera in reactors A, B, and D was lower than that in reactor E. This may indicate that, at an overall level, AA

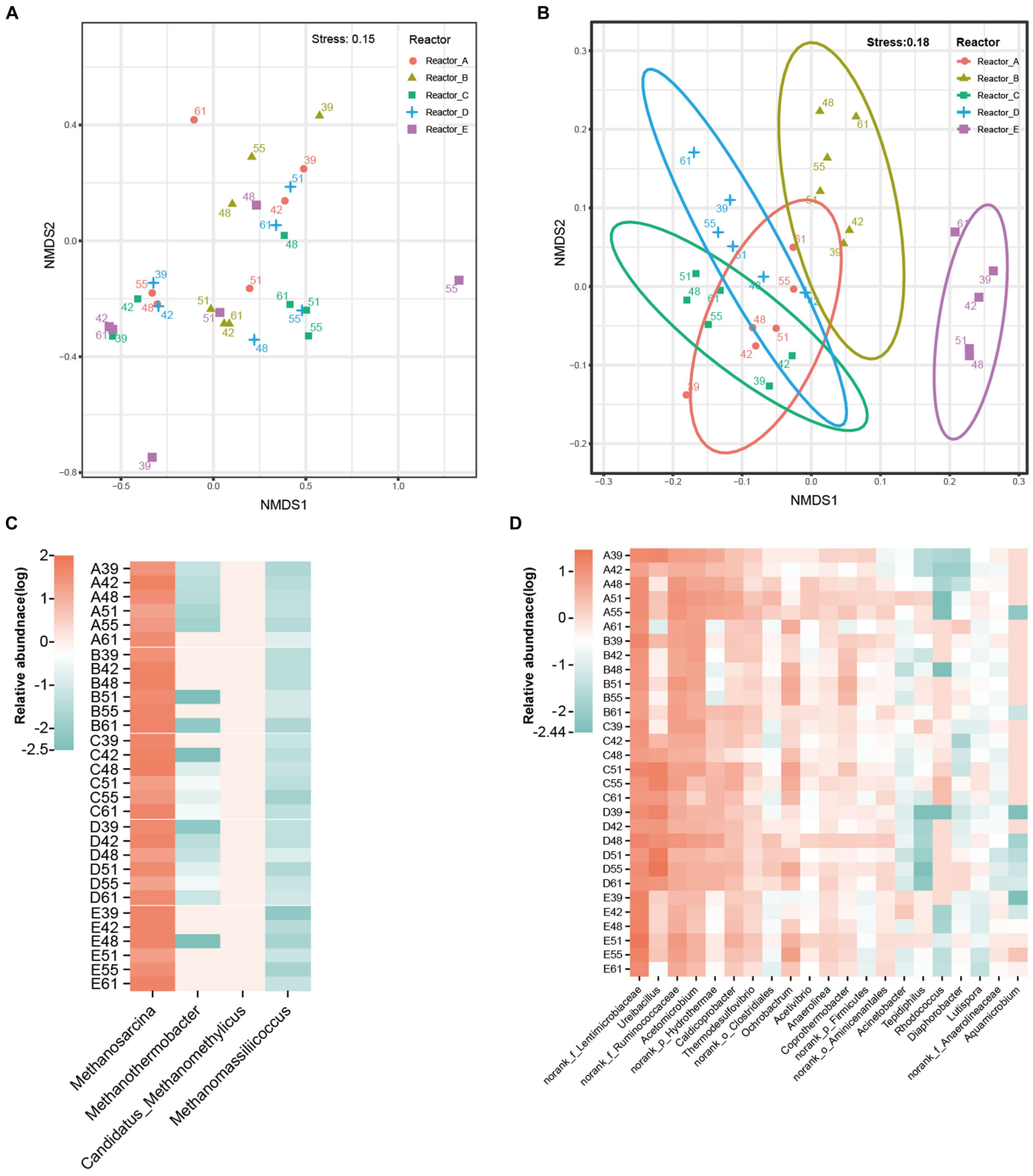

FIGURE 2
Difference of microbial communities in different reactors. **(A)** NMDS of archaeal communities, **(B)** NMDS of bacterial communities, the number of dots in the graph indicates the number of days. **(C)** archaeal genera, **(D)** major bacterial genera. norank_f_Anaerolineaceae: an unidentified genus in the family Anaerolineaceae; norank_f_Lentimicrobiaceae: an unidentified genus in the family Lentimicrobiaceae; norank_f_Ruminococcaceae: an unidentified genus in the family Ruminococcaceae; norank_o_Aminicenantales: an unidentified genus in the order Aminicenantales; norank_o_Clostridiales: an unidentified genus in the order Clostridiales; norank_p_Firmicutes: an unidentified genus in the phylum Firmicutes; norank_p_Hydrothermae: an unidentified genus in the phylum Hydrothermae.

additions reduced positive cooperation among community members, especially for those communities supplied with high-cost AAs. The average proportion of positive interactions of genus was higher in reactor D than in reactors B and C. This may be caused by a significant decrease in the degree of genus under conditions of all AAs complementation (Table 2). In terms of the number of interactions (including both positive and negative correlations) among genera in the different reactors, the mean number of interactions among genera in reactors A, B, C, D, and E were 5.1, 3.5, 3.7, 3.1, and 5.8, respectively. The number of interactions among genera was significantly higher in

10.3389/fmicb.2024.1368215

TABLE 2 The key parameters in networks of five reactors.

Reactor	Total nodes	Total links	Total positive links	Average clustering coefficient	Average degree	Average betweenness
A	66	215	120	0.425	6.51	44.38
B	57	146	78	0.344	5.12	50.45
C	59	157	90	0.37	5.32	71.88
D	57	132	71	0.335	4.63	68.9
E	72	245	134	0.36	6.8	62.9

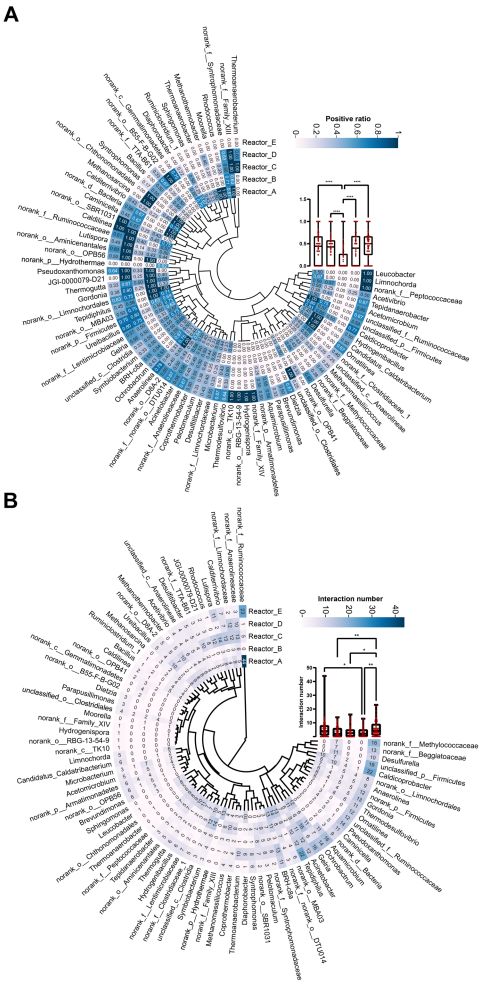

FIGURE 3
The interaction relationship among genus in each reactor. **(A)** The proportion of positive relationships of each genus. **(B)** The number of interaction relationships of each genus. "*": $p < 0.05$; "**": $p < 0.01$; "****": $p < 0.0001$. The whiskers on a box plot indicate the range from the lowest to the highest value. Bottom to top of the box indicates 25th, 50th, and 75th percentile, respectively.

control reactor E than in AA-supplemented reactors especially reactor D with all AA supplementation (Figure 3B). Thus, AA supplementation reduced the interactions among genera in communities, and the effect of all AA supplementation was more significant and the low-cost AAs the least.

To further examine the differences in the interactions of the dominant genera under different AA supplementation conditions, we selected three dominant methanogen genera *Methanosarcina*, *Methanothermobacter*, and *Methanomassiliicoccus*, and three bacterial genera *Ureibacillus*, norank_f_Lentimicrobiaceae, and norank_f_Ruminococcaceae, respectively, and mapped their interactions with other genera in different reactors (Supplementary Figure S2). It was noticeable that the reciprocal profiles of each genus were significantly different in the different reactors. For example, *Methanosarcina* and *Methanothermobacter* did not interact with other genera in the control reactor E, whereas significant interactions were formed with some genera in the AA-supplemented reactors. The bacterial genus norank_f_Ruminococcaceae had significant interactions with 44 and 33 genera in reactors A and E, respectively, while no interactions were formed with any genus in reactor B, which was supplemented with medium-cost AAs. This suggests that AAs with different synthetic costs had different effects on the interactions that dominant genera formed with the remaining community members.

To explore whether keystone genera change in the co-generation network of different reactors under different conditions of AA supplementation, the keystone genera in each system were identified by calculating the Zi (within-module connectivity) and Pi (among-module connectivity) of the different genera in each of the interaction networks (Guimerà and Nunes Amaral, 2005; Figure 4). Model hubs (high Zi, low Pi) have a high degree of connectivity only within the model they are in and little connectivity with other model hubs. Connectors (low Zi, high Pi) may play an important role in connecting other models. Network hubs (high Zi, high Pi) have many links both within the model they are in and within other models. The number of connectors in reactors A and C was relatively high for complementary low-cost and high-cost AAs. norank_f_Ruminococcaceae was a connector in reactor C, while it was a network hub in reactor A, which corresponded to its much higher number of reciprocal relationships in reactor A than in reactor C. This may indicate that low-cost AAs enhanced the ecological role of norank_f_Ruminococcaceae. In addition, the three keystones mentioned above were not present in the co-occurrence network in Reactor D, which was supplemented with all AAs. Notably, the composition of keystone genera varied considerably across reactors, with very few genera able to exist in two of the five networks (Figure 4F), suggesting that there were significant differences in the effects of AAs with different synthetic costs on the ecological status of members in a community.

4 Discussion

We constructed five acetate-fed methanogenic reactors. Four of them were supplemented with low-synthesis-cost AAs,

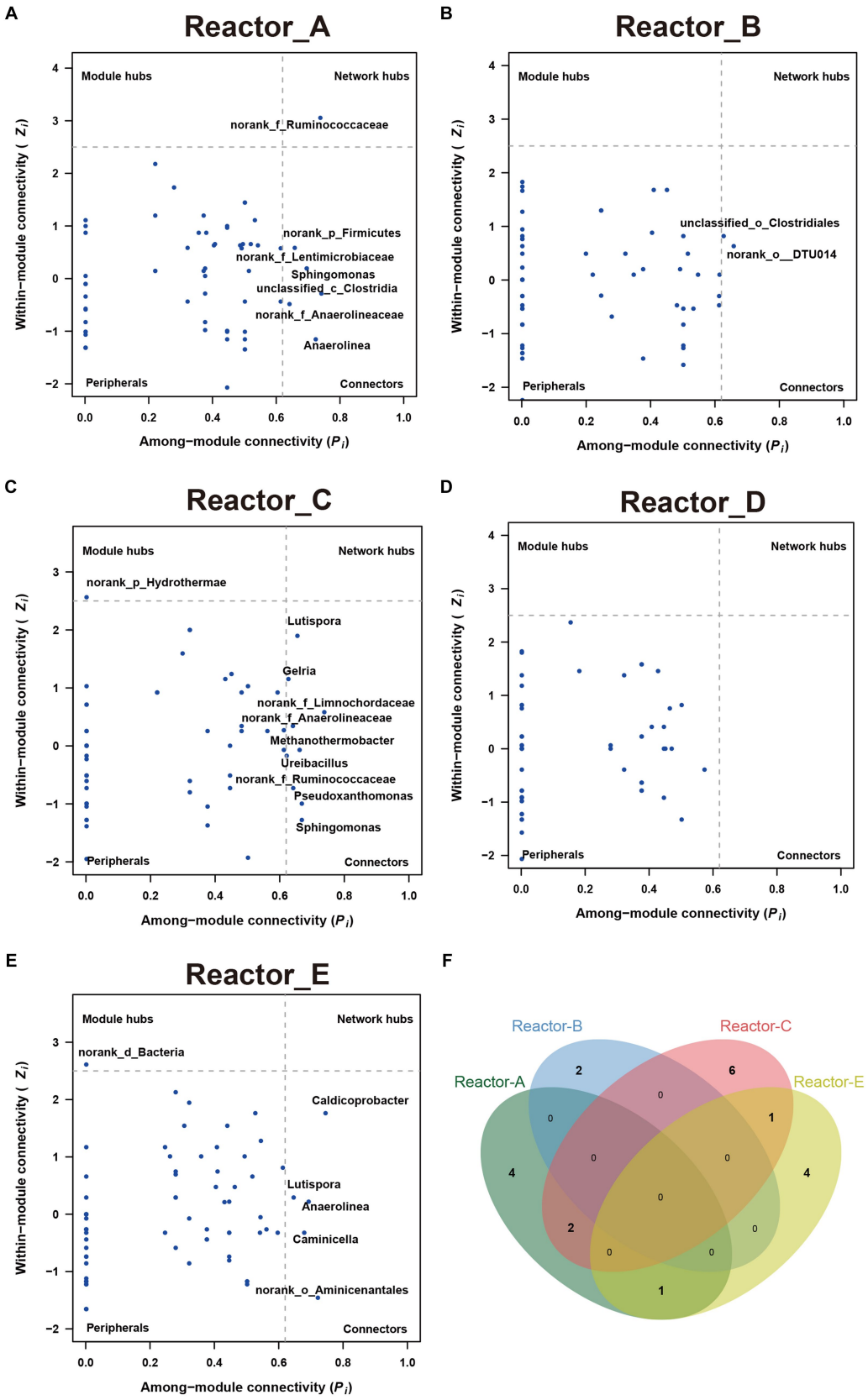

FIGURE 4
The keystones genus in communities in each reactor **(A–E)** show the key-stone genera in each reactor. **(F)** The Venn diagram of the key-stone genera (i.e., module hubs, network hubs and connectors) in reactors A, B, C and E.

medium-synthesis-cost AAs, high-synthesis-cost AAs, all 20 kinds of AAs, respectively, and one was used as a control reactor with no AA added. We compared the differences in biogas production, microbial community composition, and co-occurrence network of members during the stable operation phase of each reactor.

Differences in biogas production and composition among reactors may be due to modulation of microbial metabolic activity by different AAs rather than using AAs as an added carbon source. Because, AAs synthesis is an energy-intensive metabolic process. In an energy-limited anaerobic environment, using trace AAs (around 10^{-4} M, three orders of magnitude lower compared to the supplied carbon source acetate) as a carbon source for energy metabolism rather than protein synthesis is an unreasonable survival strategy. Compared to bacterial community, the variability in the abundance of methanogenic archaea and the interaction relationships with the rest of the members were not significant from reactor to reactor. This variability may be related to the difference in energy accessibility among methanogens and bacteria in reactors. In methanogenic reactors where acetate is the sole carbon source, the methanogen *Methanosarcina* has high acetate accessibility because of both the acetate trophic pathway and the hydrogen trophic pathways (Schink, 1997; Yao et al., 2021), leading to their absolute dominance in communities. Low energy accessibility or stress conditions promote microorganisms to interact more with each other (share more public goods, e.g., AAs, cobalamin) to cope with unfavorable conditions, which is an optimized survival strategy (Piccardi et al., 2019; Zhao et al., 2023). It is clear that the number of interaction relationships of the bacterial genera with lower energy accessibility in our reactors was significantly higher than that of *Methanosarcina* (Supplementary Figures S3a–e). In addition, *Methanosarcina* was able to synthesize most of AAs itself (Yao et al., 2021) and the high energetic accessibility makes *Methanosarcina* not highly exogenous AA dependent. Therefore, the supplementation with different cost AAs had a lower effect on the number of interactions of *Methanosarcina* than other members (Supplementary Figure S3f).

Compared to *Methanosarcina*, bacterial genera in the community (e.g., SAOB) are at a disadvantage in the competition for acetate and therefore adopt a survival strategy that reduces their ability to synthesize AAs (especially high-cost AAs). In our previous study (Yao et al., 2021), we found that SAOBs generally cannot synthesize the majority of the 20 AAs, especially those with medium and high synthetic costs. This increases the AA's dependence of SAOBs and then reduces its metabolic activity. Under the conditions of AAs supplementation (especially with high-cost AAs), the number of interactions and the proportion of positive interactions of potential SAOBs (judging from genus names, not including other unknown potential SAOBs in the communities) with the remaining members of the community were reduced (Supplementary Figure S4). This indicates that adding AAs alleviated SAOB's AA dependence on other members. In addition, compared to *Methanosarcina*, SAOBs, which have a lower capacity for AAs synthesis, benefited more from obtaining AAs from external AA supplementation. In turn, the metabolic activity and the competitiveness of acetate of SAOBs were therefore enhanced. Consequently, SAOBs converted more acetic acid to H_2 and CO_2 in the high-cost and all AAs supplemented reactors (Figure 1).

Supplementation of different cost AAs significantly reduced the level of interactions among microbial members especially when all 20 AAs were supplemented (Figure 3B). This may indicate that AA supplementation reduced the AA exchange-based cooperation among members. This phenomenon was also found in the study of Hoek et al. (2016), where the relationship among a pair of strains based on AA exchange was transformed from an obligatory mutualism to a competitive exclusion as the number of available AAs in the environment increased. In our study, the supplementation of different cost AAs all reduced the proportion of positive interactions among members, with the most significant effect being achieved by the supplementation of AAs with high synthesis cost. In our previous study, very few members in the acetate-degrading anaerobic microbial community were able to synthesize high-cost AAs (Yao et al., 2021). This phenomenon was similarly found in the study of Mee et al. (2014) and in the synthetic syntrophic community, biosynthetically costly AAs tended to promote stronger synergistic interactions. Thus, an increase in the accessibility of high-cost AAs in the environment is likely to reduce positive cooperation among members based on the exchange of high-cost AA, thus significantly reducing the number of interaction relationships among community members. This also suggests that AAs, which are more expensive to synthesize, can have a greater impact on the interactions among microbial community members.

In studying the impact of public good accessibility on microbial members' interaction relationships and community structure, most of the previous research subjects used synthetic microbial floras formed by auxotrophs from model strains [*E. coli* (Mee et al., 2014) or *Saccharomyces cerevisiae* (Hoek et al., 2016)]. These studies enable a quantitative description of effects in terms of direct observables, such as the number of strains. Conclusions can be supported by mathematical modelling. However, these auxotrophs are genomically almost identical. This means that they overlap almost perfectly in ecological niches, resulting in intense competition among strains when the environment is altered (Hoek et al., 2016). In the present study, an acetate-degrading methanogenic microbial community enriched without AAs supply was used as the object of study. Most of members in the community were AA auxotrophs and formed AA exchange interactions with each other (Yao et al., 2021). In addition to this, there are large differences in energy acquisition among these members (Zeng et al., 2024), while avoiding overlapping ecological niches. Thus, in our results, changes in AA accessibility in the environment had a more pronounced effect on bacterial genera with low energy accessibility and did not lead to the collapse of the microbial community.

Of course, many issues are still in need of further investigation in future studies. Firstly, tracking the incorporation of stable isotope-labelled AAs in the microbial proteome may give us a deeper understanding of AAs utilization of community members. It is possible to reveal the community members who are more likely to obtain AAs from external sources and which AAs are more easily absorbed and utilized by community members. This will undoubtedly help us to better explain the effects of AAs on the structure and function of microbial communities. Secondly, considering the diversity of AAs synthetic pathways, grouping AAs by characterizing amino acid synthetic pathways (e.g., precursors) would also probably lead to interesting findings., Thirdly, the calculation of the relative abundance of microbial members has some bias. The methods such as BarBIQ (Jin et al., 2023) that can quantitatively characterize the absolute abundance of community members should be employed in the future study.

In addition, acetate-degrading methanogenic microbial community in this study is one kind of diverse natural microbial communities. Whether the conclusions in the present study can be applied to other natural microbial communities is not clear. Therefore, more microbial communities with different characteristics need to be investigated in future studies.

5 Conclusion

The acetate-degrading methanogenic microbial community was supplemented with different combinations of AAs with different synthesis costs. This resulted in changes to the structure of the microbial community and the interactions among microbial members. Bacterial genera which had low energy accessibility were likely affected more in interaction relationships and abundance compared to methanogens with high energy accessibility. The increase in AA accessibility reduced the number of interaction relationships within the microbial community. This effect was more significant when more kinds of AAs were supplemented. The positive correlation among community members was reduced with increased accessibility of AAs. This effect became more pronounced as the synthesis cost of AA increased.

Data availability statement

The datasets presented in this study can be found in online repositories. The names of the repository/repositories and accession number(s) can be found at: NCBI – PRJNA1078993.

Author contributions

JY: Writing – original draft, Writing – review & editing. QZ: Funding acquisition, Writing – review & editing. MG: Supervision, Writing – review & editing. Y-QT: Project administration, Supervision, Writing – review & editing.

Funding

The author(s) declare that financial support was received for the research, authorship, and/or publication of this article. This study was funded by the National Natural Science Foundation of China (no. 51678378) and the Ministry of Science and Technology of China (no. 2016YFE0127700).

Conflict of interest

QZ was employed by the company SINOPEC.

The remaining authors declare that the research was conducted in the absence of any commercial or financial relationships that could be construed as a potential conflict of interest.

Publisher's note

All claims expressed in this article are solely those of the authors and do not necessarily represent those of their affiliated organizations, or those of the publisher, the editors and the reviewers. Any product that may be evaluated in this article, or claim that may be made by its manufacturer, is not guaranteed or endorsed by the publisher.

Supplementary material

The Supplementary material for this article can be found online at: https://www.frontiersin.org/articles/10.3389/fmicb.2024.1368215/full#supplementary-material

References

Akashi, H., and Gojobori, T. (2002). Metabolic efficiency and amino acid composition in the proteomes of *Escherichia coli* and *Bacillus subtilis*. *Proc. Natl. Acad. Sci. USA* 99, 3695–3700. doi: 10.1073/pnas.062526999

D'Souza, G., and Kost, C. (2016). Experimental evolution of metabolic dependency in bacteria. *PLoS Genet.* 12:e1006364. doi: 10.1371/journal.pgen.1006364

Embree, M., Liu, J. K., Al-Bassam, M. M., and Zengler, K. (2015). Networks of energetic and metabolic interactions define dynamics in microbial communities. *Proc. Natl. Acad. Sci. U. S. A.* 112, 15450–15455. doi: 10.1073/pnas.1506034112

Feng, K., Peng, X., Zhang, Z., Gu, S., He, Q., Shen, W., et al. (2022). iNAP: an integrated network analysis pipeline for microbiome studies. *iMeta* 1:e13. doi: 10.1002/imt2.13

Friedman, J., and Alm, E. J. (2012). Inferring correlation networks from genomic survey data. *PLoS Comput. Biol.* 8:e1002687. doi: 10.1371/journal.pcbi.1002687

Guimerà, R., and Nunes Amaral, L. A. (2005). Functional cartography of complex metabolic networks. *Nature* 433, 895–900. doi: 10.1038/nature03288

Hoek, T. A., Axelrod, K., Biancalani, T., Yurtsev, E. A., Liu, J., and Gore, J. (2016). Resource availability modulates the cooperative and competitive nature of a microbial cross-feeding mutualism. *PLoS Biol.* 14:e1002540. doi: 10.1371/journal.pbio.1002540

Jin, J., Yamamoto, R., and Shiroguchi, K. (2023). High-throughput identification and quantification of bacterial cells in the microbiota based on 16S rRNA sequencing with single-base accuracy using BarBIQ. *Nat. Protoc.* 19, 207–239. doi: 10.1038/s41596-023-00906-8

McMurdie, P. J., and Holmes, S. (2013). Phyloseq: an R package for reproducible interactive analysis and graphics of microbiome census data. *PLoS One* 8:e61217. doi: 10.1371/journal.pone.0061217

Mee, M. T., Collins, J. J., Church, G. M., and Wang, H. H. (2014). Syntrophic exchange in synthetic microbial communities. *Proc. Natl. Acad. Sci. U. S. A.* 111, E2149–E2156. doi: 10.1073/pnas.1405641111

Newman, M. E. (2004). Fast algorithm for detecting community structure in networks. *Phys. Rev. E Stat. Nonlinear Soft Matter Phys.* 69:066133. doi: 10.1103/PhysRevE.69.066133

Olesen, J. M., Bascompte, J., Dupont, Y. L., and Jordano, P. (2006). The smallest of all worlds: pollination networks. *J. Theor. Biol.* 240, 270–276. doi: 10.1016/j.jtbi.2005.09.014

Piccardi, P., Vessman, B., and Mitri, S. (2019). Toxicity drives facilitation among 4 bacterial species. *Proc. Natl. Acad. Sci. U. S. A.* 116, 15979–15984. doi: 10.1073/pnas.1906172116

Schink, B. (1997). Energetics of syntrophic cooperation in methanogenic degradation. *Microbiol. Mol. Biol. Rev.* 61, 262–280.

Yao, J., Wang, M., Wang, L., Gou, M., Zeng, J., and Tang, Y. Q. (2022). Co-inoculation with beneficial microorganisms enhances tannery sludge bioleaching with *Acidithiobacillus thiooxidans*. *Environ. Sci. Pollut. Res. Int.* 29, 48509–48521. doi: 10.1007/s11356-022-19236-5

Yao, J., Zeng, Y., Wang, M., and Tang, Y.-Q. (2021). Energy availability determines strategy of microbial amino acid synthesis in volatile fatty acid–fed anaerobic methanogenic chemostats. *Front. Microbiol.* 12:744834. doi: 10.3389/fmicb.2021.744834

Zeng, Y., Zheng, D., Li, L.-P., Wang, M., Gou, M., Kamagata, Y., et al. (2024). Metabolism of novel potential syntrophic acetate-oxidizing bacteria in thermophilic methanogenic chemostats. *Appl. Environ. Microbiol.* 90:e0109023. doi: 10.1128/aem.01090-23

Zengler, K., and Zaramela, L. S. (2018). The social network of microorganisms - how auxotrophies shape complex communities. *Nat. Rev. Microbiol.* 16, 383–390. doi: 10.1038/s41579-018-0004-5

Zhao, Y., Liu, Z., Zhang, B., Cai, J., Yao, X., Zhang, M., et al. (2023). Inter-bacterial mutualism promoted by public goods in a system characterized by deterministic temperature variation. *Nat. Commun.* 14:5394. doi: 10.1038/s41467-023-41224-7

Zheng, D., Wang, H.-Z., Gou, M., Nobu, M. K., Narihiro, T., Hu, B., et al. (2019). Identification of novel potential acetate-oxidizing bacteria in thermophilic methanogenic chemostats by DNA stable isotope probing. *Appl. Microbiol. Biotechnol.* 103, 8631–8645. doi: 10.1007/s00253-019-10078-9

Zhu, X., Campanaro, S., Treu, L., Seshadri, R., Ivanova, N., Kougias, P. G., et al. (2020). Metabolic dependencies govern microbial syntrophies during methanogenesis in an anaerobic digestion ecosystem. *Microbiome* 8:22. doi: 10.1186/s40168-019-0780-9

frontiers | Frontiers in Microbiology

TYPE Original Research
PUBLISHED 12 April 2024
DOI 10.3389/fmicb.2024.1345000

Check for updates

OPEN ACCESS

EDITED BY
Hao Li,
Jining Medical University, China

REVIEWED BY
Volker Siegfried Brozel,
South Dakota State University, United States
Shrivardhan Dheeman,
MVN University, India
Martha Helena Ramírez-Bahena,
University of Salamanca, Spain

*CORRESPONDENCE
Liangbo Li
✉ llb100@126.com
Rongshao Huang
✉ hrshao802@163.com

RECEIVED 27 November 2023
ACCEPTED 21 March 2024
PUBLISHED 12 April 2024

CITATION
Cao K, Chen J, Li Q, Gu P, Li L and Huang R (2024) Bacteria from nodules of *Abrus mollis* Hance: genetic diversity and screening of highly efficient growth-promoting strains.
Front. Microbiol. 15:1345000.
doi: 10.3389/fmicb.2024.1345000

COPYRIGHT
© 2024 Cao, Chen, Li, Gu, Li and Huang. This is an open-access article distributed under the terms of the Creative Commons Attribution License (CC BY). The use, distribution or reproduction in other forums is permitted, provided the original author(s) and the copyright owner(s) are credited and that the original publication in this journal is cited, in accordance with accepted academic practice. No use, distribution or reproduction is permitted which does not comply with these terms.

Bacteria from nodules of *Abrus mollis* Hance: genetic diversity and screening of highly efficient growth-promoting strains

Kexin Cao[1], Jianhua Chen[2], Qiuling Li[2], Peng Gu[2], Liangbo Li[2]* and Rongshao Huang[1]*

[1]College of Agriculture, Guangxi University, Nanning, Guangxi, China, [2]College of Pharmacy, Guangxi University of Chinese Medicine, Nanning, Guangxi, China

Introduction: *Abrus mollis* Hance. (AM) is an important species used in southern Chinese medicine. It is mainly found in Guangdong and Guangxi provinces in China, and it is effective in the treatment of hepatitis. Endophytic bacteria are known to affect the growth and quality of medicinal plants. However, there are limited reports describing endophytic bacteria related to AM.

Methods: In the present study, Illumina-based 16S rRNA gene sequencing was used to investigate the endophytic bacterial communities of root nodules of AM at five sampling sites in Guangxi. In addition, 179 strains of endophytic bacteria were isolated and categorized into 13 haplotypes based on recA sequence analysis.

Results: The phylogeny of the 16S rRNA gene sequences revealed a predominance of nonrhizobial endophytes. Microbial diversity analysis showed that Proteobacteria was the dominant phylum in all samples, while Bradyrhizobium was the dominant genus in different samples. An efficient strain, *Rhizobium tropici* FM-19, was screened and obtained through greenhouse experiments. The AM plants inoculated with this strain showed the best growth performance and high nitrogen fixation and nodulation capacity. Notably, total phenols and total flavonoids, important active components in AM, increased by 30.9 and 42.7%, respectively, after inoculation with *Rhizobium tropici* FM-19.

Discussion: This study provides insights into the complex microbial diversity of AM nodules and provides strain information for the efficient cultivation of AM.

KEYWORDS

***Abrus mollis* Hance., root nodule, endophytic bacteria, microbial diversity, rhizobium**

1 Introduction

The genus *Abrus* is a member of the legume family, with 12 species distributed throughout the world and four species in China, namely, *Abrus cantoniensis* Hance., *Abrus mollis* Hance., *Abrus pulchellus* Wall. and *Abrus precatorius* Linn. *Abrus mollis* Hance. (AM) is used in Chinese herbal medicine and is mainly distributed in Guangdong and Guangxi (Cao et al., 2023). It is also the main raw material for the hepatitis treatment drug "Jigucao capsule." People often use AM as an ingredient in soups and herbal teas to promote health (Fu et al., 2018). AM has been known to cure liver diseases, such as liver injury (Yuan et al., 2014), hepatitis (Hu et al., 2019), nonalcoholic fatty liver (Yan et al., 2016) and other diseases, in clinical applications.

Nitrogen is one of the most important nutrients needed for plant growth. Adequate nitrogen availability can help plants flourish and improve photosynthesis, which plays a vital role in plant growth and development (Ahluwalia et al., 2021). Some nitrogen-fixing microorganisms in nature can convert nitrogen into forms that can be absorbed and utilized by plants, a process known as biological nitrogen fixation (BNF) (Singh et al., 2022). Rhizobial symbiotic nitrogen fixation, as the most efficient nitrogen fixation system in nature, fixes approximately 40 million tons of pure nitrogen annually, accounting for 65% of total biological nitrogen fixation (Herridge et al., 2018). As the most valuable nitrogen fixation system, rhizobial symbiotic nitrogen fixation has been widely applied in many countries where soybeans and forages are grown, and a significant reduction in the use of chemical nitrogen fertilizers has been achieved (Guan et al., 2012). The number of newly discovered rhizobia is increasing, but the studies are concentrated in common crops such as soybean and alfalfa. In contrast, relatively little research has been done on leguminous medicinal plants. With the increasing emphasis on the development of traditional Chinese medicine (TCM) in China, research on rhizobia in leguminous medicinal plants has been increasing. In recent years, an increasing number of scholars have studied the rhizobial symbiotic system of leguminous medicinal plants. For these plants, the nitrogen produced by BNF in the plant participates in primary and secondary metabolic pathways to promote the synthesis of active ingredients (Feng et al., 2021). Tang et al. (2017) inoculated the legume *Sophora tonkinensis* Gagnep. with rhizobia, and the plants showed significant increases in the major components matrine and oxmatrine. In addition, the nitrogen fixation effect of the rhizobial symbiosis system can satisfy the nitrogen demand for medicinal plant cultivation, and at the same time, it can effectively improve plant resistance to drought, low temperature and salt stress (Jiang et al., 2019). Therefore, it is very important to study the leguminous medicinal plant–rhizobial nitrogen fixation system to discover new rhizobial resources, to screen efficient related strains and to apply the strains in agricultural production. By utilizing the full capacity of rhizobial resources in medicinal plants, the green, healthy and sustainable development of medicinal plants can be ensured in the future.

The study of endophytic of root nodules is mainly based on the traditional microbial culture method. This method is mainly used by homogenizing the root nodules and inoculating onto isolation media in order to obtain pure cultures of endophytic. Finally, morphological and molecular characterization were performed to determine the taxonomic status of the strains. This method is very simple and convenient, however, some microorganisms are difficult or unculturable to culture. So it may lead to a large amount of missing information about root nodules endophytic, and the development of high-throughput sequencing technology provides a new method to solve this research bottleneck. Currently, high-throughput sequencing technology is less used in root nodules endophytes diversity. Zhang et al. (2021) investigated the diversity of endophytes in *Hippophae tibetana* root nodules using high-throughput sequencing technology, and found that *Frankia* were the dominant taxa in *Hippophae tibetana* root nodules. However, high-throughput sequencing technology has not been applied to the study of endophytes diversity in AM root nodules.

In this study, high-throughput sequencing was used to evaluate the endophytic bacterial community and diversity of AM nodules in different regions of Guangxi Province, China. In addition, the soil physicochemical properties of different AM habitats were determined and analyzed to reveal the effects of different ecological environments on the diversity of endophytic bacteria in AM rhizobia. Finally, a greenhouse experiment was conducted to determine growth and physiological and biochemical changes in the inoculated plants, to explore the growth-promoting effect of rhizobia on AM and to screen for efficient growth-promoting strains. This work may enable the exploration of rhizobial resources specific to AM and contribute to the efficient development of rhizobium–AM symbiosis.

2 Materials and methods

2.1 Root nodule collection

Root nodules were sampled in June 2022 from AM plants in Lingshan County (LS), Pingnan County (PN), Fumian County (FM), Yuzhou County (YZ) and Nanning City (Nn) in Guangxi Province. The details of the five root nodule collection sites and soil physicochemical properties are shown in Table 1. Five points were selected as representative of each sampling site and the soil was carefully dug through the AM roots using a shovel. About 20 g of large and full, fresh root nodules were collected from each site. At the same time, about 200 g of soil within 5 cm of the roots and 10 cm deep was collected and put into a sealed bag for physicochemical

TABLE 1 Details and soil physicochemical properties of the root nodule sites.

	LS	PN	FM	YZ	Nn
Altitude (m)	70	70	118	78.5	100
longitude	109.1349	110.2646	109.5821	110.0331	108.3801
latitude	22.2329	23.4638	22.3246	22.8621	22.394
pH	4.1	4.8	5.0	4.7	5.0
Organic matter (g/kg)	53.3	37.5	35.0	33.0	19.6
Total P (%)	0.069	0.102	0.127	0.035	0.053
Total K (%)	0.93	1.39	1.11	2.19	0.15
Hydrolysable N (mg/kg)	100.1	97.3	93.9	83.5	81.7
Available P (mg/kg)	43.6	220.5	88.5	2.2	174.5
Available K (mg/kg)	126	135	236	170	102

characterization. The root nodules were transported in an ice box to a laboratory and stored at 4°C until further use.

2.2 DNA extraction

The root nodules were surface-sterilized using methods reported by Du et al. (2021). Specifically, the root nodules were washed thoroughly with sterile water, immersed in 70% ethanol for 3 min, washed with fresh sodium hypochlorite solution (2.5% available Cl^-) for 5 min with agitation, rinsed three times with 70% ethanol for 30 s, and finally washed five times with sterile distilled water. Fifty microliters of the final rinse water was applied to LB medium, and the medium was examined for bacterial growth after incubation at 30°C for 72 h. If there was no bacterial growth, the surface disinfection procedure was confirmed to be effective, and the samples were used for further analysis.

Total genomic DNA from samples was extracted using the CTAB method. DNA concentration and purity were monitored on 1% agarose gels. According to the concentration, DNA was diluted to 1 ng/μL using sterile water.

2.3 Amplicon library preparation and sequencing

Purified amplicons were pooled in equimolar ratios and paired-end sequenced by Novogene Co., Ltd. (Beijing, China) using an TruSeq® DNA PCR-Free Sample Preparation Kit (Illumina, United States) following manufacturer's recommendations. Raw 16S rRNA gene sequencing reads were demultiplexed, quality-filtered by fastq version 0.20.0, and merged by FLASH version 1.2.7. Operational taxonomic units (OTUs) with a 97% similarity cut-off were clustered using Uparse v7.1, and chimeric sequences were identified and removed. The taxonomy of each OTU representative sequence was analyzed by RDP Classifier version 2.2 against the 16S rRNA database using a confidence threshold of 0.7.

2.4 Data analysis

Alpha diversity was calculated including Chao, ACE, Shannon, and Simpson indices using QIIME software (Version 1.7.0). The sequences were clustered into operational taxonomic units (OTUs) at a similarity level of 97% by UPARSE to generate rarefaction curves and to calculate the richness and diversity indices (Gu et al., 2018). The Ribosomal Database Project (RDP) Classifier tool was used to classify all sequences into different taxonomic groups (Wang et al., 2007). β-diversity was visualized using principal coordinates analysis (PCoA) and non-metric multidimensional scaling (NMDS) based on the distance matrix, with the calculation of the Euclidean and BrayCurtis algorithm, respectively. To investigate similarities among different samples, OTU information was analyzed using Bray–Curtis-based principal coordinate analysis (PCoA) (Zhang et al., 2019). Representative sequences of OTUs were compared and analyzed by the RDP Classifier algorithm at each level (phylum, class, family, and genus) (Jiang et al., 2013). The linear discriminant analysis effect size (LEfSe) technique was used to identify biomarkers with statistically significant differences among groups (Segata et al., 2011). RDA was used to analyze the relationships between the bacterial community and environmental factors (Wang et al., 2015).

2.5 Rhizobium isolation and culture conditions

For rhizobium isolation, root nodules collected from each sampling point were rinsed with running water until adhering soil particles were completely removed, and the root nodules were then washed with distilled water. The root nodules were immersed in 95% ethanol for 30 s to eliminate surface tension, the ethanol was poured off, and the samples were immersed in 0.2% $HgCl_2$ solution for 5 min and finally rinsed 5–6 times with sterile water. Root nodules (0.5 g) were crushed with 4.5 mL of sterile water under aseptic conditions. The suspensions were diluted by a gradient to 10^{-3}, and 100 μL of suspension was plated on yeast extract mannitol agar (YMA: mannitol 10.0 g, yeast extract 3.0 g, K_2HPO_4 0.25 g, KH_2PO_4 0.25 g, $MgSO_4.7H_20$ 0.2 g, NaCl 0.1 g, agar 10 g, and distilled water 1,000 mL; pH 7.2). All the inoculated YMA plates were cultured upside down at 28°C until single colonies appeared. Then, the purified cultures were suspended in sterilized 50% (*v/v*) glycerol and maintained at-80°C for long-term storage.

2.6 Symbiotic characteristics of the isolates

The genomic DNA of each isolate was extracted using a TIANGEN genomic DNA extraction kit for bacteria (TIANGEN, China) and was used as the template to amplify *rec A* sequences with the primer pair rec A 41F/640R (Liu et al., 2021). The amplification products were sequenced by Beijing Tsingke Biotechnology Co., Ltd. All the obtained sequences were aligned using ClustalW integrated in MEGAX, and the *recA* haplotypes were classified through cluster analysis to select representative strains (Li et al., 2015). Each representative strain of AM plants was tested in greenhouse-based pot experiments. The AM seeds were soaked in 0.1% Hg_2Cl solution for 10 min for surface disinfection, rinsed 5–6 times with sterile water and then cooled naturally in 50°C distilled water. Once the seeds had imbibed the water, they were placed in a sterile germination box and germinated in a 25°C incubator. The seedlings were repotted into pots with sterilized substrate (vermiculite:seedling substrate = 1:2) once they reached a height of 1–2 cm and were inoculated with the desired rhizobial liquid inoculum (suspended in distilled water, 10^8 cells/mL) after true leaves had formed. Each plant was inoculated with 10 mL of rhizobial liquid inoculum every 10 days after the first inoculation for a total of 3–5 times. Plants inoculated with distilled water were included as controls. Each treatment was repeated three times. Sixty days after inoculation, the plants were removed from the soil and rinsed with tap water.

2.7 Agronomic traits and physicochemical analysis of plants

Agronomic parameters such as fresh weight, dry weight, and nodule weight after AM plant harvest were observed. The roots of fresh plants were cut from the first true leaves, and the fresh weights of the aboveground and underground parts of the plants were

measured. The plants were then dried in an oven until they reached a constant weight, and the dry weight of the plants was recorded. For nodulation data, the mature nodules of each plant were washed with distilled water and weighed, and an average was computed. Analysis of variance (ANOVA) was performed on the growth and biochemical parameter data. Duncan's test (IBM SPSS Statistics 19, United States) was used to test for significant differences between treatment means.

3 Results

3.1 OTU composition of the bacterial community

After read-quality filtering, a total of 1,501,042 high-quality sequences (clean tags) remained and were queried. The total number of bases was 538,864,653, and the average read length was 409 bp. In addition, to obtain the taxonomic information corresponding to each OTU, the RDP Classifier algorithm was used to annotate OTUs at the phylum to genus level (Table 2).

Rarefaction curves, combined with the estimated coverage values, suggested that the data were sufficient to capture most of the bacterial diversity in the samples. To visualize the differences in OTUs in root nodules from different origins, a detailed Venn diagram of the distribution of common or unique OTUs from different origins was constructed, which is shown in Supplementary Figure S1. The number of OTUs obtained was highest in PN, followed by FM, while the lowest number of OTUs was present in YZ. OTUs common to root nodules taken from the five locations represented 6.69% (315) of the total number of OTUs, and the remaining OTUs were shared between or unique to the samples. PN contained the most specific OTUs, accounting for 9.84% (463) of its total OTUs, indicating that PN had the highest abundance of specific bacterial groups. Furthermore, PN and FM jointly had 2044 OTUs, 71.15 and 71.95% of their total OTUs, respectively, indicating that more bacterial taxa were shared between them than were unique. Nn and FM shared 1,200 OTUs, accounting for 62.73 and 42.24%, respectively, showing similarities between the two. LS and YZ jointly had 560 OTUs, accounting for 22.24 and 59.51% of their total OTUs, respectively, suggesting similarities in these two communities.

3.2 Alpha diversity analysis of bacterial communities

To further assess the abundance and diversity of the endophytic bacterial community in root nodules, the alpha diversity of samples was calculated, and the results are detailed in Table 3. The alpha diversity indices included the Shannon, Simpson and Chao1 indices. The Chao1 index was used to estimate the abundance of species, with a larger value indicating higher community richness (Baláž and Balážová, 2012). The Chao1 index indicated that the abundance of bacterial communities was in the order PN > FM > LS > Nn > YZ. The Shannon index was used to evaluate bacterial diversity, where the larger the values were, the higher the community diversity (Braga and Diniz, 2015). The Shannon index of the bacterial community in PN was the highest, followed by that in LS, while the Shannon index in FM was the lowest. The Simpson index was used to characterize the diversity and uniformity of the species distribution within a community, with greater values indicating higher community diversity (Chen et al., 2022). The Simpson index indicated that the bacterial community diversity was in the order PN > LS > YZ > Nn > FM. This result was consistent with that of the Shannon index, but it was slightly different from that of the Chao1 index.

TABLE 2 The endophytic bacterial OTU composition of the five root nodule locations.

Sample	Phylum	Class	Order	Family	Genus
PN	35	77	174	231	334
Nn	35	78	162	229	332
LS	36	81	172	258	353
YZ	21	42	93	136	199
FM	40	89	178	246	332

3.3 Beta diversity analysis of bacterial communities

The similarity or difference in the root nodule community structure of plants from different origins was studied by using the Bray–Curtis-based PCoA method (Yue et al., 2022). To investigate differences in endophytic bacterial community structure in root nodules taken from the 5 locations, PCoA was used to map the two-dimensional distribution of root nodules, as shown in Figure 1. The distance between each pair of samples reflects the similarity of their community structures. PCoA 1 and PCoA 2 explained 40.43 and 27.07% of the variation, respectively. The PCoA results showed that the distances between samples LS, FM and PN were short, which indicated that the structures of the endophytic bacterial communities in samples LS, FM and PN were similar. Sample YZ was obviously separated from the other samples, indicating that its community structure was very different, and the same was true for its alpha diversity. This may have occurred due to the unique growth environment of AM. The soil organic matter content of YZ was lowest among the five sample collection sites, which resulted in a decrease in the type and quantity of bacterial communities.

3.4 Microbial taxonomic analysis at the phylum level

The bacterial communities were highly diverse at the phylum level, with up to 47 bacterial phyla distributed among the five regions. The relative abundance of Proteobacteria was the highest in the five samples, accounting for 74.55, 73.49, 71.07, 74.72 and 80.24% in PN, Nn, LS, YZ and FM, respectively. The relative abundance of Cyanobacteria in PN (2.53%), Nn (5.65%), YZ (8.03) and FM (5.52%) was significantly lower than that in LS (17.19%). The relative abundance of Firmicutes in Nn (13.40%) and YZ (13.07%) was significantly higher than that in PN (1.92%), LS (2.22%) and FM (1.42%) (Figure 2A). Comparing the relative abundance of bacterial communities of all groups at the phylum level, some differences were observed (Figure 3). The relative frequencies of unidentified bacteria ($p = 0.029$), Actinobacteria ($p = 0.045$), Chloroflexi ($p = 0.035$) and

TABLE 3 Operational taxonomic unit (OTU; 97% similarity cutoff) richness and diversity indices of different samples associated with root nodules.

Sample	OTUs observed	Shannon index	Simpson index	Chao 1 index	Coverage (%)
PN	1901.67 ± 133.52^{a}	5.94 ± 0.62^{a}	0.85 ± 0.04^{a}	2364.20 ± 94.55^{a}	98.90%
Nn	844.67 ± 153.56^{bc}	2.58 ± 0.23^{b}	0.47 ± 0.04^{bc}	1095.11 ± 147.47^{bc}	99.40%
LS	1294.00 ± 340.20^{ab}	4.57 ± 0.13^{a}	0.62 ± 0.04^{b}	1692.33 ± 425.56^{ab}	99.10%
YZ	521.33 ± 53.07^{c}	2.63 ± 0.40 ^{b}	0.56 ± 0.06^{bc}	656.10 ± 70.47 ^{c}	99.70%
FM	1478.33 ± 337.34^{ab}	2.32 ± 0.67^{b}	0.40 ± 0.08^{c}	1985.34 ± 399.55^{ab}	98.93%

Differences in bacterial alpha diversity based on a 16S rDNA sequence assignment dataset with a 97% sequence similarity threshold in upland root nodules. Values were tested using analysis of variance (ANOVA) with three replicates in each treatment. Data for the same diversity index followed by the same lowercase letter are not significantly different at the $p = 0.05$ level.

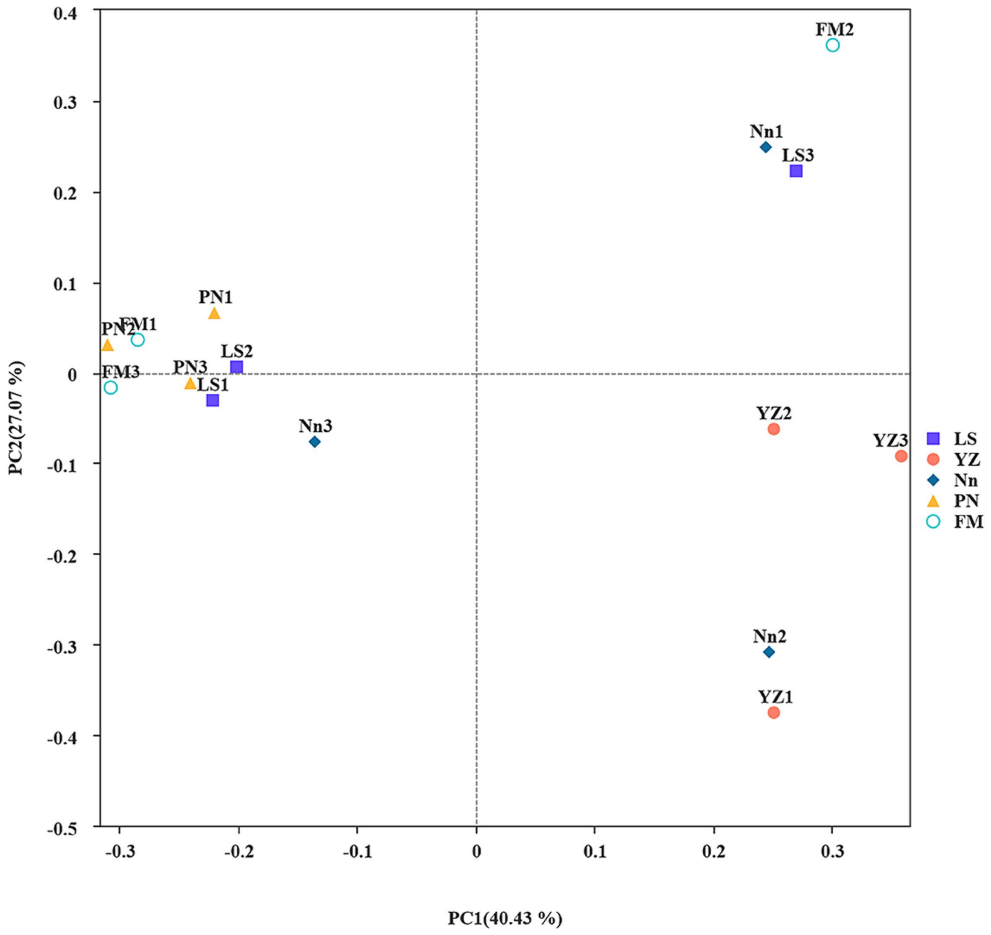

FIGURE 1
Principal coordinate analysis (PCoA): Ecological differences between the different groups and samples in the case of mixed samples at the level of 97% sequence similarity. The abscissa and ordinates represent the contribution rates of principal components 1 and 2, respectively, to the distribution of the samples. Each point in the figure represents a sample, and points of the same color come from the same group.

Nitrospirae ($p = 0.047$) were higher in PN than in YZ. At the same time, the relative abundances of unidentified_Bacteria ($p = 0.037$), Actinobacteria ($p = 0.042$), Chloroflexi ($p = 0.044$) and Nitrospiota ($p = 0.043$) were significantly higher than those of Nn. The relative abundance of Actinobacteria ($p = 0.041$) was significantly higher in PN than in FM. In addition, no significant differences in PN were found for the other two groups at the phylum level. Chloroflexi had a significantly lower relative abundance in FM than in YZ ($p = 0.018$) and had a significantly lower relative abundance in FM than in Nn ($p = 0.021$) and LS ($p = 0.034$).

3.5 Microbial taxonomic analysis at the class and family levels

The bacterial communities were more diverse at the class level (Figure 2B). Moreover, the bacterial groups and the relative abundance of bacteria in root nodules from various sources were different. The bacterial community of PN mainly included 56.15% Alphaproteobacteria, 18.36% Gammaproteobacteria, 2.58% Bacteroidia, and 2.52% Cyanobacteria. The bacterial community of Nn was mainly composed of 68.07% Alphaproteobacteria, 10.22%

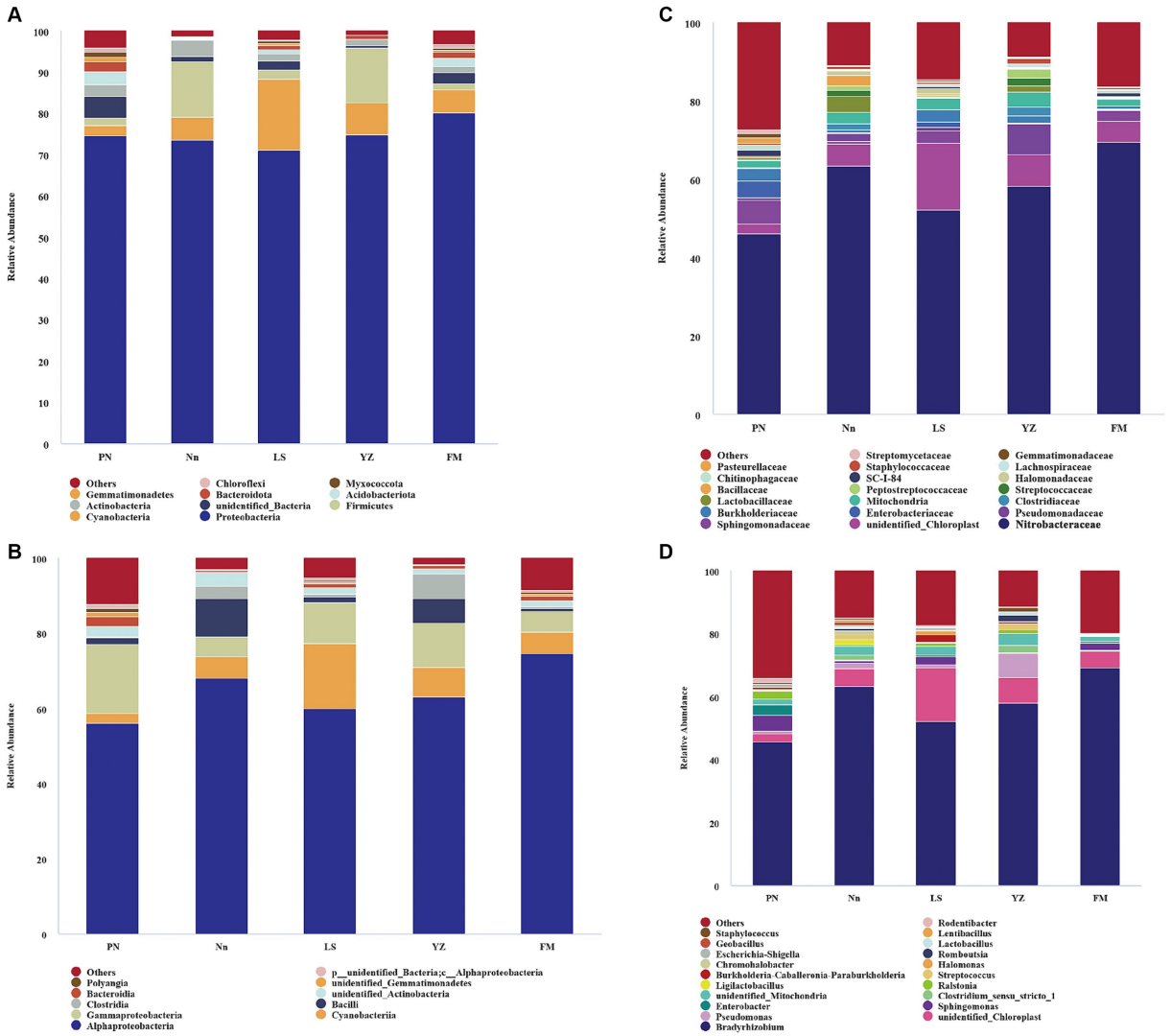

FIGURE 2
The relative abundance of bacteria at different levels. Bacterial groups at the phylum level **(A)**; bacterial groups at the class level **(B)**; bacterial groups at the family level **(C)**; bacterial groups at the genus level **(D)**. The analysis method is based on the relative abundance of species at the family and genus levels, using the ggplot2 package of R (v3.6.0) software to perform histogram analysis of species composition. Species with a relative abundance of less than 1% are represented by "others" in the legend.

Bacilli, 5.64% Cyanobacteria, and 5.43% Gammaproteobacteria. That of LS was mainly composed of 60.04% Alphaproteobacteria, 17.18% Cyanobacteria, and 11.03% Gammaproteobacteria. In YZ, 62.99% Alphaproteobacteria, 11.73% Gammaproteobacteria and 8.02% Cyanobacteria were observed.

There were differences in the composition of endophytic bacterial communities in root nodules from different sources at the family level, mainly in terms of relative abundance (Figure 2C). Specifically, the relative abundance of Xanthobacteraceae in PN (46.02%) was significantly lower than that in Nn (63.3%) and FM (69.37). The relative abundance of Sphingomonadaceae in PN, LS and FM was 5.98, 3.07 and 2.61%, respectively, and it was less than 1% in both Nn and YZ. The relative abundance of Enterobacteriaceae was 4.23% in PN and 1.28% in LS, while it was less than 1.00% in Nn, YZ and FM. Burkholderiaceae had a relative abundance of less than 1.00% in both Nn and FM.

3.6 Microbial taxonomic analysis at the genus level

The species evolutionary tree of the top 50 genera is shown in Supplementary Figure S2. These 50 bacterial genera belonged to eight phyla: Firmicutes (16 genera), Proteobacteria (14), Myxococcota (2), Verrucomicrobiota (1), Actinobacteria (11), Cyanobacteria (1), Bacteroidota (2) and Actinobacteria (3). Further analysis revealed that the endophytic bacterial communities showed high diversity at the genus level among root nodules from different sources (Figure 2D). The genus *Bradyrhizobium* was the dominant group in all samples, with a relative abundance of 45.79% in PN, 63.23% in Nn, 52.04% in LS, 58.14% in YZ and 69.17% in FM. The relative abundances of *Pseudomonas* in YZ and Nn were 7.76 and 1.99%, respectively, while they were less than 1.00% in Nn, PN and FM. The relative abundances of *Sphingomonas* and *Enterobacter* ranked second and third in PN, at

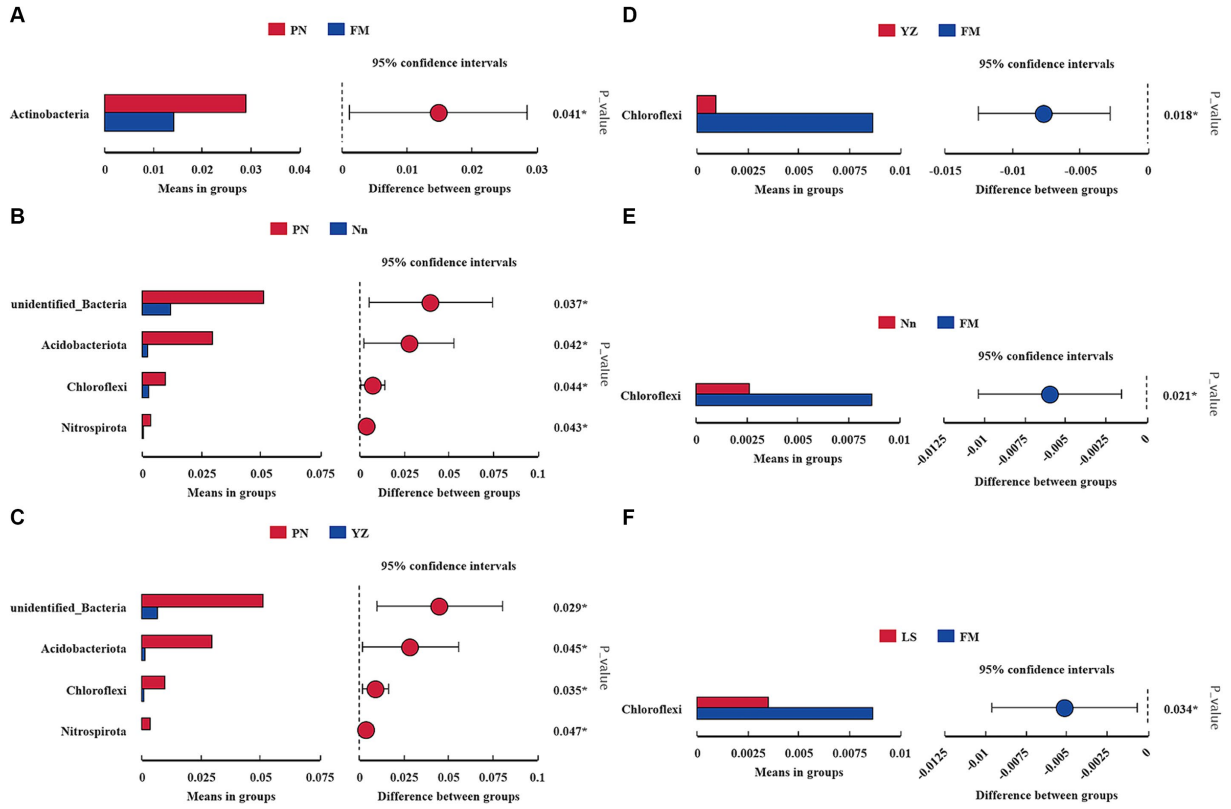

FIGURE 3
Comparison of the abundance of dominant bacterial genera in different samples. * indicates a significant difference at a p value < 0.05. The x-axis represents the mean proportion of the genus, and the y-axis shows the dominant bacterial genera. Comparison between PN and FM **(A)**. Comparison between PN and Nn **(B)**. Comparison between PN and YZ **(C)**. Comparison between YZ and FM **(D)**. Comparison between Nn and FM **(E)**. Comparison between LS and FM **(F)**.

5.13 and 3.22%, respectively, well above those of the other groups. The relative abundance of *Ralstonia* in PN and YZ was 2.54 and 1.13%, respectively, but it was less than 1.00% in FM, Nn and LS.

These results show that the endophytic bacterial communities of root nodules from different origins had abundant diversity and that the dominant taxa were essentially the same. Root nodules in different regions tend to have rich endophytic bacterial communities.

3.7 Analysis of the influence of environmental factors on community structure and diversity

To further explore the influence of environmental factors on the endophytic bacterial community structure and diversity in the samples, the relationships between environmental factors and dominant bacteria were analyzed by RDA, with the soil physiochemical and environmental factors used as variables (Figure 4A). The effects of environmental factors on the endophytic bacteria in root nodules in the RDA diagram were characterized mainly by the length of the environmental factors, while the degree of influence on each strain was reflected by the cosine value of the angle. The content of organic matter (OM, $p = 0.008$) in soil was found to have significant effects on the endophytic bacteria in root nodules. The Spearman correlation coefficient was used to analyze the correlations of the top 10 genera with soil physiochemical and environmental factors (Figure 4B). The longitude and latitude of the environmental factors were negatively correlated with *Bradyrhizobium*, and the altitude was negatively correlated with *Ralstonia*. Available K (AK) and total K (K) were significantly negatively correlated with *Clostridium_sensu_stricto_1*, and AK was significantly negatively correlated with *Streptococcus* and very significantly negatively correlated with *Pseudomonas*. Available P (AP) was significantly negatively correlated with *unidentified_Chloroplast*. Hydrolysable N (HN) and organic matter (OM) were positively correlated with *Sphingomonas* and *Enterobacter*.

3.8 Rhizobial strain isolation and selection of representative strains

A total of 179 (G^-) purified strains were obtained from the five sampling sites after isolation and identification by Gram staining; the number of isolates obtained from the sites varied from 9 in FM to 58 in PN. Thirteen *rec* A haplotypes, among which one was found in only one strain and LS-47 was found in 61 strains, were classified according to *rec* A sequence analysis, and one randomly selected representative for each haplotype was used for the subsequent phylogenetic analyses (Figure 5A). The phylogenetic analyses of bacterial isolates were conducted by the alignment of 16S rRNA sequences using the BLAST search

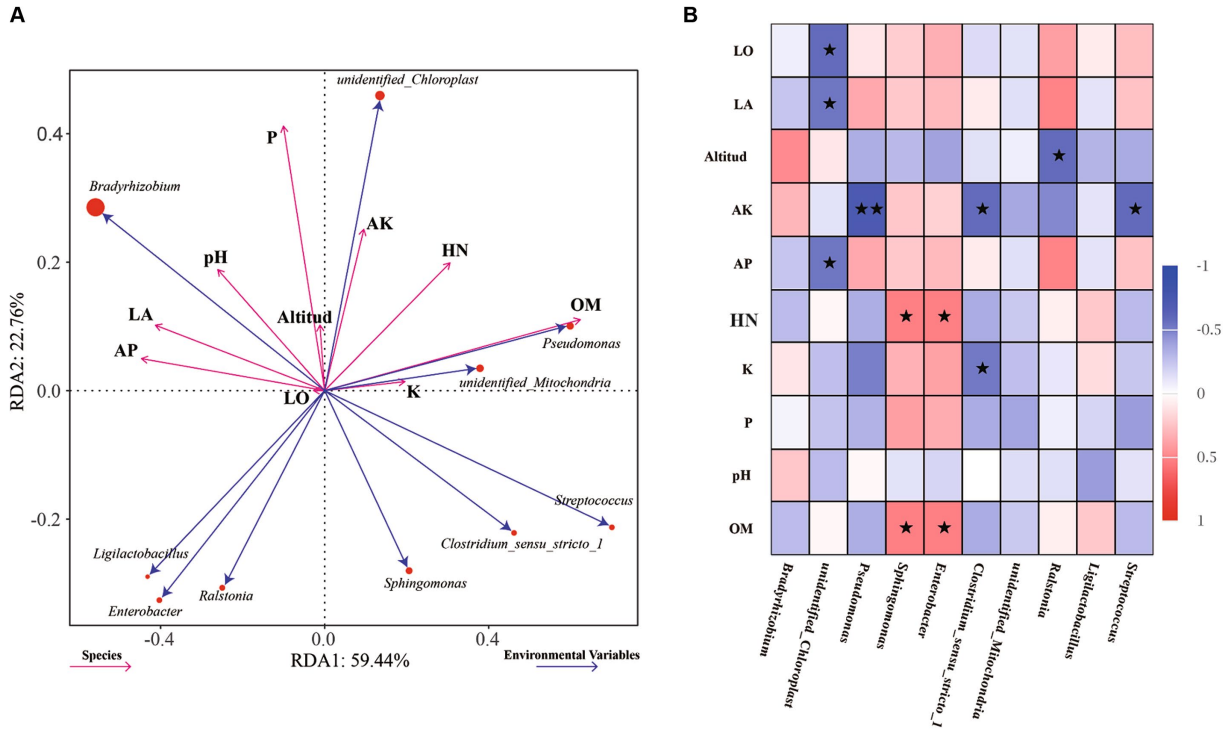

FIGURE 4
RDA of dominant endophytic bacteria and environmental factors of AC nodule samples: Environmental factors are indicated by arrows, with the lengths of the connection between the arrow and origin representing the degrees of correlation between environmental factors, community distribution and species distribution. The greater the length is, the stronger the correlation. The influence of environmental factors on bacteria is reflected by the cosine of the angle. The smaller the angle is, the stronger the correlation **(A)**. Correlations between the abundances of the top 10 genera and soil physicochemical and environmental factors were analyzed using Spearman's correlation coefficient, * indicates significance at a *p* value <0.05, ** indicates significance at a *p* value <0.01 **(B)**.

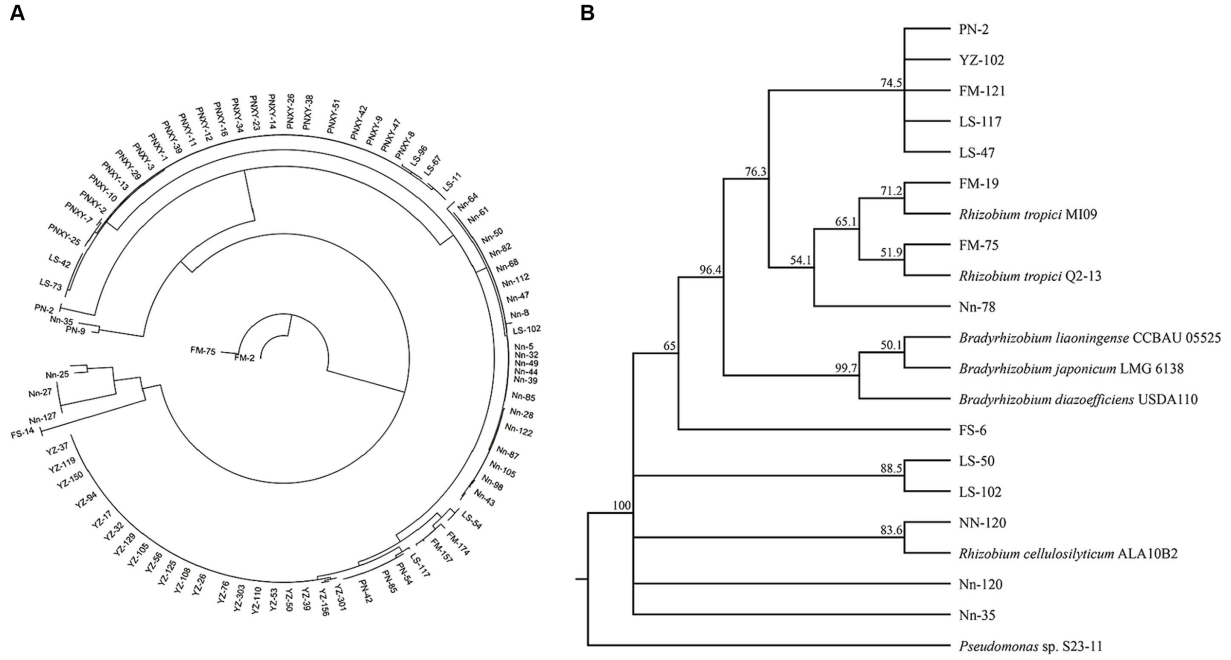

FIGURE 5
Neighbor-joining (NJ) phylogenetic tree based on *recA* gene sequences showing the clustering relationships of isolates **(A)**. Neighbor-joining (NJ) phylogenetic tree based on 16S rRNA gene sequences showing the relationships of isolated bacteria and reference strains (GenBank database). Bootstrap values (1,000 replicates) are indicated above the branches **(B)**.

function in the GenBank database. The results in Figure 5B show that four rhizobial strains and nine rhizobial endophytic bacterial strains co-occurred in twelve haplotypes. The isolates FM-19 (PP325808) and FM-75 (PP325810) were grouped with *Rhizobium tropici*. The isolate Nn-120 was close to *Rhizobium cellulosilyticum* (PP325880).

3.9 Greenhouse experiment for the assessment of nodulation efficiency and plant growth

Rhizobial strain inoculation had significant positive effects on the growth and nodulation of AM plants compared to uninoculated controls 60 days after plant emergence. *Rhizobium tropici* FM-19 inoculation significantly enhanced the plant biomass, dry weight of nodules and nodule nitrogenase activity over those of the control. Interestingly, *Rhizobium tropici* FM-75 inoculation significantly enhanced the nodule number over that in the control, while nodules of plants subjected to FM-19 inoculation were fuller than those of FM 75-inoculated plants. Inoculation with FM-19 increased the shoot fresh weight (FW), shoot dry weight (DW), root FW and root DW of plants by 157.4, 126.5, 154.3 and 79.8%, respectively, compared with those of the uninoculated control (Figure 6A). In addition, the number of nodules, nodule DW and nodule nitrogenase activity increased by 98.0, 279.5 and 121.5%, respectively (Figure 6B). The total phenolic and total flavonoid contents of stems were increased by inoculation with *Rhizobium*, but this response was further enhanced with FM-19 application. The largest increase in total phenolics (30.9%) and total flavonoids (42.7%) was recorded for stems with FM-19 inoculation (Figure 6C).

4 Discussion

High-throughput sequencing provides a convenient and effective way to study the diversity of plant endophytes, which is conducive to the identification of low-abundance species and can reveal the structure of microbial communities in target environments in a comprehensive way and provide relevant biological information (Wang et al., 2021). However, traditional culture methods are still considered the main way to obtain target strains and show advantages in yielding endophytic bacterial resources with potential applications. For example, some endophytic bacteria with growth-promoting properties have been isolated by pure culture methods, and these endophytic bacteria can produce a variety of physiologically active metabolites, which have broad potential for development and application (Pavithra et al., 2022; Santos et al., 2022; Tori et al., 2023). Microbial endophytes play an important role in promoting the ecological functions, health, and growth of plants, especially *Rhizobium*, which can facilitate symbiotic nitrogen fixation. However, there are limited reports on the endophytic microbial populations present in AM nodules. Therefore, in this study, Illumina MiSeq was used to sequence the V3-V4 variable region of the bacterial 16S rRNA gene to study the diversity of endophytic bacteria in AM nodules. A total of 179 rhizobial isolates were isolated from root nodules of AM grown at the 5 sampling sites. Liu et al. (2021) found that *recA* could be widely used to define rhizobial haplotypes. We defined *recA* gene sequences with 100% sequence similarity as the same genotype and categorized the isolated bacteria into 13 groups. The 16S-derived data reflect a predominance of *Bradyrhizobium* with more than 50% in almost all samples. However, *Bradyrhizobium* was not isolated in our results. During the incubation, by the third day of incubation, colonies had grown all over the plate with the minimum concentration of suspension. So we had to culture and preserve these single colonies in pure form in advance, which may have contributed to the fact that we did not obtain *Bradyrhizobium*. As stated by the experts, they need at least 3–4 days to form colonies during sub-culturing, and even longer when isolated from the wild. Because they need at least 3–4 days to form colonies during successional cultures, and longer if isolated from the field.

The results showed that the symbiotic nitrogen-fixing rhizobia present within the nodules mainly belonged to *Rhizobium*, *Ensifer*, *Bradyrhizobium*, *Mesorhizobium*, *Azorhizobium* and

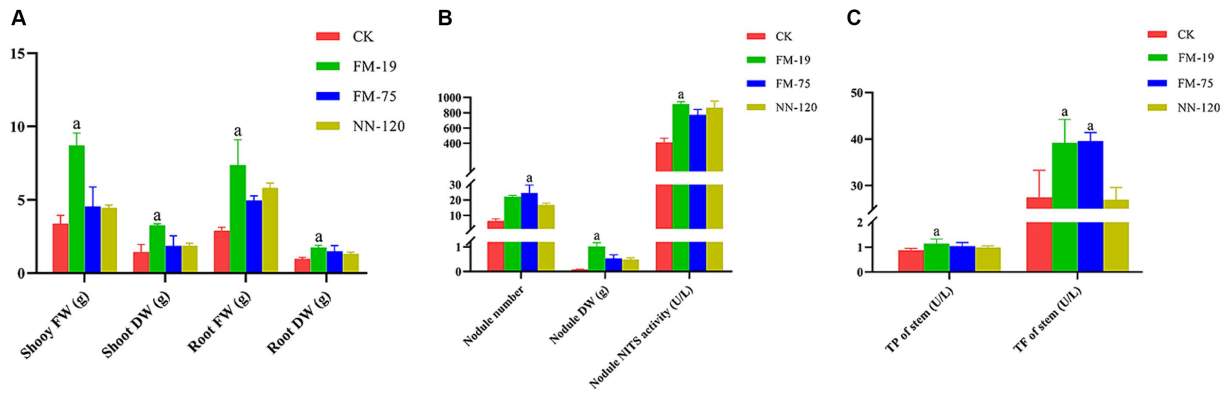

FIGURE 6
Plant parameters influenced by *Rhizobium* strain inoculation: shoot fresh weight (FW), shoot dry weight (DW), root fresh weight (FW) and root dry weight (DW) **(A)**; nodule number, nodule dry weight (DW) and nodule nitrogenase (NITS) activity **(B)**; total phenolics (TP) in stems and total flavonoids (TF) in stems **(C)**. The red column represents CK, green column represents FM-19 treatment, blue column represents FM-75 treatment and yellow-green column represents NN-120 treatment.

Methylobacterium in Alphaproteobacteria and to *Burkholderia* and *Cupriavidus* in Betaproteobacteria. The nonnitrogen fixing bacteria were mainly from *Bacillus*, *Pseudomonas*, *Enterobacter*, *Chryseobacterium* and *Sphingobacterium* (Mouradi et al., 2016). Some of the endophytic bacteria detected in the AM nodules in this study were the same as those found in the other plant endophytes mentioned above, especially at the phylum level, and were similar to those found in soybean nodules (Akifumi et al., 2017), which mainly contain the phyla Proteobacteria, Firmicutes, Actinobacteria, and Bacteroidetes, suggesting that the endophytic bacteria present in AM nodules were somewhat similar to those present in the nodules of other plants in terms of their community composition. Many *Bradyrhizobium* have been isolated from other legume hosts and subsequently named after the host plant. For example, Ramírez-Bahena et al. (2009) isolated *Bra. pachyrhizi* from nodules of yams; Chahboune et al. (2011) isolated *Bra. cytisi* from *Cytisus villosus*; and Wang et al. (2013) isolated a new species, *Bra. daqingense*, from soybean. In this study, the 16S-derived data reflect a predominance of *Bradyrhizobium* with more than 50% in almost all samples. The dominant phylum in the AM nodules collected from five different locations was Proteobacteria because Proteobacteria are able to utilize a wider variety of substrates than other bacteria (Chao et al., 2015). However, in terms of environmental factors, we found opposite trends between Proteobacteria and Firmicutes, suggesting that Proteobacteria and Firmicutes have opposite environmental preferences, which is consistent with the findings of Zhang et al. (2018). These nonrhizobial endophytes are considered opportunists since they can infect nodules when rhizobia induce nodule formation (Leite et al., 2017). In addition, the predominance of nonrhizobial isolates was attributed to the genus *Pseudomonas*. This result is consistent with the findings of Cardoso et al. (2018), who showed that the genus *Pseudomonas* is one of the most dominant genera in several legume nodules. *Pseudomonas* is commonly classified as a plant bacterial endophyte and can reduce Fusarium root rot and promote soybean growth (Dengqin et al., 2023).

The root system is the main organ in plants for absorbing water and nutrients, and inoculation with *Rhizobium* promotes root system growth and the absorption and utilization of nutrients and water by the root system. Rasheeda et al. (2023) showed that inoculation with rhizobial strains significantly increased the root length and root volume of *Vigna radiata* compared to a control, and similar findings were obtained in the present study. Plant inoculation with rhizobial strains increases photosynthetic capacity and improves water and nutrient absorption, which ultimately results in an increase in plant biomass. The symbiotic interaction between AM and *Rhizobium* is the result of mutual selection over a long period of evolution and adaptation to the environment. In this study, we showed that AM inoculation with three different strains of rhizobia under the same conditions did not have the same growth effect, although all of the rhizobia could symbiotically colonize AM and perform nitrogen fixation. This result suggests differences in symbiotic matching between rhizobia and host plants (Igolkina et al., 2019). The full capacity for symbiotic nitrogen fixation and the promotion of plant growth and active ingredients can be achieved only by the selection of suitable strains. The rhizobia isolated in this study were from different regions, each with its own habitat. Although AM was the host for all these rhizobia, there were genotypic differences in the AM grown in different regions, and thus, inoculation under the same conditions produced inconsistent results. With *Astragalus sinicus,* the inoculum match and nitrogen fixation capacity of different rhizobia also varied considerably (Burghardt et al., 2017). Nine strains of rhizobia belonging to three species were isolated and obtained in this study and were identified as *Rhizobium tropici* and *Rhizobium cellulosilyticum*. In greenhouse experiments, *Rhizobium tropici* exhibited strong growth-promoting properties and positive effects on total flavonoid and total phenol accumulation in AM. Banuelos et al. (2023) found that *Rhizobacteria tropici* could secrete riboflavin, which affects AMF symbiosis and promotes the growth of *Phaseolus vulgaris* L. Similarly, Diez-Mendez et al. (2015) found that *Rhizobium cellulosilyticum* as a coinoculant enhances *Phaseolus vulgaris* grain yield under greenhouse conditions. Notably, both *Rhizobacteria tropici* and *Rhizobium cellulosilyticum* were first identified in AM and show strong growth promotion in AM, which has a large impact on the crop management of AM. However, multisite field trials are required to demonstrate the success of this technology under natural field conditions.

5 Conclusion

In this study, the bacterial diversity and composition of AM nodules were elucidated for the first time using high-throughput sequencing methods. The content of OM in soil was found to have significant effects on endophytic bacteria in AM nodules. *Bradyrhizobium* was the dominant genus in all samples, and among the environmental factors, longitude and latitude were negatively correlated with *Bradyrhizobium*. In addition, the results of a greenhouse experiment demonstrated that the *Rhizobium tropici* FM-19 isolated in this study had a highly significant growth-promoting effect on AM and could significantly increase the accumulation of total phenols and total flavonoids in AM plants.

Data availability statement

The data presented in the study are deposited in the NCBI Short Read Archive (SRA) database repository, accession number PRJNA1091308.

Author contributions

KC: Data curation, Writing – original draft. JC: Methodology, Writing – review & editing. QL: Investigation, Writing – review & editing. PG: Visualization, Writing – review & editing. LL: Conceptualization, Funding acquisition, Writing – review & editing. RH: Conceptualization, Funding acquisition, Writing – review & editing.

Funding

The author(s) declare financial support was received for the research, authorship, and/or publication of this article. This research was funded by the Science and Technology Major Project of Guangxi (Grant nos. AA23023035, AA22096029).

Conflict of interest

The authors declare that the research was conducted in the absence of any commercial or financial relationships that could be construed as a potential conflict of interest.

Publisher's note

All claims expressed in this article are solely those of the authors and do not necessarily represent those of their affiliated organizations, or those of the publisher, the editors and the reviewers. Any product that may be evaluated in this article, or claim that may be made by its manufacturer, is not guaranteed or endorsed by the publisher.

Supplementary material

The Supplementary material for this article can be found online at: https://www.frontiersin.org/articles/10.3389/fmicb.2024.1345000/full#supplementary-material

References

Ahluwalia, O., Singh, P. C., and Bhatia, R. (2021). A review on drought stress in plants: implications, mitigation and the role of plant growth promoting rhizobacteria. *Resour. Environ. Sustain.* 5:100032. doi: 10.1016/j.resenv.2021.100032

Akifumi, S., Yusuke, U., Ui, O., Emon, Y., Hideyuki, S., Kiwamu, M., et al. (2017). Assessment of bacterial communities of black soybean grown in fields. *Commun. Integr. Biol.* 10:e1378290. doi: 10.1080/19420889.2017.1378290

Baláž, M., and Balážová, M. (2012). Diversity and abundance of bird communities in three mountain forest stands: effect of the habitat heterogeneity. *Pol. J. Ecol.* 465, 299–304. doi: 10.3354/meps09902

Banuelos, J., Martínez-Romero, E., Montaño, N. M., and Camargo-Ricalde, S. L. (2023). *Rhizobium tropici* and riboflavin amendment condition arbuscular mycorrhiza colonization in *Phaseolus vulgaris L. Agronomy* 13:876. doi: 10.3390/agronomy13030876

Braga, L., and Diniz, I. R. (2015). Importance of habitat heterogeneity in richness and diversity of moths (Lepidoptera) in Brazilian savanna. *Environ. Entomol.* 44, 499–508. doi: 10.1093/ee/nvv026

Burghardt, L. T., Guhlin, J., Chun, C. L., Liu, J., Sadowsky, M. J., Stupar, R. M., et al. (2017). Transcriptomic basis of genome by genome variation in a legume-rhizobia mutualism. *Mol. Ecol.* 26, 6122–6135. doi: 10.1111/mec.14285

Cao, K., Chen, J., Huang, R., Lu, R., Zhou, X., Bu, Y., et al. (2023). Metabolomics analysis reveals the differences between *Abrus cantoniensis* Hance and *Abrus mollis* Hance. *BMC Plant Biol.* 23:375. doi: 10.1186/s12870-023-04372-y

Cardoso, P., Alves, A., Silveira, P., Silveira, P., Fidalgo, C., Freitas, R., et al. (2018). Bacteria from nodules of wild legume species: phylogenetic diversity, plant growth promotion abilities and osmotolerance. *Sci. Total Environ.* 645, 1094–1102. doi: 10.1016/j.scitotenv.2018.06.399

Chahboune, R., Carro, L., Peix, A., Barrijal, S., Velazquez, E., and Bedmar, E. J. (2011). *Bradyrhizobium cytisi* sp. nov., isolated from effective nodules of *Cytisus villosus*. *Int. J. Syst. Evol. Microbiol.* 61, 2922–2927. doi: 10.1099/ijs.0.027649-0

Chao, A., Jing-wen, S., Xiu-bin, W., Guo-qing, L., Ping, H., and Wei, Z. (2015). Advances in the study of the relationship between plant rhizodeposition and soil microorganism. *J. Plant Nutr. Fertil.* 21, 1343–1351. doi: 10.11674/zwyf.2015.0530

Chen, C., Guo, G., Li, M., Liang, X., and Gu, Y. (2022). Diversity of endophytic bacteria of mulberry (*Morus L.*) under cold conditions. *Front. Microbiol.* 13:923162. doi: 10.3389/fmicb.2022.923162

Dengqin, W., Dan, Z., Yunfeng, Z., Zheng, Y., Xiaoling, W., Jing, S., et al. (2023). Characterization of rhizosphere *Pseudomonas chlororaphis* IRHB3 in the reduction of *fusarium* root rot and promotion of soybean growth. *Biol. Control* 186:105349. doi: 10.1016/j.biocontrol.2023.105349

Diez-Mendez, A., Menéndez, E., García-Fraile, P., Celador-Lera, L., Rivas, R., and Rivas, R. (2015). *Rhizobium cellulosilyticum* as a co-inoculant enhances *Phaseolus vulgaris* grain yield under greenhouse conditions. *Symbiosis* 67, 135–141. doi: 10.1007/s13199-015-0372-9

Du, J., Wang, T., Zhou, Q., Wu, J., Li, G., Li, G., et al. (2021). Graphene oxide enters the rice roots and disturbs the endophytic bacterial communities. *Ecotoxicol. Environ. Saf.* 192:110304. doi: 10.1016/j.ecoenv.2020.110304

Feng, Y., Wu, P., Liu, C., Peng, L., Wang, T., Wang, C., et al. (2021). Suppression of LjBAK1-mediated immunity by SymRK promotes rhizobial infection in *Lotus japonicus*. *Mol. Plant* 14, 1935–1950. doi: 10.1016/j.molp.2021.07.016

Fu, Y., Yang, J., Cunningham, A. B., Towns, A. M., Zhang, Y., Yang, H., et al. (2018). A billion cups: the diversity, traditional uses, safety issues and potential of Chinese herbal teas. *J. Ethnopharmacol.* 222, 217–228. doi: 10.1016/j.jep.2018.04.026

Gu, Y., Wang, Y., Sun, Y., Zhao, K., Xiang, Q., Yu, X., et al. (2018). Genetic diversity and characterization of arsenic-resistant endophytic bacteria isolated from *Pteris vittata*, an arsenic hyperaccumulator. *BMC Microbiol.* 18:42. doi: 10.1186/s12866-018-1184-x

Guan, F., Qiu, H., Chen, J., and Lin, X. (2012). Rhizobium inoculants: research progress and development status. *Chin. J. Ecol.* 31, 755–759. doi: 10.13292/j.1000-4890.2012.0144

Herridge, D. F., Peoples, M. B., and Boddey, R. M. (2018). Global inputs of biological nitrogen fixation in agricultural systems. *Plant Soil* 311, 1–18. doi: 10.1007/s11104-008-9668-3

Hu, X., Niu, Y., Chen, M., Feng, J., Shen, W., Jiang, Z., et al. (2019). Preventive effects of total flavonoid C-glycosides from *Abrus mollis* on nonalcoholic fatty liver disease through activating the PPARα signaling pathway. *Planta Med.* 85, 678–688. doi: 10.1055/a-0895-5838

Igolkina, A. A., Bazykin, G. A., Chizhevskaya, E. P., and Provorov, N. A. (2019). Andronov EE. Matching population diversity of rhizobial *nodA* and legume *NFR5* genes in plant–microbe symbiosis. *Ecol. Evol.* 9, 10377–10386. doi: 10.1002/ece3.5556

Jiang, H., Li, R., Peng, W., Zhang, B., Liu, X., and Liu, S. (2019). Genetic diversity of rhizobia Isolated from root nodules of wild *Astragalus adsurgens pall* in west of Sichuan, China. *Southwest China J. Agric. Sci.* 32, 1910–1917. doi: 10.16213/j.cnki.scjas.2019.8.035

Jiang, X. T., Peng, X., Deng, G. H., Sheng, H. F., Wang, Y., Zhou, H. W., et al. (2013). Illumina sequencing of 16S rRNA tag revealed spatial variations of bacterial communities in a mangrove wetland. *Microb. Ecol.* 66, 96–104. doi: 10.1007/s00248-013-0238-8

Leite, J., Fischer, D., Rouws, L., Fernandes-Júnior, P., Hofmann, A., Kublik, S., et al. (2017). Cowpea Nodules Harbor non-rhizobial bacterial communities that are shaped by soil type rather than plant genotype. *Front. Plant Sci.* 7:02064. doi: 10.3389/fpls.2016.02064

Li, X., Li, Y., Jiang, N., Wu, H., Song, W., Xu, H., et al. (2015). Genetic diversity of the rhizobia and screening of high-efficient growth-promoting strains isolated from *Sesbania cannabina* in Rudong County. *Acta Microbiol Sin.* 55, 1105–1116. doi: 10.13343/j.cnki.wsxb.20140574

Liu, G., Liu, X., Liu, W., Gao, K., Chen, X., Wang, E., et al. (2021). Biodiversity and geographic distribution of rhizobia Nodulating with *Vigna minima*. *Front. Microbiol.* 12:665839. doi: 10.3389/fmicb.2021.665839

Mouradi, M., Bouizgaren, A., Farissi, M., Latrach, L., Qaddoury, A., Ghoulam, C., et al. (2016). Seed osmopriming improves plant growth, nodulation, chlorophyll fluorescence and nutrient uptake in alfalfa (*Medicago sativa* L.) – rhizobia symbiosis under drought stress. *Sci. Hortic.* 213, 232–242. doi: 10.1016/j.scienta.2016.11.002

Pavithra, R., Anandham, R., Manikandan, A., Gopal, N. O., Thiyageswari, S., and Vincent, (2022). Plant growth promoting potential of Rhizobial and non-Rhizobial endophytes and their influence on groundnut germination in drought stress under in-vitro conditions. *Int. J. Plant Soil Sci.* 34, 348–361. doi: 10.9734/ijpss/2022/v34i2231386

Ramírez-Bahena, M. H., Peix, A., Rias, R., Camacho, M., Rodrıguez-Navarro, D. N., Mateos, P. F., et al. (2009). *Bradyrhizobium pachyrhizi* sp. nov. and *Bradyrhizobium jicamae* sp. nov., isolated from effective nodules of *Pachyrhizus erosus* [J]. *Int. J. Syst. Evol. Microbiol.* 59, 1929–1934. doi: 10.1099/ijs.0.006320-0

Rasheeda, S. M., Isabella, S. J. M., Senthil, K. P., Gayathri, R., and Veena, G. K. (2023). Rhizobium mayense sp. Nov., an efficient plant growth-promoting nitrogen-fixing bacteria isolated from rhizosphere soil. *Environ. Res.* 220:115200. doi: 10.1016/j.envres.2022.115200

Santos, S. D. S., Silva, A. A. D., Polonio, J. C., Polli, A. D., Orlandelli, R. C., Oliveira, J. A. D. S., et al. (2022). Influence of plant growth-promoting endophytes *Colletotrichum siamense* and *Diaporthe masirevici* on tomato plants (*Lycopersicon esculentum mill.*). *Mycology* 13, 257–270. doi: 10.1080/21501203.2022.2050825

Segata, N., Izard, J., Waldron, L., Gevers, D., Miropolsky, L., Garrett, W. S., et al. (2011). Metagenomic biomarker discovery and explanation. *Genome Biol.* 12:R60. doi: 10.1186/gb-2011-12-6-r60

Singh, R. K., Singh, P., Sharma, A., Guo, D., Upadhyay, S. K., Song, Q., et al. (2022). Unraveling nitrogen fixing potential of endophytic diazotrophs of different Saccharum species for sustainable sugarcane growth. *Int. J. Mol. Sci.* 23:6242. doi: 10.3390/ijms23116242

Tang, M., Min, D., Li, G., and Li, L. (2017). Biological characterization of rhizobium and its effect of different strains on the medicinal active components of

Sophora tonkinensis Gagnep. *Jiangsu Agric. Sci.* 45, 131–134. doi: 10.15889/j.issn.1002-1302.2017.01.037

Tori, L., LambertPaul, J., Ewa, O., Małgorzata, W., Jaco, V., and Sofie, T. (2023). Community profiling of seed endophytes from the Pb-Zn Hyperaccumulator *Noccaea caerulescens* and their plant growth promotion potential. *Plan. Theory* 12:643. doi: 10.3390/plants12030643

Wang, X., Cui, H., Shi, J., Zhao, X., Zhao, Y., and Wei, Z. (2015). Relationship between bacterial diversity and environmental parameters during composting of different raw materials. *Bioresour. Technol.* 198, 395–402. doi: 10.1016/j.biortech.2015.09.041

Wang, Q., Garrity, G. M., Tiedje, J. M., and Cole, J. R. (2007). Naive Bayesian classifier for rapid assignment of rRNA sequences into the new bacterial taxonomy. *Appl. Environ. Microb.* 73, 5261–5267. doi: 10.1128/AEM.00062-07

Wang, J. Y., Wang, R., Zhang, Y. M., Liu, H. C., Chen, W. F., Wang, E. T., et al. (2013). Bradyrhizobium daqingense sp.nov., isolated from soybean nodules[J]. *Int. J. Syst. Evol. Microbiol.* 63, 616–624. doi: 10.1099/ijs.0.034280-0

Wang, Z., Zhu, Y., Jing, R., Wu, X., and Liu, Y. (2021). High-throughput sequencing-based analysis of the composition and diversity of endophytic bacterial community in seeds of upland rice. *Arch. Microbiol.* 203, 609–620. doi: 10.1007/s00203-020-02058-9

Yan, W., Han, Q., Guo, P., Wang, C., and Zhang, Z. (2016). Simultaneous detection of flavonoids, phenolic acids and alkaloids in abri herba and abri mollis herba using liquid chromatography tandem mass spectrometry. *Phytochem Analysis* 27, 50–56. doi: 10.1002/pca.2598

Yuan, X., Lin, L., Zhang, X., and Deng, S. (2014). Abrusamide a and B, two hepatoprotective isomeric compounds from *Abrus mollis* Hance. *Phytochem. Lett.* 7, 137–142. doi: 10.1016/j.phytol.2013.11.003

Yue, H., Zhao, L., Yang, D., Zhang, M., Wu, J., Zhao, Z., et al. (2022). Comparative analysis of the endophytic bacterial diversity of *Populus euphratica* Oliv. In environments of different salinity intensities. *Microbiol. Spectr.* 10:e0050022. doi: 10.1128/spectrum.00500-22

Zhang, L., Cai, Y., Jiang, M., Dai, J., Guo, X., Li, W., et al. (2019). The levels of microbial diversity in different water layers of saline Chagan Lake, China. *J. Oceanol Limnol* 38, 395–407. doi: 10.1007/s00343-019-9027-7

Zhang, B., Du, N., Li, Y., Shi, P., and Wei, G. (2018). Distinct biogeographic patterns of rhizobia and non-rhizobial endophytes associated with soybean nodules across China. *Sci. Total Environ.* 643, 569–578. doi: 10.1016/j.scitotenv.2018.06.240

Zhang, A., Yin, Y., Kong, W., Zhu, X., and Sun, K. (2021). Diversity of endophytes associated with *hippophae tibetana* root nodules based on high-throughput sequencing. *Acta Ecol. Sin.* 41, 8212–8221. doi: 10.5846/stxb202012163198

frontiers | Frontiers in Microbiology

TYPE Original Research
PUBLISHED 04 September 2024
DOI 10.3389/fmicb.2024.1391428

Check for updates

OPEN ACCESS

EDITED BY
Zhenlin Han,
University of Hawaii at Manoa, United States

REVIEWED BY
Yanrui Ye,
South China University of Technology, China
Elena K. Perry,
Genentech Inc., United States
Wenbo Wang,
University of Jinan, China

*CORRESPONDENCE
Yali Huang
✉ huangyali2291@163.com

†These authors have contributed equally to this study and share first authorship

RECEIVED 25 February 2024
ACCEPTED 23 July 2024
PUBLISHED 04 September 2024

CITATION
Niu H, Yuan M, Chen X, Zhao J, Cui Y, Song Y, Zhou S, Song A and Huang Y (2024) Deciphering the differences of bacterial communities between high- and low-productive wheat fields using high-throughput sequencing. *Front. Microbiol.* 15:1391428. doi: 10.3389/fmicb.2024.1391428

COPYRIGHT
© 2024 Niu, Yuan, Chen, Zhao, Cui, Song, Zhou, Song and Huang. This is an open-access article distributed under the terms of the Creative Commons Attribution License (CC BY). The use, distribution or reproduction in other forums is permitted, provided the original author(s) and the copyright owner(s) are credited and that the original publication in this journal is cited, in accordance with accepted academic practice. No use, distribution or reproduction is permitted which does not comply with these terms.

Deciphering the differences of bacterial communities between high- and low-productive wheat fields using high-throughput sequencing

Hongjin Niu[1†], Min Yuan[2†], Xiaobo Chen[3†], Jingwei Zhao[1], Yushuang Cui[1], Yao Song[3], Sihao Zhou[1], Alin Song[4] and Yali Huang[1*]

[1]School of Environmental Science and Engineering, Hebei University of Science and Technology, Shijiazhuang, China, [2]College of Life Sciences, North China University of Science and Technology, Tangshan, China, [3]College of Food Science and Biology, Hebei University of Science and Technology, Shijiazhuang, China, [4]Institute of Agricultural Resources and Regional Planning, Chinese Academy of Agricultural Sciences, Beijing, China

Microbial communities have been demonstrated to be essential for healthy and productive soil ecosystems. However, an understanding of the relationship between soil microbial community and soil productivity levels is remarkably limited. In this study, bulk soil (BS), rhizosphere soil (RS), and root (R) samples from the historical high-productive (H) and low-productive (L) soil types of wheat in Hebei province of China were collected and analyzed by high-throughput sequencing. The study highlighted the richness, diversity, and structure of bacterial communities, along with the correlation networks among different bacterial genera. Significant differences in the bacterial community structure between samples of different soil types were observed. Compared with the low-productive soil type, the bacterial communities of samples from the high-productive soil type possessed high species richness, low species diversity, complex and stable networks, and a higher relative abundance of beneficial microbes, such as *Pseudoxanthomonas*, unclassified Vicinamibacteraceae, *Lysobacter*, *Massilia*, *Pseudomonas*, and *Bacillus*. Further analysis indicated that the differences were mainly driven by soil organic matter (SOM), available nitrogen (AN), and electrical conductivity (EC). Overall, the soil bacterial community is an important factor affecting soil health and crop production, which provides a theoretical basis for the targeted regulation of microbes in low-productivity soil types.

KEYWORDS

wheat, Illumina HiSeq sequencing, bacterial community, network analysis, mantel test

1 Introduction

Wheat is the second most widely grown crop across the world, with 200 million hectares under cultivation, and is a staple food for approximately 35 to 40% of the population globally, providing 20% of calories and protein in the human diet. Wheat plays an important role in the food supply of many countries across the world (Husenov et al., 2021). In China, wheat, as the

main food crop, is planted in an area of 23.57 million hectares, accounting for approximately 25% of the country's total grain production. Increasing wheat yield is of great significance in stabilizing food security for China and even for the world (Li et al., 2023). Despite the widespread cultivation of wheat in China, its production is hindered mostly by soil fertility exhaustion, agricultural deterioration, and unfavorable cropping circumstances. Low soil fertility is considered to be the main constraint to wheat production and yield in China (Liu C. L. et al., 2015; Duan et al., 2016; Li J. et al., 2019).

Hebei Province is one of the largest agricultural production regions in China, accounting for 9.48% of China's winter wheat planting area and 10.72% of China's total grain production (Ren D. et al., 2018; Zhang et al., 2023). However, 60% of the grain fields in Hebei province are low-productive soil types, which seriously restricts the increase in the total wheat yield (Yan et al., 2016). The fertility of the soil has a direct impact on plant growth, either by physically influencing root growth and exposure to the soil solution or indirectly by regulating mineralization, nutrient retention in the soil, and the association between soil and plant water (Li et al., 2016; Chi et al., 2021). Additionally, fertile and productive soil sustains a diverse and dynamic community of biota, which contributes to nutrient cycling and retention and the preservation of soil structure (Pellegrino et al., 2020).

The fertility of soil can be compromised by the interplay of physical, chemical, and biological factors, ultimately leading to a detrimental effect on the development of crops (Xiao et al., 2022). While physical and chemical indicators of soil are commonly used to assess soil quality by farmers and researchers, biological indicators are often considered underrepresented (Buckland et al., 2018). However, the soil bacteria, as a biological indicator, play a crucial role in the creation and reinforcement of soil aggregates, leading to improved water infiltration, root penetration, and nutrient mobility, thus enhancing the soil structure (Guo et al., 2018; Belimov et al., 2022; Rabbi et al., 2022; Lu et al., 2023). An appropriately structured soil accelerates root growth and absorption of nutrients in plants, hence enhancing soil fertility. On the other hand, several studies have demonstrated that there is a mutual influence between soil chemical properties, microbial activity, and community structure (Rousk et al., 2010; Fanin and Bertrand, 2016; Veldkamp et al., 2020). Fan et al. found that the relative abundances of Actinobacteria, Chloroflexi, and Rokubacteria significantly decreased with increasing levels of desertification, whereas the opposite trend was detected for Proteobacteria (especially Alphaproteobacteria and Gammaproteobacteria) and Bateroidetes (Fan et al., 2020). As described previously, soil microbiota plays a crucial role in sustainable agriculture and crop production; combining chemical and microbiological indicators may be a good approach to characterize soil fertility gradients (Philippot et al., 2023).

Bacterial communities in soil, rhizosphere, and root are essential for the health of the soil and plant growth. However, the bacterial communities in different soil zones may be different in response to the same environmental factors. The abundance and diversity of bacteria were significantly developed by chemical fertilizer inputs in the rhizosphere compared with those in the bulk soil (Xiao et al., 2024). The addition of nitrogen significantly reduced bacterial diversity in the phyllosphere, rhizosphere soil, and bulk soil samples but not in the root endophytes and altered the community composition of bacteria and fungi in all four compartments. Cultivars could affect the community composition of root-associated bacteria and fungi. Soil saline also had an effect on the microbial community of bulk and rhizosphere soils than root endophytes (Sun et al., 2021). Although many studies showed that environmental factors, such as fertilizer input, saline, drought, and plant cultivars, have different effects on the microbial communities of different soil types, there are few reports on the specific relationship between soil fertility levels and the microbial community from the bulk soil, rhizosphere soil, and root samples. Identifying the reduced beneficial microflora and the enriched harmful microflora in the low-productive soil type can serve as a focal point for altering soil microflora and establishing a scientific basis for fostering healthy soil conditions, thereby enhancing wheat production. To clarify the relationship between soil fertility types and soil microbial characteristics, based on the crop yield statistics for 10 consecutive years, we collected samples from the historical high- and low-productive soil types of wheat in Hebei Province, performed bacterial 16S rRNA amplicon sequencing, and analyzed the bacterial communities in the current study.

2 Materials and methods

2.1 Description of the experimental area

The study area is located within Hebei province in China (36°05′N–42°40′N, 113°27′E–119°50′E). The average annual temperature in the province is 10–20°C, and the average annual precipitation is 484.5 mm. The planting area of wheat in Hebei province is 2.23 million hectares, with the proportion of high-productive fields being 27.6% and low-productive fields being 35.8%. The high- and low-productive fields were determined by the crop yield statistics for 10 consecutive years.

2.2 Sample collection

In May 2022, we randomly selected 17 wheat farmlands from 6 counties in Hebei province, which is located in the northeast of China. Eight farmlands with high productivity and nine farmlands with low productivity were selected in this study. High-productive fields were located in Zhao county, Luancheng county, and Xinjin county, respectively. Low-yield fields were located in Guangzong county, Wei county, and Nangong county, respectively (Hebei Provincial Bureau of Quality and Technical Supervision, 2021). The average annual yield of wheat in high- and low-productive fields in this study is 9,000–10,500 and 6,750–8,250 $kg \cdot ha^{-1}$, respectively. Randomly selected 2–3 wheat farmlands with a straight-line distance of more than 10 km are considered as sample points in each county and designated them as biological replicates. In each sampling plot, five wheat plants were collected using an "S" pattern and combined into one sample (Figure 1). The whole wheat root was completely uprooted with a shovel, which was re-sterilized between sample plots and transported to the laboratory in a sterile sealing bag on ice. The bulk soil samples (BS) were collected using a shaking method. The rhizosphere soil samples(RS)were collected using a sterilized brush to accumulate the soil adhered to the surface of fine roots, which had a thickness of approximately

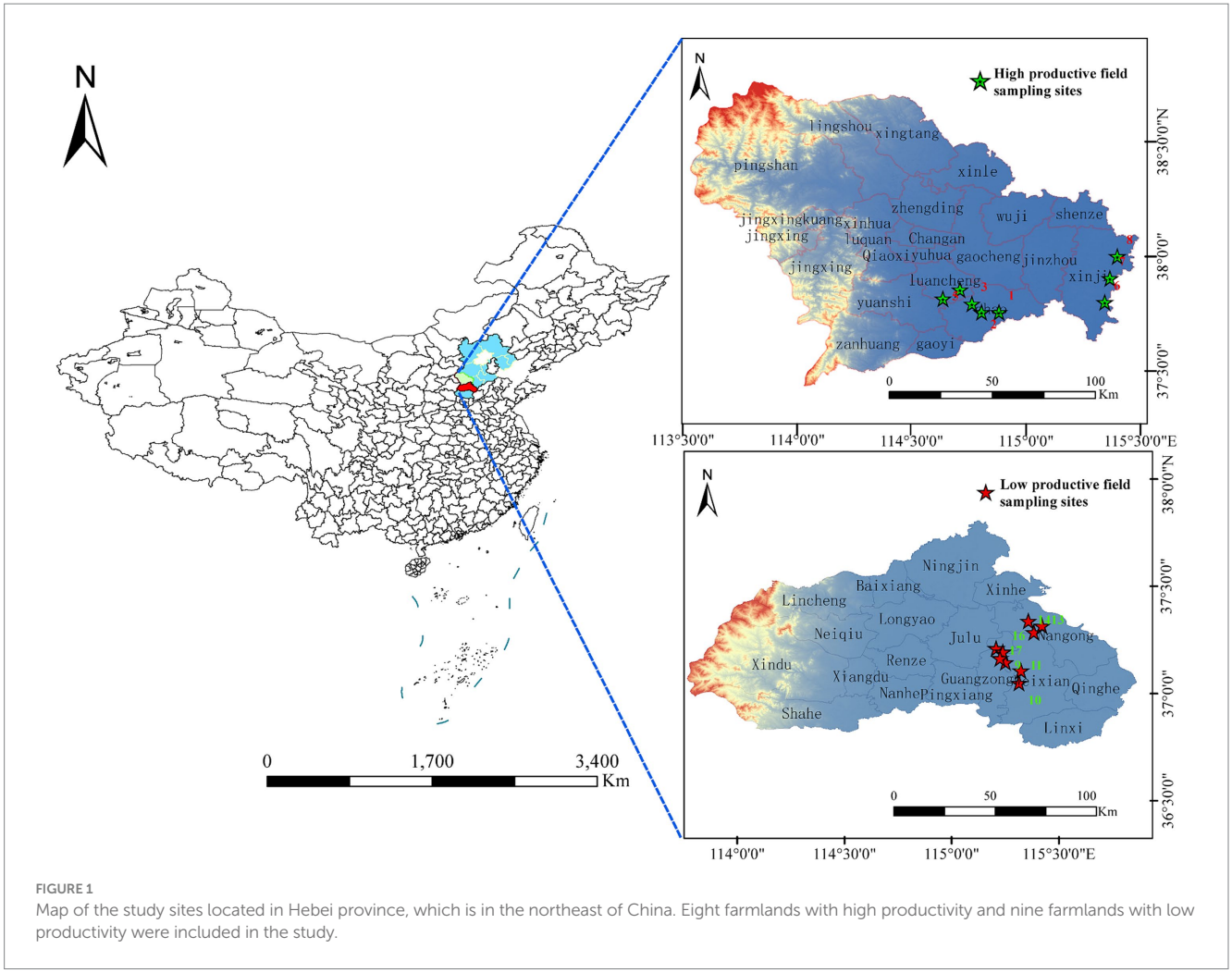

FIGURE 1
Map of the study sites located in Hebei province, which is in the northeast of China. Eight farmlands with high productivity and nine farmlands with low productivity were included in the study.

1–2 mm. For root samples (R), the roots were washed three times using sterile water and then sonicated in a sterilized tube for 3 min at 60 Hz (sonication for 60 s, break for 30 s), to remove the microbes from the rhizoplane. After removing litter, stones, and soil earthworms, all bulk soil samples were sieved through a 2-mm mesh and divided into two parts: one part was stored at −80°C for microorganism analysis and the other part was air-dried for the determination of soil chemical properties. The rhizosphere soil samples and root samples were stored at −80°C for microorganism analysis.

2.3 Sample analyses

2.3.1 Soil chemical analyses

The analyses of bulk soil chemical properties were conducted as follows: The pH was measured by a pH meter (PB-10, Beijing, China), and electrical conductivity was measured by a conductivity meter (DDS-307A, Shanghai Leici, China), with a soil to water ratio of 1: 2.5 (w/v). Soil available phosphorus (AP), available potassium (AK), available nitrogen (AN), and soil organic matter (SOM) were determined as previously described (Yan et al., 2021). Principal component analysis (PCA) of soil chemical properties was analyzed by R (version 4.4.2) (Qin et al., 2022).

2.3.2 DNA extraction, PCR amplification, and Illumina HiSeq sequencing

The total DNA of each sample was extracted using the PowerSoil DNA Isolation Kit. The bacterial 16S rRNA V3–V4 region of each sample was amplified using primers 338F (5′-ACT CCT ACG GGA GGC AGC A-3′) and 806R (5′-GGA CTA CHV GGG TWT CTA AT-3′). The PCR products were purified with a DNA gel extraction kit (Axygen, Shanghai, China) and verified by 1.8% agarose gel electrophoresis. Finally, an Illumina HiSeq 2,500 platform (Illumina, Inc., San Diego, CA, United States) was used to perform high-throughput sequencing at Biomarker Technologies Corporation (Beijing, China). Raw image data files obtained in the current study were transformed into the original sequence reads using base calling analysis. The sequence information and corresponding sequencing quality information were stored in FASTQ (fq) file format. All sequences were deposited in the NCBI Sequence Read Archive with the BioProject ID PRJNA 1081352.

2.3.3 Statistical and bioinformatics analyses

Trimmomatic (version 0.33) was used to filter the raw reads obtained from sequencing, with parameters of SLIDINGWINDOW:50:20 and MINLEN:215. Then, cutadapt (version 1.9.1) was used to obtain clean reads by removing primer sequences. Then, raw FASTQ files were further processed using QIIME software

(version 1.8.0) for demultiplexing, quality filtering, and data analysis. The high-quality sequences were obtained by filtering the raw tags using FLASH (Magoc and Salzberg, 2011) and were further clustered using DADA2. The tags were calculated using QIIME for bacterial α-diversity analysis (Callahan et al., 2016; Bolyen et al., 2019). Non-metric multidimensional scaling (NMDS) of bacterial β-diversity was performed at the ASV level based on the Bray_Curtis algorithm (Looft et al., 2012). Kruskal–Wallis test in the linear discriminant analysis (LDA) effect size (LEfSe) method was performed to detect the potential indicators. The taxa with significant differences between low- and high-productive soil samples were determined by LDA ≥ 3.5 and $p < 0.05$ (Segata et al., 2011). SPSS 17.0 was used to test differences in soil chemical properties and bacterial α-diversity indices between low- and high-productive soil samples using the independent samples t-test. The co-occurrence network of bacterial communities was constructed according to the relative abundance files at the genus level. The genera were filtered based on the abundance size and the correlation, which was calculated using the Spearman correlation coefficient. In this study, the genera with abundance of >0.1%, correlation of >0.1, and p-value of <0.05 were selected to construct the network. R software was used to transform the relative abundance table at the genus level into a correlation coefficient matrix. Then, Gephi 0.10.1 software was used to visualize the network based on the correlation coefficient matrix. Ultimately, the role of nodes was determined and classified according to the connectivity among modules (Pi) and connectivity within modules (Zi). The nodes with Zi < 2.5 and Pi ≥0.62 are categorized as connectors (key taxa) (Deng et al., 2012). The Mantel test was used to analyze the interrelationship between soil chemical properties and bacterial communities.

3 Results

3.1 Soil chemical properties

Soil chemical properties usually serve as an important indicator of soil fertility type. In this study, the chemical properties of the high- and low-productive soil type samples were determined. The contents of SOM, AN, and AP in the low-productive soil type samples were significantly lower than those in the high-productive soil type samples, but the soil EC was higher than that in the high-productive soil type samples ($p < 0.05$). However, there were no significant differences in pH and AK contents among the different types of soils (Table 1). Principal component analysis (PCA) showed that two-dimensional PCA for soil chemical properties could explain 76.77% of the total variance of soil fertility types of all samples, and the chemical properties showed obvious changes along the first axis of PCA, with the high-productive soil type samples on the left and the low-productive soil type samples on the right, indicating a good differentiation between the two soil type samples in terms of soil chemical properties (Figure 2).

3.2 Richness and diversity of the bacterial community

A total of 1,547,961 effective sequences were obtained in the bacterial community analysis of 51 samples. The coverage value of each sample was higher than 99.99%, implying sufficient sequencing depths for assessing bacterial biodiversity in all samples. Bacterial communities were analyzed by comparing the ASVs (ASV quantities), diversity indices (Shannon and Simpson), and richness indices (ACE and Chao1) between low- and high-productive soil types within bulk soil, rhizosphere soil, and root samples, respectively. Although no significant differences were observed between low- and high-productive soil type samples, a larger number of ASVs were obtained in the high-productive soil type samples than in the low-productive soil type samples within bulk soil, rhizosphere soils, and root soil groups (Table 2). Meanwhile, a Venn diagram was used to show the differences in the bacterial community based on unique and shared ASVs across the two groups with each subgroup. The numbers of shared ASVs by the two different groups within BS, RS, and R subgroups were 1,223, 1,268, and 460, respectively. The numbers of unique ASVs of the low-productive soil type samples in the BS, RS, and R subgroups (259, 282, and 11) were lower than those of the high-productive soil type samples (307, 298, and 15), indicating that the species richness decreased in the low-productive soil type (Figure 3A).

3.3 Bacterial community β-diversity

To visualize the differences in community structure between high- and low-productive soil type samples, NMDS and analysis of similarities (ANOSIM) were conducted at the ASV level. The results showed that the eight repetitions from the high-productive group and the nine repetitions from the low-productive group were clustered together, respectively, indicating that the bacterial community structure in this study had good representativeness (Figure 3B). In the bulk soil and rhizosphere soil samples, a clear separation was observed between high- and low-productive soil type samples within each sample type (bulk soil: $R = 0.74$, $p = 0.001$; rhizosphere soil: $R = 0.68$, $p = 0.001$). However, in the root samples, the degree of separation between bacterial communities decreased (root: $R = 0.19$, $p = 0.01$). These results indicated that the soil microbial community structure of bacteria has a strong relation with soil fertility.

3.4 Bacterial community composition

The microbial community structure in the bulk soil, rhizosphere soil, and root samples was analyzed at the bacterial phylum level in both high- and low-productive soil type samples. In the bulk soil

TABLE 1 Soil chemical properties of the high- and low-productive soil type samples.

Groups	SOM/ (g·kg^{-1})	AN/ (mg·kg^{-1})	AP/ (mg·kg^{-1})	AK/ (mg·kg^{-1})	EC/ (μS·cm^{-1})	pH
H	26.56 ± 1.15*	153.43 ± 5.97*	21.73 ± 1.55*	169.51 ± 13.76	267.00 ± 7.76	7.82 ± 0.11
L	16.71 ± 1.39	83.15 ± 14.24	12.63 ± 1.67	173.35 ± 14.89	553.50 ± 48.83*	7.72 ± 0.10

H, high-productive soil type samples; L, low-productive soil type samples; SOM, Soil Organic Matter; AN, Available Nitrogen; AP, Available Phosphorus; and AK, Available Potassium. The results were given as mean ± SD (standard deviation). Statistical significances were determined by the Independent-samples T Test (*$p < 0.05$).

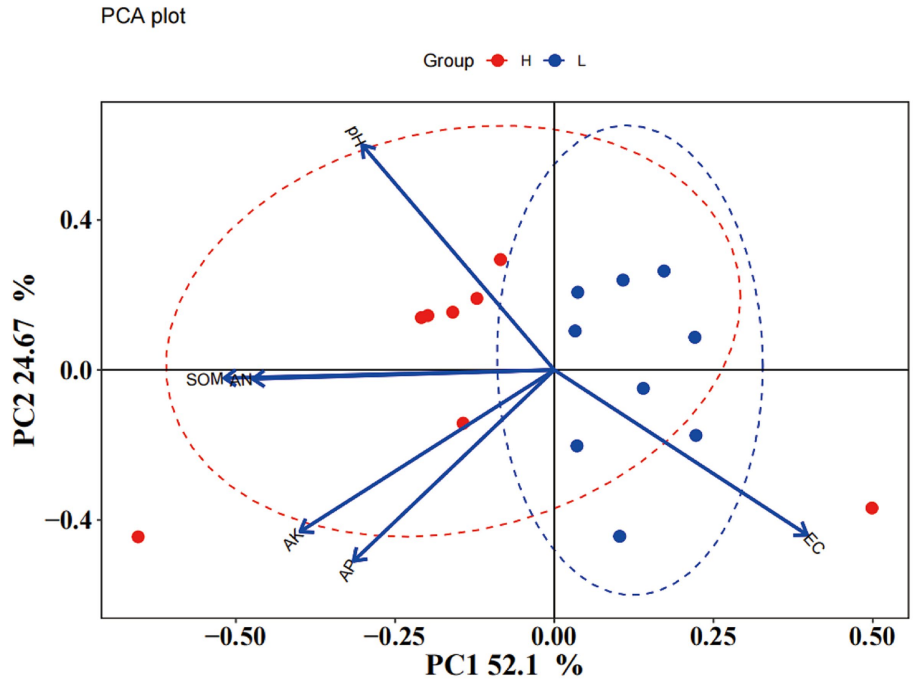

FIGURE 2
Principal component analysis (PCA) of soil properties.

TABLE 2 Richness and diversity of the high- and low-productive soil types samples.

	Samples	Sequence numbers	ASVs	ACE	Chao1	Simpson	Shannon	Coverage/%
BS	HBS	39,726 ± 1,284	644 ± 30	645.27 ± 30.48	646.68 ± 31.95	0.9967	8.76 ± 0.08	99.99
	LBS	38,020 ± 2,786	635 ± 71	636.46 ± 71.34	637.76 ± 72.44	0.9967	8.78 ± 0.18	99.99
RS	HRS	43,182 ± 2,261	677 ± 55	678.90 ± 55.38	680.21 ± 55.93	0.9963	8.76 ± 0.19	99.99
	LRS	37,721 ± 2699**	645 ± 66	646.31 ± 66.43	649.86 ± 65.66	0.9968	8.79 ± 0.18	99.99
R	HR	13,260 ± 1775	263 ± 31	263.39 ± 31.13	263.42 ± 31.07	0.9934	7.65 ± 0.20	99.99
	LR	10,773 ± 1153**	239 ± 48	239.07 ± 48.51	238.98 ± 48.54	0.9923	7.48 ± 0.40	99.99

The results were presented as mean ± SD (standard deviation). Statistical significances were determined by the independent samples *t*-test. The differences between low- and high-productive soil types within bulk soil, rhizosphere soil, and root samples are indicated by * for $p < 0.05$ and ** for $p < 0.01$.

samples, the abundance and order of the top 10 dominant phyla were similar, with the highest abundance of Proteobacteria, Acidobacteriota, Actinobacteriota, Bacteroidota, and Gemmatimonadota, accounting for more than 85% of the overall relative abundance. Among the high abundance of phyla, Gemmatimonadota was significantly higher in the low-productive soil type samples than in the high-productive soil type samples. Moreover, among the low-abundance phyla, the relative abundance of Dadabacteria, Desulfobacterota, and Campylobacterota was significantly higher than that of the high-productive soil type samples (Supplementary Table S1). The dominant phyla in the rhizosphere soil samples were the same as in the bulk soil samples, and there was no significant difference in the abundance in the dominant phyla of soil bacteria between high- and low-productive soil type samples, but Firmicutes were highly significantly different ($p < 0.001$) with abundances of 0.75% in the high-productive soil type samples and 0.10% in the low-productive soil type samples (Supplementary Table S3). In the root samples, Proteobacteria were highly enriched with an abundance of 85.57 to 86.04%, followed by Bacteroidota, and comparative analyses of all bacterial phyla of the two productive soil type samples revealed that none of the bacterial groups showed significant differences (Supplementary Table S5; Figure 4A). From the above analyses, it can be observed that the differences between bacterial community decreased sequentially from bulk soil and rhizosphere soil to root samples at different levels of productivity.

At the genus level, the dominant genera in the bulk soil samples were similar at both high- and low-productive soil type samples, with *Sphingomonas*, unclassified Vicinamibacteraceae, *Allorhizobium*, *Massilia*, *Lysobacter*, *Pseudoxanthomonas*, *Pseudomonas*, and unclassified Gemmatimonadaceae. Among them, the relative abundance of *Sphingomonas* and unclassified Gemmatimonadaceae in the bulk soil samples of the low-productive soil type samples was significantly increased, while the relative abundance of unclassified

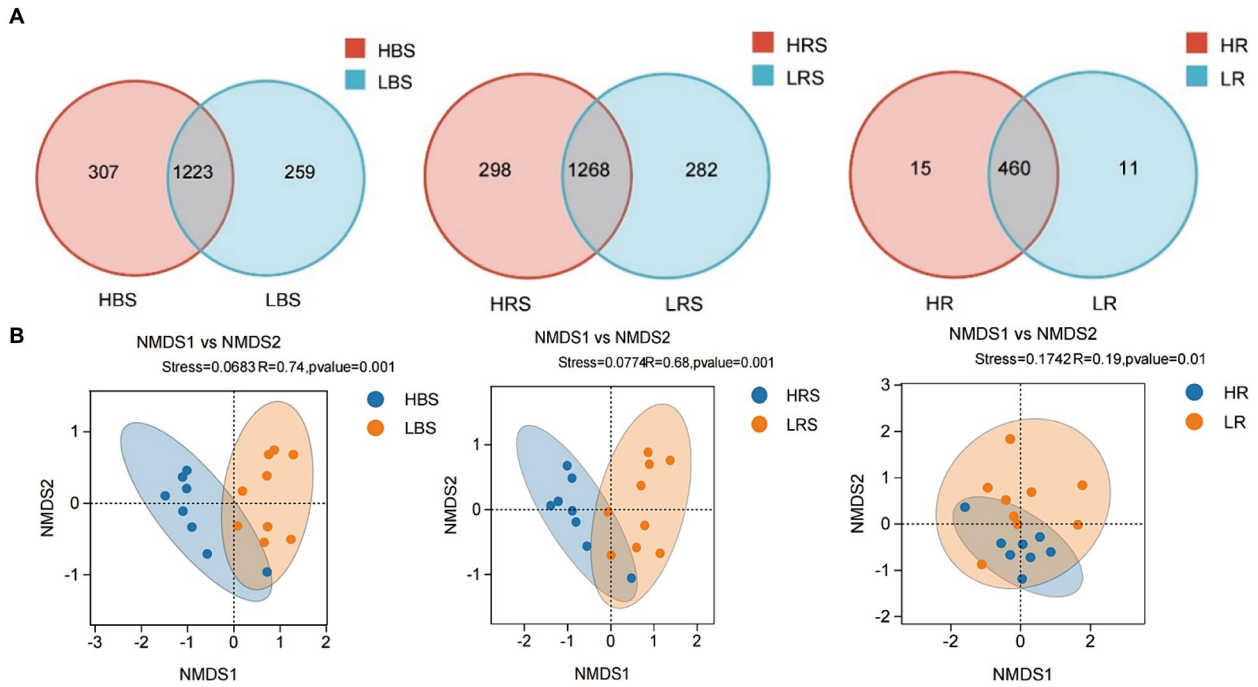

FIGURE 3
(A) Venn diagram of the composition of bacterial communities in the BS, RS, and R samples. Different colors represented different treatments. The numbers in overlapping and non-overlapping sections referred to the quantity of common ASVs and unique ASVs of samples from different types of soil. **(B)** Non-Metric Multi-Dimensional Scaling (NMDS) analysis of the high-productive and low-productive soil type groups in the bulk soil, rhizosphere soil, and root samples, respectively. The scatter plot of 8 samples from the high-productive group and 9 samples from the low-productive soil type group represented the bacterial ASV community composition. The distance between points represented the degree of difference based on unweighted UniFrac similarities in each group.

Vicinamibacteraceae, *Pseudoxanthomonas*, and *Lysobacter* significantly decreased ($p < 0.01$) (Supplementary Table S2). Analysis of bacterial community composition at the genus level and abundance of the rhizosphere soil samples between high- and low-productive soil type samples revealed that the significant transformation of bacteria in the low-productive soil type samples compared to the high-productive soil type samples was the same as in the bulk soil samples, with unclassified Gemmatimonadaceae and *Sphingomonas* increasing by 38.86 and 27.68%, respectively. *Pseudoxanthomonas*, unclassified Vicinamibacteraceae, and *Lysobacter* were decreased by 53.74, 37.83, and 12.81%, respectively (Supplementary Table S4). Analysis of microbial community composition within the root samples revealed that the abundance of bacterial community within the root samples varied considerably from the soil samples, with *Lysobacter* increasing and *Massilia* and *Pseudomonas* significantly decreasing in the root samples of the low-productive soil type samples (Supplementary Table S6; Figure 4B).

3.5 Indicator bacteria for two productive soil type samples

Indicator bacteria are usually treated as specialized communities that represent microbial communities with statistically significant differences. In the bulk soil samples, there are more potential biomarkers in the low-productive soil type samples than those in the high-productive soil type samples; the phylum Proteobacteria together with its three main orders (Rhizobiales, Xanthomonadaceae, and PLTA13) and the order Vicinamibacterales and its genus unclassified Vicinamibacterales (phylum Acidobacteriota) were enriched in the HBS, while the family Pyrinomonadaceae together with its order Pyrinomonadales, order Myxococcales (phylum Myxococcota), order Gemmatimonadales (phylum Gemmatimonadota), and order *Sphingomonas* (Proteobacteria) was dominant in the LBS (Figure 4C). In addition, in the rhizosphere soil samples, the relative abundance of the family Pyrinomonadaceae (phylum Acidobacteriota), order Gemmatimonadales (phylum Gemmatimonadota), and order Sphingomonadales (Proteobacteria) were also dominant in the LRS. However, in the HRS, the order Bacillales was specifically enriched together with its family Bacillaceae and the genus *Bacillus* (phylum Firmicutes) (Figure 4D).

3.6 Co-occurrence network structure of bacterial communities

We explored the bacterial co-occurrence patterns using network analysis. Six networks were comprised of bulk soil, rhizosphere soil, and root samples of the high- and low-productive soil type samples, respectively (Figure 5). The quantities of total nodes and total links in the low-productive soil type samples were higher than those in the high-productive soil type samples, except for the HR at total links. Additionally, the bacterial networks of the low-productive soil type samples had a lower average clustering coefficient than those of the high-productive soil type samples, indicating that the bacterial

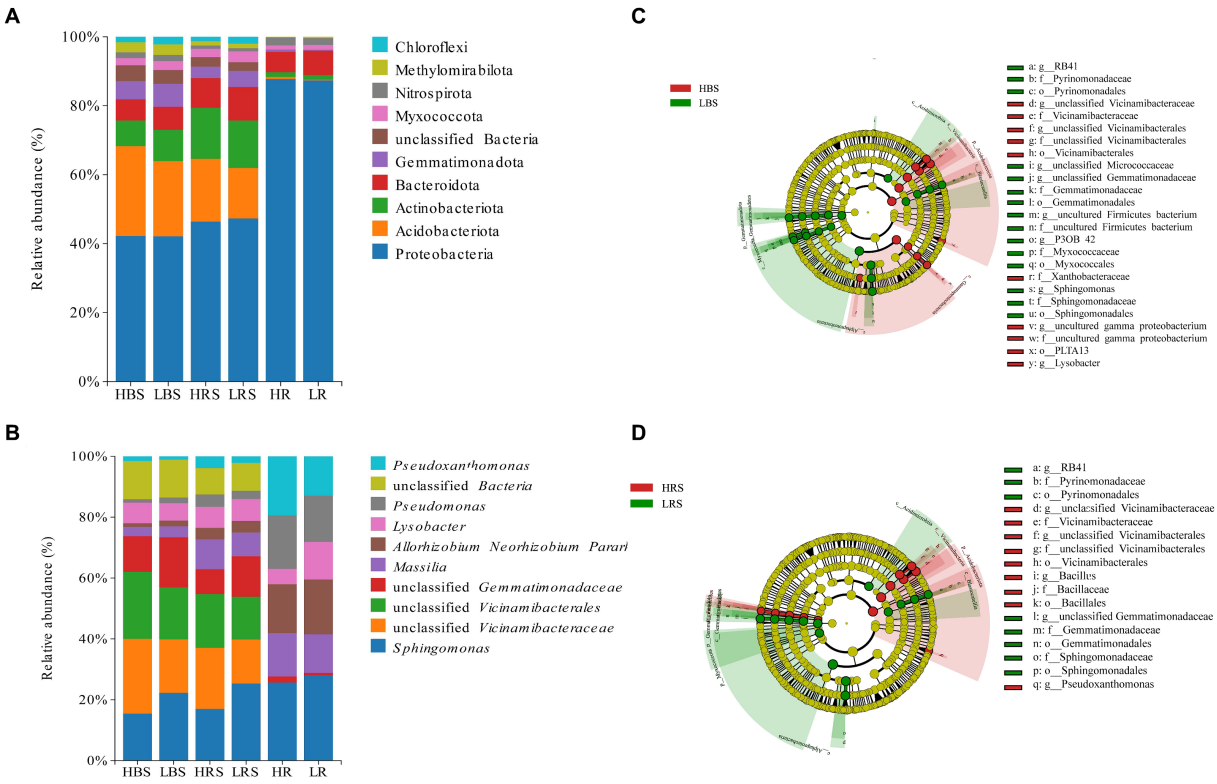

FIGURE 4
Relative abundances on **(A)** phylum and **(B)** genus levels of bacteria of different soil and root samples. Cladogram based on LEfSe analysis (LDA > 3.5) of the **(C)** bulk soil samples bacterial community and **(D)** rhizosphere soil samples, showing that bacteria that significantly differ between groups, color-coded in red and green. The classification levels from phylum to genus are organized concentrically, with the innermost circle representing phylum and the outermost representing genus. The yellow circle represents ASVs with no significant difference.

network of the low-productive soil type samples was simpler. The co-occurrence analyses for the bulk soil and rhizosphere soil samples showed an augment in graph density for the low-productive soil type samples, indicating that bacteria of the bulk soil and rhizosphere soil samples in low-productive soil type samples are closely connected. This may be due to lower module numbers in the low-productive soil type samples, resulting in lower average path lengths and greater susceptibility to external environmental factors. Moreover, the rhizosphere soil samples of the low-productive soil type samples have a higher number of negative links, indicating a more competitive correlation among bacteria in the LRS network. However, for the root samples of the low-productive soil type samples, the graph density was decreased, suggesting that the LR networks had prominent 'small-world' modularity and hierarchy of their topological properties. As a consequence, the inter-bacterial network of the bulk soil and rhizosphere soil samples in the low-productive soil type samples is simpler and more unstable. Additionally, the LR exhibited small-world characteristics, rendering a more efficient whole system in the root samples from the low-productive soil type samples (Table 3).

Based on Spearman's correlations, we further selected the genus with a correlation of >0.6 and a *p*-value of <0.05 and analyzed the microbial networks of bacteria in different groups. The results showed that a few nodes were designated as a connector in the respective networks, and the connectors were defined as key taxa ($Zi \leq 2.5$, $Pi > 0.62$). In the bulk soil samples, the high-productive soil type samples had two connectors, both belonging to the Proteobacteria, while the low-productive soil type samples had four connectors. In addition to Proteobacteria, Chloroflexi (as one of the main carbon-fixing phyla) and Bacteroidota were determined to be connectors in the low-productive soil type samples. This phototrophic mode is a stress-resistant strategy under nutrient-deficiency conditions, indicating that the low-productive soil type samples need to include other phyla to enhance bacterial interactions. In contrast, in the rhizosphere soil samples, there were four connectors in both high- and low-productive soil type samples. Compared with the low-productive soil type samples where all connectors are Proteobacteria, the high-productive soil type samples also include Acidobacteria and Bacteroidetes in their connectors, with Bacteroidetes being the primary degraders of complex carbohydrate biomass. In the root samples, the connectors of both high- and low-productive soil type samples are Proteobacteria. In summary, there are significant differences in key species at different productivity levels, which are mainly manifested in the bulk soil and rhizosphere soil samples, and these two ecological niches have different nutritional availability and needs (Table 4).

3.7 Relationships between bacterial communities and soil chemical properties

The Mantel test was performed to assess the relationship between bacterial communities and environmental factors,

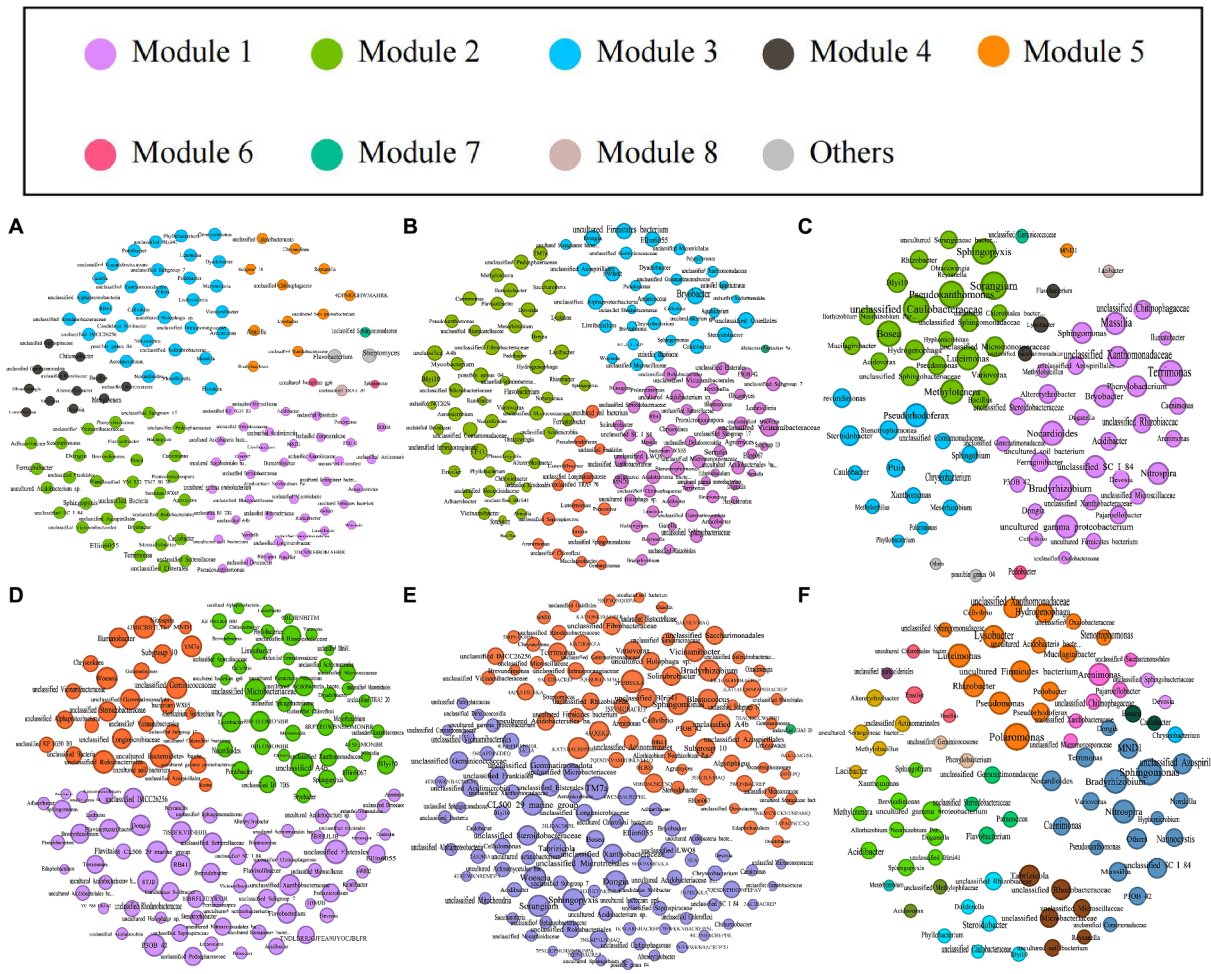

FIGURE 5
The networks of co-occurring bacterial in the bulk soils, rhizosphere soils, and root samples in both high- and low-productive soil type samples of six groups, **(A)** HBS, **(B)** HRS, **(C)** HR, **(D)** LBS, **(E)** LRS, and **(F)** HR, based on correlation analysis. The co-occurring networks are colored by module. Within each panel, the node size corresponds proportionally to its degree of connectivity.

including six chemical properties: pH, EC, SOM, AN, AP, and AK. The changes in the bacterial community structure between high- and low-productive soil type samples in the bulk soil and rhizosphere soil samples were associated with SOM (bulk soil: $R = 0.767$, $p = 0.001$; rhizosphere soil: $R = 0.683$, $p = 0.001$), AN (bulk soil: $R = 0.699$, $p = 0.001$; rhizosphere soil: $R = 0.608$, $p = 0.001$), and soil EC (bulk soil: $R = 0.325$, $p = 0.019$; rhizosphere soil: $R = 0.361$, $p = 0.010$) (Table 5). In addition, the heatmap was used to further analyze the correlation between environmental factors and bacterial genera. In the bulk soil and rhizosphere soil samples, unclassified Gemmatimonadaceae and *Sphingomonas* showed significant negative correlations with AN, respectively. Unclassified Vicinamibacteraceae and *Lysobacter* exhibited a significant positive correlation with SOM and AN. In the root samples, a significant negative correlation was found between *Massilia* and EC. From the above analyses, it can be observed that soil fertility indices such as SOM, AN, and EC were the main factors affecting the soil bacterial community. The interaction between soil fertility index and bacteria would determine the soil productivity (Figure 6).

4 Discussion

4.1 Correlations between microbial communities and soil properties

Soil microbes are vital components of agricultural ecosystems, and their abundance and diversity are correlated with soil fertility. Increasing the application of organic fertilizers significantly enhances both soil organic matter content and microbial diversity (Karami et al., 2012; Ai et al., 2015; Tkacz et al., 2015). Below-ground interactions by the maize–peanut intercropping increased the number of beneficial soil bacteria and diversity of bacterial communities (Simpson and Shannon indices), which were conducive to improving the supply capacity of soil nutrients (N and P) and the stability of the soil microbial ecosystems (Li et al., 2007). Continuous cropping, mono-nutrient depletion, and declining soil fertility led to a decrease in soil microbial abundance (Chao1 index) and diversity (Shannon index), which promoted the growth of soil harmful microorganisms (Zhao et al., 2016). In this study, compared with the high-productive soil type samples, the bacterial richness indices (ACE and Chao1) in the bulk

TABLE 3 Topological properties of co-occurring bacterial networks and their corresponding random networks.

Network metrics	BS		RS		R	
	HBS	LBS	HRS	LRS	HR	LR
Number of nodes	137	141	157	163	81	86
Number of edges	817	912	1,037	1,282	255	224
Number of positive correlations (%)	53.00	53.07	53.52	49.06	52.94	62.50
Number of negative correlations (%)	47.00	46.93	46.48	50.94	47.06	37.50
Average path length (APL)	2.812	2.616	2.651	2.571	3.576	3.539
Graph density	0.088	0.092	0.085	0.097	0.079	0.061
Network diameter	6	5	6	6	9	8
Average clustering coefficient (avg CC)	0.451	0.419	0.422	0.417	0.47	0.478
Number of modules	10	3	5	3	10	16
Modularity (M)	6.256	6.510	6.114	−273.055	6.330	1.839

soil, rhizosphere soil, and root samples in the low-productive soil type samples were lower than those in the high-productive soil type samples, indicating that the lack of nutrients in the low-productive soil type samples may affect the growth and abundance of certain microorganisms.

However, in the current study, the bacterial diversity indices (Shannon and Simpson) in the low-productive soil type samples were higher than those in the high-productive soil type samples. Similar results were also obtained from previous research studies. For example, the diversity of bacterial communities decreased due to the increase in the amount of soil nitrogen; the Shannon diversity index of inter-root soil bacterial communities in plants was higher under low nitrogen conditions than that at high nitrogen levels, probably due to the suppression of beneficial interactions between the microbiome and non-leguminous plants under high fertilizer conditions (Kavamura et al., 2018). In addition, Sun et al. (2015) showed that soil nutrient content was low in the no-fertilizer treatment for 30 consecutive years, and bacterial abundance (16S rRNA gene copy number) was correspondingly low but phylogenetic diversity (PD) was high, which was manifested by higher bacterial diversity and analyzed that soil pH was the strongest driver of bacterial diversity.

In summary, bacterial diversity is influenced by various factors. In certain situations, nutrient deficiency may lead to decreased bacterial richness. Conversely, under specific conditions where the proliferation of certain bacterial communities is suppressed, bacterial diversity might increase in the low-productive soil type samples.

4.2 Relation between soil chemical properties and microbial community structure

In recent years, several studies on the differences in microbial communities in various types of farmlands have been conducted. Bandara et al. compared the differences in root microbial communities between high-yield and low-yield sites in soybean farms in Pennsylvania. The high-yield sites had more root-colonizing bacteria that increase plant growth, and the soil conditions were not ideal for symbiotic nitrogen fixation in low-yield sites (Bandara et al., 2021). Our study further analyzed the bacterial community structures of the high- and low-productive soil type samples in Hebei province of China. The dominant bacterial phyla in different productive soil types were consistent, such as Proteobacteria, Acidobacteriota, Actinobacteria, Bacteroidota, and Gemmatimonadota. These bacterial phyla are common in soils of various habitats and play essential roles in nutrient cycling, such as carbon, nitrogen, and phosphorus cycling (Li Y. et al., 2019; Ibrahim et al., 2020; Xue et al., 2020; Yan et al., 2021). Among them, Proteobacteria exhibited the highest abundance and played a crucial role in nutrient cycling in environments rich in organic matter (Ren C. J. et al., 2018). Meanwhile, Actinobacteria and Bacteroidota played dominant roles in the decomposition of soil organic matter (Six et al., 2004). Gemmatimonadota play an important role in nutrient transformation. Gemmatimonadota can transform inorganic nutrient elements into organic forms through its metabolism, such as nitrate into amino acids (Ibrahim et al., 2020).

Although the dominant bacteria of the high- and low-productive soil type samples were similar, there were obvious differences in the abundance of some bacteria between the two soil fertility samples. Members of Acidobacteria, especially those in the family Pyrinomonadaceae and order Pyrinomonadales, order Myxococcales (phylum Myxococcota), order Gemmatimonadales (phylum Gemmatimonadota), and order Sphingomonadales (Proteobacteria) were significantly more abundant in the low-productive soil type samples compared to the high-productive soil type samples. Acidobacteria were considered oligotrophic microorganisms, which thrive in low-nutrient soil, leading to a high abundance in the low-productive soil type samples (Jackson et al., 2007). Certain groups within the phylum Gemmatimonadota can adapt to dry conditions. Given the low water retention capacity of the low-productive soil type samples due to the soil structure, this adaptation might explain the increased abundance of these groups (Yan et al., 2021). Additionally, there was a notable increase in the abundance of Sphingomonas (a class within Proteobacteria) in the low-productive soil type samples. This bacterium is among the top five root pathogens (Deng et al., 2022). Conversely, there was a significant decrease in the abundance of certain groups in the phylum Actinobacteria, such as those in the order Rhizobiales, the family Xanthomonadaceae, and the genera *Lysobacter* and *Pseudoxanthomonas*. The genus *Lysobacter* exhibited strong antagonistic activity against various plant pathogenic fungi, bacteria, and nematodes and became a new type of biocontrol bacteria

10.3389/fmicb.2024.1391428

TABLE 4 Nodes identified as connectors of bacterial networks (HBS, LBS, HRS, LRS, HR, and LR).

Genus	Role	Abundance (%)	Degree	Phyla	Zi value	Pi value
HBS						
Unclassified Xanthobacteraceae	Connector	0.0139	9	Proteobacteria	0.4975	0.6400
Steroidobacter	Connector	0.0086	19	Proteobacteria	0.4954	0.6400
LBS						
Unclassified Chloroflexi	Connector	0.0093	13	Chloroflexi	0.0000	0.6400
Sphingomonas	Connector	0.0693	17	Proteobacteria	0.4902	0.6667
Terrimonas	Connector	0.0079	17	Bacteroidota	1.1180	0.6563
Unclassified SC I 84	Connector	0.0060	16	Proteobacteria	−1.1180	0.6250
HRS						
Unclassified Comamonadaceae	Connector	0.0076	20	Proteobacteria	−0.8492	0.6250
Unclassified Vicinamibacteraceae	Connector	0.0619	31	Acidobacteriota	0.8235	0.6250
Pedobacter	Connector	0.0096	7	Bacteroidota	−0.4611	0.6667
Unclassified Xanthobacteraceae	Connector	0.0088	12	Proteobacteria	−0.8018	0.7222
LRS						
Cellvibrio	Connector	0.0056	26	Proteobacteria	−1.0394	0.6250
BIyi10	Connector	0.0062	15	Proteobacteria	0.4103	0.6667
Altererythrobacter	Connector	0.0212	6	Proteobacteria	0.0000	0.6250
HR						
Altererythrobacter	Connector	0.0268	7	Proteobacteria	0.0000	0.6667
Bradyrhizobium	Connector	0.0138	12	Proteobacteria	1.1674	0.6667
Pseudorhodoferax	Connector	0.0092	11	Proteobacteria	0.3529	0.6627
Pseudomonas	Connector	0.0593	7	Proteobacteria	0.0000	0.6250
LR						
Cellvibrio	Connector	0.0167	6	Proteobacteria	−0.4590	0.6250
Altererythrobacter	Connector	0.0316	5	Proteobacteria	1.2585	0.6250
Bradyrhizobium	Connector	0.0130	11	Proteobacteria	1.1893	0.6400
Sphingopyxis	Connector	0.0100	5	Proteobacteria	0.0000	0.6667
Acidibacter	Connector	0.0164	5	Proteobacteria	0.0000	0.6667

The topological importance of each node is determined by two attributes: the within-module connectivity Zi, which gauges how strongly a node is connected to others within its module, and the among-module connectivity Pi, which measures the extent of a node's connections to nodes in different modules.

TABLE 5 Mantel analysis of environmental factors and bacterial genera.

Environment	BS		RS		R	
	R	P	R	P	R	P
pH	0.102	0.195	0.168	0.139	0.016	0.435
EC	0.325	0.019	0.361	0.010	0.221	0.097
SOM	0.767	0.001	0.683	0.001	0.190	0.106
AN	0.699	0.001	0.608	0.001	0.129	0.167
AP	−0.051	0.586	−0.032	0.457	−0.069	0.570
AK	0.091	0.184	0.006	0.366	−0.021	0.446

with biocontrol potential (Hayward et al., 2010). Furthermore, in the rhizosphere soil samples of the low-productive soil type samples, the abundance of *Bacillus*, a genus within Firmicutes, was significantly lower than that in the high-productive soil type samples. Rhizobiales, which are capable of symbiotic nitrogen fixation in leguminous plants, leading to increased nitrogen absorption by plant roots, demonstrated higher abundance in the low-productive soil type samples (Masson-Boivin and Sachs, 2018). *Bacillus* are saprotrophic microorganisms, have preferable biocontrol and growth-promoting potential, and are a potential strain to control wheat root rot caused by *F. oxysporum* (Xiong et al., 2015). The abundance of these microorganisms serves as an indicator of the health of soil microbial communities. Kandasamy

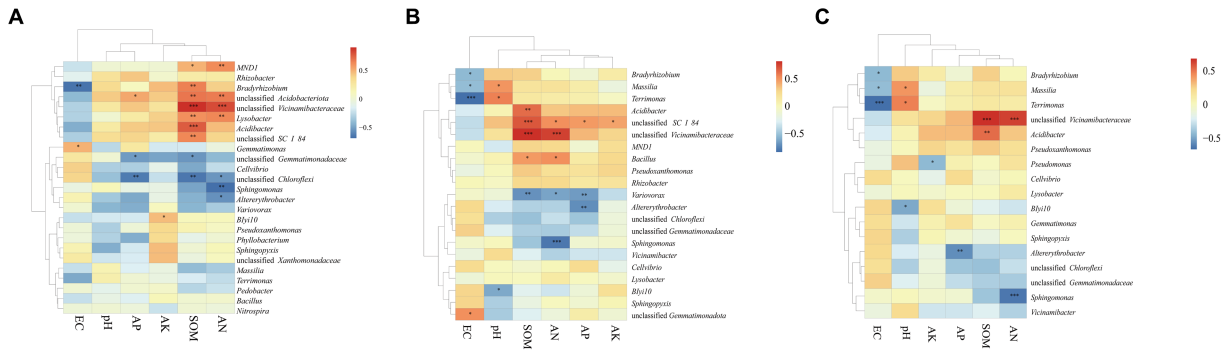

FIGURE 6
Correlation-based heatmap method reveals the relation between environmental factors and bacterial genera in the **(A)** BS, **(B)** RS, and **(C)** R. The different colors and intensities were adjusted based on associations among traits.

et al. (2019) found that introducing key microorganisms from high-productive soil type samples altered the original microbial characteristics in the low-productive soil type samples, thereby enhancing soil biological health and yield. These findings lay the foundation for constructing healthy microbial communities in the low-productive soil type samples and targeted the regulation of soil microbes.

4.3 Shifts of structure in co-occurrence network for different productive soil types

In ecological environments, microorganisms cannot survive in an isolated environment, and they form complex network systems through interactions (Liu J. J. et al., 2015; Liu et al., 2016). In these intricate ecosystems, microbial interactions are more crucial for ecological functionality than microbial abundance and diversity (Zhao et al., 2022a). In recent years, researchers predominantly focused on microbial diversity and community structure in ecosystems, neglecting interactions between microbial communities. However, the functionality of microbial communities in complex ecosystems was not analyzed comprehensively in these studies. Based on the differences between bacterial communities in wheat-planting soil and root samples from different soil types in Hebei province, the inter-species interactions were further analyzed in this study. Co-occurrence network analysis was used to explore the interactions within bacterial communities in the high- and low-productive soil type samples. The results indicated that compared with the high-productive soil type samples, the low-productive soil type samples exhibited lower average clustering coefficients, fewer modules, and longer average path lengths, indicating decreased complexity in bacterial coexistence networks. The complexity of the microbial symbiotic network in the ecosystem is influenced by many factors. Zheng et al. (2021) showed that the occurrence of *Ralstonia solanacearum* has reduced the complexity of its microbial network compared with that in healthy tobacco plants. Although this study did not statistically analyze the occurrence of wheat root rot disease in the low-productive soil type samples, the reduced complexity of the bacterial network to some extent may reflect the unhealthy condition of soil microbial communities in the low-productive soil type samples.

However, the reduced complexity of the microbial network does not necessarily imply weakened interactions among microbial communities. Zhao et al. (2022b) observed enhanced microbial interactions during the composting process despite the decreased complexity and diversity of microbial networks during high-temperature fermentation. Similarly, Yuan et al. (2021) found increased microbial interactions despite decreased microbial diversity with increasing temperatures. The current study also revealed higher average degrees in the co-occurrence networks of the bulk soil and rhizosphere soil samples in the low-productive soil type samples, indicating tighter connections among soil microbes. In addition, the LR exhibited small-world characteristics, which could allow the effects of a perturbation to distribute rapidly through the entire network, rendering a more efficient system, consistent with the findings by Yuan et al.

Key taxa within soil microbial network modules play a crucial role in maintaining the stability of functional microbial communities (Zhou et al., 2010). Due to their specific roles in different substance cycles in soil, these key taxa are vulnerable to disruption caused by changes in soil environments (Steele et al., 2011). Changing the hub species (that is, species that are associated with many other species) would impact the community structure, such as rebuilding microbial co-occurrence networks (Faust and Raes, 2012). Therefore, analyzing key taxa in different habitats is essential. Fan et al. (2019) found that long-term fertilization suppressed the growth of nitrogen-fixing microbial clusters (modules), leading to reduced soil nitrogen-fixing functionality and indicating that fertilizer regulation of soil ecological functions might occur through the growth of specific microbial modules. Similar conclusions were drawn in the research by Wagg et al. These studies indicate that higher microbial community diversity and more complex microbial network significantly increased soil ecosystem function related to carbon and nutrient cycling (Wagg et al., 2019). In this study, significant differences in key bacterial species were found between samples from the high- and low-productive soil types, especially in the bulk soil and rhizosphere soil samples, where the differences were more pronounced. Except for the Proteobacteria phylum (a key phylum in the high-productive soil type samples), other phyla microorganisms such as Chloroflexi and Bacteroidota were also served as connectors to increase the microbial interactions in the bulk soil samples from low-productive soil types. In contrast, in the rhizosphere soil and root samples, key species in the low-productive soil type samples belonged

to Proteobacteria. The results indicated low capacities for specific enrichment of dominant keystone strains, and other genera microorganisms may be used to establish network interactions in the low-productive soil type samples due to a lack of key genera.

In summary, the enhanced understanding of soil bacterial communities will aid in regulating the balance of soil ecosystems and provide a theoretical reference for further targeted regulation mechanisms in the low-productive soil type samples. However, to further identify the direct impact of soil environmental variables on microbial communities, future research should consider trait-based approaches. For instance, dose–response relationships between soil variables and microbial growth should be quantified. Alternatively, modern multi-omics technology such as metagenomics, metatranscriptomics, and metabolomics can provide a better understanding of microbial communities and their functionality, revealing possibilities for manipulating microbial communities to enhance crop nutrient utilization efficiency and reduce fertilizer usage.

Data availability statement

The names of the repository/repositories and accession number(s) can be found below: https://www.ncbi.nlm.nih.gov/sra/PRJNA1081352.

Author contributions

HN: Writing – original draft, Conceptualization, Investigation, Software. MY: Writing – review & editing, Conceptualization. XC: Writing – review & editing, Investigation. JZ: Methodology, Writing – review & editing. YC: Investigation, Writing – review & editing. YS: Investigation, Writing – review & editing. SZ: Investigation, Writing – review & editing. AS: Writing – review & editing. YH: Writing – review & editing, Investigation, Methodology, Software.

Funding

The author(s) declare financial support was received for the research, authorship, and/or publication of this article. The authors are grateful for the support of the National Key R&D Program of China (2021YFD1901004).

Conflict of interest

The authors declare that the research was conducted in the absence of any commercial or financial relationships that could be construed as a potential conflict of interest.

Publisher's note

All claims expressed in this article are solely those of the authors and do not necessarily represent those of their affiliated organizations, or those of the publisher, the editors and the reviewers. Any product that may be evaluated in this article, or claim that may be made by its manufacturer, is not guaranteed or endorsed by the publisher.

Supplementary material

The Supplementary material for this article can be found online at: https://www.frontiersin.org/articles/10.3389/fmicb.2024.1391428/full#supplementary-material

References

Ai, C., Liang, G. Q., Sun, J. W., Wang, X., He, P., Zhou, W., et al. (2015). Reduced dependence of rhizosphere microbiome on plant-derived carbon in 32-year long-term inorganic and organic fertilized soils. *Soil Biol. Biochem.* 80, 70–78. doi: 10.1016/j.soilbio.2014.09.028

Bandara, A. Y., Weerasooriya, D. K., Trexler, R. V., Bell, T. H., and Esker, P. D. (2021). Soybean roots and soil from high- and low-yielding field sites have different microbiome composition. *Front. Microbiol.* 12:675352. doi: 10.3389/fmicb.2021.675352

Belimov, A. A., Shaposhnikov, A. I., Azarova, T. S., Syrova, D. S., Kitaeva, A. B., Ulyanich, P. S., et al. (2022). Rhizobacteria mitigate the negative effect of aluminum on pea growth by immobilizing the toxicant and modulating root exudation. *Plants* 11:2416. doi: 10.3390/plants11182416

Bolyen, E., Rideout, J. R., Dillon, M. R., Bokulich, N. A., Abnet, C. C., al-Ghalith, G. A., et al. (2019). Reproducible, interactive, scalable and extensible microbiome data science using QIIME 2. *Nat. Biotechnol.* 37, 852–857. doi: 10.1038/s41587-019-0209-9

Buckland, K. R., Reeve, J. R., Creech, J. E., and Durham, S. L. (2018). Managing soil fertility and health for quinoa production and weed control in organic systems. *Soil Tillage Res.* 184, 52–61. doi: 10.1016/j.still.2018.07.001

Callahan, B., McMurdie, P., Rosen, M., Han, A. W., Johnson, A. J. A., and Holmes, S. P. (2016). DADA2: high-resolution sample inference from Illumina amplicon data. *Nat. Methods* 13, 581–583. doi: 10.1038/nmeth.3869

Chi, Q.-D., Wang, J., Liu, Y.-Q., Zhao, J., Cheng, Y., Cai, Z.-C., et al. (2021). Varying interactive effects of climate, soil properties, and gross nitrogen dynamics on biomass production between the topsoil and the subsoil in natural grassland ecosystems. *Eur. J. Soil Biol.* 104:103299. doi: 10.1016/j.ejsobi.2021.103299

Deng, Y., Jiang, Y. H., Yang, Y., He, Z., Luo, F., and Zhou, J. (2012). Molecular ecological network analyses. *BMC Bioinformatics.* 13:113. doi: 10.1186/1471-2105-13-113

Deng, X. H., Zhang, N., Li, Y. C., Zhu, C., Qu, B., Liu, H., et al. (2022). Bio-organic soil amendment promotes the suppression of by inducing changes in the functionality and composition of rhizosphere bacterial communities. *New Phytol.* 235, 1558–1574. doi: 10.1111/nph.18221

Duan, Y., Xu, M., Gao, S., Liu, H., Huang, S., and Wang, B. (2016). Long-term incorporation of manure with chemical fertilizers reduced total nitrogen loss in rain-fed cropping systems. *Sci. Rep.* 6:33611. doi: 10.1038/srep33611

Fan, K., Delgado-Baquerizo, M., Guo, X., Wang, D., Wu, Y., Zhu, M., et al. (2019). Suppressed N fixation and diazotrophs after four decades of fertilization. *Microbiome* 7:143. doi: 10.1186/s40168-019-0757-8

Fan, M., Li, J., Tang, Z., and Shangguan, Z. (2020). Soil bacterial community succession during desertification in a desert steppe ecosystem. *Land Degrad. Dev.* 31, 1662–1674. doi: 10.1002/ldr.3545

Fanin, N., and Bertrand, I. (2016). Aboveground litter quality is a better predictor than belowground microbial communities when estimating carbon mineralization along a land-use gradient. *Soil Biol. Biochem.* 94, 48–60. doi: 10.1016/j.soilbio.2015.11.007

Faust, K., and Raes, J. (2012). Microbial interactions: from networks to models. *Nat. Rev. Microbiol.* 10, 538–550. doi: 10.1038/nrmicro2832

Guo, Y. S., Furrer, J. M., Kadilak, A. L., Hinestroza, H. F., Gage, D. J., Cho, Y. K., et al. (2018). Bacterial extracellular polymeric substances amplify water content variability at the pore scale. *Front. Environ. Sci.* 6:93. doi: 10.3389/fenvs.2018.00093

Hayward, A. C., Fegan, N., Fegan, M., and Stirling, G. R. (2010). Stenotrophomonas and lysobacter: ubiquitous plant-associated gamma-proteobacteria of developing significance in applied microbiology. *J. Appl. Microbiol.* 108, 756–770. doi: 10.1111/j.1365-2672.2009.04471.x

Hebei Provincial Bureau of Quality and Technical Supervision (2021). DBDB13/t 5406–2021. Classification diagnosis of main indicators of farmland fertility.

Husenov, B., Asaad, S., Muminjanov, H., Garkava-Gustavsson, L., and Johansson, E. (2021). Sustainable wheat production and food security of domestic wheat in Tajikistan:

implications of seed health and protein quality. *Int. J. Environ. Res. Public Health* 18:5751. doi: 10.3390/ijerph18115751

Ibrahim, M. M., Tong, C. X., Hu, K., Zhou, B., Xing, S., and Mao, Y. (2020). Biochar-fertilizer interaction modifies N-sorption, enzyme activities and microbial functional abundance regulating nitrogen retention in rhizosphere soil. *Sci. Total Environ.* 739:140065. doi: 10.1016/j.scitotenv.2020.140065

Jackson, R. B., Fierer, N., and Schimel, J. P. (2007). New directions in microbial ecology. *Ecology* 88, 1343–1344. doi: 10.1890/06-1882

Kandasamy, S., Liu, E. Y. R., Patterson, G., Saldias, S., Ali, S., and Lazarovits, G. (2019). Introducing key microbes from high productive soil transforms native soil microbial community of low productive soil. *Microbiology* 8:e895. doi: 10.1002/mbo3.895

Karami, A., Homaee, M., Afzalinia, S., Ruhipour, H., and Basirat, S. (2012). Organic resource management: impacts on soil aggregate stability and other soil physico-chemical properties. *Agric. Ecosyst. Environ.* 148, 22–28. doi: 10.1016/j.agee.2011.10.021

Kavamura, V. N., Hayat, R., Clark, I. M., Rossmann, M., Mendes, R., Hirsch, P. R., et al. (2018). Inorganic nitrogen application affects both taxonomical and predicted functional structure of wheat rhizosphere bacterial communities. *Front. Microbiol.* 9:1074. doi: 10.3389/fmicb.2018.01074

Li, Y., Fang, F., Wei, J. L., Wu, X., Cui, R., Li, G., et al. (2019). Humic acid fertilizer improved soil properties and soil microbial diversity of continuous cropping Peanut: a three-year experiment. *Sci. Rep.* 9:12014. doi: 10.1038/s41598-019-48620-4

Li, M., Jordan, N. R., Koide, R. T., Yannarell, A. C., and Davis, A. S. (2016). Meta-analysis of crop and weed growth responses to arbuscular mycorrhizal fungi: implications for integrated weed management. *Weed Sci.* 64, 642–652. doi: 10.1614/WS-D-16-00050.1

Li, J., Li, Z., Li, X., Tang, X., Liu, H., Li, J., et al. (2023). Effects of spraying KH2PO4 on flag leaf physiological characteristics and grain yield and quality under heat stress during the filling period in winter wheat. *Plan. Theory* 12:1801. doi: 10.3390/plants12091801

Li, L., Li, S. M., Sun, J. H., Zhou, L. L., Bao, X. G., Zhang, H. G., et al. (2007). Diversity enhances agricultural productivity via rhizosphere phosphorus facilitation on phosphorus-deficient soils. *Proc. Natl. Acad. Sci. USA* 104, 11192–11196. doi: 10.1073/pnas.0704591104

Li, J., Zelong, W., and Yuan, J. (2019). Impact of agro-farming activities on microbial diversity of acidic red soils in a camellia Oleifera Forest. *Rev. Bras. Ciênc. Solo* 43:e0190044. doi: 10.1590/18069657rbcs20190044

Liu, C. C., Liu, Y. G., Guo, K., Wang, S., Liu, H., Zhao, H., et al. (2016). Aboveground carbon stock, allocation and sequestration potential during vegetation recovery in the karst region of southwestern China: a case study at a watershed scale. *Agric. Ecosyst. Environ.* 235, 91–100. doi: 10.1016/j.agee.2016.10.003

Liu, J. J., Sui, Y. Y., Yu, Z. H., Shi, Y., Chu, H., Jin, J., et al. (2015). Soil carbon content drives the biogeographical distribution of fungal communities in the black soil zone of Northeast China. *Soil Biol. Biochem.* 83, 29–39. doi: 10.1016/j.soilbio.2015.01.009

Liu, C. L., Wu, Y. Z., and Liu, Q. J. (2015). Effects of land use on spatial patterns of soil properties in a rocky mountain area of northern China. *Arab. J. Geosci.* 8, 1181–1194. doi: 10.1007/s12517-013-1233-6

Looft, T., Johnson, T. A., Allen, H. K., Bayles, D. O., Alt, D. P., Stedtfeld, R. D., et al. (2012). In-feed antibiotic effects on the swine intestinal microbiome. *Proc. Natl. Acad. Sci.* 109, 1691–1696. doi: 10.1073/pnas.1120238109

Lu, J., Li, S., Wu, X., Liang, G., Gao, C., Li, J., et al. (2023). The dominant microorganisms vary with aggregates sizes in promoting soil carbon accumulation under straw application. *Arch. Agron. Soil Sci.* 69, 1–17. doi: 10.1080/03650340.2021.1955354

Magoc, T., and Salzberg, S. L. (2011). FLASH: fast length adjustment of short reads to improve genome assemblies. *Bioinform.* 27, 2957–2963. doi: 10.1093/bioinformatics/btr507

Masson-Boivin, C., and Sachs, J. L. (2018). Symbiotic nitrogen fixation by rhizobia – the roots of a success story. *Curr. Opin. Plant Biol.* 44, 7–15. doi: 10.1016/j.pbi.2017.12.001

Pellegrino, E., Gamper, H. A., Ciccolini, V., and Ercoli, L. (2020). Forage rotations conserve diversity of arbuscular mycorrhizal fungi and soil fertility. *Front. Microbiol.* 10:2969. doi: 10.3389/fmicb.2019.02969

Philippot, L., Chenu, C., Kappler, A., Rillig, M. C., and Fierer, N. (2023). The interplay between microbial communities and soil properties. *Nat. Rev. Microbiol.* 22, 226–239. doi: 10.1038/s41579-023-00980-5

Qin, J., Bian, C., Duan, S., Wang, W., Li, G., and Jin, L. (2022). Effects of different rotation cropping systems on potato yield, rhizosphere microbial community and soil biochemical properties. *Front. Plant Sci.* 13:999730. doi: 10.3389/fpls.2022.999730

Rabbi, S. M. F., Warren, C. R., Macdonald, C., Trethowan, R. M., and Young, I. M. (2022). Soil-root interaction in the rhizosheath regulates the water uptake of wheat. *Rhizosphere* 21:100462. doi: 10.1016/j.rhisph.2021.100462

Ren, C. J., Wang, T., Xu, Y. D., Deng, J., Zhao, F., Yang, G., et al. (2018). Differential soil microbial community responses to the linkage of soil organic carbon fractions with respiration across land-use changes. *For. Ecol. Manag.* 409, 170–178. doi: 10.1016/j.foreco.2017.11.011

Ren, D., Yang, Y., Yang, Y., Richards, K., and Zhou, X. (2018). Land-water-food nexus and indications of crop adjustment for water shortage solution. *Sci. Total Environ.* 626, 11–21. doi: 10.1016/j.scitotenv.2018.01.071

Rousk, J., Brookes, P. C., and Bååth, E. (2010). Investigating the mechanisms for the opposing pH relationships of fungal and bacterial growth in soil. *Soil Biol. Biochem.* 42, 926–934. doi: 10.1016/j.soilbio.2010.02.009

Segata, N., Izard, J., Waldron, L., Gevers, D., Miropolsky, L., Garrett, W. S., et al. (2011). Metagenomic biomarker discovery and explanation. *Genome Biol.* 12:R60. doi: 10.1186/gb-2011-12-6-r60

Six, J., Bossuyt, H., Degryze, S., and Denef, K. (2004). A history of research on the link between (micro)aggregates, soil biota, and soil organic matter dynamics. *Soil Tillage Res.* 79, 7–31. doi: 10.1016/j.still.2004.03.008

Steele, J. A., Countway, P. D., Xia, L., Vigil, P. D., Beman, J. M., Kim, D. Y., et al. (2011). Marine bacterial, archaeal and protistan association networks reveal ecological linkages. *ISME J.* 5, 1414–1425. doi: 10.1038/ismej.2011.24

Sun, A., Jiao, X.-Y., Chen, Q., Wu, A. L., Zheng, Y., Lin, Y. X., et al. (2021). Microbial communities in crop phyllosphere and root endosphere are more resistant than soil microbiota to fertilization. *Soil Biol. Biochem.* 153:108113. doi: 10.1016/j.soilbio.2020.108113

Sun, R. B., Zhang, X. X., Guo, X. S., Wang, D., and Chu, H. (2015). Bacterial diversity in soils subjected to long-term chemical fertilization can be more stably maintained with the addition of livestock manure than wheat straw. *Soil Biol. Biochem.* 88, 9–18. doi: 10.1016/j.soilbio.2015.05.007

Tkacz, A., Cheema, J., Chandra, G., Grant, A., and Poole, P. S. (2015). Stability and succession of the rhizosphere microbiota depends upon plant type and soil composition. *ISME J.* 9, 2349–2359. doi: 10.1038/ismej.2015.41

Veldkamp, E., Schmidt, M., Powers, J. S., and Corre, M. D. (2020). Deforestation and reforestation impacts on soils in the tropics. *Nat. Rev. Earth Environ.* 1, 590–605. doi: 10.1038/s43017-020-0091-5

Wagg, C., Schlaeppi, K., Banerjee, S., Kuramae, E. E., and van der Heijden, M. G. A. (2019). Fungal-bacterial diversity and microbiome complexity predict ecosystem functioning. *Nat. Commun.* 10:4841. doi: 10.1038/s41467-019-12798-y

Xiao, J., Chen, S. Y., Sun, Y., Wu, S., Liang, W., and Yang, S. (2022). Effects of mechanical weeding on soil fertility and microbial community structure in star anise (Hook.F.) plantations. *PLoS One* 17:e0266949. doi: 10.1371/journal.pone.0266949

Xiao, R., Huang, D., du, L., Tang, X., Song, B., Yin, L., et al. (2024). Molecular insights into linkages among free-floating macrophyte-derived organic matter, the fate of antibiotic residues, and antibiotic resistance genes. *J. Hazard. Mater.* 471:134351. doi: 10.1016/j.jhazmat.2024.134351

Xiong, W., Zhao, Q. Y., Zhao, J., Xun, W., Li, R., Zhang, R., et al. (2015). Different continuous cropping spans significantly affect microbial community membership and structure in a vanilla-grown soil as revealed by deep pyrosequencing. *Microb. Ecol.* 70, 209–218. doi: 10.1007/s00248-014-0516-0

Xue, Y. F., Tian, J., Quine, T. A., Powlson, D., Xing, K., Yang, L., et al. (2020). The persistence of bacterial diversity and ecosystem multifunctionality along a disturbance intensity gradient in karst soil. *Sci. Total Environ.* 748:142381. doi: 10.1016/j.scitotenv.2020.142381

Yan, H., Ji, Y., Liu, J., Liu, F., Hu, Y., and Kuang, W. (2016). Potential promoted productivity and spatial patterns of medium- and low-yield cropland land in China. *J. Geogr. Sci.* 26, 259–271. doi: 10.1007/s11442-016-1267-2

Yan, T. T., Xue, J. H., Zhou, Z. D., and Wu, Y. (2021). Biochar-based fertilizer amendments improve the soil microbial community structure in a karst mountainous area. *Sci. Total Environ.* 794:148757. doi: 10.1016/j.scitotenv.2021.148757

Yuan, M. M., Guo, X., Wu, L., Zhang, Y., Xiao, N., Ning, D., et al. (2021). Climate warming enhances microbial network complexity and stability. *Nat. Clim. Chang.* 11, 343–348. doi: 10.1038/s41558-021-00989-9

Zhang, X., Chen, K., and Li, K. (2023). Detection of meteorological influence on bread wheat quality in Hebei province, China based on the gradient boosting decision tree. *Front. Plant Sci.* 14:1083665. doi: 10.3389/fpls.2023.1083665

Zhao, Y. P., Lin, S., Chu, L. X., Gao, J., Azeem, S., and Lin, W. (2016). Insight into structure dynamics of soil microbiota mediated by the richness of replanted. *Sci. Rep.* 6:26175. doi: 10.1038/srep26175

Zhao, Y. X., Lou, Y. C., Qin, W. Z., Cai, J., Zhang, P., and Hu, B. (2022a). Interval aeration improves degradation and humification by enhancing microbial interactions in the composting process. *Bioresour. Technol.* 358:127296. doi: 10.1016/j.biortech.2022.127296

Zhao, Y. X., Zhuge, C. X., Weng, Q., and Hu, B. (2022b). Additional strains acting as key microbes promoted composting process. *Chemosphere* 287:132304. doi: 10.1016/j.chemosphere.2021.132304

Zheng, Y. F., Han, X. B., Zhao, D. L., Wei, K., Yuan, Y., Li, Y., et al. (2021). Exploring biocontrol agents from microbial keystone taxa associated to suppressive soil: a new attempt for a biocontrol strategy. *Front. Plant Sci.* 12:655673. doi: 10.3389/fpls.2021.655673

Zhou, J., Deng, Y., Luo, F., He, Z., Tu, Q., and Zhi, X. (2010). Functional molecular ecological networks. *MBio* 1:e00169–10. doi: 10.1128/mbio.00169-10

Frontiers in Microbiology

Explores the habitable world and the potential of microbial life

The largest and most cited microbiology journal which advances our understanding of the role microbes play in addressing global challenges such as healthcare, food security, and climate change.

Discover the latest Research Topics

See more →

Frontiers

Avenue du Tribunal-Fédéral 34
1005 Lausanne, Switzerland
frontiersin.org

Contact us

+41 (0)21 510 17 00
frontiersin.org/about/contact